THE PHYSICAL REVIEW

VOLUME 75 Second Series NUMBER 10

MAY 15, 1949

Published for the

AMERICAN PHYSICAL SOCIETY

by the

AMERICAN INSTITUTE OF PHYSICS

Lancaster, Pa. and New York, N. Y.

A journal of ex

Published by the American Institute of P
for the
AMERICAN PHYSICAL SOCI

Officers

President

E. W. Loomis
University of Illinois
Urbana, Illinois

Vice-President

I. I. Rabi
Columbia University
New York, New York

Secretary

K. K. Darrow
Bell Telephone Laboratories
Office:
Columbia University
New York 27, New York

Treasurer

G. B. Pe
Columbia University
New York 27, New York

Local Secretary
for the Pacific Coast

I. Kaplan
University of California at
Angeles
Los Angeles, California

Managing Editor

John T. Tate
University of Minnesota
Minneapolis, Minnesota

The Physical Review
Entered as second-class matter
acceptance for mailing at special

REVIEW

published by E. L. Nichols

BOARD OF EDITORS

Associate Editors

A. Goldsmith
M. Phillips
F. Watanabe

should be submitting
Minnesota. This
charge of $4 per page
instructions will be
concerning papers in the
Publication Manager,
New York 22, New York.

Subscription Price

Single Numbers

complete year is
to July, 1939;
1920–December, 1
January, 1942–December,

Back

back numbers should be
Pennsylvania, or to the
New York 22, New York.

of members if the
order; in this case
Institute of Physics.
Cornell University,

Entered as second-class matter, December, Publication
Pennsylvania, under the
233, P.L. & R., authorized

THE
PHYSICAL REVIEW

A journal of experimental and theoretical physics established by E. L. Nichols in 1893

SECOND SERIES, VOL. 75, No. 10 MAY 15, 1949

Characteristics of the Fission Product Cs^{135}

NATHAN SUGARMAN
*Los Alamos Scientific Laboratory, University of California, Los Alamos, New Mexico**

and

Institute for Nuclear Studies, University of Chicago, Chicago, Illinois

(Received February 2, 1949)

Two samples of Xe^{135} of high intensity were prepared at the Los Alamos homogeneous pile. The decay products of the gas contained a Cs activity presumed to be Cs^{135}. The half-life of Cs^{135} was found to be $(2.1\pm0.7)\times10^6$ yr. and the maximum energy of its β^--radiations 0.21 Mev. No γ-radiations were detected. The capture cross section of Cs^{135} for pile neutrons was determined to be 14.5 ± 4 barns.

INTRODUCTION

IN earlier fission product studies the attempts to detect radiation from Se^{79}, Pd^{107}, I^{129}, and Cs^{135} were unsuccessful. On the assumption that the half-lives of all four species were long, minimum half-lives were estimated from the failure to detect the radiations and the factors limiting observation.[1] Chief among the latter have been the detection apparatus for extremely soft β^--radiation and the strength of the sources prepared.

The three earlier experiments designed to measure the half-life of Cs^{135} have given minimum half-life estimates ranging from 1200 years to 3.5×10^6 years. In the first experiment Finkle and Sugarman[2] isolated an iodine sample from irradiated uranium and after decay of the 6.7-hr. I^{135} and 9.2-hr. Xe^{135} analyzed for Cs. No radiations were detected by a mica end-window counter. On the assumption that the radiations of Cs^{135} would have been detected in this apparatus, a minimum half-life for Cs^{135} was calculated to be 1200 years. In a similar experiment Glendenin and Metcalf[3] estimated the half-life as >2000 years. In a third experiment Engelkemeir[4] looked for radiations from Cs^{135} in the decay products of 30 millicuries of 9.2-hr. Xe^{135}. The absence of radiations in a mica end-window counter led to a half-life estimate of $>3.5\times10^6$ years for β^--particles sufficiently energetic to penetrate the 3.5-mg/cm² mica window and the ~12-mg/cm² Cs carrier source without appreciable loss in intensity. The Cs sample was also examined with a windowless counter and if a β^--energy of 30 kev was assumed, the minimum half-life estimate fell to 2.5×10^4 years.

In the present experiments, two samples of Xe^{135}, containing 36 curies and 30 curies of activity, were prepared at the Los Alamos homogeneous pile.[5] After decay of the Xe activity, the decay products were examined for Cs activity. A new Cs activity was found, the maximum energy of the β^--radiations being 0.21 ± 0.01 Mev as determined by Feather analysis of the Al absorption curve. The timing of the experiments was such as to indicate that the new activity is Cs^{135}, the daughter of 9.2-hr. Xe^{135}. The half-life for Cs^{135} calculated from the observed activity and the total activity of the Xe parent is $(2.1\pm0.7)\times10^6$ yrs. This value is not inconsistent with the limiting value set by Engelkemeir[4] if one considers the loss in intensity arising

* The Xe^{135} samples were prepared during the summer of 1948 when the author was a consultant to the Los Alamos Scientific Laboratory.

[1] "Nuclei formed in fission," issued by The Plutonium Project, J. Am. Chem. Soc. **68**, 2411 (1946); Rev. Mod. Phys. **18**, 513 (1946).

[2] B. Finkle and N. Sugarman, Plutonium Project Record, **9B**, 7.40.1 (1946).

[3] L. E. Glendenin and R. P. Metcalf, Plutonium Project Report, CC-2219 (1945).

[4] D. W. Engelkemeir, Plutonium Project Record, **9B**, 7.40.2 (1946).

[5] R. F. Christy, AEC declassified document, MDDC No 72 (June 18, 1946).

TABLE I. Activity of 9.2-hr. Xe^{135} prepared at water boiler.

Experiment	Gas cell	Activity of 9.2-hr. Xe^{135} at time of bulb filling (c/min.)	Counting geometry*	Fraction of gas in cell	Calculated activity of 9.2-hr. Xe^{135} at bulb filling time (dis/sec.)
1	1	14,000 (1st filling)	0.033	5.73×10^{-9}	1.23×10^{12}
	2	12,870 (1st filling)	0.033	5.14×10^{-9}	1.26×10^{12}
		14,200 (2nd filling)	0.033	5.14×10^{-9}	1.39×10^{12}
2	1	11,800 (1st filling)	0.033	5.88×10^{-9}	1.01×10^{12}
		13,800 (2nd filling)	0.033	5.88×10^{-9}	1.18×10^{12}
	2	11,700 (1st filling)	0.033	5.26×10^{-9}	1.12×10^{12}

*Average counting geometry of cell determined from measurements with a U_3O_8 β^--standard.

from the absorption of the β^--rays in the source and counter window.

PREPARATION OF Xe^{135}

In the operation of the Los Alamos homogeneous pile (water boiler) the active Kr and Xe isotopes formed in the fission process are swept out of solution and discarded. This pile is, therefore, a convenient source of gaseous fission products freed from the host of non-volatile active products formed in fission. The separation of 9.2-hr. Xe^{135} from the gases emanating from the water boiler during its operation presents a formidable shielding problem because of the many short-lived Kr and Xe activities. The radiation hazard can be substantially reduced if advantage is taken of the fact that only two of the gaseous fission products have parents of appreciable half-life, namely, 5.3-day Xe^{133} growing from a 22-hr. I^{133} and 9.2-hr. Xe^{135} from 6.7-hr. I^{135}. The active gases produced during the operation of the boiler are removed quite efficiently by the internal bubbling from the radiation decomposition of the water. These gases are discarded. If one gas-sweeps the boiler after its operation and examines the sweeping gas, the only fission products which should be present are those whose parents are sufficiently long-lived to continue generating these species, namely, Xe^{133} and Xe^{135}.

In the isolation of the Xe samples the boiler was operated for some twelve hours. The gases during this period were discarded. The boiler was shut down and the solution swept with He for about 30 minutes at a rate of 50 l/hr. to remove any residual gases. This gas was also discarded. The solution was then swept with He for five hours and the gas was passed through a vacuum line for collection of the Xe^{133} and Xe^{135} activities growing from their I parents during this interval.

The vacuum line for collecting of Xe was shielded by two inches of lead and consisted of a liquid NaOH trap for removal of acid vapor and spray, two glass wool traps for removal of spray, a Drierite trap for removal of the bulk of the water vapor, a dry ice cooled trap for removal of the residual water vapor, an activated charcoal trap cooled by dry ice for adsorption of Xe, and a Toepler pump and 1-l bulb for collection of the Xe after desorption from the charcoal.

After five hours of sweeping at the rate of ~30 l/hr. the He flow was stopped. At this time the activity on the charcoal trap was ~35 r/hr. at ~2 ft. Little activity was present elsewhere in the line except for the NaOH trap which had an observed level of ~2 r/hr. in contact. The dry ice was removed from the charcoal trap and the charcoal allowed to warm up to room temperature. Most of the air swept out of the boiler and adsorbed on the trap is removed but very little Xe is desorbed. To desorb the Xe the trap was heated by passing current through the resistance wire wound around it. The active Xe and residual air thus desorbed from the charcoal were transferred to a 1-l bulb on the line by means of the Toepler pump. The activity level of the Xe at this time corresponded roughly to 10 curies of Ra as measured with a radiation survey meter.

The bulb containing the Xe was then attached to another lead-shielded vacuum line for the transfer of a small aliquot of the gas to a counting cell. This vacuum line consisted of three 1-l bulbs, including the one containing the Xe, joined by sections of small volume. The volume of the bulbs and of each section of the line was measured. A small aliquot of the original gas (~2 ml) was diluted with air and expanded into a 1-l bulb. A small aliquot of this gas was again diluted with air and expanded into the third 1-l bulb. Finally, a small aliquot of the twice-expanded gas was transferred to a counting cell for measurement of the radioactivity.

The two counting cells were of glass, 2 cm across and 1 cm deep, with a wide flange for sealing of a 3-mg/cm² mica window. A micro stopcock was sealed at the bottom of each cell. The volumes of the cells were 3.09 ml and 2.65 ml. The average fractions of the original gas transferred to the cells after the dilution process were 5.8×10^{-9} and 5.2×10^{-9} in the two experiments. The radioactivity in the cells was measured with a 3-mg/cm² mica end-window counter at ~3.3 percent geometry.

Absorption and decay curves taken on the Xe samples showed that the major activity (94 percent) at the time of isolation was the 9.2-hr. Xe^{135}. The other activity present was the 5.3-day Xe^{133}. Two experiments were performed, in each of which samples of Xe^{135} in high intensity were prepared.

In each experiment, both gas cells were filled from the same diluted gas mixture and the activity in each was measured for some time. One of the cells was then emptied and a new diluted gas mixture was prepared by a different dilution procedure and the cell was refilled and the activity followed. The purpose in filling the cell from a new gas dilution was to test the dilution technique and the homogeneity of the gas. The data from the two experiments appear in Table I. The data are not corrected for the absorption or scattering of the β^--radiations because of the difficulty in estimating these corrections. Much of the error will, however, cancel since the two effects contribute oppositely to the observed counting rate.

The discrepancy in the activity of a cell from two different fillings arises from the difference in the dilution technique for each filling, the technique so designed as to give the maximum discrepancy from the inhomogeneity in the diluted gas mixture. Averaging the results from each experiment, weighing the two fillings equally, one finds that the total 9.2-hr. Xe^{135} activity present at the time the bulb was filled was 36 curies in experiment 1 and 30 curies in experiment 2. The estimated error in these values is ~20 percent. Much of this error comes from the uncertainty in the counting geometry and scattering and absorption corrections for the β^--radiations.

RADIOACTIVITY OF Cs^{135}

About a week after the preparation of the Xe^{135} samples, the bulbs containing the active Xe were washed with dilute acetic acid solution. The acid wash solution was introduced into the bulbs and shaken vigorously in order to wash the decay products out of the gas phase and from the walls. This process was repeated five times. The combined wash solutions from each bulb were examined for radioactivity some two months later. Samples were prepared for radioactivity detection by evaporation and by chemical analysis for radio-Cs. The analysis consisted of addition of Cs carrier to an aliquot of the wash solution, $CsClO_4$ precipitations, $Fe(OH)_3$ scavengings, precipitations of a mixed $CsI\text{-}BiI_3$ compound, and finally precipitation of cesium cobaltinitrite.[6] Measurements with a 2-mg/cm² mica end-window tube showed the presence of activity in the evaporated samples and the Cs precipitates. The absorption characteristics of the radiations of the evaporated samples were the same as those from the chemically separated Cs samples, and the level of activity in the evaporated samples from an aliquot of solution agreed with that of the Cs samples after self-absorption corrections were made. Analysis by the Feather method[7] of the Al absorption curve of the radiations of this activity led to an estimate of the maximum β^--ray energy of 0.21 ± 0.01 Mev (Fig. 1). The γ-counting rate was less than 1 c/min. for a Cs sample of 600 β^- c/min. This result indicates the absence of γ-rays of moderate energy in high yield.

Assignment of the new Cs activity to Cs^{135} is very probable from the way in which it was prepared. This assignment is consistent with the timing of the experiments in which the He gas-sweeping of the pile was retained for Xe adsorption after discarding the first half-hour sweeping to eliminate active gases from short-lived halogens. The only Cs isotopes which should be present in the decay products of the gas are Cs^{133} arising from the decay of Xe^{133} and Cs^{135} from Xe^{135}. Since Cs^{133} is a naturally occurring stable isotope, assignment of the activity to Cs^{133} would mean that the expected mode of decay would be isomeric transition. The shape of the Al absorption curve of the Cs activity is characteristic of a β^- spectrum rather than that of a conversion electron spectrum. The mass assignment of 135 appears most probable.

The half-life of Cs^{135} was determined from the measured activity of an aliquot of the wash solution and the previously determined Xe^{135} activity of the samples. Small aliquots of each wash solution were evaporated on 2-mil platinum foils and counted. No decay in the activity of the Cs samples was observed over a period of three months. Corrections for geometry, backscattering,[8] and absorp-

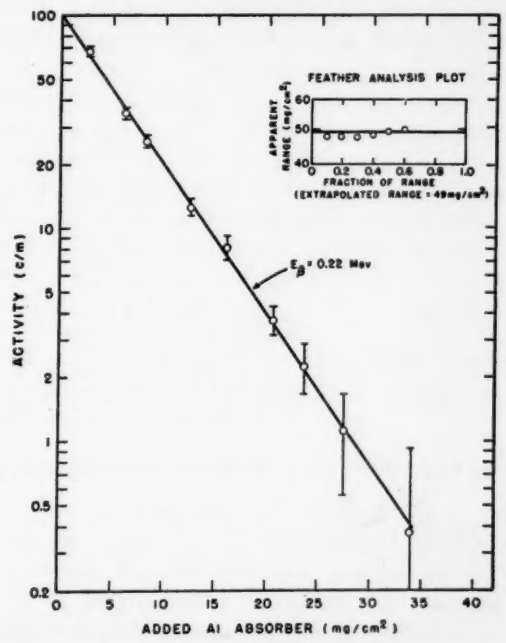

FIG. 1. Aluminum absorption curve of Cs^{135}. At zero added Al absorber the absorber thickness is about 3 mg/cm² from the counter window and air gap.

[6] Nathan Sugarman, J. Chem. Phys. **17**, 11 (1949).
[7] N. Feather, Proc. Camb. Phil. Soc. **34**, 599 (1938).
[8] Engelkemeir, Seiler, Steinberg, Winsberg, and Novey, Plutonium Project Record, **9B**, 2.4 (1946).

TABLE II. Half-life of Cs^{135}.

Experiment	Average activity of 3 samples (c/min.)	Aliquot	Counting geometry	Absorption correction (1-mg/cm² air, 2-mg/cm² mica)	Back-scattering correction	Total activity Cs^{135} in wash solution (dis/sec.)	Total activity 9.2-hr. Xe^{135} originally present (dis/sec.)	Half-life Cs^{135} (years)
1	111.0	0.02	0.175	1.71	0.67	600	1.32×10^{12}	2.30×10^{6}
2	116.5	0.02	0.175	1.71	0.67	635	1.12×10^{12}	1.85×10^{6}

tion of the β^--radiation in the 1-mg/cm² air and 2-mg/cm² mica window of the counter were made. The average half-life of Cs^{135} determined from these measurements is 2.1×10^6 years. The error estimated in the half-life of Cs^{135} is ~35 percent which includes the error in the Xe^{135} activity. The data are given in Table II.

NEUTRON CAPTURE CROSS SECTION OF Cs^{135}

Aliquots of the Cs^{135} wash solutions were irradiated in the thimble of the Argonne heavy water pile for about four days for the production of Cs^{136}. Radiochemical analyses for Cs were performed on the irradiated solutions three days after the end of the irradiation. Decay and absorption measurements on the Cs samples showed the presence of the 13.7-day Cs^{136} activity.[9] The cross section of Cs^{135} for the capture of pile neutrons was determined to be 13.7 barns from samples of the Cs solution from experiment 1, and 15.3 barns for the Cs solution from experiment 2. The average cross section is 14.5 barns with an estimated error of ~30 percent.

Some of the work on which this document was based was supported by the joint program of the ONR and the AEC.

ACKNOWLEDGMENT

It is a pleasure to acknowledge the assistance given the author in the work done at the Los Alamos Scientific Laboratory by Dr. S. Katcoff, Messrs. F. L. Benson and J. W. Starner, and especially Mr. J. A. Bridge who devised the techniques for remote control operation of the apparatus.

[9] L. E. Glendenin, private communication on nuclear characteristics of Cs^{136}.

On the g_J Values of the Alkali Atoms*

The Hyperfine Structure of the Alkali Atoms

P. KUSCH
Columbia University, New York, New York

AND

H. TAUB
Columbia University and The City College of New York, New York

(Received January 20, 1949)

Measurements have been made on the ratios of the g_J values of the alkali atoms. It is found that the g_J values of Li^6, Li^7, Na and K^{39} are identical to within one part in 40,000. The g_J of Rb and Cs, however, are greater than the g_J of the other alkalis by 5 and 13 parts in 100,000 respectively. Effects which modify the g_J value of an atom may be expected to depend on the detailed electronic configuration of an atom. Since the g_J values of Li, Na and K are shown, in present experiments, to be equal, it can be presumed, in view of the different electronic structures of these atoms, that perturbing effects are negligible and that the g_J values of these atoms are, in fact, equal to the electron spin gyromagnetic ratio.

INTRODUCTION

THIS paper describes a precision determination of the ratios of the g_J values of the alkali atoms. The measurement was undertaken because the g_J values of one or more of the alkali atoms enter into the experimental determination of at least two important physical quantities, the spin gyromagnetic ratio of the electron and the gyromagnetic ratio of the proton.

In a recent experiment, Kusch and Foley[1] have measured the spin gyromagnetic ratio of the electron by a determination of the ratios of the total electronic g values of two different atomic energy states. Interpretation of the data of those experiments depends on the assumption that the g_J values are properties of an ideal state and are not characteristic, to a significant extent, of a particular atomic system. In particular, the result depends on the ratio of the g_J of indium in the $^2P_{\frac{1}{2}}$ state to that of sodium in the $^2S_{\frac{1}{2}}$ state and on the ratio of the g_J of gallium in the $^2P_{\frac{1}{2}}$ state to that of sodium in the $^2S_{\frac{1}{2}}$ state. The two ratios yield the same value for the spin gyromagnetic ratio of the electron, and from this agreement it may be inferred that perturbations which affect the g_J values of the two $^2P_{\frac{1}{2}}$ states are identical. Since this is not likely to be the case if the perturbations are large, it follows that the g_J values are very nearly those characteristic of a pure $^2P_{\frac{1}{2}}$ state. In a similar way, if it can be shown that the g_J value of sodium is common to most of the alkali atoms, it can again be assumed that its g_J value is characteristic of a pure $^2S_{\frac{1}{2}}$ state and the interpretation of the result of Kusch and Foley becomes much more significant than it is in the absence of the indicated information.

In the paper following the present paper, Taub and Kusch[2] present a determination of the gyromagnetic ratio of the proton, g_H, in terms of the g_J value of indium in the $^2P_{\frac{1}{2}}$ state and in terms of the g_J value of caesium in the $^2S_{\frac{1}{2}}$ state. By use of the ratio $g_J(^2P_{\frac{1}{2}}, \text{In})/g_J(^2S_{\frac{1}{2}}, \text{Na})$ previously reported[1] and by use of the ratio $g_J(^2S_{\frac{1}{2}}, \text{Cs})/g_J(^2S_{\frac{1}{2}}, \text{Na})$ reported in this paper, it is possible to find the value of g_H in terms of the g_J of sodium. Since the results of the present experiment indicate that the g_J value of sodium does not deviate to a significant extent from the spin gyromagnetic ratio, it is possible to find the g value of the proton in terms of the spin gyromagnetic ratio of the electron and hence in terms of the fundamental quantity, the orbital gyromagnetic ratio of the electron.

As has been pointed out before, a precision measurement of the absolute value of a gyromagnetic ratio is not feasible with currently available methods, because of the difficulty of producing magnetic fields which are known in terms of absolute standards to a high order of precision. The ratios of g values may, however, be measured with extremely high precision.

The general experimental procedures employed in the measurements here reported are identical to those previously discussed.[1]

THE HYPERFINE STRUCTURE OF THE ALKALI ATOMS

In order to determine the ratios of the g_J values of any two atoms by an observation of appropriately chosen lines in the h.f.s. spectra of the two atoms, it is necessary to know the interaction constants which determine the frequencies of the lines in a magnetic field. These constants, when $J=\frac{1}{2}$, are $\Delta\nu$, the zero field separation of the two levels for which $F=I+\frac{1}{2}$ and $F=I-\frac{1}{2}$, and the

* Publication assisted by the Ernest Kempton Adams Fund for Physical Research of Columbia University.

[1] P. Kusch and H. M. Foley, Phys. Rev. 74, 250 (1948).

[2] H. Taub and P. Kusch, Phys. Rev. 75, 1481 (1949).

TABLE I. Values of $\Delta\nu$ and g_J/g_I.

Atom	$\Delta\nu\times10^{-6}$ (sec.$^{-1}$)	g_J/g_I
Li^6	228.208±0.005	−4472±3
Li^7	803.512±0.015	−1693.7±0.8
Na^{23}	1771.61±0.03	−2487.8±2.5
K^{39}	461.723±0.010	−14130±100
Rb^{85}	3035.7±0.15	−6853±40
Rb^{87}	6834.1±1.0	−2016±7
Cs^{133}	9192.76±1.0	−5018±3

ratio g_J/g_I. These quantities can be determined directly from an observation of the h.f.s. spectrum of the atom in question.

For the purposes of this experiment as well as for the requirements of the experiment on the determination of the g value of the proton, the values of $\Delta\nu$ of Li^6, Li^7, Na^{23}, K^{39} and Cs^{133} have been redetermined. The $\Delta\nu$ of Li^6, Li^7 and K^{39} have been measured by the method of observing the transitions, $\Delta F=\pm1$, $\Delta m=\pm1$ at very weak fields. This method has been extensively discussed by Kusch and Millman.[3] We find that the values of $\Delta\nu$ are the following:

$$Li^6(228.208\pm0.005)\times10^6 \text{ sec.}^{-1}$$
$$Li^7(803.512\pm0.015)\times10^6 \text{ sec.}^{-1}$$
$$K^{39}(461.723\pm0.010)\times10^6 \text{ sec.}^{-1}.$$

The $\Delta\nu$ of Na^{23} and Cs^{133} are inconveniently high (1770 and 9190 mc) for a direct measurement of this quantity at weak fields. Large $\Delta\nu$ have been determined[4] in the past by measurement at intermediate fields of lines described by the low field quantum numbers $(F,m)\leftrightarrow(F,m\pm1)$ or of lines described by the high field quantum numbers $(m_J,m_I)\leftrightarrow(m_J,m_I\pm1)$. The Breit-Rabi formula, which describes[3] the energy levels of an atom in a state in which $J=\frac{1}{2}$, permits a determination from such data of $\Delta\nu$ and of the ratio g_J/g_I. This method is of rather poor precision since a fractional error in the observation of the line frequencies may appear as a much larger fractional error in $\Delta\nu$.

Another procedure, not heretofore employed in the determination of $\Delta\nu$, is, however, available. This procedure depends on the fact that some of the lines $(F,m)\leftrightarrow(F,m\pm1)$ attain a maximum frequency at characteristic values of the magnetic field. (See, for example, some curves in references 3 and 4, which indicate the dependence of the frequency of such lines on magnetic field.)

The frequency of a line arising from the transition $(I\pm\frac{1}{2},m)\leftrightarrow(I\pm\frac{1}{2},m-1)$ is given by:

$$f=(\Delta\nu/2)\{[1+4mx/(2I+1)+x^2]^{\frac{1}{2}} -[1+4(m-1)x/(2I+1)+x^2]^{\frac{1}{2}}\}\pm g_I\mu_0H/h, \quad (1)$$

where

$$x=(g_J-g_I)\mu_0H/h\Delta\nu. \quad (2)$$

All the lines appear as components of doublets of frequency separation $2g_I\mu_0H$, except when the magnetic level $m=\pm(I+\frac{1}{2})$ is involved in the transition. The mean frequency of the doublet, f_m, is as given by Eq. (1) except that the term $g_I\mu_0H$ does not occur. If we call $x_1=-2m/(2I+1)$ and $x_2=-2(m-1)/(2I+1)$, the value of x at which f_m has a maximum is given by:

$$x=(x_1x_2+1)/(x_1+x_2) +[(x_1x_2+1)^2/(x_1+x_2)^2-1]^{\frac{1}{2}}. \quad (3)$$

The value of $f_m/\Delta\nu$ may then be determined by Eq. (1). It can be shown that a maximum occurs only when $-(I-\frac{3}{2})\leqslant m\leqslant0$, $-(I-\frac{1}{2})\leqslant m-1\leqslant-1$. In the case of Na^{23} where $I=\frac{3}{2}$, the only line for which a maximum occurs is the line $(F,0)\leftrightarrow(F,-1)$. For Cs where $I=7/2$, a maximum will occur for the lines $(F,-2)\leftrightarrow(F,-3)$, $(F,-1)\leftrightarrow(F,-2)$ and $(F,0)\leftrightarrow(F,-1)$.

From an observation of the maximum mean frequency of a doublet it is thus possible to determine $\Delta\nu$ with the same precision as that with which the frequency has been measured. This method of determining $\Delta\nu$ has a marked advantage over other methods since in the region of field at which the frequency is a maximum, the line frequencies are almost entirely field independent. Accordingly, small inhomogeneities in the magnetic field will not affect the width and shape of the lines. A significant measurement of a line frequency may be made to a precision limited only by the accuracy of the frequency measuring equipment and by the natural width of the lines, and the possibility of systematic error arising from unsymmetrical broadening is avoided. It is not necessary to determine the frequency of the line at precisely the maximum, for $f/\Delta\nu$ varies very slowly with field in the neighborhood of the maximum. Accordingly, from an approximate knowledge of g_J/g_I and from the measured doublet separation $2g_I\mu_0H$, it is possible to find an approximate value of H. If $\Delta\nu$ is also approximately known, x may be found to a sufficiently good degree of approximation to permit the determination of a new value of $\Delta\nu$ with a precision limited only by the precision of frequency determination. If observations of the frequencies of both components of a doublet are made over a fairly large range of field on either side of the field for maximum frequency, it is possible to determine the value of g_J/g_I; for if an incorrect value of g_J/g_I is assumed, the calculated value of $\Delta\nu$ will be either an increasing or a decreasing function of field and g_J/g_I may be adjusted until the calculated value of $\Delta\nu$ is independent of field.

For the case of Cs, the maximum mean frequency of the doublet $(F,-2)\leftrightarrow(F,-3)$ occurs at $x=0.1(11+(21)^{\frac{1}{2}})=1.55926$. At this field and for this line, $2f/\Delta\nu=0.1((12)^{\frac{1}{2}}-(7)^{\frac{1}{2}})(11+(21)^{\frac{1}{2}})^{\frac{1}{2}}$ which

[3] Kusch, Millman, and Rabi, Phys. Rev. **57**, 765 (1940).
[4] S. Millman and P. Kusch, Phys. Rev. **58**, 438 (1940).

gives a mean doublet frequency of about 1485 mc. This is inconveniently high. The maximum mean frequency of the doublet $(F,-1)\leftrightarrow(F,-2)$ occurs at $x=0.5(3+(5)^{\frac{1}{2}})=2.618034$. At this field, $2f/\Delta\nu=0.5((5)^{\frac{1}{2}}-2)(3+(5)^{\frac{1}{2}})^{\frac{1}{2}}=0.27009$. This corresponds to a line frequency of about 1240 mc. The field of 8600 gauss is readily attained in our apparatus.

In the course of three independent runs, twenty-five individual observations were made of the frequencies of each member of the doublet at values of x ranging from 2.4 to 2.75. This range included not only the value of the field at which the mean of the doublet attains a maximum frequency, but included also the fields at which each component of the doublet separately attains a maximum frequency. From the maximum of the mean a value $\Delta\nu=9192.76\times10^6$ sec.$^{-1}$ is obtained. This known value of $\Delta\nu$ permits a calculation to be made, in terms of g_J/g_I, of the maximum frequency of each component of the doublet. We thus find that $g_J/g_I=-5018$. Using this value of the ratio g_J/g_I, the twenty-five values of $\Delta\nu$ calculated from the individual observations give a mean $\Delta\nu$ as stated above with an average deviation of 0.10×10^6 sec.$^{-1}$. Further, the individually calculated $\Delta\nu$ show no variation with magnetic field as would be expected if the value g_J/g_I had been incorrectly chosen. We take $\Delta\nu(\mathrm{Cs})=(9192.76\pm0.10)\times10^6$ sec.$^{-1}$ and $g_J/g_I=-5018\pm3$. The precision measures attached to the values are considerably greater than the probable error deduced from the internal consistency of the data and are given because of a small uncertainty in the frequency of the quartz crystal against which all frequencies were measured.

As an additional check, measurements have also been made at intermediate fields ($x\sim0.6$) of the frequencies of the four lines $(F,3)\leftrightarrow(F,2)$ and $(F,-2)\leftrightarrow(F,-3)$. From these data we find $\Delta\nu(\mathrm{Cs})=9192.51\times10^6$ sec.$^{-1}$ and $g_J/g_I=-5017$. The discrepancy between this value of $\Delta\nu$ and the one previously given can be accounted for by an error in the mean frequency of the doublet $(F,3)\leftrightarrow(F,2)$ of 1 part in 10^5. We consider the agreement to be good; the agreement indicates that the frequencies of lines are given by Eq. (1) to a very high order of precision.

Further evidence of the validity of our procedures can be obtained by a comparison of the present result with the ratio $g_I(\mathrm{Cs})/g_I(\mathrm{Li}^7)=0.33743$ recently measured by Bitter[5] by use of the nuclear absorption method. All nuclear g values heretofore published, and obtained[6] by molecular beam methods, assume that the g_J values of the alkali atoms are equal to g_s which is, in turn, assumed to be exactly 2. If we use the previously published value of $g_I(\mathrm{Li}^7)$ and the new value of $g_I(\mathrm{Cs})$ obtained by making the same assumption about g_J, we find for the ratio the value 0.3375. The agreement of our value with that of Bitter is well within our experimental error and indicates the possibility of obtaining accurate values of the ratio g_J/g_I by the indicated procedures.

TABLE II. Observations from which the ratios of the g_J values of the alkali atoms are calculated.

Run	Atom	Line		Calc. H'
I	Li^7	(2,−1)	(2,−1)	604.479
		(2,−2)	(1,−1)	604.486
	Na	(2,−1)	(2,−2)	604.460
II	Li^7	(2,−1)	(2,−2)	509.088
		(2,−2)	(1,−1)	509.090
	Li^6	(3/2,−3/2)	(3/2,−1/2)	509.097
	Na	(2,−1)	(2,−2)	509.084
III	Li^7	(2,−1)	(2,−2)	605.236
		(2,−2)	(1,−1)	605.232
	K^{39}	(2,−1)	(2,−2)	605.246
		(2,−2)	(1,−1)	605.201
IV.	Na	(2,−1)	(2,−2)	603.584
		(2,−2)	(1,−1)	603.604
	Cs	(F, 1)	(F, 0)	603.684
V	Na	(2,−1)	(2,−2)	603.525
		(2,−2)	(1,−1)	603.534
	Cs	(F, 1)	(F, 0)	603.583
VI	Na	(2,−1)	(2,−2)	603.237
	Cs	(F, 1)	(F, 0)	603.329
		(F, 3)	(F, 2)	603.305
VII	Na	(2,−1)	(2,−2)	603.881
	Cs	(F, 1)	(F, 0)	603.971
		(F, 3)	(F, 2)	603.957
VIII	Na	(2,−1)	(2,−2)	603.930
	Cs	(F,−1)	(F,−2)	604.001
		(F, 2)	(F, 1)	604.024
IX	Na	(2,−1)	(2,−2)	603.707
	Rb^{87}	(F, 0)	(F,−1)	603.724
	Rb^{85}	(F, 1)	(F, 0)	603.732
X	Na	(2,−1)	(2,−2)	603.891
	Rb^{87}	(F, 0)	(F,−1)	603.930
	Rb^{85}	(F, 1)	(F, 0)	603.941

For Na the only lines which have a maximum frequency are the components of the doublet $(F,0)\leftrightarrow(F,-1)$. The mean frequency of the doublet has a maximum at $x=2+\sqrt{3}=3.732$. This corresponds to a field of 2360 gauss. At this field $2f/\Delta\nu=(2-\sqrt{3})^{\frac{1}{2}}$, and the mean frequency is about 458 mc. The mean of a number of observations in the region of maximum frequency gives $\Delta\nu(\mathrm{Na}^{23})=(1771.61\pm0.03)\times10^6$ sec.$^{-1}$. The value of $g_I(\mathrm{Na}^{23})$ given by Millman and Kusch[4] has been used, and we find it to be entirely consistent with our data.

In the experiments to be described in the next section of this paper we use the values of $\Delta\nu$ and g_J/g_I given in Table I. All quantities are taken from previously published work[3,4,6] except where new measurements are presented in this paper.

[5] F. Bitter, Phys. Rev. **75**, 1326 (1949).
[6] S. Millman and P. Kusch, Phys. Rev. **60**, 91 (1941).

THE ELECTRONIC g VALUES OF THE ALKALI ATOMS

In this section are discussed the results of the intercomparison of the g_J values of the atoms Li^6, Li^7, Na^{23}, K^{39}, Rb^{85}, Rb^{87} and Cs^{133}, in their ground states. The general experimental procedures are similar to those previously described.[1] The atomic beam apparatus is fitted with a special oven chamber which permits the rapid interchange of ovens. Suitable lines in the h.f.s. spectrum of each of two alkali atoms are measured in succession at a suitably chosen magnetic field. Since the magnetic field always drifts to some extent during the time required to make the necessary observations, all of the lines are measured several times in rotation and from a suitable reduction of data, line frequencies are found which correspond to some fixed magnetic field. From the observed frequencies of the lines, from the known zero field h.f.s. separation and from the known ratio g_J/g_I, it is possible, by application of Eq. (1), to find the value of $H'=\mu_0 H/h \times 10^{-6}$ at which the lines were observed. The nominal g_J of the atom is assumed in this calculation. If the g_J values of the two atoms depart from their nominal values, g_J^0, by differential amounts, the values of H' will differ. However, under the conditions of the experiment, H' is the same for both atoms; hence the g_J ratio is adjusted to make H' the same. Suppose that $H_1'-H_2'=\Delta H'$. Then $g_{J1}/g_{J2}=(1+\Delta H'/H')g_{J1}^0/g_{J2}^0$.

In Table II are recorded the results of the observations of lines in the spectra of each of two alkali atoms at the same value of the magnetic field. The quantity H' has been found by assuming that $g_J=2$. In the cases of Cs and Rb, H' has been calculated from the mean frequency of the doublet listed in Table II. In the cases of Cs and Rb, the effect of uncertainties in the $\Delta\nu$ is trivial, since the lines are observed in the Zeeman region or in the low intermediate field region and the $\Delta\nu$ enters the calculation only as a small correction term. In cases where two lines, not components of the same doublet, are measured, it is possible, provided g_J/g_I is known, to find H' without prior knowledge of $\Delta\nu$, since the $\Delta\nu$ may itself be calculated from the two observed line frequencies. Adopting this procedure in case *I*, we find $\Delta\nu(Li^7)=803.509\times10^6$ sec.$^{-1}$ and $H'=604.478$. Of the three determinations of the $\Delta\nu$ of Li^7 which are possible from the data of Table II, this one deviates by the largest amount from the previously given value of 803.512×10^6 sec.$^{-1}$. By comparison of the value of $H'=604.478$ with the values given for run *J* in Table II, it is seen that the value of H' derived from measurements on the line $(2,-2)\leftrightarrow(1,-1)$ is excessively sensitive to the assumed value of $\Delta\nu$ and the values of H' derived from this line are therefore not used in further deductions. The same considerations apply to the case of K^{39}, where the internally obtained $\Delta\nu(K^{39})=461.731\times10^6$ sec.$^{-1}$ and $H'=605.248$. Evidently the very small difference between this value of $\Delta\nu$ and that given in Table I has changed the apparent H' found from the line $(2,-2)\leftrightarrow(1,-1)$ by a very large amount. From the two runs, *IV* and *V*, we find that the $\Delta\nu$(Na) is 1771.59 and 1771.60×10^6 sec.$^{-1}$, and here again the line $(2,-2)\leftrightarrow(1,-1)$ is discarded in further deductions. It is to be noted, however, that the very good agreement of the $\Delta\nu$'s calculated from these data with the values more directly obtained is good indication of the validity of the data.

From the runs *I*, *II* and *III* we conclude that the g_J of Li^6, Li^7, Na^{23} and K^{39} are identical to within 1 part in 40,000. However, in the runs *IV–VIII* the mean $\Delta H'=H'(Cs)-H'(Na)=0.081\pm0.004$. Note that eight different lines in the spectrum of Cs have been measured. We conclude that $g_J(Cs)/g_J(Na)=1+\Delta H'/H'=1.000134\pm0.000007$, where the precision measure is the statistical probable error.

Inspection of the runs *IX* and *X* indicates that $g_J(Rb)>g_J(Na)$. The apparent discrepancy between the g_J of Rb^{87} and the g_J of Rb^{85} is within the experimental error of the observations. We conclude from these observations that $g_J(Rb)/g_J(Na)=1.00005\pm0.00001$, where the precision measure is again the statistical probable error.

DISCUSSION

Relativistic effects which influence the g_J value of an electron have been considered by Margenau[7] and others. The g_J values are reduced by about 1 part in 10^5 and the reduction is roughly the same for all the alkali atoms.[1,8] The order of magnitude of this effect is too small to be detected in the present experiments.

The fact that the g_J of Li, Na and K are identical seems to indicate that, within the precision of these measurements, the g_J of these atoms is equal to the spin gyromagnetic ratio, g_s. For if perturbations were to affect the value of g_J, they would presumably affect the different atoms by different amounts. The larger g_J values of Rb and Cs presumably arise from some perturbation. The possible origin of such perturbations has been previously discussed.[1] It is not possible, at the present time, to give a quantitative theory of the effect.

We are indebted to Miss Zelda Marblestone who has reduced much of the data used in this series of experiments.

---

[7] H. Margenau, Phys. Rev. **57**, 383 (1940).
[8] M. Phillips, Phys. Rev. **60**, 100 (1941).

The Magnetic Moment of the Proton*

H. TAUB
Columbia University and The City College of New York, New York

AND

P. KUSCH
Columbia University, New York, New York

(Received January 20, 1949)

The molecular beam magnetic resonance method has been employed to measure, in the same magnetic field, the frequency corresponding to a reorientation of the proton in the molecule NaOH and the frequency corresponding to a transition between certain of the h.f.s. levels of the ground state of both the atoms Cs^{133} and In^{115}. From these data are calculated the ratio of the g factor of the proton, g_H, to the g factor of total electronic angular momentum, g_J, with the result $g_H/g_J(Cs, {}^2S_{\frac{1}{2}}) = 15.1911\times10^{-4}$ and $g_H/g_J(In, {}^2P_{\frac{1}{2}}) = 45.6877\times10^{-4}$. From a knowledge of the ratios $g_J(Cs^{133})/g_J(Na^{23})$ and $g_J(In^{115})/g_J(Na^{23})$ two entirely independent values of the ratio $g_H/g_J(Na^{23})$ have been obtained:

From indium
$g_H/g_J(Na) = 15.1923\times10^{-4}$.
From caesium
$g_H/g_J(Na) = 15.1931\times10^{-4}$.

From the known value of $g_s/g_l = 2(1.00116)$, where g_s and g_l are, respectively, the g factors of electron spin and of orbital angular momentum, and on the basis of the assumptions that $g_s = g_J$ and that $g_l = 1$, we find,

$g_H = 30.4206\times10^{-4} \pm 0.005$ percent.

Including a small diamagnetic correction, the magnetic moment of the proton, μ_H, is

$\mu_H = (15.2106\times10^{-4} \pm 0.005$ percent) Bohr magneton.

INTRODUCTION

THIS paper describes a determination, with high precision, of the magnetic moment of the proton. The data of this experiment yield directly the ratio of the gyromagnetic ratio of the proton, g_H, to the g_J (g of total electronic angular momentum) of indium in the ground state (${}^2P_{\frac{1}{2}}$) and to the g_J of caesium in the ground state (${}^2S_{\frac{1}{2}}$). The ratios (g_J/g_l), where g_l is the g of orbital angular momentum, are known for both indium and caesium from the experiments of Kusch and Foley[1] and Kusch and Taub.[2] Accordingly, the ratio g_H/g_l may be found, and, on the assumption that g_l is identically unity, the value g_H and the ratio μ_H/μ_0 may be calculated, where μ_H is the magnetic moment of the proton and μ_0 the Bohr magneton.

The magnetic moments of nuclei generally, and in particular the magnetic moments of the proton, neutron and deuteron, serve as an important guide to theoretical considerations concerning the forces between fundamental nuclear particles. Aside from the obvious importance of a precise knowledge of the proton moment as a fundamental physical constant, a value of the proton moment permits a precise determination of the neutron, deuteron and triton moments μ_N, μ_D and μ_T from the precisely known ratios μ_N/μ_H,[3] μ_D/μ_H[4] and μ_T/μ_H.[5] Further, the application to nuclear spectroscopy of the methods of nuclear absorption and nuclear induction have yielded precise values of the ratios of magnetic moments of a number of nuclei from which the value of the magnetic moments of the nuclei may be determined with the knowledge of the magnetic moment of the proton. In addition, a measurement of the proton moment permits a calculation of the fine structure constant, α, to be made with the aid of calculations of Fermi,[6] Breit[7] and Meyerott[8] and from a knowledge of the h.f.s. constant of hydrogen, measured by Nafe and Nelson.[9]

The experiment described in this paper is, in principle, identical to an earlier experiment of Millman and Kusch[10] in which the value g_H was compared to the g_J values of the atoms Na^{23}, Rb^{85} and Cs^{133}, all in the ground state, (${}^2S_{\frac{1}{2}}$). In the present experiment, by the application of improved techniques, by the more propitious selection of atoms, and from a more extensive body of data, the ratio μ_H/μ_0 has been determined with a precision

* Publication assisted by the Ernest Kempton Adams Fund for Physical Research of Columbia University.

[1] P. Kusch and H. M. Foley, Phys. Rev. **74**, 250 (1948).
[2] P. Kusch and H. Taub, Phys. Rev. **75**, 1477 (1949).
[3] Bloch, Nicodemus, and Staub, Phys. Rev. **74**, 1025 (1948).
[4] Bloch, Levinthal, and Packard, Phys. Rev. **72**, 1125 (1947).
[5] Bloch, Graves, Packard, and Spence, Phys. Rev. **71**, 551 (1947).
[6] E. Fermi, Zeits. f. Physik **60**, 320 (1930).
[7] G. Breit, Phys. Rev. **35**, 1447 (1930).
[8] G. Breit and E. R. Meyerott, Phys. Rev. **72**, 1023 (1947).
[9] J. E. Nafe and E. B. Nelson, Phys. Rev. **73**, 718 (1948).
[10] S. Millman and P. Kusch, Phys. Rev. **72**, 1023 (1947).

far exceeding the precision of the earlier experiment. Further, present knowledge concerning the g_J ratios of alkali atoms[2] avoids the error of the previous assumption that the g_J value of the ground state of all the alkalis is exactly equal to g_s. In addition, present knowledge of the spin gyromagnetic ratio of the electron in terms of the orbital gyromagnetic ratio of the electron permits a determination of the g value of the proton in terms of the fundamental quantity, the orbital gyromagnetic ratio of the electron.

A direct determination of the magnetic moment of the proton, μ_H, in terms of absolute standards is to be preferred to the present determination which is indirect and which serves to determine the ratio μ_H/μ_0 rather than the absolute value of μ_H. However, a precise determination of the absolute value of μ_H is not feasible, with currently available techniques, on account of the difficulty of making an absolute determination of the intensity of a magnetic field. The ratios of g values may, on the other hand, be determined with a precision comparable to the precision with which one can measure the frequencies of spectral lines. Nevertheless, it is to be noted that in certain calculations, such as in the calculation of the fine structure constant, α, the ratio μ_H/μ_0 is precisely the quantity which is required, and, in addition, of course, the present determination of μ_H/μ_0 yields the absolute value of μ_H with the same precision with which μ_0 is known.

A direct measurement of g_H in terms of the g_J of sodium or lithium would yield the most direct determination of g_H, since for these atoms $g_J=g_s$. However, technical reasons make such a determination extremely difficult and subject to large experimental error. The procedure employed in the present experiments, is to measure g_H in terms of the g_J of caesium and indium. The precise values of these g_J values in terms of the more fundamental quantities g_s and g_I is not known. The value of g_H in terms of g_s is found, however, by a determination of the auxiliary ratios of the g_J of indium to that of sodium and of the g_J of caesium to that of sodium. All the required ratios of g values can be measured to a high degree of precision and the net result is of considerably greater precision than could be obtained by a comparison of g_H to the g_J of sodium directly. The details of the procedure and the reasons which dictate the choice of atoms are discussed below.

THE RATIO g_H/g_J

In a sufficiently strong magnetic field the nuclear spins in a molecule will be decoupled from one another and also from the molecular rotation. In this case, if the net electronic angular momentum is zero, the energy levels due to the interaction of a nuclear magnetic moment with the applied field, H, will be $W=m_I g_N \mu_0 H$, in which m_I and g_N are the magnetic quantum number and the nuclear g factor respectively. An oscillating magnetic field perpendicular to the fixed field will induce transitions for which $\Delta m_I=\pm 1$. Accordingly, in a molecule which contains hydrogen, a nuclear transition due to the proton may be observed at a frequency,

$$f_H=g_H\mu_0 H/h. \tag{1}$$

The energy levels in a magnetic field of the hyperfine structure of an atom for which the quantum number of total orbital angular momentum J is equal to $\frac{1}{2}$ are described by the Breit-Rabi[11] formula:

$$W_{I\pm\frac{1}{2},m_F}=-h\Delta\nu/2(2I+1)+[h\Delta\nu/(g_J/g_I-1)]m_F x \pm(h\Delta\nu/2)[1+(4m_F x)/(2I+1)+x^2]^{\frac{1}{2}}, \tag{2}$$

in which I is the nuclear spin, $\Delta\nu$ is the separation, in frequency units, at zero field, of the two levels which are characterized by the values of the total angular momentum $F=I\pm J=I\pm\frac{1}{2}$, m_F is the projection in the direction of the magnetic field of the total angular momentum, g_J and g_I are respectively the Landé g factors of orbital angular momentum of the atom and of the nuclear spin, and x is defined by

$$x=g_J[1-g_I/g_J]\mu_0 H/h\Delta\nu. \tag{3}$$

If, at a particular magnetic field, a measurement is made of the frequency of a line which results from a transition between levels described by the Breit-Rabi formula, a value of x may be calculated from Eq. (2) in terms of $\Delta\nu$ and the ratio g_J/g_I. A determination, in the same magnetic field, of the frequency, f_H, of a proton resonance permits the determination of the ratio g_H/g_J since, from Eqs. (1) and (3),

$$g_H/g_J=f_H[1-g_I/g_J]/x\Delta\nu. \tag{4}$$

Since the quantities $\Delta\nu$ and g_J/g_I may be determined with no assumptions whatsoever concerning the value of g_J, the ratio g_H/g_J is likewise independent of assumptions concerning g_J.

GENERAL EXPERIMENTAL CONSIDERATIONS

In order that it be possible to observe a nuclear resonance in a molecular beam apparatus, it is necessary that the deflection of the molecular beam, in the inhomogeneous fields of the deflecting magnets, be at least of the order of magnitude of the widths of the slits and detector wire which define the beam. However, since the ratio of the magnetic moment of an atom to the magnetic moment of a nucleus is of the order of the ratio of the Bohr to the nuclear magneton, deflecting fields, adequate to insure sufficient deflection of molecules, will, in

[11] G. Breit and I. I. Rabi, Phys. Rev. 38, 2082 (1931).

general, cause atoms to strike the pole faces of the magnets. Since a readjustment of the deflecting fields may cause an appreciable change in the value of the homogeneous transition field, an adjustment of the deflecting fields to permit in turn an examination of nuclear and atomic resonances, may introduce large systematic errors in the results of an experiment in which a constant transition field is assumed. If, however, one takes advantage of the fact that at characteristic values of the magnetic field, certain states in the hyperfine structure of atoms may have zero magnetic moment,[12] one may, by the appropriate choice of atom and state, use deflecting fields adequate for the molecules and not excessive for the atoms.

It is desirable that comparison of the proton resonance frequency and the atomic resonance frequency be made in as high a magnetic field as possible. For, since the width of the proton resonance is constant and independent of the field, the ratio of the uncertainty in the proton resonance frequency to the frequency itself will decrease as the frequency increases. The maximum field, however, which may be employed is dictated by the maximum field at which the calibrating atom provides a line sufficiently field sensitive to determine with precision the value of the quantity x and which originates in a state which has a zero moment.

Of the states which exhibit zero moments at a particular value of the field, not all are available for the purpose at hand, since states whose moment increases with increasing magnetic field are, in principle, non-focusing states.[13] That is, atoms in such states have the property, that if they deviate from the line along which they have zero moment, the induced moment in the atoms is such as to occasion forces which will cause still further deviations.

All of the lines which have been measured in this experiment result from transitions in which $\Delta m_J=0$ and $\Delta m_I=\pm 1$, first, because transitions of the type $\Delta m_J=\pm 1$ lie for the most part in a frequency range which is neither conveniently attained nor measured, and secondly, because a considerable part of the advantage which might accrue from the high field sensitivity of the frequencies of such lines is canceled by the fact that slight deviations from homogeneity in the transition magnet cause these lines to have excessive widths.

Altogether then, the choice of atom to whose g_J value g_H is to be compared is dictated by the consideration that the atom provide the most field sensitive lines at the highest possible field, that the frequency involved shall not lie in an excessively inconvenient range, and that at least one of the terminal states of the transition shall have a zero moment at a field adequate to insure reasonable deflections of the molecular beam. In strong fields, the energies of the h.f.s. states may be written as $W_{m_J,m_I}=m_I g_I\mu_0 H+m_J g_J\mu_0 H+(\Delta W/I+\frac{1}{2})m_I m_J$, so that transitions of the type $\Delta m_J=0$, $\Delta m_I=\pm 1$ approach asymptotically the frequencies ν (strong field) $=(\Delta\nu/2I+1)\pm g_I\mu_0 H$ as the magnetic field increases. The field sensitivity of these lines decreases, in general, with increasing field, being a maximum at zero field. The character of the field dependence of the line frequencies is determined largely by the extent to which the coupling between the magnetic moment of the nucleus and the magnetic field produced by electrons is broken down by the externally applied magnetic field. At weak fields, the energy of the states may be written $W_{F,m_F}=W_F+m_F g_F\mu_0 H$, so that lines corresponding to transitions $\Delta F=0$, $\Delta m_F=\pm 1$ have frequencies given by ν (weak field) $=g_F\mu_0 H$, where g_F is the g factor for a state of quantum number $F=I\pm J$. Since $|g_F|\sim g_J/2I+1$, ν(weak field) $=g_J\mu_0 H/(2I+1)$. The ratio of the field sensitivity of these lines at low and high fields is then equal to $(g_J/g_I(2I+1))$. At intermediate fields the field sensitivity will be intermediate between the two values. A quantity which measures the extent of the decoupling of nuclear and orbital magnetic moment is precisely the quantity x which is introduced as a dimensionless parameter in the Breit-Rabi formula. From these considerations, it can be seen that indium is an atom ideally suited for the purpose of providing highly field dependent lines at strong fields. The ground state of In^{115} is a $^2P_{\frac{1}{2}}$ state for which the nominal value of g_J is $\frac{2}{3}$. Accordingly, from the definition of x it appears that a value of x sufficiently small to assure the existence of field sensitive lines will correspond to a higher absolute value of the magnetic field in the case of In^{115} in the $^2P_{\frac{1}{2}}$ state than will be the case for atoms in the $^2S_{\frac{1}{2}}$ state of comparable $\Delta\nu$ for which the nominal g_J value is 2. In addition, since the $\Delta\nu$ of In is large (greater than that of any of the alkali atoms) the field to be obtained for any x is correspondingly large. It is to be noted, however, that the maximum field at which an atomic line is suitable for use in the present application is limited not only by the fact that the field sensitivity decreases with increasing field but also by the consideration that at strong fields the sensitivity of such lines depends to a marked extent on the ratio g_J/g_I, which is, in most cases, not known with sufficient precision to permit its use as an important factor in the determination of x.

The $^2P_{\frac{1}{2}}$ state of indium offers another advantage over $^2S_{\frac{1}{2}}$ states in that it permits the use of large deflecting fields. For an atom whose hyperfine structure is described by the Breit-Rabi formula,

[12] V. W. Cohen, Phys. Rev. 46, 713 (1934).
[13] I. I. Rabi, Phys. Rev. 49, 324 (1936).

zero moments occur nominally at values of x given by $x=-(2m_F/2I+1)$ for negative values of m_F. Since the occurrence of zero moments is determined by the quantity x rather than by the magnetic field directly, the $^2P_{\frac{1}{2}}$ state provides atoms of zero moment at much higher fields than is the case with the $^2S_{\frac{1}{2}}$ state. As an example, the zero moment peaks for In^{115}, in the $^2P_{\frac{1}{2}}$ state, $I=9/2$, $\Delta\nu\sim11{,}000\times10^6$ sec.$^{-1}$, occur,[14] for $m=-4, -3, -2, -1$ at $H\sim10{,}000$, 7500, 5000, 2500 gauss respectively, while for Cs^{133} in the $^2S_{\frac{1}{2}}$ state, $I=7/2$, $\Delta\nu\sim9000\times10^6$ sec.$^{-1}$, the zero moment peaks for $m=-3, -2, -1$ occur[15] at $H\sim2300$, 1500 and 750 gauss respectively.

In^{115} in the $^2P_{\frac{1}{2}}$ state offers, then, the best choice of atom among those available for study by current techniques for a precise determination of g_H in terms of an atomic g_J, while Cs^{133} in the $^2S_{\frac{1}{2}}$ state offers a somewhat less attractive choice. We have, however, used the Cs atom as a second comparison atom, principally to ascertain from the internal consistency of the results, the general validity of the procedures employed in this experiment.

THE DETERMINATION FROM ATOMIC SPECTRA OF THE SIGN OF g_J/g_I

An error in the sign of the quantity g_J/g_I will obviously introduce a large systematic error in the determination of the ratio g_H/g_J. The sign of g_J/g_I for Cs^{133} is known to be negative from the results of two independent experiments.[15,16] No previous reliable determination of the sign of g_J/g_I for In^{115} is available. The following considerations, however, provide a means by which the sign of g_J/g_I may be determined from an examination of the h.f.s. spectrum.

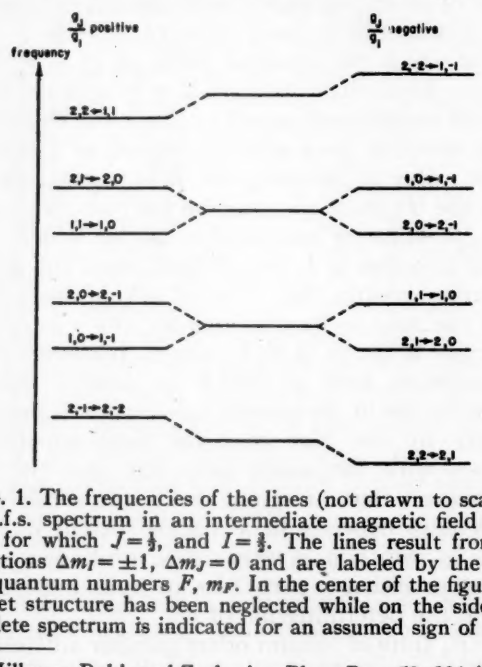

FIG. 1. The frequencies of the lines (not drawn to scale) in the h.f.s. spectrum in an intermediate magnetic field of an atom for which $J=\frac{1}{2}$, and $I=\frac{3}{2}$. The lines result from the transitions $\Delta m_I=\pm1$, $\Delta m_J=0$ and are labeled by the weak field quantum numbers F, m_F. In the center of the figure the doublet structure has been neglected while on the sides the complete spectrum is indicated for an assumed sign of g_J/g_I.

If the ratio g_J/g_I is negative, the zero field energy of the state $F=I+J$ must be higher than the energy of the state $F=I-J$. In this case, the quantity $\Delta\nu$ and the parameter x, in the Breit-Rabi formula, must both be taken as positive. If, however, g_J/g_I is positive, the zero field energy of the state $F=I-J$ is higher than that of the state $F=I+J$ and both $\Delta\nu$ and x become negative.

The energy levels of an atom for which g_J/g_I is negative together with the spectrum resulting from transitions of the type $\Delta m_J=0$, $\Delta m_I=\pm1$ have been described in several papers[17,18] on h.f.s. spectroscopy by the atomic beam magnetic resonance method. All the lines are components of doublets with the exception of lines which involve the state $F=I+J$, $m_F=\pm(I+J)$. The doublet separation arises from the term $[h\Delta\nu/(g_J/g_I-1)]m_Fx=m_Fg_I\mu_0H$ in the Breit-Rabi formula, and the components of the doublets are displaced symmetrically by an amount $g_I\mu_0H$ from the position they would occupy if this term were neglected.

In Fig. 1 are shown schematically the lines resulting from the transitions $\Delta m_J=0$, $\Delta m_I=\pm1$, in which, for convenience, the nuclear spin has been taken to be $\frac{3}{2}$. The lines in the center of the figure indicate the spectrum when the term $g_I\mu_0H$ is ignored. The lines on the right indicate the spectrum when a negative g_J/g_I is assumed, while the lines on the left indicate the spectrum for a positive g_J/g_I. The components of the doublets have the same frequencies in both cases for a fixed x value, although the magnetic field which corresponds to the x will be somewhat different in the two cases. From observations on lines which are components of doublets, it is possible to find $\Delta\nu$, x and the absolute value of g_J/g_I. The positions of the single lines may then be predicted assuming either a positive or negative sign for g_J/g_I and the observed positions of the single lines will reveal which of the assumptions is correct.

For g_J/g_I negative, the states for which $F=I+J$ and m_F is negative will be the focusing states while for g_J/g_I positive, the states of $F=I-J$ and m_F positive will be the focusing states. However, in both cases a $\Delta m_I=\pm1$ transition from a focusing state will be the lower frequency component of a doublet. If it is therefore not possible as Hardy and Millman[19] claim to have done, to determine the sign of g_J/g_I by noting which of the components of a doublet is more intense under an experimental condition in which the deflecting fields are adjusted

[14] Millman, Rabi, and Zacharias, Phys. Rev. **53**, 384 (1938).
[15] S. Millman and J. R. Zacharias, Phys. Rev. **51**, 1049 (1937).
[16] Kusch, Millman, and Rabi, Phys. Rev. **55**, 1176 (1939).
[17] Kusch, Millman, and Rabi, Phys. Rev. **57**, 765 (1940).
[18] S. Millman and P. Kusch, Phys. Rev. **58**, 438 (1940).
[19] T. C. Hardy and S. Millman, Phys. Rev. **61**, 459 (1942).

so that one of the states involved in the transition has zero moment.

Measurements have been made at a nominal $x \sim 0.65$ of the frequencies, at fixed field, of the set of indium lines $(4,-3 \leftrightarrow 4,-4)$, $(4,-1 \leftrightarrow 4,-2)$, $(5,-1 \leftrightarrow 5,-2)$, and $(5,5 \leftrightarrow 5,4)$, the first three lines being components of doublets and the last being a single line. The doublet components permit a calculation of $\Delta\nu$ independently of any assumption concerning the sign or magnitude of g_J/g_I and the relative position of the single line then permits a determination of the sign of g_J/g_I. It is found that g_J/g_I In^{115} is indeed negative as previously stated.[19]

THE CALIBRATING ATOMS

The value of the $\Delta\nu$ and the ratio g_J/g_I for Cs^{133} used in the calculations involved in this experiment are $\Delta\nu = 9192.76 \pm 0.10$ mc and $g_J/g_I = -5018 \pm 3.0$. These values are discussed in a previous paper[2] and the experiment there discussed was motivated in part by the requirements of the present experiment.

A redetermination has been made of the $\Delta\nu$ of In^{115} using the method described by Kusch and Taub.[2] Observations were made of the frequencies of both components of a doublet in a region of field at which the mean frequency of a doublet attains a maximum. For this purpose, the doublet $(F,-3 \leftrightarrow F,-4)$ has been employed. The maximum frequency of the mean of this doublet occurs at an $x = 1.4$ and has a value $\Delta\nu\sqrt{2}/10$. The value of the magnetic field corresponding to this value of x is about 17,000 gauss, while the line frequency is about 1600 mc. Ten observations on each of the doublet components over a range of x from 1.35 to 1.48 gives a mean $\Delta\nu$ of 11,409.50 mc with an average deviation of 0.10 mc. The ratio g_J/g_I, on the other hand, has been determined by three independent observations of the separation of the components of two other doublets in a region of field where the line frequency is markedly field dependent. The mean frequency of the doublet gives the value of x and the doublet separation at once determines g_J/g_I. At $x \sim 0.65$, the doublet $(F,4 \leftrightarrow F,3)$ yields $g_J/g_I = -1005.2$ and the doublet $(F,3 \leftrightarrow F,2)$ yields $g_J/g_I = -1004.7$; at $x \sim 0.6$, the doublet $(F,3 \leftrightarrow F,2)$ gives $g_J/g_I = -1005.4$. We take $\Delta\nu = (11,409.50 \pm 0.10)$ mc and $g_J/g_I = -1005.1 \pm 0.5$; the precision measures assigned are a conservative estimate of the possible error. It is to be noted, that if an incorrect value of g_J/g_I is assumed, the calculated $\Delta\nu$ from measurements on the doublet components of the line $(F,-3 \leftrightarrow F,-4)$ will exhibit an increase or a decrease with field. The ten measured values, however, show no such field dependence, but only a statistical fluctuation.

An extensive series of observations has been made on the lines of indium, $\Delta F = 0$, $\Delta m_F = \pm 1$ at values of x of 0.6 and 0.65, for the purpose of providing an independent determination of $\Delta\nu$. Since the ratio g_J/g_I has been found by independent observation, it is sufficient to measure the frequencies of two lines, not components of the same doublet, to determine both $\Delta\nu$ and x. The parameter x is determined from the ratio of the line frequencies, and it is desired, for maximum precision, that the ratio be as field dependent as possible. Evidently, certain pairs of lines will give a better precision than others. Even for the best choice of available lines, the fractional uncertainty in the calculated $\Delta\nu$ may be as much as three times the fractional uncertainty in the observed line frequency. Evidence has appeared as a result of the analysis of the data that the measured frequencies of the most field sensitive lines, which are also the lines of highest frequency, are systematically too low. The effect is not evident from a single run, but appears as a result of statistical analysis. That is, a single run yields a value of $\Delta\nu$ which differs from the more exactly determined value of $\Delta\nu$ by an amount well within the uncertainty of the determinations. The $\Delta\nu$ is, however, consistently higher than the accurately known value. Analysis of a large body of data shows that the effect depends markedly on the field dependence of the line frequency. It is believed that the effect arises from inhomogeneities in the magnetic field which cause an unsymmetrical broadening of lines. An estimate of the maximum error which this effect can introduce into determinations of x from observations made on a single line is about one part in 25,000. Such an error in x would be directly reflected in the determination of the ratio g_H/g_J. Our observations on the ratio g_H/g_J have included measurements of a number of atomic lines of In at several different magnetic fields and the field dependence of the line frequency varied by a factor of 3 over the range of observation. The systematic error resulting from the shift is, in most of these cases, certainly less than 1 part in 25,000. The high degree of internal consistency among the observations leads to the conclusion that the effect is entirely negligible compared to the over-all precision of our result.

APPARATUS AND PROCEDURE

The apparatus used in this experiment to determine the ratio of g_H to the g_J of indium is identically the apparatus used by Kusch and Foley[1] in their determination of the intrinsic magnetic moment of the electron, while the experiment on the determination of the ratio of g_H to g_J of caesium was performed after the original homogeneous transition magnet had been replaced by a new magnet. The original magnet was made of Armco iron and had tapered Permendur pole pieces, which served to increase the maximum attainable field in the gap to about 21,000 gauss. Since it was felt that

TABLE I. Results of the individual determinations of the ratio $g_H/g_J(In^{115}, {}^2P_{\frac{1}{2}})$ and the circumstances under which the individual determinations were made. The atomic transitions are designated by the weak field quantum numbers F, m_F.

Run	Nominal x	Nominal magnetic field (gauss)	In^{115} transition	$g_H/g_J(In^{115}, {}^2P_{\frac{1}{2}})\times10^4$ Field direction N	Field direction R
1	0.65	8000	(5, −2) (5, −3)	45.6921	45.6967
2	0.65	8000	(5, −3) (5, −4)	45.6867	45.6871
3	0.85	10,000	(5, −2) (5, −3)	45.6862	45.6913
4	0.85	10,000	(5, −1) (5, −2)	45.6870	45.6846
5	1.0	12,000	(5, −1) (5, −2)	45.6853	45.6860
6	0.65	8000	(5, −3) (5, −4)	45.6875	45.6823
7	0.65	8000	(5, −2) (5, −3)	45.6864	45.6879
			Average N	45.6873	
			Average R		45.6880
			Over-all average	45.6877	
			Statistical probable error	0.0007	

inhomogeneities in the Permendur contributed in some measure to the lack of perfect homogeneity of the field, the new magnet, which has essentially the same geometry as the original one, is made entirely of Armco iron. That a worth while improvement has been made in the field homogeneity by the magnet replacement is evidenced by the reduced width, with the new magnet, of field sensitive lines.

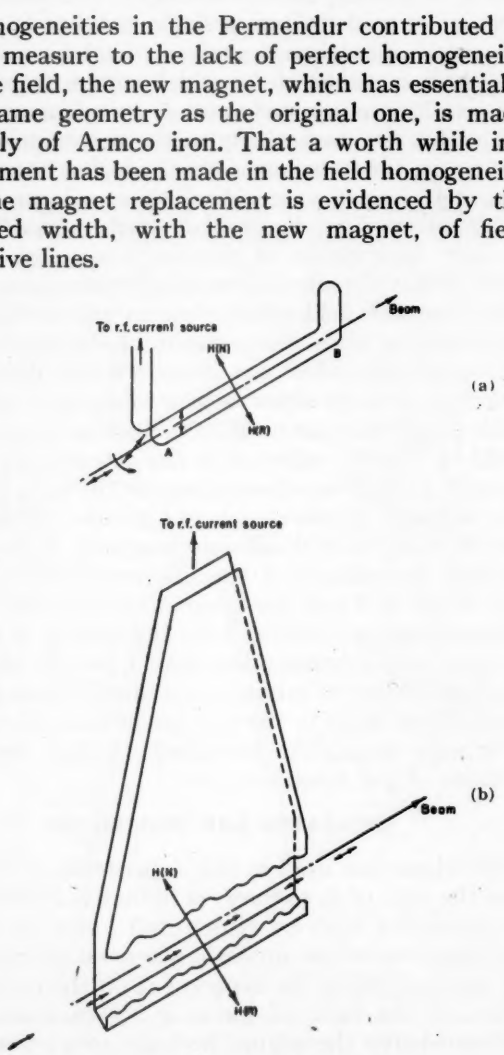

FIG. 2. Arrangements for superimposing an oscillating magnetic field on the fixed magnetic field. The orientations of the fixed and alternating fields are indicated by the arrows. (a) The two wire arrangement which exhibits marked Millman effect. (b) The parallel plane arrangement in which the Millman effect is suppressed.

An iron oven loaded with a mixture of powdered calcium and caesium chloride provided a caesium beam. An indium beam was obtained by evaporating indium from a graphite lined molybdenum oven, while a silver oven loaded with NaOH provided a beam in which a proton resonance could be observed. For the purpose of permitting consecutive measurements in rapid sequence of the proton resonance and a line of the spectrum of the atom employed, the double oven arrangement previously described[1] was again employed.

All of the data of this experiment consist of the frequency in a fixed magnetic field of a line in the h.f.s. spectrum of an atom and the frequency in the same magnetic field of a proton resonance. No precise knowledge of the magnitude of the magnetic field is required, but, as a matter of practice, data on the current through the magnetizing coil serves to correct for the drift of the magnetic field during the course of a run.

The frequency of any line measured in this experiment was determined by an observation of the frequency at which a maximum decrease in beam intensity occurred, or by an observation of the mean of the frequencies of two points on either side of the minimum which were symmetrical with respect to reduction in beam intensity. It was not feasible to make a detailed plot of beam intensity as a function of frequency in taking the data because the time consumed in making the necessary observations would seriously prejudice the essential requirement that atomic and molecular line be observed in the same magnetic field. To permit corrections to be made for field drift, the current through the coils of the magnet which produces the homogeneous field was carefully monitored with the aid of a Leeds & Northrup Type K potentiometer and a precision shunt. The errors in determining the frequency of a line occasioned by line width and beam unsteadiness are statistical in character, and the error may then be materially reduced by numerous repetitions of observations. All frequency measurements were made on a General Radio heterodyne frequency meter, type 620A. This instrument may be used to measure a particular frequency with an accuracy of about 1 part in 50,000. Since the limitation on accuracy imposed by line widths exceeded in general the limitation imposed by the wave meter, there was no advantage to be gained from the use of better frequency measuring equipment.

The data from which g_H/g_J is found, were obtained in the following manner. From four to eight separate and individual observations were taken of the frequency of the appropriate atomic line. At the instant one observer read the line frequency, a second observer read the corresponding value of the magnet current. The ovens having

been interchanged, the same procedure was followed in reading the frequency of the proton resonance. The series of observations were then repeated alternately on the atomic and molecular lines until at least three sets of observations had been made on the atomic line and at least two on the molecular line. The drift of the magnetic field, while in principle undesireable, nevertheless required that a line be read at a slightly different frequency on each occasion, and therefore served the useful purpose of making each individual line reading independent of the others, and of eliminating prejudice on the part of the observer, who was not aware of the nature of the drift. Further, since the errors made in reading the wave meter are statistical in character, the mean of a set of frequencies which require the use of differing parts of the scale will be of an accuracy appreciably better than the accuracy of an individual reading.

It has been noted experimentally that, in general, for small amplitudes of the radio frequency current which provides the oscillating magnetic field, the intensity of a line increases with increasing current and the width of the line remains approximately constant. For large r-f currents, on the other hand, the intensity remains approximately constant while the line increases in width with increasing current and may on occasion exhibit asymmetries. The exact adjustment of the current to a predetermined value is at best a difficult procedure. We have, however, in all cases, reduced the r-f current to a point where further reduction would have resulted in a marked decrease in line intensity.

The data taken in the manner described was interpreted on the assumption that the magnetic field varied linearly with magnet current. That this assumption is reasonable is supported by the fact that even at the largest fields employed, where the drift was most pronounced, the range of field over which the assumption of linearity was required to hold rarely exceeded three parts in one thousand. At lower fields, the drift was very much less and in some cases negligible. The validity of this assumption is further supported by the precision with which the points of a plot of magnetic field *versus* field current fall on a straight line, the magnetic field being determined by the measured frequency of a field sensitive atomic line. And finally, the validity of the assumption is borne out by the consistency of the data generally.

In the previous experiment[10] on the determination of the proton moment, the oscillating magnetic field which produces transitions was produced by the two wire arrangement illustrated in Fig. 2a. However, such an arrangement, on account of end effects will produce in a spectral line a spurious auxiliary line which may or may not be resolved from the main line. This is the so-called Millman[20] effect. The direction and magnitude of the displacement of the auxiliary line and its relative intensity will depend on the velocity of the beam, the amplitude of the oscillating current and the geometry of the wires. The shift may be reversed by a reversal of the fixed field. If the auxiliary line is not resolved its presence will nevertheless serve to broaden the line and shift it from the position it would occupy in the absence of the Millman effect. The magnitude of the Millman effect is unaffected by the frequency of the line. With the wire arrangement of Fig. 2a, described by Millman, for which the distance AB was of the order 6 cm and for which the end effects were confined to about $\frac{1}{2}$ cm at each end, displacements of the order of 10^4 cycles per second had been observed. A frequency of 10^4 c.p.s. is an appreciable fraction of the frequencies encountered in molecular spectroscopy. It is therefore necessary that the correct frequency of a line be determined by taking the average of the frequencies measured for each of the two possible directions of the fixed magnetic field since, all other experimental conditions remaining fixed, the direction of the line shift reverses with reversal of the field. In the earlier experiment on the proton moment, measurements of g_H were made with the field in each of the two directions and the average of the two values was accepted as the correct value. In that experiment the proton moment as calculated from data taken for each of the field directions differs by amounts of the order of 1 part in 1000. In the present experiment it was not evident that the cancellation of Millman effect error accomplished by taking an average would eliminate the error to the precision which was contemplated for these experiments. Accordingly, the arrangement used in the present experiment for superimposing an oscillating field on the fixed field is that illus-

TABLE II. Results of the individual determinations of the ratio $g_H/g_J(Cs^{133}, {}^2S_{\frac{1}{2}})$ and the circumstances under which the individual determinations were made. In every case the atomic transition $(4, -1)\leftrightarrow(4, -2)$ was employed.

Run	Nominal x	Nominal magnetic field (gauss)	$g_H/g_J(Cs^{133}, {}^2S_{\frac{1}{2}})$ Field direction N	Field direction R
1	1.0	3300	15.1910	
2	1.0	3300	15.1927	
3	1.0	3300	15.1908	15.1914
4	1.0	3300		15.1888
5	1.0	3300	15.1900	15.1911
6	1.2	4000	15.1902	
7	1.2	4000	15.1919	15.1929
8	1.2	4000	15.1915	
	Average N		15.1912	
	Average R			15.1911
	Over-all average		15.1911	
	Statistical probable error		0.0003	

[20] S. Millman, Phys. Rev. **55**, 628 (1939).

trated in Fig. 2b. The Millman effect occurs because the magnetic field produced by the oscillating current is such that a moving molecule in the beam sees a field in the neighborhood of the ends of the "hairpin," which rotates about an axis parallel to the main field. A comparison of figures indicates that the Millman effect disappears for a perfect symmetry of the hairpin of Fig. 2b and for a symmetrical approach of the beam to the hairpin and is, in any event, appreciably smaller for the arrangement of Fig. 2b than for the arrangement of Fig. 2a. Most importantly, however, the data presented below exhibits no Millman effect whatsoever so that no uncertainties arise on this account.

RESULTS

In the experiment on the determination of the ratio of g_H to the g_J of In^{115} in the $^2P_{\frac{1}{2}}$ state measurements were made under the conditions indicated in Table I for each of seven runs. It is to be noted that measurements have been made on three lines at three different magnetic fields. In each case, the choice of line was dictated by the considerations discussed above. The inhomogeneous, deflecting fields were set to refocus the state which had a zero moment at the higher field, that is, the state with the m_F number of larger absolute magnitude. The data taken with the field direction N and the data with the field R, where N and R are arbitrary designations of field direction, give the same value of g_H/g_J to better than 1 part in 50,000 and the discrepancy is too small to be meaningful. Since no Millman effect occurs we may consider each separate entry in Table I as an independent experimental value of g_H/g_J. The over-all average of these fourteen independent observations is $g_H/g_J(\text{In}) = 45.6877\times10^{-4}$ and the probable error, computed by the usual statistical procedures, is 0.0007×10^{-4}, or about 1 part in 65,000.

In the comparison of g_H to the g_J of Cs^{133} in the ground state, measurements were made under the conditions noted in Table II. In every case, an attempt was made to have a complete run consist, as was the case with indium, of a determination of g_H with the fields in each of the two directions. The blank spaces in Table II do not represent rejected data, but are rather the result of experimental difficulties which required the termination of a run before completion. The parenthetical comment should be made that an experiment was successful only upon the simultaneous satisfactory operation of a large number of elements. The fact that all runs involving indium are complete is the result of an extraordinarily long run of good luck. Here again the difference between normal and reverse field directions is too small to be meaningful and provides further evidence of the absence of Millman effect. The over-all average of eleven independent determinations gives $g_H/g_J(\text{Cs}) = 15.1911\times10^{-4}$ with a probable error of 0.0003×10^{-4}, which is about 1 part in 50,000.

g_H IN TERMS OF g_J(Na)

The most direct results of the present experiment are the quantities $g_H/g_J(\text{In}) = 45.6877\times10^{-4}$ and $g_H/g_J(\text{Cs}) = 15.1911\times10^{-4}$. It is to be noted that these two experimental results are entirely independent. The essential part of the apparatus, namely the transition field, was different in the two determinations and the range of magnetic field used in the two determinations differed widely. To reduce the results of the two sets of observations to a common standard we use the ratio $g_J(\text{Cs})/g_J(\text{Na}) = 1.000134$ determined by Kusch and Taub,[2] and the ratio $g_J(\text{Na})/g_J(\text{In}) = 3(1.00243)$ determined by Kusch and Foley.[1] These ratios lead to the results:

From comparison with In:

$$g_H/g_J(\text{Na}) = 15.1923\times10^{-4};$$

From comparison with Cs:

$$g_H/g_J(\text{Na}) = 15.1931\times10^{-4}.$$

The discrepancy between the two measured quantities arrived at by two independent procedures is one part in 19,000. This high degree of consistency is of the greatest significance in establishing the general validity of the experimental procedures and of the interpretation of the data. Equal weight is given to each of the separate determinations, so that

$$g_H/g_J(\text{Na}) = 15.1927\times10^{-4}\pm0.005 \text{ percent},$$

the precision measure, which is twice as large as that required to include both the individual determinations, will be justified in a following section.

THE MAGNETIC MOMENT OF THE PROTON

The experiment discussed in the previous paper[2] leads to the result that $g_J(\text{Na}) = g_s$, the spin gyromagnetic ratio of the electron. The experimental value of the quantity g_s is 2(1.00119);[1] this value is in agreement, within experimental error, with the result calculated by Schwinger,[21] that $g_s = 2(1+\alpha/2\pi) = 2(1.00116)$. No sufficient grounds exist on the basis of which a choice can be made between the two values. Purely as a matter of convention the theoretical value of g_s is adopted. A simple application of this factor leads to the value of the gyromagnetic ratio of the proton:

$$g_H = 30.4206\times10^{-4}\pm0.005 \text{ percent}.$$

As will be pointed out later a small diamagnetic correction of 0.002 percent increases the value of

[21] J. Schwinger, Phys. Rev. 73, 416 (1948).

the moment obtained from the experimentally observed g value. Accordingly,

$$\mu_H = (15.2106 \times 10^{-4} \pm 0.005 \text{ percent}) \text{ Bohr magnetons.}$$

It is to be emphasized that the precision measure depends on the data of the present series of experiments alone. No attempt is made to include in this measure any uncertainties arising from the interpretation of $g_J(\text{Na})$ as g_s or any uncertainties in the value of g_s itself.

It is common practice to express the values of nuclear magnetic moments in terms of nuclear magnetons. This is, from the point of view of the present experiments, an artificial procedure since it demands the insertion of the quantity M/m into a result which is independent of any of the constants of atomic physics except the value of g_s. If we use $M/m = 1836.57$[22] we find

$$\mu_H = 2.7935 \text{ nuclear magnetons.}$$

In an experiment in which μ_H is determined by the observation of the resonant frequency of the proton in a known magnetic field it is not of importance whether the moment is expressed in Bohr or nuclear magnetons, since in one case the experimental quantity e/mc must be applied and in the other case the quantity e/Mc. At present no obvious choice of either value can be made.

Using for the absolute value of the Bohr magneton the value $\mu_0 = (0.92731 \pm 0.00017) \times 10^{-20}$ erg/gauss, the absolute value of the magnetic moment of the proton is found to be

$$\mu_H = (1.4105 \times 10^{-23} \pm 0.02 \text{ percent}) \text{ erg/gauss.}$$

From the data of the present experiments, no information as to the sign of μ_H is obtained. However, μ_H is known to be positive from several previously reported lines of evidence. The value of g_H discussed in this paper is the absolute value of the quantity.

PRECISION

The statistical probable error in $g_H/g_J(\text{Cs})$ is, as stated above, 1 part in 50,000, while the p.e. in $g_J(\text{Cs})/g_J(\text{Na})$, as given by Kusch and Taub is 1 part in 150,000. The p.e., then, in $g_H/g_J(\text{Na})$ is about 1 part in 50,000. A review of the published data of Kusch and Foley[1] from which the quantity $g_J(\text{In})/g_J(\text{Na})$ is derived reveals a p.e. of about 1 part in 80,000. The published precision measure for this ratio, 1 part in 10,000, is clearly pessimistic and this extremely pessimistic view does not appear to be justified, especially in view of the subsequent history of the apparatus used in that experiment. It is to be noted further, that if the g_J values of atoms are characteristic of the atomic state rather than of the particular atom, then it is to be expected that $g_J(\text{In } {}^2P_{\frac{1}{2}})/g_J(\text{Na } {}^2S_{\frac{1}{2}}) = g_J(\text{Ga } {}^2P_{\frac{1}{2}})/g_J(\text{Na } {}^2S_{\frac{1}{2}})$. The remarkable agreement between these measured quantities (Kusch and Foley give $g_J(\text{Na})/g_J(\text{In}) = 3(1.00243)$; $g_J(\text{Na})/g_J(\text{Ga}) = 3(1.00242)$) is strong evidence to the effect that the precision of determination of these ratios is appreciably in excess of the stated precision. If we accept the p.e. of 1 part in 80,000 in $g_J(\text{In})/g_J(\text{Na})$ then the p.e. of $g_H/g_J(\text{Na})$ obtained from the In data, is, as in the case of the Cs data, about 1 part in 50,000. The p.e. of the mean is, then, 1 part in 70,000 and the precision measure of 1 part in 20,000, given above, is not only twice as large as is required to include both individual determinations, but is also 3.5 times as large as the p.e.

A straightforward numerical calculation based on Eqs. (1) and (2) reveals that the uncertainties in the $\Delta\nu$'s and the ratios g_J/g_I for In and Cs introduce no error in the value g_H/g_J, in each case, of magnitude sufficient to effect the proton moment to the precision here contemplated. The largest error in the ratio $g_H/g_J(\text{In})$ arising from an error in the $\Delta\nu$ and g_J/g_I of In occurs for the case $x \sim 1.0$ where the line $(5, -1 \leftrightarrow 5, -2)$ was used. Here, the assumption of an error of 0.10 mc in $\Delta\nu$ gives rise to an error of about 1 part in 100,000 in $g_H/g_J(\text{In})$, while an error of 0.5 in g_J/g_I causes an error of 1 part in 80,000. For all other x values and lines employed the resultant error is very much smaller. Similarly, an assumed error of 0.10 mc in the $\Delta\nu$ of Cs causes an error in the value $g_H/g_J(\text{Cs})$ calculated at $x \sim 1.0$ of 1 part in 90,000 and, at $x = 1.2$, an error of 1 part in 50,000. Further, an error of 3 in $(g_J/g_I)\text{Cs}$ produces an error of only 1 part in 500,000 at $x \sim 1.0$ and 1 part in 300,000 at $x \sim 1.2$.

All the errors discussed above are purely statistical errors, and the possibility of systematic errors must be considered. Since the present experiment consists entirely of the measurement of spectral lines in a fixed magnetic field, the only sources of systematic error which suggest themselves are errors in the frequency measuring equipment, errors occasioned by some circumstance associated with part of the apparatus which determines the frequencies of the observed lines, that is, the homogeneous transition magnet and the possibility that the center of the observed molecular line does not, in fact, correspond to the frequency $g_I\mu_0 H/h$ because of interactions which give an unsymmetrical broadening of the line. The frequency measuring equipment had been periodically checked against the standard signals broadcast by WWV and the instability of the equipment is not great enough to introduce significant error. However, inhomogenei-

[22] J. W. M. DuMond and E. R. Cohen, Rev. Mod. Phys. 20, 82 (1948).

ties in the transition field, which have a marked effect on line width might conceivably result in an unsymmetrical broadening of the lines. That such effects occur has been previously noted but sufficient evidence exists from the measurements of the $\Delta\nu$ of indium that the effects play a negligible part in the apparent value of g_H/g_J. The possibility of error from such sources, is, in addition, quite remote, in view of the wide variety of circumstances, with respect to the transition magnet, under which data has been taken in the present experiment and and in view of the history generally of the apparatus employed. The data for the determination of the ratio g_H/g_J(In) was taken using the original transition magnet of the apparatus, while all other data, including the data for the determination of the g_J ratios for the alkali atoms, described in a previous paper,[2] was taken after the replacement of the original magnet with the new one. It is to be noted that the dependence of the data on the characteristics of the transition magnet is so critical that the replacement of this magnet constitutes the creation of an almost entirely new apparatus. Second, the agreement between the ratio g_H/g_J from data taken for each of the two directions of the magnetic fields is convincing evidence that no systematic shift of line frequencies occurs, since it seems unlikely that such a reversal of fields would not affect the magnitude of a systematic error occasioned by field inhomogeneities and the disposition of the hairpin in the magnet. Most importantly, the extremely good agreement between the values g_H/g_J obtained through completely separate channels, that is, through the combinations of four completely independent experiments on the determination of g_H/g_J(In), g_J(In)/g_J(Na), g_H/g_J(Cs) and g_J(Cs)/g_J(Na), militates against the occurrence of systematic error.

A further source of systematic error which suggests itself is the possibility of a perturbation of the $^2P_{\frac{1}{2}}$ levels of indium by the $^2P_{3/2}$ state, separated from the lower state by about 2000 cm^{-1}. Such a perturbation might arise on account of the existence of matrix elements $(J|\mu_N \cdot H_e|J+1)$ between the two states, $J=\frac{1}{2}$, $J=\frac{3}{2}$, of the interaction between the nuclear moment and the field at the nucleus due to the electron. Mann and Kusch[23] of this laboratory have recently measured the intervals, at zero field, of the four levels of the $^2P_{3/2}$ state of indium. They have found that to a precision of 1 part in 100,000 the frequencies of the three zero field lines agree with the frequencies calculated using only the elements diagonal in J of the interaction $\mu_N \cdot H_e$ and the interaction due to the quadrupole moment of the nucleus. The matrix elements, non-diagonal in J, which are proportional to the magnetic field serve at any particular field to shift all the levels by exactly the same amount and hence have no effect either on line frequencies or on the determination of magnetic field from the measured frequency of a line.

Finally we must inquire whether the proton resonance curve observed in NaOH is entirely symmetrical about the frequency $f_H = g_H \mu_0 H$. The natural width of the resonance under the circumstances which prevailed in this experiment is estimated to be of the order of 10 kc. The observed half width is of the order of 40 kc and this broadening is caused by interactions internal to the molecule. The only perturbing, internal interactions which are presently contemplated in a molecule in which the net electronic angular momentum is zero are the interactions between the nuclear spins, the interaction between the nuclear spins and the magnetic field which arises from molecular rotation and the interaction of a nuclear quadrupole moment with an electric field gradient at the position of the nucleus. Since the oxygen nucleus has no magnetic moment, the Hamiltonian from which the energy levels may be calculated is entirely similar to the Hamiltonian which has been applied to the molecule HD.[24] In both cases one nucleus is the proton which has a magnetic moment but no quadrupole moment, while the other nucleus has both magnetic moment and electric quadrupole moment.

The result of a first order calculation using this Hamiltonian is that the single line which would result from the reorientation of the magnetic moment of the proton is split on account of the internal interactions into a set of lines $(2J+1)(2I+1)$ in number. J is the quantum number of molecular rotation and I is the spin of the other nucleus. What is important for our purpose is to note that the multiplet of lines which results are disposed entirely symmetrically about the frequency $f_H = g_H \mu_0 H$. The individual lines are not observed in the present experiment because the interval between lines is very much smaller than the resolution of the apparatus.

In second order, small asymmetries begin to appear, but second order corrections are completely negligible in the present case on account of the large fields which were employed. Proton resonances were observed at frequencies varying from 15 to 50 mc. The width of the line is constant and of the order of 40 kc. Accordingly, first order perturbation energy terms are smaller than the zero order energies, even in the worst case, by a factor of 15 mc/40 kc$\sim$400. And second order corrections, since they result from the same interactions as are responsible for first order terms, are less than the zero order energy by a factor $(400)^2$.

[23] A. K. Mann and P. Kusch (private communication).

[24] Kellogg, Rabi, and Ramsey, Phys. Rev. **57**, 677 (1940).

These considerations, above the fact that the proton resonance as observed experimentally exhibits no asymmetry, and the consistency of results of measurements made over a range of magnetic field from 3000 to 12,000 gauss leads to the conclusion that the proton resonance curve is entirely symmetrical about the frequency $f_H = g_H \mu_0 H$.

THE FINE STRUCTURE CONSTANT

The hyperfine splitting of a $^2S_{\frac{1}{2}}$ state which results from the interaction of the nuclear moment with the perturbing magnetic field at the nucleus due to the electron is given by Fermi[6] as

$$\Delta\nu = (8\pi/3h)(2I+1/I)\mu_e\mu_N\psi^2(0),$$

where I is the nuclear spin, μ_e and μ_N are respectively the electronic and nuclear magnetic moments in absolute units and $\psi(0)$ is the Schrödinger wave function evaluated at $r=0$. In the Fermi formula the assumption is made that the mass of the nucleus is infinite. Breit and Meyerott[8] have calculated that the finite mass of the nucleus may properly be taken into account by including a factor $(m_r/m_0)^3$, in which m_r is the reduced mass and m_0 is the rest mass of the electron. It has also been shown by Breit[7] that the Fermi formula must be modified by the inclusion of a relativistic correction factor $(1+\frac{3}{2}\alpha^2)$. Including these factors, writing $\mu_e = \mu_0(\mu_e/\mu_0)$, and replacing μ_0 and $\psi(0)$ by equivalent combinations of physical constants, we have finally for $\Delta\nu$ of hydrogen,

$$\Delta\nu_H = 4/3(2I+1/I)cR_\infty(m_r/m_0)^3 \times(\mu_H/\mu_0)(\mu_e/\mu_0)\alpha^2(1+3\alpha^2/2).$$

In this expression α is the fine structure constant, c is the velocity of light, and R_∞ is the Rydberg constant for infinite mass.

Using the Nafe-Nelson[6] value $\Delta\nu_H = (1420.410 \pm 0.006)\times 10^6$ sec.$^{-1}$, the values $\mu_e/\mu_0 = 1.00116$, $\mu_H/\mu_0 = (15.2106\times 10^{-4})\pm 0.005$ percent and the values of the physical constants recommended by DuMond and Cohen,[22] $M/m_0 = 1836.57\pm 0.20$; $R_\infty = (109{,}737.30\pm 0.05)$ cm^{-1}; $c = (2.99776\pm 0.00004)\times 10^{10}$ cm sec.$^{-1}$, we have, $\alpha^2 = 5.3246\times 10^{-5}$ or,

$$1/\alpha = 137.043\pm 0.003$$

in which the precision measure assigned includes only the uncertainty in the measured ratio μ_H/μ_0. This value is to be compared to the values $1/\alpha = 137.021\pm 0.0007$ given by DuMond and Cohen and 137.030 ± 0.016 given by Birge.[25]

THE GYROMAGNETIC RATIOS AND MAGNETIC MOMENTS OF OTHER NUCLEI

The ratio of two nuclear g's may, in general, be determined more conveniently and to a much higher order of precision than the absolute g value of a particular nucleus. Accordingly, a large body of data is available in which the g value of a

[25] R. T. Birge, Rev. Mod. Phys. 13, 233 (1941).

TABLE III.* Nuclear gyromagnetic ratios and magnetic moments in terms of the Bohr magneton (without diamagnetic correction) and the magnetic moments in units of the nuclear magneton (with diamagnetic correction).

Nucleus	Spin	$\lvert g\rvert = \frac{\mu/\mu_0}{I}$ ×10^4 (obs.)	μ/μ_0 ×10^4 (obs.)	Diamagnetic correction (%)	μ/μ_N (corr.)	Precision (%)	Reference**
$_0N^1$	1/2	20.8381	−10.4191		−1.91354	0.0066	3
$_1H^1$	1/2	30.4206	15.2103	0.0018	2.79353	0.0050	
$_1H^2$	1	4.66975	4.66975	0.0018	0.857648	0.0050	4
$_1H^3$	1/2	32.4477	16.2239	0.0018	2.97968	0.0051	5
$_2He^3$	1/2	23.2	11.6	0.0046	2.13	0.92	a
$_3Li^6$	1	4.4769	4.4769	0.0081	0.82228	0.011	2, b
$_3Li^7$	3/2	11.8222	17.7333	0.0081	3.25711	0.011	b
$_4Be^9$	3/2	4.27	−6.41	0.0122	−1.177	0.38	c
$_5B^{10}$	3	3.269	9.806	0.0168	1.8012	0.036	b
$_5B^{11}$	3/2	9.7604	14.641	0.0168	2.6893	0.021	b
$_6C^{13}$	1/2	7.6487	3.8243	0.0219	0.7025	0.021	b
$_7N^{14}$	1	2.20	2.20	0.0275	0.404	0.50	10
$_7N^{15}$	1/2	3.05	±1.53	0.0275	±0.280	1.0	d
$_9F^{19}$	1/2	28.619	14.309	0.0401	2.6291	0.011	b
$_{11}Na^{22}$	3	3.1679	9.5038	0.0546	1.7464	0.012	2, e
$_{11}Na^{23}$	3/2	8.0462	12.0694	0.0546	2.21784	0.011	b
$_{13}Al^{27}$	5/2	7.9264	19.816	0.0709	3.6419	0.011	b
$_{15}P^{31}$	1/2	12.315	6.1573	0.0891	1.1318	0.011	b
$_{17}Cl^{35}$	3/2	2.9812	4.472	0.109	0.8222	0.032	b
$_{17}Cl^{37}$	3/2	2.48	3.72	0.109	0.683	0.44	f
$_{19}K^{39}$	3/2	1.418	2.13	0.131	0.391	0.3	16
$_{19}K^{40}$	4	1.755	−7.02	0.131	−1.291	0.3	2, k
$_{19}K^{41}$	3/2	0.780	1.171	0.131	0.215	0.3	2, 17
$_{29}Cu^{63}$	3/2	8.063	12.095	0.239	2.2266	0.021	b
$_{29}Cu^{65}$	3/2	8.637	12.955	0.239	2.3850	0.021	b
$_{29}Ga^{69}$	3/2	7.294	10.940	0.262	2.0145	0.036	i
$_{31}Ga^{69}$	3/2	7.25	10.87	0.262	2.001	0.25	j
$_{31}Ga^{71}$	3/2	9.264	13.895	0.262	2.559	0.048	i
$_{31}Ga^{71}$	3/2	9.21	13.81	0.262	2.543	0.20	j
$_{35}Br^{79}$	3/2	7.622	11.432	0.309	2.1061	0.043	b, g
$_{35}Br^{81}$	3/2	8.214	12.322	0.309	2.2700	0.032	b
$_{37}Rb^{85}$	5/2	2.9378	7.345	0.333	1.3534	0.032	b
$_{37}Rb^{87}$	3/2	9.953	14.930	0.333	2.7510	0.021	b
$_{49}In^{113}$	9/2	6.610	29.74	0.489	5.489	0.051	19
$_{49}In^{115}$	9/2	6.624	29.81	0.489	5.502	0.05	1
$_{53}I^{127}$	5/2	6.088	15.220	0.545	2.8105	0.029	i
$_{55}Cs^{133}$	9/2	3.989	17.951	0.573	3.316	0.032	b
$_{56}Ba^{135}$	3/2	3.018	4.527	0.587	0.8364	0.29	h
$_{56}Ba^{137}$	3/2	3.376	5.064	0.587	0.9354	0.29	h
$_{81}Tl^{203}$	1/2	17.385	8.6927	0.98	1.6121	0.011	b
$_{81}Tl^{205}$	1/2	17.557	8.7784	0.98	1.6280	0.011	b

* Most of the g values listed in this table have been calculated from the measured ratios of g values. Exceptions occur in the following instances.

N^{15}: The g of N^{15} has been determined by the direct calibration of a magnetic field in terms of absolute standards.

Li^6, K^{40}, K^{41}, In^{113}: The g values of these nuclei have been calculated from the relationship $g_1/g_2 = (2I_2+1)/(2I_1+1)(\Delta\nu_1/\Delta\nu_2)$ in terms of the measured g values of the more abundant isotopes, the spins and the appropriate hyperfine structure interaction constants, $\Delta\nu$.

In^{115}: The g value of In^{115} has been calculated from

$$g_I(In^{115}) = \frac{g_I(In^{115})}{g_J(In^{115},\ ^2P_{\frac{1}{2}})}\,\frac{g_J(In^{115},\ ^2P_{\frac{1}{2}})}{g_J(Na,\ ^2S_{\frac{1}{2}})}\,g_J(Na,\ ^2S_{\frac{1}{2}}),$$

assuming $g_J(Na) = g_s = 2(1.00116)$.

Ga^{69}, Ga^{71}: The g values of these isotopes were calculated on the one hand from the ratios $g(Ga^{71})/g(Ga^{69})$ and $g(Ga^{71})/g(Na^{23})$, measured be Pound (see reference i) and on the other hand from the ratios $g_I(Ga^{69,71})/g_J(Ga^{69,71},\ ^2P_{\frac{1}{2}})$, measured by Becker and Kusch (see reference j). Since the g values calculated from these two sets of measurements disagree by an amount which is larger than the sum of the assigned errors, both sets of values have been listed. The results obtained by Pound by the use of the nuclear absorption method are more precise than those obtained by Becker and Kusch by the application of the method of atomic h.f.s. spectroscopy. The ratios of the g values of the two isotopes as determined by the two methods are very nearly the same. Unpublished results of Kusch and Foley yield for $g_I(Ga^{69})$ a value very close to that obtained by Becker and Kusch, and it is believed that the indicated discrepancy is real and does not arise from an excessively optimistic estimate of the precision of the spectroscopic result.

** Numbered references refer to footnotes in text.

[a] H. L. Anderson and A. Nowick, Phys. Rev. 73, 919 (1948).
[b] F. Bitter, Phys. Rev. 75, 1326 (1949).
[c] Kusch, Millman, and Rabi, Phys. Rev. 55, 666 (1939).
[d] J. R. Zacharias and J. M. B. Kellogg, Phys. Rev. 57, 570 (1940).
[e] L. Davis, Phys. Rev. 74, 1193 (1948).
[f] P. Kusch and S. Millman, Phys. Rev. 56, 527 (1939).
[g] R. V. Pound, Phys. Rev. 72, 1273 (1947).
[h] R. H. Hay, Phys. Rev. 60, 75 (1941).
[i] R. V. Pound, Phys. Rev. 73, 1112 (1948).
[j] G. Becker and P. Kusch, Phys. Rev. 73, 584 (1948).
[k] J. R. Zacharias, Phys. Rev. 61, 270 (1942).

particular nucleus has been measured in terms of a g value which is well known, notably $g(H^1)$, $g(Li^7)$ and $g(Na^{23})$. In view of the present determination, with high precision of the ratio of the magnetic moment of the proton to the Bohr magneton, it seems desirable, whenever possible, to calculate, in terms of the Bohr magneton, the g values and magnetic moments of other nuclei. In Table III are tabulated the values of the gyromagnetic ratios and the magnetic moments of all nuclei for which data is currently available from molecular and atomic beam experiments and from experiments using the techniques of nuclear induction and absorption.

The first and second columns of Table III list the nuclei (and neutron) and their spins. In each case, except He^3, the spins have been determined by reliable experimental procedures, while in the case of He^3 there seems to be little doubt, on theoretical grounds, that the spin is $\frac{1}{2}$. The third column lists the magnitude of the g values or the absolute value of the ratio of the magnetic moment in units of the Bohr magneton to the spin. The fourth column lists the magnetic moment in terms of the Bohr magneton. The signs of the moments are known except in the case of N^{15}

The fifth column gives the correction which must be applied because of the diamagnetic effect of the electrons of the atom. This correction serves in every case to increase the g value and the moment. Lamb[26] has calculated the magnitude of this effect and finds that

$$g(\text{corrected}) = g(\text{measured})[1+(e/3\ mc^2)v(0)] \cong g(\text{measured})(1+0.319\times10^{-4}Z^{4/3}),$$

in which $v(0)$ is the electrostatic potential at the nucleus which is produced by the electrons. For hydrogen $v(0)$ may be calculated exactly with the result that the factor 0.319 is replaced by 0.178 while in the cases $Z=19$, 20, 26, 29, 37, 55, 74 and 81 the value of $v(0)$ which has been given explicitly by Hartree and others[27] requires the replacement of the factor 0.319 by the factors 0.259, 0.259, 0.263, 0.268, 0.270, 0.274, 0.277 and 0.280 respectively. The diamagnetic corrections listed in Table III are calculated by linear interpolations between these values. In each case, of course, the accuracy of the diamagnetic correction may be improved by using the exact value of $v(0)$ and by making more detailed considerations concerning the contribution to the diamagnetic effect of the outermost electrons. On account of the uncertainties in the diamagnetic corrections, and in order to keep experimental numbers distinct from theoretical calculations, the diamagnetic corrections have not been included in the g values and moments listed in the third and fourth columns of Table III. It is to be noted that in the calculation of the frequencies at which lines occur in the h.f.s. spectrum of atoms and molecules the uncorrected g values are precisely the values which are required.

The sixth column lists the moments in units of the nuclear magneton. The diamagnetic correction has been applied to these moments and for the conversion factor from Bohr to nuclear magnetons we have used the ratio $M/m=1836.57$ given by DuMond and Cohen.[22] The seventh column lists the precision measure which is the square root of the sum of the squares of the precision measures which have been assigned to the individual numbers or ratios from which the g values and moments have been calculated. The uncertainty in the ratio M/m and the uncertainties in the diamagnetic corrections have not been included in the precision measure.

We are pleased to acknowledge our indebtedness to Professor H. M. Foley for several clarifying discussions concerning perturbations of atomic states. We are grateful also to Miss Zelda Marblestone who performed a considerable part of the numerical computation involved in this experiment.

[26] W. E. Lamb, Jr., Phys. Rev. 60, 817 (1941).

[27] The references are listed in F. Seitz, *Modern Theory of Solids* (McGraw-Hill Book Company, Inc., New York, 1940), p. 251, except for the case $Z=26$, which is given by M. Manning and L. Goldberg, Phys. Rev. 53, 662 (1938).

Production of π-Mesons in Nucleon-Nucleon Collisions

L. L. FOLDY
Case Institute of Technology, Cleveland, Ohio

AND

R. E. MARSHAK
University of Rochester, Rochester, New York

(Received December 23, 1948)

The cross section for the production of π-mesons in nucleon-nucleon collisions is calculated at energies just above the threshold. The process is treated in complete analogy with photonic bremsstrahlung: the π-meson field is coupled to the nucleon and an empirical potential between the two nucleons ensures momentum and energy conservation. The nuclear potential is taken from the Berkeley experiments on neutron-proton scattering at 90 Mev. In this treatment the symmetric scalar theory yields zero cross section if the recoil of the nucleons is neglected. The symmetric pseudoscalar theory (with pseudovector coupling) leads to the results given in Tables I–III. The cross section obtained is several orders of magnitude smaller than the cross section obtained by Morette and Peng on the basis of a thoroughgoing field-theoretic approach.

1. INTRODUCTION

IN connection with the construction of the large synchro-cyclotrons, a theoretical prediction of the cross section for the production of π-mesons in nucleon-nucleon collisions is desirable. A comparison with experiment of the predicted angular distribution and energy spectrum of the π-mesons will throw light on certain properties of the π-meson and the nature of its coupling with nucleons.

Although it is now apparent that the fundamental idea of the two-meson hypothesis is correct[1] (in accordance with which only the π-meson is produced in a nucleon-nucleon collision whereas the μ-meson has a negligible interaction with nucleons and arises solely as a decay product of the π-meson), a reliable meson theory of nuclear forces still does not exist. The possibility of using one kind of meson to explain the tensor character of nuclear forces while at the same time avoiding the inevitable $1/r^3$ singularity has not yet been demonstrated. Moreover, it is possible that several kinds of mesons are strongly coupled to nucleons and the resulting field theory of nuclear forces may become quite complicated.

In view of the uncertain status of meson field theories, we have adopted a different approach to the problem of meson production. We have not treated meson production as a third-order process in which one real meson is created and one virtual meson is created and destroyed, as Morette and Peng[2] have done. Instead, we have regarded meson production as a second-order process in which one step consists of the creation of a meson by one of the nucleons, and the other step consists of the scattering of the resulting nucleon by the second nucleon via the nuclear potential between them. The advantage of our approach is twofold: (1) the nuclear potential may be chosen so as to give the best fit to those scattering experiments which involve momenta transfers coming into play in the meson problem (e.g. the Berkeley neutron-proton experiments at 90 Mev,[3] and (2) the cross section only depends on the square of the coupling constant rather than the sixth power so that the correct value of the coupling constant is not as crucial.

It might be objected that our method of calculation neglects the "exchange" terms taken into account in the consistent third-order field-theoretic calculation. These "exchange" terms arise from the creation of the real meson in the second step (in the scheme of perturbation theory) while the virtual meson is created in the first step and destroyed in the third. The "ordinary" terms in which the virtual meson is created and destroyed in the first two steps or the last two steps comprise the terms which are essentially taken into account by our method. Fortunately, it can be shown[4] that the "exchange" terms are of order (μ/M) (μ is the mass of the π-meson, M is the nucleonic mass) compared to the "ordinary" terms in the energy region with which we are concerned—directly above the threshold—so that the error incurred is small. Of course, if the non-relativistic approximation for the nucleons, in which the recoil momenta of the nucleons are neglected, leads to a vanishing cross section for a particular type of coupling, the "ex-

[1] R. E. Marshak, Phys. Rev. **75**, 700 (1949).
[2] C. Morette and H. W. Peng, Proc. Roy. Irish Acad. **51A**, 217 (1948).
[3] Hadley, Kelly, Leith, Segrè, Wiegand, and York, Phys. Rev. **73**, 1114 (1948); Brueckner, Hartsough, Hayward, and Powell, Phys. Rev. **75**, 555 (1949).
[4] This can be shown by writing out the different types of perturbation-theoretic terms or by means of a more direct method developed by R. P. Feynman; we are indebted to Professor Feynman for performing the calculation at our request.

change" terms will be as important, possibly more important, then the ordinary terms, in determining the final result.[5]

2. METHOD OF CALCULATION

We consider the production of π-mesons by the collision of two nucleons when the nucleons possess energies just above the threshold for production (i.e. $2\mu c^2$ or 290 Mev[6]). Although, even at these energies, the velocities of the nucleons are not small compared to the velocity of light, we employ the nonrelativistic approximation for the nucleons. This is consistent with the neglect of the "exchange" terms referred to in the introduction. For the interaction of the two nucleons with each other we use a symmetrical potential of the most general type which does not contain tensor forces. It is possible to include convergent tensor forces in the theory but we have not done so because the best fit with the neutron-proton scattering cross section at 90 Mev, from which we shall take our potential, is obtained by neglecting tensor forces.[7] The most general charge-independent central-force interaction can be written in the form:

$$V(r)=V^{(1)}(r)+\sigma_1\cdot\sigma_2 V^{(2)}(r)+\tau_1\cdot\tau_2 V^{(3)}(r)+(\sigma_1\cdot\sigma_2)(\tau_1\cdot\tau_2)V^{(4)}(r), \quad (1)$$

where the $V^{(i)}$ may all be distinct and contain the radial dependence of the forces. For the coupling of the π-meson with the nucleon, we first treat the case of a symmetric pseudoscalar field with pseudovector coupling. We then consider the case of a symmetric scalar field with scalar coupling. Other types of coupling can be investigated in a similar fashion, but the symmetric scalar and pseudoscalar fields will serve as illustrations.

Since the nucleon may be a proton or neutron and may have either direction of spin, we use a four-component wave function for the nucleon, namely, $\psi_\rho=(\psi_1, \psi_2, \psi_3, \psi_4)$ and four-component representations of the ordinary spin operators and the isotopic spin operators, namely:

$$\sigma_x=\begin{pmatrix}0&1&0&0\\1&0&0&0\\0&0&0&1\\0&0&1&0\end{pmatrix},\quad \sigma_y=\begin{pmatrix}0&-i&0&0\\i&0&0&0\\0&0&0&-i\\0&0&i&0\end{pmatrix},$$

$$\sigma_z=\begin{pmatrix}1&0&0&0\\0&-1&0&0\\0&0&1&0\\0&0&0&-1\end{pmatrix}, \quad (2)$$

and

$$\tau_x=\begin{pmatrix}0&0&1&0\\0&0&0&1\\1&0&0&0\\0&1&0&0\end{pmatrix},\quad \tau_y=\begin{pmatrix}0&0&-i&0\\0&0&0&-i\\i&0&0&0\\0&i&0&0\end{pmatrix},$$

$$\tau_z=\begin{pmatrix}1&0&0&0\\0&1&0&0\\0&0&-1&0\\0&0&0&-1\end{pmatrix}. \quad (3)$$

These operators satisfy the relations:

$$\sigma_i\sigma_j+\sigma_j\sigma_i=2\delta_{ij};\quad \tau_i\tau_j+\tau_j\tau_i=2\delta_{ij};\quad \sigma_i\tau_j-\tau_j\sigma_i=0. \quad (4)$$

Any operator in the ordinary spin-isotopic spin space may be expressed as a linear combination of the sixteen linearly independent matrices: 1, σ_i, τ_i, $\sigma_i\tau_j$, including the operators in (1). The total Hamiltonian for symmetric pseudoscalar mesons may then be written in second quantized form as follows (we set $\hbar=c=1$ and use the summation convention throughout):

$$H=\int dx\Big\{\frac{1}{2M}(\nabla\psi_\rho^*)\cdot(\nabla\psi_\rho)+\tfrac{1}{2}[\pi_i^2+(\nabla\phi_i)^2+\mu^2\phi_i^2]+(4\pi)^{\frac{1}{2}}\frac{g}{\mu}\psi_\rho^*(\tau_{p\mu})_i(\sigma_{\mu\nu}\cdot\nabla\phi_i)\psi_\nu+\int\psi_\rho^*(x)\psi_\sigma^*(x')J_{\rho\mu}{}^\alpha J_{\sigma\nu}{}^\alpha \times V^{(\alpha)}(x-x')\psi_\mu(x)\psi_\nu(x')dx'\Big\}. \quad (5)$$

In (5), ϕ is the meson wave function, π the canonically conjugate momentum, g the meson-nucleon coupling constant and J^α represents the operators for $\alpha=1, 2, 3, 4$, respectively (i.e. $V=J_1{}^\alpha\cdot J_2{}^\alpha V^{(\alpha)}$). The commutation rules for the ψ and ϕ are

$$[\psi_\rho^*(x),\psi_\sigma(x')]_+=-i\delta_{\rho\sigma}\delta(x-x'),\quad [\psi_\rho(x),\psi_\sigma(x')]_+=[\psi_\rho^*(x),\psi_\sigma^*(x')]_+=0,\quad [\pi_i(x),\phi_j(x')]=-i\delta_{ij}\delta(x-x'), \quad (6)$$

all other quantities commuting.

We expand the wave functions in Fourier series in a box of volume Ω. For the nucleon, we have

$$\psi_\rho(x)=\Omega^{-\frac{1}{2}}A_p{}^m u_\rho{}^m e^{ip\cdot x},\quad \psi_\rho^*(x)=\Omega^{-\frac{1}{2}}A_p{}^{m*}u_\rho{}^{m*}e^{-ip\cdot x}, \quad (7)$$

where

$$u_\rho{}^{m*}u_\rho{}^{m'}=\delta_{mm'},\quad u_\rho{}^{m*}u_\sigma{}^m=\delta_{\rho\sigma}.$$

The u's may conveniently be taken to be

$$u^1=\begin{pmatrix}1\\0\\0\\0\end{pmatrix},\quad u^2=\begin{pmatrix}0\\1\\0\\0\end{pmatrix},\quad u^3=\begin{pmatrix}0\\0\\1\\0\end{pmatrix},\quad u^4=\begin{pmatrix}0\\0\\0\\1\end{pmatrix}, \quad (8)$$

[5] W. Horning and M. Weinstein, Phys. Rev. **72**, 251 (1947).
[6] Private communication from R. Serber.
[7] R. Serber and R. Christian, private communication; see, however, the note added in proof at the end of this paper.

where the superscripts 1, 2, 3, 4 represent proton spin up, proton spin down, neutron spin up, neutron spin down, respectively.

For the meson, we have

$$\phi_i(x)=\Omega^{-\frac{1}{2}}(2\omega_k)^{-\frac{1}{2}}(a_k{}^s v_i{}^s+a_{-k}{}^{s*}v_i{}^{s*})e^{ik\cdot x},$$
$$\pi_i(x)=i\Omega^{-\frac{1}{2}}(\tfrac{1}{2}\omega_k)^{\frac{1}{2}}(a_k{}^{s*}v_i{}^{s*}-a_{-k}{}^s v_i{}^s)e^{-ik\cdot x}, \quad (9)$$

with

$$\omega_k=(\mu^2+k^2)^{\frac{1}{2}}$$

and where

$$v_i{}^{s*}v_j{}^s=\delta_{ij}, \quad v_i{}^{s*}v_i{}^{s'}=\delta_{ss'}.$$

It is convenient to choose

$$v^1=\begin{pmatrix}1/\sqrt{2}\\ +i/\sqrt{2}\\ 0\end{pmatrix}, \quad v^2=\begin{pmatrix}1/\sqrt{2}\\ -i/\sqrt{2}\\ 0\end{pmatrix}, \quad v^3=\begin{pmatrix}0\\ 0\\ 1\end{pmatrix}, \quad (10)$$

where the superscripts 1, 2, 3 represent positive, negative and neutral mesons, respectively.

The operators satisfy the commutation rules:

$$[A_p{}^{m*}, A_{p'}{}^{m'}]_+=\delta_{mm'}\delta_{pp'},$$
$$[A_p{}^{m*}, A_{p'}{}^{m'*}]_+=[A_p{}^m, A_{p'}{}^{m'}]_+=0, \quad (11)$$
$$[a_k{}^s, a_{k'}{}^{s'*}]=\delta_{ss'}\delta_{kk'},$$

all other quantities commuting.

The Hamiltonian now takes the form

$$H=A_p{}^{m*}A_p{}^m E_p+(a_k{}^s a_k{}^{s*}+a_k{}^{s*}a_k{}^s)\omega_k/2$$
$$+\frac{i(4\pi)^{\frac{1}{2}}g}{\mu\Omega^{\frac{1}{2}}(2\omega_k)^{\frac{1}{2}}}(u^{m*}|\tau_i(\sigma\cdot k)|u^{m'})A_p{}^{m*}A_{p'}{}^{m'}$$
$$\times(a_k{}^s v_i{}^s+a_{-k}{}^{s*}v_i{}^{s*})\delta(p-p'-k)$$
$$+A_p{}^{m*}A_{p'}{}^{m'*}A_{p''}{}^{m''}A_{p'''}{}^{m'''}V_{p''-p}{}^{(\alpha)}$$
$$(u^{m*}|J^\alpha|u^{m''})\cdot(u^{m'*}|J^\alpha|u^{m'''})$$
$$\times\delta(p+p'-p''-p'''), \quad (12)$$

where

$$V_P{}^{(\alpha)}=\frac{1}{\Omega}\int V^{(\alpha)}(x)e^{iP\cdot x}dx.$$

We shall calculate to first order in V and g the transition probability from a state in which we have two nucleons with momenta p_0 and $-p_0$ and in spin states m_1 and m_2, respectively, to a state in which we have two nucleons with momenta $p-\frac{1}{2}k$ and $-p-\frac{1}{2}k$ and in spin states m_1' and m_2', respectively, and a meson with momentum k and isotopic spin state s. The transition scheme is

$$(p_0, m_1)(-p_0, m_2)\begin{cases}\nearrow (p-\frac{1}{2}k, m_1')(-p+\frac{1}{2}k, m'')\\ \nearrow (-p-\frac{1}{2}k, m_2')(p+\frac{1}{2}k, m'')\\ \searrow (p_0, m_1)(-p_0-k, m'')(k, s)\\ \searrow (-p_0, m_2)(p_0-k, m'')(k, s)\end{cases}\searrow\nearrow (p-\tfrac{1}{2}k, m_1')(-p-\tfrac{1}{2}k, m_2')(k, s). \quad (13)$$

The transition scheme (13) would yield eight distinct matrix elements if we did not take advantage of the assumption that $p_0\ll M$. Making this assumption, we may neglect $\frac{1}{2}k$ compared with $p\pm p_0$ so that $p^2=p_0{}^2-M\omega_k$ and we may replace $V_{p\pm p_0\pm\frac{1}{2}k}{}^{(\alpha)}$ by $V_{p\pm p_0}{}^{(\alpha)}$. With this approximation, neglecting the nucleonic recoil energies and summing over m''. the transition matrix element reduces to

$$H'=\frac{i(4\pi)^{\frac{1}{2}}g}{\mu\Omega^{\frac{1}{2}}\omega_k(2\omega_k)^{\frac{1}{2}}}\{V_{p-p_0}{}^{(\alpha)}[(m_1|J^\alpha|m_1')$$
$$\cdot(m_2|K^\alpha|m_2')+(m_1|K^\alpha|m_1')\cdot(m_2|J^\alpha|m_2')]$$
$$+V_{p+p_0}{}^{(\alpha)}[(m_1|J^\alpha|m_2')\cdot(m_2|K^\alpha|m_1')$$
$$+(m_1|K^\alpha|m_2')\cdot(m_2|J^\alpha|m_1')]\}, \quad (14)$$

where

$$K^{\alpha*}=J^\alpha(\tau_i v_i{}^{s*})(\sigma\cdot k)-(\tau_i v_i{}^{s*})(\sigma\cdot k)J^\alpha. \quad (14a)$$

Before proceeding, we must make our notation a little more specific. The quantity J^1 is a scalar, J^2 and J^3 are vectors, while J^4 is a tensor. We may adopt a uniform notation if we use two tensor indices as follows:

$$\begin{aligned}&J^1: \quad J_{ik}{}^1=\delta_{ik}/\sqrt{3},\\ &J^2: \quad J_{ik}{}^2=\sigma_i\delta_{ik},\\ &J^3: \quad J_{ik}{}^3=\tau_i\delta_{ik},\\ &J^4: \quad J_{ik}{}^4=\sigma_i\tau_k.\end{aligned} \quad (15)$$

Then,

$$H'=-\frac{ig(4\pi)^{\frac{1}{2}}}{\mu\Omega^{\frac{1}{2}}\omega_k(2\omega_k)^{\frac{1}{2}}}\{V_{p-p_0}{}^{(\alpha)}[(m_1|J_{ik}{}^\alpha|m_1')$$
$$\times(m_2|K_{ik}{}^\alpha|m_2')$$
$$+(m_1|K_{ik}{}^\alpha|m_1')(m_2|J_{ik}{}^\alpha|m_2')]$$
$$+V_{p+p_0}{}^{(\alpha)}[(m_1|J_{ik}{}^\alpha|m_2')(m_2|K_{ik}{}^\alpha|m_1')$$
$$+(m_1|K_{ik}{}^\alpha|m_2')(m_2|J_{ik}{}^\alpha|m_1')]\}. \quad (16)$$

Taking the absolute square of H' and summing over the final spin states of the nucleons, we get (since

$J_{ik}{}^{\alpha}=J_{ik}{}^{\alpha}$)

$$|H'|^2=-\frac{2\pi g^2}{\mu\Omega\omega_k{}^3}$$
$$\times\{[V_{p-p_0}{}^{(\alpha)}V_{p-p_0}{}^{(\beta)}+V_{p+p_0}{}^{(\alpha)}V_{p+p_0}{}^{(\beta)}]$$
$$\times[(m_1|J_{ik}{}^{\alpha}J_{jl}{}^{\beta}|m_1)(m_2|K_{ik}{}^{\alpha}K_{jl}{}^{\beta*}|m_2)$$
$$+(m_1|J_{ik}{}^{\alpha}K_{jl}{}^{\beta*}|m_1)(m_2|K_{ik}{}^{\alpha}J_{jl}{}^{\beta}|m_2)$$
$$+(m_1|K_{ik}{}^{\alpha}K_{jl}{}^{\beta*}|m_1)(m_2|J_{ik}{}^{\alpha}J_{jl}{}^{\beta}|m_2)$$
$$+(m_1|K_{ik}{}^{\alpha}J_{jl}{}^{\beta}|m_1)(m_2|J_{ik}{}^{\alpha}K_{jl}{}^{\beta*}|m_2)]$$
$$+2V_{p-p_0}{}^{(\alpha)}V_{p+p_0}{}^{(\beta)}[(m_1|J_{ik}{}^{\alpha}K_{jl}{}^{\beta*}|m_2)$$
$$\times(m_2|K_{ik}{}^{\alpha}J_{jl}{}^{\beta}|m_1)+(m_1|J_{ik}{}^{\alpha}J_{jl}{}^{\beta}|m_2)$$
$$\times(m_2|K_{ik}{}^{\alpha}K_{jl}{}^{\beta*}|m_1)+(m_1|K_{ik}{}^{\alpha}K_{jl}{}^{\beta*}|m_2)$$
$$\times(m_2|J_{ik}{}^{\alpha}J_{jl}{}^{\beta}|m_1)+(m_1|K_{ik}{}^{\alpha}J_{jl}{}^{\beta}|m_2)$$
$$\times(m_2|J_{ik}{}^{\alpha}K_{jl}{}^{\beta*}|m_1)]\}. \quad (17)$$

If we now introduce the projection operators:

$$\Lambda=\begin{cases}\frac{1}{2}(1+\tau_z) \text{ if the particle is a proton}\\ \frac{1}{2}(1-\tau_z) \text{ if the particle is a neutron}\end{cases} \quad (18)$$

and average over the initial spin states, we find

$$|H'|^2=-\frac{\pi g^2}{2\mu^2\Omega\omega_k{}^3}$$
$$\{[V_{p-p_0}{}^{(\alpha)}V_{p-p_0}{}^{(\beta)}+V_{p+p_0}{}^{(\alpha)}V_{p+p_0}{}^{(\beta)}]$$
$$\times[Sp(J_{ik}{}^{\alpha}J_{jl}{}^{\beta}\Lambda_1)Sp(K_{ik}{}^{\alpha}K_{jl}{}^{\beta*}\Lambda_2)$$
$$+Sp(J_{ik}{}^{\alpha}J_{jl}{}^{\beta}\Lambda_2)Sp(K_{ik}{}^{\alpha}K_{jl}{}^{\beta*}\Lambda_1)$$
$$+Sp(J_{ik}{}^{\alpha}K_{jl}{}^{\beta*}\Lambda_1)Sp(K_{ik}{}^{\alpha}J_{jl}{}^{\beta}\Lambda_2)$$
$$+Sp(J_{ik}{}^{\alpha}K_{jl}{}^{\beta*}\Lambda_2)Sp(K_{ik}{}^{\alpha}J_{jl}{}^{\beta}\Lambda_1)]$$
$$+2V_{p-p_0}{}^{(\alpha)}V_{p+p_0}{}^{(\beta)}[Sp(J_{ik}{}^{\alpha}K_{jl}{}^{\beta*}\Lambda_2K_{ik}{}^{\alpha}J_{jl}{}^{\beta}\Lambda_1)$$
$$+Sp(J_{ik}{}^{\alpha}J_{jl}{}^{\beta}\Lambda_2K_{ik}{}^{\alpha}K_{jl}{}^{\beta*}\Lambda_1)$$
$$+Sp(K_{ik}{}^{\alpha}K_{jl}{}^{\beta*}\Lambda_2J_{ik}{}^{\alpha}J_{jl}{}^{\beta}\Lambda_1)$$
$$+Sp(K_{ik}{}^{\alpha}J_{jl}{}^{\beta}\Lambda_2J_{ik}{}^{\alpha}K_{jl}{}^{\beta*}\Lambda_1)]\}. \quad (19)$$

The subscripts 1 and 2 on Λ refer to the nucleons with momenta p_0 and $-p_0$, respectively. The evaluation of the spurs in (19) is straightforward and yields the results (we have written $\Lambda=\frac{1}{2}(1+\delta\tau_z)$ where $\delta=+1$ for proton and $\delta=-1$ for neutron and $\epsilon^s=-i(v_1{}^{s*}v_2{}^s-v_2{}^{s*}v_1{}^s)$):

$$P_1{}^{\alpha\beta}(\Lambda_1,\Lambda_2,s)\equiv Sp(J_{ik}{}^{\alpha}J_{jl}{}^{\beta}\Lambda_1)Sp(K_{ik}{}^{\alpha}K_{jl}{}^{\beta*}\Lambda_2)$$
$$=-16k^2\begin{pmatrix}0 & 0 & 0 & 0\\ 0 & 2(1+\epsilon^s\delta_2) & 0 & 2\delta_1\delta_2(v_3{}^s)^2\\ 0 & 0 & [2(1-\delta_1\delta_2(v_3{}^s)^2)+\epsilon^s(\delta_1+\delta_2)] & 0\\ 0 & P_1{}^{24} & 0 & [2(2-\delta_1\delta_2(v_3{}^s)^2)+\epsilon^s(\delta_2+3\delta_1)]\end{pmatrix}, \quad (20a)$$

$$P_2{}^{\alpha\beta}(\Lambda_1,\Lambda_2,s)\equiv Sp(J_{ik}{}^{\alpha}J_{jl}{}^{\beta}\Lambda_2)Sp(K_{ik}{}^{\alpha}K_{jl}{}^{\beta*}\Lambda_1)=P_1{}^{\alpha\beta}(\Lambda_2,\Lambda_1,s), \quad (20b)$$

$$P_3{}^{\alpha\beta}(\Lambda_1,\Lambda_2,s)\equiv Sp(J_{ik}{}^{\alpha}K_{jl}{}^{\beta*}\Lambda_1)Sp(K_{ik}{}^{\alpha}J_{jl}{}^{\beta}\Lambda_2)=-16k^2\begin{pmatrix}0 & 0 & 0 & 0\\ 0 & -P_1{}^{24} & 0 & -P_1{}^{22}\\ 0 & 0 & 0 & -P_1{}^{33}\\ 0 & -P_1{}^{22} & -P_1{}^{33} & -P_1{}^{24}\end{pmatrix}, \quad (20c)$$

$$P_4{}^{\alpha\beta}(\Lambda_1,\Lambda_2,s)\equiv Sp(J_{ik}{}^{\alpha}K_{jl}{}^{\beta*}\Lambda_2)Sp(K_{ik}{}^{\alpha}J_{jl}{}^{\beta}\Lambda_1)=P_3{}^{\alpha\beta}(\Lambda_2,\Lambda_1,s), \quad (20d)$$

$$Q_1{}^{\alpha\beta}(\Lambda_1\Lambda_2,s)\equiv Sp(J_{ik}{}^{\alpha}K_{jl}{}^{\alpha*}\Lambda_2K_{ik}{}^{\beta}J_{jl}{}^{\beta}\Lambda_1)$$
$$=-16k^2\begin{pmatrix}0 & 0 & 0 & 0\\ 0 & 0 & [1+\epsilon^s\delta_2-\delta_1\delta_2(v_3{}^s)^2] & -Q_1{}^{23}\\ 0 & Q_1{}^{23} & -[\delta_1\delta_2(1-(v_3{}^s)^2)+(\epsilon^s/2)(\delta_1+\delta_2)] & -[1+\delta_1\delta_2(1-2(v_3{}^s)^2)+(\epsilon^s/2)(3\delta_1+\delta_2)]\\ 0 & Q_1{}^{24} & Q_1{}^{34} & [2-\delta_1\delta_2(1+(v_3{}^s)^2)+(\epsilon^s/2)(3\delta_1-\delta_2)]\end{pmatrix}, \quad (21a)$$

$$Q_2{}^{\alpha\beta}\equiv Sp(J_{ik}{}^{\alpha}J_{jl}{}^{\beta}\Lambda_2K_{ik}{}^{\alpha}K_{jl}{}^{\beta*}\Lambda_1)=-16k^2\begin{pmatrix}0 & 0 & 0 & 0\\ 0 & 0 & Q_1{}^{23} & Q_1{}^{24}\\ 0 & Q_1{}^{23} & -Q_1{}^{23} & -Q_1{}^{23}+Q_1{}^{24}\\ 0 & Q_1{}^{24} & -Q_1{}^{23}+Q_1{}^{24} & [2+\delta_1\delta_2(1-3(v_3{}^s)^2)+\frac{3}{2}\epsilon^s(\delta_1+\delta_2)]\end{pmatrix}, \quad (21b)$$

$$Q_3^{\alpha\beta}\equiv Sp(K_{ik}{}^{\alpha}K_{jl}{}^{\beta*}\Lambda_2 J_{ik}{}^{\alpha}J_{jl}{}^{\beta}\Lambda_1)=-16k^2\begin{pmatrix}0 & 0 & 0 & 0\\ 0 & 0 & [1+\epsilon^s\delta_1 & -Q_3{}^{23}\\ & & -\delta_1\delta_2(v_3{}^s)^2] & \\ 0 & Q_3{}^{23} & -Q_1{}^{33} & -[1+(\epsilon^s/2)(\delta_1-\delta_2)-\delta_1\delta_2]\\ 0 & Q_3{}^{24} & Q_3{}^{34} & Q_2{}^{44}\end{pmatrix}, \quad (21c)$$

$$Q_4^{\alpha\beta}\equiv Sp(K_{ik}{}^{\alpha}J_{jl}{}^{\beta}\Lambda_2 J_{ik}{}^{\alpha}K_{jl}{}^{\beta*}\Lambda_1)=-16k^2\begin{pmatrix}0 & 0 & 0 & 0\\ 0 & 0 & Q_3{}^{23} & Q_3{}^{24}\\ 0 & Q_3{}^{23} & Q_1{}^{23} & -Q_1{}^{23}+Q_1{}^{33}\\ 0 & Q_3{}^{24} & -Q_1{}^{23}+Q_1{}^{33} & Q_1{}^{33}+2Q_1{}^{23}\end{pmatrix}. \quad (21d)$$

If we now sum the P's and Q's, and use the notation

$$S_1{}^{\alpha\beta}=\sum_{n=1}^{4}P_n{}^{\alpha\beta}, \quad S_2{}^{\alpha\beta}=\sum_{n=1}^{4}Q_n{}^{\alpha\beta},$$

we get

$$S_1{}^{\alpha\beta}=-32k^2A^s(\Lambda_1,\Lambda_2)\begin{pmatrix}0 & 0 & 0 & 0\\ 0 & 1 & 0 & -1\\ 0 & 0 & 1 & -1\\ 0 & -1 & -1 & 2\end{pmatrix};$$
$$S_2{}^{\alpha\beta}=-32k^2A^s(\Lambda_1,\Lambda_2)\begin{pmatrix}0 & 0 & 0 & 0\\ 0 & 0 & 1 & -1\\ 0 & 1 & 0 & -1\\ 0 & -1 & -1 & -2\end{pmatrix}, \quad (22)$$

where

$$A^s(\Lambda_1,\Lambda_2)=2+\epsilon^s(\delta_1+\delta_2)-2\delta_1\delta_2(v_3{}^s)^2. \quad (22a)$$

The quantity $A^s(\Lambda_1,\Lambda_2)$ characterizes the relative probabilities for the production of the various types of charged mesons in the different nucleon-nucleon collisions and Table I lists its values.

Our theory (which is a weak coupling theory) correctly gives zero probability for the production of negative and positive mesons in proton-proton and neutron-neutron collisions, respectively. The equality of the number of neutral mesons and the number of charged mesons produced in a neutron-proton collision follows naturally, whereas the unexpected zero probability for the production of neutral mesons in like-particle collisions is a consequence of a subtle cancellation of matrix elements.

Since the density of final states is

$$\frac{\Omega M p d\Omega_p}{16\pi^3}\cdot\frac{\Omega k\omega_k d\Omega_k d\omega_k}{8\pi^3}$$

the differential cross section for the production of mesons of type s becomes

$$d\sigma^s(\Lambda_1,\Lambda_2)=\left(\frac{\sqrt{2}gMk}{4\pi^2\mu\omega_k}\right)^2\left(\frac{kp}{p_0}\right)A^s(\Lambda_1,\Lambda_2)$$
$$\cdot\int d\Omega_p\{[(V_{p-p_0}{}^{(2)})^2+(V_{p+p_0}{}^{(2)})^2]$$
$$+2(V_{p-p_0}{}^{(2)}V_{p+p_0}{}^{(3)}+V_{p+p_0}{}^{(2)}V_{p-p_0}{}^{(3)})$$
$$-(V_{p-p_0}{}^{(2)}+V_{p+p_0}{}^{(4)})^2-(V_{p-p_0}{}^{(4)}+V_{p+p_0}{}^{(2)})^2$$
$$+[(V_{p-p_0}{}^{(3)})^2+(V_{p+p_0}{}^{(3)})^2]$$
$$-(V_{p-p_0}{}^{(3)}+V_{p+p_0}{}^{(4)})^2-(V_{p-p_0}{}^{(4)}+V_{p+p_0}{}^{(3)})^2$$
$$+2(V_{p-p_0}{}^{(4)}+V_{p+p_0}{}^{(4)})^2\}d\Omega_k d\omega_k. \quad (23)$$

Equation (23) is the general expression for the differential cross section for the production of pseudoscalar mesons of type s in a collision of two nucleons of types Λ_1 and Λ_2, respectively. That the angular distribution of the mesons is uniform in the center of mass system, independent of any particular assumption about the V's is evident, and follows directly from our approximation of neglecting $\frac{1}{2}k$ compared with $p\pm p_0$.

The method of calculation which has just been used for symmetric pseudoscalar mesons with pseudovector coupling can easily be extended to the case of symmetric scalar mesons with scalar coupling. The total Hamiltonian (5) is replaced by

$$H=\int dx\left\{\frac{1}{2M}(\nabla\psi_\rho{}^*)\cdot(\nabla\psi_\rho)+\tfrac{1}{2}[\pi_i{}^2+(\nabla\phi_i)^2+\mu^2\phi_i{}^2]\right.$$
$$+(4\pi)^{\frac{1}{2}}f\psi_\rho{}^*(\tau_{\rho\mu})_i\phi_i\psi_\rho+\int dx'\psi_\rho{}^*(x)\psi_\sigma{}^*(x')$$
$$\left.\times(J_{\rho\mu}{}^{\alpha}\cdot J_{\sigma\nu}{}^{\alpha})V^{(\alpha)}(x-x')\psi_\mu(x)\psi_\nu(x')\right\}. \quad (24)$$

Proceeding in exactly the same fashion as for the pseudoscalar case, we obtain an expression for $|H'|^2$ identical with (19) except that f^2 replaces $(g/\mu)^2$ and $K^{\alpha*}$ is defined by $[J^{\alpha}(\tau_i v_i{}^{s*})-(\tau_i v_i{}^{s*})J^{\alpha}]$ instead of (14a). Evaluation of the spurs then leads

TABLE I. Values of $A^s(\Lambda_1,\Lambda_2)$.

	p-p collision ($\Lambda_1=\Lambda_2=1$)	n-n collision ($\Lambda_1=\Lambda_2=-1$)	n-p collision ($\Lambda_1=\pm1$, $\Lambda_2=\mp1$)
pos. meson ($s=1$)	4	0	2
neg. meson ($s=2$)	0	4	2
neutral meson ($s=3$)	0	0	4

TABLE II. Values of total cross section for Yukawa potential.

(E_0/E_t)	1.25	1.50	2.00
$\frac{\sigma_T{}^s(\Lambda_1,\Lambda_2)}{(g^2/\hbar c)A^s(\Lambda_1,\Lambda_2)}$	$4.4\cdot10^{-31}$ cm²	$4.4\cdot10^{-30}$ cm²	$2.0\cdot10^{-29}$ cm²

to the following values for the P's and Q's (see Eqs. (20a)–(21d)):

$$P_1{}^{\alpha\beta}(\Lambda_1,\Lambda_2,s)=-16A^s(\Lambda_1,\Lambda_2)\begin{pmatrix}0&0&0&0\\0&0&0&0\\0&0&1&0\\0&0&0&3\end{pmatrix}, \quad (25a)$$

$$P_2{}^{\alpha\beta}(\Lambda_1,\Lambda_2,s)=P_1{}^{\alpha\beta}(\Lambda_2,\Lambda_1,s), \quad (25b)$$

$$P_3{}^{\alpha\beta}(\Lambda_1,\Lambda_2,s)=-P_1{}^{\alpha\beta}(\Lambda_1,\Lambda_2,s), \quad (25c)$$

$$P_4{}^{\alpha\beta}(\Lambda_1,\Lambda_2,s)=P_3{}^{\alpha\beta}(\Lambda_2,\Lambda_1,s). \quad (25d)$$

$$Q_1{}^{\alpha\beta}(\Lambda_1,\Lambda_2,s)=-8B^s(\Lambda_1,\Lambda_2)\begin{pmatrix}0&0&0&0\\0&0&0&0\\0&0&1&3\\0&0&3&-3\end{pmatrix}, \quad (26a)$$

$$Q_2{}^{\alpha\beta}(\Lambda_1,\Lambda_2,s)=-8B^s(\Lambda_1,\Lambda_2)\times\begin{pmatrix}0&0&0&0\\0&0&0&0\\0&0&-1&-3\\0&0&-3&3\end{pmatrix}, \quad (26b)$$

$$Q_3{}^{\alpha\beta}(\Lambda_1,\Lambda_2,s)=Q_2{}^{\alpha\beta}(\Lambda_1,\Lambda_2,s), \quad (26c)$$

$$Q_4{}^{\alpha\beta}(\Lambda_1,\Lambda_2,s)=Q_1{}^{\alpha\beta}(\Lambda_1,\Lambda_2,s), \quad (26d)$$

where $A^s(\Lambda_1,\Lambda_2)$ is defined by (22a) and

$$B^s(\Lambda_1,\Lambda_2)=2\delta_1\delta_2(-1+(v_3{}^s)^2)-\epsilon^s(\delta_1+\delta_2).$$

If we now sum the P's and Q's, we find $S_1{}^{\alpha\beta}\equiv0$ and $S_2{}^{\alpha\beta}\equiv0$. Hence, in the present approximation, the symmetric scalar theory yields zero cross section. This result was discovered independently by W. S. MacAfee.[8] This means, of course, that one must take account of the recoil of the nucleons in order to get a non-vanishing cross section on the symmetrical scalar theory.[5] However, if this is done, it is no longer self-consistent to neglect the "exchange" terms compared to the "ordinary" terms (see Introduction). We have, therefore, not calculated the meson production cross section on the basis of the symmetric scalar theory.[9]

3. RESULTS AND DISCUSSION

We apply formula (23) to calculate the π-meson production cross section on the basis of two different assumptions regarding the spatial behavior of the four V's: a Yukawa potential for all four V's and a square-well potential for all four V's. These two assumptions are taken from the work of Serber and Christian[7] who have obtained the best fit of the experimental angular distribution for neutron-proton scattering at 90 Mev. Serber and Christian find for the best Yukawa potential:

$$V(r)=\tfrac{1}{2}(1+P_M)({}^ag)^2(e^{-Kr}/r), \quad (27)$$

where $K=0.87\mu$, $({}^1g)^2=0.280$, $({}^3g)^2=0.404$ and P_M is the Majorana operator. Translated into our notation, (27) becomes:

$$V(r)=\{3(c_1+c_3)+(-3c_1+c_3)\sigma_1\cdot\sigma_2+(c_1-3c_3)\tau_1\cdot\tau_2+(-c_1-c_3)\sigma_1\cdot\sigma_2\tau_1\cdot\tau_2\}e^{-Kr}/16r, \quad (28)$$

where $c_1=({}^1g)^2$, $c_3=({}^3g)^2$. Substitution of (28) into (23) yields the differential cross section for the production of pseudoscalar mesons:

$$d\sigma^s(\Lambda_1,\Lambda_2)=\frac{(c_1-c_3)^2}{2\pi}\left(\frac{gMk}{\mu\omega_k}\right)^2\left(\frac{kp}{p_0}\right)A^s(\Lambda_1,\Lambda_2)\times\left\{\frac{1}{(K^2+p^2+p_0{}^2)^2-4p_0{}^2p^2}-\frac{\tanh^{-1}[2p_0p/(K^2+p^2+p_0{}^2)]}{2p_0p(K^2+p^2+p_0{}^2)}\right\}d\Omega_kd\omega_k, \quad (29)$$

where $k=(\omega_k{}^2-\mu^2)^{\frac{1}{2}}$ and $p=(p_0{}^2-M\omega_k)^{\frac{1}{2}}$. The total cross section, $\sigma_T{}^s(\Lambda_1,\Lambda_2)$, can easily be evaluated; we find the results given in Table II for three values of the incident energy E_0. In Table II the incident energy is measured in units of the threshold energy E_t, chosen as 290 Mev[8], i.e., the mass of the π-meson is taken as 145 Mev. The quantity $A^s(\Lambda_1,\Lambda_2)$ is given by Table I while $(g^2/\hbar c)$ can be taken from Pauli;[10] the product $(g^2/\hbar c)A^s$ is of order unity. The rapid increase of cross section is characteristic of the pseudoscalar theory.

TABLE III. Values of total cross section for square well potential.

(E_0/E_t)	1.25	1.50	2.00
$\frac{\sigma_T{}^s(\Lambda_1,\Lambda_2)}{(g^2/\hbar c)A^s(\Lambda_1,\Lambda_2)}$	$8.4\cdot10^{-31}$ cm²	$9.6\cdot10^{-30}$ cm²	$1.7\cdot10^{-29}$ cm²

A corresponding calculation has been performed for a square-well potential using the constants determined by Serber and Christian,[7] namely:

$$V(r)=\tfrac{1}{2}(1+P_M)^aJ(r), \quad (30)$$

where

$$\left.\begin{aligned}{}^1J(r)&=0.166\mu\\{}^3J(r)&=0.252\mu\end{aligned}\right\}\text{ for } r\leq1.5/\mu$$

[8] Cornell doctoral dissertation under H. A. Bethe; we are indebted to Professor Bethe for informing us of Mr. MacAfee's result.

[9] See L. W. Nordheim and G. Nordheim, Phys. Rev. **54**, 254 (1938) and reference 5.

[10] W. Pauli, *Meson Theory of Nuclear Forces* (Interscience Publishers, Inc., New York, 1946).

and

$$^{a}J(r)=0 \text{ for } r>1.5/\mu.$$

Table III gives the results[11] for the same range of values for the incident energy of the nucleon as Table II.

Comparison of Tables II and III makes manifest the rather expected insensitivity of the meson production cross section to the shape of the nuclear potential as long as the nucleon-nucleon scattering experiments are fitted at high energies. For both the square-well and Yukawa potentials, the meson production cross section turns out to be surprisingly small. This result is in striking contrast to the result obtained by Morette and Peng[2] on the basis of a third-order field-theoretic perturbation calculation. Morette and Peng obtain a meson production cross section of the order of 10^{-27} cm^2 at an incident nucleon energy of twice the threshold energy.

The large discrepancy between the two results has been discussed by one of the authors (R.E.M.) with Dr. Morette. Dr. Morette has reexamined the details of her calculation and arrived at the conclusion that the "exchange" terms are responsible for the large cross section predicted by the field-theoretic treatment. This is a consequence of the fact that whereas the δ-interaction terms between the two nucleons are effectively subtracted out from the "ordinary" terms, they are not subtracted out from the "exchange" terms so that the latter make the largest contributions to the cross section. This is contrary to our statement in the introduction and is due to the singularities which arise in present-day meson field theories of nuclear forces. In a correct convergent field theory of nuclear forces, the "exchange" terms should not be large compared to the "ordinary" terms, except for accidental cancellations as in the symmetric scalar theory.

[11] The fluctuations due to the sine and cosine functions (arising from the Fourier transform of the square well) were averaged out.

We believe that the small cross sections—not necessarily those predicted by the symmetric pseudoscalar theory—will correspond to experiment. We feel that the value of our method lies precisely in its correlation of the meson production cross section with the nucleon-nucleon scattering cross section at high energies and its bypassing of the existing singular field theories of nuclear forces. The quantitative cross section and the energy spectrum of the mesons just above the threshold should therefore contribute to our knowledge of the meson-nucleon coupling. We do not believe, however, that our results and calculations along similar lines (for other types of meson-nucleon coupling and more complicated (tensor) forms of nuclear interaction) will shed light on the correct meson theory of nuclear forces.

The authors are indebted to Dr. E. Caianiello for assistance with the numerical calculations. This work was carried out last summer at the University of Rochester and was assisted by the joint program of the Office of Naval Research and the Atomic Energy Commission.

Note added in proof: One of the authors (L.L.F.) has investigated the effect of tensor forces on the angular distribution of the mesons produced in nucleon-nucleon collisions. Toward this end, a calculation was performed with the neutral pseudoscalar theory (pseudovector coupling) with the same approximations as were made above with a phenomenological interaction of the form:

$$(\sigma_1\cdot\text{grad})(\sigma_2\cdot\text{grad})U(r) = \tfrac{1}{3}S_{12}\left[\frac{d^2U}{dr^2}-\frac{1}{r}\frac{dU}{dr}\right]+\tfrac{1}{3}\sigma_1\cdot\sigma_2\left[\frac{d^2U}{dr^2}+\frac{2}{r}\frac{dU}{dr}\right],$$

where S_{12} is the tensor force operator. The results indicate that in contrast to the isotropic angular distribution predicted for central forces, a force of the above type yields a $(\sin^2\theta)$ angular distribution where θ is the angle between the direction of emission of the meson and the direction of the incident nucleon. By adding to the above interaction a central force which cancels out the central part, the resulting angular distribution becomes $(\frac{4}{3}-\sin^2\theta)$. Hence, in the first instance, the emission of mesons perpendicular to the direction of the nucleons is favored while for a pure tensor force, emission parallel to this direction is favored.

Reactions Induced by Slow Neutron Irradiation of Europium

RICHARD J. HAYDEN, JOHN H. REYNOLDS,* AND MARK G. INGHRAM
Argonne National Laboratory and University of Chicago, Chicago, Illinois
(Received February 10, 1949)

A sample of europium which had been subjected to slow neutron irradiation was analyzed using mass spectrometric techniques. By using a modified isotopic dilution technique, i.e., adding a standard containing known relative abundances of normal samarium, europium, and gadolinium the complete chemical and isotopic analysis of the irradiated sample was obtained. Combining this nuclide composition and certain radioactivity measurements the thermal neutron cross sections, half-lives and branching ratios of five of the europium isotopes were calculated. The results were $\sigma_{151}=5200$ barns, $\sigma_{152}=3200$ barns, $\sigma_{153}=240$ barns, $\sigma_{154}=880$ barns, $\sigma_{155}=7900$ barns, $T_{\frac{1}{2}}(152)=5.3$ years, $T_{\frac{1}{2}}(154)=5.4$ years, $T_{\frac{1}{2}}(155)=1.7$ years, K/β^- ratio for 9.2-hr. $Eu^{153}=0.22$, K/β^- ratio for 5.3-year $Eu^{152}=2.8$, and K/β^- ratio for 5.4-year $Eu^{154}<0.05$. All these results are believed to be good to ± 15 percent.

INTRODUCTION

SLOW neutron induced activities in europium have been studied by several investigators.[1–6] However, because of the complex nature of the radiations induced a more complete analysis of the problem is desirable. Of special interest are the following problems: (1) The determination of the ratio of K-capture to beta-decay for the (n, γ) induced activities of europium. Previous investigation of these branching ratios have been based on a determination of x-ray counter efficiencies. (2) The determination of the characteristic radiations of the long lived Eu^{152} and long lived Eu^{154}. This problem exists since up to this time all studies of these radiations have been made on a mixture of these two long lived activities. (3) The determination of the half-lives of Eu^{152} and Eu^{154}. These measurements have been heretofore uncertain because of the length of both half-lives and because of the intimate mixture of the two isotopes. (4) The determination of the neutron absorption cross sections of the stable and active europium isotopes. This investigation was undertaken to provide answers to these problems.

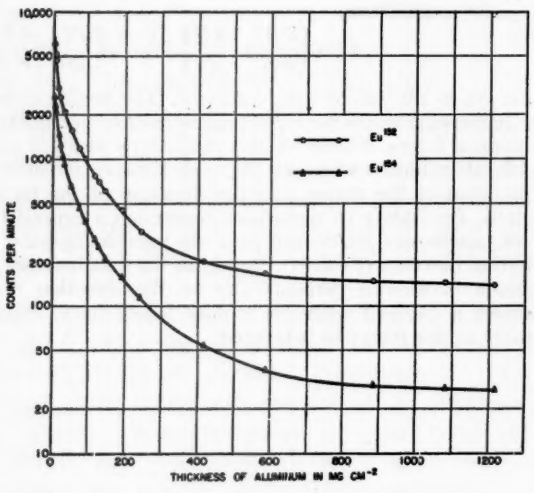

FIG. 1. Aluminum absorption curves taken from mass spectrographically separated samples of 5.3-year Eu^{152} and 5.4-year Eu^{154}.

I. SAMPLE AND IRRADIATIONS

The europium used in this analysis was an Eu_2O_3 sample prepared by Dr. J. K. Marsh of Oxford. It was obtained from Johnson, Matthey and Company who distribute it as Laboratory Number 11,158, Catalog Number F.606. The spectrographic analysis supplied with the material stated that ytterbium was the only rare earth impurity detectable. A mass spectrometric analysis showed additional impurities of the order of one part in 10,000 of samarium, gadolinium, dysprosium, lanthanum, and praseodymium. With the exception of the lanthanum, the effects of which will be later discussed, these impurities did not effect the accuracy of measurement. Two separate neutron irradiations of portions of this material were made. The first of these was a short bombardment in the thermal neutron flux of the Argonne heavy water pile. From this bombardment the mass assignment of the 9.2-hr. activity was obtained. The second sample was subjected to long slow neutron irradiation in a graphite moderated pile. All the other results reported in this paper were obtained from this sample.

II. MASS ASSIGNMENT OF EUROPIUM ACTIVITIES

The mass of radioactive isotopes may be determined by separating the isotopes of an active sample by means of a mass spectrograph and investigating the activity corresponding to each

* National Research Council Fellow.
[1] M. L. Pool and L. L. Quill, Phys. Rev. **53**, 437 (1938).
[2] W. Z. Bothe, Zeits. f. Naturforschung, **1**, 179 (1946).
[3] R. J. Hayden and M. G. Inghram, Phys. Rev. **70**, 89 (1946).
[4] M. G. Inghram and R. J. Hayden, Phys. Rev. **71**, 130 (1947).
[5] J. M. Cook, R. G. Shreffler, and C. M. Fowler, Phys. Rev. **72**, 1209 (1947); **73**, 78 (1948).
[6] Franklin B. Shull, Phys. Rev. **74**, 917 (1948).

mass position. This method was employed in our investigation of the europium activities. The mass spectrograph and techniques employed have been described by Lewis and Hayden.[7,8] Briefly the method is as follows: A portion of the material to be investigated is irradiated with neutrons to obtain the desired activity. The sample is then dissolved in nitric acid and an aliquot placed on the filament source of the mass spectrograph. By operation of the spectrograph the isotopes are separated according to mass and deposited on a photographic plate called the original plate. After removal from the spectrograph this plate is placed face to face with a second photographic plate called the transfer plate. With the passage of time the radioactive decay particles emitted from the active isotopes on the original plate give rise to developable images on both plates. Upon development the original plate shows the active lines and the normal mass spectrum of the irradiated element, while the transfer plate shows only the radioactive lines. By comparison of these two plates and, if necessary, by observation of the radioactive decay at the various mass positions, the masses of the active isotopes produced by the irradiation can be deduced.

In order to determine the mass number of the 9.2-hr. europium, first reported by Pool and Quill,[1] a sample of europium was irradiated with slow neutrons for eight hours in the Argonne heavy water pile.[8] A longer irradiation would have brought up the long lived europium activities in the sample without appreciably increasing the amount of 9.2-hr. activity. A portion of this irradiated material was run through the mass spectrograph and original and transfer plates were obtained. A decay curve from another aliquot of the irradiated sample obtained while the transfer was taking place, showed that at least 95 percent of the activity of the sample was of 9.2-hr. half-life. A comparison of the two plates showed that the activity deposited is of mass number 152. The simple decay curve showed that the activity in the sample and hence the activity deposited was of 9.2-hr. half-life. The ratio of ion intensity in the oxide to the metal position proved that the 9.2-hr. element was europium. Thus we conclude that the 9.2-hr. activity is associated with a europium isotope of mass number 152.

In an attempt to assign the 5–8-year europium activity first reported by Scheichenberger to a specific isotope it was discovered that there were two long lived (n, γ) induced activities in europium, one at mass number 152 and one at mass number 154. This preliminary work has been previously reported by the authors.[4] For the present work the europium sample which had been subjected to long slow neutron bombardment was separated on a photographic plate by the mass spectrograph and two transfer plates were obtained six months apart. The transfer plate obtained shortly after the end of the irradiation showed activity at masses 152, 154, 155, and 156. The later transfer showed lines only at masses 152, 154, and 155. The fact that the 156 line does not appear in the later transfers proves that this activity has a half-life of less than one month. The next paragraph will describe further work on this isotope. The fact that the 152, 154, and 155 lines did not change between the two exposures proves that the half-lives of these isotopes is considerably greater than one month. The Eu^{155} is therefore quite probably the two-year europium first discovered in fission by Winsberg[9] and shown to be a result of Eu^{155} by one of the authors.[8] In this case, however, the activity was produced by a second-order (n, γ) reaction on Eu^{153}. Previous estimates of the half-lives of Eu^{152} and Eu^{154} were Fajans and Voigt's value of 5–8 years[10] and Krisberg, Pool, and Hibdon's value of greater than 20 years.[11] Both of these measurements, however, were made on a mixture of Eu^{152} and Eu^{154} of unknown relative concentration. Values for the half-lives of these isotopes and for Eu^{155} are deduced later in this paper.

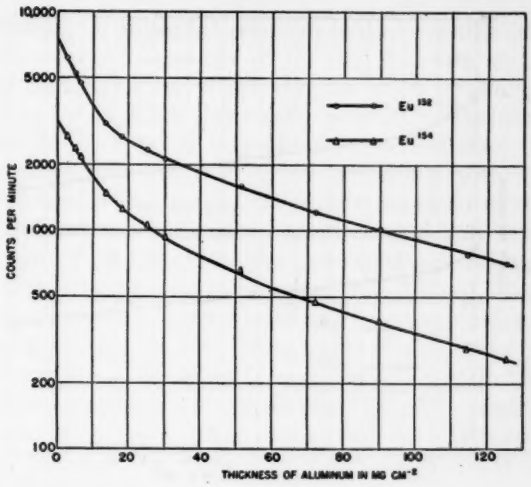

FIG. 2. Aluminum absorption curves taken from mass spectrographically separated samples of 5.3-year Eu^{152} and 5.4-year Eu^{154}. Expanded scale.

Winsberg,[12,13] working with fission europium found an activity of 15.4-day half-life which he

[7] L. G. Lewis and R. J. Hayden, Rev. Sci. Inst. 19, 599 (1948).
[8] Richard J. Hayden, Phys. Rev. 74, 650 (1948).
[9] L. Winsberg, Manhattan Project Report CC-2000 (August, 1944).
[10] K. Fajans and A. F. Voigt, Phys. Rev. 60, 533 (1941).
[11] N. L. Krisberg, M. L. Pool, and C. T. Hibdon, Phys. Rev. 74, 44 (1948).
[12] L. Winsberg, Manhattan Project Report CN-2126 (September, 1944).
[13] L. Winsberg, Manhattan Project Report CC-2310, pp. 231–244 (January, 1945).

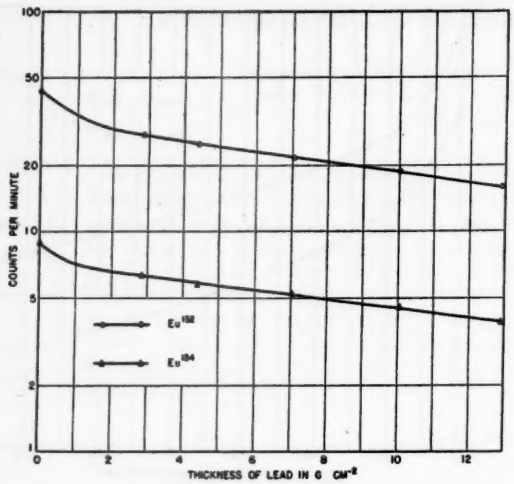

FIG. 3. Lead absorption curves taken from mass spectrographically separated samples of 5.3-year Eu^{152} and 5.4-year Eu^{154}. Zero thickness corresponds to 1000 mg cm^{-2} of aluminum shielding at the counter.

ascribed to Eu^{156}. To verify that the Eu^{156} formed in neutron bombardment of normal europium has a half-life of 15.4 days, a series of transfers were taken from one original plate. The duration of these successive exposures were such as to give a constant number of disintegrations at the mass 156 position if the half-life were 15.4 days. The fact that the intensities at masses 152, 154, and 155 increased while that at 156 remained constant proved that half-life of the europium deposited at mass 156 on the plate is 15.4±4 days. This is, therefore, the same activity reported by Winsberg as a fission product, and proves conclusively that the 15.4-day activity is associated with a europium isotope of mass number 156.

III. CHARACTERISTIC RADIATIONS OF LONG LIVED Eu^{152} AND LONG LIVED Eu^{154}

The characteristic radiations of the long lived activities formed by slow neutron irradiation of europium have been the subject of several investigations.[2,5,6] In all cases the sample studied contained appreciable amounts of both long lived Eu^{152} and long lived Eu^{154}, so that correlation of a particular radiation with a specific isotope was difficult. Shull, in the most extensive of these investigations,[6] used a magnetic two-directional focusing beta-ray spectrometer to obtain the beta-spectrum, the conversion line spectrum, and the photoelectron spectrum. He reported ten conversion lines in the combined activities with the strongest intensities at 73.1, 74.4, 114.0, and 119.6 kev and nine γ-transitions, including γ-rays at energies 0.243, 0.342, 0.959, 1.082, and 1.402 Mev. A Fermi plot of the continuous beta-ray spectrum indicated the presence of two beta-groups with energies of 0.75 and 1.6 Mev. Shull concluded that "The low energy conversion lines observed in 5–8-year europium, which are probably caused by two transitions of approximately equal energy must definitely be associated with Eu^{152}, not Eu^{154}," and "The 0.751-Mev β^--spectrum of the 5–8-year europium must also be associated with Eu^{152}." It is the purpose of this section to describe measurements made of the characteristic radiations of separated isotopes of Eu^{152} and Eu^{154}.

For the study, the isotopes of a portion of the heavily irradiated europium sample were separated with the 60° mass spectrograph in a manner similar to that used for determining the mass assignments. However, instead of the separated isotopes being deposited on a photographic plate, they were deposited on thin aluminum. The locations of the active deposits on this aluminum were then obtained by means of the photographic transfer technique, and the activities completely isolated by mechanically cutting the aluminum between the active deposits. A subsequent photographic transfer served as a check on the accuracy of the cuts. The samples of Eu^{152} and Eu^{154} thus obtained were introduced separately into a vertical lead shield end window counter system of standard design and the absorption curves shown in Figs. 1, 2, and 3 obtained. In the course of this work, three such isotope separations were made; the results were identical in all three cases.

In order to determine the degree of separation, for example, the amount of Eu^{152} activity scattered to the Eu^{154} position, a section of the original aluminum plate two mass units below the Eu^{152} mass position was isolated and counted; the counting rate was less than one percent of the total Eu^{152} activity so that for counting purposes the isolated deposits were "pure."

The aluminum absorption curves shown in Fig. 1, and in expanded scale in Fig. 2 were obtained under identical conditions in an end window counter of 2.6 mg thickness and a calculated geometry of about 16 percent. The lead absorption curves shown in Fig. 3 were obtained under identical conditions in an end window counter of 2.6 mg thickness and a calculated geometry of 5 percent. In order to suppress all betas the counter window was here shielded with 1000 mg/cm^2 of aluminum.

The first conclusion which may be drawn from these curves is that both radiations are complex and that not all the γ-rays are associated with the Eu^{152} as was suggested by Shull.

Secondly, from Fig. 2 it is evident that both Eu^{152} and Eu^{154} have soft components with ranges of less than 30 mg/cm^2 corresponding to energies of less than 165 kev. These are undoubtedly the strong conversion lines reported by Shull. The result, however, is contrary to the first of Shull's conclusions, i.e., that the low energy conversion lines must

definitely be associated with Eu^{152}. Further, in the case of Eu^{154} where, as will be shown later, the fraction of K-capture is less than 5 percent of the β^--disintegrations, there must be more than one soft conversion electron per disintegration. Otherwise it is difficult to account for the high ratio at zero thickness of total counts to extrapolated higher energy counts. Thus if we assume, as seems reasonable from Shull's work, that the 74.4- and 114.0-kev conversion lines are due to Eu^{152}, it appears probable that the 73.1- and 119.6-kev conversion lines are associated with the decay of Eu^{154}.

Referring to Fig. 1, it is evident that the beta-end points are obscured both in Eu^{152} and Eu^{154} by semi-penetrating γ-rays so as to preclude any beta-energy assignments. From intensity considerations however, using Shull's data for the ratio of the 0.751 to 1.6-Mev betas, it is quite reasonable to assign the former to Eu^{152} and the latter to Eu^{154}.

From the lead absorption curves it is apparent that both radiations have at least two high energy γ-rays. The half-thickness of the high energy Eu^{152} γ-rays is 12.8 ± 0.4 g/cm^2 and that of the Eu^{154} 14.4 ± 1.2 g/cm^2. Thus it appears that the highest energy γ-ray observed by Shull is associated with Eu^{154}.

Unfortunately there is not sufficient activity to justify using these separated samples for beta-ray spectroscopic work. However, using the method of cadmium shielded irradiations, or very long slow neutron bombardment, it should be possible to produce Eu^{154} preferentially for which a complete analysis is more feasible.

Muehlhause[14] has studied the 9.2-hr. Eu^{152} and long lived Eu^{152} and Eu^{154} for K-capture by critical absorption methods. He found K-capture in both activities. His results showed that the branching ratio, i.e., K-capture of β^--emission ratio is 10.22 times greater in long lived Eu^{152} and Eu^{154} than that in 9.2-hr. Eu^{152}. We have rechecked this result and agree with his value within two percent. In the calculations to follow we will assume Muehlhause's value.

IV. NUCLIDE COMPOSITION OF THE IRRADIATED EUROPIUM SAMPLE

As will be shown in Section V, a knowledge of the nuclide composition of an irradiated sample before and after irradiation, together with a knowledge of the conditions of the irradiation, is, in general, sufficient to determine neutron absorption cross sections, nuclide half-lives, and nuclide branching ratios for many of the observed nuclides. The procedures required to make a mass spectrometric determination of nuclide composition, i.e., of both element and isotope abundance are the following. A standard solution is made which contains weighed amounts of all the elements in the original sample for which relative nuclide analysis is to be made. Each element in the standard solution must be of different isotopic composition than the corresponding element in the unknown solution. A portion of this standard solution is mixed with a portion of the unknown solution and the mass spectra of all three samples are observed. As long as only relative nuclide analyses are desired, these data alone are usually sufficient for the analysis. No knowledge of the mixing ratio of the standard and unknown solutions is necessary. Later in this section methods of calculation of the nuclide composition from these data will be discussed; first, however, the europium measurements will be described.

The mass spectrometer used for determining the nuclide composition was the same as that used previously by the authors in measuring the normal isotopic abundances of some of the rare earths.[15,16] Briefly, it consisted of a 60°, 6″ radius of curvature single focusing mass spectrometer using a surface ionization type of source. The resolved ion currents corresponding to the various mass positions were amplified with a vibrating reed electrometer and recorded on a Brown Electronic Strip Chart Recorder, so that permanent records of isotope abundances were obtained.

The analysis of the heavily irradiated europium sample gave currents corresponding to isotopes of mass numbers 151, 152, 153, 154, 155, 167, 168, 169, 170, 171, and 172. The ratio 151/153 was constant throughout the run. Since with a surface ionization type of source the ratio of ion currents due to adjacent rare earths is a marked function of time, it was concluded that these two peaks were due solely to europium, which emits predominately as Eu^+. The lines at masses 152 and 154 were found to increase with time relative to the 153. This effect was attributed to the presence of several elements, europium plus gadolinium or samarium or both, at these positions. The intensity of the 155 line compared to any other position was not constand and relative to the 153 it grew with time. This behavior was attributed to a contribution at 155 as a result of LaO^+. No correction could be made for this and so the 155 peak height was circumvented in the calculations. The peaks at 167 and 169 were always very small. They were caused by the slight europium emission of the form EuO^+. The lines at 170, 171, and 172 were proportional throughout the run. Since the europium contributions here would be negligible all these masses should be attributed to GdO^+. The 168 peak fraction-

[14] C. Muehlhause, Manhattan Project Report CP-3750 (January, 1947).

[15] M. G. Inghram, R. J. Hayden, and D. C. Hess, Phys. Rev. 72, 967 (1947).

[16] David C. Hess, Phys. Rev. 74, 773 (1948).

ated with time relative to any other peak. Since its fractionation relative to the 170 was too large to be accounted for by a change in the small $Eu^{152}O^+$ current both Gd^{152} and Sm^{152} occur in the sample. That no normal Sm or Gd impurities occurred in the sample is amply shown by the complete lack of the peaks which should be observed from Sm^{147+} and $Gd^{158}O^+$ if normal samarium and gadolinium were present.

A standard solution of europium, gadolinium, and samarium was made by mixing together weighed amounts of normal Eu_2O_3, Gd_2O_3, and Sm_2O_3 and dissolving this mixture in nitric acid. An aliquot of this solution was mixed with an aliquot of a nitric acid solution of the irradiated europium. This mixture was analyzed by the mass spectrometer. The same lines as before and, in addition to these, the previously non-appearing members of the Sm^+, SmO^+, and GdO^+ spectra were observed. The Gd^+ spectrum was not observed except in very weak intensity just before the end of the run. By observation of the new 151/153 ratio the amount of these isotopes in the original sample relative to the amount added was calculated. The ratio of Gd^{154} present to gadolinium added was obtained from the 170 peak. This was found to fractionate very closely with the normal $Gd^{158}O^+$ peak. Utilizing also the $Sm^{147}O^+$ peak and the method of simultaneous equations later described, it was deduced that the greatest amount of Sm^{154} which could be present in the irradiated sample was less than 5 percent of the amount of Gd^{154} in the irradiated sample. In other words the branching ratio of Eu^{154} is less than 0.05. The relative amounts of Gd^{155} and Gd^{156} present were obtained by comparing the 171 and 172 peaks to the 170 peak in the original run. The situation at mass 152 was clarified by observing the change in the 152 line (europium and samarium) and the 168 line (gadolinium and samarium) with time, and so relating the amounts Eu^{152}, Gd^{152}, and Sm^{152} to the standards Eu^{153} (added), Gd^{158}, and Sm^{147}. This gave two separate measurements of the relative amount of Sm^{152} present. These agreed to within 5 percent.

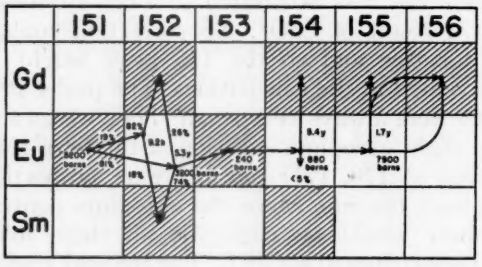

FIG. 4. Summary of reactions induced by slow neutron irradiation of europium, showing cross sections in units of 10^{-24} cm², half-lives, and branching ratios. See also footnote to Table I.

The following mathematical analysis summarizes the methods by which the relative nuclide composition of the unknown sample is obtained. Let i and j be two mass numbers where no lines other than those caused by element k occur in the mixture of standard and unknown samples. Let the superscript (1) refer to the unknown sample, (2) refer to the standard sample, and (3) refer to a mixture of the samples. Let a_{ik} and a_{jk} be the fractional abundances of the nuclides i, k and j, k in the element k. Further define $\alpha_{ijk} \equiv a_{ik}/a_{jk}$. Then it is easily shown that, where $N_{ik}^{(1)}$ is the number of atoms of the nuclide characterized by i, k which have been introduced into the mixture by the unknown sample, and where $N_k^{(2)}$ is the total number of atoms of element k introduced into the mixture from the standard sample, that we have

$$N_{ik}^{(1)} = a_{jk}^{(2)} \alpha_{ijk}^{(1)} \frac{(\alpha_{ijk}^{(3)} - \alpha_{ijk}^{(2)})}{(\alpha_{ijk}^{(1)} - \alpha_{ijk}^{(3)})} N_k^{(2)} \equiv b_{ijk} N_k^{(2)}. \quad (1)$$

The quantity b_{ijk} may here be calculated from the observed quantities α and $a_{jk}^{(2)}$. For element s suppose that different masses q and r play the roles of i and j above. Then a similar expression will be obtained for $N_{qs}^{(1)}$. The ratio of these expressions is given by

$$N_{ik}^{(1)}/N_{qs}^{(1)} = b_{ijk}/b_{qrs}(N_k^{(2)}/N_s^{(2)}). \quad (2)$$

Thus the relative abundances of the nuclides characterized by i, k and q, s in the unknown sample depends only on the mass spectrometrically determinable quantities b_{ijk} and b_{qrs} and on the relative numbers of atoms $N_k^{(2)}/N_s^{(2)}$ of elements k and s present in the standard sample. This ratio is determined by weighing the samples used in making the standard solution, and, from the known atomic weights of the compounds used, computing the relative amounts of k and s present. A knowledge of the mixing ratio of unknown and standard solutions is here unnecessary to determine $N_{ik}^{(1)}/N_{qs}^{(1)}$.

Consider now the analysis of a composite peak at mass m to which n elements give contributions. We assume that the unknown solution and the available standard solution are such that for every element k in the solutions there exist masses $i \neq m$ and $j \neq m$ which satisfy at least one of the following conditions: Case 1: At mass i only the element k occurs in the standard solution and no element occurs in the unknown solution. Case 2: At mass i only the element k occurs in the standard solution and at i and j only k occurs in the unknown solution. These assumptions are not the most general which might be made but they are sufficient for the europium analysis. An example of Case 1 in this analysis is the $Sm^{152}O^+ - Gd^{152}O^+$ conflict at $m = 168$. The "free position" i for samarium is mass 163 where $Sm^{147}O^+$ occurs in the standard spectrum

and nothing is present in the irradiated spectrum. The $Gd^{158}O^+$ peak in the normal spectrum at $i=176$ establishes the free position for gadolinium. In the case of the $Sm^{152+}-Eu^{152+}$ conflict at $m=152$ the samarium satisfies the first condition with $i=147$ while the europium satisfies Case 2 with $i=151$ and $j=153$. For both cases we have for the peak heights P in arbitrary units at various mass positions

$$P_m^{(3)}=\sum_k A_k N_{mk}^{(3)}, \tag{3}$$

$$P_{ik}^{(3)}=A_k N_{ik}^{(3)}, \tag{4}$$

where the quantities A_k are proportionality factors depending only on the element k and the summation in (3) extends over all elements contributing to the peak at mass m. Letting

$$\alpha_{mik}^{(3)}=N_{mk}^{(3)}/N_{ik}^{(3)}$$
$$=(N_{mk}^{(1)}+N_{mk}^{(2)}/N_{ik}^{(1)}+N_{ik}^{(2)}), \tag{5}$$

we have substituting (4) and (5) in (3)

$$P_m^{(3)}=\sum_k \alpha_{mik}^{(3)} P_{ik}^{(3)}. \tag{6}$$

Because of the fractionation effects in the surface ionization source the relative peak heights for the various elements in the mixture change markedly with time. However, though the P's and their ratios are changing, Eq. (6) must be satisfied at any time. Thus if n measurements of the peak heights are made at different times throughout the run, n linear equations of type (6) would result. These may be solved for the n quantities α_{mik}. In case (1) where $N_{ik}=0$ reduction of Eq. (5) gives

$$N_{mk}^{(1)}=a_{ik}^{(2)}[\alpha_{mik}^{(3)}-\alpha_{mik}^{(2)}]N_k^{(2)}. \tag{7}$$

In case (2) a solution of the type described by Eq. (1) is possible at masses i and j. This result substituted into (5) gives

$$N_{mk}^{(1)}=[\alpha_{mik}^{(3)}(b_{ijk}+a_{ik}^{(2)})-a_{mk}^{(2)}]N_k^{(2)}, \tag{8}$$

where b_{ijk} is defined in Eq. (1). From Eqs. (1), (7), and (8) relative nuclide compositions are obtained, as in (2) by taking ratios.

Since the isotopic abundances of samarium, europium, and gadolinium are different in the irradiated and normal sample all the quantities a, α, and b involved are determinate. Thus straightforward application of the methods outlined above leads to a determination of the relative nuclide composition of the irradiated europium sample, complete except for the Eu^{155}.

V. DETERMINATION OF CROSS SECTIONS, HALF-LIVES, AND BRANCHING RATIOS

The values of the nuclide composition make it possible to calculate the thermal neutron absorption cross sections for all the europium isotopes observed, the half-lives of Eu^{152}, Eu^{154}, and Eu^{155}, the ratio of the number of atoms of Eu^{151} going into the long and short lived isomeric states of Eu^{152} upon thermal neutron absorption, and the branching ratio of the europium activities. The decay and absorption scheme which leads to the observed nuclides is shown in Fig. 4.

In order to calculate the unknown quantities it is necessary to set up a mathematical formulation of the changes (indicated in Fig. 4) which are taking place at time t in the pile. The differential equations so obtained must be integrated over the time of irradiation τ and corrected for the decay of certain of the nuclides in the time T since the end of the irradiation. Let $N_1(t)$ be the number of atoms of Eu^{151} present at time t, $N_2(t)$ be the number of Eu^{152} atoms, etc. Primes on the N's will denote gadolinium of similar mass and double primes samarium. σ_1, σ_2, σ_3, σ_4, σ_5, and λ_2, λ_4, λ_5 are the thermal neutron cross sections and the decay constants, respectively, for the corresponding europium isotopes, a is the fraction of Eu^{152} formed which is long lived, b is the fraction of 9.2-hr. Eu^{152} decaying to gadolinium, c is the fraction of long lived Eu^{152} decaying to gadolinium, and Φ is the thermal neutron flux. The equations describing conditions at time t during the irradiation are

$$dN_1/dt=-\sigma_1\Phi N_1, \tag{9}$$

$$dN_2/dt=-(\sigma_2\Phi+\lambda_2)N_2+a\sigma_1\Phi N_1, \tag{10}$$

$$dN_3/dt=-\sigma_3\Phi N_3+\sigma_2\Phi N_2, \tag{11}$$

$$dN_4/dt=-(\sigma_4\Phi+\lambda_4)N_4+\sigma_3\Phi N_3, \tag{12}$$

$$dN_5/dt=-(\sigma_5\Phi+\lambda_5)N_5+\sigma_4\Phi N_4, \tag{13}$$

$$dN_2'/dt=c\lambda_2 N_2+(1-a)b\sigma_1\Phi N_1, \tag{14}$$

$$dN_4'/dt=\lambda_4 N_4, \tag{15}$$

$$dN_6'/dt=(\sigma_5\Phi+\lambda_5)N_5, \tag{16}$$

$$dN_2''/dt=(1-a)(1-b)\sigma_1\Phi N_1+(1-c)\lambda_2 N_2. \tag{17}$$

In writing Eq. (16) the simplifications were made that (1) the half-life of Eu^{156} is zero and (2) the cross section of Gd^{155} is infinite. Since Eu^{156} has been observed in fission to have a half-life of 15.4 days,[12] and since measurements were made at a time several times that long after removal of the sample from the pile, and since the use of Eq. (16) is only to calculate $N_6'(\tau+T)$ the first of these simplifications introduces no errors into the calculation. Because σ_5' is so large (57,000 barns),[17] because the contribution to Gd^{156} via the Gd^{155} route turns out a good deal smaller than the contribution via the Eu^{156} route, and because the amount of Gd^{156} formed by decay after the end of irradiation

[17] R. E. Lapp, J. R. Van Horn, and A. J. Dempster, Phys. Rev. 71, 745 (1947).

is considerably larger than even the *total* Gd^{155} formed (most of which soon goes to Gd^{156}), the errors resulting from the second simplification are also negligible.

To solve the Eqs. (9)–(13) we will derive a general expression for $N_k(\tau+T)$, where τ is the time of irradiation during which the previous equations hold and T is the time after the end of the irradiation during which radioactive decay occurs. During the irradiation the general differential equations are

$$\begin{aligned}&\frac{dN_1}{dt}=-(\sigma_1\Phi+\lambda_1)N_1\\&\frac{dN_j}{dt}=-(\sigma_j\Phi+\lambda_j)N_j+\sigma_{j-1}\Phi N_{j-1}\quad j=2,\,3,\,\cdots k.\end{aligned}\tag{18}$$

Applying the Laplace transform

$$\bar{N}_j(s)=\int_0^\infty e^{-st}N_j(t)dt\tag{19}$$

to these equations we have, where N_{j0} is the initial value of N_j,

$$\begin{aligned}&(s+\sigma_1\Phi+\lambda_1)\bar{N}_1=N_{10}\\&-\sigma_{j-1}\Phi\bar{N}_{j-1}+(s+\sigma_j\Phi+\lambda_j)\bar{N}_j=N_{j0}\quad j=2,\,3,\,\cdots k.\end{aligned}\tag{20}$$

Solving the linear Eqs. (20) for $\bar{N}_k$ we obtain

$$\begin{aligned}&\bar{N}_1=\frac{N_{10}}{s+\sigma_1\Phi+\lambda_1}\\&\bar{N}_k=\frac{N_{k0}}{s+\sigma_k\Phi+\lambda_k}+\sum_{j=1}^{k-1}N_{j0}\Phi^{k-j}\left[\prod_{i=j}^{k-1}\sigma_i\right]\prod_{i=j}^{k}\frac{1}{s+\sigma_i\Phi+\lambda_i}\quad k=2,\,3,\,\cdots.\end{aligned}\tag{21}$$

Expanding the last product in the expression for $\bar{N}_k$ by partial fractions we have, assuming $(\sigma\Phi+\lambda)$ is not exactly the same for any two isotopes,

$$\begin{aligned}&\bar{N}_1=\frac{N_{10}}{s+\sigma_1\Phi+\lambda_1}\\&\bar{N}_k=\frac{N_{k0}}{s+\sigma_k\Phi+\lambda_k}+\sum_{j=1}^{k-1}N_{j0}\Phi^{k-j}\left[\prod_{i=j}^{k-1}\sigma_i\right]\sum_{m=j}^{k}\prod_{\substack{i=j\\i\neq m}}^{k}\frac{1}{\sigma_i\Phi+\lambda_i-\sigma_m\Phi-\lambda_m}\left(\frac{1}{s+\sigma_m\Phi+\lambda_m}\right).\end{aligned}\tag{22}$$

Applying inverse Laplace transforms to these equations we have at time t

$$\begin{aligned}&N_1(t)=N_{10}\exp[-(\sigma_1\Phi+\lambda_1)t]\\&N_k(t)=N_{k0}\exp[-(\sigma_k\Phi+\lambda_k)t]+\sum_{j=1}^{k-1}N_{j0}\Phi^{k-j}\left[\prod_{i=j}^{k-1}\sigma_i\right]\sum_{m=j}^{k}\prod_{\substack{i=j\\i\neq m}}^{k}\frac{\exp[-(\sigma_m\Phi+\lambda_m)t]}{\sigma_i\Phi+\lambda_i-\sigma_m\Phi-\lambda_m},\end{aligned}\tag{23}$$

and at a time T after irradiation time τ

$$\begin{aligned}&N_1(\tau+T)=N_{10}\exp[-(\sigma_1\Phi+\lambda_1)\tau]\exp(-\lambda_1T)\\&N_k(\tau+T)=\exp(-\lambda_kT)\left\{N_{k0}\exp[-(\sigma_k\Phi+\lambda_k)]\tau+\sum_{j=1}^{k-1}N_{j0}\Phi^{k-j}\left[\prod_{i=j}^{k-1}\sigma_i\right]\sum_{m=j}^{k}\prod_{\substack{i=j\\i\neq m}}^{k}\frac{\exp[-(\sigma_m\Phi+\lambda_m)\tau]}{\sigma_i\Phi+\lambda_i-\sigma_m\Phi-\lambda_m}\right\}.\end{aligned}\tag{24}$$

Utilizing the general solutions (24) for the Eqs. (9)–(13) we have five equations, of increasingly complicated algebraic nature for $N_1(\tau+T)$, $N_2(\tau+T)$, $N_3(\tau+T)$, $N_4(\tau+T)$, and $N_5(\tau+T)$. Wherever σ_1 appears in (24) representing contributions to Eu^{152} (long) or beyond a result of the original

Eu^{151} it must be replaced in the solution of the five special equations of $a\sigma_1$. Four more equations are obtained by direct integration of (14)–(17) with the now known N's substituted on the right-hand side. A tenth equation is obtained by integration of the differential equation

$$dN_5'/dt=\lambda_5 N_5, \tag{25}$$

which prevails after the irradiation. Three final equations are obtained from (1) the value (2600) of the cross section for normal europium which was computed from the best estimate of $\Phi\tau$ as obtained from known absorbers irradiated with the europium; (2) the ratio of the beta-counting rates at masses 152 and 154 as described in Section III; and (3) the ratio of the branching ratios in 9.2-hr. Eu^{152} and long lived $Eu^{152}+Eu^{154}$ as given by Muehlhause. It should be pointed out that this definition is such that the x-ray counting efficiencies cancel. The three additional equations are

$$\frac{N_{10}\sigma_1+N_{30}\sigma_3}{N_{10}+N_{30}}=\sigma_T, \tag{26}$$

$$\frac{\lambda_2}{\lambda_4}=\frac{1}{c}\frac{(dN_2/dt)_\beta N_4(\tau+T)}{(dN_4/dt)_\beta N_2(\tau+T)}, \tag{27}$$

$$\frac{[(dN_2/dt)+(dN_4/dt)]_\beta}{(dN_2/dt)_K}\frac{(dN_2^*/dt)_K}{(dN_2^*/dt)_\beta}=\frac{c}{1-c}\frac{1-b}{b}\left[1+\frac{N_{30}\sigma_3\lambda_4}{N_{10}\sigma_1 ac\lambda_2}\right]. \tag{28}$$

In these equations subscripts K and β refer to the K-capture and beta-disintegration rates respectively; the superscript * denotes the 9.2-hr. isomer and terms without superscripts refer to the long lived activities.

The foregoing equations allow calculation of all the quantities of interest without involving counter efficiencies or use of $N_5(\tau+T)$. Considering the unknowns in the equations to be σ_1, σ_2, σ_3, σ_4, σ_5, λ_2, λ_4, λ_5, a, b, c, and $N_5(\tau+T)$ a numerical solution of the equations was carried out.

TABLE I. Pile neutron absorption cross sections, half-lives and branching ratios of the europium isotope.

Mass	151	152	153	154	155
$\sigma\times10^{24}$ cm² (see note (a))	5200	3200	240	880	7900
$T_{\frac{1}{2}}$ in years	—	5.3	—	5.4	1.7
K/β-ratios	—	0.22 (9.2 hr.) 2.8 (5.3 year)	—	<0.05	—

[a] These values of the pile neutron cross sections are all related linearly to the assumed value of 2600×10^{-24} cm² for the absorption cross section of normal europium. Thus an error in this value will enter linearly in all the cross sections. However it will leave the branching ratios and half-lives unchanged.

VI. CONCLUSIONS

The results of this calculation are summarized in Table I and Fig. 4. The values obtained for the constants a, b, and c, respectively, imply that of the Eu^{152} formed 81 percent has a half-life of 5.3 years and 19 percent has a half-life of 9.2 hr. Of the 9.2-hr. Eu^{152} formed 82 percent decays by beta-emission to gadolinium and 18 percent by K-capture to samarium. Of the 5.3-year Eu^{152} formed 26 percent decays by beta-emission and 74 percent by K-capture.

Because of the complexity of the computations necessary to arrive at these values no systematic analysis of error was carried out. However, the following possible sources of error were considered: (1) weighing errors in the preparation of the standard solution; (2) random and systematic errors in the nuclide composition chart as a result of mass spectrometer errors; and (3) different counting efficiencies for the activities deposited at 152 and at 154. We believe the cumulative effect of these errors is such that all the above values are good to 15 percent.

ACKNOWLEDGMENTS

We wish to express our appreciation to Professor A. J. Dempster for his helpful discussions during the course of this problem, to Mr. C. Muehlhause and Mr. Edward der Matiosian for the use of their special krypton counters and critical absorbers, and to Mr. A. Orstrom for his aid in the design and construction of the critical components of the apparatus.

An Interpretation of the Resonance Scattering of Neutrons by Cobalt in Terms of the Breit-Wigner Equation*, †

F. G. P. SEIDL**
Argonne National Laboratory, Chicago, Illinois
(Received November 22, 1948)

The neutron transmission of a Co foil (8.67 mg/cm²) was measured for epi-thermal pile neutrons which were filtered through various thicknesses of B^{10}. The detector consisted of an annular BF_3 counter. As used for the transmission measurements this counter was set up to count only neutrons scattered by a second Co foil (9.55 mg/cm²). The counter sensitivity as a function of neutron energy was studied. Effective total cross sections of 3100 b and over were calculated from observed transmissions. By means of B^{10} absorption, a resonance was located at 108±10 ev and this was associated with resonance scattering of the neutrons. The total resonance cross section σ_0 was estimated to be 12,500 ±1250 b and the magnitude of the resonance scattering, expressed by $\gamma\cdot\sigma_s(E_r)$, was estimated to be ~45,000 ev-b, here γ denotes the total level width and $\sigma_s(E_r)$ denotes the elastic scattering cross section at resonance. The neutron transmission was calculated from the single-level Breit-Wigner equation for the case where scattering is the predominant process. This equation was written in a conventional form involving, besides energy dependence, the parameters Γ, R, and j; where the neutron width is $\Gamma(E/E_r)^{\frac{1}{2}}$; where $4\pi R^2$ represents the scattering from the surface of the initial nucleus, and where j is the spin quantum number of the compound nucleus. Calculated transmissions agreed with experimental transmissions in two instances: (1) $\Gamma=2.0\pm0.1$ ev, $R=+0.93\times10^{-12}$ cm, $j=4$, and (2) $\Gamma=5.0\pm0.5$ ev, $R=+0.97\times10^{-12}$ cm, $j=3$. However, the value $\sigma_0=12{,}500$ ±1250 b is consistent only with $j=4$. A negative R will mean that the minimum of the "dispersion" curve $\sigma_s(E)$ *vs.* E occurs above the resonance energy E_r and such was found to be inconsistent with the data. Finally, mention is made of the similar scattering resonance which takes place in manganese, $E_r\approx300$ ev; here σ_0 lies between 4000 and 5000 b and $\Gamma\sim10$ ev.

I. INTRODUCTION

A STRONG scattering of neutrons by cobalt has been reported,[1] and this effect was attributed to a resonance interaction with neutrons of energies in the neighborhood of $E_r=115\pm5$ ev. The value of E_r has been determined at Columbia University by means of the modulated-cyclotron time-of-flight technique.[2]

Both the measurements of the total cross section of cobalt for neutrons of energies about 115 ev, and the measurements which demonstrate that the interaction is predominantly scattering, now have been extended. The purpose of extending these measurements was to obtain a sufficiently accurate value of the total resonance cross section to allow an estimate of the total angular momentum j of the resonance state of the compound nucleus. Moreover, it was desirable to see how well the data could be fitted to a single-level Breit-Wigner equation by adjusting the parameters Γ and R which denote the neutron width at E_r and the equivalent nuclear radius.

II. APPARATUS[3]

Figure 1 illustrates the experimental arrangement. The incident neutrons consisted of a collimated beam coming from a hole in the concrete shield of the Argonne heavy-water pile. Thermal neutrons were eliminated by passing the beam through a sheet of cadmium which was located near the iron shutter (see *D*, Fig. 1). The incident neutron beam travelled down the axis of the apparatus and through the central tube (I.D. $1\frac{7}{8}$ inches) of an annular BF_3 counter (*AC*, Fig. 1). When nothing was situated at the position *S* (see Fig. 1), the incident beam would pass through without affecting the counter. Neutrons were detected only after being scattered out of the incident beam into the neutron-sensitive region *AC*. The scattering was produced by a substance (e.g. a thin cobalt foil) placed at the center of the annular counter (*S*, Fig. 1). The neutrons most likely to be counted were those most strongly scattered out of the incident beam; consequently, the detector system, as composed of a thin cobalt scattering foil and the annular BF_3 counter plus its paraffin reflector, was especially sensitive to neutrons of resonance energy where the cobalt scattering cross section is very large.

The annular counter was constructed of 2*S* aluminum. Its sensitive region lay between the central tube of O.D. 2 inches and an outer tube of I.D. slightly under 4 inches. This region was enclosed by welding to each end an aluminum disk

* This document is based on work performed under Contract Number W-31-109-eng-38 for the AEC at the Argonne National Laboratory.

† The calculations described in Section VII were carried out at Brookhaven National Laboratory under the auspices of the AEC.

** Now at Brookhaven National Laboratory, Upton, Long Island, New York.

[1] S. P. Harris, A. S. Langsdorf, Jr., and F. G. P. Seidl, Phys. Rev. **72**, 866 (1947).

[2] C. S. Wu, L. J. Rainwater, and W. W. Havens, Jr., Phys. Rev. **71**, 174 (1947).

[3] The design of the apparatus, particularly the annular counter, had been undertaken by A. S. Langsdorf, Jr. Its construction was carried out by S. P. Harris, G. E. Thomas, Jr., H. Schroeder, and the author.

having a central hole of $1\frac{7}{8}$-inch diameter which matched the hole through the inner tube and permitted an open path through the center of the counter. The collecting electrode consisted of a cylindrical grid of 2-mil Kovar wires running longitudinally, and it was supported between the inner and outer tube by an insulated aluminum frame. Within the counter all sharp edges were rounded and the surfaces were polished. The assembly was filled to 15 cm of mercury pressure with pure BF_3 of normal isotopic composition, and the counter was operated in the proportional region.

A two-inch thick paraffin neutron reflector (*P*, Fig. 1) surrounded the counter. The object of the reflector was to cause the response to be more nearly independent of neutron energy, and it also served to increase the sensitivity.

Monitoring of the incident neutron beam was accomplished by a uranium-235 fission counter placed at the region *M* in Fig. 1.

The electronic equipment was of standard design. The mechanical registers for the annular counter and the fission monitor were preceded by a scale-of-512 circuit.

The heavy borax-paraffin shield (*B*, Fig. 1) and the cadmium sheet which surrounded the paraffin reflector reduced the background due to stray neutrons. Another source of background would have been the scattering of neutrons from the incident beam by the air contained in the central tube of the counter; this was eliminated by sealing off each end of the central tube with thin aluminum foils (AL, Fig. 1) and evacuating the region. The last procedure itself reduced the total background by about a factor of ten. Moreover, the shield (*Sh*, Fig. 1) was introduced so that neutrons which were scattered through a small angle by a foil at *f* would not reach the annular counter *AC*.

The alignment of the apparatus was tested frequently during the investigation. This was accomplished by placing at *S* (Fig. 1), a graphite sector ($\sim\frac{1}{4}$ inch thick) which occupied about $\frac{1}{4}$ of the cross-sectional area of the central tube; this sector would only scatter into the annular counter neutrons travelling along that quarter of the central tube which it intercepted. By rotating the sector in quarter-revolution steps about the direction of the incident beam, and by observing the counting rate at each step, asymmetries in the alignment could be detected and suitable adjustments would be made.

III. THE ENERGY DEPENDENCE OF THE COUNTING RATE

The energy dependence of the counting rate was described by a function $\varphi(E)$, E being the incident neutron energy in ev. $\varphi(E)$ included both the energy dependence of the neutron flux and the energy variation of the sensitivity of the annular counter plus the paraffin reflector; it did not contain any energy dependence of the cross section of the scatterer. In order to determine an empirical expression for $\varphi(E)$, the cobalt scattering foil at *S* was replaced by a thin graphite disk, and a study was made of the scattering by graphite as the incident flux was changed in a known way. The manner in which the graphite scattering varied with the flux depended upon the form of $\varphi(E)$. Modifications of the flux were achieved by inserting various thicknesses of B^{10} in the incident beam[4] (*b*, Fig. 1).

Because of the action of the paraffin reflector, the counter response was expected to be more nearly constant than $1/v$, v being the incident neutron velocity. Therefore, the sensitivity of counter and reflector was first conjectured to behave as $1+a/E^{\frac{1}{2}}$, a being determinable by means of a best fit with the experimental data. The epi-thermal pile flux was known to vary as $1/E$; thus $\varphi(E)$, which included both the $1/E$ flux variation and the sensitivity, became

$$\varphi(E)=1/E+a/E^{\frac{1}{2}}. \quad (1)$$

In the energy range from 0.01 ev to 1000 ev, the total B^{10} cross section has been found to be almost entirely due to capture which varies as $1/v$, and it is to be expected that the capture cross section will continue to vary as $1/v$ up to much higher energies.[5] Accordingly, the result of inserting boron in the incident beam was to multiply the intensity by the factor

$$\exp[-(0.294+37.3/E^{\frac{1}{2}})B], \quad (2)$$

where B is the thickness of B^{10} in g/cm² and E is

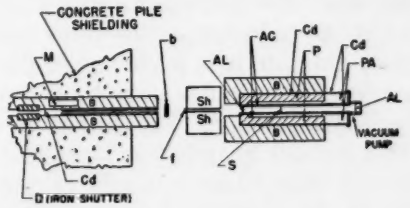

FIG. 1. Experimental arrangement. Legend:

AL—aluminum foil
S—scattering foil
D—approximate position of iron shutter
f—filter foil
Cd—cadmium sheet
b—boron—10 absorber
M—monitor
P—paraffin
AC—annular counter
PA—location of pre-amplifier
B—borax-paraffin neutron shield
Sh—"neutron shield"

[4] The B^{10} was in the form of disks made by compressing a mixture of fine-grain lead powder and crystalline boron powder which had been enriched to about 70 percent B^{10} atoms per mole of boron. The disks contained 71.3 percent by weight of lead and 28.7 percent of boron.

[5] H. H. Goldsmith, H. W. Ibser, and B. T. Feld, Rev. Mod. Phys. **19**, 259 (1947). This paper contains a résumé of cross-section measurements for various elements and includes references to the original works.

TABLE I. Typical transmission data for a thin cobalt foil f.

Detector foil at S mg/cm²	Filter foil at f mg/cm²	B Thickness of B^{10} absorber g/cm²	Position of Cd filter	Counting rate per unit monitor count*
9.55 Co	none	none	in	0.2812
9.55 Co	8.67 Co	none	in	0.2316
9.55 Co	none	none	in	0.2848
9.55 Co	8.67 Co	none	in	0.2304
9.55 Co	8.67 Co	0.148	in	0.1415
9.55 Co	none	0.148	in	0.1728
9.55 Co	8.67 Co	0.148	in	0.1449
9.55 Co	none	0.148	in	0.1735
9.55 Co	8.67 Co	0.148	in	0.1440
9.55 Co	none	0.148	in	0.1741
9.55 Co	none	none	in	0.2837
9.55 Co	8.67 Co	none	in	0.2290
9.55 Co	none	0.635	in	0.0623
9.55 Co	8.67 Co	0.635	in	0.0594
9.55 Co	none	0.635	in	0.0630
9.55 Co	8.67 Co	0.635	in	0.0578
none	8.67 Co	none	in	0.0683
none	none	none	in	0.0698
none	none	0.148	in	0.0486
etc.	etc.	etc.	etc.	etc.

* Corrected for dead time according to $N_0=N/(1-Nt)$, where N_0 is the true counting rate, N the observed rate, and t the dead time of the apparatus; in this case $t=24$ microseconds.

expressed in ev. The quantity 0.294 pertains to the scattering by all the material in the boron disk.[6] The constant 37.3 expressing the absorption was calculated from cross-section values given in reference 5 and made use of the value 18.7 percent as the isotopic abundance of B^{10} in normally occurring boron.[7]

The effect of the cadmium was approximated by assuming the neutron flux to vanish abruptly for all energies below 0.35 ev. Above 0.35 ev the flux was supposed to be unaffected. Later (Section VII), in calculating the neutron transmission of a thin cobalt foil when $B=0$, it was necessary to consider the effect of the cadmium cut-off more carefully.

For pure graphite it is known that the neutron capture cross section is less than 0.1 percent of the scattering cross section. The latter is equal to 4.80 b and remains relatively independent of E up to about 0.1 Mev.[5] Consequently the energy dependence of the graphite scattering cross section was neglected, and the intensity scattered by a thin disk of graphite situated at S (see Fig. 1) was assumed to be proportional to

$$\exp[-0.294B]\int_{0.35\text{ ev}}^{E_M}(1/E+a/E^{\frac{1}{2}})\times\exp[-37.3B/E^{\frac{1}{2}}]dE+F(B), \quad (3)$$

where E_M is an equivalent maximum energy above which $\varphi(E)$ effectively vanishes. $F(B)$ represents a contribution in the incident beam due to the fission neutrons ($\gtrsim$1 Mev).

A good match was obtained with experiment if

$$E_M=(10.0\pm0.5)\times10^4\text{ ev}, \quad a\approx0.78, \quad F(B)\approx0. \quad (4)$$

The exact value of a was not critical, provided it was close to unity. For the above values expression (3) is plotted as a function of B in Fig. 2;†† the indicated points are experimental.

The results given in (4) show that the neutron sensitivity of the annular counter surrounded by a paraffin reflector is relatively independent of energy, especially in the region of 100 ev. Thus the response of the arrangement illustrated in Fig. 1 as a function of neutron energy must be controlled by the energy dependence of the scattering cross section of the scatterer located at S. When this scatterer is a thin cobalt foil which possesses a very large scattering cross section for neutrons of energies about 115 ev, the apparatus will be selectively responsive to the cobalt resonance-scattered neutrons.

$F(B)\approx0$ was further justified by means of certain measurements carried out at the Argonne Laboratory by G. E. Thomas, Jr. The total cross sections σ_t for lead, graphite, and beryllium showed a regular decrease with increasing B, and this effect was attributed to the fast neutrons which constituted a progressively larger fraction of the incident beam as B was increased. By subtracting intensity data obtained with larger B from those obtained with smaller B, the influence of the fast neutrons could be minimized and Thomas's results were brought into accord with other measurements.[8] The relative magnitude of $F(0)$ was estimated to be that required to cause the decrease of σ_t with B as observed by Thomas. Thus,

$$F(0)\Big/\int\varphi(E)dE\approx0.027\pm0.003. \quad (5)$$

IV. TRANSMISSION MEASUREMENTS

The neutron transmission of a thin cobalt foil (8.67 mg/cm²) located at f in Fig. 1 was measured

[6] The measurement of the scattering by a typical boron disk was made during a set of experiments previously described; cf. H. V. Lichtenberger, R. G. Nobles; G. D. Monk, H. Kubitschek, and S. M. Dancoff, Phys. Rev. 72, 164A (1947); also the AEC declassified report AECD-1781.

[7] The isotopic composition of boron varies from sample to sample. Investigations by H. G. Thode, J. Macnamara, F. P. Lossing, and C. B. Collins, J. Am. Chem. Soc. 70, 3008 (1948), show the ratio B^{11}/B^{10} to vary as much as from 4.27 to 4.42. The work of M. G. Inghram, Phys. Rev. 70, 653 (1946), is in agreement, the mean result being that 18.8 percent of normally occurring boron atoms are B^{10}. The value used above, i.e., 18.7 percent, is a sort of average of these measurements.

†† Actually Eq. (3) multiplied by $\exp[-0.294B]$ is plotted in Fig. 2.

[8] For recent measurements of the cross section of lead cf. W. W. Havens, Jr., I. I. Rabi, and L. J. Rainwater, Phys. Rev. 72, 634 (1947).

for various modifications of the incident flux. Again the energy distribution of the flux was varied by filtering the incident beam through various thicknesses of B^{10} (b, Fig. 1), and a cadmium foil was always placed in the beam to remove thermal neutrons. A second thin cobalt foil (9.55 mg/cm²) was situated at S (Fig. 1); thus the detecting system was most sensitive to cobalt resonance-scattered neutrons.

The cobalt foils were prepared electrolytically from chemically pure materials. A spectrochemical analysis revealed that the most abundant impurities were 1 percent Fe, 0.1 percent Cu, 0.05 percent Al, and 0.05 percent Ni by weight, and other impurities appeared to be considerably less. The foils had the undesirable feature of being pitted with many small holes of diameters about 10^{-3} cm; however, it was estimated on the basis of relative areas that the error introduced into the transmission measurements because of the holes was negligible.

A small portion of data which illustrates the sequence of readings is set out in Table I.

Table II shows the results of the transmission measurements. $T(\delta, B)$ denotes the transmission of a foil of thickness δ atoms/cm² for epi-thermal pile neutrons which have penetrated B g/cm² of B^{10}. In this case δ was always the same, i.e. $8.86\times10^{+19}$ atoms/cm² corresponding to 8.67 mg/cm². The counting rates per unit monitor count, corrected both for dead time and for background, are denoted by $I(\delta, B)$ and $I(0, B)$; the latter represents the intensity when the foil f was removed. The errors given for the $T(\delta, B)$ were calculated from the standard deviations of the means of the measurements of $I(\delta, B)$ and $I(0, B)$.

In order to minimize the effects of fast neutrons, the intensities were corrected for the scattering by the boron absorbers, and the resulting values obtained for larger B were subtracted from those obtained with smaller B. In Table III the subtractions are indicated for certain of the possible combinations; the corresponding transmissions and σ_{eff} follow. The errors stated in Table III were again based upon the standard deviations of the means of the $I(\delta, B)$ and $I(0, B)$.

V. THE RESONANCE ENERGY BY MEANS OF BORON ABSORPTION

Upon the passage of a monochromatic neutron beam through one or more of the boron disks of total B^{10} thickness equal to B g/cm², its intensity will be depleted by the factor (2). From the form of (2), the variation of intensity of the monochromatic beam traversing B g/cm² should be exponential with the absorption coefficient $\mu=0.294+37.3/E_r^{\frac{1}{2}}$. Thus, if E_r is unknown, a measurement of the absorption coefficient μ will enable E_r to be calculated.

TABLE II. Neutron transmission of a thin cobalt foil f for epi-thermal pile neutrons which were filtered through various amounts of boron.

Thickness of B^{10} absorber B g/cm²	Characteristic values of the flux distribution E_s* ev	E_m** ev	Transmission of foil f	Effective total cross section σ_{eff}† barns
0.000	—	—	0.759±0.005	3100±75
0.148	33	7.5	0.758±0.006	3100±90
0.157	36	8.4	0.759±0.006	3100±90
0.313	163	33.6	0.781±0.007	2800±100
0.635	835	138.0	0.852±0.018	1800±230

* A neutron of energy E_s has the probability $1/s$ of penetrating the corresponding B^{10} thickness.
** Assuming a $1/E$ epi-thermal incident neutron spectrum, E_m is the most probable energy of a neutron traversing the corresponding B^{10} thickness.
† $\sigma_{eff}=ln\,[1/T(\delta, B)]/\delta$.

With a thin cobalt foil at S, the apparatus of Fig. 1 would detect mostly cobalt resonance-scattered neutrons. Nevertheless, to a lesser degree it also detected neutrons of energies away from resonance; this was because the flux of neutrons about 115 ev constituted only a very small fraction of the total flux incident on the foil S, and in the off-resonance case the greater numbers of incident neutrons tended to counterbalance the much smaller cross section. Consequently, a rigorous procedure was introduced in order to obtain the effects of a strictly monochromatic beam. The manner of isolating the resonance neutrons will now be described.

Clearly a thin cobalt foil, when placed in the incident beam at f, will have little effect except on neutrons of energies for which the cobalt cross section is very large; e.g. in order that a cobalt foil of 8.67 mg/cm² may cause a decrease in intensity of a collimated neutron beam by 1 percent the

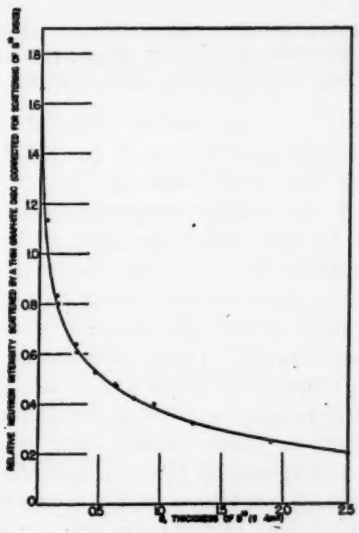

FIG. 2. Curve calculated from $\phi(E)$, the empirical expression for the energy variation of the product of flux and sensitivity. The points are experimental.

TABLE III. Neutron transmission of a thin cobalt foil f for pile neutrons which were filtered through B_1 g/cm² of B^{10} minus those filtered by B_2 g/cm² of B^{10}.

Combination of B^{10} absorbers† B_1-B_2 g/cm²	Characteristics of resulting flux Fb*	Fa**	Intensities $I(0, B_1)-I(0, B_2)$	$I(\delta, B_1)-I(\delta, B_2)$	Transmission $T(\delta)$	Effective total cross section σ_{eff} barns
0.000–0.148	0.84	0.16	0.0819±0.0009	0.06225±0.00110	0.760±0.016	3100±230
0.000–0.635	0.68	0.32	0.1772±0.0009	0.13120±0.0010	0.740±0.007	3400±100
0.148–0.313	0.49	0.51	0.0465±0.0006	0.03335±0.00080	0.717±0.020	3750±300
0.148–0.635	0.36	0.64	0.0953±0.0006	0.06895±0.00080	0.724±0.010	3660±150
0.157–0.313	0.48	0.52	0.0384±0.0006	0.02730±0.0008	0.711±0.024	3850±370
0.313–0.635	0.23	0.77	0.0488±0.0005	0.03560±0.0006	0.730±0.014	3560±220

* Fb denotes the fraction of the resulting flux distribution extending *below* the cobalt resonance at 115±5 ev.
** Fa denotes the fraction of flux *above* 115 ev.
† In all cases the neutrons were first filtered through cadmium.

average cross section per cobalt atom would have to be 114 b. Hence, if intensities measured with a thin cobalt foil (8.67 mg/cm²), located at f in Fig. 1, are subtracted from intensities measured under similar conditions but with the foil removed, there will be a mutual cancellation except for neutrons of energies in the neighborhood of resonance. Such measurements have been carried out for eight values of B with a 9.67-mg/cm² cobalt foil at S. The results are plotted in Fig. 3. Sufficient measurements were taken at each B to enable the standard deviations of the means to be calculated and these are shown in Fig. 3 as vertical lines extending above and below each point. From the slope of the semi-logarithmic plot (Fig. 3) of resonance neutron intensity *vs.* B, it was found that $E_r=108\pm10$ ev.

The scattering of the points beyond the indicated errors is ascribed to uncertainties in the values of B. However, the above value of E_r agrees with the results found at Columbia University[2] and shows that the values of B assigned to the several boron disks should not contain systematic errors greater than about 5 percent.

VI. AN ESTIMATE OF THE TOTAL RESONANCE CROSS SECTION AND THE MAGNITUDE OF THE SCATTERING RESONANCE

The results in this section depend upon an analysis into two components of the total neutron scattering by the cobalt foil at S: (1) a monochromatic or resonance component due only to neutrons of energies close to 115 ev, and (2) a component which behaves like the scattering by graphite, i.e., a potential-scattering part. Since the detecting system is especially sensitive to resonance-scattered neutrons and in light of the large values of σ_{eff} which are given in Table III, it might appear that the off-resonance scattering could be nelected in estimating σ_0 from those data taken with moderate thicknesses of boron; however, such a procedure would introduce into the estimate of σ_0 errors of 20 percent and greater (cf. the difference between $T(\delta)$ and T_0 which is discussed in the following paragraphs). Accordingly, the scattering by cobalt of epi-thermal neutrons was separated into two parts, r and p, which were distinguishable because they varied with the incident energy E in different ways.[9] The energy dependence was studied by changing B, the thickness of B^{10}, through which the incident beam was passed. r was associated with resonance neutrons and was *defined* to be that component of the total scattering which varied as $\exp[-(0.294+37.3/E_r^{\frac{1}{2}})B]$. The component of scattering which remained after subtracting r from the total was designated p.

The ratio r/p was measured in the following manner. $I(C_o, B)$ represented the average counting rate per unit monitor count when a 9.55-mg/cm² cobalt foil was placed at S, and $I(G, B)$ was the similar quantity when the cobalt at S was replaced by a graphite disk of thickness 150 mg/cm². Both these quantities were corrected for background and dead time. The experimental value for r/p was obtained from an analysis of $I(C_o, B)$ as a function of B. By definition

$$I(C_o, B)=r(B)+p(B), \tag{6}$$

and it was assumed that

$$p(B)=kI(G, B), \tag{7}$$

k being a constant. From (6) and (7)

$$r/p=r(0)/p(0)=I(C_o, 0)/kI(G, 0)-1. \tag{8}$$

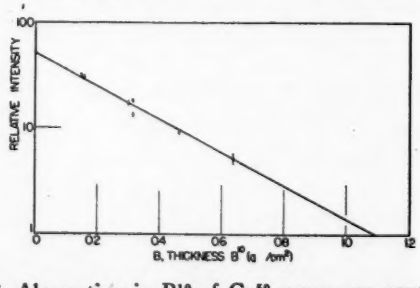

FIG. 3. Absorption in B^{10} of Co^{59} resonance neutrons (obtained by a differential experiment using a thin Co^{59} filter). From slope $E_r=108$ ev±10.

[9] The method of separating the total scattering into r and p was suggested by the somewhat similar treatment of absorption data by S. M. Dancoff; see also reference 6.

Equation (6) was written as

$$r(B)=I(C_o, B)-kI(G, B). \quad (9)$$

The factor k was determined empirically to be such a value that when the measured values of $I(C_o, B)$ and $I(G, B)$ were substituted in (9), the expression for $r(B)$ varied exponentially with B. In Fig. 4 $\ln[r(B)]$ is plotted as a function of B for $k=0.038$. The energy associated with $r(B)$ was found from the slope of the best straight line through the points in Fig. 4, and this energy came out to be 112 ev (see Section V). The agreement with other determinations of the resonance energy E_r lends justification to the above treatment. The errors indicated in Fig. 4 were based upon the standard deviations of the means of $I(C_o, B)$ and $I(G, B)$.

A sufficient number of individual measurements of $I(C_o, B)$ and $I(G, B)$ were made at each B so that the standard deviations of the mean $I(C_o, B)$ were always under 1 percent except for $B>0.5$ g/cm², and the standard deviations of the mean $I(G, B)$ were always less than 0.5 percent. The same values of $I(G, B)$ were used to determine $\varphi(E)$ (cf. Section III).

Using $k=0.038$ it was found that

$$r/p=2.42. \quad (10)$$

The error in k is probably not more than 5 percent.

The quantity p may be imagined to arise from an equivalent energy-independent scattering cross section σ_p which was calculated by the expression

$$k=\sigma_p\tau_{Co}/[1-e^{-(\sigma_s\tau)_G}], \quad (11)$$

which is the ratio of the scattering by $\sigma_p\tau_{Co}$ to that by the graphite disk. The subscripts "Co" and "G" respectively designate quantities pertaining to cobalt and graphite, and τ denotes thickness in atoms/cm². If $k=0.038$, then $\sigma_p=13.7$ b.

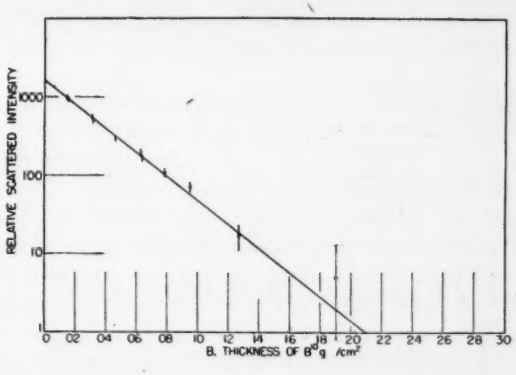

FIG. 4. Absorption in B^{10} of Co^{59} resonance neutrons (obtained by subtracting potential scattering). From slope $E_r=112$ ev.

The manner in which the total resonance cross section σ_0 was estimated is discussed below. The experimental transmission $T(\delta)$ was chosen for those cases where the off-resonance scattering should be least; i.e., for the two rows in Table III corresponding to $B_1-B_2=0.148-0.313$ and $0.157-0.313$. The average for the two cases is $T(\delta)=0.714\pm0.016$.

The data which are plotted in Fig. 3 show that the only resonance which has an appreciable effect upon the counting rate lies about 110 ev (see Section VII). Moreover, it was assumed that once a neutron has been scattered out of the incident beam by a thin cobalt foil at S, its probability of detection is independent of its initial energy E other than any such dependence contained in the function $\varphi(E)$. Then $T(\delta)$ was written

$$T(\delta)=\frac{P+R_0\int_{res}\sigma_s(E)e^{-\sigma_t(E)\cdot\delta}[1-e^{-\sigma_t(E)\cdot\tau}]dE/\sigma_t(E)}{P+R_0\int_{res}\sigma_s(E)[1-e^{-\sigma_t(E)\cdot\tau}]dE/\sigma_t(E)}, \quad (12)$$

where P denotes scattering of off-resonance neutrons and δ and τ respectively denote the thicknesses of foil f and foil S in number of atoms per cm². $\sigma_s(E)$ is the cross section for elastic scattering and $\sigma_t(E)$ is the total cross section. Here the foil f was so thin that its effect was not included in the P in the numerator of (12). Since the data had been corrected for scattering by the boron disks, it was unnecessary to consider terms of the type $\exp[-0.294B]$ and

$$P=\frac{p\int_{0.35\text{ ev}}^{10^5}(\exp[-37.3B_1/E^{\frac{1}{2}}]-\exp[-37.3B_2/E^{\frac{1}{2}}])(1/E+0.78/E^{\frac{1}{2}})dE}{\int_{0.35\text{ ev}}^{10^5}(1/E+0.78/E^{\frac{1}{2}})dE}, \quad (13)$$

$$R=R_0\int_{res}\sigma_s(E)[1-e^{-\sigma_t(E)\cdot\tau}]dE/\sigma_t(E), \quad (14)$$

$$R=r(\exp[-37.3B_1/E_r^{\frac{1}{2}}]-\exp[-37.3B_2/E_r^{\frac{1}{2}}]). \quad (15)$$

TABLE IV. Values of T_0 for several values of σ_0.

σ_0 barns	T_0 Eq. (20)
9,000	0.726
10,000	0.707
11,000	0.689
12,000	0.673
13,000	0.658

Using (10) and Eqs. (12) through (15)

$$T_0=\frac{\int_{\text{res}}\sigma_s(E)e^{-\sigma_t(E)\cdot\delta}[1-e^{-\sigma_t(E)\cdot\tau}]dE/\sigma_t(E)}{\int_{\text{res}}\sigma_s(E)[1-e^{-\sigma_t(E)\cdot\tau}]dE/\sigma_t(E)}=0.666\pm0.019. \quad (16)$$

The error stated for T_0 in (16) was calculated from the relation (17);

$$\Delta T_0/T_0=(1.569[\Delta T(\delta)/T(\delta)]^2+1.050\times10^{-2}(\Delta k/k)^2)^{\frac{1}{2}}. \quad (17)$$

It is important to note that the error in T_0 does not depend very strongly upon the error in k and depends even less on the error in B which has not been included in (17). However, the effect of the errors in values of B may be included as an addition to Δk.

By neglecting the potential scattering and the interference between potential and resonance scattering $\sigma_t(E)$ may be approximated in the resonance region by

$$\sigma_t(E)=\sigma_0/(1+\zeta^2), \quad (18)$$

where

$$\zeta=2(E-E_r)/\gamma, \quad (19)$$

E being the incident neutron energy, and γ the total level width. Thus

$$T_0=\frac{\int_{-\infty}^{+\infty}e^{-\sigma_0\delta/(1+\zeta^2)}[1-e^{-\sigma_0\tau/(1+\zeta^2)}]d\zeta}{\int_{-\infty}^{+\infty}[1-e^{-\sigma_0\tau/(1+\zeta^2)}]d\zeta}. \quad (20)$$

The integrals may now be evaluated in terms of Bessel functions of imaginary arguments;[10] e.g.

$$\int_{-\infty}^{+\infty}[1-e^{-\sigma_0\tau/(1+\zeta^2)}]d\zeta=\pi\sigma_0\tau e^{-\sigma_0\tau/2}[J_0(i\sigma_0\tau/2)-iJ_1(i\sigma_0\tau/2)]. \quad (21)$$

The values of T_0 corresponding to several values of σ_0 are set out in Table IV for the case of $\delta=0.886\times10^{20}$ atoms/cm^2 and $\tau=0.976\times10^{20}$ atoms/cm^2.

[10] This was pointed out to the author by A. S. Langsdorf, Jr.; see also M. Born, *Optik* (Verlag. Julius Springer, Berlin, 1933), Eqs. (7) and (11), p. 489.

TABLE V. Maximum possible resonance cross sections *vs.* E_r.

Max. σ_0 if $j=3$	E_r ev	Max. σ_0 if $j=4$
12,700 b	90	16,300 b
11,400	100	14,600
9900	115	12,700
9500	120	12,200
8100	140	10,500

Interpolating between the values for $\sigma_0=12{,}000$ b and 13,000 b, we find that (16) corresponds to

$$\sigma_0=12{,}500\pm1250 \text{ b}. \quad (22)$$

Calculations similar to the one above also have been made for $B_1-B_2=0.000-0.148$ and $0.148-0.635$ g/cm^2. In these cases $\sigma_0=14{,}800\pm2000$ b and $11{,}700\pm1000$ b, respectively.

According to the Breit-Wigner equation (see Section VII) the total cross section at resonance cannot exceed $4\pi G\lambda_r^2$ where $2\pi\lambda_r$ is the resonance wave length of the incident neutron in the center of mass reference frame. G is a statistical factor equal to $(2j+1)/(2i+1)(2s+1)$ where j is the total angular momentum quantum number of the compound nucleus, and i and s are respectively the spin quantum numbers of the initial nucleus[11] and incident particle. In order that $\sigma_t(E_r)$ approach $4\pi G\lambda_r^2$, it is necessary for elastic scattering to be the predominate resonance process; i.e. $\sigma_t(E_r)\approx\sigma_s(E_r)$. Values of max. $\sigma_0=4\pi G\lambda_r^2$ were calculated for several values of E_r and for the two possible spins of the compound nucleus; i.e. $j=3$ and $j=4$. These results are given in Table V. It is of considerable interest to note that *within the statistical error the estimated resonance cross section σ_0 is consistent only with $j=4$.*

The magnitude of the cobalt scattering resonance was expressed as $\gamma\cdot\sigma_s(E_r)$ where γ represents the total level width. An estimate of $\gamma\cdot\sigma_s(E_r)$ was obtained from a relation between this quantity and r/p. The relation was derived by assuming that the total scattering by a thin cobalt foil could be *completely* described by two components: (1) a component r due solely to neutrons of energies very close to E_r, and (2) a component p which arises entirely from an energy-independent scattering cross section σ_p. As will be pointed out later the total scattering can only approximately be described in this way. Expressions for r and p were taken to be

$$r=S_0\int_{\text{res}}\varphi(E)\sigma_s(E)[1-e^{-\sigma_t(E)\cdot\tau}]dE/\sigma_t(E), \quad (23)$$

$$p=S_0\sigma_p\tau\int_{0.35\text{ ev}}^{10^5}\varphi(E)dE, \quad (24)$$

[11] For Co^{59} $i=7/2$, cf. J. Mattauch, *Nuclear Physics Tables* (Interscience Publishers, Inc., New York, 1946), p. 112. Co^{59} constitutes 100 percent of normally occurring cobalt.

where S_0 is a constant depending upon the absolute values of the incident neutron flux and detector sensitivity, and $\varphi(E)$ is given by (1) and (4). But it was assumed that r was due only to resonance neutrons; hence,

$$r \approx [S_0 \varphi(E_r) \gamma \sigma_s(E_r)/2\sigma_0] \times \int_{-\infty}^{+\infty} [1 - e^{-\sigma_0 \tau/(1+\zeta^2)}] d\zeta. \quad (25)$$

From (24) and (25) it was possible to show that

$$\gamma \cdot \sigma_s(E_r) \approx \frac{1037 \sigma_p}{f(\sigma_0 \tau)} \cdot \frac{r}{p}. \quad (26)$$

The constant 1037 came from an evaluation of

$$[2/\pi \varphi(E_r)] \int_{0.35 \text{ ev}}^{10^5} \varphi(E) dE$$

using (1) and (4) and $E_r = 115$ ev. Moreover, the definition of $f(\sigma_0 \tau)$ is

$$f(\sigma_0 \tau) = e^{-\sigma_0 \tau/2} [J_0(i\sigma_0 \tau/2) - iJ_1(i\sigma_0 \tau/2)]. \quad (27)$$

The function (27) is not very sensitive to σ_0 since, if σ_0 is varied from 8000 b to 13,000 b, $f(\sigma_0 \tau)$ will only change from 0.836 to 0.761. According to (10) and (22) and using $\sigma_p = 13.7$ b,

$$\gamma \cdot \sigma_s(E_r) \approx 44{,}700 \text{ ev-b}, \quad (28)$$

or

$$\gamma \sim 3.5 \text{ ev}. \quad (29)$$

In general because of the thermal motion of the target nuclei, the observed width will be increased over the intrinsic γ (i.e. Doppler broadening). The magnitude of this effect has been estimated in terms of the quantity

$$\Delta = E - \tfrac{1}{2} M_n v^2 \approx M_n v u_v, \quad (30)$$

where M_n and v denote the neutron mass and velocity, and u_v represents the component parallel to v of the velocity of the cobalt nucleus. The magnitude of u_v was obtained from

$$\tfrac{1}{2} M_A u_v^2 \approx \epsilon,$$

where, excluding the zero-point energy, ϵ denotes the average energy per degree of freedom in a cobalt crystal and M_A is the mass of the cobalt atom. ϵ was evaluated from the Debye theory of specific heats.[12]

[12] See J. E. Mayer and M. G. Mayer, *Statistical Mechanics* (John Wiley & Sons, New York, 1941), p. 251. The Debye temperature of cobalt was taken to be $\Theta_D = 385°$K, cf. Landolt-Börnstein, *Physikalische Chemie Tabellen* (Verlag. Julius Springer, Berlin, 1931), Eg II b, p. 1233.

Thus,

$$\Delta \approx 0.38 \text{ ev}. \quad (31)$$

Since, the approximate Doppler width Δ is considerably less than the value (29), the Doppler effect was neglected.

Another measurement of r/p was undertaken by a different method; i.e. the scattering of neutrons by cobalt and graphite were compared when the incident beam was and was not passed through a cadmium foil. The cobalt and graphite were located alternatively at S (see Fig. 1) and their respective thicknesses were 9.55 mg/cm² and 150 mg/cm². It was possible to estimate r/p from the relative scattering of the two substances and the result is:

$$r/p = 6.2. \quad (32)$$

Equation (32) contains a correction for the small amount by which the cadmium foil depleted the epi-thermal beam and also for the fact that the cadmium cut-off energy was not sharp. The above p corresponds to a scattering cross section $\sigma_p = 6.6 \pm 0.1$ b. According to (26), (22), and (32)

$$\gamma \cdot \sigma_s(E_r) \approx 55{,}000 \text{ ev-b}. \quad (33)$$

Neither (28) nor (33) are exact. In this regard it may be mentioned that, if the cobalt resonance scattering arises from a single level, then according to (28) and (33) the width of this level must be exceptionally large. However, when γ is so large, Eqs. (24) and (25) together cannot be an exact description of the total scattering; because either r is defined as the monochromatic component for the resonance energy E_r and some of the energy-dependent scattering will overlap into p, or p is strictly associated with an energy-independent scattering cross section and r will require a more complicated expression which involves some dependence upon B. The estimate given by (28) was obtained by rigorously defining r as a monochromatic component; while that of (33) was based upon the strict association of p with an energy-independent cross section σ_p which behaved like the graphite scattering cross section. Note that in the former case $\sigma_p = 13.7$ b and in the latter $\sigma_p = 6.6$ b.

In the case of the resonance interaction between neutrons and cobalt, the value of σ_0 given in (22) placed the spin quantum number of the compound nucleus at $j = 4$ within the statistical errors. However, difficulties have appeared in the attempt to calculate $\gamma \cdot \sigma_s(E_r)$, cf. the difference between (28) and (33), and these depreciate the method used to obtain σ_0. Consequently, the next attempt was to relate the experimentally observed transmissions $T(\delta)$ and the single-level Breit-Wigner equation more correctly than was done by (12) and (22). A description of the more exact treatment will be found in Section VII.

VII. FITTING OF THE BREIT-WIGNER EQUATION TO THE EXPERIMENTAL TRANSMISSIONS BY NUMERICAL INTEGRATIONS

According to the Breit-Wigner theory,[13] the energy dependence of the cross section exhibits certain peaks or resonances which are associated with energy levels of the compound nucleus. For light nuclei and small incident kinetic energies E the resonances are found to be spaced relatively far apart. In this case and when the orbital angular momentum of the incident particle relative to the initial nucleus is zero, the cross sections for the various possible processes which may occur after the absorption of a neutron of energy in the neighborhood of a resonance are expressed by the "single-level" equations given below. The equations are simplest if the incident particles are neutrons which do not have to overcome an electrostatic repulsion before entering a nucleus.

$$\sigma_s(E)=\pi G\lambda\!\!\!^{-}_r\Gamma\frac{\lambda\!\!\!^{-}_r\Gamma+4R\cdot(E-E_r)}{(E-E_r)^2+\gamma^2/4}+4\pi R^2; \quad (34)$$

$$\sigma_a(E)=\pi G\lambda\!\!\!^{-}_r\Gamma\frac{\lambda\!\!\!^{-}\gamma_a}{(E-E_r)^2+\gamma^2/4}. \quad (35)$$

$\sigma_s(E)$ denotes the neutron elastic scattering cross section. $\sigma_a(E)$ includes the neutron inelastic scattering as well as the cross section for neutron absorption with the emission of a different kind of particle or of a γ-ray. γ is the total width and very closely equals the width of the resonance peak at half maximum. Moreover,

$$\gamma=\Gamma(E/E_r)^{\frac{1}{2}}+\gamma_a, \quad (36)$$

where $\Gamma(E/E_r)^{\frac{1}{2}}$ is the neutron width, and γ_a is the partial width corresponding to processes other than elastic scattering. $2\pi\lambda\!\!\!^{-}$ denotes the wave length of the incident neutron; at resonance $\lambda\!\!\!^{-}=\lambda\!\!\!^{-}_r$. G is a statistical factor equal to $(2j+1)/(2i+1)(2s+1)$. The probability that the incident neutron may be reflected at the surface of the nucleus without ever combining with the latter is included in the elastic scattering by the quantity $4\pi R^2$. The contributions from more than one resonance are not contained in expressions (34) and (35).

Provided $\lambda\!\!\!^{-}_r$ and $\lambda\!\!\!^{-}$ are always expressed in the center-of-mass frame, the forms of Eqs. (34) and (35) will be the same regardless of whether the energies and widths are written in terms of the center-of-mass frame or the laboratory frame.[14] In what follows, the energies and widths shall be expressed in the laboratory frame and the $\lambda\!\!\!^{-}$ shall be expressed in the center-of-mass frame; i.e. E will be the incident kinetic energy of the neutron relative to the cobalt nucleus.

According to (28) and (33) $\gamma\gtrsim 3$ ev; however, it is doubtful that γ_a can be much larger than ~ 0.1 ev. Furthermore, the estimate (22) of the total resonance cross section σ_0 shows it to be the order of $4\pi G\lambda\!\!\!^{-}_r{}^2$, and σ_0 can approach this value only if elastic scattering is the predominant resonance process. Therefore, it was written that

$$\gamma\approx\Gamma(E/E_r)^{\frac{1}{2}}\gg\gamma_a. \quad (37)$$

The transmission $T(\delta, B)$ of the thin cobalt foil f of thickness δ atoms/cm^2 for epi-thermal neutrons which were filtered through B g/cm^2 of B^{10} was written as

$$T(\delta,B)=\frac{\int_E c(E)\varphi(E)\exp[-37.3B/E^{\frac{1}{2}}]dE e^{-\sigma_t(E)\cdot\delta}\sigma_s(E)[1-e^{-\sigma_t(E)\cdot\tau}]/\sigma_t(E)}{\int_E c(E)\varphi(E)\exp[-37.3B/E^{\frac{1}{2}}]dE\sigma_s(E)[1-e^{-\sigma_t(E)\cdot\tau}]/\sigma_t(E)}, \quad (38)$$

where

$$\varphi(E)=1/E+a/E^{\frac{1}{2}}, \quad (39)$$

and

$$c(E)=\exp\{-50/[1+300(E-0.176)^2]\}. \quad (40)$$

In setting up (38) it was assumed that, once a neutron was scattered, its probability of being counted was independent of its incident energy E other than any such dependence included in the function $\varphi(E)$.

The factor $c(E)$ represented the effect of the cadmium foil which had been introduced in the incident beam to eliminate the thermal neutrons. The constants in (40) were taken from E_r and γ of the cadmium resonance.[5] However, for all cases except $B=0$ it was shown to be sufficient to set $c(E)=1$ and to use $E_m=5$ ev as the inferior limit of integration.

The object in calculating $T(\delta, B)$ was to find one or more sets of values for Γ, R, G which would

[13] G. Breit and E. P. Wigner, Phys. Rev. **49**, 519 (1936); H. Bethe and G. Placzek, Phys. Rev. **51**, 450 (1937); P. L. Kapur and R. Peierls, Proc. Roy. Soc. **A166**, 277 (1938); H. Feshbach, D. C. Peaslee and V. F. Weisskopf, Phys. Rev. **71**, 145 (1947); E. P. Wigner and L. Eisenbud, Phys. Rev. **72**, 29 (1947); etc.

[14] If quantities in the $c-m$ frame are primed and quantities in the laboratory frame remain unmarked, then

$$E'=M_AE/(M_A+M_n) \quad \text{and} \quad \gamma'=M_A\gamma/(M_A+M_n),$$

M_A and M_n being respectively the masses of initial nucleus and incident neutron. For the neutron-cobalt interaction $(M_A+M_n)/M_A=1.017$.

TABLE VI. Illustrates the agreement between the experimental transmissions and those calculated from the Breit-Wigner equation using the indicated values of Γ, R and j.

Γ ev	R cm $\times 10^{-12}$	j†	B g/cm²	$T(\delta, B)$ Calculated	Experimental
2.0±0.1	+0.93	4	0.000*	0.757	0.759±0.005
			0.148	0.757	0.758±0.006
			0.157	0.758	0.759±0.006
			0.313	0.786	0.781±0.007
			0.635	0.858	0.852±0.018
1.8±0.1	−0.56	3	0.000*	0.778	0.759±0.005
			0.148	0.757	0.758±0.006
			0.635	0.820	0.852±0.018
5.0±0.5	+0.97	3	0.000*	0.753	0.759±0.005
			0.148	0.754	0.758±0.006
			0.313	0.774	0.781±0.007
			0.635	0.831	0.852±0.018

* Referring to Eq. (39), it was found to be more correct to use $a=1.00$ in these cases than $a=0.78$ as reported in Section III; this difference arose from expression (40) which describes the effect of the Cd more accurately and which was not used in the analysis described in Section III.
† j is the spin quantum number of the compound nucleus.

cause the calculated $T(\delta, B)$ as a function of B to agree with the experimental values given in Table II. Only two values of G are possible, i.e. $\frac{9}{16}$ or $\frac{7}{16}$ corresponding to the cases where the incident neutron spin is aligned parallel or anti-parallel to that of the cobalt nucleus. Furthermore, an energy-independent component of the cobalt cross section equal to 6.7±0.3 b was found from the experiments by Wu, Rainwater, and Havens[2] over the energy range from ~5 ev down to 0.1 ev. This last fact was used to limit the arbitrariness of Γ and R by assuming that $\sigma_s(E)=6.7$ b for, say, $E\sim 4$ ev. The assumption that the value 6.7 b constituted the scattering cross section for $E\sim 4$ ev was checked approximately by means of the apparatus shown in Fig. 1.[15]

In Eq. (38) it was desired to set $\sigma_i(E)=\sigma_s(E)$ for E in the neighborhood of E_r and to express $\sigma_s(E)$ by the single-level Eq. (34). However, at Columbia University recent measurements on the neutron transmission of cobalt as a function of E indicated the existence of one or more higher resonances in the neighborhood of 4000 ev.[16] Consequently, it was necessary to consider what effect this would have on the scattered intensity as measured by the

[15] A comparison was made of the scattering of 4.8-ev neutrons by a cobalt foil situated at S (Fig. 1) to that by a graphite disk situated in place of the cobalt. Neutrons of energies near 4.8 ev were isolated by means of their differential absorption in a 1½-mil gold foil which was moved in and out of the incident beam at f, cf. isolation of cobalt resonance neutrons, Section V. The ratio of cobalt scattering to graphite scattering was denoted by k and $k=[\sigma_s(1-\exp(-\sigma_i\tau))/\sigma_i]_{Co}/[1-\exp(-\sigma_s\tau)]_G$. The best measurement on the apparatus of Fig. 1 gave $k=0.92\pm0.10$; while, as calculated from values obtained by the Columbia group and using $\sigma_s=4.80$ b for graphite, $k=0.94\pm0.05$. The isolation of 4.8-ev neutrons by differential absorption in gold is, of course, only possible because of the strong gold resonance for 4.8-ev neuterons.

[16] The author is grateful to W. W. Havens, Jr., and L. J. Rainwater for the use of their data prior to publication.

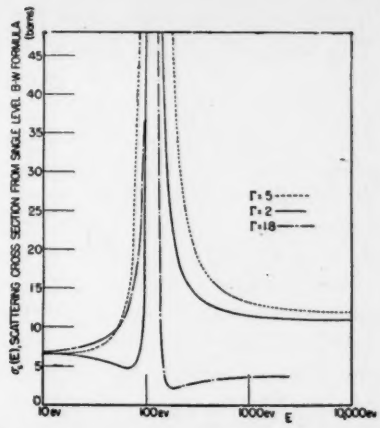

FIG. 5. Curves showing the variation with incident neutron energy of the scattering cross section calculated from the single-level Breit-Wigner formula for three pairs of values for Γ and R. The curve for $\Gamma=1.8$ ev is also for $R<0$. In the cases of $\Gamma=2$ ev and $\Gamma=5$ ev, $R>0$.

apparatus of Fig. 1. Hence, an attempt was made to fit the intensity data of Fig. 3, which had been corrected for scattering by the boron disks, to the expression $A_1\exp[-3.55B]+A_2\exp[-0.585B]$. The absorption coefficients 3.55 and 0.585 were computed respectively for resonance energies of 115 ev and 4000 ev. The ratio A_2/A_1 was found to be -0.004 ± 0.025, where 0.025 is the standard deviation of the mean. It was then estimated from the standard deviation that the errors in the calculated transmissions which arose because of neglecting the higher resonances should be less than 1 percent. Thus, it was possible to use the one-level Eq. (34) for $\sigma_s(E)$ and the calculations were carried out accordingly.

The first calculations of $T(\delta, B)$ were made for the case of $B=0.148$ g/cm² of B^{10}. After obtaining three sets of values for Γ and R which brought about a match between the calculated and experimental $T(\delta, 0.148)$, the corresponding $T(\delta, B)$ were

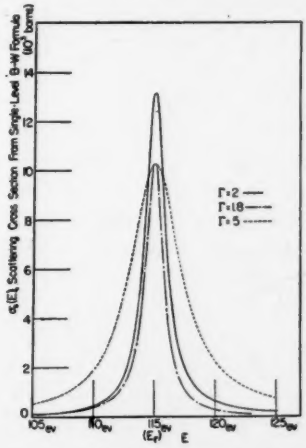

FIG. 6. The above curves are continuations of those in Fig. 5 up to the peak values of $\sigma_s(E_r)$ at $E=E_r=115$ ev.

calculated for the other B. The results are given in Table VI. The "errors" quoted for the Γ are such that, if a particular Γ were to be varied by an amount outside these "errors" and if the corresponding R were adjusted so as to maintain the relation $\sigma_s(4\text{ ev})=6.7$ b, then the resulting calculated $T(\delta, B)$ would be changed by more than the error of the experimental $T(\delta, B)$. All the numerical integrations of (38) were carefully checked and these should not contain errors greater than 1 percent. However, the effects of any higher resonances were neglected and, as has been mentioned, they could introduce into the calculated values of $T(\delta, B)$ an error of 1 percent.

Equation (34) is plotted in Figs. 5 and 6 for the three sets of values Γ, R, and j set out in Table VI.

VIII. CONCLUSION

According to Table VI the variation of $T(\delta, B)$ with B may be accounted for by a single scattering resonance in cobalt at $E_r=115$ ev. The observed transmissions are fitted best if $\Gamma=2.0\pm0.1$ ev, $R=+0.93\times10^{-12}$ cm, and $j=4$, where $\Gamma(E/E_r)^{\frac{1}{2}}$ is the neutron width, R is an equivalent nuclear radius and j is the total angular momentum quantum number of the compound nucleus. These numbers are in agreement with the value of the total resonance cross section σ_0 which was obtained from a less exact treatment; i.e. $\sigma_0=12{,}500\pm1250$ b. Nevertheless, the set $\Gamma=5.0\pm0.5$ ev, $R=+0.97\times10^{-12}$ cm, and $j=3$ cannot be entirely excluded in light of possible errors. As concerns Table VI, this last fit would be better if Γ were increased slightly, e.g. $\Gamma=5.5$ or 6 ev. The case of $\Gamma=2$ and $j=4$ corresponds to $\gamma\cdot\sigma_s(E_r)\approx26{,}000$ ev-b, and that of $\Gamma=5$ and $j=3$ to $\gamma\cdot\sigma_s(E_r)\approx50{,}000$ ev-b. The last is closer to the values of $\gamma\cdot\sigma_s(E_r)$ given by (28) and (33); but these estimates are not accurate enough to decide which value of Γ and therefore which j is more appropriate. In short the present analysis can only be taken as a strong indication that for the 115-ev resonance state in cobalt, the spin quantum number of the compound nucleus is $j=4$.

The values for negative R (i.e. $\Gamma=1.8$ ev, $R=-0.56\times10^{-12}$ cm, $j=3$) are unlikely because as is evident from Table VI the calculated $T(\delta, B)$ do not vary with B in the same manner as the experimental $T(\delta, B)$. Besides the magnitude of $\gamma\cdot\sigma_s(E_r)$ derived from this set is 18,000 ev-b which is much less than (28) and (33). Another possibility of negative R exists for $\Gamma<1$ ev and $j=4$; however, this case has not been computed for two reasons: (1) the Γ would be comparable in size to the Doppler width, see Eq. (31), and this would introduce considerable difficulties into the calculations; (2) such a small Γ is incompatible beside the large value of $\gamma\cdot\sigma_s(E_r)$, see Eqs. (28) and (33).

IX. APPENDED NOTE ON THE RESONANCE SCATTERING BY MANGANESE

Corresponding to the resonance scattering by cobalt, a similar phenomenon has been observed in manganese for neutrons of about 300 ev.[1,17–19] Since the first publications, additional data on the manganese resonance have been obtained at the Argonne National Laboratory by S. P. Harris and the author. These data were taken before the completion of the apparatus shown in Fig. 1, and at that time the neutrons were detected by means of the resonance activation of thin ($\sim$11 mg/cm^2) manganese foils. The transmission $T(\delta, B)$ of thin layers of $MnSO_4$ dissolved in D_2O was investigated as a function of B, the thickness of B^{10} in the incident beam. The measurements were made on manganese layers ranging in thickness from $\delta=0.2\times10^{+20}$ atoms per cm^2 to $1.5\times10^{+20}$ atoms per cm^2. An analysis of these transmission data indicated that for manganese σ_0 lies between 4000 b and 5000 b and that $\Gamma\sim10$ ev. Again as for cobalt, the peak cross section of this resonance appears to approach the theoretical upper limit of $4\pi G\lambda_r^2$.

X. ACKNOWLEDGMENT

The author wishes to thank Dr. A. S. Langsdorf, Jr., of Argonne National Laboratory for his stimulating discussions and to reiterate that the apparatus in Fig. 1 was largely designed by him. The author also expresses his gratitude to Dr. Hartland S. Snyder of Brookhaven National Laboratory for several valuable suggestions regarding the calculations of $T(\delta, B)$, and to Miss Jean H. Snover who was responsible for carrying out the numerical integrations.

[17] M. Goldhaber and A. A. Yalow, Phys. Rev. **69**, 47A (1946); N. H. Barbre and M. Goldhaber, Phys. Rev. **71**, 141A (1947).

[18] F. G. P. Seidl, S. P. Harris, and A. S. Langsdorf, Jr., Phys. Rev. **72**, 168A (1947).

[19] For the determination of E_r for manganese, see L. J. Rainwater, W. W. Havens, Jr., C. S. Wu, and J. R. Dunning, Phys. Rev. **71**, 65 (1947).

Relativistic Terms in the Interaction between Nucleons in Pseudoscalar and Vector Meson Theory

L. VAN HOVE
*Institute for Theoretical Physics, Copenhagen, Denmark**

(Received January 3, 1949)

The second-order interaction between nucleons in the pseudoscalar and vector meson theory is calculated, all terms being taken into account. It is shown that in both cases the exact expression for the interaction caused by virtual exchange of mesons involves contact interaction terms which cancel the well-known direct coupling terms of the Hamiltonian. The remaining interaction is essentially different from the expressions given by usual derivations. Its singularity for small separations r of the nucleons, usually obtained to be in r^{-3} for pseudoscalar and vector fields, is reduced for the former and not for the latter, so that no singularity can be removed by a mixture of the mentioned fields. For pseudoscalar mesons, all interaction terms are proportional to some power of the nucleon velocity, whereas for vector mesons there is a non-vanishing static approximation in r^{-1}. It seems impossible from the present treatment to draw precise and reliable conclusions about the deuteron.

I. INTRODUCTION

THE forces between nucleons resulting from meson fields are usually calculated either by neglecting all velocity-dependent variables of the nuclear particles (static interaction),[1] or by neglecting only recoil energies of the nucleons in emission and absorption of virtual mesons.[2] In the latter case the perturbation method is used and the first non-vanishing part of the interaction is of second order in the coupling constants. Our purpose is the investigation of the second-order interaction, all terms being taken into account. We treat here the cases of pseudoscalar and vector meson fields; for both types of mesons the consideration of all terms makes it possible to separate from the interaction caused by virtual exchange of mesons expressions proportional to $\delta(\mathbf{r})$, where $\mathbf{r}$ is the relative position vector of two nucleons. Such expressions are usually called contact interaction terms. When the Lagrange function describing interacting nucleon and meson fields contains only coupling terms between nucleons and mesons and no term of direct coupling between nucleons, it is a well-known fact that the derived Hamiltonian contains direct coupling terms. These give rise to contact interactions between nucleons, and, as we shall see, cancel exactly the contact interaction terms mentioned above. The remaining second-order interaction turns out to be essentially different from the usual expressions. Its singularity for small values of the nucleon separation r, which was found to be in r^{-3} for both pseudoscalar and vector fields, is reduced for the former but not for the latter. Hence no singularity is removed in the relativistic region by mixing both fields, as was done for the static approximation by Møller and Rosenfeld.[1]

Our treatment of the second-order interaction is completely independent of the neutral or charged character of the mesons and of the corresponding charge dependence of nuclear forces. For the sake of simplicity we shall consider neutral mesons, and consequently the meson field will be described by real wave functions. The isotopic spin of the nucleons will play no part, and we may consider nucleons of definite charge which, we assume, obey the Dirac equation.

II. PSEUDOSCALAR MESON FIELD. EMISSION AND ABSORPTION MATRIX ELEMENTS

The Lagrange function of interacting nucleon and pseudoscalar meson fields is the sum of two terms for the free particles and a coupling term in which we take both types of coupling, pseudoscalar and pseudovector:

$$L = L_{\text{free nucl.}} + L_{\text{free mes.}} + L_1, \tag{1}$$

$$L_{\text{free nucl.}} = -(1/2i)\int [\psi^*(\boldsymbol{\alpha}\cdot\operatorname{grad}\psi) - (\operatorname{grad}\psi^*\cdot\boldsymbol{\alpha})\psi + \psi^*(\partial\psi/\partial t) - (\partial\psi^*/\partial t)\psi + 2iM\psi^*\beta\psi]d_3\mathbf{x}, \tag{2}$$

$$L_{\text{free mes.}} = -\tfrac{1}{2}\int [(\operatorname{grad} U\cdot\operatorname{grad} U) - (\partial U/\partial t)^2 + \kappa^2 U^2]d_3\mathbf{x}, \tag{3}$$

$$L_1 = -\int \psi^*\{f_1\rho_2 U + [f_2/\kappa] \times [(\boldsymbol{\sigma}\cdot\operatorname{grad} U) + \rho_1(\partial U/\partial t)]\}\psi d_3\mathbf{x}. \tag{4}$$

The pseudoscalar U and the spinor ψ are the wave functions for mesons and nucleons; κ and M denote

* This work was performed during a stay in Copenhagen while the author was on leave from the University of Brussels, Belgium.

[1] C. Møller and L. Rosenfeld, Kgl. Danske Vid. Sels. Math.-Fys. Medd. **17**, 8 (1940).

[2] N. Kemmer, Proc. Roy. Soc. **A166**, 127 (1938).

their respective masses in natural units ($\hbar=c=1$); α, $\beta=\rho_3$, ρ_1, ρ_2, $\sigma=\rho_1\alpha=\alpha\rho_1$ are the usual Dirac matrices; the coupling constants f_1 and f_2 have no dimension in our units; the integrals are taken over three-dimensional space.

With the variable $\Pi=\delta L/\delta(\partial U/\partial t)$ canonically conjugage to U, the Hamiltonian is

$$H=H_{\text{free nucl.}}+H_{\text{free mes.}}+H_1+H_{\text{dir.}}, \tag{5}$$

$$H_{\text{free nucl.}}=(1/2i)\int[\psi^*(\alpha\cdot\text{grad}\psi)-(\text{grad}\psi^*\cdot\alpha)\psi +2iM\psi^*\beta\psi]d_3\mathbf{x}, \tag{6}$$

$$H_{\text{free mes.}}=\tfrac{1}{2}\int[(\text{grad}\,U\cdot\text{grad}\,U) +\Pi^2+\kappa^2U^2]d_3\mathbf{x}, \tag{7}$$

$$H_1=\int\psi^*\{f_1\rho_2U+[f_2/\kappa] \times[(\sigma\cdot\text{grad}\,U)+\rho_1\Pi]\}\psi d_3\mathbf{x}, \tag{8}$$

$$H_{\text{dir.}}=\tfrac{1}{2}(f_2/\kappa)^2\int(\psi^*\rho_1\psi)^2d_3\mathbf{x}. \tag{9}$$

Apart from the meson-nucleon interaction expressed by H_1, it contains a direct coupling $H_{\text{dir.}}$ between nucleons.

We use momentum representation and take all wave functions periodical with unit period in spatial coordinates. The plane wave states of the mesons will be denoted by their momentum $\mathbf{k}$, the corresponding energy being $\epsilon_k=(\kappa^2+k^2)^{\frac{1}{2}}$. The nucleon plane wave states are written

$$\psi_m=\chi_m\exp(i\mathbf{p}_m\cdot\mathbf{x}). \tag{10}$$

$\mathbf{p}_m$ is the momentum of state m, and χ_m a matrix of four rows and one column satisfying Dirac equation

$$(\alpha\cdot\mathbf{p}_m+\beta M)\chi_m=E_m\chi_m, \tag{11}$$

where E_m is the energy of the state.

The operator H_1 accounts for emission and absorption of a meson by a nucleon. The matrix elements for these processes are obtained in the usual way by expansion of U and ψ in plane waves and use of the production and annihilation operators for mesons and nucleons. This gives the known expressions

$$(H_1)_{n+k\leftarrow m}=(H_1)_{m\leftarrow n+k}^*=[1/(2\epsilon_k)^{\frac{1}{2}}]\chi_n^* \times[f_1\rho_2-i(f_2/\kappa)(\sigma\cdot\mathbf{k}-\rho_1\epsilon_k)]\chi_m,$$

where the meson momentum $\mathbf{k}$ is equal to the momentum change $\mathbf{p}_m-\mathbf{p}_n$ of the emitting or absorbing nucleon. By means of $\mathbf{k}=\mathbf{p}_m-\mathbf{p}_n$, $\sigma=\alpha\rho_1=\rho_1\alpha$, Eq. (11), and $\rho_1\beta=-\beta\rho_1=-i\rho_2$, we have successively

$$\begin{aligned}
&i\chi_n^*(\sigma\cdot\mathbf{k}-\rho_1\epsilon_k)\chi_m\\
&=i\chi_n^*\rho_1(\alpha\cdot\mathbf{p}_m)\chi_m-i\chi_n^*(\alpha\cdot\mathbf{p}_n)\rho_1\chi_m-i\epsilon_k\chi_n^*\rho_1\chi_m\\
&=i\chi_n^*\rho_1(E_m-M\beta)\chi_m-i\chi_n^*(E_n-M\beta)\rho_1\chi_m\\
&\qquad\qquad-i\epsilon_k\chi_n^*\rho_1\chi_m\\
&=i(E_m-E_n-\epsilon_k)\chi_n^*\rho_1\chi_m-2M\chi_n^*\rho_2\chi_m,
\end{aligned}$$

and the matrix elements become

$$(H_1)_{n+k\leftarrow m}=(H_1)_{m\leftarrow n+k}^*=[1/(2\epsilon_k)^{\frac{1}{2}}]\chi_n^* \times[f_3\rho_2-i(f_2/\kappa)(E_m-E_n-\epsilon_k)\rho_1]\chi_m, \tag{12}$$

with $f_3=f_1+(2M/\kappa)f_2$.

III. SECOND-ORDER INTERACTION IN PSEUDOSCALAR THEORY

In the Hamiltonian (5), the term H_1 of first order in the coupling constants is carried over to higher order by the canonical transformation $\exp(iS)$, defined in momentum representation by

$$S_{r'\leftarrow r}=i(H_1)_{r'\leftarrow r}/(E_r-E_{r'}). \tag{13}$$

E_r, $E_{r'}$ are the eigenvalues of the (diagonal) matrix $H_{\text{free nucl.}}+H_{\text{free mes.}}$. Apart from terms of order three and more in f_1 and f_2, the new Hamiltonian is

$$\exp(iS)H\exp(-iS) =H_{\text{free nucl.}}+H_{\text{free mes.}}+H_2+H_{\text{dir.}}, \tag{14}$$

where H_2 is found to be

$$(H_2)_{r'\leftarrow r}=\tfrac{1}{2}\sum_{r''}[[1/(E_r-E_{r''}]+[1/(E_{r'}-E_{r''})]] \times(H_1)_{r'\leftarrow r''}(H_1)_{r''\leftarrow r}. \tag{15}$$

The matrix elements $(H_1)_{r''\leftarrow r}$ and $(H_1)_{r'\leftarrow r''}$ are given by (12), and the energy difference multiplying ρ_1 in this expression becomes equal (apart possibly from the sign) to the denominators $E_r-E_{r''}$ and $E_{r'}-E_{r''}$ of (15), respectively. The formal simplification thus introduced results in the appearance in H_2 of a contact interaction term. To see it, let us consider the simple case of a two-nucleon system with center of gravity at rest, and write down the matrix element of H_2 for an arbitrary transition $\Phi\rightarrow\Psi$ of the system. We expand Φ and Ψ in plane wave states (10):

$$\begin{aligned}
\Phi&=(1/\sqrt{2})\sum_{m_1,\,m_2}\Phi_{m_1m_2}\psi_{m_1}{}^{(1)}\psi_{m_2}{}^{(2)},\\
\Psi&=(1/\sqrt{2})\sum_{n_1,\,n_2}\Psi_{n_1n_2}\psi_{n_1}{}^{(1)}\psi_{n_2}{}^{(2)},
\end{aligned} \tag{16}$$

where the upper suffixes refer to the two particles.

The non-vanishing terms of the sums (16) satisfy

$$\Phi_{m_1m_2}=-\Phi_{m_2m_1},\quad \Psi_{n_1n_2}=-\Psi_{n_2n_1},$$
$$\mathbf{p}_{m_1}+\mathbf{p}_{m_2}=\mathbf{p}_{n_1}+\mathbf{p}_{n_2}=E_{m_1}-E_{m_2}=E_{n_1}-E_{n_2}=0. \tag{17}$$

Introducing (12) into (15) and using (17) one gets, after some calculation,

$$(H_2)_{\Psi\leftarrow\Phi}=-(f_2/\kappa)^2\sum\Psi_{n_1n_2}{}^*\chi_{n_1}{}^{(1)*}\chi_{n_2}{}^{(2)*}\times\rho_1{}^{(1)}\rho_1{}^{(2)}\chi_{m_1}{}^{(1)}\chi_{m_2}{}^{(2)}\Phi_{m_1m_2}+(W_1+W_2)_{\Psi\leftarrow\Phi}, \tag{18}$$

$$(W_1)_{\Psi\leftarrow\Phi}=-f_3{}^2\sum\Psi_{n_1n_2}{}^*\chi_{n_1}{}^{(1)*}\chi_{n_2}{}^{(2)*}\times[\rho_2{}^{(1)}\rho_2{}^{(2)}/[\epsilon_k{}^2-(E_{m_1}-E_{n_1})^2]]\times\chi_{m_1}{}^{(1)}\chi_{m_2}{}^{(2)}\Phi_{m_1m_2}, \tag{19}$$

$$(W_2)_{\Psi\leftarrow\Phi}=i(f_2f_3/\kappa)\sum\Psi_{n_1n_2}{}^*\chi_{n_1}{}^{(1)*}\chi_{n_2}{}^{(2)*}\times[(E_{m_1}-E_{n_1})/[\epsilon_k{}^2-(E_{m_1}-E_{n_1})^2]]\times(\rho_1{}^{(1)}\rho_2{}^{(2)}+\rho_2{}^{(1)}\rho_1{}^{(2)})\chi_{m_1}{}^{(1)}\chi_{m_2}{}^{(2)}\Phi_{m_1m_2} \tag{20}$$

with $\mathbf{k}=\mathbf{p}_{m_1}-\mathbf{p}_{n_1}$. The first term of $(H_2)_{\Psi\leftarrow\Phi}$ in (18) does not depend explicitly on $\mathbf{p}_{m_1}$ and $\mathbf{p}_{n_1}$. Therefore, it gives an interaction energy proportional to $\delta(\mathbf{r})$, $\mathbf{r}$ being the relative position vector of the two nucleons. As can be seen immediately, that term is equal to $(-H_{\text{dir.}})_{\Psi\leftarrow\Phi}$ and the complete second-order interaction is

$$W=H_2+H_{\text{dir.}}=W_1+W_2. \tag{21}$$

For large relative momentum p or small relative distance r, the expectation value $\langle W_1\rangle$ becomes proportional to p or r^{-1} and $\langle W_2\rangle$ becomes proportional to p^2 or r^{-2}. For any real transition of the two-nucleon system, occurring with conservation of energy, the matrix element of W_2 vanishes. In particular, it has no diagonal elements in momentum representation and hence can be carried over to fourth order by canonical transformation. One will also observe that, according to (19) and (20), the second-order interaction vanishes for $f_3=f_1+(2M/\kappa)f_2=0$. A slightly longer calculation shows that all these features are still valid in an arbitrary system of reference, where the center of gravity of the particles is not at rest.

IV. AN ALTERNATIVE METHOD

Dyson[3] has shown that the pseudovector coupling term in (8) can be transformed into a pseudoscalar coupling term by a canonical transformation. This transformation $\exp(iS')$ is defined, in momentum representation, by a formula similar to (13):

$$S_{r'\leftarrow r}{}'=i(H_1')_{r'\leftarrow r}/(E_r-E_{r'}), \tag{22}$$

where H_1' differs from H_1 by the constant of pseudoscalar coupling:

$$H_1'=\int\psi^*\{-(2M/\kappa)f_2\rho_2U+(f_2/\kappa)[(\boldsymbol{\sigma}\cdot\operatorname{grad}U)+\rho_1\Pi]\}\psi d_3\mathbf{x}.$$

As a consequence of (12), the matrix elements (22) reduce to the simple form

$$(S')_{n+k\leftarrow m}=(S')_{m\leftarrow n+k}{}^*=[1/(2\epsilon_k)^{\frac{1}{2}}][f_2/\kappa]\chi_n{}^*\rho_1\chi_m.{}^4$$

The transformed Hamiltonian up to second-order terms is

$$\exp(iS')H\exp(-iS')=H_{\text{free nucl.}}+H_{\text{free mes.}}+H_1''+H_2'+H_{\text{dir.}}, \tag{23}$$

where H_1'' involves pseudoscalar coupling only:

$$H_1''=f_3\int(\psi^*\rho_2\psi)Ud_3\mathbf{x},\quad f_3=f_1+(2M/\kappa)f_2,$$

and $H_2'+H_{\text{dir.}}$ gives a vanishing contribution to the second-order interaction between nucleons. Starting now with (23), the procedure of Section III gives the second-order interaction by means of canonical transformation $\exp(iS'')$ with $S''=S-S'$, S and S' being defined in (13) and (22), respectively. Instead of (21), one gets

$$W'=W_1,$$

given by (19). The discrepancy between W and W' is, of course, formally due to the difference between the transformation $\exp(iS)$ used in the preceding section and the product $\exp(iS'')\exp(iS')$ used here. In fact, the transformation V defined by

$$\exp(iS'')\exp(iS')=V\exp(iS)$$

removes the W_2 term from W and carries it over to fourth-order interaction.

One should expect the two methods to have the same physical consequences in second-order approximation; this is in agreement with the mentioned vanishing of all diagonal elements of W_2 and of its elements corresponding to real transitions. The deuteron problem will be discussed in the last section.[5]

[3] F. J. Dyson, Phys. Rev. **73**, 929 (1948). The author is greatly indebted to Dr. Luttinger who called his attention to Dyson's method and pointed out to him that it gives W_1 instead of W_1+W_2 as second-order interaction. Dyson investigates the case $f_1=0$. The generalization to $f_1\neq0$ which we give here is quite immediate.

[4] This explains why S can be written in closed form in coordinate space as is done by Dyson.

[5] The conclusion of Dyson's treatment that pseudovector coupling has the same second-order effects as pseudoscalar coupling was previously reached by E. C. Nelson, Phys. Rev. 60, 830 (1941), who transforms the Lagrange function (1) by means of the equations of motion deduced from it. This procedure seems not convincing to the present author, because the equations of motion deduced from the new Lagrange function are not equivalent to the previous ones.

V. VECTOR MESON FIELD

The Lagrange function of interacting nucleon and vector meson fields is again of form (1), but $L_{\text{free mes.}}$ and L_1 have to be replaced by

$$L_{\text{free mes.}}{}^{v}=-\tfrac{1}{2}\int[(\operatorname{curl}\mathbf{U}\cdot\operatorname{curl}\mathbf{U})-(\{(\partial\mathbf{U}/\partial t)-\operatorname{grad}U_0\}\cdot\{(\partial\mathbf{U}/\partial t)-\operatorname{grad}U_0\})+\kappa^2(\mathbf{U}\cdot\mathbf{U}-U_0^2)]d_3\mathbf{x},$$

$$L_1{}^{v}=-\int\psi^*\{g_1(\boldsymbol{\alpha}\cdot\mathbf{U}+U_0)+[g_2/\kappa][(\boldsymbol{\beta\sigma}\cdot\operatorname{curl}\mathbf{U})-(\boldsymbol{\gamma}\cdot\{(\partial\mathbf{U}/\partial t)-\operatorname{grad}U_0\})]\}\psi d_3\mathbf{x}.$$

The four wave functions $\mathbf{U}$, U_0 describe the mesons, g_1 and g_2 are dimensionless coupling constants, and $\boldsymbol{\gamma}$ is defined as usually: $\boldsymbol{\gamma}=-i\boldsymbol{\beta\alpha}=i\boldsymbol{\alpha\beta}$. Introduction of

$$\boldsymbol{\Pi}=\delta L/\delta(\partial\mathbf{U}/\partial t)$$

and elimination of U_0 by means of the field equations give the Hamiltonian of form (5), the three last terms being now

$$H_{\text{free mes.}}{}^{v}=\tfrac{1}{2}\int[(\operatorname{curl}\mathbf{U}\cdot\operatorname{curl}\mathbf{U})+\kappa^2(\mathbf{U}\cdot\mathbf{U})+(1/\kappa^2)(\operatorname{div}\boldsymbol{\Pi})^2+(\boldsymbol{\Pi}\cdot\boldsymbol{\Pi})]d_3\mathbf{x},$$

$$H_1{}^{v}=\int\psi^*\{g_1(\boldsymbol{\alpha}\cdot\mathbf{U}-(1/\kappa^2)\operatorname{div}\boldsymbol{\Pi})+(g_2/\kappa)[(\boldsymbol{\beta\sigma}\cdot\operatorname{curl}\mathbf{U})-(\boldsymbol{\gamma}\cdot\mathbf{U})]\}\psi d_3\mathbf{x},$$

$$H_{\text{dir.}}{}^{v}=\tfrac{1}{2}(g_1/\kappa)^2\int(\psi^*\psi)^2d_3\mathbf{x}+\tfrac{1}{2}(g_2/\kappa)^2\int((\psi^*\boldsymbol{\gamma}\psi)\cdot(\psi^*\boldsymbol{\gamma}\psi))d_3\mathbf{x}.$$

Instead of transforming the matrix elements of $H_1{}^{v}$ by means of (11), as was done in Section II for H_1, it seems more convenient to deduce first the second-order interaction between two nucleons with center of gravity at rest. A canonical transformation defined by the formula analogous to (13) gives to the Hamiltonian the form (14), $H_{\text{free mes.}}$, $H_{\text{dir.}}$, and H_2 being replaced, respectively, by $H_{\text{free mes.}}{}^{v}$, $H_{\text{dir.}}{}^{v}$, and a matrix $H_2{}^{v}$ which is easily deduced.[6] For an arbitrary transition $\Phi\rightarrow\Psi$ of the two-nucleon system, using (16) and (17), one gets

$$(H_2{}^{v})_{\Psi\leftarrow\Phi}=-\sum\Psi_{n_1n_2}{}^{*}\chi_{n_1}{}^{(1)*}\chi_{n_2}{}^{(2)*}[1/[\epsilon_k{}^2-(E_{m_1}-E_{n_1})^2]]\{g_1{}^2[(\boldsymbol{\alpha}^{(1)}\cdot\boldsymbol{\alpha}^{(2)})+(1/\kappa^2)\{k^2+(\boldsymbol{\alpha}^{(1)}\cdot\mathbf{k})(\boldsymbol{\alpha}^{(2)}\cdot\mathbf{k})\}]$$
$$+(g_2/\kappa)^2[\epsilon_k{}^2(\boldsymbol{\gamma}^{(1)}\cdot\boldsymbol{\gamma}^{(2)})-(\boldsymbol{\gamma}^{(1)}\cdot\mathbf{k})(\boldsymbol{\gamma}^{(2)}\cdot\mathbf{k})+(\boldsymbol{\gamma}^{(1)}\cdot\boldsymbol{\gamma}^{(2)})(\boldsymbol{\alpha}^{(1)}\cdot\mathbf{k})(\boldsymbol{\alpha}^{(2)}\cdot\mathbf{k})+k^2\beta^{(1)}\beta^{(2)}]$$
$$+i(g_1g_2/\kappa)[((\boldsymbol{\gamma}^{(1)}-\boldsymbol{\gamma}^{(2)})\cdot\mathbf{k})(1-(\boldsymbol{\alpha}^{(1)}\cdot\boldsymbol{\alpha}^{(2)}))-i\beta^{(1)}(\boldsymbol{\alpha}^{(2)}\cdot\mathbf{k})+i\beta^{(2)}(\boldsymbol{\alpha}^{(1)}\cdot\mathbf{k})]\}\chi_{m_1}{}^{(1)}\chi_{m_2}{}^{(2)}\Phi_{m_1m_2}. \quad (24)$$

$\mathbf{k}$ is defined as $\mathbf{p}_{m_1}-\mathbf{p}_{n_1}$. By means of (11) and of the properties of Dirac matrices, the expression (24) can be transformed. The main points of the calculation can be found in the appendix. The final result is

$$(H_2{}^{v})_{\Psi\leftarrow\Phi}=(-H_{\text{dir.}}{}^{v}+W_1{}^{v}+W_2{}^{v}+W_3{}^{v})_{\Psi\leftarrow\Phi}, \quad (25)$$

$$(W_1{}^{v})_{\Psi\leftarrow\Phi}=-\sum\Psi_{n_1n_2}{}^{*}\chi_{n_1}{}^{(1)*}\chi_{n_2}{}^{(2)*}\frac{g_3{}^2[(\boldsymbol{\alpha}^{(1)}\cdot\boldsymbol{\alpha}^{(2)})-1-\beta^{(1)}\beta^{(2)}]+(g_1{}^2-g_2{}^2)\beta^{(1)}\beta^{(2)}}{\epsilon_k{}^2-(E_{m_1}-E_{n_1})^2}\chi_{m_1}{}^{(1)}\chi_{m_2}{}^{(2)}\Phi_{m_1m_2}, \quad (26)$$

$$(W_2{}^{v})_{\Psi\leftarrow\Phi}=(g_2g_3/\kappa)\sum\Psi_{n_1n_2}{}^{*}\chi_{n_1}{}^{(1)*}\chi_{n_2}{}^{(2)*}\frac{(E_{m_1}-E_{n_1})(\boldsymbol{\alpha}^{(1)}\cdot\boldsymbol{\alpha}^{(2)})-2(E_{m_1}+E_{n_1})}{\epsilon_k{}^2-(E_{m_1}-E_{n_1})^2}\times(\beta^{(1)}+\beta^{(2)})\chi_{m_1}{}^{(1)}\chi_{m_2}{}^{(2)}\Phi_{m_1m_2}, \quad (27)$$

$$(W_3{}^{v})_{\Psi\leftarrow\Phi}=-(g_2/\kappa)^2\sum\Psi_{n_1n_2}{}^{*}\chi_{n_1}{}^{(1)*}\chi_{n_2}{}^{(2)*}\left[1-\frac{8E_{m_1}E_{n_1}}{\epsilon_k{}^2-(E_{m_1}-E_{n_1})^2}\right]\beta^{(1)}\beta^{(2)}\chi_{m_1}{}^{(1)}\chi_{m_2}{}^{(2)}\Phi_{m_1m_2}, \quad (28)$$

with $g_3=g_1+(2M/\kappa)g_2$, and the total second-order interaction is given by $W^{v}=W_1{}^{v}+W_2{}^{v}+W_3{}^{v}$.

For large relative momentum p or small relative distance r, the expectation values $\langle W_1{}^{v}\rangle$, $\langle W_2{}^{v}\rangle$, and $\langle W_3{}^{v}\rangle$ behave, respectively, as $p\sim r^{-1}$, $p^2\sim r^{-2}$, and $p^3\sim r^{-3}$. All three expressions have nonvanishing diagonal terms and consequently are of physical importance in second-order approximation.

VI. DISCUSSION OF THE RESULTS

Although obviously the second-order interactions W and W^{v} deduced in the foregoing sections differ from the usual expressions[1,2] only by some contact interaction terms and by quantities negligible in the approximations involved in the usual derivations, the expressions we have obtained look very different

[6] H. J. Bhabha, Proc. Roy. Soc. A166, 501 (1938).

from the usual ones. Starting with our expressions, which are exact in second order, it is possible to get the static part of the interaction between nucleons, by making from Eqs. (19) and (20) for the pseudoscalar field and (26) to (28) for the vector field:

$$E_{m1}\sim E_{n1}\sim M,\quad \rho_1\sim 0,\quad \rho_2\sim 0,\quad \alpha\sim 0,\quad \beta\sim 1. \tag{29}$$

For the pseudoscalar field, the second-order interaction vanishes completely in this static approximation, whereas for the vector field one gets the pure Yukawa potential $e^{-\kappa r}/r$ and a contact interaction, i.e., an expression essentially different from the usual one. This shows how much the expression of the static interaction depends on the way of deriving it, although, of course, the difference, apart from some contact interaction terms, must vanish for vanishing nucleon velocities. By thinking, for example, of Kemmer's derivation of the usual static interaction,[2] one could perhaps say that it corresponds to the static approximation for infinitely heavy nucleons: $M\gg\kappa$, whereas when putting (29) in our Eqs. (19), (20), and (26) to (28), we assume a given and finite value for M/κ (this ratio comes in the coupling constants f_3 and g_3).

As regards the deuteron problem, a first question is whether one can get reliable information about the ground state of the deuteron by putting the interactions W or W^v derived above in a two-particle Dirac equation. This seems doubtful, for, as shown in Sections III and IV for the pseudoscalar case, the non-diagonal elements of second-order interaction are not uniquely defined in the treatment using canonical transformations (W can be made equal to W_1+W_2 or to W_1), and these elements strongly influence the eigenvalues of the wave equation. By instance, in the pseudoscalar case, the r^{-1} singularity of W_1 is low enough to account for the existence of a ground state,[7] whereas W_1+W_2, with its r^{-2} singularity, excludes the possibility of any ground state with finite binding energy. The procedure, so successful in electrodynamics, of putting the static interaction in the wave equation and treating non-static effects as perturbations, here also meets with difficulties: one has to choose a definite expression for the static interaction, and the latter may happen to vanish, as we have observed for the pseudoscalar case. Accordingly, for a satisfactory discussion of the deuteron problem, a new line of approach seems desirable.[8]

Nevertheless, a few general conclusions can be attained. For the pseudoscalar meson, apart from the W_2 term given in (20) and deprived of physical effects of second order, both types of coupling (in f_1 and f_2) give the same second-order interaction. This is in agreement with Nelson[5] and Dyson's[3] conclusion. For the vector meson, g_1 and g_2 couplings give essentially different interactions. For small separations r of the nucleons, the second-order interaction has a r^{-3} singularity for the vector meson, whereas for the pseudoscalar field the singularity is not higher than r^{-2} and probably in r^{-1}. This makes it hopeless to discard the inadmissible singularities in the relativistic region by mixing vector and pseudoscalar fields, as was done by Møller and Rosenfeld[1] for the static interaction as usually defined. The same conclusion was reached by Hu[9] for the approximate expressions obtained when neglecting recoil energies and disregarding contact interaction terms.

ACKNOWLEDGMENT

The author's thanks are due the Belgian "Centre Interuniversitaire de Physique Nucléaire," who awarded the grant enabling him to stay in Copenhagen. He is greatly indebted to Professor N. Bohr for his kind hospitality, and to him as well as to Professor W. Pauli, Professor C. Møller, Dr. N. Hu, Dr. A. Bohr, and Dr. J. M. Luttinger for many stimulating discussions and suggestions.

APPENDIX

The following equations connect quantities which may be replaced by each other in the curly bracket of (24). The quantities are equal only when introduced into (24). The deduction uses Eqs. (11) and (17) and relation $\mathbf{k}=\mathbf{p}_{m1}-\mathbf{p}_{n1}$, and runs exactly as the deduction of (12).

$$(\alpha^{(1)}\cdot\mathbf{k})=E_{m1}-E_{n1};\quad (\alpha^{(2)}\cdot\mathbf{k})=E_{n1}-E_{m1};$$

$$(\gamma^{(1)}\cdot\mathbf{k})=2iM-i(E_{m1}+E_{n1})\beta^{(1)};$$

$$(\gamma^{(3)}\cdot\mathbf{k})=-2iM+i(E_{m1}+E_{n1})\beta^{(2)};$$

$$\begin{aligned}(\gamma^{(1)}\cdot\gamma^{(2)})&(\alpha^{(1)}\cdot\mathbf{k})(\alpha^{(2)}\cdot\mathbf{k})\\ &=(\gamma^{(1)}\cdot\gamma^{(2)})[(\alpha^{(1)}\cdot\mathbf{p}_{m1})(\alpha^{(2)}\cdot\mathbf{p}_{m1})+(\alpha^{(1)}\cdot\mathbf{p}_{n1})(\alpha^{(2)}\cdot\mathbf{p}_{n1})\\ &\qquad-(\alpha^{(1)}\cdot\mathbf{p}_{m1})(\alpha^{(2)}\cdot\mathbf{p}_{n1})-(\alpha^{(1)}\cdot\mathbf{p}_{n1})(\alpha^{(2)}\cdot\mathbf{p}_{m1})];\end{aligned}$$

$$\begin{aligned}(\gamma^{(1)}\cdot\gamma^{(2)})&(\alpha^{(1)}\cdot\mathbf{p}_{m1})(\alpha^{(2)}\cdot\mathbf{p}_{m1})\\ &=-(\gamma^{(1)}\cdot\gamma^{(2)})(E_{m1}-M\beta^{(1)})(E_{m1}-M\beta^{(2)});\end{aligned}$$

$$\begin{aligned}(\gamma^{(1)}\cdot\gamma^{(2)})&(\alpha^{(1)}\cdot\mathbf{p}_{n1})(\alpha^{(2)}\cdot\mathbf{p}_{n1})=(\alpha^{(1)}\cdot\mathbf{p}_{n1})(\alpha^{(2)}\cdot\mathbf{p}_{n1})(\gamma^{(1)}\cdot\gamma^{(2)})\\ &=-(E_{n1}-M\beta^{(1)})(E_{n1}-M\beta^{(2)})(\gamma^{(1)}\cdot\gamma^{(2)});\end{aligned}$$

$$\begin{aligned}&-(\gamma^{(1)}\cdot\gamma^{(2)})[(\alpha^{(1)}\cdot\mathbf{p}_{m1})(\alpha^{(2)}\cdot\mathbf{p}_{n1})+(\alpha^{(1)}\cdot\mathbf{p}_{n1})(\alpha^{(2)}\cdot\mathbf{p}_{m1})]\\ &=(\alpha^{(1)}\cdot\alpha^{(2)})[-(\alpha^{(2)}\cdot\mathbf{p}_{n1})(E_{m1}-M\beta^{(1)})\\ &\qquad+(\alpha^{(1)}\cdot\mathbf{p}_{n1})(E_{m1}-M\beta^{(2)})]\beta^{(1)}\beta^{(2)}\\ &=\{[-2(\alpha^{(1)}\cdot\mathbf{p}_{n1})+(\alpha^{(2)}\cdot\mathbf{p}_{n1})(\alpha^{(1)}\cdot\alpha^{(2)})](E_{m1}-M\beta^{(1)})\\ &\qquad+[2(\alpha^{(2)}\cdot\mathbf{p}_{n1})-(\alpha^{(1)}\cdot\mathbf{p}_{n1})(\alpha^{(1)}\cdot\alpha^{(2)})](E_{m1}-M\beta^{(2)})\}\beta^{(1)}\beta^{(2)}\\ &=\{[2(M\beta^{(1)}-E_{n1})+(M\beta^{(2)}-E_{n1})(\alpha^{(1)}\cdot\alpha^{(2)})](E_{m1}-M\beta^{(1)})\\ &\qquad+[2(M\beta^{(2)}-E_{n1})+(M\beta^{(1)}-E_{n1})(\alpha^{(1)}\cdot\alpha^{(2)})]\\ &\qquad\qquad\times(E_{m1}-M\beta^{(2)})\}\beta^{(1)}\beta^{(2)};\end{aligned}$$

whence

$$\begin{aligned}(\gamma^{(1)}\cdot\gamma^{(2)})(\alpha^{(1)}\cdot\mathbf{k})(\alpha^{(2)}\cdot\mathbf{k})&=-(E_{m1}-E_{n1})^2(\gamma^{(1)}\cdot\gamma^{(2)})\\ &\quad-4E_{m1}E_{n1}\beta^{(1)}\beta^{(2)}+2M[(E_{n1}-E_{m1})(\alpha^{(1)}\cdot\alpha^{(2)})\\ &\quad+(E_{m1}+E_{n1})](\beta^{(1)}+\beta^{(2)})+4M^2[(\alpha^{(1)}\cdot\alpha^{(2)})-\beta^{(1)}\beta^{(2)}].\end{aligned}$$

Introducing into (24), one readily obtains Eqs. (25) to (28).

[7] This does not mean that an acceptable ground state effectively exists for the W_1 interaction.

[8] The author is indebted to Professor N. Bohr, Dr. A. Bohr, and also to Dr. J. M. Luttinger for an illuminating discussion of this rather delicate point.

[9] Ning Hu, Phys. Rev. 67, 339 (1945).

The Microwave Absorption Spectrum of Oxygen*

M. W. P. STRANDBERG, C. Y. MENG,** AND J. G. INGERSOLL
Research Laboratory of Electronics, Massachusetts Institute of Technology, Cambridge, Massachusetts
(Received January 31, 1949)

Measurements of the absorption of 5-mm radiation in oxygen gas have been made. The experimentally observed magnitude and shape of the absorption may be satisfactorily compared with the theoretical curves of Van Vleck for an assumed line breadth $\Delta\nu=0.015$ to 0.02 cm^{-1}. Observations of the absorption in mixtures of oxygen and nitrogen indicate a disparity of O_2 and N_2 collision cross sections. It is suggested that nitrogen causes an anomalous narrowing of the oxygen absorption line breadth.

INTRODUCTION

THE existence of an absorption band in the millimeter region resulting from molecular oxygen has been predicted and discussed at some length by Van Vleck.[1] Measurements made by Beringer[2] have given a preliminary confirmation of the existence of this absorption band, as have those of Lamont.[3] A more detailed investigation of the absorption of 5-mm radiation by oxygen will be reported here.

As Van Vleck has pointed out, the oxygen molecule is a $^3\Sigma$ ground state, since it has one unit of spin angular momentum. As a consequence of this resultant spin, it has a magnetic moment equal to two Bohr magnetons. This permanent magnetic moment is the cause of the paramagnetism observed in oxygen, and it also allows the molecule to couple to the magnetic field of an electromagnetic wave. The unit of spin angular momentum perturbs the rotational state since it is coupled to the rotational motion of the molecule. The unit electron spin has three spatial orientations with respect to the given molecular rotational angular momentum vector, K, so that each rotational level is split into three states, $J=K+1$, K, and $K-1$, each J state of this so-called ρ-type triplet arising from a different orientation of the spin with respect to the rotational motion of the molecule. The energy difference between successive J terms in any of these triplets is about 2 cm^{-1} (with the single exception of $J=0\rightarrow1$ difference which is about 4 cm^{-1}). Selection rules for magnetic dipole transitions allow induced transitions between these successive members of the triplet ($\Delta J=\pm1$) so that for each value of the rotational angular momentum quantum number K there are two absorption frequencies in the 2-cm^{-1} region. The population of the various rotational levels follows Boltzmann statistics, and it may be shown that the most populated state at room temperatures is that one for which $K=13$. States with $K\cong25$ still have significant populations however. The O^{16} nucleus has zero nuclear spin angular momentum, so that symmetry considerations demand that K have only odd values. Thus, with two absorption lines for each value of K, there are about 25 lines which overlap at atmospheric pressure and which contribute significantly to the absorption in the 2-cm^{-1} region. Van Vleck[1] has calculated the shape and magnitude of the absorption for various values of the line-broadening parameter $\Delta\nu$. The theory uses the values of the triplet spacings as determined from optical spectroscopy and is totally determined except for line-broadening or line-breadth parameter $\Delta\nu$. The intensity is not sensitive to the assumed triplet spacings but it is a strong function of the line breadth $\Delta\nu$. For this reason, previous measurements[2,3] have obtained the magnitude of the absorption at a few scattered points and have inferred the line breadth $\Delta\nu$ from this intensity. The measurements below are an extension of previous measurements in that the theory is essentially checked by comparing both the intensity and structure of the measured and computed absorption.

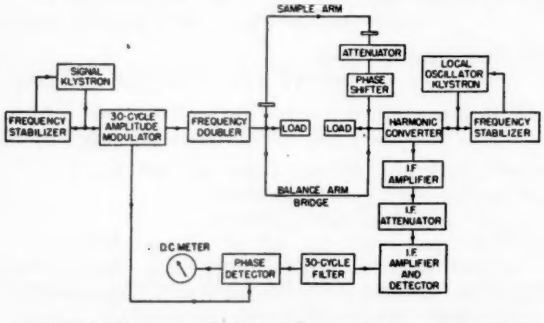

FIG. 1. Block diagram of absorption measurement apparatus.

APPARATUS

A balanced microwave bridge was used to measure the absorption. Five-mm power was obtained from the second harmonic generated in a non-linear silicon crystal driven by a 1-cm reflex

* This research has been supported in part by the Signal Corps, the Air Materiel Command, and ONR.
** Now at National Tsing Hua University, Peiping, China.
[1] J. H. Van Vleck, Phys. Rev. **71**, 413 (1947).
[2] Robert Beringer, Phys. Rev. **70**, 53 (1946).
[3] H. R. L. Lamont, Phys. Rev. **74**, 353 (1948); also private communication.

klystron oscillator. A block diagram of the apparatus is shown in Fig. 1. The 5-mm radiation was then divided between two nearly identical wave guides and recombined in a bridge T-junction. One output arm of the T fed a matched load and the other fed a harmonic converter. The converter mixed the incoming 5-mm radiation with the second harmonic of another 1-cm local oscillator, and the heterodyne signal current was fed to a 24-Mc/sec. amplifier. Provisions were made for inserting a step-attenuator pad in the amplifier cascade after three stages of amplification.

Both the signal oscillator and local oscillator were frequency-stabilized to a high mode of a 3-cm cavity using a Pound[4] and, later, a Zaffarano[5] circuit. The frequency of the signal-generator fundamental was measured with the M.I.T. frequency standard.[6] The signal-generator fundamental was amplitude-modulated with a rotating attenuator at 30 cycles/sec. The detected output from the receiver could then be filtered for the 30-cycle modulations. This modulation was amplified and converted to d.c. with a phase detector. The signal was read on a milliammeter and the 30-cycle modulation merely provided a convenient monitoring current to amplify after filtering.

In operation, the sample arm of the bridge was filled with tank oxygen at 80 cm Hg, and the bridge balanced for no receiver output by means of the r-f phase shifter and attenuator in the sample arm. The sample was then pumped out and the bridge rebalanced as well as possible by slowly admitting tank argon into the sample arm to an appropriate pressure. The final minimum was achieved with readjustment of the r-f phase shifter. The use of argon for rebalancing allowed the bridge to work under constant impedance conditions. This procedure proved necessary for accuracy. Argon was chosen because its dielectric constant is similar to that of oxygen. Since argon is monatomic, it has no absorption in the region of these measurements. Check measurements on nitrogen using argon as a balancing agent disclosed no absorption greater than 1 db/km. The minimum signal current was noted and the phase shifter was readjusted to give a maximum output; the 24-Mc/sec. step attenuator was then introduced, and the current-output reading was made as nearly equal to that observed at minimum balance as was possible. The attenuator had a minimum change of 1 db and the readings were taken to 0.5 db by interpolation. The attenuator reading then gave the value of the maximum-to-minimum power ratio as:

$$\text{db} = 10 \log(P_{\max}/P_{\min}).$$

It can be shown that the attenuation in the gas may be calculated as:

$$\Delta P/P = 4\alpha^{\frac{1}{2}}/(1+\alpha^{-\frac{1}{2}})^2,$$

where ΔP = power absorbed, P = incident power on sample, $\alpha = P_{\max}/P_{\min}$.

The path length was 6.15 m and, when correction has been made for changing from a guided path to a free-space path, the attenuation γ in db/km is

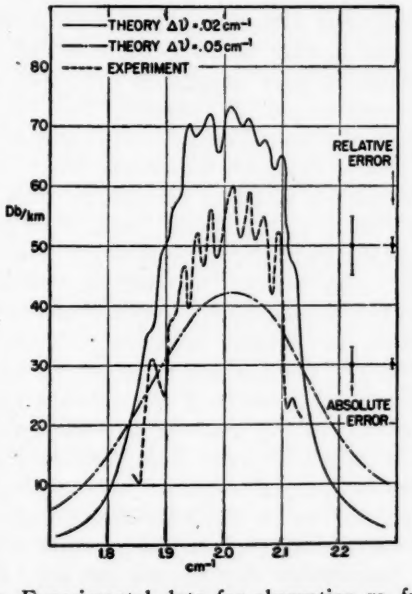

FIG. 2a. Experimental data for absorption *vs.* frequency, in pure oxygen at 80 cm Hg, plotted with a computed curve for $\Delta\nu = 0.05$ cm^{-1} and 0.02 cm^{-1}.

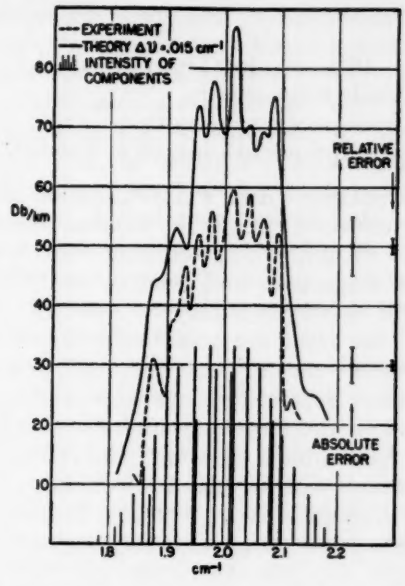

FIG. 2b. Experimental data for absorption *vs.* frequency, in pure oxygen at 80 cm Hg, plotted with a computed curve for $\Delta\nu = 0.015$ cm^{-1}.

[4] R. V. Pound, Proc. I.R.E. **35**, 1405 (1947).
[5] W. G. Tuller, W. C. Galloway, and F. P. Zaffarano, Proc. I.R.E. **36**, 794 (1948).
[6] M. W. P. Strandberg, T. Wentink, and R. L. Kyhl, Phys. Rev. **75**, 270 (1949).

given as:

$$\gamma = -10(\lambda_0/l\lambda_g)\log(1-\Delta P/P) \text{ db/km},$$

λ_g = guide wave-length,
λ_0 = free-space wave-length,
l = absorption-path length in kilometers.

A stable balance with a P_{max}/P_{min} of 60 db could be readily obtained; this is the balance required to read to 2.5 db/km. The attenuator was correct to ±1 db in magnitude and relative readings were good to the setting accuracy of ±0.5 db. Stated otherwise, the data are good to ±10 percent in absolute value and to less than ±5 percent in relative value. Several readings were made at each frequency and the frequency intervals were about 0.003 cm^{-1}. Readings at about 100 different frequency settings with oxygen at 80-cm Hg pressure, were used to compile the final results. Readings were also made at some frequencies for oxygen-nitrogen mixtures.

ABSORPTION OF PURE OXYGEN

The data obtained for pure oxygen at 80-cm Hg pressure are shown plotted in Fig. 2(a), together with two curves of predicted absorption at 80-cm Hg pressure for line breadths $\Delta\nu = 0.02$ cm^{-1} and 0.05 cm^{-1}. The curve for $\Delta\nu = 0.02$ cm^{-1} is derived from that of Lamont[3] which was computed using the new Babcock evaluation of the triplet energy differences. It is in slightly better agreement with the experimental data than the curve of Van Vleck for which the older values of Dieke and Babcock were used. The curve of absorption for $\Delta\nu = 0.05$ cm^{-1} at 80-cm Hg pressure is derived from that of Van Vleck.[1]

A line breadth of 0.05 cm^{-1} is obviously too high. The curves match rather well for a line breadth of 0.02 cm^{-1}, although the experimental absorption is about 20 percent low. Figure 2(b) shows the plotted experimental data, together with a computed curve for $\Delta\nu = 0.015$ cm^{-1}. The structure of these two curves registers rather well. The magnitude of the measured absorption is low, in this case by about 35 percent. The discrepancy in magnitude is not unreasonable. In a similar case, the observed absorption in H_2O at 0.74 cm^{-1} is 10 to 20 percent below the theoretical value, depending upon the value of the electric dipole moment used.[7,8] So it may be said that, assuming a line breadth of 0.015 cm^{-1}, there is a satisfactory agreement between theoretical and experimental values of the 2 cm^{-1} absorption in O_2 at 80 cm Hg and 283°K.

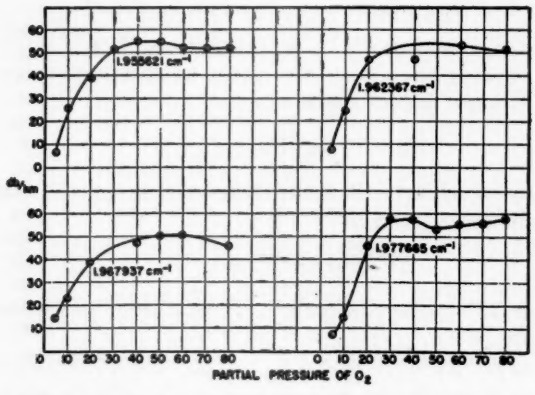

FIG. 3. Curves of absorption in oxygen nitrogen mixtures *vs.* oxygen partial pressure taken at various frequencies.

It may be noted that the line breadth predicted from the collision cross section given by kinetic theory is about 0.04 cm^{-1}. There is a certain amount of difficulty in justifying a line breadth smaller than that given by the mean free time. For simple microwave spectra, it has been generally found that the observed line breadths are greater than those predicted by the mean free time because of dipole-dipole perturbations. In the absence of large dipole interactions, line breadths narrower than those computed from kinetic theory are possible if all collisions are not effective in interrupting the absorption processes. Since the molecular translational energy follows a Boltzmann distribution from energy considerations some collisions are conceivably ineffective, hence a narrower line breadth. This point should undoubtedly be further investigated theoretically.

OXYGEN NITROGEN MIXTURE

Measurements were also made of the absorption in oxygen diluted with nitrogen. This was done to determine the scaling factor needed to reduce the measurements on pure oxygen to their air equivalent (21 percent O_2, 79 percent N_2). We had expected to find a simple linear relationship between pure and dilute oxygen absorption. Since O_2 and N_2 collision cross sections should be nearly the same, the line breadth should remain essentially constant with a constant total pressure. The reduction in absorption would then vary proportionally to the number of absorbing oxygen molecules.

Absorption in oxygen nitrogen mixtures was measured in the fashion described above for pure oxygen. The total pressure of the mixture was held constant at 80 cm Hg and the partial pressure of oxygen was varied between 5 and 80 cm Hg. The relationship between absorption and oxygen partial pressure proved to be complex. Several curves of absorption *versus* oxygen partial pressure taken at different frequencies are shown in Fig. 3. The behavior of the absorption with varying oxygen content is difficult to justify with any simple picture of the absorption process.

In Van Vleck's notation, the data of Fig. 3 were

[7] J. H. Van Vleck, Phys. Rev. **71**, 425 (1947).
[8] M. W. P. Strandberg, R.L.E. Report No. 85, Sept. 25, 1948.

taken for the region between the $K_-=9$, $K_+=3$ and the $K_-=7$, $K_+=5$ transitions. Since the characteristic line breadth is the only factor undetermined in the Van Vleck-Weisskopf theory, there remains only the possibility of variation of this parameter with nitrogen dilution. If the line breadth were to increase with increasing dilution, the curves of Fig. 3 would have the opposite curvature, i.e., a curvature away from the axis of partial pressure. If the line breadth were to decrease with increasing oxygen dilution (a situation which might be accounted for by a decrease in dipole-dipole interaction), the curvature toward the partial-pressure axis would possibly not be so great as that observed. The interval 1.950 cm^{-1} to 1.976 cm^{-1} is 0.026 cm^{-1} wide and a decrease in line breadth much below 0.015 cm^{-1} would tend to decrease the absorption in the least resonance region of 1.963 cm^{-1}. However, the $K_-=7$ line (1.976 cm^{-1}) and the $K_+=3$ line (1.950 cm^{-1}) may be closer together than we have assumed from Babcock's analysis; or the line breadth for those two lines may be different from the average line breadth of 0.015 cm^{-1}. A variation of line breadth with rotational energy state is certainly understandable; the possibility of such a phenomenon has been pointed out by Van Vleck and Weisskopf,[9] and has been demonstrated experimentally in the case of ammonia by Bleaney and Penrose.[10] It should be noted that the case of ammonia is unusual, since there are large diagonal dipole matrix elements which presumably make the line breadth a function of the rotational state. Similar elements for oxygen should be too small to consider by virtue of the hundredfold-smaller magnetic dipole moment of oxygen.

It can be readily seen from Fig. 3 that dilute oxygen ($\sim$25 percent O_2) does behave like an absorbing gas with constant line breadth, since the absorption becomes proportional to the oxygen partial pressure. In highly diluted oxygen, the collisions which interrupt the radiation process are predominantly those between oxygen and nitrogen molecules; so that if the anomalous behavior of the absorption in O_2-N_2 mixtures containing a high percentage of O_2 is, in fact, caused by a line narrowing phenomenon, one would be led to believe that the characteristic line breadth for oxygen absorption is smaller in the case where nitrogen is the interrupting agent than it is in pure oxygen. The difference in the line breadths might be a factor of four, but this is only a guess.

A conclusive check on the experiments would be that obtained from a comparison of the integrated absorption for various concentrations of oxygen. The integrated absorption is independent of the line breadth and must be a linear function of the number of absorbing molecules. It would seem difficult to fulfill such a requirement with data such as are given in Fig. 3. However, it must be remembered that the integrated intensity may still be decreasing as a result of decreasing skirt absorption. In short, we have too little data for mixtures of oxygen and nitrogen to be able to apply the criterion of appropriate variation of the integrated intensity. Measurements of this type are sufficiently tedious to discourage us from carrying them out and, furthermore, observations on individual lines at low pressures seem to be more useful in developing a model for the processes taking place.

It has been pointed out above that the line breadth, $\Delta\nu\cong 0.015$ cm^{-1}, is less than the kinetic-theory value of 0.04 cm^{-1}. Any further narrowing caused by a preponderance of O_2-N_2 collisions, though certainly possible, is hard to visualize in any simple fashion.

It should also be noted that Bleaney and Penrose,[10] found anomalous values for the collision cross sections, or line widths, in ammonia nitrogen mixtures. The supposedly similar cross sections for ammonia argon and ammonia oxygen collisions determined from the line breadths are smaller by a factor of two. This large discrepancy worried these experimenters enough to cause them to remeasure the ammonia nitrogen value, but they found no error and let the matter stand. Unfortunately, these experiments are of little value here, since the effect Bleaney and Penrose observe is in the wrong direction (i.e., they observe nitrogen broadening) and the collision cross sections are for interaction with ammonia. The point remains that in two cases, those of oxygen and ammonia, dilution of an absorbing gas with nitrogen has indicated an anomalous behavior of the nitrogen molecules.

Briefly it may be said that measurements made on pure oxygen cannot be reduced to atmospheric absorption by a simple multiplication with the fraction representing the number of oxygen molecules present. The variation of the absorption in oxygen-nitrogen mixtures is not readily understandable. At low oxygen concentration, the absorption does vary proportionally to the partial pressure of oxygen, as might be expected. On the other hand, in mixtures with a high percentage of oxygen, the absorption becomes almost independent of the partial pressures of the oxygen over a region several line breadths wide. Qualitatively, this independence of absorption on the concentration of oxygen might be due to a variation arising from a difference between O_2-O_2 and N_2-O_2 collisions, but the phenomenon cannot be quantitatively explained on the basis of available data. Further, the measurements presented here are not in good agree-

[9] J. H. Van Vleck and V. F. Weisskopf, Rev. Mod. Phys. 17, 227 (1945).

[10] B. Bleaney and R. P. Penrose, Phys. Soc. Proc. 59, 418 (1947); 60, 540 (1948)

ment with previously published experimental data. Beringer[2] found that the absorption in oxygen-nitrogen mixtures is proportional to the oxygen partial pressure. Lamont[3] measured directly the absorption in the atmosphere and found it to be about 15 db/km. On the basis of our experiments, we would predict the absorption resulting from oxygen in the atmosphere to be about 30 to 40 db/km.

A good deal of work remains to be done. Studies of the absorption in pure oxygen at low pressures should be carried out to determine the exact transition frequencies, any shift of frequency with pressure, any dependence of the line breadth upon rotational state, and any anomalous dependence of the line breadth on pressure. We intend to carry on further researches along these lines in this laboratory. The data given above from an incomplete study of the absorption phenomena in oxygen and are presented at this time so that the material already at hand might be made available without further delay to those interested in the problem.

ACKNOWLEDGMENT

The authors would like to express their appreciation of several stimulating discussions with J. H. Van Vleck on the subject matter of this paper.

PHYSICAL REVIEW VOLUME 75, NUMBER 10 MAY 15, 1949

Radiations from Ge^{77} and Ge^{71} *

C. E. MANDEVILLE, Y. H. WOO,** M. V. SCHERB,*** W. B. KEIGHTON,**** AND E. SHAPIRO
Bartol Research Foundation of the Franklin Institute, Swarthmore, Pennsylvania

(Received February 10, 1949)

The 12-hour Ge^{77} was found to emit beta-rays of energy 1.74 Mev and γ-rays of 0.5 Mev. Beta-gamma-coincidences were measured in the 12-hour period. The 40-hour positron emitter is not formed by slow neutrons on germanium. The 11-day Ge^{71} decays with the emission of the x-rays of gallium following orbital electron capture. Previously obtained absorption curves have given evidence of emission of charged particles by the 11-day period. This misinterpretation is discussed.
See note added in proof.

INTRODUCTION

THE measurements of this paper were accumulated during 1948 and the early part of 1949 and resulted from the exposure of four different quantities of GeO_2 in the Oak Ridge pile. Two activities, 12 hours and 11 days, were found in the germanium fraction, and the 40-hour daughter of the 12-hour period was found in the arsenic fraction. Owing to the distance of the laboratory from Oak Ridge, observations were never begun at a time less than twenty hours after removal of the irradiated material from the pile. The third sample of GeO_2 was irradiated for only twelve hours so as to enhance the intensity of the shorter germanium period. The first, second, and fourth samples were exposed for longer but unspecified periods as indicated by the fact that the 11-day activity was several times more intense in each case than in the third sample. Chemical separations were carried out for the removal of Ni, Fe, Cu, Ag, Na, Ca, and Ga as possible impurities.

Ge^{77}

The 12-hour Ge^{77} was found to emit beta-rays and gamma-rays. An absorption measurement of the beta-rays carried out within twenty-five hours after removal of the irradiated material from the pile is plotted in Fig. 1. The end point occurs at 0.78 g/cm², 1.74 Mev as calculated by Feather's equation.[1] This value is to be compared with a K-U extrapolation of cloud-chamber data giving 1.9 Mev,[2] and an aluminum absorption measurement giving 2.0 Mev.[3] The activity of the irradiated GeO_2 was followed in a single Geiger counter, shielded by 0.26 g/cm² of absorber, including wall thickness of the counter. This absorber thickness excluded from the counting rate the beta-rays of the forty-hour As^{77} which emits no gamma-rays. The decay curve is shown in Fig. 2 where it is clear

* Assisted by the joint program of the ONR and the AEC.
** Guest physicist, Bartol Research Foundation, on leave of absence from National Central University and Academia Sinica, Nanking, China.
*** Now at Princeton University, Princeton, New Jersey.
**** Also of the Department of Chemistry, Swarthmore College, Swarthmore, Pennsylvania.

[1] N. Feather, Proc. Camb. Phil. Soc. 34, 599 (1938).
[2] R. Sagane, G. Miyamoto, and M. Ikawa, Phys. Rev. 59, 904 (1941).
[3] E. P. Steinberg and D. W. Engelkemeir, Plutonium Project Report, "*Nuclei formed in fission*," Rev. Mod. Phys. 18, 513 (1946).

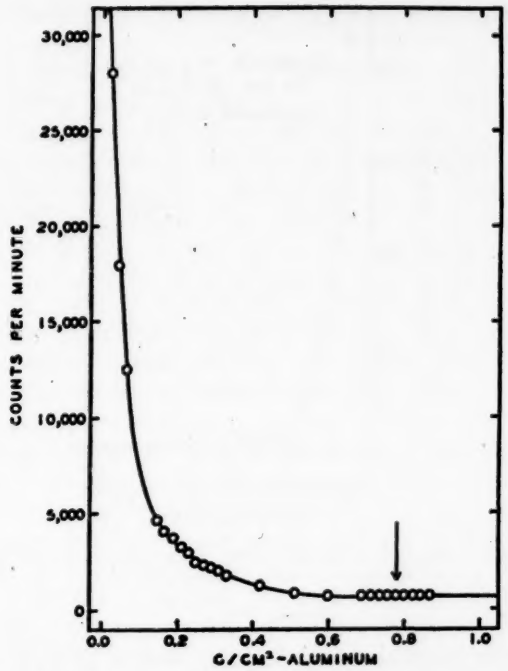

FIG. 1. Absorption in aluminum of the hard beta-rays of Ge^{77}. The end point corresponds to an energy of 1.74 Mev.

that only two periods, twelve hours and eleven days are present. No effects were observed from the 1.2-Mev positrons and accompanying annihilation radiation of the 40-hour Ge^{69}. This is consistent with the conclusion of McCown, Woodward, and Pool[4] that the 40-hour Ge^{69} is not produced by deuteron bombardment of germanium.

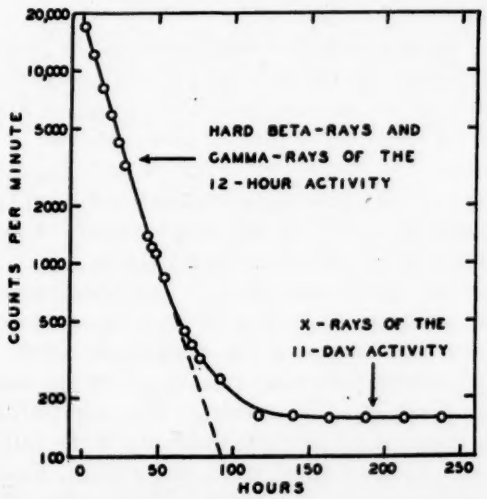

FIG. 2. Decay of the 12-hour Ge^{77}. The counter was shielded by 0.26 g/cm² of aluminum so as to suppress any effects from As^{77}. This decay curve shows that the 1.2-Mev positron emitter of 40-hour half-period is not formed by slow neutrons on germanium.

[4] D. A. McCown, L. L. Woodward, and M. L. Pool, Phys. Rev. 74, 1311 (1948).

The beta-gamma-coincidence rate of the 12-hour Ge^{77} is given in Fig. 3 as a function of the surface density of aluminum placed before the beta-ray counter. It is seen to rise from a relatively low value at zero absorber thickness to 0.3×10^{-3} coincidence per beta-ray at an absorber thickness of about 100 mg/cm² and remains constant thereafter. The reduced coincidence rate below 100 mg/cm² is attributed to the presence of the x-rays of the 11-day Ge^{71} and the nuclear beta-rays of As^{77}. The beta-rays of As^{77} actually have a range of 0.192 g/cm² in aluminum, but at the time of the beta-gamma-coincidence measurements, the number of As^{77} beta-rays having a range in excess of 100 mg/cm² was small as compared with the number of hard beta-rays of Ge^{77} present. The coincidences per minute were observed to decay with the 12-hour half-period of Ge^{77} at all points along the curve, showing that the beta-rays of As^{77} are non-coincident with any gamma-radiation. The gamma-ray counter of the beta-gamma-coincidence counting arrangement was calibrated by the beta-gamma-coincidence rate of Sc^{46} (2 Mev of de-excitation energy). This calibration showed that the beta-gamma-coincidence rate of 0.3×10^{-3} coincidence per beta-ray beyond 100 mg/cm² corresponds to a de-excitation energy of 0.5 Mev; that is, the hard beta-rays of Ge^{77} lead to an excited state 0.5 Mev above the ground state of the As^{77} nucleus. When the gamma-rays of Ge^{77} were absorbed in lead, an energy of 0.5 Mev was obtained, in agreement with the value predicted by the coincidence rate.

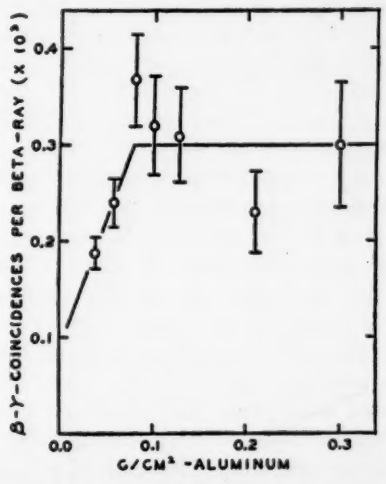

FIG. 3. The beta-gamma-coincidence rate of the 12-hour Ge^{77} as a function of the surface density of aluminum placed before the beta-ray counter. The coincidence rate below 100 mg/cm² is reduced owing to the presence of the beta-rays of As^{77} and the x-rays of Ge^{71}. Beyond 100 mg/cm², the beta-gamma-coincidence rate indicates that the hard beta-rays of Ge^{77} are followed by 0.5 Mev of gamma-ray energy.

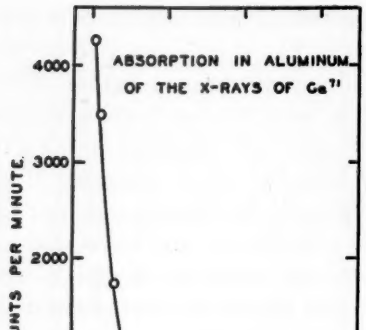

FIG. 4(a). Absorption in aluminum of the x-rays of Ge^{71}. The similarity of this curve to that of Fig. 4(b) led to an early misinterpretation of the data.

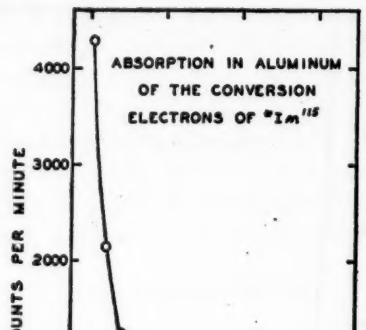

FIG. 4(b). Absorption in aluminum of the conversion electrons of the 4-hour isomer of indium (115).

Ge^{71}

The 11-day Ge^{71} was first reported by Seaborg, Livingood, and Friedlander,[5] who found the radiation to consist primarily of charged particles having an energy of 0.6 Mev. As stated by them, it seemed plausible that these were conversion electrons following K electron capture. Negatron emission by Ge^{71} was excluded by the fact that there exists no stable As^{71}. In the course of studying the radiations of the first three quantities of GeO_2, the absorption curve of Fig. 4(a) was obtained. On comparing its shape with those of some thirty-five nuclear beta-ray spectra having end points ranging from 0.15 to 2.22 Mev, it was concluded that the curve of 4(a) could not be that of a nuclear beta-ray spectrum. On the other hand, the curve shape was almost identical with that of the 0.338-Mev[6] conversion electrons of $*In^{115}$, shown in Fig. 4(b). The two curves strongly resemble each other in shape, half-value thickness, and extrapolated end point. It was concluded that the radiation of Ge^{71} was indeed conversion electrons following K electron capture. This view was strengthened when coincidences between the supposed conversion electrons and x-rays were noted. To ascertain whether the x-rays were from the gallium residual nucleus, 150 mg of aluminum were placed before the source to exclude the supposed conversion electrons, and critical absorption measurements were carried out on the residual x-ray activity. The radiation was much more heavily absorbed in copper than in zinc. This would be characteristic of the gallium $K\alpha$-line. The picture seemed fairly logical, and a preliminary abstract of these conclusions was given.[7]

Neither the writers nor Seaborg, Livingood, and Friedlander could dectect any gamma-radiation. This suggested that the supposed gamma-ray was very nearly totally converted. This feature could not be explained by a $0 \rightarrow 0$ transition, because the ground state of the Ga^{71} residual nucleus has a spin of $\frac{3}{2}$. A search was made for an isomeric state of the Ga^{71} residual nucleus, but measurements carried out within 20 minutes after the germanium-gallium separation showed no activity in the gallium fraction.

Since no satisfactory explanation of the conversion coefficient of the supposed converted gamma-ray was reached, it was decided to prepare a fourth unit of Ge^{71} and make further observations. In the meantime, the paper by Pool *et al.*[4] appeared, reporting no charged particles whatever from Ge^{71}. This conclusion was reached from a study of decay curves and cloud-chamber observations.

After the fourth unit of Ge^{71} had been properly aged to avoid any 12-hour or 40-hour effects the critical absorption curves of Fig. 5 were obtained. The zinc and copper foils were placed before the source with no aluminum intervening. The rapid absorption in copper can be explained only if the bulk of the radiation is assumed to be the gallium $K\alpha$-line. This confirms the conclusion of the Ohio State University group that only K capture x-rays are emitted by the 11-day Ge^{71}. The previously reported "conversion electron-(x-ray)" coincidences[7] were

[5] G. T. Seaborg, J. J. Livingood, and G. Friedlander, Phys. Rev. **59**, 320 (1941).
[6] J. L. Lawson and J. M. Cork, Phys. Rev. **57**, 982 (1940).
[7] Woo, Mandeville, Scherb, and Keighton, Bull. Am. Phys. Soc. **24**, No. 1, 13 (1949).

actually (x-ray)—(x-ray) coincidences as might be expected.†

If the curve of 4(a) is treated as that of a nuclear beta-ray spectrum, the end point could reasonably occur near 0.2 g/cm² or about 0.6 Mev as it appeared to Seaborg, Livingood, and Friedlander.††

Note added in proof: Shortly after the writers submitted this paper for publication, they became aware of the study of the radiations of Ge^{71} made by L. Seren, H. N. Friedlander, and S. H. Turkel, Phys. Rev. **72**, 888 (1947). Those authors describe in the fine print of Table III of their paper critical absorption measurements identical with those of the present report, which show that only the x-rays of gallium are emitted by Ge^{71}. They also state specifically that no electrons or beta-rays are to be found in the radiations of Ge^{71} so that the only mode of decay is that of orbital electron capture. These data are apparently also contained in a restricted version of the work of Seren *et al.* which is referred to in connection with Ge^{71} in the recent isotopic table compiled by Seaborg and Perlman.

APPENDIX: CHEMICAL PROCEDURE FOR THE SEPARATION OF GERMANIUM AND ARSENIC AND THE PURIFICATION OF THE GERMANIUM FRACTION

Germanium oxide from the pile was fused with K_2CO_3 and Na_2CO_3 in a nickel crucible, and the melt was dissolved in cold H_2O. After filtering out insoluble material, 50 mg of As_2O_3, dissolved in K_2CO_3 solution, was added as a carrier. To the solution was added one-half volume of 48 percent hydrofluoric acid. The new solution was then saturated with H_2S to precipitate the arsenic. The As_2O_3 precipitate was washed with 16 percent hydrofluoric acid and with water. It was dissolved in ammonium hydroxide and several drops of H_2O_2, diluted with water, made 6 normal with HCl and again precipitated with H_2S. The precipitate was washed with water, hydrofluoric acid, water, alcohol, and dried.

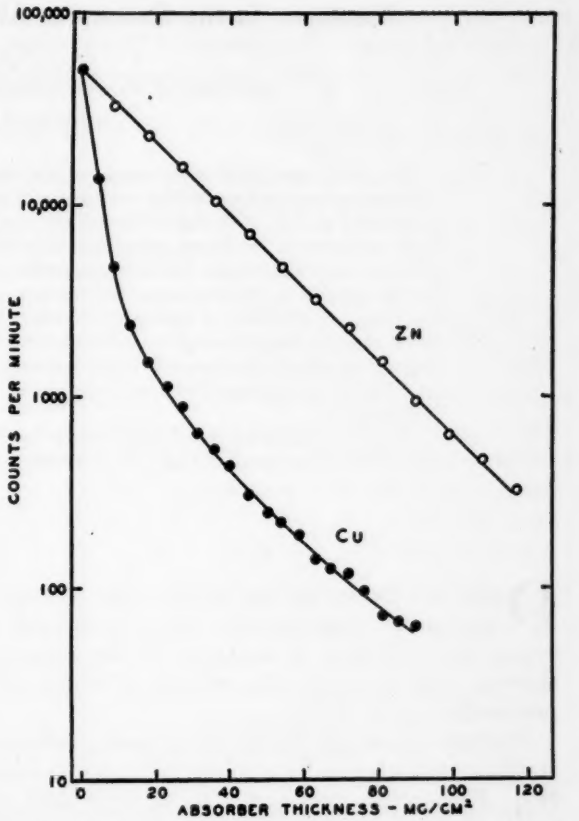

FIG. 5. Critical absorption of the x-rays of the 11-day Ge^{71}. The heavy absorption in copper indicates that most of the radiation is the gallium $K\alpha$-line.

The filtrate containing germanium was evaporated, after adding H_2SO_4 to expel the hydrofluoric acid. The residue was dissolved in water, and the acid concentration was adjusted to 25 percent free H_2SO_4. GeS_2 was precipitated with H_2S, washed with water, dissolved in hot $(NH_4)_2S$ and filtered. After adding H_2O_2 the solution was evaporated, the residue moistened with H_2SO_4, heated to expel $(NH_4)_2SO_4$ and free acid, and ignited to GeO_2. The procedure followed should have removed Ni, Fe, Cu, Ag, Ca, and Na from the GeO_2.

† Thought to be "K–L" coincidences.

†† L. C. Miller and L. F. Curtiss, Phys. Rev. **70**, 983 (1946), report 0.6 Mev beta-rays and 0.5 Mev gamma-rays as the radiations of the 11-day Ge^{71}. It seems probable that they have incorrectly assigned the beta-rays of As^{77} and the gamma-rays of Ge^{77} to Ge^{71}.

Neutrons in the Extensive Air Showers of the Cosmic Radiation

VANNA COCCONI TONGIORGI
Laboratory of Nuclear Studies, Cornell University, Ithaca, New York
(Received February 7, 1949)

Neutrons associated with extensive air showers have been studied by recording delayed coincidences among Geiger-Müller counters and proportional BF_3 counters. The experiments have been performed at 260, 3260 and 4300 m above sea level. It has been shown that in the extensive showers both neutrons of moderate energies and radiations capable of producing such neutrons are present. The number of neutrons and neutron-producers in showers of different sizes is roughly proportional to the number of the electrons. The neutron-producers cannot be, at least in a large fraction, either electrons, or photons, or μ-mesons. Nuclear interactions induced by fast neutrons and protons are consequently thought to give the main contribution to the neutron production observed. The total neutron-producing-radiation is of the order of 2–3 percent of the electronic component of the showers at 3260 m. Its altitude variation is consistent with the assumption that nucleons constitute its main component.

The multiplicity of the neutron production in lead is very high: ~60 neutrons of energies between 2 and 15 Mev are produced at a time on the average.

I.

DURING the spring and the summer of 1948, a group of experiments were performed to prove the existence of neutrons in the extensive showers and to study the process in which their production takes place.

Preliminary measurements have been made practically at sea level (Ithaca, New York, 260 m elevation, barometric pressure 1007 g/cm²) and the results have been reported in two Letters to the Editor.[1,2] The existence in the showers of neutrons of energies smaller than 10–15 Mev was demonstrated and evidence was obtained of their being produced mostly by a penetrating radiation. Yet, as the frequencies of the phenomena we were dealing with are very low at sea level, a confirmation of these results seemed very desirable.

Further experiments have been performed part at Echo Lake, Colorado (3260 m elevation, barometric pressure 708 g/cm²) and part on the top of Mt. Evans, Colorado (4300 m, barometric pressure 616 g/cm²).

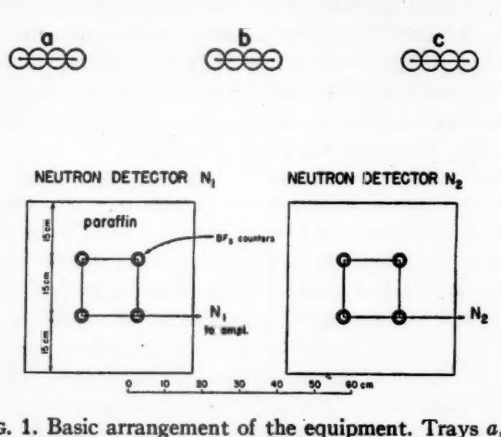

FIG. 1. Basic arrangement of the equipment. Trays *a*, *b*, *c* select extensive showers; the BF_3 counters embedded in paraffin detect neutrons.

Besides confirming the results obtained at sea level, an aim of these experiments was to study the distribution of neutrons in the showers and to get further information about the nature of the neutron-producer-radiation.

II. EXPERIMENTAL ARRANGEMENT

For all the measurements, the experimental procedure was in principle the same as that briefly described in reference 1. The basic arrangement of the equipment is drawn in Fig. 1.

Three trays of G-M counters, *a*, *b* and *c*, were placed in a horizontal plane at the vertices of a triangle of 3–4-meter side. The counters were always kept at constant temperature. Extensive air showers were recorded by concidences $S=a+b+c$, with a resolving time of 10 μsec.

The neutron detectors used consisted of paraffin blocks in which BF_3 proportional counters were placed. Two identical detectors, N_1 and N_2, were used, each built as follows: in a wooden box ($45\times50\times45$ cm³) paraffin was cast in a solid block, leaving four cylindrical holes barely containing the neutron counters. The box was completely covered by aluminum foil, which provided an electrical shield for the counters and constituted on the front and back sides of the box, two shielded compartments, in which the pieces of equipment that had to be close to the counters were placed (cathode followers, filters on the high voltage supply to the counters, etc.).

The construction of the neutron counters is shown in Fig. 2. Brass tubing of 2.5 cm diameter, 0.5-mm walls, was used. The central wire was tungsten, 0.1 mm diameter, 46-cm effective length. The arrangement of Kovar seals at both ends of the counters, shown in the figure, provided the wire

[1] V. Tongiorgi Cocconi, Phys. Rev. **73**, 923 (1948).
[2] V. Tongiorgi Cocconi, Phys. Rev. **74**, 226 (1948).

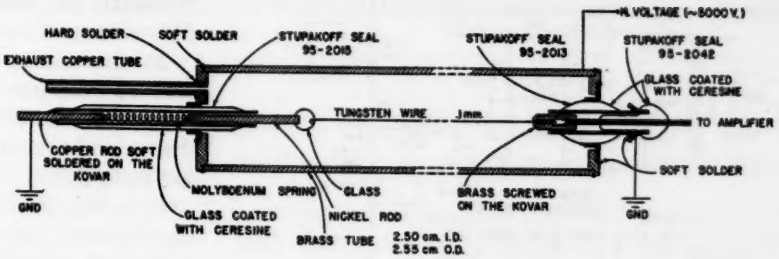

FIG. 2. Construction of the neutron counters.

with guard rings. This was particularly important, as the counters were designed to work at quite high voltage (5000 volts).

We noticed that dust or humidity could produce discharges along the surface of the Kovar seals. All the glass portions, therefore, after careful cleaning, were covered with ceresine. This arrangement worked very satisfactorily all the time.

Solid complex boron trifluoride—calcium fluoride ($BF_3 \cdot CaF_2$), the boron being enriched in B^{10}, was obtained from the Oak Ridge Laboratory. By heating it above 260°C in vacuum, the boron trifluoride is released as a gas, 96 percent of which is $B^{10}F_3$.

The gas was purified first in a NaF cell cooled down in dry ice, the NaF having been outgassed by heating it at 200°C. Further purification was obtained by freezing the gas in a liquid air trap and pumping the residues out. The operation of freezing and defreezing was repeated several times.*

In order to have good efficiency we chose to fill our counters at rather high pressure; 1.5 atmos. BF_3 plus 0.3 atmos. argon were put in. The argon was added to lower the thresholds.

The efficiency η of our counters, i.e. the probability of recording a slow neutron crossing the counter along a path of average length (the average length across the counter is the diameter), was calculated with the formula

$$\eta = 1 - e^{-pL\sigma d},$$

where p = pressure of BF_3 in atmos., L = Löschmidt's number, σ = cross sections for $(n,\alpha)B^{10}$ reaction, d = diameter of the counter. It was found to be: $\eta \approx 0.3$.

In our filling system 12 counters could be filled at a time on a manifold. The counters filled together always showed very similar behavior. With the amplifier gains used in the course of the experiments, they had neutron thresholds close to 4500 volts, operating voltages around 5000 volts with plateaus of 200–300 volts and Geiger thresholds around 5500 volts.

A typical counting rate *versus* voltage curve at fixed gain is drawn in Fig. 3.

High voltage up to 6000 volts was supplied to the counters by a voltage doubler rectifier, the output of which was regulated by a 6C6 pentode, as shown in Fig. 4. The fluctuations of the output were ~3 percent of the percent fluctuations of the a.c. line, i.e., smaller than ±15 volts for variations of the a.c. line (115 volts) of ±10 volts. At Ithaca, where the variations of the a.c. line are often larger than ±10 volts, a magnetized iron regulator was used at the input of the rectifier.

The arrangement of several counters in parallel inside the paraffin was always used in order to improve the geometrical efficiency of the system, that is the probability that a neutron entering the paraffin reaches the counters.

The block diagram of the recording circuit is shown in Fig. 5. The pulses from the two neutron detectors N_1 and N_2 were fed, through cathode followers and coax cables, into Mod. 100 amplifiers, then into pulse discriminators and blocking oscillators (pulse width at the output 1.5 μsec.). These pulses were then put in coincidence, through crystal diodes, with the coincidences $S=a+b+c$ delayed by 7 μsec. and shaped in a square pulse ~160 μsec. wide. Delayed coincidences $S+N_1$ and $S+N_2$ were recorded, as well as coincidences $S+N_1+N_2$ and showers S. The delay was introduced in order to remove the background due to slow protons, stars, bunches of electrons, etc., which could strike the proportional counters when an extensive shower occurs. The neutrons lost because of this delay are

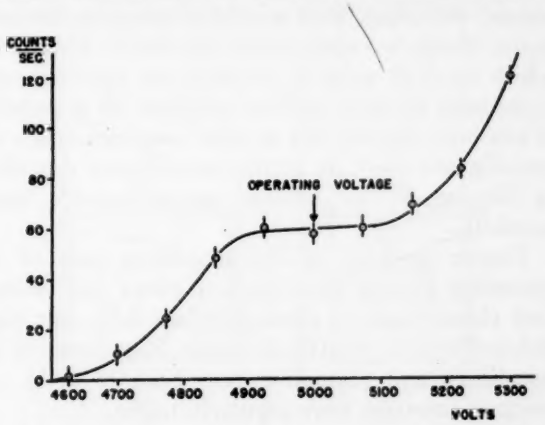

FIG. 3. Counting rate *versus* voltage at fixed gain for the BF_3 proportional counters.

* We are indebted to Mr. J. Bistline for suggesting this technique and filling some of our counters.

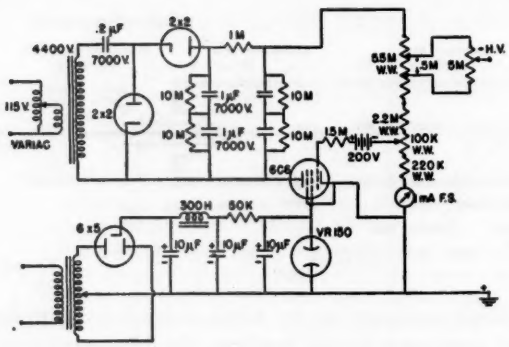

FIG. 4. Diagram of the high voltage regulated power supply for the BF_3 counters.

negligible (a few percent), owing to the large lifetime of such particles in the detector.

Several runs with Cd-shields (0.75 mm thick) around the neutron counters always gave zero background for the coincidences $S+N_1$, $S+N_2$ and $S+N_1+N_2$.

The duration of the square pulse, hence the resolving time, of the coincidences $S+N_1$ and $S+N_2$ (160 μsec.) is comparable with the lifetime of the neutrons in the system of paraffin and BF_3 constituting the detector. A larger gate would give higher probability of recording neutrons associated with the showers, but would introduce an undesirable larger fraction of chance coincidences.

In the following sections we shall always call efficiency of the apparatus to record coincidences $S+N$, the over-all efficiency ϵ, which results from the product of the efficiency η of the neutron counters to record slow neutrons, times the probability α that a neutron falling on the paraffin is slowed down and reaches the counters, times the efficiency k of the coincidence circuit, depending on the introduced delay and on the resolving time of the coincidences. We calculated $\eta=0.3$ and $k=0.7$ and we tried to determine α by measuring the efficiency of our detector for a (Ra+Be) neutron source. We think that $\alpha=0.1$ is a reasonable estimate. Hence we have $\epsilon=\eta\cdot\alpha\cdot k\simeq 0.02$. This value which we shall write ϵ_4, refers to the basic arrangement with the four neutron counters all in parallel. When only the two left or right counters inside the paraffin are used, as in the experiments described in Section V, we assume $\alpha_2=\alpha/2=0.05$, hence $\epsilon_2=0.01$.

Proper working of the amplifiers and of the recording circuit was checked every day with a test circuit built to provide pulses 0.01 volt high, delayed by 0, 3, 10, 100, 200 μsec. Bias curves of the amplifiers and plateau curves both of G-M and neutron counters were regularly taken.

The whole apparatus was placed at Ithaca in an annex covered by a roof of few g/cm² of light material; at Echo Lake in a wooden shack; at Mt. Evans it was arranged inside a large truck.

In the course of the experiments different absorbers were put around one or both of the neutron detectors. In Fig. 6 the arrangements used are drawn and the nature and thickness of the absorbers are indicated.

It is important to keep in mind that in all our experiments, the neutrons recorded are particles of moderate energies. The energy range explored depends, of course, on the amount of paraffin surrounding the BF_3 counters; neutrons of too high energy are not slowed down, while neutrons of too low energy are brought to rest before reaching the counters. We think that the lower and upper energy limits of our detector (arrangement I) lie roughly around 2 and 15 Mev, respectively.

III. LOCAL PRODUCTION OF NEUTRONS IN ASSOCIATION WITH EXTENSIVE SHOWERS

At Echo Lake measurements have been taken with the neutron detector N_1 successively put in arrangements I, II, III, IV (Fig. 6), while detector N_2 was kept always in arrangement I for sake of comparison and test of proper working of the whole apparatus.

Trays a, b, c selecting extensive showers had effective surface $s=2000$ cm². The average rate of the showers recorded, corrected for chance coincidences, was 570 h^{-1}.

The recorded rates (h^{-1}) of $S+N_1$ are collected in Table I. All the results, in this table and in the following ones, are corrected for chance coincidences, and standard errors are indicated. The correction for chance coincidence is roughly 17 percent of the observed rates for arrangements I and III, ~8 percent for II and IV.

The comparison of rates I and II, as well as of rates III and IV, gives evidence of a strong production in the absorber Σ (2″ lead) of neutrons genetically correlated with some component of the extensive showers.

Further measurements have been taken in arrangement IV with the 2″ lead replaced by 2″ iron and 2″ carbon (graphite). The results are in Table

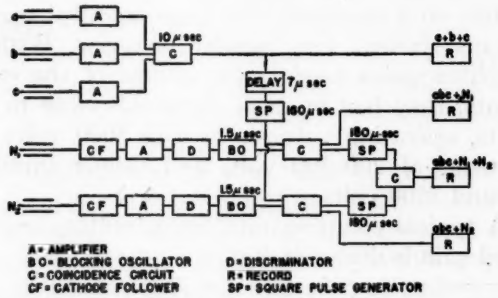

FIG. 5. Block diagram of the recording circuit.

TABLE I. Coincidence rates for arrangements I, II, III, and IV.

Arrangement	I	II	III	IV
$S+N_1(h^{-1})$	0.500±0.028	3.48±0.24	0.367±0.043	2.97±0.23

II. Table II shows that local production of neutrons in association with extensive showers takes place in all absorbers. The yield per g/cm² is 0.046 h^{-1} in lead, 0.026 h^{-1} in iron and 0.020 h^{-1} in carbon. If neutron production is observed in C, it is reasonable to assume that neutrons are produced also in air, while the shower is traveling through the atmosphere.

Hence we conclude that *in the extensive showers neutrons are present, as well as a radiation capable of producing them.*

IV. ORIGIN OF NEUTRONS ASSOCIATED WITH EXTENSIVE SHOWERS

The results of Section III raise the question of which is the radiation chiefly responsible for the production of the observed neutrons. The photons present in the extensive showers may generate neutrons through (γ, n) reactions. Recent experiments[3] have shown that the yields of (γ, n) reactions are very large in nuclei with large Z.

Furthermore, neutrons may be produced by nuclear evaporations or other processes induced by particles interacting with nuclei. Neutrons have actually been observed in association with μ-mesons stopped in heavy materials.[4] π-mesons are known to undergo capture by nuclei, giving rise to nuclear evaporations. Fast neutrons and protons are thought to be able to produce stars and penetrating showers, in which neutrons of moderate energies originate.[5] To get information on this problem, measurements have been made at Echo Lake with the neutron detector N_1 put also in arrangements V and VI, the extensive showers being always recorded by counters of 2000 cm² area.

Essentially the same series of arrangements, I, II, III, IV, V, VI had previously been run at Ithaca.

In order to facilitate both the comparison with those preliminary results reported in reference 2 and the discussion of the present data, the rates $S+N_1$ obtained at Ithaca and at Echo Lake in all six arrangements are collected in Table III.

The two series at Ithaca and at Echo Lake show the same general behavior. The results at Ithaca have extremely large statistical uncertainty and the

TABLE II. Coincidence rates for arrangement IV with various absorbers.

Σ	0	2″ C 8 g/cm²	2″ Fe 39 g/cm²	2″ Pb 56 g/cm²
$S+N_1(h^{-1})$	0.367±0.043	0.53±0.068	1.38±0.12	2.97±0.23

arrangement of the absorbers was not quite identical with that in the series run at Echo Lake, so that we do not think that a comparison of the details at the two stations is highly reliable. In the following we shall base the discussion on the series obtained at Echo Lake.

First, by comparing the difference between arrangements I and II with that between arrangements III and V it appears that the neutrons locally produced in lead do not have, in the great majority, energies large enough to reach the detector, when the paraffin B is added to it; this means energies not larger than 10–20 Mev.

Furthermore, as the two rates IV and VI are the same, within the statistical errors, while rate V is almost six times lower and comparable with rate II, the experiments show that the production of the neutrons recorded with arrangement VI takes place essentially in the lead Σ, not in Σ′, and that the neutron-producer-radiation can cross the 7.5 cm Pb constituting Σ′, without being strongly absorbed.

Since the electrons and photons constituting the soft component of the extensive showers are reduced in such an absorber to ~10 percent of their initial intensities, we think that the observed behavior

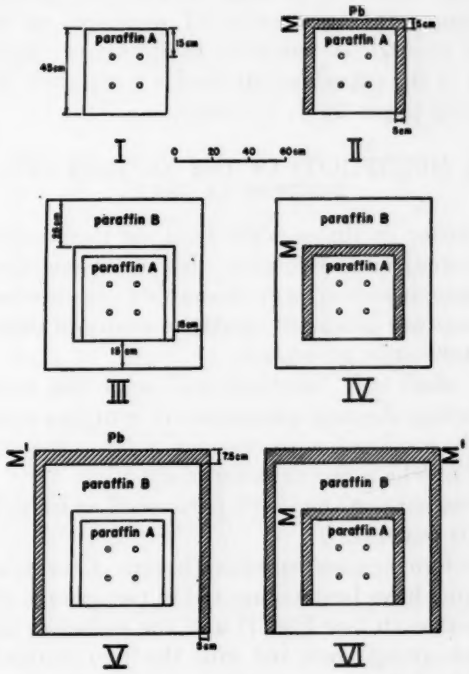

FIG. 6. Arrangements of absorbers around the neutron detectors in various experiments.

[3] M. L. Perlman and G. Friedlander, Phys. Rev. **74**, 442 (1948).
[4] R. D. Sard, W. B. Ittner, A. M. Conforto, and M. F. Crouch, Phys. Rev. **74**, 97 (1948); G. Groetzinger and G. W. McClure, Phys. Rev. **74**, 341 (1948).
[5] G. Cocconi, V. Cocconi Tongiori, and K. Greisen, Phys. Rev. **74**, 1867 (1948).

TABLE III. Coincidence rates $S+N_1$ at Ithaca and at Echo Lake.

	Station \ Arrangement	I	II	III	IV	V	VI
$S+N_1$	Ithaca	0.119±0.008	0.278±0.050	0.017±0.008	0.198±0.040	0.023±0.012	0.199±0.040
(h^{-1})	Echo Lake	0.500±0.028	3.48 ±0.24	0.367±0.043	2.97 ±0.23	0.584±0.090	3.39 ±0.25

cannot be explained on the basis of neutron production only through (γ, n) reactions. It is reasonable to assume that processes of this kind occur, but their contribution to the observed neutrons, though probably not negligible, is certainly not the predominant one. In order to justify the experimental results IV and VI one is led to think that the absorption of the electrons and photons in the lead Σ' happens to be roughly compensated by multiplication in the same lead of some other radiation, which is the means principally responsible for production of neutrons; furthermore, also a small tail of the neutrons produced in Σ' may contribute to rate VI.

Hence, the conclusion is reached that *neutrons associated with extensive showers are generated, in a large fraction, by radiation different from electrons and photons, with rather high penetration in lead.*

We consider this point as the basis for the interpretation and the discussion of all our further experiments.

We think that too little is known about the cross sections for (γ, n) reactions, as well as about the nature, intensity and behavior of the radiations different from electrons and photons present in the extensive showers, to hope to solve the problems concerning the production of neutrons on theoretical ground. A tentative quantitative interpretation of the experimental results is reported in the following paper by J. Levinger.

V. MULTIPLICITY OF THE NEUTRON PRODUCTION IN LEAD

In order to throw some light on the process in which neutrons associated with extensive showers originate, it seemed very desirable to know whether neutrons are produced singly, or many of them are simultaneously generated.

We shall call "multiplicity" ν of the neutron production the average number of neutrons simultaneously produced with energies lying in the energy range to which our detector is sensitive.

An experiment has been performed at Echo Lake for this purpose.

The four neutron counters in one of the neutron detectors have been connected in two groups of two counters each (see Fig. 7) and the pulses n_1 and n_2 of each group were fed into the two channels of cathode followers, amplifiers, etc., described in Section II.

The over-all efficiency of the system (paraffin+2 counters) is estimated to be $\epsilon_2=0.01$, as explained in Section II.

Extensive showers $S=a+b+c$ were always recorded by G-M counters of area $s=2000$ cm². Their rate was 570 h^{-1}.

Coincidences $S+n_1$, $S+n_2$ and $S+n_1+n_2$ were recorded, once in arrangement III, once in arrangement IV. The average $S+n$ of the rates $S+n_1$, and $S+n_2$, and the rate $S+n_1+n_2$ are reported in Table IV for both arranements, as well as the difference IV–III. This difference is thought to be independent of the contributions due both to neutrons present in the showers before reaching the detector, and to neutrons produced in the paraffin; in other words, it refers only to neutrons produced in the lead Σ. The correction for chance coincidences was 17 percent of the recorded rate $S+n$ in arrangement III, 6 percent in arrangement IV. Chance coincidences $S+n_1+n_2$ were negligible.

With the assumption that the neutrons emitted from a nucleus are isotropically distributed, one may write:

$$\frac{S+n_1+n_2}{S+n}=1-\exp[-(\nu-1)\cdot\epsilon_2\cdot\omega/4\pi]. \quad (1)$$

where ω is the solid angle subtended by the detector at the absorber.
From the data IV–III one gets:

$$(\nu-1)\epsilon_2\cdot\omega/4\pi=0.20. \quad (2)$$

By introducing $\epsilon_2=0.01$ and $\omega/4\pi=0.3$, the multiplicity in lead is found to be of the order of magnitude of 60.

The question arises whether a single primary particle is responsible for the production of all those neutrons, or several neutron-producers fall simultaneously on the lead and generate each a few neutrons.

We think that the first hypothesis receives a strong support by the following argument. Since the area s' of the neutron detector ($s'=2250$ cm²) is practically equal to the area $s=2000$ cm² of the

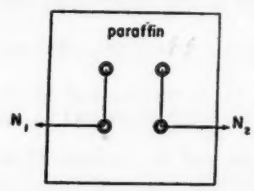

FIG. 7. Arrangement of the neutron detector for investigating the multiplicity of the neutron production.

counters a, b and c recording the extensive showers, the number of electrons and photons falling on s', when a shower is recorded, has a low probability of being larger than one or two.

As it was shown in Section IV, the neutron-producer-radiation does not belong in a large fraction to the electron component, which constitutes more than 97 percent of the ionizing particles in the extensive showers.

Now, if only one or few electrons can fall in the average on s' when a shower occurs, certainly not more than one ionizing neutron-producer can strike the lead Σ. As for the non-ionizing particles (fast neutrons) which could also produce neutrons, no direct information is available. But evidence has been obtained (see Section VII) that the *total* neutron-producer-radiation does not represent more than a few percent of the electron component. Hence, the conclusion is reached that the high number of neutrons simultaneously observed under lead have great probability of arising from a process originated by a *single* particle. It is difficult to think of such a large number of neutrons coming out from a single nucleus. Many nuclei have probably to be excited and simultaneously evaporated.

A likely picture is that a single heavy particle makes a nuclear disintegration in which not only neutrons are produced, but also protons and π-mesons. All of those secondaries have the possibility of causing further nuclear disintegrations, hence further neutron production, either in the lead or in the large block of paraffin.

It may be noted that it is particularly hard to account for the high average multiplicity observed, if the neutron production is by γ-rays. Even if several γ-rays strike the apparatus each time a neutron is recorded, one is forced to consider cross sections for reactions such as (γ, qn) with $q=5$ or more, which are very small compared with the (γ, n) cross sections.

We want to recall that a very high multiplicity has been obtained[5] also for the neutrons associated with *penetrating* showers locally generated in lead. In that case it is known that the originating particles are not photons, because the local penetrating showers were not associated with extensive air showers, and the primaries were absorbed more strongly in carbon than in lead.

The experiment with arrangement III gives $\nu \approx 1$ for the neutron production in paraffin. The statistical uncertainly in the results is, however, very large.

VI. NEUTRONS AND NEUTRON PRODUCERS IN SHOWERS OF DIFFERENT DENSITIES

On the basis of the experiments described in Section III, the extensive showers are thought to contain both neutrons of moderate energies produced in the air and radiation capable of producing such neutrons in materials surrounding the detecting apparatus.

TABLE IV. Coincidences in arrangements III and IV.

Arrangement	$S+n$ (h^{-1})	$S+n_1+n_2$ (h^{-1})
III	0.172±0.073	0
IV	2.19 ±0.19	0.372±0.075
IV–III	2.018	0.372

A study was attempted of the intensity of the neutrons and of the neutron-producers in showers of different mean densities.

At Mt. Evans (4300 m) experiments have been performed with the neutron detector in arrangements I, III and IV, the extensive showers being recorded by counters of different surfaces in order to select showers of different mean-particle-densities. Counter areas $s=100$ cm², $s=500$ cm² and $s=2000$ cm² have been used. Since, in first approximation, a counter of area s records showers of mean density $\bar{\Delta} \approx 1/S$, we recorded showers having, in the average, 100, 20 and 5 particles/m², respectively.

In Table V the rates S and the rates $S+N_1$ for arrangement I and for the difference (IV–III) are collected. We shall discuss first the arrangement (IV–III), that selects essentially the events in which neutrons are locally produced in the lead Σ, and is therefore independent of neutron production in air, in paraffin B and in the detector.

Consider an extensive shower in which the density of the electron is Δ and the density of the neutron-producers is Δ_p. When the neutron-producers cross the thickness x of the absorber Σ in which their mean free path is λ, the density of neutron-producers *interacting* with the nuclei of the absorber is $\Delta_p(1-e^{-x/\lambda})$. In every interaction ν neutrons are produced on the average; if the efficiency of the neutron detector for each one of those neutrons is ϵ_4 and the solid angle subtended by the detector at the absorber is ω, the probability of recording such a neutron-shower is $(1-e^{-\nu\epsilon_4\cdot(\omega/4\pi)})$. If s' is the surface of the neutron-detector, the probability of detecting the neutron-producers, by recording the neutrons produced by them, is given by

$$\pi(N)=1-\exp(-\Delta_p(1-e^{-x/\lambda})(1-e^{-\nu\epsilon_4\cdot(\omega/4\pi)})\cdot s'). \quad (3)$$

The same extensive shower is recorded by the system of the three G-M counters a, b and c, whose area is s, with the probability

$$\pi(S)=(1-e^{-\Delta s})^3.$$

Hence, the probability of a coincidence $S+N$ is given by

$$\pi(S+N)=(1-e^{-\Delta s})^3 \times(1-\exp(-\Delta_p(1-e^{-x/\lambda})(1-e^{-\nu\epsilon_4\cdot(\omega/4\pi)})s')).$$

TABLE V. Coincidence rates $S+N_1$ in arrangement I and IV–III, in showers of different average density.

	1	2	3	4	5	6
			Arrangement I		Arrangement (IV–III)	
Surface s	S (h^{-1})	γ	$S+N_1$ (h^{-1})	R	$S+N_1$ (h^{-1})	R
100 cm²	16	1.40	0.286±0.086	0.00030±0.00009	0.89±0.22	0.00104±0.00026
500 cm²	126	1.35	0.68 ±0.13	0.00038±0.00007	2.53±0.51	0.00155±0.00032
2000 cm²	1010	1.30	1.20 ±0.14	0.00028±0.00004	6.16±1.14	0.00155±0.00029

Now we can proceed as follows: we assume that Δ_p is proportional to Δ in showers of different size, that is the ratio $\rho=\Delta_p/\Delta$ is a constant independent of the size of the showers. This implies that the differential density spectrum

$$g(\Delta)d\Delta=K\Delta^{-(\gamma+1)}d\Delta,$$

known to hold in first approximation for the electrons in the extensive showers, holds also for the neutron producers, with a different K, but with the same γ. Then formula (3) can be written

$$\pi(N)=1-\exp(-\rho\Delta(1-e^{-x/\lambda})(1-e^{-\nu\epsilon_4\cdot(\omega/4\pi)})\cdot s')=1-e^{-R\Delta s'}$$

with

$$R=\rho(1-e^{-x/\lambda})(1-e^{-\nu\epsilon_4\cdot(\omega/4\pi)}) \qquad (4)$$

and the counting rates S and $S+N$ can be related by the expression

$$\frac{S+N}{S}=\frac{\int_0^\infty \Delta^{-(\gamma+1)}(1-e^{-\Delta s})^3(1-e^{-R\Delta s'})d\Delta}{\int_0^\infty \Delta^{-(\gamma+1)}(1-e^{-\Delta s})^3 d\Delta}. \qquad (5)$$

From the experimental data, R can be calculated. If the assumption of proportionality of Δ_p to Δ is correct, the same R must be found for showers of different mean densities.

From the data of columns 1 and 5 of Table V, by using formula (5), the values R reported in column 6 have been deduced. For s' we have used the top area 45×50 cm² of the paraffin block of the detector; for γ, we introduced the values indicated in column 2, which are deduced from other experiments[6] performed this summer.

As column 6 shows, R is constant, within the statistical errors, while the mean electron density varies by a factor ~20. Hence we are led to conclude that on the average, the density of neutron producers in extensive showers is roughly proportional to the density of the electrons in the showers. Probably both neutron producers and electrons are proportional in number, roughly, to the energy of the primary particle that generates the shower.

This result, of course, is deduced with the hypotheses that both the multiplicity ν of the neutron production and the efficiency ϵ_4 of the detector (i.e. the average neutron energy) are fixed quantities for all showers. Such an assumption seems necessary for lack of any information.

Consider now arrangement I. The values of R deduced from the data of columns 1 and 3 with formula (5) are collected in column 4. They are constant within the statistical errors. Arrangement I is the most suitable to give information about neutrons associated with extensive showers, present in a shower before it reaches the detecting apparatus, though the contribution due to neutrons generated in the materials constituting the detector is probably far from being negligible.

On the basis of the constancy of R, we can deduce that, at least in first approximation, also the neutrons present in a shower developing in the air are proportional in number to the electrons of the shower. If one assumes that the local production of neutrons in the detector is negligible, formula (4) can be written

$$R=\rho_n(1-e^{-\epsilon_4})$$

by introducing $\nu=1$, $\omega/4\pi=1$ and putting $\rho_n=\rho(1-e^{-x/\lambda})$; with $R=0.00032$ and $\epsilon_4=0.02$, one finds: $\rho_n=\sim 0.016$, that is the density in air of neutrons with energies between 2 and 15 Mev, belonging to an extensive shower, is of the order of 1–2 percent of the average electron density in the same shower.

VII. TENTATIVE DEDUCTION OF THE RATIO NEUTRON-PRODUCERS/ELECTRONS

From the value of R deduced from the difference of the rates $S+N_1$ obtained in arrangements IV and III (see Table V), the ratio ρ = neutron-producer-density/electron density could be calculated, provided that the absorption coefficient of the neutron producers in lead is known.

In fact, from formula (4) of Section VI one has

$$\rho=\frac{\Delta_p}{\Delta}=\frac{R}{(1-e^{-\nu\epsilon_4\cdot(\omega/4\pi)})}\cdot\frac{1}{(1-e^{-x/\lambda})}$$

where x thickness of Σ, is 56 g/cm². Also if ν and ϵ_4 are not well known, the product $\nu\epsilon_4$, better still the *average* of $(1-e^{-\nu\epsilon_4\cdot(\omega/4\pi)})$, is quite well known, since the experiment described in Section V gives the

[6] G. Cocconi and V. Cocconi Tongiorgi, Phys. Rev. 75, 1058 (1949).

average of $(1-e^{-(\gamma-1)\epsilon_2\cdot(\omega/4\pi)})$ and since the assumption $\epsilon_4=2\epsilon_2$ is surely good in first approximation. We have therefore, by using (2) in Section V, and the average of the values obtained for R in column 6 of Table V (Section VI):

$$\rho=\frac{0.0014}{1-e^{-0.42}}\cdot\frac{1}{(1-e^{-x/\lambda})}=0.0045\frac{1}{1-e^{-x/\lambda}}. \quad (6)$$

No information is available about the mean free path in lead of neutron producers.

Let us suppose that the neutron producers are the most penetrating particles present in the extensive showers, very likely μ-mesons, which are known to penetrate more than 7″ Pb with a mean free path $\lambda\approx 3000$ g/cm².[7] Then we should have $\rho\approx 0.23$; that is, the average density of the neutron producers should be ~23 percent of the density of the electrons in the showers. This is certainly not true, as the penetrating component of the extensive showers which has the characteristic described above, is only 1–2 percent of the electronic component.

Then, the great majority of the neutron-producers consist neither of the soft component (electrons and photons), nor of the very penetrating component (μ-mesons) of the extensive showers.

Nucleonic particles are consequently thought to be the particles able to generate a large fraction of the observed neutrons. For nucleonic particles a mean free path in lead of a few hundred g/cm² can be assumed. If we put in (6) $\lambda=300$ g/cm², we get $\rho\approx 0.026$ so that the neutron producers should roughly be 2–3 percent of the electrons in the showers, which is a reasonable order of magnitude. This figure is probably too high to be accounted for only with protons; one has to think of a large fraction of neutron-producers consisting of fast neutrons, which, however, is a very plausible hypothesis.

The presence of fast neutrons and protons in the extensive showers has never been experimentally proved, as far as we know, either in a direct or in an indirect way. We think that our results give rather reliable indirect evidence that fast neutrons and protons do exist in the extensive showers, in total number of the order of 2–3 percent of the number of electrons.

VIII. ALTITUDE VARIATION OF THE NEUTRON PRODUCERS

Coincidences $S+N$ for arrangements III and IV have been measured at Ithaca (260 m), Echo Lake (3260 m) and Mt. Evans (4300 m), always with extensive showers recorded by counters of area $s=2000$ cm².

The rates $(S+N)$ for the difference IV–III, which refers to neutrons locally generated in Σ, as well as the rates S of the showers at the three stations are reported in Table VI. The values of R have been calculated by using formula (5) of Section VI, with the values of γ indicated in the table. As the data show, the extensive shower rates are reduced by a factor 11.4 between 260 m and 3260 m, and by a factor 1.7 between 3260 m and 4300 m. The showers recorded at 260 m with average electron density Δ are those that at 3260 m had average density Δ' such that $(\Delta'/\Delta)^{\gamma}=11.4$ (where $\gamma=1.35$ is the exponent of the density spectrum of the extensive showers) and at 4300 m had average density Δ'' such that $(\Delta''/\Delta)^{\gamma}=1.7$. Hence the average density of the electrons is reduced by a factor $(1.7)^{1/\gamma}\simeq 1.5$ from Mt. Evans to Echo Lake and by a factor $(11.4)^{1/\gamma}\simeq 5$ from Echo Lake to Ithaca. This means by a factor ~7.5 from 260 m to 4300 m altitude.

TABLE VI. Rates of extensive showers S and of coincidences $S+N$ at different elevations above sea level.

	S (h^{-1})	$S+N$ (h^{-1})	γ	R
Ithaca 260 m	53	0.21±0.11	1.36	0.00111±0.00058
Echo Lake 3260 m	570	2.60±0.37	1.33	0.0012 ±0.0002
Mt. Evans 4300 m	1010	6.16±1.14	1.30	0.00155±0.00029

For the comparison of the neutron data, we assume that the efficiency of the detector is the same at all altitudes, as well as the multiplicity of the neutron production. Then, by using the values obtained for R at the three stations, it is found that the average density of the neutron-producers varies by a factor $\sim 7.5\times 155/111\approx 10.5\pm 50$ percent from 260 to 4300 m altitude. The statistical uncertainty is extremely large; yet, the result is not inconsistent with the assumption that the neutron producers are fast nucleons, and confirms that μ-mesons do not play a substantial role in neutron production.

IX. CONCLUSIONS

The results obtained in the described experiments can be summarized as follows:

(a) In the extensive showers neutrons are present. The number of neutrons in the energy range between 2 and 15 Mev present in an extensive shower in the air is of the order of magnitude of 1 percent of the number of electrons belonging to the shower.

(b) Local production of neutrons in association with extensive showers has been observed in Pb, Fe and C and likely takes place in any material. In Pb a high number of neutrons (roughly 60) are produced simultaneously.

(c) Radiation capable of producing neutrons of moderate energy exists in the extensive showers. It

[7] G. Cocconi, V. Cocconi Tongiorgi, and K. Greisen, Phys. Rev. 75, 1063 (1949).

cannot consist only of photons giving rise to neutrons through (γ, n) reactions. A large fraction of the neutron-producers must be rather penetrating particles. μ-mesons are, on the other hand, out of the question as substantial contributors to neutron production. Hence, nucleonic particles—fast neutrons and protons—are thought to be present in the showers and responsible for the production of most of the neutrons observed.

(d) A rough evaluation shows that the intensity of the total neutron-producer-radiation is of the order of magnitude of 2–3 percent of the intensity of the electronic component of the showers.

(e) Neutrons and neutron-producers in showers of different sizes are in first approximation, proportional in number to the electrons.

(f) The density of the neutron producers present in the extensive showers varies by a factor ~ 11 from 260 m to 4300 m above sea level, which is not inconsistent with the neutron producers being nucleonic particles.

The author wishes to thank Professor K. Greisen and Mr. J. Levinger for many helpful discussions on the problem. She is grateful to the Research Corporation for a grant which covered the expense of performing the experiment described above. The cost of constructing the apparatus was provided through an ONR contract. The facilities of the Inter-University High Altitude Laboratories, and the help of Professors Cohn and Iona of Denver University, were an invaluable aid in performing the experiment.

PHYSICAL REVIEW VOLUME 75, NUMBER 10 MAY 15, 1949

Analysis of Neutrons in Extensive Showers

JOSEPH S. LEVINGER
Physics Department, Cornell University, Ithaca, New York
(Received February 7, 1949)

V. Cocconi-Tongiorgi has shown in the preceding paper that there are neutrons in cosmic-ray extensive showers, and that some of these neutrons are produced locally, while some are present in the atmosphere. In this paper we analyze the experimental measurements into elementary factors: the transmission of the neutrons through paraffin, the production of neutrons in paraffin, the production of neutrons in lead, the transmission of neutron producers through paraffin, the transmission of neutron producers through lead, and neutrons present in the atmosphere. We find that the neutrons detected have a transmission corresponding to a mean energy of roughly 3 Mev. In the arrangement of neutron counters in paraffin, the counting rate due to local neutron production in the paraffin is comparable to the counting rate due to neutrons in the atmosphere. Our results are in agreement with those of V. Cocconi Tongiorgi.

THE association of neutrons with extensive cosmic-ray showers has been shown by V. T. Cocconi. She has also shown that neutrons are produced locally by a penetrating component in the showers.[1]

Since several processes occur simultaneously in the experimental arrangements, it is difficult to make a quantitative analysis of these experimental results. Arrangement I (see Fig. 6, preceding paper) consists of neutron counters in paraffin, and will record neutrons present in the atmosphere, neutrons produced in the paraffin block, or neutrons produced locally in material near the paraffin. Arrangement II consists of the paraffin block with neutron counters, surrounded by a layer of lead. The difference between these two arrangements represents primarily neutrons produced locally in the lead layer; but the lead can have several other small effects: it can absorb neutrons present in the atmosphere; it can absorb or multiply the neutron producers that produced neutrons in the paraffin in arrangement I; it can increase the efficiency of the neutron counting by acting as a reflector keeping neutrons in the paraffin by scattering. Statements of the effects measured by the other four arrangements become more complicated.

We shall analyze the experimental results into elementary factors, by writing down the equations for the counting rate in each arrangement in terms of these factors, and then solving this set of simultaneous equations. The results of this analysis are not very certain; the analysis is presented mainly because it is believed to be a useful method in this type of experiment.

Since V. Cocconi-Tongiorgi used six experimental arrangements, giving six simultaneous equations, we can solve for at most six unknown factors. The success of this analysis depends on having chosen the most important six factors. Our provisional

[1] Vanna Cocconi-Tongiorgi, Phys. Rev. 75, 1532 (1949).

choice is

factor A: transmission of neutrons by 25 cm paraffin (layer B),
factor B: counting rate due to production of neutrons per cm of paraffin,
factor C: counting rate due to production of neutrons per cm of lead,
factor D: transmission of neutron-producers by 25 cm paraffin (layer B), (1)
factor E: transmission of neutron-producers by 7.5 cm lead (layer Σ'),
factor F: counting rate due to neutrons present in the atmosphere, or produced locally, outside the paraffin-lead arrangements.

The counting rate for the 6 different arrangements of lead and paraffin employed by V. Cocconi Tongiorgi can be written in terms of these six factors as follows:

$$\mathrm{I} = F + 30B$$

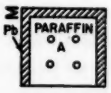

$$\mathrm{II} = F + 30B[1 - 2/3(1-E)] + 5C$$

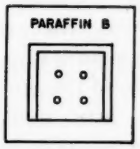

$$\mathrm{III} = FA + (30+\lambda)BD$$

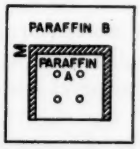

$$\mathrm{IV} = FA + 30BD[1 - 2/3(1-E)] + 5CD + \lambda BD \quad (2)$$

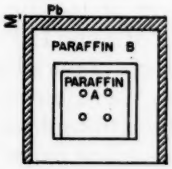

$$\mathrm{V} = FA + 30BDE + 7.5CA + \lambda BED$$

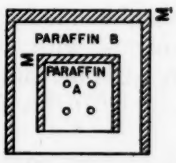

$$\mathrm{VI} = FA + 30BD[1 - 5/3(1-E)] + 5CDE + 7.5CA + \lambda BED$$

We shall repeat the equation for the sixth arrangement in words: neutrons present in the atmosphere (F) are transmitted through the upper paraffin layer with transmission factor A; in addition neutrons are produced in the 30 cm of paraffin near the counters, but the neutron producers must be transmitted through the upper paraffin layer, and through both lead layers; neutrons are also produced in the 5 cm of lead in the lower layer, but the neutron producers must be transmitted through the upper layers of lead and paraffin; neutrons are also produced in the upper layer of lead, and the neutrons must be transmitted through the upper layer of paraffin; and finally, neutrons are produced in one mean free path (λ) of the upper layer of paraffin, but the neutron producers must be transmitted through the upper layer of lead, and most of the 25 cm of paraffin.

These equations need certain explanations, and qualifications: (i) We have taken the production of neutrons in the paraffin near the counters as $30B$; this is on the assumption that the neutrons are produced mainly in the forward downward direction, so that only the 30 cm of paraffin above the lower counters is effective in the production of neutrons. (ii) We find below that the transmission of neutrons through the upper paraffin layer is small. The effective region of the upper paraffin layer in producing neutrons that will be counted is then a thickness of a mean free path λ near the center paraffin. (iii) We have called E the transmission factor for the neutron producers through the top layer of 7.5 cm of lead. Assuming that the absorption of neutron producers is directly proportional to the thickness of the lead, we have $(1-\frac{2}{3}(1-E))$ as the transmission through $\frac{2}{3}$ as much lead in the lower layer; and $(1-5/3(1-E))$ as the transmission through both lead layers. (iv) We have taken the production of neutrons in the top layer of lead as 1.5 times the production of neutrons in the lower layer, since this is the ratio of their thicknesses. This is neglecting the fact that the upper layer of lead has an area about three times as great as that of the lower layer, and therefore is being struck by many more neutron producers. If the neutrons were produced isotropically in the lab system, and if the paraffin scattering had no substantial effects, this neglect of the difference in area could be justified. For the other extreme of neutron production in a very narrow cone (much less than 5°) our procedure would also be correct. In the intermediate region, the larger area of the upper layer would result in more neutron counts. We shall find below that this uncertainty in the production of neutrons for the upper layer affects mainly the determination of A, the transmission for neutrons in paraffin.

In our equations we are assuming that the efficiency of the counting arrangement does not depend on how or where the neutrons are produced, so long as they reach the inner paraffin. Since all our quantities would be multiplied by the same factor for counting efficiency, this factor is neglected.

Further, the numerical values used for the thicknesses of the lead layers apply to the Echo Lake

TABLE I. Analysis of measurements.

Factor	Ithaca	Echo Lake
A (neutron transmission by 25 cm paraffin)	0.023±0.07	0.043±0.035
B (neutron production in 1 cm paraffin)	0.0003±0.00005/hr.	0.011±0.002/hr.
C (neutron production in 1 cm lead)	0.04±0.01/hr.	0.59±0.06/hr.
D (transmission neutron-producers by 25 cm par.)	1.1±0.4	0.88±0.10
E (transmission neutron-producers by lead)	1.0±0.3 (for 6 cm lead)	1.08±0.12 (for 7.5 cm lead)
F (neutrons present in the atmosphere)	0.11±0.02/hr.	0.17±0.06/hr.

measurements. For the earlier Ithaca measurements, the lead layers were 4 cm and 6 cm thick, respectively, instead of the 5 cm and 7.5 cm used at Echo Lake.

The equations can be solved by successive approximations. We used the cycle

$$B=[\mathrm{III}-\mathrm{I}A]/[(30+\lambda)D-30A]. \quad (3)$$

In Eq. (3) make the preliminary assumptions: A about equal to 0.05, and therefore $\lambda=8$ cm; and $D=1$.

$$F=\mathrm{I}-30B \quad (4)$$

using the approximate value of B from Eq. (3).

$$C=\tfrac{1}{5}[\mathrm{II}-\mathrm{I}+20B(1-E)]. \quad (5)$$

Here we use our approximate value for B, and further assume that $1-E=0$; that is, that the neutrons are produced primarily by a penetrating component. We can then solve for the transmission of the neutron producers in lead

$$1-E=[(\mathrm{IV}-\mathrm{III})-(\mathrm{VI}-\mathrm{V})]/5CD, \quad (6)$$

$$A=[1/7.5C][\mathrm{V}-\mathrm{III}+BD(1-E)(30+\lambda)]. \quad (7)$$

Finally,

$$D=[\mathrm{IV}-FA-\lambda B]/\{30B[1-\tfrac{2}{3}(1-E)]+5C\}. \quad (8)$$

We take the values of the 6 factors from these 6 equations, and repeat the solutions again. We have found that this method of solution converges rapidly: two, or at most three, cycles are generally sufficient to obtain a consistent answer.

In this paper we shall analyze the neutrons in coincidence with extensive showers. Measurements were made at Ithaca, and Echo Lake by V. Cocconi Tongiorgi with results given in Table III of the preceding paper. Analyzing these measurements using Eq. (3) through (8), we have the results given in Table I.

The errors given in Table I are determined from combining the standard errors given by V. Cocconi Tongiorgi neglecting additional errors that may be introduced by a faulty analysis.

Inspection of Table I leads to several conclusions. First, the statistical errors of the measurements at Ithaca are so large, due to the low counting rate, that a detailed quantitative analysis hardly seems worth while. We find that the transmission of the neutrons through paraffin is probably less than 0.1, but may easily be negligible. There is definitely neutron production in the lead layer, and in the paraffin layer, as well. The transmission of the neutron producers is something like unity for both lead and paraffin absorbers. Some neutrons are present in the atmosphere. These statements are all consistent with the qualitative conclusions reached by V. T. Cocconi;[2] and do not go far beyond these conclusions.

The statistical errors of the Echo Lake measurements are much smaller. The small transmission value of neutrons through 25 cm of paraffin ($A=0.043\pm0.035$) shows that the neutrons counted are of moderate energy. (If allowance is made for the larger area of the upper lead layer, this would further decrease the value for the transmission, as shown by Eq. (7).) Our crude estimate of the energy is based on the assumption that any neutron scattered by the protons in the upper paraffin layer would be slowed down so much that it would not reach the counters at the center of the inner paraffin layer. A transmission of 0.043 then corresponds to a mean free path of 8 cm, or a mean neutron energy of roughly 3 Mev.

Our analysis shows that there is appreciable neutron production in the inner layer of paraffin. With arrangement I the counting rate at Echo Lake due to production of neutron in the 30 cm of paraffin near the counter is twice as great as the counting rate due to neutrons present in the atmosphere. V. Cocconi Tongiorgi (Section III, preceding paper) finds a production of neutron counts of 0.020/hr. for 1 g/cm² of carbon. This agrees within the large statistical errors of the measurements with the production by the carbon nuclei in paraffin: factor B is 0.011/hr. for 1 cm paraffin, or 0.016/hr. for 1 g/cm² of carbon.

Our value for the production of neutron counts in the inner layer of lead is in agreement with the value obtained by V. T. Cocconi (Section III, preceding paper). In her paper the difference of counting rates in arrangements IV and III (or arrangements II and I) is taken as the production of neutron counts in the inner lead layer. This is

[2] Vanna T. Cocconi, Phys. Rev. 74, 226 (1948).

completely justified by our detailed analysis. In Eq. (5), the term $20B$ is much less than the difference (II−I), and the term $(1-E)$ is also very small, so that V. Cocconi Tongiorgi's analysis is justified.

The transmission of neutron producers is unity, within the statistical errors, through both 25 cm of paraffin, and 7.5 cm of lead. This result can be obtained by a simple inspection of the counting rates in the various arrangements, as shown by V. Cocconi Tongiorgi in the preceding paper.

Our analysis is successful in separating the factors for neutron production in the paraffin near the counters from neutrons present in the atmosphere. The counting rate due to neutrons present in the atmosphere at Echo Lake is the same, within statistical errors, as the increase of counting rate due to the production of neutrons in 2 inches of graphite. We could interpret the neutrons in the atmosphere, in coincidence with the extensive showers, as being produced in an equivalent layer of air above the apparatus. If air is as effective as graphite in neutron production, for 1 g/cm², the counting rate for neutrons in the atmosphere corresponds to the production of neutrons in 8 g/cm² of air, or 100 m of air above the apparatus.

Three of the factors found by our detailed analysis of the data were found by V. Cocconi-Tongiorgi by a simple inspection of the counting rates in the various arrangements: the production of neutrons in the inner layer of lead or other material, the transmission of neutron producers through paraffin, and the transmission of neutron producers through lead. A detailed analysis was needed to obtain the transmission of neutrons through 25 cm of paraffin, and to separate the counting rate in arrangement I into that due to neutrons present in the atmosphere, and that due to neutron production in the paraffin.

It is clear that the larger the number of experimental arrangements used in the experiments, the greater the certainty with which a detailed analysis can be carried out. For instance, we were unable to select four factors, of the six used in this analysis, to fit the Mt. Evans data given in Table V of the accompanying paper. It would be desirable to have more experimental arrangements than unknown factors, so that we could check the consistency of the analysis.

ACKNOWLEDGMENT

The author is grateful to V. Cocconi-Tongiorgi and K. I. Greisen for many discussions on this problem. Some of this work was done while the author was a research associate under an ONR contract.

Precision Measurements of Gamma-Rays from I^{131} with the 2-Meter Focusing Curved Crystal Spectrometer*

DAVID A. LIND, JAMES BROWN, DAVID KLEIN, DAVID MULLER, AND JESSE DUMOND
Norman Bridge Laboratory of Physics, California Institute of Technology, Pasadena, California

(Received January 24, 1949)

With the 2-meter curved crystal focusing spectrometer three nuclear gamma-ray lines from I^{131} have been found to have wave-lengths $(34.033\pm0.01)\cdot10^{-11}$ cm, $(154.671\pm0.01)\cdot10^{-11}$ cm, $(43.622\pm0.02)\cdot10^{-11}$ cm which when converted to energies give 364.18 ± 0.1, 80.133 ± 0.005, 284.13 ± 0.1 expressed in kev. The sum of the last two energies equals the first to an accuracy of a part in 4500, thus verifying a decay scheme proposed by Metzger and Deutsch in which the 80- and 284-kev lines form a cascade between the same pair of excited levels of Xe^{131} as the initial and final levels for the 364-kev line. An alternative proposal seems also thus to be invalidated. The intensities of the lines are discussed, and a method of calibrating the efficiency of the multicellular Geiger counter as a function of wave-length depending on the use of such cascades is proposed. This is probably the first time that a precision test of the Ritz combination principle as applied to nuclear gamma-rays has been possible. It also furnishes an excellent internal check of the reliability of the wave-length scale of the 2-meter curved crystal spectrometer.

USING a nearly "carrier-free" source of I^{131}, five independent precision measurements of its 364-kev and three of its 80-kev lines had been made at this laboratory with the 2-meter focusing curved crystal spectrometer,[1] when news reached us of a new disintegration scheme of F. Metzger and M. Deutsch[2] showing at least two additional lines. The stronger of these at 284-kev was immediately sought and, in spite of considerable source decay, we were still able to obtain one precision measurement on it. Two weeks later, G. E. Owen, D. Moe, and C. S. Cook published[3] results indicating four gamma-ray lines from this same source, only three of which coincide with those of Metzger and Deutsch to the precision to be expected. It seems likely that at least five lines exist, and each of these groups has missed one line that the other has found. In both cases the work was done with magnetic β-ray spectrometers, the precision of the energy determinations being probably of the order of a percent or so. The Metzger-Deutsch proposal indicates that the sum of the quantum energies of the 284- and 80-kev lines, which form a cascade, should just equal the energy of the 364-kev line whereas the Owen-Moe-Cook proposal suggests that exact equality should exist between two cascade pairs, 80 kev+364 kev and 284 kev+163 kev. The two schemes are shown in Fig. 1. The higher precision of the 2-meter focusing spectrometer offers an opportunity to test and discriminate between these schemes. To give an idea of the high reproducibility of these measurements we give in Table I the results of the individual measurements before and after corrections for small errors in the screw and in the carriage mechanism of the instrument. Each "reading" measures the distance in nominal scale x units between the centers of two complete delineations of the line profile (as reflected to the left and to the right of the (310) planes of the quartz crystal). This, divided by two and by the instrument screw conversion factor (1.000230 rev. per x.u. obtained by calibration with x-rays[4]), gives the wave-length in x.u. (Siegbahn scale). This is then converted to absolute units (10^{-11} cm) in the column, λ_g, by means of the factor $\lambda_g/\lambda_s=1.002030$ and the final column gives the energy in kev from the formula kev$=(12394.2\times10^{-11})/(\lambda_g$ cm).

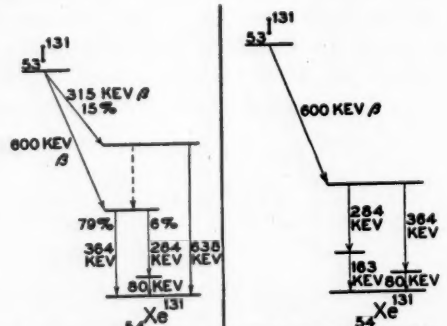

FIG. 1. Disintegration schemes of I^{131} of Metzger and Deutsch and Owen, Moe, and Cook.

It is easy to verify that the energies of the 80- and 284-kev lines add up to equality with that of the 364-kev line *to a part in 4500* which is about the precision to be expected from the single observation on the weak 284-kev line. The precision measures we have assigned are based chiefly on possible systematic errors in the calibration of the instru-

* Assisted by the joint program of the ONR and the AEC.
[1] Jesse W. M. DuMond, Rev. Sci. Inst. **18**, 626 (1947); Jesse W. M. DuMond, David A. Lind and E. Richard Cohen, Rev. Sci. Inst. **18**, 617 (1947); DuMond, Lind, and Watson, Phys. Rev. **73**, 1392 (1948).
[2] F. Metzger and M. Deutsch, Phys. Rev. **74**, 1640 (1948).
[3] Owen, Moe, and Cook, Phys. Rev. **74**, 1879 (1948).
[4] Watson, West, Lind and DuMond, Phys. Rev. **75**, 505 (1949).

TABLE I. Results of independent measurements before and after corrections for small errors in the screw and in the carriage mechanism of the instrument.

Run No.	Reading	Screw	Corrections Periodic	Level	Corrected reading	Wt.	Average	X.U. (Siegbahn)	λ_γ in 10^{-11} cm	Energy kev
1	67.950	−0.001	+0.001	+0.014	67.964	1				
2	67.940	−0.001	+0.001	+0.002	67.942	1				
3	67.921	−0.001	+0.001	+0.006	67.927	1				
4	67.950	−0.001	+0.001	+0.010	67.960	1			34.033	364.18
5	67.933	−0.001	+0.001	+0.004	67.937	1	67.946	33.965	±0.01	±0.1
1	308.785	+0.002	+0.002	+0.008	308.797	1				
2	308.785	+0.002	+0.001	+0.010	308.798	1			154.671	80.133
3	308.765	+0.002	+0.001	+0.018	308.786	½	308.795	154.362	±0.01	±0.005
1	87.096	−0.002	+0.003	−0.006	87.091	1	87.091	43.535	43.622 ±0.02	284.13 ±0.1

ment rather than on the excellent reproducibility. We shall only be able to measure Owen, Moe, and Cook's 163-kev line when our program permits a repetition experiment with a new source, but the present results obviously give strong positive support to the Metzger and Deutsch scheme and seem, therefore, to exclude the other. The advantage of the higher precision crystal method is well exemplified here.

We have also estimated the intensity ratios (photons per unit time) of the three lines we have measured with the following results (Table II).

TABLE II. Estimated intensity ratios.

Line	*R* observed	*N*	Counter efficiency
364 kev	1.000	1.000	25% (Estimated)
80 kev	0.273	0.049	6.8%
284 kev	0.143	0.087	25% (Estimated)

R is the relative intensity (in counts per unit time) *taken from the spectral curves* after subtracting background and making correction for source decay. This result must still be corrected (1) for the differing efficiency of the multicellular Geiger counter, and (2) for the differing reflection coefficient of the crystal at different wave-lengths. Fortunately, the law as regards the crystal reflection coefficient is quite well established by the work of D. A. Lind,[5] as yet unpublished, done in this laboratory. It has been shown to vary as λ^2. To date we have measured the efficiency of the nine-cell multicellular Geiger counter at one energy only, 510-kev. The result obtained was 30 percent. This was done by coincidence methods with two such counters utilizing the simultaneous, oppositely directed pairs of annihilation photons from the same source of Cu^{64} with which a precision study of annihilation radiation was recently made.[6] From theory we estimate that the efficiency for the 364- and 284-kev lines should be only slightly less than this, about 25 percent, but the counter efficiency for the 80-kev line should be quite low, about 4 or 5 percent, because many photoelectrons will fail to be ejected into the gas from the 15-mil thick lead partitions. The column in Table II marked *N* gives the relative activities (photons per unit time) of the three lines after the crystal and estimated counter corrections have been made. This then represents the relative activities of the lines *at the source.* (Because of the small depth and high specific activity of our source we believe its self-absorption is negligible.) In computing the column, *N*, the cascade relationship of the 80- and 284-kev lines seems so firmly established by our wave-length measurements that we feel justified in taking *as a valuable datum* the exact *equality* of the activities associated with these two lines. The relative numbers of quanta associated with the two lines must be corrected for their internal conversion coefficients, however. We thus obtain with considerable certainty *the absolute efficiency of the counter at 80-kev*, namely, 6.8 percent. By the use of a number of such cascades it seems possible that quite reliable curves of counter efficiency *vs.* energy can eventually be obtained. These results indicate then that the ratio of the activity associated with the 284- +80-kev cascade to the activity of the 364-kev line is as 0.087 to 1.00, which agrees as well as can be expected with the ratio reported by Metzger and Deutsch, 0.076 to 1.00.

[5] David A. Lind, thesis, Pasadena (1948).
[6] DuMond, Lind and Watson, Phys. Rev. 75, 1226 (1949).

On the Origin of Solar Radio Noise

ANDREW V. HAEFF
Naval Research Laboratory, Washington, D. C.
(Received November 22, 1948)

The observed anomalous radio-frequency radiations from the sun are associated with sun spot activity and are believed to be generated within intermingling streams of charged particles issuing from active areas of the sun. Such streams have the property of greatly amplifying initial space-charge fluctuations over a range of frequencies determined by the density and velocity distribution of particles in the stream. The theory of generation of radio energy resulting from space-charge interaction between streams of charged particles is reviewed and applied to the solution of the solar radio noise problem. From estimates of average density and velocity distribution of solar particles the frequency of the most intense radiation (30 to 60 megacycles) and the absolute value of radiation intensity at the surface of the earth (7 to 2)$\times 10^{-22}$(watt/cm^2/cycle/sec.) are computed and found to agree well with measurements. The most probable spectral distribution of the anomalous solar radiation is derived in the form

$$E/E_m = (\lambda/\lambda_m)^2 \exp\{2[1-(\lambda/\lambda_m)]\},$$

where E_m is the maximum intensity corresponding to the wave-length λ_m.

I. INTRODUCTION

RECENT studies of solar radiation by means of radio telescopes[1] indicate that in addition to a steady component corresponding to radiation from a black body at a temperature of about 6000°K, there occur bursts of intense radiation within the radio spectrum which are associated with solar flares. While the steady radiation originates over the entire surface of the sun, the source of these anomalous bursts appears to lie in the vicinity of sun spots. The intensity of anomalous radiations, as measured at the surface of the earth, exceeds the normal radiation by a factor of 10^6 to 10^7 in the frequency region below 50 megacycles.[1]

It has been suggested by several investigators[2] that the abnormally intense radiations are caused by oscillations of the electron gas or plasma existing in the outer layers of solar atmosphere and corona. It has also been suggested that the electron plasma is excited by the passage of fact electrons or other corpulscles originating in the sun spots. It has always been assumed, however, that the frequency of such radiation must be near the natural frequency of oscillation of the electron plasma.[2] Furthermore, no detailed picture of the mechanism of excitation of the plasma has ever been given.

It is the purpose of this paper to present a description of a new mechanism of generation of radio energy which is believed to be responsible for the observed anomalous solar noise, and to interpret the observed data on the intensity of solar radiation and its spectral distribution in terms of the new theory.

II. MECHANISM OF GENERATION OF RADIO ENERGY BY STREAMS OF CHARGED PARTICLES

Consider a stream of electrons of velocity v_1 injected into an electron cloud moving with velocity v_2. Because of Coulomb forces between electrons the two streams will interact. In addition to a familiar scattering due to individual electron encounters there occurs additional scattering due to interaction of electrons with electric fields associated with space-charge waves. As was shown by the author in a recent paper[3] this space-charge-wave and electron interaction is a first-order effect considerably larger than that due to "collisions" and is believed responsible for the observed abnormally high temperature of electron clouds.[4]

As is shown in reference 3, the space-charge-wave interaction in streams of charged particles results, under certain conditions, in imparting to the space occupied by the streams the characteristics of a medium having negative attenuation. This means, that under such conditions an initial perturbation which may exist in the stream (such as caused by statistical fluctuations, for example) will be amplified in an exponential manner as the disturbance propagates along the stream. The amplification process continues until the available energy is exhausted. This energy is derived from the kinetic energy of the particles in the stream so that the energy spectrum of the composite electron cloud will be substantially modified after a prolonged coexistence of streams of different energy. The kinetic energy is thus partially transformed into the energy of the electromagnetic fields associated with space-charge waves and can be observed as

[1] E. V. Appleton and J. S. Hey, Phil. Mag. **37**, 73–84 (1946).
[2] I. S. Shklovsky, Astronom. J. (U.S.S.R.) **23**, 333–347 (1946).
[3] A. V. Haeff, Naval Research Laboratory Report No. R-3306, June 24, 1948.
[4] A. V. Haeff, Phys. Rev. **74**, 1532 (1948).

radiation emanating from the streams of charged particles.

As is shown in Appendix I which reproduces for the convenience of the reader the pertinent details of the author's previous analysis[3] of space-charge-wave and particle interaction effects, the amplitude of perturbation V at a distance z from its origin can be expressed as

$$V = V_0 \cos(\omega t - \omega z/v) \cdot (\cosh \gamma_r z + \cos \gamma_i z) \cdots \quad (1)$$

where V_0 is the initial amplitude of the disturbance of frequency ω; v is the average velocity of the inhomogeneous electron stream, and γ_r and γ_i are the real and the imaginary components of the propagation constant. When $\gamma_r z \gg 1$ the increase in energy of the original disturbance, or the energy gain, G, can be approximated as

$$G = (V/V_0)^2 = e^{2\gamma_r z} \cdots . \quad (2)$$

In the case of two-velocity streams the amplifying properties can be indicated by the value of the "inhomogeneity factor," (see Appendix I) which is defined as the ratio of the fractional velocity difference δ/v of the two components of the stream, to the fractional plasma frequency ω_1/ω, or

$$x = (\delta/v) \cdot (\omega/\omega_1) \cdots . \quad (3)$$

The real component of the propagation constant has finite value when the inhomogeneity factor lies within the range from 0 to $\sqrt{2}$.* The inhomogeneous electron gas or plasma having the inhomogeneity factor within this range will behave as a medium of negative attenuation where original perturbation can be amplified to an extent limited only by the length of the stream and the amount of energy available for the process.

Since streams of charged particles which are present in sun spots consists of electrons, alpha-particles, ionized helium atoms or other charged particles, and resemble the inhomogeneous streams discussed in the above theory it is reasonable to assume that space-charge-wave and particle interaction takes place in these streams and can be responsible for abnormal radiations characterized by energy distributions corresponding to very high temperatures of the plasma when observed over a limited range of frequencies. It is important to note that the frequency of the disturbance which can be amplified by the space-charge interaction within inhomogeneous clouds does not have to be near the plasma frequency as has been always assumed by previous investigators.[2] In fact, as long as the inhomogeneity factor does not exceed a critical value ($\sqrt{2}$ for the case $\omega_1 = \omega_2$), disturbances of all frequencies are amplified to some degree up to the limiting frequency.

Since the length, z, of the streams of solar particles along which the space-charge wave amplification can take place, is quite large, it is clear that a limit to amplification or to the maximum amount of energy that can be generated and eventually radiated will be set not by the magnitude of the attenuation constant but by the amount of available energy which can be converted from the kinetic energy of the particles in the stream into the electromagnetic energy of the field of the space-charge waves. The available energy can be estimated in the following manner. Because of collisions and space-charge wave scattering the energy spectrum of the composite stream gradually changes. After a prolonged travel of the stream a final energy distribution will be attained which can be characterized by the condition that the real component of the propagation constant becomes equal to 0, so that no more kinetic energy of the particles can be transformed into the electromagnetic energy of the space-charge wave field. As shown in Appendix II, a stream of particles having a continuous velocity distribution such that $d\omega_n^2/dv = K$ (const.) has zero value of the real component of the propagation constant. Other distributions, for example $dv/d\omega_n = 0$ also show no amplifying properties. Experimental results obtained with the Electron Wave Tubes[3] indicate that the "true" final distribution is rather complex and resembles the first-mentioned but with superposition of the Maxwellian distribution.

If it is assumed that the stream is initially composed of two components, one having a current I_1 and velocity corresponding to potential V_1, and the other a current I_2 and potential V_2, and that the final composition of the stream is characterized by the condition $d\omega_n^2/dv = \text{const.}$, then the maximum rate at which the kinetic energy of the particles in the stream can be converted into the energy of electromagnetic fields, is (see Appendix III):

$$P = \tfrac{1}{2}(V_1 - V_2) \cdot (I_1 - I_2) \cdots . \quad (4)$$

In general, it is reasonable to assume that the available energy is of the order of the initial difference of energy of the components of the stream so that

$$P \approx \Delta V \cdot I. \quad (4')$$

This energy is the total available energy so that the energy per unit frequency range will depend upon the frequency band width over which amplification takes place. As was shown by the author in reference 3, the band width (defined as the frequency range over which the amplification is within 3 decibels of the amplification at the optimum frequency) is proportional to the optimum

* A more general solution (when $\omega_1 \neq \omega_2$) gives a still wider range of the inhomogeneity factor over which amplification of energy can take place although the frequency band width is reduced. See "General Solution of the Two-Beam Electron Wave Tube Equation" by A. V. Haeff, H. Arnett, and W. Stein, submitted to the Proc. I. R. E.

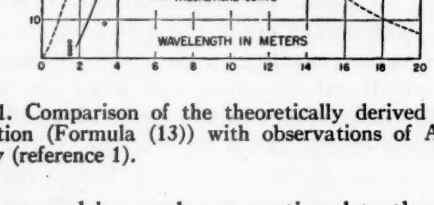

FIG. 1. Comparison of the theoretically derived spectral distribution (Formula (13)) with observations of Appleton and Hey (reference 1).

frequency and inversely proportional to the square root of the product of propagation constant and the effective length z of the stream, i.e.

$$\Delta f = f/(\gamma_1 z)^{\frac{1}{2}}. \tag{5}$$

In the case of streams of solar particles, the effective length of the streams is limited by saturation effects and it can be assumed that the product $(\gamma_1 z)$ remains approximately constant. Therefore, we may assume that the band width is proportional to the optimum frequency, and the power per unit band width is

$$P/\Delta f \propto P/f. \tag{6}$$

It is reasonable to assume that clouds of varying compositions are generated by the sun spot activity. Therefore, there exists a certain space and time distribution of clouds having different particle density, velocity and inhomogeneity. Each individual cloud having a particular value of the inhomogeneity factor will amplify mostly those disturbances where frequency lies in the vicinity of

$$\omega_{opt} = \tfrac{1}{2}\sqrt{3}\omega_1 v/\delta. \tag{7}$$

that is, for which the inhomogeneity factor is near its optimum value. The frequency at which maximum intensity of radiation from a particular cloud will be expected should correspond to the difference in velocity (2δ), to the average value of space charge density (and thus of the corresponding plasma frequency ω_1), and to the average velocity of particles (v). The over-all spectral distribution can then be determined by averaging over all clouds both in time and space.

The problem of finding the frequency at which maximum intensity of radiation is to be expected then reduces to the problem of determining the average velocity of particles, their charge to mass ratio, their density and the most probable difference in energy of the component streams.

The study of magnetic storms indicates that sun spot activity sometimes causes streams of particles originating from the surface of the sun to arrive at the earth. The magnetic field due to current generated by these streams of charged particles is responsible for variations of the earth magnetic field. From measurements of the magnitude of these magnetic disturbances it has been estimated[5] that the cross section of the streams when they arrive at the earth is limited to an area of $(100\text{–}200)^2$ kilometers and the total current is of the order of $5\cdot 10^5$ amperes. Thus the average current density is of the order of $(5-1.25)\cdot 10^{-10}$ amp./cm^2. Neglecting focusing effects of the earth magnetic field and assuming that the particles propagate from the sun in radial directions so that the particle density decreases as the inverse square of the distance from the sun, we arrive at the estimate of the average current density at the surface of the sun:

$$I_s = (92.9\cdot 10^6/0.43\cdot 10^6)^2\cdot(5-1.25)10^{-10} = (23-5.75)10^{-6}\ \text{amp./cm}^2. \tag{8}$$

It has been noted that the beginning of the magnetic storms takes place usually about one day after intense flares are observed at the sun. This indicates that the particles emanating from the sun move with an average velocity of the order of

$$v = [92.9\cdot 10^6(\text{miles})/24(\text{hours})] = 2.5\times 10^8\ \text{cm/sec}. \tag{9}$$

It has been shown that solar particles which arrive at the earth are either ionized helium or hydrogen atoms.[5] Whatever the nature of these particles it is reasonable to assume that at the origin of a corpuscular stream there existed a corresponding stream of electrons moving with the same average velocity. Assuming that the initial temperature of the particles corresponds to the observed surface temperature of the solar disk (6000°K), the most probable value of the velocity difference of the electrons would be approximately

$$2\delta \approx (3k_0 T/m)^{\frac{1}{2}} = 5.4\times 10^7\ \text{cm/sec}. \tag{10}$$

where k_0 is Boltzmann's constant.

Using the above estimated values of the current density, the average velocity and the most probable value of the velocity difference we can compute from Eq. (7) the frequency at which maximum energy will be generated in such an electron cloud:**

[5] M. N. Gnevyshev, Astronom. J. (U.S.S.R.), **25**, 109–122 (1948).

** It is interesting to note that the same frequency will be obtained if it is assumed that the streams consist of ionized hydrogen, for example, rather than electrons. Indeed:

$$[\omega]_{\text{ions}} = \tfrac{1}{2}\sqrt{3}(\omega)_{\text{ions}}(v/\delta)_{\text{ions}} = \tfrac{1}{2}\sqrt{3}(\omega)_{\text{electrons}}(m/M)^{\frac{1}{2}}\frac{v}{\delta_{ei}(m/M)^{\frac{1}{2}}} = [\omega]_{\text{electrons}}.$$

where $[\omega]_{\text{ions}}$ and $[\omega]_{\text{electrons}}$ represent optimum frequency in the case of ion or electron streams, respectively, and $(\omega)_{\text{ion}}$ and $(\omega)_{ei}$ represent the corresponding plasma frequencies.

$$\omega = \tfrac{1}{2}\sqrt{3}\omega_1 v/\delta = 1.22\times10^{14}(I_s/v)^{\frac{1}{2}}\cdot(v/\delta)$$
$$= 1.22\times10^{14}[(23-5.75)10^6/2.5\cdot10^8]^{\frac{1}{2}} \times(2.5\times10^8/2.7\times10^7)$$
$$= (32-64) \text{ megacycles.} \quad (11)$$

Considering the uncertainties in estimates of cloud density and velocity this value checks surprisingly well with the frequency of 50 megacycles corresponding to maximum of solar radio noise as observed by Appleton and Hey.[1]

In order to estimate the time and space averaged spectral distribution of the abnormal radio noise we may proceed as follows. We assume that the average density and velocity are the same for all clouds but that different clouds have different velocity difference. The probability that a cloud has a velocity difference 2δ is $e^{-k\delta}$, and the available energy in such a cloud is proportional to δ according to the relation (4′). Since the band width is proportional to the optimum frequency f (Eq. 5), and this frequency is inversely proportional to δ, (from 7) the energy per unit frequency range will be proportional to δ^2. Since $\delta \approx 1/f \approx \lambda$ we finally arrive at the result that the energy density of abnormal noise when averaged over space and time can be represented as

$$E_\lambda = A\lambda^2 e^{-k\lambda}\cdots \quad (12)$$

where A and k are constants. By differentiation of Eq. (12), k can be expressed in terms of the wave-length λ_m at which maximum of energy density E_m is observed. Expressing the energy density at a wave-length λ in units of energy density E_m at the optimum wave-length λ_m, we obtain the following relation:

$$E/E_m = (\lambda/\lambda_m)^{\frac{1}{2}} \exp[-2(\lambda/\lambda_m - 1)]. \quad (13)$$

This relation is plotted in Fig. 1 which also shows experimental points obtained by Appleton and Hey.[1] The maximum of the theoretical curve has been made to coincide approximately with the observed value. Considering the fact that the theoretical assumption of the constancy of the average density and velocity of particles in the clouds is only a convenient approximation, and also considering the fact that the experimental data are rather incomplete, the agreement between the theory and observations is believed to be as good as can be expected at this stage of the study.

On the basis of the theory given in this paper it is also possible to estimate the absolute value of the radiation density. The power generated per square centimeter of the cross section of the solar stream can be computed from Eq. (4′):

$$P_s \approx \Delta V\cdot I = 0.8(\text{volt})(23-5.75)10^{-6}(\text{amp./cm}^2)$$
$$= (18-4.6)10^{-6} \text{ watt/cm}^2. \quad (14)$$

With the peak of intensity occurring at 50 megacycles the effective band width (taken from Fig. 1) is about 106 megacycles so that the power density (per cycle per second) E_s at the active area of sun is

$$E_s = P_s/\Delta f = (17-4.3)10^{-14}$$
$$\text{watt/cm}^2\text{/cycle/sec.} \quad (15)$$

As reported by Appleton and Hey[1] the area of the active sun spot (S) during the period of their observations was estimated to be about 2×10^{-3} of the area of the sun's hemisphere:

$$S = 2.10^{-3}\cdot 2\pi(0.432\times10^6)^2$$
$$= 2.35\times10^9 \text{ sq. miles.} \quad (16)$$

Assuming that the whole area of the sun spot was effective in generating abnormal radiations the power density E_e at the earth's surface (a distance $R = 92.9\times10^6$ miles away) can be easily computed to be

$$E_e = E_s S/4\pi R^2 = (17.0-4.3)10^{-14}$$
$$\times[2.35\times10^9/4\pi(92.9\times10^6)^2]$$
$$= (7.7-2)10^{-22} \text{ watt/cm}^2\text{/cycle/sec.} \quad (17)$$

which agrees well with the observed value of 10^{-22} watt/cm^2/cycle/sec. as measured by Appleton and Hey.[1]

Figure 2 shows the theoretical curve of the spectral distribution of the abnormal radiations as computed in this paper, (Eq. (13)) together with experimental observations in the radio spectrum and the theoretical "Black Body" solar spectrum at 6000°K.

Some recent observations by J. P. Hagen and his coworkers at the Naval Research Laboratory indicate that appreciable excess noise is generated during the existence of active sun-spots at wavelengths even below 1 cm. This indicates that particle streams of higher density than estimated in the present paper can also be produced.

Because of a rather good agreement between the theoretical results and the observed data, it is believed that a more detailed analysis of abnormal solar radiations on the basis of the present theory

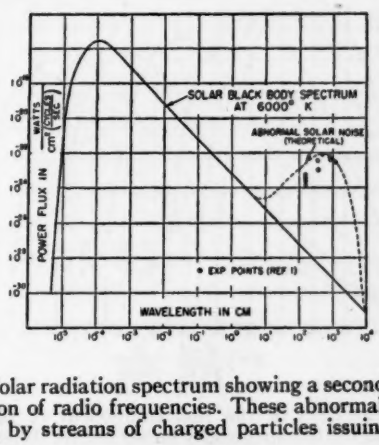
SOLAR BLACK BODY SPECTRUM AT 6000° K
ABNORMAL SOLAR NOISE (THEORETICAL)
POWER FLUX IN WATTS CM² (CYCLE/SEC)
• EXP POINTS (REF 1)
WAVELENGTH IN CM

FIG. 2. Solar radiation spectrum showing a second maximum in the region of radio frequencies. These abnormal radiations are caused by streams of charged particles issuing from sun spots.

will be profitable. It is also hoped that experimental data giving instantaneous spectral distribution over wide frequency bands will be available in the future to permit a more direct analysis.

APPENDIX I.

Theory of Space-Charge Wave and Particle Interaction

Consider that n-streams of charged particles of charge densities ρ_n moving in the z-direction with velocities v_n are injected into a space common to all streams. Taking into account only first order perturbations, we define the space charge densities, currents and velocities as follows

$$\rho_n' = \rho_n + \bar{\rho}_n, \tag{1a}$$

$$v_n' = v_n + \bar{v}_n, \tag{2a}$$

$$i_n' = i_n + \bar{i}_n = i_n + \bar{\rho}_n v_n + \bar{v}_n \rho_n. \tag{3a}$$

The first symbols represent average or d.c. quantities, and the marked symbols represent first order perturbation quantities which are assumed to vary with time and distance in an exponential manner similar to the variation of the field $\bar{E}$:

$$\bar{E} = \bar{E}_0 e^{-\Gamma z + j\omega t} \tag{4a}$$

where Γ is the propagation constant, and ω is the frequency of the disturbance having an initial amplitude $\bar{E}_0$ at the origin ($z=0$). The Poisson's equation

$$\left(\nabla \cdot \epsilon \bar{E} = \sum_1^n \rho_n'\right),$$

the equation expressing conservation of charge $((\partial/\partial t)\rho_n' + (\partial/\partial z) i_n' = 0)$ and the force equation

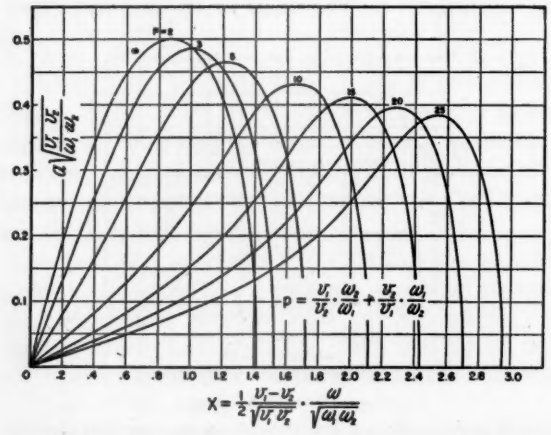

FIG. 3. Variation of the real component of propagation constant with the inhomogeneity factor (x), for different values of the distribution index (p).

$m(dv_n'/dt) = m[(\partial v_n'/\partial t) + v_n(\partial v_n'/\partial z)] = e\bar{E}$ give:

$$-\epsilon\Gamma\bar{E} = \sum_1^n \rho_n \tag{5a}$$

$$j\omega\rho_n = \Gamma\bar{i}_n \tag{6a}$$

$$j\omega\bar{v}_n - v_n\Gamma\bar{v}_n = (e/m)\bar{E}. \tag{7a}$$

By using (3a) and (6a) we obtain

$$j\omega\bar{\rho}_n = \Gamma(\bar{\rho}_n v_n + \bar{v}_n\rho_n)\cdots \tag{8a}$$

so that

$$\bar{v}_n = \bar{\rho}_n/\Gamma\rho_n(j\omega - \Gamma v_n). \tag{9a}$$

When (9a) is substituted into (7a) we obtain

$$\bar{\rho}_n = -\frac{[(e/m)\rho_n]}{(\omega + j\Gamma v_n)^2}\Gamma\bar{E} \tag{10a}$$

so that (5a) can be written as

$$\Gamma\bar{E} = \sum_1^n \frac{[(e/m)(\rho_n/\epsilon)]}{(\omega + j\Gamma v_n)^2}\Gamma\bar{E}. \tag{11a}$$

Excluding trivial solutions ($\Gamma=0$ and $\bar{E}=0$) and replacing space charge densities by electron plasma frequencies defined as

$$\omega_n = [(e/m)(\rho_n/\epsilon)]^{\frac{1}{2}} \tag{12a}$$

we obtain the following equation from which Γ can be determined:

$$\sum_1^n \frac{\omega_n^2}{(\omega + j\Gamma v_n)^2} = 1. \tag{13a}$$

In the case of a continuous distribution of velocities (13a) can be replaced by

$$\int_{v_1}^{v_2} \frac{d\omega_n^2/dv}{(\omega + j\Gamma v)^2} dv = 1. \tag{14a}$$

In the case of only two streams of plasma frequencies ω_1 and ω_2, and velocities v_1 and v_2 the solution of (13a) can be written explicitly when $\omega_1=\omega_2$ or when $\omega_1/v_1=\omega_2/v_2$:

$$\Gamma = \alpha[x^2 + 1 \pm (4x^2+1)^{\frac{1}{2}}]^{\frac{1}{2}} \tag{15a}$$

where for the case $\omega_1=\omega_2$

$$\alpha = \frac{\omega_1}{\frac{1}{2}(v_1+v_2)} \quad \text{and} \quad x = \frac{\frac{1}{2}(v_1-v_2)}{\frac{1}{2}(v_1+v_2)} \cdot \frac{\omega}{\omega_1} = \frac{\delta\omega}{v\omega_1}, \tag{16a}$$

and, for the case $\omega_1/v_1=\omega_2/v_2$,

$$\alpha = \left(\frac{\omega_1\omega_2}{v_1 v_2}\right)^{\frac{1}{2}} \quad \text{and} \quad x = \frac{\frac{1}{2}(v_1-v_2)}{(v_1 v_2)^{\frac{1}{2}}} \cdot \frac{\omega}{(\omega_1\omega_2)^{\frac{1}{2}}}. \tag{17a}$$

The factor x is called the inhomogeneity factor. It

defines amplifying properties of the space traversed by electron streams. The general solution of the two-stream case when $\omega_1 \neq \omega_2$ and $\omega_1/v_1 \neq \omega_2/v_2$ is given by Haeff, Arnett, and Stein[6] from which Fig. 3 is reproduced. This figure shows the real component of the normalized propagation constant (γ_r/α) plotted against the inhomogeneity factor x for different values of the "distribution index" p defined as $p=v_1\omega_2/v_2\omega_1+v_2\omega_1/v_1\omega_2$ and expressing the current distribution between the two streams. Maximum amplification of the space-charge-waves occurs when $\omega_1=\omega_2$ or when $\omega_1/v_1=\omega_2/v_2$ and the inhomogeneity factor is equal to $\frac{1}{2}\sqrt{3}$. Therefore, the frequency of optimum amplification is given by

$$\omega_{opt}=\tfrac{1}{2}\sqrt{3}v\omega_1/\delta \text{ when } \omega_1=\omega_2. \tag{18a}$$

APPENDIX II

Zero-Gain Velocity Distribution

If the velocity distribution in the inhomogeneous stream is such that $d\omega_n^2/dv=k$ then the solution of Eq. (14a) of Appendix I gives

$$1=\int_{v_1}^{v_2}\frac{kdv}{(\omega+j\Gamma v)^2}=\frac{k}{j\Gamma}\left(\frac{1}{\omega+j\Gamma v_2}-\frac{1}{\omega+j\Gamma v_1}\right)$$

$$=\frac{k(v_1-v_2)}{(\omega+j\Gamma v_2)(\omega+j\Gamma v_1)} \tag{19a}$$

or, since

$$\omega_n=\int_{v_1}^{v_2}\frac{d\omega_n}{dv}dv=\int_{v_1}^{v_2}kdv=k(v_2-v_1). \tag{20a}$$

Equation (19a) can be written as

$$\Gamma^2-j\Gamma\frac{v_1+v_2}{v_1v_2}\omega-\frac{\omega^2-\omega_n^2}{v_1v_2}=0. \tag{21a}$$

The solution of (21a) gives

$$\Gamma=j\frac{\omega}{v_1}\left\{\frac{1}{2}\left(1+\frac{v_1}{v_2}\right)\right.$$

$$\left.\pm\left[\frac{1}{4}\left(1-\frac{v_1}{v_2}\right)^2+\frac{v_1}{v_2}\left(\frac{\omega_n}{\omega}\right)^2\right]^{\frac{1}{2}}\right\}. \tag{22a}$$

Since the sum under the radical is always a positive quantity, the propagation constant Γ is always imaginary, regardless of velocity range or the magnitude of current. Therefore if the velocity distribution in the stream can be expressed as $d\omega_n^2/dv=k$, then no space charge amplification can take place.

APPENDIX III

Estimate of Available Power

If it is assumed that the original velocity distribution is such that current I_1 is produced by charges moving with velocity v_1 corresponding to a potential V_1, and the current I_2 by charges of velocity v_2 corresponding to a potential V_2, then the total power carried by the stream at the origin is

$$P_1=I_1V_1+I_2V_2. \tag{23a}$$

Assuming the final distribution to be as described in the Appendix II, the total power carried by the stream at the end will be

$$P_2=\int_{V_1}^{V_2}V(dI/dV)dV. \tag{24a}$$

But from the expression defining the distribution of current

$$d\omega_n^2/dv=k=e/m\epsilon(dI/vdv), \tag{25a}$$

we find that

$$I=I_1+I_2=\int_{v_1}^{v_2}(m/e)\epsilon kvdv$$

$$=(\epsilon k/2)(m/e)(v_2^2-v_1^2)=\epsilon k(V_2-V_1), \tag{26a}$$

and

$$\frac{dI}{dV}=\frac{dI}{dv}\cdot\frac{dv}{dV}=\frac{m}{e}\epsilon k\frac{vdv}{dV}=\epsilon k=\frac{I_1+I_2}{V_2-V_1}. \tag{27a}$$

Therefore,

$$P_2=\int_{V_1}^{V_2}\frac{I_1+I_2}{V_2-V_1}VdV=\tfrac{1}{2}(V_1+V_2)(I_1+I_2). \tag{28a}$$

Finally, the available power, or the power that can be converted from kinetic energy of the charged particles in the stream into the field energy of the space-charge waves and eventually radiated, is

$$P=P_1-P_2=(I_1V_1+I_2V_2)$$

$$-\tfrac{1}{2}(V_1+V_2)(I_1+I_2)=\tfrac{1}{2}(V_1-V_2)(I_1-I_2). \tag{29a}$$

[6] A. V. Haeff, H. Arnett, and W. Stein, submitted to the Proc. I. R. E. in Nov. 1948.

Transmission of Elastic Pulses in Metal Rods*

D. S. HUGHES, W. L. PONDROM, AND R. L. MIMS**
Department of Physics, University of Texas, Austin, Texas
(Received January 20, 1949)

Pulses are generated at one end of a cylindrical rod by a quartz crystal. A second crystal at the opposite end is used as a detector. The transmission time is studied as a function of rod length, diameter, and material. In general a single input pulse gives rise to several pulses at the detector. For the dimensions and rise times used, all of the arrivals are explicable in terms of transmission with either the dilatational or rotational velocity of the material or a combination of both. The rotational and dilatational velocities can be computed from these data and hence the elastic constants of the material.

INTRODUCTION

A QUICK accurate method of measuring the elastic constants of solids has been the objective of much research, and many special methods have been evolved which are applicable to special conditions. The authors desiring a method applicable to small cylindrical samples have investigated the transmission of sharp pulses through samples of this form. Under certain conditions, all of the elastic constants of an isotropic solid may be determined from the transmission of pulses from one end of the cylindrical sample to the opposite end. It is necessary that the material be capable of transmitting pulses of the requisite rise time, i.e., 0.2 to 0.6 μsec., but only longitudinal excitation and detection is necessary. Good results have been obtained with steel, brass, aluminum, and Lucite.

THEORY OF THE EXPERIMENTAL METHOD

A block diagram of the apparatus is shown in Fig. 1. The cylindrical rods are driven by an x cut quartz crystal pressed against one end, and a similar crystal used as a detector or "pick-up" is pressed against the opposite end. These crystals are 1⅛ inch in diameter and have a fundamental frequency of 3.5 megacycles for free longitudinal vibration in the direction of thickness.

A model TS-100/AP oscilloscope[1] is used as the basic time standard. This instrument has a circular sweep of 12.368 μsec. per revolution which is generated continuously from an 80.86-kc crystal oscillator. A trigger circuit can be synchronized at any submultiple of this frequency lying between 300 and 1500/sec. This circuit generates pulses accurately synchronized with the circular sweep and having a rise time of 0.1 μsec., duration 0.6 μsec., and amplitude of +100 volts or −70 volts. These trigger pulses can be used to synchronize a Brooton model 300-pulse generator, which in turn excites the crystal. The pulses from this generator can be varied in amplitude[2] and duration but have a longer rise time than those from the trigger generator of the TS-100/AP oscilloscope.

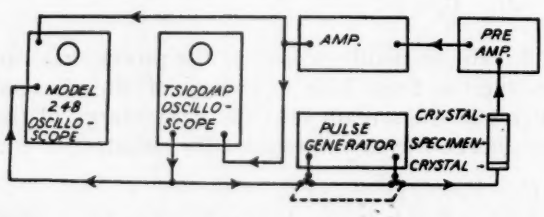

FIG. 1. Block diagram of apparatus.

The pick-up crystal is connected to a preamplifier and amplifier similar to that described by Jordan and Bell.[3] The output of this amplifier is connected to the vertical deflection plates of the Dumont model 248 oscilloscope and to the radial deflection electrode of the TS-100/AP oscilloscope. The fixed sweeps of the model 248 instrument are triggered from the pulse generator of the TS-100/AP instrument.

Using the 100-μsec. fixed sweep and 10-μsec. markers on the model 248 instrument the time of arrival of each pulse train can be read to 1 μsec. The character of the pulses is also easily checked with this presentation.

The TS-100/AP oscilloscope is used for the precise measurement of arrival times. The accuracy of reading this unit varies with the sharpness and amplitude of the arrival. For the better defined pulses different observers could repeat to about 0.03 μsec. The continuously running circular sweep causes no confusion of data from different revolutions because the instrument is provided with a variable delay intensity gate which allows the operator to select any desired revolution after the

* This work was supported by the ONR under Contract N6onr-266.
** Employed under research grant from Shell Oil Company.
[1] Radiation Laboratory Series Vol. 21, *Electronic Instruments* (McGraw-Hill Book Company, Inc., New York, 1948), pp. 626–634.
[2] A control has been added to this instrument which varies the screen grid potential of its output amplifier. This controls the pulse amplitude and has a slight influence on the rise time of the pulses.
[3] W. H. Jordan and P. R. Bell, "General purpose linear amplifier," Rev. Sci. Inst. 18, 703 (1947).

trigger and examine it separately. The trace is blanked out for all revolutions but the desired one.

A photographic record of the display obtained on the Model 248 oscilloscope is shown in Fig. 2. Traces *I* and *VIII* are simply records of the 10-μsec. markers. Trace *II* was taken with the two crystals in contact. The start of the pulse train is the small down-kick followed by a damped wave train (frequency about 1 megacycle). Trace *III* shows the arrivals with a steel rod 3.645 cm in diameter and 5.080 cm in length placed between the crystals. Traces *IV*, *V*, and *VI* are for rods of the same diameter, cut from the same stock, having lengths of 10.160 cm, 15.240 cm, 20.320 cm, and 25.400 cm, respectively. A clear sharp arrival at the points marked *A* with a character very similar to that of the directly coupled crystals in trace *II* is found for all rods. In addition there are clearly defined arrivals marked *B*, and on the longer rods arrivals marked *C*. For the longer rods many more such arrivals are visible on the TS-100/AP display. These arrive later than 100 μseconds after the trigger and are not recorded in this photograph. These arrivals can be brought into view on the model 248 display by triggering the 100-μsec. sweep from the delayed gate of the TS-100/AP oscilloscope. Table I shows the arrival times of all wave groups that could be clearly identified. On the basis of character these have been separated into two groups. Members of the first group show a character similar to the directly coupled crystal signal and their arrival times are denoted t_A, t_B, t_C, etc. in order of arrival. Members of the second group are indicated at *P* on traces *III* and *IV* and occur at much larger times on the longer rods. These are characterized by longer wave trains than those of the first group. These arrival times are given as t_P, t_Q, t_R, etc.

The arrival time, t_A, is evidently linear with rod length, and the corresponding velocity is 5886 meters/sec. This is much too high for a wave transmitted with the so-called bar-velocity, V_E, given by

$$V_E=(E/\rho)^{\frac{1}{2}}, \tag{1}$$

where E is Young's modulus and ρ is the density of the material. However, if we assume that this is a true dilatational wave, its velocity, V_D, should be given by

$$V_D=[(K+4\mu/3)/\rho]^{\frac{1}{2}}, \tag{2}$$

where K is the bulk modulus and μ is the shear modulus of the material. A computation of this velocity using handbook values of K and μ is in close agreement with the above experimental figure, and thus fits the hypothesis satisfactorily.

The arrivals at t_B, t_C, t_D, etc. are somewhat different. It is apparent from Table I, that the velocity of the waves corresponding to these arrivals is also

TABLE I. Arrival times of wave groups. $D=3.645$ cm, t in μsec

Rod No.	L cm	t_A	t_B	t_C	t_D	t_P	t_Q	t_R	t_S
20	2.54	4.27				13.05			
21	5.08	8.69				25.91	35.68		
22	10.16	17.23	27.15			51.90	61.51		
23	15.24	25.89	35.66			77.73	87.29		
24	20.32	34.72	44.34	53.86	63.32	103.58	113.10	122.88	
25	25.40	43.16	53.00	62.27	71.55	129.43	138.95	148.35	158.43

V_D, because the time intervals t_B-t_A, t_C-t_B, etc. are the same for all the various lengths of rods. These must then correspond to delayed wave trains, and, since the above intervals are equal for all of these rods, the delay is independent of the length of the rods.

Figure 3 is similar in all respects to Fig. 2 except that steel rods 2.540 cm in diameter were used. The corresponding data on arrivals are shown in Table II, and it is apparent that the arrivals at t_A correspond to the same velocity, V_D, as before. However, the intervals t_B-t_A, t_C-t_B, etc. from Table II are shorter than those of Table I but are constant for the rods considered in Table II. These intervals are shorter than those of Table I in the ratio 2.540/3.645 and lead to the conclusion that the delay is directly proportional to the diameter of the rods. It is thus apparent that these wave groups traveled during some part of the path in a direction oblique to the axis of the rod so as to traverse the diameter of the rod.

A rational explanation is obtainable from a consideration of the effect of the free surfaces bounding the rod. The driving crystal would be expected to generate a group of plane waves of dilatation at the driven boundary traveling very nearly parallel to the free cylindrical wall of the rod. It is well known that such waves cannot alone satisfy the free boundary condition, but must be accompanied by rotational waves.[4] In the present situation these rotational waves must travel very nearly at an angle θ relative to the normal of the boundary where θ is given by

$$\sin\theta=V_R/V_D, \tag{3}$$

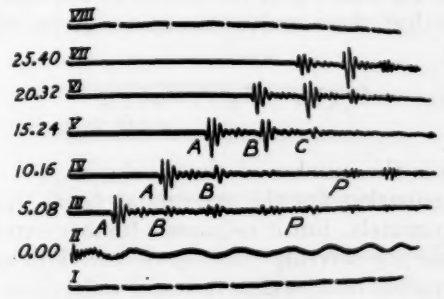

FIG. 2. Pulses through cold rolled steel rods 3.645 cm in diameter.

[4] *Handbuch der Physik*, Band VI (Verlag. Julius Springer, Berlin, 1928), pp. 323–324.

TABLE II. Arrival times of wave groups. $D=2.540$ cm, t in μsec.

Rod No.	L cm	t_A	t_B	t_C	t_D	t_P	t_Q	t_R	t_S
14	2.54	4.21							
15	5.08	8.53	15.03				32.40	38.96	
16	10.16	17.19	23.75	30.30	37.04		52.38		
17	15.24	25.79	32.65	38.87	45.82		83.95		
18	20.32	34.44	41.25	47.24			110.38	117.10	
19	25.40	43.04	49.57	56.21	63.13		136.17	142.91	149.78

and V_R the velocity of rotational waves is given by

$$V_R=(\mu/\rho)^{\frac{1}{2}}. \tag{4}$$

Such a rotational wave must eventually strike the opposite side of the rod and there give rise to a reflected rotational wave and a dilatational wave at grazing reflection in order to satisfy the boundary conditions. This dilatational wave is the first delayed arrival corresponding to the time t_B.[5]

Referring to Fig. 4 and using the principles of geometrical optics, the above process corresponds to a path such as $\langle bqrd\rangle$, where $\langle bq\rangle$ and $\langle rd\rangle$ are traversed as dilatational waves, and $\langle qr\rangle$ is traversed as a rotational wave. There is an uncountably infinite set of such paths ($\langle astc\rangle$ and $\langle buvd\rangle$ are further examples) but all have the same travel time. The delay, Δt, incurred in taking the path $\langle bqrd\rangle$ instead of the path $\langle bc\rangle$ (traversed as a dilatational wave) is readily seen to be given by

$$\Delta t=(1/V_R)(D/\cos\theta)-(1/V_D)(D\sin\theta/\cos\theta), \tag{5}$$

where D is the diameter of the rod. Upon elimination of θ with Eq. (3) we find

$$\Delta t=D[(V_D^2-V_R^2)^{\frac{1}{2}}/V_DV_R]. \tag{6}$$

The above analysis is by no means limited to one such delay; the delayed dilatational wave may be carried through the same reasoning to yield a twice delayed dilatational wave corresponding to the path $\langle bqrstc\rangle$ in Fig. 4 and yet again to yield a dilatational wave delayed three times corresponding to the path $\langle bqrstuvd\rangle$ of Fig. 4, etc. Since the time for the undelayed dilatational wave to travel the length of the rod is L/V_D where L is the length of the rod, it is obvious that these arrival times are given by the relation

$$t=(L/V_D)+nD[(V_D^2-V_R^2)^{\frac{1}{2}}/V_DV_R], \qquad n=0,1,2,\cdots, \tag{7}$$

where n is the number of times delayed.

This equation fits the arrivals at t_A, t_B, t_C, etc. quite accurately, but it requires a further extension to include the arrivals at t_P, t_Q, t_R, etc. This extension is readily obtained in terms of reflections from the ends of the rods.

[5] This transfer of mode process has been used in the making of delay lines. See *Supersonic Solid Delay Lines* NDRC Div. 14 OEMsr-262 Report No. 932 (April 30, 1946).

Referring to Table I, it is evident that the relations

$$t_P=3t_A,\quad t_Q=3t_A+\Delta t,\quad t_R=3t_A+2\Delta t,\quad t_S=3t_A+3\Delta t$$

are very closely satisfied. In other words t_P corresponds to a wave pulse which traversed the length of the rod three times as a dilatational wave, t_Q corresponds to a wave which traversed the rod in the same manner except delayed once, etc. Occasionally still higher types such as $5t_A+n\Delta t$, etc. are observed, but accurate reading of the arrival time is difficult.

From the above considerations it is apparent that all the arrival times considered can be represented by the equation

$$t=m(L/V_D)+nD[(V_D^2-V_R^2)^{\frac{1}{2}}/V_DV_R], \qquad n=0,1,2,3,\text{ etc.}, \quad m=1,3,5,\text{ etc.} \tag{8}$$

However, m and n are subject to the restriction

$$mL\geqslant nD\tan\theta, \tag{9}$$

since the wave must advance along the axis of the rod a distance $D\tan\theta$ during each delay, and the wave travels a total axial distance of mL.

The principles of geometrical optics employed here are generally valid when the wave-length is small compared to the smallest dimension involved. This condition is satisfied for the rods of Figs. 2 and 3, because the pulses involved consist of a frequency spectrum of roughly 1–5 megacycles, which corresponds to a dilatational wave-length of 0.12 cm to 0.6 cm in steel. However, a much more lucid justification for their use in the present instance is the simple fact that the transmitted pulses are so short that it is impossible for the first delayed wave train to interfere with the undelayed wave train, etc.

The situation when the successive wave trains interfere has also been investigated to some extent. Figure 5 is a photographic record obtained for the transmission of these same pulses through a series of samples of drill rod 15.240 cm in length and having diameters of 2.54, 1.27, 0.635, 0.3125, and 0.1565 cm, respectively.

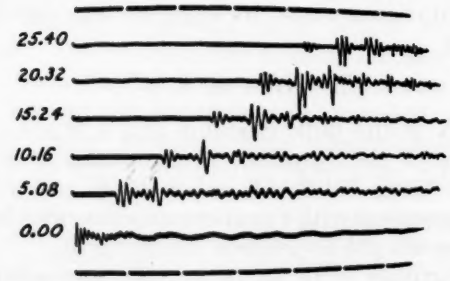

FIG. 3. Pulses through cold rolled steel rods 2.540 cm in diameter.

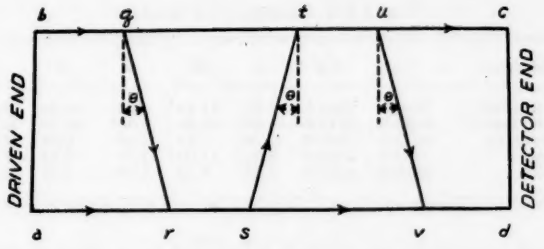

FIG. 4. Possible wave paths in rod.

The 2.54-cm and 1.27-cm rods give the characteristic patterns described above except that the undelayed wave is attenuated as the diameter decreases. This wave appears to be absent for the 0.635-cm rod but it can be seen on the oscilloscope screen. For the two smaller rods it could not be detected above the background. The characteristic decrease in delay with decrease in diameter is clearly shown, and, as this means production of more delayed wave trains for a rod of given length, the rapid decay of the primary (undelayed) wave pulse with decrease in diameter is certainly to be expected. However, the time of arrival of the undelayed wave does not change by any detectable amount. The traces for the 0.3125 cm and 0.1565 cm rods clearly indicate the interference possible between the various wave trains when the delay is shorter than the pulse duration.

These experimental results are in no way contrary to the theory of unending simple harmonic progressive waves on an infinite cylindrical bar as described by Pochhammer.[6] For such a wave interference would have its full effect. The infinite number of delayed wave trains would bring about complete destructive interference unless the delay, Δt, is exactly an integral number of vibrations. This is precisely the nature of the motions which are permitted in Pochhammer's solution. Using the methods employed by Cooper,[7] one should be able to pass from the steady state solutions of Pochhammer to the solution of the present transient problem.

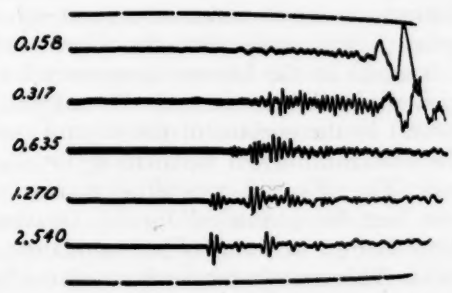

FIG. 5. Pulses through drill rods 15.240 cm in length.

[6] L. Pochhammer, J. F. Math. (Creele), Bd. 81 (1876), p. 324 also A. E. H. Love, Mathematical Theory of Elasticity, p. 287–291.
[7] J. L. B. Cooper, Phil. Mag. 38, 1–22 (1947).

EXPERIMENTAL RESULTS

The principles of geometrical optics must be regarded as exact as far as the travel times of first arrivals are concerned. However, experimental error possibilities are fairly numerous in apparatus of the sort employed here. Consequently, a least squares solution was made in fitting the data of Table I and that of Table II to Eq. (8). For this purpose Eq. (8) was replaced by

$$t=\epsilon+m\beta L+n\alpha D, \tag{10}$$

where

$$\beta=1/V_D, \quad \alpha=(V_D^2-V_R^2)^{\frac{1}{2}}/V_D V_R,$$

and ϵ was a possible error in determining the time zero.

For the data of Tables I and II the following values of ϵ, α, and β were obtained (α and β are expressed in μsec./cm and ϵ in μsec.).

	ϵ	α	β
Table I	0.090	2.6176	1.7007
Table II	−0.063	2.6083	1.6971

These values together with the appropriate integers m and n will reproduce the data in the corresponding tables with a probable error of 0.05 μsec. when substituted into Eq. (10). This figure is satisfactorily close in view of the reading errors to be expected with the TS-100/AP oscilloscope.

From the definitions of α and β it is evident that V_D and V_R can be calculated from

$$V_D=1/\beta, \tag{11}$$

$$V_R=(\alpha^2+\beta^2)^{-\frac{1}{2}}. \tag{12}$$

The bulk modulus, K, and rigidity modulus, μ, can then be calculated from V_D, V_R and the density ρ by using Eqs. (2) and (4). The Young's modulus, E, and Poisson's ratio, σ, can then be found from the

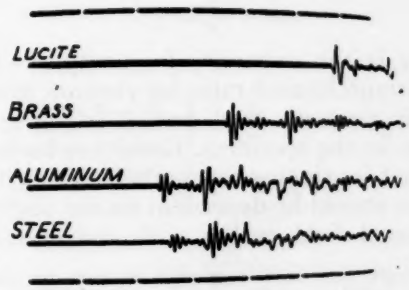

FIG. 6. Pulses through rods 2.540 cm in diameter, 15.240 cm in length.

equations

$$E=9\mu K/(3K+\mu), \tag{13}$$

$$\sigma=\frac{1}{2}\left(\frac{3K-2\mu}{3K+\mu}\right). \tag{14}$$

To date several materials other than the above samples of steel have been examined using a single rod 15.24 cm long and 2.540 cm in diameter. The totality of results is summarized in Table III. The velocities are given in meters/sec., and the elastic moduli in units of 10^{11} dynes/cm². The densities used are given in g/cm³. Figure 6 is a photograph of the traces obtained with the additional materials with a cold rolled steel rod of the same length and cross section for comparison.

TABLE III. Summary of results.

Material	V_D	V_R	ρ	K	μ	E	σ
C. R. Steel I	5880.0	3203.5	7.82	16.34	8.025	20.69	0.289
C. R. Steel II	5892.2	3211.8	7.82	16.39	8.067	20.79	0.289
Aluminum	6379.0	3100.0	2.70	7.47	2.60	6.98	0.345
Brass	4283.0	2033.0	8.56	11.02	3.54	9.59	0.355
Lucite	2640.0	1269.0	1.18	5.70	1.90	5.13	0.350

PHYSICAL REVIEW VOLUME 75, NUMBER 10 MAY 15, 1949

Ferromagnetic Resonance at Microwave Frequencies in an Iron Single Crystal*

ARTHUR F. KIP AND ROBERT D. ARNOLD
Research Laboratory of Electronics, Massachusetts Institute of Technology, Cambridge, Massachusetts
(Received January 19, 1949)

Ferromagnetic resonance absorption in a single iron crystal has been observed at 23,675 and 9260 Mc/sec., using an external magnetic field applied perpendicular to the r-f magnetic field in the plane of the crystal surface. A variation in the resonance field is found which depends on the angle the magnetic field makes with the crystal axes. The results agree well with the theory of Kittel which predicts that an angular variation in resonance will result from the effects of crystal anisotropy. In the case of the lower frequency, deviations from the expected angular variation and a second resonance peak are shown to be the result of incomplete alignment of the magnetization with the direction of applied field. A calculation of the first-order anisotropy constant computed on the basis of this deviation agrees well with the known value.

INTRODUCTION

THE first experiment showing a microwave resonant absorption in iron was performed by Griffiths.[1] In this experiment a thin film of iron was applied to one end of a microwave resonant cavity. An external magnetic field was applied parallel to the surface of the thin film. With a constant microwave frequency, it was found that a maximum power absorption occurred for a particular value of external applied field.

Kittel[2] has discussed the theory of ferromagnetic resonance absorption and has shown that the resonance condition is given by

$$\omega_0=\gamma(BH)^{\frac{1}{2}}, \tag{1}$$

where ω_0 is the resonance frequency, $\gamma=ge/2mc$ = magnetomechanical ratio for electron spin, H is the static magnetic field, and B is the magnetic induction in the specimen. Kittel has further predicted that for single crystals the magnetic field for resonance should be dependent on the angle which the external field makes with the crystal axis, owing to the effect of anisotropy. In the present experiments the resonance phenomenon was investigated, using a single Fe–Si crystal, with the purpose of determining the effect of the known anisotropy of the crystal on resonance absorption.

THEORY

Before presenting the results of these experiments, a short discussion of the theory, as developed by Kittel, will be given. Ferromagnetic resonance absorption is to be expected, by analogy with the Purcell-Bloch nuclear resonance experiment, when the applied field is such that the microwave frequency is equal to the Larmor frequency for electron spin. It is shown that the demagnetization field normal to the surface of the crystal must be taken into account when calculating the Larmor frequency. The effect of crystalline anisotropy on resonance can be accounted for by treating the anisotropy energy in terms of an equivalent magnetic field. This treatment leads to the effective demagnetizing factor which is to be included in the calculation of the Larmor frequency, and results in a modification of Eq. (1).

In an infinite plane cubic crystal, the modified equation for resonance in the (100) plane is found

* This work has been supported in part by the Signal Corps, the Air Materiel Command and the ONR.
[1] J. H. E. Griffiths, Nature 158, 670 (1946).
[2] C. Kittel, Phys. Rev. 73, 155 (1948).

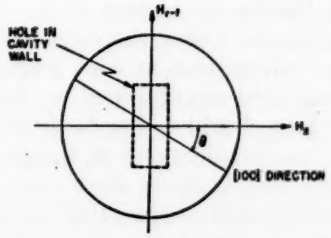

FIG. 1. Sketch showing crystal mounted over hole in cavity giving directions of r-f and external magnetic fields and the [100] direction in the crystal.

by Kittel to be

$$\omega_0=\gamma\{[H_s+4\pi M_s+(2K_1/M_s)] \times[H_s-(2K_1/M_s)\cos 4\theta]\}^{\frac{1}{2}}. \quad (2)$$

Here M_s is the saturation magnetization, K_1 is the first-order anisotropy term (anisotropy energy/unit volume $=(K_1/4)\sin^2 2\theta$), H_s is the applied magnetic field, and θ is the angle between the magnetization and the [100] direction of the crystal.

In this treatment it is assumed that the external applied field is always great enough so that the magnetization is saturated and oriented parallel to the external field. On these assumptions, using a constant frequency, one expects that the field for resonance in the (001) plane will vary with $\cos 4\theta$, since $H_s \ll 4\pi M_s$ at the frequencies used. This will give a maximum field for resonance in the [110] direction and a minimum in the [100] direction.

EXPERIMENTAL ARRANGEMENT

The apparatus used in this experiment consisted of a resonant cavity arranged so that one surface of the iron crystal acted as part of one wall of the cavity, a reflex klystron for generating microwave power, and measuring equipment for determining the variation in absorption of power as the external magnetic field was varied.

The resonant cavity was constructed from a piece of brass wave guide shorted at one end and coupled through an adjustable iris to the wave guide leading to the generator. The cavity was one guide wavelength long and was excited in the TE_{102} mode. The Fe–Si crystal (approximately 3.85 percent Si), kindly loaned to us by Dr. R. M. Bozorth of the Bell Telephone Laboratories, was in the form of a circular plate 2.2 cm in diameter and 0.022 cm in thickness. The plane of the surface was within a few degrees of the (001) plane of the crystal.

Figure 1 shows the arrangement of the iron crystal in the wall of the cavity. A rectangular hole was cut in the narrow wall of the cavity so that the iron crystal placed against the hole would have an r-f magnetic field tangent to its surface plane. The cavity was placed between the poles of an electromagnet so that the external field was in the plane of the crystal, perpendicular to the r-f field in the crystal plane. By rotating the crystal about an axis perpendicular to its plane it was possible to change the angle θ between the external field direction and the [100] direction in the crystal plane. A very thin mica disk was placed between the crystal and cavity wall to prevent variation in the cavity Q due to variable contact between crystal and cavity.

A reflection method was used to measure relative power absorption in the crystal, as follows. The cavity containing the iron crystal was connected to the microwave power source by a wave guide, with sufficient attenuation inserted to isolate the source from the effects of changing load. A change in power absorbed in the crystal caused a change in the Q of the cavity, which changed the fraction of power reflected from the cavity. A directional coupler inserted in the guide between power source and cavity was oriented so as to pick up only the power reflected from the cavity. The signal thus received could then be related to the relative power absorbed in the crystal for each value of applied magnetic field. In order to measure the signal obtained from the directional coupler, a 1000 cycle per second square wave modulation was applied to the signal generator, so that power picked up through the directional coupler could be detected by a crystal and the resulting 1000 cycle signal amplified through a narrow band amplifier and read on a meter.

The details of the method of measurement were as described in an earlier paper,[3] except that in these experiments a directional coupler was used instead of a magic T for measuring the power reflected from the test cavity. The data obtained consisted of measurements of the relative power absorption as a function of external magnetic field, from which could be plotted the magnitude of applied magnetic field necessary for maximum absorption *versus* the orientation of the crystal.

The applied magnetic field was determined by measuring the a.c. voltage induced in a small rotating coil placed in the field. Details are given in reference 3.

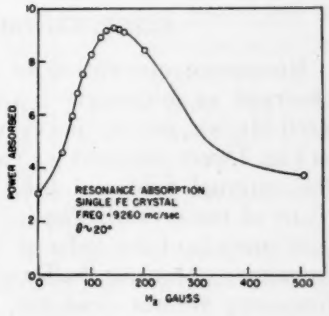

FIG. 2. Resonance absorption in an iron single crystal, showing relative power absorbed *vs.* applied magnetic field.

[3] R. D. Arnold and A. F. Kip, Phys. Rev. **75**, 1199 (1949).

TABLE I. Comparison of observed and calculated resonance fields at $\theta=0°$ and 45°. Calculations are from Eq. (2), using $\gamma/2\pi=2.80$ Mc/gauss, $M_s=1575$ gauss, $K_1=2.8\times10^5$ ergs/cm³.

Frequency	θ	Resonance field Calculated	Experimental
23,675 Mc/sec.	0°	2765 gauss	2530 gauss
23,675	45°	3393	3290
9260	0°	182	70
9260	45°	875	830

EFFECT OF STRAINS IN THE SINGLE CRYSTAL

It should be mentioned that original measurements gave a very broad resonance effect, and showed essentially no effect of orientation on the magnetic field required for the absorption maximum. The crystal was therefore returned to the Bell Laboratories where it was electrolytically polished in an effort to remove any surface strains. Both before and after this treatment, examination was made of the domain structure by H. J. Williams of the Bell Laboratories, using the colloid technique. In both cases, maze patterns characteristic of strained surfaces were found. However, after polishing, the resonance effect was found to be a strong function of orientation and, as will be shown, the detailed results indicate that the strains played at most a minor role after the crystal surface had been polished. All data given below were obtained on the polished crystal.

MAGNETIC FIELD CORRECTION

A correction must be applied to the values of magnetic fields obtained in these experiments, because we used a finite size of sample rather than an infinite plane. The result of this is that the demagnetizing field due to the edge surface of the crystal reduces the effective applied field by a calculable amount. Using the equations of Osborn[4] for the demagnetizing factors of a very flat oblate spheroid, and assuming a saturation magnetization of 1575 gauss, we find that for our crystal the effective magnetic field is obtained by subtracting 154 gauss from the applied field. All fields given have been corrected in this way.

EXPERIMENTAL RESULTS

Resonance absorption in the iron crystal was observed at microwave frequencies of 23,675 and 9260 Mc/sec. Absorption curves such as those shown in Fig. 2 were obtained for various angles θ between the external field and the [100] direction in the plane of the crystal. The half-width of the absorption curve is of the order of 200 gauss for the lower frequency. Accurate half-width data at the higher frequency are not available, but the half-widths at the two frequencies are known to be of the same order of magnitude. Using the values of H_s giving the maximum absorption at each angle, the resonance magnetic field was obtained as a function of θ, as shown in Figs. 3 and 4. For both frequencies it is seen that the predications of theory are qualitatively borne out. Thus for $\theta=0°$, 90°, 180°, 270° (external field parallel to the [100] or [010] directions) the resonance field is a minimum. For angles 45° from these angles (external field parallel to the [110] or [1$\bar{1}$0] directions) the resonance field is a maximum. (On the graphs, results are plotted only from 0° to 180°.)

Table I gives the results of our experiments compared with calculations from Kittel's equation. Resonant fields are given for applied field in the [100] and [110] directions in the (001) plane. The values of the various constants used in the calculations are given with the table.

The results at the higher frequency are seen to agree reasonably well with the theoretically determined values for resonant field. As shown in Fig. 3, the variation of resonance field with θ is accurately in accord with $\cos4\theta$, showing that the magnetization is aligned with the external field for all values of θ.

Examination of the curves for both frequencies shows that maximum and minimum values for resonance fields do not exactly repeat at 90° intervals. This effect can be explained on the basis that the crystal face is not exactly in the (001) plane. With the crystal set at 0° there is actually a small angle between the [100] direction and the external field, due to the error in the crystal surface. Rotation of 180° will give the same angle, but rotation of 90° will give a different angle. Thus resonance fields at angles 180° apart should be equal, but those 90° apart should be slightly different. This is in agreement with experimental results.

Results at the lower frequency (Fig. 4) show a number of deviations from the simple results at the higher frequency. In the first place the variation of resonant field with angle no longer follows the $\cos4\theta$ variation. In the second place, a second reso-

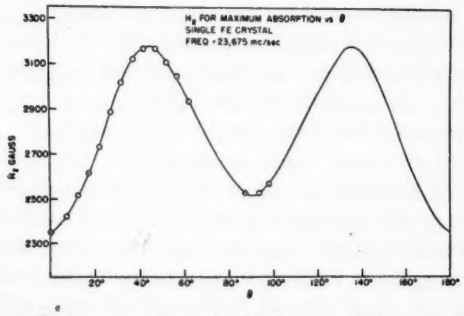

FIG. 3. Resonance magnetic field *vs.* angle between applied field and [100] direction in iron crystal, where frequency = 23,675 Mc/sec.

[4] J. A. Osborn, Phys. Rev. 67, 351 (1945).

nance occurs at angles near the [110] direction, at lower applied fields than for the expected resonance. Figure 5 shows a typical resonance curve at a particular angle, illustrating the appearance of the second resonance. Each of the foregoing phenomena will be discussed below.

The deviation from $\cos 4\theta$ variation of resonant field with angle at the lower frequency is readily accounted for as follows: with the relatively low applied fields used, the torque of anisotropy prevents alignment of the direction of magnetization with the applied field for some angles of applied field. We assume, however, that the magnitude of static magnetization is at its saturation value.

The effective field producing resonance is the component of H_s in the direction of magnetization, $H_s \cos\beta$, where β is the angle between H_s and the direction of magnetization, and the resonance condition depends upon the angle α between the [100] direction and the direction of magnetization instead of upon θ. (See Fig. 6.) It is to be noted that when the external field is in the [100] or [110] direction,

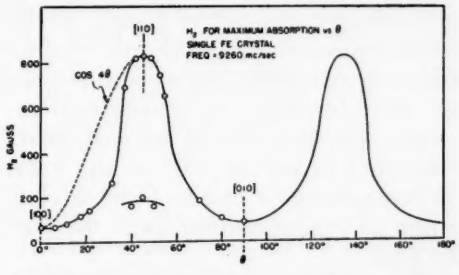

FIG. 4. Resonance magnetic field *vs.* angle between applied field and [100] direction in iron crystal, where frequency =9260 Mc/sec.

$\beta=0°$. This follows from the fact that the first-order anisotropy energy per unit volume is given by $f=(K_1/4)\sin^2 2\theta$ so that the torque $\partial f/\partial\theta$ becomes zero at $\theta=0°$ and $\theta=45°$. It follows that the anisotropy forces which cause the direction of magnetization to deviate from the direction of H_s disappear at these angles.

It is possible to check the validity of this explanation of the departure from $\cos 4\theta$ dependence by deriving from our experiment the anisotropy force constant and comparing this with the known value. To do this we first determine the value of α for each point on the experimental curve by comparison with the $\cos 4\theta$ curve (as shown in Fig. 4). The angle α for a given point on the experimental curve is obtained by finding the point on the $\cos 4\theta$ curve where the ordinate has a value $H_s \cos\beta$. The abscissa of this point is α. The torque acting to align the magnetization away from the [100] direction is $M_s H_s \sin\beta$. For all values of α this torque must equal the torque of anisotropy which tends to align the magnetization in the [100] direction. A plot of

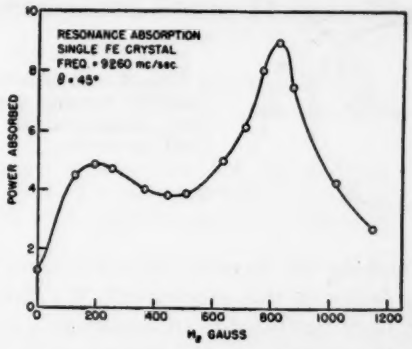

FIG. 5. Resonance absorption curve at 9260 Mc/sec. showing double peak which occurs when θ is near 45°.

$M_s H_s \sin\beta$ *versus* α obtained from the experimental data is shown in Fig. 7, where $M_s=1575$ gauss is used for the saturation magnetization. This should be the same as the curve for the torque of anisotropy, given by $K_1/2 \sin 4\alpha$. The experimental curve is seen to be approximately the expected shape. The value of K_1 evaluated from the experimental data is 3.0×10^5 ergs/cm^3. This is to be compared with the value 2.8×10^5 which has been obtained by H. J. Williams, using a single crystal of approximately the same composition as ours. Failure to get exact agreement is not surprising in view of the known fact that the simple picture we have assumed to describe the magnetization in a single crystal breaks down at low applied fields.[5]

The appearance of the second resonance peak at low fields when θ is near 45° can be qualitatively explained in the following manner. Consider the case where the applied magnetic field is in the [110] direction ($\theta=45°$). As the field is increased from zero, the value of α will change. Figure 7 can be used to determine the value of α for each value of H_s. The value of the resonance field can be determined for each value of α, using the known variation of resonance field with angle. In addition, $H_s \cos\beta$, the effective component of the applied field, can be calculated for each value of α. Comparison of these last two quantities shows that for fields around 200 gauss, the effective field is close enough to the resonance field to cause appreciable absorption in view of the width of the resonance curve. As the applied field is increased, however, the angle α increases very rapidly so that the effective applied field is very far below the field required for resonance. Absorption is thus lowered until the field has been increased to such an extent that the normal resonance at $\theta=45°$ begins to show. The double peak shown in Fig. 5 is in very good agreement with calculations made on this basis.

It should be noted that lack of knowledge of precise values of M_s and K_1 precludes the possi-

[5] A. von Engel and M. S. Wills, Proc. Roy. Soc. **A188**, 464 (1947).

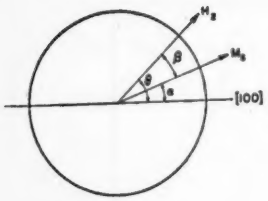

FIG. 6. Angular relationships among applied field, magnetization, and [100] direction.

bility of making an accurate determination of the effective g factor in this experiment. We have used the value of γ resulting from assuming $g=2$, but any value of g within, say, 10 percent of this would give equally good fit with the equations.**

At the lower frequency used, an additional observation was made which has not been shown on the curves. The resonance fields reported were determined using only one side of the crystal. When the crystal was reversed to expose the opposite face to the microwave field, results were in agreement with the results using the original side, except that an additional resonance peak was found for certain orientations of the crystal. The field required for this peak was of the order of 40 percent higher than for the normal resonance. The magnitude of the absorption and the field required for resonance was found to vary rapidly with angle, indicating that the effect was due to localized regions on the surface which behaved differently from the normal crystal surface, and whose effects disappeared as rotation of the crystal moved them out of the rectangular slit opening into the cavity. The normal resonance curve was unaffected, indicating that only a small fraction of the exposed area of the crystal behaved anomalously. This result has been attributed to small regions under stress, on the surface of one side of the crystal, which alter the anisotropy energy and hence affect the resonance fields. No observations were made of the stressed side of the crystal using the higher frequency.

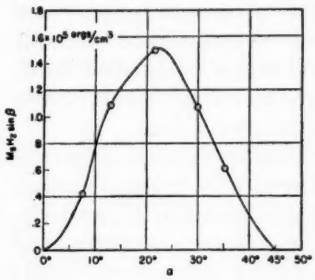

FIG. 7. Experimental curve showing anisotropy torque as a function of the angle α.

CONCLUSIONS

The results of these experiments show conclusively that the effects of anisotropy can be accounted for along the lines suggested by Kittel. In the case of the lower frequency used, a simple modification of the theory is necessary, taking into account the fact that the direction of magnetization may deviate from the direction of applied field. The second resonance peak observed at the lower frequency is explained as a result of the deviation of the direction of magnetization from the direction of applied field.

The authors wish to express their appreciation to Dr. Kittel for numerous very helpful discussions of the results of these experiments.

** Comparison of data taken at the two frequencies, assuming M_s and g to be the same in the two cases, allows elimination of M_s from the equation. The value of g obtained in this way is 2.14 ± 0.08.

Equations of State of Elements Based on the Generalized Fermi-Thomas Theory*

R. P. FEYNMAN,** N. METROPOLIS, AND E. TELLER***
Los Alamos Scientific Laboratory, University of California, Los Alamos, New Mexico
(Received January 21, 1949)

The Fermi-Thomas model has been used to derive the equation of state of matter at high pressures and at various temperatures. Calculations have been carried out both without and with the exchange terms. Discussion of similarity transformations lead to the virial theorem and to correlation of solutions for different Z values.

I. INTRODUCTION

THE Fermi-Thomas statistical model of the atom has been used by several investigators[1] for approximate calculations of potential fields and charge densities in metals as a function of lattice spacing. The method has also served as a starting point for the study of the behavior of matter under extremely high pressures as found, for example, in stars.

In its original form, the theory makes several simplifying assumptions: the effect of exchange forces is not taken into account, and the temperature of electrons and nuclei is taken as zero degrees absolute, $T=0$. With these simplifications, a set of universal potential functions may be found, applicable to all atomic numbers, Z, by a simple change in scale of linear dimensions.

Dirac[2] has extended the theory to include the effects of exchange forces. However, the solutions of the modified equation do not lend themselves to the above mentioned similarity transformation and it is necessary to obtain separate solutions for each Z.

Marshak and Bethe[3] have carried through a perturbation treatment of the simple Fermi-Thomas equation to include temperatures corresponding to several electron volts.

In the following, we present first a set of solutions for the simple Fermi-Thomas equation without exchange forces and for $T=0$. Although these numerical solutions are known, they have been calculated again because they are the unperturbed solutions in subsequent perturbation calculations. Hence, rather precise values are needed. A set of solutions was given for the case with exchange effects, but with $T=0$ as before, for several Z values by Slater and Krutter and by Jensen. To make more accurate interpolation possible we have obtained further solutions for $Z=6$ and 92. The various solutions for a given Z correspond to a series of atomic volumes. The value of the potential at the boundary is simply related to the pressure. Consequently a pressure-volume (or -density) relation can be obtained for that element. These new solutions with previously calculated ones[4] permit rather reliable interpolation for $P-v$ relations corresponding to any Z value. A set of numerical solutions is also given for the perturbation problem corresponding to non-zero temperatures. Finally solutions are given for the case of very high temperatures where the perturbation treatment is no longer valid and the complete equation must be considered.

II. SIMPLE FERMI-THOMAS METHOD

We consider first the simple Fermi-Thomas equation without exchange effects and for temperature, $T=0$,

$$d^2\phi/dx^2=\phi^{\frac{1}{2}}/x^{\frac{1}{2}}. \tag{1}$$

This equation is derived with the assumption that at each point in coordinate space there exists a relation between the electron density ρ_e and the potential V, namely

$$\rho_e=8\pi/3h^3[2m(E-eV)]^{3/2}, \tag{1a}$$

where m is the electronic mass and E the total energy. This relation is in turn obtained from the postulate that the electron wave functions in a small volume element behave like plane waves and that the electrons satisfy the Pauli exclusion principle. Spherical symmetry is assumed; x is the distance from the nucleus measured in units of

$$\mu=a_0(9\pi^2/128Z)^{\frac{1}{3}}=0.88534a_0/Z^{\frac{1}{3}}, \tag{1b}$$

where a_0 is the Bohr radius for hydrogen. ϕ is essentially the potential multiplied by $r=\mu x$; more precisely

$$Ze^2\phi=(E_0-eV)r, \tag{2}$$

where E_0 is the maximum total energy.

* This document is based on work performed at Los Alamos Scientific Laboratory of the University of California under Government Contract W-7405-Eng-36 and the information contained therein will appear in the National Nuclear Energy Series as part of the contribution of the Los Alamos Scientific Laboratory.
** Now at Cornell University, Ithaca, New York.
*** Now at the University of Chicago, Chicago, Illinois.
[1] J. C. Slater and H. M. Krutter, Phys. Rev. **47**, 559 (1935); H. Jensen, Zeits. f. Physik **111**, 373 (1938) and additional references given there.
[2] P. A. M. Dirac, Proc. Cambridge Phil. Soc. **26**, 376 (1930).
[3] R. E. Marshak and H. A. Bethe, Ap. J. **91**, 239 (1940).
[4] H. Jensen, G. Meyer-Gossler and H. Rohde, Zeits. f. Physik **110**, 277 (1938); see also, J. C. Slater and H. M. Krutter, reference 1.

TABLE I. Coefficients of the series solution for the Fermi-Thomas equation. a_2 is the initial slope. See Eq. (4).

$$a_3=\frac{4}{3}$$
$$a_4=0$$
$$a_5=\frac{2}{5}a_2$$
$$a_6=\frac{1}{3}$$
$$a_7=\frac{3}{70}a_2^2$$
$$a_8=\frac{2}{15}a_2$$
$$a_9=\frac{2}{27}-\frac{1}{252}a_2^3$$
$$a_{10}=\frac{1}{175}a_2^2$$
$$a_{11}=\frac{31}{1485}a_2+\frac{1}{1056}a_2^4$$

The boundary conditions may be written

$$\phi(0)=1 \tag{3}$$

and at the surface of the atom, since the potential gradient is zero,

$$d\phi/dx=\phi/x. \tag{3a}$$

In an actual crystal, the solutions of spherical symmetry are, of course, not strictly valid. It is more appropriate to surround each nucleus with a polyhedron containing an average number of electrons sufficient to neutralize the nuclear charge.

In many cases, the polyhedron may be replaced in good approximation by a sphere. Then condition (3a) is valid on the surface of this sphere and the radius $R(=\mu x_0)$ is defined as the atomic radius. It is to be noted that use of this procedure need not be restricted to crystals of pure elements.

ϕ may be expanded about the origin in a semi-convergent power series of the form

$$\phi=1+a_2x+a_3x^{\frac{3}{2}}+a_4x^2+\cdots. \tag{4}$$

Once a value is selected for the initial slope, i.e., a_2, the remaining coefficients are determined. Expressions for the first few coefficients in terms of a_2 are given in Table I. For a particular value of a_2, ϕ approaches the x-axis asymptotically. This solution corresponds to the free atom. For numerically smaller initial slopes, solutions are obtained for atoms of finite radius. Numerically greater initial slopes yield solutions for ions.

For the numerical integration it is convenient to introduce a change of independent variable,

$$x=w^2/2.$$

This, in effect, makes the interval for each step of the numerical integration conveniently small near the origin where ϕ changes appreciably, and automatically increases the interval farther out where the function changes more slowly. To initiate the numerical integration routine, the series given by (4) is rewritten in terms of w; it is evaluated at two points $w=0.88$ and $w=0.92$, hence the derivative is obtained at $w=0.90$. This procedure is more accurate than the evaluation of the derivative from the differentiation of the series. Intervals are taken as $\Delta w=0.04$. The error in each step is $<0.00002_5$ in ϕ.

In Table II, numerical solutions are given corresponding to eight values of the initial slope. ϕ is given at intervals $\Delta w=0.08$. These values are frequent enough for most purposes; if values for intermediate w values are desired, quadratic interpolation is adequate.

In Table III the values of a_2 are given corresponding to these solutions together with values for the atomic radius x_0 and for $\phi(x_0)$. The last two solutions, in which ϕ reaches zero, correspond to ions.

Finally one can obtain a pressure-volume relation based on this model with the aid of the following virial theorem,[5]

$$(\tfrac{3}{2})Pv=\text{kinetic energy}+(\tfrac{1}{2})(\text{potential energy}), \tag{5}$$

where P is pressure (dynes/cm^2) and

$$v=(4\pi/3)(\mu x_0)^3 \text{ cm}^3,$$

the volume. One can easily show that

$$Pv=(e/15)(Z^2e^2/\mu)x_0^{1/2}\phi^{5/2}(x_0). \tag{6}$$

Thus, having chosen a Z value, one can substitute values for x_0 and $\phi(x_0)$ from Table III and obtain a series of points on a $P-v$ diagram in this approximation. We shall return to a more complete discussion of equations of state after we have discussed the effects of exchange.

III. FERMI-THOMAS-DIRAC EQUATION

Dirac[2] has introduced modifications to the original Fermi-Thomas theory to include effects of exchange. Instead of Eq. (1) we have now to consider

$$d^2\psi/dx^2=x(\epsilon+\psi^{\frac{1}{2}}/x^{\frac{1}{2}})^3. \tag{7}$$

x has the same meaning as before,

$$\epsilon=(3/32\pi^2)^{\frac{2}{3}}Z^{-\frac{4}{3}}=0.211873Z^{-\frac{4}{3}}.$$

The potential without exchange effects, denoted by V_0, is connected with ψ by the relation

$$eV_0=E_0+2me^4/h^2-Ze^2\psi/\mu x.$$

Equation (7) is obtained by including in the expression for the average potential energy of an

[5] This is to be discussed in Section VI.

TABLE II. Numerical solutions of the Fermi-Thomas equation (without exchange effects). The initial slope a_2 for the various solutions is shown. The independent variable is $w=(2x)^{\frac{1}{2}}$, where x is the conventional Fermi-Thomas variable.

w	Case 1 $-a_2=1.58806$	Case 2 1.58842	Case 3 1.58856	Case 4 1.58865	Case 5 1.58870	Case 6 1.58874	Case 7 1.58884	Case 8 1.58876
0.92	0.64693	0.64676	0.64670	0.64666	0.64665	0.64663	0.64657	0.64661
1.00	0.60732	0.60712	0.60704	0.60699	0.60698	0.60695	0.60689	0.60693
1.08	0.56886	0.56862	0.56853	0.56847	0.56845	0.56842	0.56835	0.56840
1.16	0.53179	0.53151	0.53140	0.53133	0.53130	0.53127	0.53118	0.53124
1.24	0.49628	0.49595	0.49582	0.49574	0.49571	0.49567	0.49557	0.49564
1.32	0.46246	0.46207	0.46192	0.46182	0.46178	0.46173	0.46162	0.46170
1.40	0.43039	0.42994	0.42976	0.42965	0.42960	0.42954	0.42941	0.42915
1.48	0.40012	0.39959	0.39938	0.39925	0.39919	0.39913	0.39898	0.39909
1.56	0.37165	0.37103	0.37079	0.37064	0.37057	0.37049	0.37032	0.37045
1.64	0.34496	0.34424	0.34397	0.34379	0.34370	0.34361	0.34341	0.34357
1.72	0.32002	0.31919	0.31887	0.31866	0.31856	0.31845	0.31822	0.31840
1.80	0.29677	0.29581	0.29544	0.29520	0.29509	0.29496	0.29470	0.29490
1.88	0.27517	0.27405	0.27362	0.27334	0.27321	0.27307	0.27277	0.27300
1.96	0.25513	0.25384	0.25335	0.25302	0.25287	0.25271	0.25236	0.25263
2.04	0.23659	0.23511	0.23453	0.23416	0.23399	0.23380	0.23340	0.23371
2.12	0.21947	0.21777	0.21711	0.21668	0.21648	0.21626	0.21580	0.21616
2.20	0.20371	0.20175	0.20099	0.20050	0.20027	0.20001	0.19948	0.19990
2.28	0.18923	0.18697	0.18610	0.18554	0.18527	0.18498	0.18437	0.18485
2.36	0.17596	0.17337	0.17237	0.17172	0.17141	0.17108	0.17038	0.17093
2.44	0.16383	0.16086	0.15971	0.15897	0.15862	0.15823	0.15743	0.15806
2.52	0.15279	0.14939	0.14807	0.14722	0.14681	0.14637	0.14546	0.14618
2.60	0.14278	0.13888	0.13737	0.13640	0.13593	0.13543	0.13438	0.13521
2.68	0.13374	0.12928	0.12756	0.12644	0.12591	0.12533	0.12414	0.12508
2.76	0.12563	0.12054	0.11856	0.11729	0.11668	0.11602	0.11466	0.11574
2.84	0.11842	0.11259	0.11034	0.10889	0.10820	0.10744	0.10589	0.10711
2.92	0.11206	0.10541	0.10284	0.10118	0.10039	0.09953	0.09776	0.09916
3.00	0.10652	0.09894	0.09601	0.09412	0.09323	0.09225	0.09023	0.09182
3.08	0.10180	0.09316	0.08982	0.08767	0.08665	0.08553	0.08324	0.08505
3.16	0.09786	0.08802	0.08423	0.08178	0.08062	0.07935	0.07675	0.07880
3.24	0.09472	0.08351	0.07920	0.07642	0.07510	0.07365	0.07070	0.07303
3.32	0.09236	0.07960	0.07470	0.07154	0.07005	0.06841	0.06506	0.06771
3.40	0.09079	0.07629	0.07072	0.06714	0.06544	0.06358	0.05979	0.06279
3.48	0.09004	0.07354	0.06723	0.06316	0.06124	0.05914	0.05485	0.05824
3.56	0.09014	0.07137	0.06421	0.05961	0.05743	0.05505	0.05020	0.05403
3.64	0.09111	0.06978	0.06165	0.05644	0.05398	0.05129	0.04581	0.05014
3.72	0.09303	0.06876	0.05955	0.05365	0.05087	0.04784	0.04165	0.04654
3.80	0.09595	0.06833	0.05789	0.05123	0.04808	0.04466	0.03769	0.04319
3.88	0.09997	0.06851	0.05669	0.04195	0.04560	0.04174	0.03390	0.04009
3.96		0.06933	0.05594	0.04742	0.04342	0.03907	0.03026	0.03721
4.04		0.07083	0.05565	0.04603	0.04152	0.03662	0.02673	0.03453
4.12		0.07306	0.05584	0.04497	0.03989	0.03438	0.02329	0.03204
4.20		0.07608	0.05653	0.04426	0.03853	0.03234	0.01991	0.02971
4.28		0.07995	0.05775	0.04388	0.03743	0.03048	0.01658	0.02753
4.36			0.05953	0.04386	0.03660	0.02880	0.01327	0.02549
4.44			0.06193	0.04420	0.03603	0.02727	0.00996	0.02357
4.52			0.06500	0.04493	0.03573	0.02591	0.00663	0.02177
4.60				0.04606	0.03570	0.02469	0.00327	0.02007
4.68				0.04763	0.03595	0.02361	−0.00015	0.01845
4.76				0.04967	0.03650	0.02267		0.01692
4.84				0.05223	0.03736	0.02186		0.01545
4.92					0.03856	0.02118		0.01405
5.00					0.04011	0.02062		0.01270
5.08					0.04206	0.02020		0.01139
5.16					0.04443	0.01989		0.01012
5.24						0.01972		0.00886
5.32						0.01968		0.00764
5.40						0.01977		0.00643
5.48						0.01999		0.00523
5.56						0.02037		0.00403
5.64						0.02089		0.00282
5.72						0.02158		0.00160
5.80								0.00037
5.88								−0.00087
5.96								
6.04								
6.12								

TABLE III. Summary of the numerical integrations for the Fermi-Thomas equation (without exchange effects and for $T=0$). a_2 is the initial slope, x_0 is the radius of the atom, $\phi(x_0)$ is the boundary value of the ϕ function.

$-a_2$	x_0	$\phi(x_0)$
1.58806	7.385_1	0.0979_9
1.58842	8.588_0	0.0739_5
1.58856	9.565_1	0.0599_0
1.58865	10.803_8	0.0470_1
1.58870	11.963_4	0.0381_3
1.58874	15.869_5	0.0208_6
1.58884*	10.935_3	0
1.58876*	16.982_4	0

* Ions.

electron an exchange term equal to $2e^2p_0/h$, where p_0 is the maximum momentum for the coordinate point under consideration. The electron density is now connected to the electrostatic potential by the relation[6]

$$\rho_e=\frac{8\pi}{3h^3}\left\{\frac{2e^2m}{h}+\left[\frac{4e^4m^2}{h^2}+2m(E_0-eV_0)\right]^{\frac{1}{2}}\right\}^3.$$

In order to get the numerical integration of Eq. (7) started, ψ is first expanded into a semiconvergent power series about the origin. The form of this series is identical with that of Eq. (4). For convenience, we list the corresponding coefficients up to a_9 in Table IV. Again we introduce a change in independent variable $x=w^2/2$ and use the same numerical integration procedure beginning at $w=0.92$.

Slater and Krutter[1] have carried through numerical integrations for $Z=3$, 11, 29 and Jensen[4] for $Z=18$, 36, 54. We have obtained a family of six solutions for $Z=6$ and of ten for $Z=92$. The initial slopes and boundary values are shown in Tables V and VI for $Z=6$ and 92, respectively. Values for the two sets of ψ functions are listed in Tables VII and VIII at intervals of $\Delta w=0.08$. Here again quadratic interpolation is adequate to obtain ψ for intermediate w-values.

TABLE IV. Coefficients of the series solution for the Fermi-Thomas-Dirac equation. a_2 is the initial slope and $\epsilon=(3/32\pi^2)^{1/3}Z^{-2/3}=0.211873Z^{-2/3}$.

$$a_3=\frac{4}{3}$$

$$a_4=\frac{3}{2}\epsilon$$

$$a_5=\frac{2}{5}a_2+\frac{4}{5}\epsilon^2$$

$$a_6=\frac{1}{3}+\frac{a_2\epsilon}{2}+\frac{\epsilon^3}{6}$$

$$a_7=\frac{6}{35}a_2\epsilon^2+\frac{3}{70}a_2^2+\frac{5}{7}\epsilon$$

$$a_8=\frac{2}{15}a_2+\frac{77}{120}\epsilon^2$$

$$a_9=\frac{2}{27}-\frac{1}{252}a_2^3+\frac{11}{35}a_2\epsilon-\frac{1}{42}a_2^2\epsilon^2+\frac{10}{63}\epsilon^3+\frac{16}{105}\epsilon^4$$

From these results one may obtain a relation between pressure and density (or volume) for various elements at $T=0$. The pressure depends only on the minimum of the potential, $Ze\psi/r$, which is attained at the boundary of the atom. On that boundary no average force acts on the electrons, and the pressure is the same as would be caused by a density of free electrons equal to the electron density at the boundary. This electron density is in turn determined by the potential at the boundary, and one obtains for the pressure the formula

$$P=\frac{Ze^2}{10\pi\mu^4}\left(\left(\frac{\psi(x_0)}{x_0}\right)^{\frac{1}{2}}+\epsilon\right)^5\left\{1-\frac{5\epsilon/4}{(\psi(x_0)/x_0)^{\frac{1}{2}}+\epsilon}\right\}. \quad (8)$$

The relation just obtained is in effect a dependence of the pressure on the atomic volume since the value of ψ/x depends exclusively on the atomic radius and hence on the atomic volume.

In this way the pressure-density relationship is applicable to materials composed of several kinds of elements. The volume at a given pressure is obtained by adding the atomic volumes appropriate for that pressure.

In order to express pressure-density relationships for various Z values in a form which permits convenient interpolation for intermediate Z values, we follow Jensen[7] and express the pressure in units of the pressure $\bar{P}$ resulting from a uniform distribution of all the electrons of the material throughout the total available volume,[7a] i.e.,

$$P=\bar{P}f^{5/3},$$

where

$$f(\xi)=\frac{x_0^3}{3}\left(\left(\frac{\psi(x_0)}{x_0}\right)^{\frac{1}{2}}+\epsilon\right)^3\left\{1-\frac{5\epsilon/4}{(\psi(x_0)/x_0)^{\frac{1}{2}}+\epsilon}\right\}^{3/5} \quad (9)$$

where

$$\xi=Z^{-\frac{1}{3}}a_0\left(\frac{3Z}{4\pi\mu x_0}\right)^{\frac{1}{3}}=\frac{0.701}{x_0}$$

is the variable against which we plot the function f.

In Fig. 1 we have compiled the values given by Jensen for $Z=18$, 36, 54; rewritten data of Slater and Krutter in this form; and added the new calculations for $Z=6$, 92. In this way we have obtained sufficient data, so that satisfactory interpolation for any Z value is possible. Finally we have graphed our numerical values for the case without exchange.

[6] See J. C. Slater and H. M. Krutter, reference 1.

[7] See H. Jensen, reference 1, Eqs. (4a, b, c) and (5).

[7a] Explicitly, $\bar{P}=2/5(3/8\pi)^{2/3}(\hbar^2/2m)(\bar{\rho})^{5/3}$, where $\bar{\rho}$ is the uniform density of electrons.

TABLE V. Summary of the numerical results (with exchange effects) for carbon. The initial slope a_2, and the boundary values are given.*

$-a_2$	x_0	$\psi(x_0)$
1.6740	3.2617	0.23194
1.6800	3.7153	0.16946
1.6840	4.3784	0.10816
1.6858	5.1678	0.06124
1.6863	5.7291	0.03942
1.6867	7.0084	0.01079

* $x_{0(\rho=2.35)}=6.28$.

The pressure-density relations so derived are valid only at rather high pressures at which the detailed influence of the outer shell structure of the atoms has been obliterated. This usually happens at pressures exceeding ten megabars.

IV. PERTURBATION TREATMENT OF TEMPERATURE EFFECTS

If the value of the temperature is low compared to the maximum kinetic energy of electrons near the boundary between atoms, i.e., if

$$kT \ll (Ze^2/\mu)[\phi(x_0)/x_0], \tag{10}$$

the influence of the temperature can be treated by perturbation methods. The influence of this perturbation on the Fermi-Thomas distribution will now be discussed and in this discussion we shall disregard the effects of exchange. It has been shown by Ashkin[8] that the influence of the temperature perturbation and of exchange effects are very nearly additive.

Marshak and Bethe[3] have shown that the perturbation from temperature can be taken into account by modifying Eq. (1a), which connects the electron density and the electrostatic potential. They derive the expression

$$\rho_e=\frac{8\pi}{3h^3}(2m(E-eV))^{\frac{1}{2}}\left\{1+\frac{\pi^2k^2T^2}{8(E-eV)}\right\}, \tag{11}$$

where E is the Fermi energy and k is the Boltzmann constant. This leads to the corresponding differential equation for the potential

$$\frac{d^2\Phi}{dx^2}=\frac{\Phi^{\frac{1}{2}}}{x^{\frac{1}{2}}}\left[1+\frac{\zeta T^2x^2}{\Phi^2}\right], \tag{12}$$

where $(Ze^2\Phi/\mu x)=E-eV$ analogous to Eq. (2), $\zeta=\pi^2k^2\mu^2/8Z^2e^4$, and μ is given by Eq. (1b). The boundary conditions are $\Phi(0)=1$ and $d\Phi/dx=\Phi/x$. The solution of this equation can be written

$$\Phi=\phi+\zeta T^2\phi_1,$$

where ϕ is the unperturbed solution obtained in Section II and ϕ_1 satisfies the differential equation

$$\frac{d^2\phi_1}{dx^2}=\frac{3\phi^{\frac{1}{2}}\phi_1}{2x^{\frac{1}{2}}}+\frac{x^{\frac{1}{2}}}{\phi^{\frac{1}{2}}}. \tag{13}$$

Expanding $\phi_1=\sum C_nx^{n/2}$ and using the series expansion for ϕ given by Eq. (4), one finds, taking $C_2=0$, that

$$C_3=C_4=C_5=C_6=0,$$
$$C_7=(4/35);\quad C_8=0;\quad C_9=-(4/63)a_2;$$
$$C_{10}=-(13/525);\quad C_{11}=0,$$

where a_2 is the initial slope of ϕ. Here again it is

[8] J. Ashkin, unpublished report.

TABLE VI. Results of the numerical integration of the Fermi-Thomas-Dirac equation for uranium.*

$-a_2$	x_0	$\psi(x_0)$
1.60394	6.5139	0.10164
1.60444	7.4877	0.07495
1.60484	10.2143	0.03507
1.60488	11.3326	0.02623
1.60490	12.4037	0.01991
1.60491	13.3862	0.01551
1.60491_5	14.2941	0.01228
1.60492	15.6084	0.00871
1.60492_4	19.4301	0.00286
1.60500*, **		0

* $x_{0(\rho=19.0)}=16.47$.
** Ion.

TABLE VII. Solutions of the Fermi-Thomas-Dirac equation for carbon. It is to be noted that the more convenient independent variable w is used here.

	Case 1 $-a_2=1.6740$	Case 2 1.6800	Case 3 1.6840	Case 4 1.6858	Case 5 1.6863	Case 6 1.6867
w	ψ	ψ	ψ	ψ	ψ	ψ
0.92	0.62232	0.61957	0.61774	0.61691	0.61668	0.61650
1.00	0.58007	0.57676	0.57455	0.57356	0.57328	0.57306
1.08	0.53924	0.53528	0.53264	0.53145	0.53112	0.53086
1.16	0.50013	0.49543	0.49230	0.49089	0.49049	0.49018
1.24	0.46300	0.45744	0.45373	0.45206	0.45160	0.45123
1.32	0.42803	0.42146	0.41709	0.41513	0.41458	0.41414
1.40	0.39534	0.38763	0.38249	0.38018	0.37954	0.37903
1.48	0.36507	0.35602	0.34999	0.34728	0.34653	0.34593
1.56	0.33727	0.32667	0.31962	0.31644	0.31556	0.31486
1.64	0.31201	0.29962	0.29137	0.28766	0.28663	0.28581
1.72	0.28935	0.27487	0.26524	0.26091	0.25970	0.25874
1.80	0.26933	0.25242	0.24118	0.23613	0.23472	0.23361
1.88	0.25202	0.23228	0.21916	0.21327	0.21162	0.21033
1.96	0.23747	0.21442	0.19913	0.19227	0.19033	0.18884
2.04	0.22578	0.19888	0.18104	0.17304	0.17078	0.16905
2.12	0.21707	0.18565	0.16484	0.15552	0.15288	0.15087
2.20	0.21150	0.17477	0.15050	0.13964	0.13656	0.13422
2.28	0.20927	0.16630	0.13797	0.12532	0.12172	0.11901
2.36	0.21067	0.16034	0.12725	0.11251	0.10831	0.10514
2.44	0.21605	0.15701	0.11833	0.10113	0.09623	0.09254
2.52	0.22589	0.15649	0.11121	0.09114	0.08542	0.08112
2.60	0.24080	0.15903	0.10595	0.08250	0.07582	0.07081
2.68	0.26156	0.16494	0.10261	0.07518	0.06738	0.06153
2.76	0.28920	0.17465	0.10129	0.06917	0.06005	0.05321
2.84		0.18870	0.10214	0.06447	0.05378	0.04579
2.92			0.10536	0.06109	0.04857	0.03920
3.00			0.11123	0.05909	0.04438	0.03340
3.08			0.12011	0.05853	0.04123	0.02833
3.16			0.13247	0.05953	0.03914	0.02396
3.24			0.14892	0.06224	0.03814	0.02024
3.32				0.06688	0.03831	0.01714
3.40					0.03975	0.01465
3.48					0.04261	0.01275
3.56						0.01143
3.64						0.01072
3.72						0.01063
3.80						0.01123
3.88						0.01259
3.96						
4.04						
4.12						
4.20						

TABLE VIII. Solutions of the Fermi-Thomas-Dirac equation for uranium.

w	Case 1 $-\sigma_1=1.60394$ ψ	Case 2 1.60444 ψ	Case 3 1.60484 ψ	Case 4 1.60488 ψ	Case 5 1.60490 ψ	Case 6 1.60491 ψ	Case 7 1.604915 ψ	Case 8 1.60492 ψ	Case 9 1.604924 ψ	Case 10 1.60500 ψ
0.92	0.64210	0.64187	0.64169	0.64167	0.64166	0.64166	0.64165	0.64165	0.64165	0.64161
1.00	0.60189	0.60161	0.60139	0.60137	0.60136	0.60135	0.60135	0.60135	0.60134	0.60130
1.08	0.56284	0.56251	0.56225	0.56222	0.56221	0.56220	0.56220	0.56220	0.56219	0.56214
1.16	0.52521	0.52482	0.52451	0.52448	0.52446	0.52445	0.52445	0.52444	0.52444	0.52438
1.24	0.48917	0.48871	0.48834	0.48830	0.48828	0.48828	0.48827	0.48827	0.48826	0.48819
1.32	0.45485	0.45431	0.45387	0.45383	0.45381	0.45380	0.45379	0.45378	0.45378	0.45370
1.40	0.42232	0.42169	0.42118	0.42113	0.42110	0.42109	0.42108	0.42108	0.42107	0.42097
1.48	0.39164	0.39089	0.39030	0.39024	0.39021	0.39019	0.39018	0.39018	0.39017	0.39009
1.56	0.36279	0.36192	0.36123	0.36116	0.36113	0.36111	0.36110	0.36109	0.36109	0.36095
1.64	0.33578	0.33477	0.33396	0.33388	0.33384	0.33382	0.33381	0.33380	0.33380	0.33364
1.72	0.31057	0.30939	0.30846	0.30836	0.30832	0.30829	0.30828	0.30827	0.30826	0.30808
1.80	0.28710	0.28574	0.28465	0.28455	0.28449	0.28447	0.28445	0.28444	0.28443	0.28422
1.88	0.26532	0.26375	0.26249	0.26237	0.26231	0.26228	0.26226	0.26225	0.26223	0.26199
1.96	0.24517	0.24336	0.24190	0.24176	0.24169	0.24165	0.25163	0.24161	0.24160	0.24132
2.04	0.22658	0.22448	0.22280	0.22264	0.22255	0.22251	0.22249	0.22247	0.22245	0.22213
2.12	0.20947	0.20705	0.20511	0.20492	0.20483	0.20478	0.20475	0.20473	0.20471	0.20434
2.20	0.19378	0.19099	0.18875	0.18853	0.18842	0.18837	0.18834	0.18831	0.18829	0.18786
2.28	0.17946	0.17621	0.17364	0.17339	0.17326	0.17320	0.17316	0.17313	0.17311	0.17262
2.36	0.16637	0.16266	0.15970	0.15941	0.15926	0.15919	0.15915	0.15912	0.15909	0.15852
2.44	0.15452	0.15026	0.14686	0.14652	0.14635	0.14627	0.14622	0.14618	0.14615	0.14550
2.52	0.14384	0.13894	0.13503	0.13464	0.13445	0.13436	0.13430	0.13426	0.13422	0.13347
2.60	0.13427	0.12864	0.12416	0.12371	0.12349	0.12338	0.12332	0.12327	0.12323	0.12237
2.68	0.12577	0.11931	0.11417	0.11366	0.11340	0.11328	0.11321	0.11315	0.11310	0.11212
2.76	0.11831	0.11089	0.10500	0.10442	0.10413	0.10398	0.10390	0.10384	0.10378	0.10265
2.84	0.11185	0.10335	0.09660	0.09593	0.09560	0.09543	0.09534	0.09527	0.09520	0.09391
2.92	0.10637	0.09663	0.08891	0.08815	0.08776	0.08757	0.08747	0.08738	0.08731	0.08583
3.00	0.10187	0.09072	0.08188	0.08101	0.08057	0.08035	0.08023	0.08014	0.08003	0.07836
3.08	0.09834	0.08557	0.07547	0.07447	0.07397	0.07372	0.07359	0.07347	0.07337	0.07145
3.16	0.09579	0.08117	0.06963	0.06849	0.06792	0.06764	0.06748	0.06735	0.06724	0.06504
3.24	0.09424	0.07750	0.06432	0.06302	0.06238	0.06205	0.06187	0.06173	0.06160	0.05910
3.32	0.09373	0.07456	0.05952	0.05804	0.05730	0.05693	0.05673	0.05656	0.05642	0.05357
3.40	0.09430	0.07235	0.05519	0.05350	0.05266	0.05224	0.05201	0.05182	0.05165	0.04841
3.48	0.09603	0.07088	0.05130	0.04938	0.04842	0.04794	0.04768	0.04747	0.04727	0.04359
3.56	0.09900	0.07017	0.04783	0.04564	0.04456	0.04401	0.04371	0.04347	0.04325	0.03907
3.64	0.10332	0.07024	0.04476	0.04227	0.04104	0.04042	0.04008	0.03981	0.03956	0.03480
3.72		0.07114	0.04207	0.03925	0.03785	0.03714	0.03676	0.03644	0.03616	0.03077
3.80		0.07293	0.03975	0.03655	0.03496	0.03416	0.03372	0.03336	0.03305	0.02694
3.88		0.07567	0.03779	0.03415	0.03235	0.03144	0.03095	0.03054	0.03018	0.02326
3.96			0.03619	0.03205	0.03001	0.02898	0.02842	0.02796	0.02755	0.01973
4.04			0.03493	0.03024	0.02792	0.02676	0.02612	0.02560	0.02514	0.01629
4.12			0.03402	0.02870	0.02607	0.02475	0.02403	0.02344	0.02292	0.01293
4.20			0.03347	0.02742	0.02445	0.02296	0.02214	0.02148	0.02088	0.00962
4.28			0.03328	0.02642	0.02305	0.02136	0.02044	0.01969	0.01902	0.00633
4.36			0.03347	0.02568	0.02186	0.01995	0.01891	0.01806	0.01731	0.00303
4.44			0.03406	0.02521	0.02088	0.01873	0.01755	0.01659	0.01574	
4.52			0.03507	0.02502	0.02012	0.01768	0.01634	0.01526	0.01430	
4.60				0.02511	0.01955	0.01680	0.01529	0.01407	0.01298	
4.68				0.02551	0.01920	0.01608	0.01438	0.01301	0.01178	
4.76				0.02622	0.01907	0.01554	0.01361	0.01206	0.01068	
4.84				0.02728	0.01916	0.01516	0.01298	0.01124	0.00967	
4.92					0.01948	0.01495	0.01249	0.01052	0.00876	
5.00					0.02005	0.01492	0.01214	0.00991	0.00793	
5.08						0.01507	0.01192	0.00941	0.00718	
5.16						0.01541	0.01185	0.00901	0.00650	
5.24						0.01596	0.01193	0.00872	0.00589	
5.32							0.01216	0.00853	0.00534	
5.40							0.01255	0.00845	0.00485	
5.48								0.00848	0.00442	
5.56								0.00862	0.00404	
5.64								0.00889	0.00371	
5.72									0.00344	
5.80									0.00321	
5.88									0.00304	
5.96									0.00291	
6.04									0.00283	
6.12									0.00280	
6.20									0.00282	
6.28									0.00290	

convenient to make the change of independent variable $x=w^2/2$. The series solution for the perturbation function was evaluated at $w=0.48$ and was extended by a numerical procedure similar to those used above.

Three numerical solutions for ϕ_1 were obtained. They are obtained by substituting three different ϕ functions from Part II into Eq. (13). These ϕ functions may be characterized by their initial slopes $a_2=1.58856$, 1.58865, and 1.58874 (see Tables II and III). In Table IX numerical solutions are given corresponding to these three cases for the range of w that is of interest. The derivatives are also given as they are needed to satisfy the boundary conditions.

With these solutions, a series of points on a $P-v-T$ diagram may be obtained in the following manner. For a given Z, one assumes a temperature T and determines x_0, and hence atomic volume (or density), from the boundary condition $d\Phi/dx=\Phi/x$. The pressure may be obtained either by the approximate expression obtained by Marshak and Bethe or by using tables of the complete expression worked out by MacDougall and Stoner.[9] Specifically they tabulate

$$I_{3/2}(\eta)=\int_0^\infty x^{3/2}dx/(e^{x-\eta}+1).$$

The expression for the pressure in dynes/cm² is[10]

$$P=\frac{8\pi}{3h^3}(2m)^{3/2}(kT)^{5/2}I_{3/2}(\eta),$$

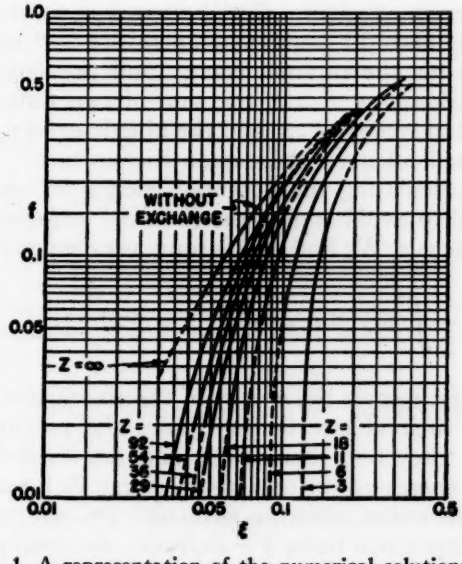

FIG. 1. A representation of the numerical solutions of the Fermi-Thomas-Dirac equation in a form that permits interpolation for intermediate Z values. f is related to pressure and ξ^3 is proportional to density (see Eq. (9)).

[9] J. MacDougall and E. C. Stoner, Phil. Trans. Roy. Soc. 237, 67 (1938).

[10] In the next section, this expression is discussed in more detail.

TABLE IX. Solutions of the temperature-perturbation equation. The unperturbed solutions associated with them may be identified by the given values of a_2. Only the interesting region is tabulated.

	(a_2=1.58856)		(a_2=1.58865)			(a_2=1.58874)	
w	ϕ_1	$\frac{d\phi_1}{dw}$	ϕ_1	$\frac{d\phi_1}{dw}$	w	ϕ_1	$\frac{d\phi_1}{dw}$
2.60	19.211		19.223		3.60	310.28	
2.64		68.757		68.833	3.64		829.73
2.68	24.712		24.730		3.68	376.66	
2.72		86.027		86.139	3.72		987.60
2.76	31.594		31.621		3.76	455.67	
2.80		107.07		107.24	3.80		1171.9
2.84	40.160		40.200		3.84	549.42	
2.88		132.61		132.84	3.88		1386.6
2.92	50.768		50.827		3.92	660.35	
2.96		163.45		163.79	3.96		1636.0
3.00	63.844		63.931		4.00	791.23	
3.04		200.55		201.04	4.04		1925.0
3.08	79.888		80.014		4.08	945.23	
3.12		245.00		245.69	4.12		2259.0
3.16	99.488		99.669		4.16	1126.0	
3.20		298.06		299.03	4.20		2644.3
3.24	123.33		123.59		4.24	1337.5	
3.28		361.16		362.51	4.28		3087.6
3.32	152.22		152.59		4.32	1584.5	
3.36		435.94		437.79	4.36		3596.6
3.40	187.10		187.61		4.40	1872.2	
3.44		524.25		526.77	4.44		4179.9
3.48	229.04		229.76		4.48	2206.6	
3.52		628.24		631.62	4.52		4847.1
3.56	279.30		280.29		4.56	2594.4	
3.60		750.30		754.77	4.60		5608.7
3.64	339.33		340.67		4.64	3043.1	
3.68		893.18		899.00	4.68		6476.7
3.72	410.79		412.59		4.72	3561.2	
3.76		1060.0		1067.4	4.76		7464.3
3.80	495.59		497.98		4.80	4158.4	
3.84		1254.4		1263.7	4.84		8586.4
3.88	595.94		599.08		4.88	4845.3	
3.92		1480.5		1491.7	4.92		9859.8
3.96	714.38		718.41		4.96	5634.1	
4.00		1743.0		1756.1	5.00		11303.0
4.04	853.82		858.90		5.04	6538.3	
4.08		2047.6		2062.1	5.08		12938.0
4.12	1017.6		1023.9		5.12	7573.4	
4.16		2401.0		2415.7	5.16		14789.0
4.20	1209.7		1217.1		5.20	8756.5	
4.24		2811.1		2823.8	5.24		16884.0
4.28	1434.6		1443.0		5.28	10107.0	
4.32		3287.5		3294.4	5.32		19256.0
4.36	1697.6		1706.6		5.36	11648.0	
4.40		3842.0		3837.0	5.40		21942.0
4.44	2005.0		2013.5		5.44	13403.0	
4.48		4489.1		4462.8	5.48		24987.0
4.52	2364.1		2370.6		5.52	15402.0	
4.56				5185.4	5.56		28443.0
4.60			2785.4		5.60	17678.0	
4.64				6020.9	5.64		32375.0
4.68			3267.1		5.68	20268.0	
4.72				6989.3	5.72		36856.0
					5.76	23216.0	
					5.80		41977.0
					5.84		

where

$$\eta=\pi\frac{\Phi(x_0)}{x_0}/(2T(2\zeta)^{\frac{1}{2}}).$$

V. EXACT TREATMENT OF TEMPERATURE EFFECTS

For the case of high temperatures the perturbation treatment given in the preceding section is not very accurate. In this section the effects of temperature will be taken into account exactly. Inasmuch as the effects of exchange for this range of temperature are relatively unimportant, we consider only the approximation in which they are neglected.

The effect of temperature is to alter the charge distribution of electrons in the atom. The number of states available to an electron of momentum p at position r is $2[4\pi p^2dp][4\pi r^2dr]/h^3$. The basis of

the simple Fermi-Thomas model at $T=0$ is to consider that all of the states up to the maximum available momentum are occupied and that the rest are empty. If the temperature is raised, the statistical analysis of Fermi and Dirac tells us that the probability that a state of momentum p, and hence of energy, $p^2/2m-eV$, is filled is

$$1/[\exp([(p^2/2m-eV)/kT]+\eta)+1],$$

where k is Boltzmann's constant and η is a constant which is determined by the condition that the total number of electrons is given. Therefore the density of electrons is

$$-\rho_e=\int_0^\infty \frac{2\cdot 4\pi p^2 dp/h^3}{\exp[(p^2/2m-eV/kT)+\eta]+1}. \quad (14)$$

Substituting this expression for the charge density into Poisson's equation we obtain

$$\frac{1}{r}\frac{d^2V}{dr^2}=\frac{16\pi^2}{h^3}\cdot e((2mkT)^{\frac{1}{2}})^3 I_{\frac{1}{2}}\left(\frac{eV}{kT}-\eta\right), \quad (15)$$

where the function $I_{\frac{1}{2}}(\eta)$ is defined by

$$I_n(\eta)=\int_0^\infty \frac{y^n dy}{\exp(y-\eta)+1} \quad (15a)$$

and arises for $n=\frac{1}{2}$ from Eq. (14) if one replaces $p^2/2mkT$ by y. It is Eq. (15) that we solve numerically.

The equation can be simplified by a change of variables. Let $s=r/c$ where

$$c=\left(\frac{h^3}{32\pi^2e^2m(2mkT)^{\frac{1}{2}}}\right)^{\frac{1}{2}}=\frac{1.602\times10^{-9}\text{ cm}}{T_{\text{kv}}^{\frac{1}{2}}}, \quad (16)$$

where T_{kv} is the temperature measured in kilovolts. The constant η in Eq. (15) can be removed by a change in the zero of potential V. Setting

$$\beta/s=(eV/kT)-\eta,$$

Eq. (15) becomes

$$d^2\beta/ds^2=sI_{\frac{1}{2}}(\beta/s). \quad (17)$$

The boundary condition is

$$d\beta/ds=\beta/s \text{ at } s=b, \quad (18)$$

where $a=cb$ is the atomic radius. At the origin, since V is to vary as Ze/r, β must approach a constant value

$$\alpha=Ze^2/kTc=0.0899Z/T_{\text{kv}}^{\frac{1}{2}}. \quad (19)$$

Because of the singular behavior of $I_{\frac{1}{2}}(\beta/s)$ as $s\to0$ (it varies as $s^{-\frac{1}{2}}$) numerical integration from the origin is laborious. To avoid this difficulty, another procedure was used. Setting $s=w^2/2$, Eq. (17) becomes,

$$(d/dw)(1/w)(d\beta/dw)=2w^3I_{\frac{1}{2}}(2\beta/w^2). \quad (20)$$

The equation was integrated from the outside ($w^2=2a/c$) inwards (to $w=0$) and no difficulties arise as the origin is approached. The limiting value of β as $w\to0$, i.e., α is easily determined. The solution is started by choosing, arbitrarily, a value of b, and of β at $s=b$ and using Eq. (18) or its equivalent $(d\beta/dw)=2\beta/w$ to get the initial value of the derivative of β. It is only after the solution is complete and the value of α is determined that the temperature (from Eq. (19)) and the density (from $a=bc$ where c is given by Eq. (16)) can be evaluated. That these turn out to be in an interesting region requires judicious choice of the initial values of b and β, but this is not a real difficulty.

The numerical procedure is similar to that described earlier. The values of $I_{\frac{1}{2}}(2\beta/w^2)$ are obtained with the help of tables of the function $I_{\frac{1}{2}}(y)$ given by MacDougall and Stoner.[9] The interval g is so chosen that the error in 2β per step which is approximately

$$\frac{g}{6}\left[\frac{d}{dw}w^3I_{\frac{1}{2}}\left(\frac{2\beta}{w^2}\right)+\frac{w}{2}\frac{d^2}{dx^2}\left(\frac{2\beta}{w^2}\right)\right]$$

is kept below 0.0001. This usually means that for large w, the interval g can be 0.05 but as the origin is approached it is frequently necessary (below $w=1.4$) to reduce it to 0.025.

The values of β as a function of w for various cases are given in Table X.

After the potential distribution V is known, we can calculate at a given temperature and density values for the internal energy and pressure. The internal energy E_{tot} is the sum of two terms, the potential energy, E_{pot}, and the kinetic energy, E_{kin}. We shall calculate these quantities in turn.

In calculating the potential energy we must be careful to avoid adding the (infinite) self-energy of the nucleus. We find, if δ is some very small radius,

$$E_{\text{pot}}=\frac{e}{2}\int_\delta^a \rho_e V\cdot 4\pi r^2dr+\tfrac{1}{2}Z[V-(Ze/r)]_{r=\delta}. \quad (21)$$

The first term is the energy of the atomic electrons, being their charge density times the potential in which they find themselves, and the second term is the energy of the nucleus of charge Ze because of its interaction with the electrons, the potential of this interaction being $V-Ze/r$, i.e., the total potential less that due to the nucleus itself. (The factor $\frac{1}{2}$ arises in the usual manner because calculating this way we count each interaction twice.) If for ρ_e, the expression given by Eq. (14) is used, the lower limit of the integral can be put equal to zero. For $[V-(Ze/r)]$ at small r, we can write its equal.

TABLE X. Solutions of the temperature dependent Fermi-Thomas equation.

	Case 1*	Case 2	Case 3	Case 4	Case 5	Case 6	Case 7	Case 8	Case 9	Case 10	Case 11
w	β	β	β	β	β	β	β	β	β	β	β
0.00	7.2021	3.9774	9.8160	6.8602	3.7659	6.8918	0.31208	5.8808	2.3570	5.2326	30.3768
0.10	7.1183	3.9324	9.6912	6.7770	3.7162	6.8136	0.27857	5.8127	2.3156	5.1661	29.8494
0.2	6.8914	3.8071	9.3559	6.5510	3.5762	6.6016	0.17822	5.6268	2.1961	4.9820	28.4774
0.3	6.5549	3.6156	8.8631	6.2118	3.3584	6.2874	0.01115	5.3472	2.0044	4.7006	26.5480
0.4	6.1386	3.3698	8.2594	5.7872	3.0736	5.8992	−0.2227	4.9964	1.7452	4.3415	24.2840
0.5	5.6676	3.0800	7.5832	5.3002	2.7302	5.4604	−0.5232	4.5922	1.4217	3.9179	21.8776
0.6	5.1615	2.7536	6.8648	4.7679	2.3338	4.9902	−0.8908	4.1492	1.0351	3.4402	19.4648
0.7	4.6352	2.3960	6.1256	4.2025	1.8872	4.5024	−1.3250	3.6773	0.5849	2.9148	17.1384
0.8	4.0985	2.0100	5.3798	3.6112	1.3906	4.0074	−1.8262	3.1828	0.0694	2.3438	14.9551
0.9	3.5572	1.5959	4.6348	2.9964	0.8419	3.5111	−2.3940	2.6684	−0.5130	1.7262	12.9442
1.0	3.0132	1.1527	3.8924	2.3567	0.2377	3.0162	−3.0288	2.1336	−1.1631	1.0576	11.1144
1.1	2.4655	0.6782	3.1494	1.6876	−0.4248	2.5229	−3.7302	1.5756	−1.8812	0.3328	9.4598
1.2		0.1702	2.3992	0.9828	−1.1481	2.0294	−4.4986	0.9902	−2.6674	−0.4530	7.9651
1.3		−0.3731	1.6328	0.2357	−1.9324	1.5328	−5.3336	0.3731	−3.5216	−1.3036	6.6084
1.4		−0.9528	0.8413	−0.5584	−2.7782	1.0224	−6.2360	−0.2804	−4.4440	−2.2194	5.3642
1.5		−1.5695	0.0167	−1.4046	−3.6856	0.5028	−7.2046	−0.9731	−5.4346	−3.2014	4.2054
1.6		−2.2234	−0.8466	−2.3030	−4.6548	−0.02762	−8.2400	−1.7048	−6.4933	−4.2498	3.1051
1.7		−2.9145	−1.7552	−3.2548	−5.6857	−0.5698	−9.3422	−2.4766	−7.6201	−5.3648	2.0387
1.8		−3.6426	−2.7084	−4.2602	−6.7783	−1.1237	−10.5110	−3.2886	−8.8150	−6.5464	0.9857
1.9		−4.4076	−3.7076	−5.3198	−7.9326	−1.6887	−11.7466	−4.1410	−10.0780	−7.7947	−0.06935
2.0		−5.2088	−4.7536	−6.4337	−9.1486	−2.2636	−13.0490	−5.0338	−11.4090	−9.1097	−1.1370
2.1		−6.0459	−5.8467	−7.6018	−10.4262	−2.8470	−14.4180	−5.9666	−12.8081	−10.4914	−2.2246
2.2		−6.9182	−6.9870	−8.8241	−11.7654	−3.4365	−15.8536	−6.9392	−14.2751	−11.9396	−3.3389
2.3		−7.8252	−8.1746	−10.1005	−13.1660	−4.0298	−17.3558	−7.9511	−15.8100	−13.4546	−4.4842
2.4		−8.7664	−9.4093	−11.4308	−14.6280	−4.6236	−18.9247	−9.0018	−17.4129	−15.0360	−5.6582
2.5		−9.7405	−10.6908	−12.8150	−16.1512	−5.2146	−20.5601	−10.0908	−19.0836	−16.6840	−6.8620
2.6		−10.7467	−12.0190	−14.2528	−17.7356	−5.7986	−22.2620	−11.2172	−20.8222	−18.3984	−8.0961
2.7		−11.7839	−13.3935	−15.7438	−19.3812	−6.3704	−24.0304	−12.3805	−22.6284	−20.1790	−9.3604
2.8		−12.8509	−14.8138	−17.2880	−21.0876	−6.9243	−25.8652	−13.5797	−24.5024	−22.0260	−10.6544
2.9		−13.9464	−16.2794	−18.8850	−22.8547	−7.4536	−27.7663	−14.8140	−26.4439	−23.9391	−11.9776
3.0		−15.0684	−17.7898	−20.5345	−24.6825		−29.7337	−16.0822	−28.4530	−25.9182	−13.3291
3.1		−16.2162	−19.3445	−22.2361	−26.5708		−31.7673	−17.3833	−30.5295	−27.9634	−14.7079
3.2		−17.3877	−20.9428	−23.9894	−28.5192		−33.8670	−18.7161	−32.6734	−30.0743	−16.1128
3.3		−18.5807	−22.5840	−25.7940	−30.5278		−36.0328	−20.0790	−34.8846	−32.2509	−17.5422
3.4		−19.7930	−24.2673	−27.6496	−32.5962		−38.2644	−21.4706	−37.1629	−34.4930	−18.9946
3.5		−21.0222	−25.9919	−29.5554	−34.7242		−40.5619	−22.8893	−39.5082	−36.8006	−20.4682
3.6		−22.2654	−27.7568	−31.5112	−36.9116		−42.9250	−24.3332	−41.9206	−39.1734	−21.9610
3.7		(−22.8912; 3.65)	−29.5612	−33.5162	−39.1580		−45.3538	−25.8002	−44.3996	−41.6112	−23.4706
3.8			−31.4037	−35.5698	−41.4632		−47.8480	−27.2881	−46.9453	−44.1140	−24.9946
3.9			−33.2834	−37.6715	−43.8269		−50.4074	−28.7945	−49.5575	−46.6813	−26.5302
4.0			−35.1988	−39.8204	−46.2487		−53.0320	−30.3166	−52.2360	−49.3131	−28.0744
4.1			−37.1488	−42.0158	−48.7283		−55.7214	(−31.0828; 4.05)	−54.9806	−52.0092	−29.6236
4.2			−39.1317	−44.2569	−51.2653		−58.4756		−57.7912	−54.7692	−31.1740
4.3			−41.1459	−46.5428	−53.8592		−61.2944		−60.6676	−57.5928	−32.7216
4.4			−43.1897	−48.8725	−56.5097				−63.6094	−60.4800	(−33.4928; 4.35)
4.5			−45.2612	−51.2450	−59.2162				−66.6165	−63.4368	
4.6			−47.3582	−53.6592	−61.9782				−69.6886	−66.4564	
4.7			−49.4786	−56.1189	−64.7952				−72.8255	−69.5388	
4.8			−51.6200	−58.6128	−67.6666				−76.0268	−72.6834	
4.9				−61.1446	−70.5918				−79.2924	−75.8899	
5.0				−63.7128	−73.5701				−82.6218	−79.1578	
5.1				−66.3158	−76.6008				−86.0146	−82.4868	
5.2				−68.9520	−79.6831				−89.4706	−85.8764	
5.3					−82.8162				−92.9893	−89.3262	
5.4					−85.9994				−96.5704	−92.8355	
5.5					−89.2316				−100.2132	−96.4039	
5.6					−92.5120				−103.9176	−100.0308	
5.7									−107.6830	−103.7156	
5.8									−111.5086	−107.4576	
5.9									−115.3942	−111.2563	
6.0									(−117.3593; 5.95)	−115.1108	
6.1										−119.0205	
6.2										−122.9845	
6.3										−127.0020	
6.4										−131.0720	

* The first part of this integration was based on Eq. (17); it was completed in the form given by Eq. (20). Only the latter is given.

$[d(Vr)/dr]_{r=0}$. Changing then to the coordinates β and s, we find

$$E_{\text{pot}} = -ZkT\int_0^{(2\beta)^{\frac{1}{2}}} (\beta - \tfrac{1}{4})w^3 I_{\frac{3}{2}}(2\beta/w^2)dw. \quad (22)$$

The integral is obtained numerically from the data of the solution.

The kinetic energy of each electron of momentum p is $p^2/2m$. Multiplying by the density of electrons and integrating over all space, we find for the kinetic energy of all electrons

$$E_{\text{kin}} = \int_0^a 4\pi r^2 dr \int_0^\infty \frac{p^2/2m \cdot 2 \cdot 4\pi p^2 dp/h^3}{\left[\exp\left(\dfrac{p^2/2m - eV}{kT} + \eta\right) + 1\right]}. \quad (23)$$

This expression can be simplified by a rather long sequence of operations. If one integrates by parts first by r, and then again by p, and then uses Eq. (14) to replace one of the integrals on p one can

TABLE XI. Summary of the numerical results for the temperature dependent Fermi-Thomas equation (see Table X). Various thermodynamics quantities are evaluated corresponding to these solutions for the case of iron.

										For Fe$_{56}$				
Case	β_b	b	α	E_{pot}/kTZ	E_{kin}/kTZ	Pv/kTZ	U/kTZ	$\frac{1}{\gamma-1}$	γ	$T_{kv}=(0.428\alpha)^{-4/3}$	$a=\frac{1.602\times10^{-9}b}{T_{kv}^{1/4}}$	$v=\frac{4\pi}{3}a^3$	ρ g/cm^3	$P_{megabars}$
1	−13.5000	5.4000	7.2021	−13.5750	7.5715	0.5227	1.2210	2.336	1.428	0.2231	$1.259A$	$8.353A^3$	11.874	581.5
2	−22.8914	6.6612	3.9774	−5.4520	3.780$_2$	0.7028	1.6014	2.278	1.439	0.4926	1.274	8.659	11.455	1665.
3	−51.6200	11.5200	9.8160	−20.2006	10.882	0.5210	1.5976	3.066	1.326	0.1476	2.977	110.54	0.8974	28.97
4	−68.9520	13.5200	6.8602	−11.6576	6.799$_8$	0.6470	1.9122	2.924	1.342	0.2381	3.101	124.91	0.7644	51.40
5	−92.5120	15.6800	3.7659	−4.2351	3.360$_0$	0.8283	2.1681	2.618	1.382	0.5297	2.944	106.88	0.9280	170.9
6	−7.4536	4.2050	6.8918	−13.0006	7.2902	0.5266	1.1017	2.092	1.578	0.2366	0.966	3.774	26.28	1375.
7	−61.2944	9.2450	0.3121	−0.0676	0.7742	0.5936	0.8165	1.654	1.605	14.660	0.757	1.816	54.62	1.66×10^5
8	−31.0828	8.2012	5.8808	−9.6867	5.7792	0.6239	1.6059	2.574	1.389	0.2923	1.787	23.893	4.154	3.179
9	−117.3593	17.7012	2.3570	−1.7505	2.2511	0.9172	2.1298	2.322	1.431	0.9892	2.844	96.30	1.030	392.4
10	−131.0720	20.4800	5.2326	−7.0961	4.7536	0.8037	2.3760	2.956	1.338	0.3416	4.292	331.04	0.2996	34.54
11	−33.4928	9.4612	30.3768	−97.300	49.0072	0.2380	0.7632	3.207	1.313	0.0326	3.567	189.52	0.5235	1.703

show finally that

$$E_{kin}=\frac{16\pi^2}{h^3m}\times\frac{a^3}{3}\int_0^\infty\frac{p^4dp}{\left[\exp\left(\frac{p^2/2m-eV_a}{kT}+\eta\right)+1\right]}-\tfrac{1}{2}E_{pot}, \tag{24}$$

where V_a is the value of the potential at the surface of the atom $r=a$. The integral is, of course, proportional to $I_{3/2}[(eV_a/kT)-\eta]$ (see Eq. (15a)).

We next compute the pressure. Since there is no field at $r=a$, all of the momentum carried across this surface (which in one second per cm^2 is P, the pressure) must be carried by electrons crossing this surface. This is the reason why computing the pressure at $r=a$ is particularly simple. At this point pressure simply appears as the pressure of a free electron gas. One obtains

$$P=\int_0^\infty\frac{\frac{1}{3}p\cdot(p/m)\cdot4\pi p^2dp/h^3}{[\exp[(p^2/2m-eV_a/kT)+\eta]+1]}. \tag{25}$$

The value of Pv per atom where $v=(4/3)\pi a^3$ is the atomic volume, is therefore

$$Pv=\frac{32\pi^2a^3}{9h^3}(2mkT)^{\frac{3}{2}}(kT)I_{3/2}\left(\frac{eV}{kT}-\eta\right)=\frac{2}{9}(ZkT)\cdot\frac{b^3}{\alpha}I_{3/2}\left(\frac{\beta_b}{b}\right), \tag{26}$$

where β_b is the value of β on the boundary $s=b$. Comparison of Eqs. (24) and (25) shows that we can express the kinetic energy as

$$E_{kin}=\tfrac{3}{2}Pv-\tfrac{1}{2}E_{pot}. \tag{27}$$

This equation will be obtained more directly by consideration of similarity transformation in Section VI.

The total energy per atom is therefore most conveniently calculated from

$$E_{tot}=\tfrac{3}{2}Pv+\tfrac{1}{2}E_{pot},$$

where Pv is computed from Eq. (26) and the potential energy E_{pot} from Eq. (22).

Actually the total energy is not interesting. What we should like to know is the excess of this energy over what the energy would be if the material were at zero temperature and pressure. That is, to find the net internal energy U we must subtract from E_{tot} the energy of a single atom at zero temperature and pressure. This energy is given by[11]

$$(3/7)(Z^2e^2/\mu)\phi'(0),$$

where μ is given by Eq. (1b) and $\phi'(0)$ has been calculated to be -1.58875 (see Section II). In terms of our present quantities,

$$Z^2e^2/\mu=kTZ(2\alpha^2/3)^{\frac{1}{3}},$$

so we have

$$U=E_{tot}+(kTZ)0.6809(2\alpha^2/3)^{\frac{1}{3}}. \tag{28}$$

In this way Pv and U have been calculated for the various conditions for which the differential equation was solved. The conditions β_b and b are given in the first two columns of Table XI. The value of α which results is given in the third column. In the next four columns the potential, kinetic, Pv and net internal energy are given in units of kTZ so that they are applicable for any Z. The ratio of the net internal energy to Pv, which we have called $1/(\gamma-1)$ is given, as well as the value of γ to which this corresponds. The ratio is written in this form in analogy to the perfect gas formulae but it is not to be assumed that in our case γ is actually the ratio of specific heats, nor the exponent in the isentropic equation $Pv^\gamma=$constant. We define γ only through the equation $U=Pv/(\gamma-1)$.

The above quantities are independent of the value of Z. But to obtain actual numerical values

[11] See Slater and Krutter, reference 1, and Section VI.

for the temperature, atomic volume, density, and pressure one must assume a definite substance.

The numerical values for these quantities for Fe_{56} (unit of density is 1 g/cm³) are given in columns 10 to 14 of Table XI. For any other atom of atomic number Z, atomic weight A, these values should be multiplied by various factors:

(i) temperature T by $(Z/26)^{4/3}$
(ii) atomic volume v by $(26/Z)$
(iii) density ρ by $(Z/26)(A/56)$
(iv) pressure P by $(Z/26)^{10/3}$.

The above calculations from the Fermi-Thomas model can be scaled, as was indicated, to apply to a substance with arbitrary Z. For any definite Z there is, however, an effect it is worth while to take into account. To the internal energy per atom, Fe, one should add $3kT/2$ to account for the kinetic energy of motion of the nuclei. For the same reason, kT should be added to Pv to account for the extra pressure developed by this motion.

VI. SIMILARITY CONSIDERATIONS

We shall summarize in this section a few simple relations which apply to the electron distributions obtained above.

The first of these relations is the virial theorem, connecting pressure P, volume v, with kinetic energy E_{kin} and potential energy E_{pot}

$$\tfrac{3}{2}Pv=\tfrac{1}{2}E_{\text{pot}}+E_{\text{kin}}. \tag{29}$$

We shall show below that in the Fermi-Thomas approximation this virial theorem is exactly satisfied. This fact has indeed been proved in the literature for some special cases.[12] The proof given here is more general.

We consider first a similarity transformation in which all charges (including the elementary charge e) are changed by the factor $(1+\epsilon)$, all distances by the factor $(1+\rho)$ and all energies by $(1+\eta)$. The quantities ϵ, ρ, η are assumed small compared to unity. The quantum of action h and the electron mass m are assumed to be unchanged.

From the expression for potential energy, the following relation obtains

$$1+\eta=(1+\epsilon)^2/(1+\rho) \quad \text{or} \quad \eta=2\epsilon-\rho.$$

The deBroglie wave-length λ, as all lengths, must change as $(1+\rho)$; thus momenta change as $1/(1+\rho)$ and kinetic energies as $1/(1+\rho)^2$. However, these energies, like potential energies, must change as $(1+\eta)$, hence we obtain

$$\eta=-2\rho \tag{30}$$

and with the above relation

$$2\epsilon=-\rho. \tag{31}$$

[12] V. Fock, Physik. Zeits. Sowjetunion 1, 747 (1932).

Equations (30) and (31) give the change in potential distribution and in energy due to a change of the charges.

If $T\neq 0$, the two similar systems to be compared must be such that the temperature should change proportionally to the energy of an electron. Hence, the entropy which changes as the heat transfer divided by temperature will remain unaltered.

We shall now treat the effect of the change of charges by a perturbation treatment. Consider first the effect of the change in all charges by the factor $(1+\epsilon)$, without altering the electron distribution. This we can consider accomplished with the aid of imaginary rigid and infinitely thin walls which subdivide the system and which prevent any change in electron densities. (It is consistent with the assumptions of the Fermi-Thomas model to localize sharply electrons even though their momentum distribution is given. Introduction of such walls is therefore permissible.) Thus densities and hence kinetic energies will remain unaltered and the change of total energy will be given by the change in potential energy, namely, $2\epsilon E_{\text{pot}}$.

As a second step we now permit the imaginary walls to readjust themselves, but we shall keep in this step the total volume unchanged. The compression and dilatation of the volume elements will introduce temperature changes which we allow to be equalized by heat conduction. Since any energy conducted away from one element must go into another, the total energy change by conduction is zero. The work done by the motion of the walls does not vanish exactly. However, the displacement of the walls is proportional to the electron density differences; since the pressure differences are also infinitesimal, the actual work performed is quadratically small. Thus the energy change introduced by changing the charge distribution remains, to the first order, $2\epsilon E_{\text{pot}}$. We also observe that the entropy change due to heat conduction described above is infinitesimal to second order, since both the amount of heat conducted and the temperature differences are infinitesimals of the first order.

In order to arrive at the same configuration reached by the similarity transformation, the volume must now be readjusted. This is done by a volume increase $(1+\rho)^3$. In this process, the entropy will be kept constant. At the same time, however, the energy of the system will decrease by an amount equal to the pressure multiplied by the volume change, i.e., by $P(3\rho v)$. Thus the total energy change is $2\epsilon E_{\text{pot}}-3\rho Pv$. Equating this with η times the original total energy we obtain

$$2\epsilon E_{\text{pot}}-3\rho Pv=\eta(E_{\text{pot}}+E_{\text{kin}}).$$

Using Eqs. (30) and (31) to express η and ρ in terms of ϵ we finally have

$$2\epsilon E_{\text{pot}}+6\epsilon Pv=4\epsilon(E_{\text{pot}}+E_{\text{kin}})$$

or

$$E_{\text{pot}}+2E_{\text{kin}}=3Pv. \tag{29}$$

The reasoning which has just been described can be applied equally to calculations with or without exchange effects. The reason is that the exchange energy, as all other potential energies, is proportional to e^2/r. The characteristic distance entering into the exchange energy happens to be the deBroglie wave-length of the fastest electron.

It is well known that the virial theorem is exactly valid for a quantum mechanical system (as well as for a classical system) when the exact equations of motion of the electrons and nuclei are taken into account. The above simple argument merely shows that the virial theorem is not invalidated by the simplifying assumptions introduced in the Fermi-Thomas method.

It is of interest to study a second similarity transformation which consists of increasing the nuclear charge and simultaneously increasing the number of electrons so that the system remains neutral. This similarity transformation describes correlations between solutions for various nuclear charges; it also leads to a further relation between the various forms of energy in the Fermi-Thomas model. The procedure to be described and the relations following from it hold only for the case where exchange forces are neglected.

It is to be noted that in this similarity transformation λ does not change like other lengths. In fact, the Fermi-Thomas equation remains unchanged, but we do not retain the detailed microscopic relations from which it is derived. The transformation consists of the following changes:

$$Z\rightarrow Z(1+\zeta), \quad r\rightarrow r(1+\rho), \quad \bar{E}\rightarrow\bar{E}(1+\eta).$$

Here $\bar{E}$ represents any form of energy per electron, and also stands for the temperature T. At the same time electron densities are changed by the factor $(1+\nu)$.

We shall consider

$$\zeta,\ \rho,\ \eta,\ \nu\ll 1.$$

It follows directly from the charge balance that

$$(1+\nu)(1+\rho)^3=1+\zeta \tag{32}$$

or

$$\nu+3\rho=\zeta.$$

Since the potential energy of an electron must change as $(1+\eta)$, we have

$$(1+\zeta/1+\rho)=1+\eta$$

or

$$\zeta-\rho=\eta. \tag{33}$$

Since the kinetic energy is proportional to the two-thirds power of the electron density, for $T=0$, we are lead to postulate

$$(1+\nu)^{\frac{2}{3}}=1+\eta$$

or

$$\tfrac{2}{3}\nu=\eta. \tag{34}$$

If we assume that the temperature T has changed by the factor $(1+\eta)$, it is easily seen that the kinetic energy per electron will transform as $(1+\eta)$.

Eliminating ν from Eqs. (32), (33), (34), we obtain

$$\rho=-\tfrac{1}{3}\zeta, \quad \eta=(4/3)\zeta.$$

If we now continue to apply such similarity transformations until there is a finite change of the nuclear charge and of the other quantities involved, we find that solutions of the Fermi-Thomas equation for different Z values are correlated by the statements that the radius changes proportionally to $Z^{-\frac{1}{3}}$; energy per electron $\bar{E}$ and temperature both change as $Z^{4/3}$. For the case $T=0$, these statements follow directly from the well-known form of the Fermi-Thomas equation. We should also note that the total energy per atom changes as $Z^{7/3}$. Thus in an infinitesimal similarity transformation the total energy per atom is multiplied by $1+7\zeta/3$.

We shall now treat the same problem by a perturbation method in the following steps.

(i) First we shall multiply the nuclear charge of a single nucleus by $(1+\zeta)$ and apply a perturbation calculation. In this step we shall keep the number of electrons, the volume, and the temperature unchanged. Due to the complete shielding of a nucleus by its electrons, assumed throughout this paper, the interaction of nuclei with each other and with electrons of other atoms need not be considered. Thus one obtains a change in energy $\zeta E_{e,N}$, where $E_{e,N}$ is the electrostatic interaction energy of electrons of an atom with its nucleus.

(ii) Second we add ζZ electrons to re-establish the charge balance. This addition gives the energy $-\zeta ZE_w$, where E_w is the work function of the solid, i.e., the energy needed to extract an electron from the solid. If one wants to apply this argument to an isolated ion, then E_w must be replaced by the ionization energy of the outermost electron.

(iii) As a third step the solid is expanded. This expansion gives rise to a change in energy of $-3\rho Pv$, where v is the atomic volume.

(iv) As a final step the temperature is raised by ηT which gives the added energy ηTC_v, where C_v is the specific heat per atom at constant volume.

The sum of these energy contributions is equal to the total energy change $(7\zeta/3)(E_{\text{pot}}+E_{\text{kin}})$ obtained from the infinitesimal similarity transformation. We have, therefore,

$$(7/3)\zeta(E_{\text{pot}}+E_{\text{kin}})=\zeta E_{e,N}-\zeta ZE_w-3\rho Pv+\eta TC_v.$$

Using the relations between η, ζ, ρ we obtain

$$(7/3)(E_{\text{pot}}+E_{\text{kin}})=E_{e,N}-ZE_w+Pv+(4/3)TC_v.$$

Using the virial theorem and introducing the relation

$$E_{\text{pot}}=E_{e,e}+E_{e,N}$$

where $E_{e,e}$ is the potential energy due to the interaction of electrons within an atom, we get

$$(5/2)Pv+(7/6)E_{e,e}+(1/6)E_{e,N} = -ZE_w+(4/3)TC_v.$$

In the special case of $T=0$ and of isolated atoms, this relation becomes particularly simple. In fact in this case $P=0$ and the ionization energy E_w is also set to zero, so that

$$E_{e,N}=-7E_{e,e}.$$

This relation had been derived by Fermi for the Fermi-Thomas equation.

ACKNOWLEDGMENT

The authors express their thanks to Miss Josephine Elliott for considerable help in preparing the tables.

PHYSICAL REVIEW VOLUME 75, NUMBER 10 MAY 15, 1949

On the Wave Equation with Small Quantum Numbers

RUDOLPH E. LANGER
Department of Mathematics, University of Wisconsin, Madison, Wisconsin
(Received December 14, 1949)

The determination of the *Eigenwerte*, and the normalization of the *Eigenfunktionen* of the one-dimensional wave equation, with a potential energy that has a single minimum, is customarily based on the use of the so-called phase integral and W.K.B. formulas. These formulas are asymptotic in character. As they have usually been applied, they accordingly lead to conclusions which can be regarded as established only when the respective quantum numbers are sufficiently large. This restriction has been both unfortunate and puzzling. For on the one hand, the cases of small or moderate quantum numbers are often peculiarly interesting while, on the other hand, the phase integral formulas have been found by trial, at least in a variety of simple cases, to give surprisingly good results even in the lower quantum number range.

It is shown in this paper how the asymptotic method should be applied when small or moderate quantum numbers are in question. In the case of the *Eigenwerte*, the characteristic equation appropriate to the lower range is derived, and a comparison of this new equation with the familiar one based on the phase integral is made. It is thus theoretically established that under certain very liberal conditions upon the potential energy the older method does give good approximations. In the special case of the harmonic oscillator the two equations are, in fact, identical. For the normalization of the *Eigenfunktionen* a method which has been used in principle by W. H. Furry is applied. It is, however, framed in a manner appropriate to the smaller quantum number range. Formulas are given for the normalized *Eigenfunktionen* over the several intervals of the variable, over the critical interval which includes the minimum of the potential energy and the turning points, as well as over the intervals remote from the turning points.

In the special case of the harmonic oscillator, the method here used gives certain exact—not merely asymptotic—results. These, therefore, supply a basis for the appraisal of the corresponding results that are obtainable by other means.

1. INTRODUCTION

THE subject of this discussion is the one-dimensional wave equation

$$(d^2u/dx^2)+\lambda^2\{E-V(x)\}u=0, \qquad (1.1)$$

in which

$$\lambda^2=8\pi^2m^2/h^2,$$

and in which $V(x)$, the potential energy, is defined over the entire x axis and has a single minimum say at a point x_0. The characteristic values E_n (*Eigenwerte*) are the values of E for which this equation admits of a solution that is bounded for all x. A solution u_n corresponding to such a characteristic value is a characteristic solution (*Eigenfunktion*) and is said to be normalized when its constant factors—which are not determined by the equation—are so adjusted that

$$\int_{-\infty}^{\infty}u_n^2dx=1. \qquad (1.2)$$

A familiar procedure for the determination of the *Eigenwerte* is based upon the phase integral and W.K.B. methods. Elementary analytical forms are used in this to represent the solutions of the differential equation asymptotically with respect to λ, in intervals which lie on opposite sides of, and are sufficiently remote from, the turning points. To account for the Stokes' phenomenon, "connection formulas" are invoked to identify the forms which represent one and the same solution in different intervals. From the fact that two such forms differently arrived at, but valid in the same interval, must be equivalent, the characteristic equation, whose roots are the *Eigenwerte*, is deduced. Quantitatively, the procedure is in brief the following.

For values of E that are larger than $V(x_0)$ but which are nevertheless exceeded by $V(x)$ for some positive and some negative x, the equation

$$E-V(x)=0$$

has two roots. These are the turning points. We shall designate them by x_1 and x_2, the subscripts being assigned so that $x_1<x_2$. The solutions of Eq. (1.1) which are bounded for all positive x are multiples of each other and are represented for all such x as are positive and large enough by the form on the right of the symbol $\leftarrow$ in the relation

$$\frac{2C}{\{E-V(x)\}^{\frac{1}{4}}}\left[\cos\left(\lambda\int_x^{x_2}\{E-V(x)\}^{\frac{1}{2}}dx-\frac{\pi}{4}\right)\right]$$
$$\leftarrow\frac{C}{\{V(x)-E\}^{\frac{1}{4}}}$$
$$\times\exp\left(-\lambda\int_{x_2}^{x}\{V(x)-E\}^{\frac{1}{2}}dx\right)[1]. \quad (1.3)$$

This same solution is represented by the form on the left of (1.3) for the values of x if such exist, which are between x_1 and x_2 and outside of neighborhoods of these points, and for which, beyond that, the phase integral

$$\lambda\int_x^{x_2}\{E-V(x)\}^{\frac{1}{2}}dx \quad (1.4)$$

has a value which is sufficiently large to make its reciprocal asymptotically negligible. A special significance attaches to the square brackets as they are used throughout this paper. The symbol $[y]$, namely, is used in the case of any expression y to denote a quantity which is asymptotically equivalent to y. In the case of the relation (1.3) and the remaining formulas of this section, this means that $[y]$ differs from y by at most terms which are of the order of magnitude of $1/\lambda$.

The solutions of Eq. (1.1) which are bounded for all negative x are, quite similarly, represented by the forms in the relation

$$\frac{C}{\{V(x)-E\}^{\frac{1}{4}}}\exp\left(-\lambda\int_x^{x_1}\{V(x)-E\}^{\frac{1}{2}}dx\right)[1]$$
$$\rightarrow\frac{2C}{\{E-V(x)\}^{\frac{1}{4}}}\left[\cos\left(\lambda\int_{x_1}^{x}\{E-V(x)\}^{\frac{1}{2}}dx-\frac{\pi}{4}\right)\right], \quad (1.5)$$

the left-hand form applying when x is large and negative, and the right-hand one for such x, if they exist, as lie between x_1 and x_2 but not too near either of these points, and at which the reciprocal of the phase integral

$$\lambda\int_{x_1}^{x}\{E-V(x)\}^{\frac{1}{2}}dx \quad (1.6)$$

is negligible. At an *Eigenwert* E a solution to which the relation (1.3) refers and one to which (1.5) refers must be multiples of each other. This requires that the constant C be numerically the same in the two formulas, and that the left-hand member of (1.3) differ at most in sign from the right-hand member of (1.5). This condition is explicitly that

$$\left[\cos\left(\lambda\int_x^{x_2}\{E-V(x)\}^{\frac{1}{2}}dx-\frac{\pi}{4}\right)\right]$$
$$=\pm\left[\cos\left(\lambda\int_{x_1}^{x}\{E-V(x)\}^{\frac{1}{2}}dx-\frac{\pi}{4}\right)\right],$$

a relation which simplifies easily into the form

$$\lambda\int_{x_1}^{x_2}\{E-V(x)\}^{\frac{1}{2}}dx=[(n+\tfrac{1}{2})\pi], \quad (1.7)$$

with n an integer. The characteristic equation based upon the phase integral is thus derived, the integer n being the quantum number. It will, however, be clear, since the derivation explicitly called for the existence of an interval between the turning points upon which the values (1.4) and (1.6) are both large, that the result (1.7) can be regarded as established only when its left-hand member is large, namely, only for large quantum numbers n.

When E is an *Eigenwert* the forms in the relations (1.3) and (1.5) describe the respective *Eigenfunktion*, and this latter will be normalized if a suitable value is assigned to the constant factor C. This value, as it has been determined[1] from the relations (1.3) and (1.5) is

$$C=\left[\left(2\int_{x_1}^{x_2}dx/\{E-V(x)\}^{\frac{1}{2}}\right)^{-\frac{1}{2}}\right]. \quad (1.8)$$

It will be clear, however, that this result, since its derivation is based upon the relations (1.3) and (1.5), can again be asserted only for quantum numbers that are sufficiently large.[2]

The restriction of the results above to the large quantum numbers is unfortunate, for the cases of the small quantum numbers are often of primary interest. We shall show in the following how the asymptotic method is to be recast to apply to these cases. The results which are to be derived will incidentally be found to include a criterion upon which can be established the fact that the formulas (1.7) and (1.8) do, in many cases, give good approximations, even in the range of the small quantum numbers. This has frequently been observed.[1]

2. THE CHARACTERISTIC VALUES

Let us assume by way of explicit hypothesis that $V'(x)$ exists for all x and is zero only at x_0, that

[1] W. H. Furry, Phys. Rev. 71, 360 (1947).
[2] Here we are evidently in disagreement with the claims made by Furry in reference 1.

$V''(x_0)$ and $V'''(x_0)$ exist, and that $V''(x_0)>0$. Let us also suppose, as we may without loss of generality, that the origin of energy values is taken so that $V(x_0)=0$. With the suitable choice of a constant M, the function $V(x)$ then fulfills a relation

$$V(x)\leqq M(x-x_0)^2 \tag{2.1}$$

on some interval which includes x_0. We shall restrict our discussion to such values of E as yield turning points which lie upon this interval, although it must be observed that this implies no restriction in some cases since the relation (2.1) may apply for all x. Except in cases of this latter kind, the range of permissible values of E may evidently be enlarged by increasing the constant M. We shall, however, suppose that the value of M remains of a moderate magnitude.

The relation (2.1) implies that

$$E-M(x-x_0)^2\leqq E-V(x).$$

Since this requires that the zeros of the left-hand member lie upon the interval joining the turning points, it follows at once that

$$\int_{x_0-(E/M)^{\frac{1}{2}}}^{x_0+(E/M)^{\frac{1}{2}}}\{E-M(x-x_0)^2\}^{\frac{1}{2}}dx\leqq\int_{x_1}^{x_2}\{E-V(x)\}^{\frac{1}{2}}dx,$$

or, since the integral on the left may be explicitly evaluated, that

$$(\pi/2M^{\frac{1}{2}})(\lambda E)\leqq\lambda\int_{x_1}^{x_2}\{E-V(x)\}^{\frac{1}{2}}dx. \tag{2.2}$$

It is our specific purpose to deal with the cases in which the phase integral is small or at most moderate in magnitude. The relation (2.2) therefore implies that for all cases which are to come into question, the values λE also remain moderate.

In Eq. (1.1) let the variable be changed by the substitution

$$z=x-x_0-(\sigma/\lambda),$$

with the constant σ determined through the formula

$$\sigma=\frac{-2V'''(x_0)(\lambda E)}{9\{V''(x_0)\}^2}. \tag{2.3}$$

The reason for this and for this specific value of σ will presently appear. It suffices for the moment to observe that the transformed equation is of the form

$$\frac{d^2u}{dz^2}-\{\lambda^2\chi_0(z)+\lambda\chi_1+\chi_2\}u=0, \tag{2.4}$$

with

$$\begin{aligned}\chi_0^2(z)&=V(z+x_0),\\ \chi_1&=-\lambda E+\sigma V'(z+x_0),\\ \chi_2&=\lambda^2\{V(z+x_0+(\sigma/\lambda))-V(z+x_0)\\ &\qquad-(\sigma/\lambda)V'(z+x_0)\}.\end{aligned} \tag{2.5}$$

The constant λ is large, whereas λE and σ are moderate or small. Equation (2.4) therefore has the following earmarks:

(i) Its coefficient $\chi_0^2(z)$, the multiplier of λ^2, has a zero of the second order at $z=0$, and is elsewhere non-vanishing.

(ii) Its coefficient χ_1, the multiplier of λ, is at most of moderate size.

(iii) Its coefficient χ_2, as a function of λ, is bounded. This becomes evident at once if it is observed that the expression within the brace in (2.5) equals a remainder of the Taylor's formula for $V(z+x_0+(\sigma/\lambda))$ in powers of σ/λ.

Having these properties, Eq. (2.4) is of a type which has been studied by the author,[3] and for which the forms of the solutions are accordingly known. By virtue of the peculiar value of σ, the relation

$$3\chi_0'(0)\chi_1'(0)-2\chi_0''(0)\chi_1(0)=0$$

is fulfilled, and Eq. (2.4) is accordingly in the normal form as that is defined in (L). The formulas as given in (L) are therefore applicable to it, and it was precisely to attain this adjustment that the change of variable was made. For use in the description of the solutions as they are given in (L), a constant k and functions φ and ξ are associated with Eq. (2.4) by the formulas

$$\begin{aligned}k&=\lambda E/2\{2V''(x_0)\}^{\frac{1}{2}},\\ \varphi&=2\chi_0+(1/\lambda)\left\{(\chi_1/\chi_0)-\left(2k\chi_0\Big/\int_0^z\chi_0dz\right)\right\},\\ \xi&=\lambda\int_0^z\varphi dz.\end{aligned} \tag{2.6}$$

The value of k, which is a mere multiple of E, is clearly moderate. The functions φ and ξ may be verified to vanish at $z=0$ to the first and second orders, respectively, and ξ is large and positive for both positive and negative values of z that are numerically large.

It is shown in (L) that the solution of Eq. (2.4) which remains bounded as $z\to\infty$ is unique except for an arbitrary constant factor, and that for values of z that are positive and sufficiently large its form is

$$u=(1/\lambda^{\frac{1}{2}}\varphi^{\frac{1}{4}})\xi^k e^{-\frac{1}{2}\xi}[1]. \tag{2.7}$$

The form of this same solution for values of z that are negative and numerically large is[4]

$$u=(1/\lambda^{\frac{1}{2}}\varphi^{\frac{1}{4}})\{[A_1]\xi^{-k}e^{\frac{1}{2}\xi}+[A_2]\xi^k e^{-\frac{1}{2}\xi}\}, \tag{2.8}$$

[3] R. E. Langer, Trans. Am. Math. Soc. **36**, 90–106 (1934). We shall refer to this paper in the text by the designation (L).

[4] We are here using a somewhat simpler notation than in (L). The symbols u, A_j, C_j, $C_j^{(1)}$, and $C_{j,2}$ here are to be identified with $u_{0,2}$, $A_{2,j}^{(0,1)}$, $C_{j,1}^{(0)}$, $C_{j,1}^{(1)}$, and $C_{j,2}^{(0)}$ there.

with the coefficients

$$A_1=\pi\{C_1C_2^{(1)}-C_2C_1^{(1)}\},$$
$$A_2=\pi\{C_1C_{2,2}-C_2C_{1,2}\},$$

in which

$$C_1=1/\Gamma(\tfrac{3}{4}-k), \qquad C_2=1/\Gamma(\tfrac{1}{4}-k),$$
$$C_1^{(1)}=-ie^{2k\pi i}/\Gamma(\tfrac{3}{4}-k), \quad C_2^{(1)}=ie^{2k\pi i}/\Gamma(\tfrac{1}{4}-k),$$
$$C_{1,2}=ie^{-(k-\frac{1}{4})\pi i}/\Gamma(\tfrac{3}{4}+k), \quad C_{2,2}=ie^{-(k+\frac{1}{4})\pi i}/\Gamma(\tfrac{1}{4}+k).$$

It is possible with the use of the standard gamma-function relation,[5]

$$\Gamma(s)\Gamma(1-s)=\pi/\sin\pi s,$$

to modify these latter evaluations into the more convenient forms

$$\begin{aligned} C_1&=(1/\pi)\Gamma(k+\tfrac{1}{4})\cos(k-\tfrac{1}{4})\pi,\\ C_2&=(-1/\pi)\Gamma(k+\tfrac{3}{4})\sin(k-\tfrac{1}{4})\pi,\\ C_1^{(1)}&=e^{2(k-\frac{1}{4})\pi i}C_1,\\ C_2^{(1)}&=-e^{2(k-\frac{1}{4})\pi i}C_2,\\ C_{1,2}&=ie^{-(k-\frac{1}{4})\pi i}/\Gamma(k+\tfrac{3}{4}),\\ C_{2,2}&=e^{-(k-\frac{1}{4})\pi i}/\Gamma(k+\tfrac{1}{4}). \end{aligned} \tag{2.9}$$

They then yield

$$A_1=(1/\pi)e^{2(k-\frac{1}{4})\pi i}\Gamma(k+\tfrac{1}{4})\Gamma(k+\tfrac{3}{4})\sin(2k-\tfrac{1}{2})\pi,$$
$$A_2=1,$$

and thus the form (2.8) is, more explicitly,

$$u=(1/\lambda^{\frac{1}{4}}\varphi^{\frac{1}{4}})\{(e^{2(k-\frac{1}{4})\pi i}/\pi)\Gamma(k+\tfrac{1}{4})\Gamma(k+\tfrac{3}{4})$$
$$\times\xi^{-k}e^{\frac{1}{4}\xi}[\sin(2k-\tfrac{1}{2})\pi]+\xi^{k}e^{-\frac{1}{4}\xi}[1]\}. \tag{2.10}$$

At a characteristic value this solution is bounded, and hence remains bounded as $z\to-\infty$. This, however, is clearly so if and only if the formula (2.10) fails to involve the term in the positive exponential $e^{\frac{1}{4}\xi}$. The symbol $[\sin(2k-\frac{1}{2})\pi]$ must therefore actually denote 0, a condition which is clearly equivalent to the relation

$$k=[(n/2)+\tfrac{1}{4}],$$

with n an integer, or, as it is expressed in terms of E,

$$E=(1/\lambda)\{2V''(x_0)\}^{\frac{1}{2}}[n+\tfrac{1}{2}]. \tag{2.11}$$

This is the characteristic equation for the *Eigenwerte* and is therefore the equation which must be taken to replace the phase integral relation (1.7) when the quantum numbers n are not large.

It is a matter of some interest to compare Eqs. (2.11) and (1.7), especially since the latter has been found by actual trial in many simple cases to be capable of giving quite good results even in the smaller quantum number range. This is easily done if $V(x)$ is subjected to a further condition—namely, that for some positive constant M_1 it fulfill the relation

$$M_1(x-x_0)^2\leqq V(x) \tag{2.12}$$

on the interval upon which the turning points lie. If this is fulfilled, the reasoning which led from the condition (2.1) to the relation (2.2) may be applied again to deduce from (2.12) the fact that

$$\lambda\int_{x_1}^{x_2}\{E-V(x)\}^{\frac{1}{2}}dx\leqq(\pi/2M_1^{\frac{1}{2}})(\lambda E).$$

If we substitute into this relation and into (2.2) the values (2.11) for E, the results combine to show that

$$\left\{\frac{V''(x_0)}{2M_1}\right\}^{\frac{1}{2}}[(n+\tfrac{1}{2})\pi]\leqq\lambda\int_{x_1}^{x_2}\{E-V(x)\}^{\frac{1}{2}}dx$$
$$\leqq\left\{\frac{V''(x_0)}{2M}\right\}^{\frac{1}{2}}[(n+\tfrac{1}{2})\pi]. \tag{2.13}$$

From this a conclusion is readily drawn. If, for a certain range of values E, the function $V(x)$ fulfills between the turning points the conditions (2.1) and (2.12), with values M and M_1 that are nearly the same, these values are also nearly the same as $\frac{1}{2}V''(x_0)$. The relations (2.13) then effectively assure the approximate fulfillment of Eq. (1.7).

Perhaps the simplest example in this connection is that of the harmonic oscillator in which $V(x)=x^2$. The conditions (2.1) and (2.12) are then fulfilled for all x with $M_1=M=\frac{1}{2}V''(x_0)$. The relations (2.13) thus reduce to precisely Eq. (1.7), which is to say that in this special case Eqs. (2.11) and (1.7) are identical.

3. THE NORMALIZATION OF THE *EIGENFUNKTIONEN*

Let us designate by E_n the characteristic value (2.11) associated with the integer n. When E has this value the function u of §2 is an *Eigenfunktion*. It is, however, not normal in the sense of Eq. (1.2). The normalized *Eigenfunktion*, which we shall designate by u_n, is, however, given by the formula

$$u_n(x)=u\Big/\left\{\int_{-\infty}^{\infty}u^2dx\right\}^{\frac{1}{2}}, \text{ with } E=E_n. \tag{3.1}$$

The calculation of this calls for the evaluation of the integral of u^2. That is feasible, at least approximately, by direct methods, since formulas which represent u in intervals that cover the entire range of x are available. We shall, however, prefer an alternative method,[1] which though indirect is both less laborious and more precise.

[5] N. Nielsen, *Handbuch der Theorie der Gammafunktion* (B. G. Teubner, Leipzig, 1906), pp. 14, 19,

When E is regarded as a free parameter and u as any corresponding solution of (1.1), the differentiation of that equation with respect to E yields the relation

$$\dot{u}''+\lambda^2\{E-V(x)\}\dot{u}+\lambda^2 u=0,$$

in which the accents denote differentiations with respect to x, and the superscribed dot denotes a differentiation with respect to E. From this and (1.1) it follows that

$$\{\dot{u}u'-\dot{u}'u\}'=\lambda^2 u. \tag{3.2}$$

Let u now be chosen in turn as a solution U which vanishes at $x=-\infty$, and as the function u of §2. In the first instance an integration of (3.2) from $-\infty$ to x gives the result that

$$\{\dot{U}U'-\dot{U}'U\}=\lambda^2\int_{-\infty}^{x}U^2dx, \tag{3.3}$$

while in the second instance, in which u vanishes at $+\infty$, the integration from x to ∞ gives

$$-\{\dot{u}u'-\dot{u}'u\}=\lambda^2\int_{x}^{\infty}u^2dx. \tag{3.4}$$

For values of z for which $|\xi|$ is not large, the solution u of (2.7) is given in (L) to be of the form

$$u=(1/\lambda^{\frac{1}{2}})[C_1Q_1(z)+C_2Q_2(z)], \tag{3.5}$$

with coefficients C_1 and C_2 as they are given in (2.9), and with

$$\begin{aligned}Q_1(z)&=\Gamma(\tfrac{1}{2})\{M_{k,-1/4}(\xi)/\varphi^{\frac{1}{2}}(z)\},\\ Q_2(z)&=\Gamma(-\tfrac{1}{2})\{M_{k,1/4}(\xi)/\varphi^{\frac{1}{2}}(z)\}.\end{aligned} \tag{3.6}$$

the symbols $M_{k,\pm 1/4}$ designating the confluent hypergeometric functions usually so denoted.[6] A solution U which vanishes at $x=-\infty$, and which therefore fulfills the requirements of (3.3), is described in (L) as having for large negative z precisely the form[7] of the right-hand member of (2.7). For z such that $|\xi|$ is not large, the form of this solution is

$$U=(1/\lambda^{\frac{1}{2}})[C_1^{(1)}Q_1(z)+C_2^{(1)}Q_2(z)], \tag{3.7}$$

the coefficients being again given in (2.9). When $E=E_n$, namely, when $k-\frac{1}{4}=n/2$, the formulas (2.9) show that $C_1^{(1)}=C_1$ and $C_2^{(1)}=C_2$. At the *Eigenwerte* the solutions U and u thus become identical, and from the relations (3.3) and (3.4) it thus follows that

$$\begin{vmatrix}\dot{U}-\dot{u} & U'-\dot{u}'\\ u & u'\end{vmatrix}=\lambda^2\int_{-\infty}^{\infty}u^2dx, \text{ when } E=E_n. \tag{3.8}$$

[6] E. T. Whittaker and G. N. Watson, *A Course of Modern Analysis* (Cambridge University Press, 1927), fourth edition, pp. 337–338.

[7] This is the solution which is designated by $u_{1,2}$ in (L).

Let us abbreviate by writing

$$D_1=C_1^{(1)}-C_1, \quad D_2=C_2^{(1)}-C_2.$$

Then

$$U-u=(1/\lambda^{\frac{1}{2}})[D_1Q_1(z)+D_2Q_2(z)],$$

and although the functions (3.6) depend upon E as well as upon z, since ξ, φ, and z are all functions of E, it is nevertheless found that

$$\dot{U}-\dot{u}=(1/\lambda^{\frac{1}{2}})[\dot{D}_1Q_1(z)+\dot{D}_2Q_2(z)], \quad \text{when } E=E_n, \tag{3.9}$$

due to the fact that at any characteristic value $D_1=D_2=0$. By virtue of (3.9) and its derivative with respect to z, the formula (3.8) is, more explicitly,

$$\int_{-\infty}^{\infty}u^2dx=\left[\frac{1}{\lambda^{5/2}}\begin{vmatrix}\dot{D}_1 & \dot{D}_2\\ C_1 & C_2\end{vmatrix}\cdot\begin{vmatrix}Q_1(z) & Q_1'(z)\\ Q_2(z) & Q_2'(z)\end{vmatrix}\right], \quad \text{when } E=E_n. \tag{3.10}$$

The Wronskian of the functions (3.6) which is here involved is easily evaluated. The formulas (3.6), together with the relation $d/dz=\lambda\varphi(d/d\xi)$, leads to the equation

$$\begin{vmatrix}Q_1(z) & Q_1'(z)\\ Q_2(z) & Q_2'(z)\end{vmatrix}=\lambda\Gamma(-\tfrac{1}{2})\Gamma(\tfrac{1}{2})\times\begin{vmatrix}M_{k,-1/4}(\xi) & (d/d\xi)M_{k,-1/4}(\xi)\\ M_{k,1/4}(\xi) & (d/d\xi)M_{k,1/4}(\xi)\end{vmatrix},$$

and the determinant on the right of this is known[6] to have the value $\frac{1}{2}$. Equation (3.10) thus simplifies into

$$\int_{-\infty}^{\infty}u^2dx=\left[\frac{\Gamma(-\frac{1}{2})\Gamma(\frac{1}{2})}{2\lambda^{\frac{1}{2}}}\begin{vmatrix}\dot{D}_1 & \dot{D}_2\\ C_1 & C_2\end{vmatrix}\right], \quad \text{when } E=E_n. \tag{3.11}$$

It is now a simple matter of computation to evaluate the determinant which remains in (3.11). The formulas (2.9) give for it directly the value

$$-(2/\pi)(dk/dE)\Gamma(k+\tfrac{1}{4})\Gamma(k+\tfrac{3}{4}).$$

This may be reduced by the gamma-function formulas[5]

$$\Gamma(s)\Gamma(s+\tfrac{1}{2})=\pi^{\frac{1}{2}}2^{1-2s}\Gamma(2s), \quad \Gamma(\tfrac{1}{2})=\pi^{\frac{1}{2}},$$

so that with (2.6) and (2.11) it gives to (3.11) the final form

$$\int_{-\infty}^{\infty}u^2dx=\left[\left\{\frac{\pi}{2\lambda V''(x_0)}\right\}^{\frac{1}{2}}\frac{n!}{2^n}\right], \text{ when } E=E_n. \tag{3.12}$$

The normalized *Eigenfunktion* corresponding to E_n

is thus

$$u_n(x)=\left[\left\{\frac{2\lambda V''(x_0)}{\pi}\right\}^{\frac{1}{4}}\left(\frac{2^n}{n!}\right)^{\frac{1}{2}}u(x)\right]. \quad (3.13)$$

The formulas for u_n may now be set forth. From (2.9) it is seen that when $E=E_n$ then

$$C_1=0, \quad C_2=(-1)^{(n+1)/2}\{n!/\pi^{\frac{1}{2}}2^n((n-1)/2)!\}, \quad \text{when } n \text{ is odd},$$
$$C_1=(-1)^{n/2}\{n!/\pi^{\frac{1}{2}}2^n(n/2)!\}, \quad C_2=0, \quad \text{when } n \text{ is even}. \quad (3.14)$$

It follows, therefore, from (3.5), (3.6), (3.13), and (3.14), that for values of x which make $|\xi|$ moderate or small

$$u_n=(2V''(x_0)/\pi)^{\frac{1}{4}}(n!/2^n)^{\frac{1}{2}}\times\{2(-1)^{(n-1)/2}/((n-1)/2)!\}\times[M_{(n/2)+1/4,\,1/4}(\xi)/\varphi^{\frac{1}{2}}(z)], \quad \text{when } n \text{ is odd},$$
$$u_n=(2V''(x_0)/\pi)^{\frac{1}{4}}(n!/2^n)^{\frac{1}{2}}\{(-1)^{n/2}/(n/2)!\}\times[M_{(n/2)+1/4,\,-1/4}(\xi)/\varphi^{\frac{1}{2}}(z)], \quad \text{when } n \text{ is even}. \quad (3.15)$$

For values of x, be they positive or negative, for which ξ is large, the formulas (3.13) and (2.7) show that

$$u_n=(2V''(x_0)/\pi)^{\frac{1}{4}}(2^n/n!)^{\frac{1}{2}}\times\{\xi^{(n/2)+\frac{1}{4}}/\varphi^{\frac{1}{2}}(z)\}e^{-\frac{1}{2}\xi}[1]. \quad (3.16)$$

An analysis of this method and of its basis in (L) shows[8] that in the special case of the harmonic oscillator the formulas (3.15) are not merely asymptotically valid, but that, even upon the omission of the square brackets, they are exact for all x. This is so, morever, without any limitations upon the quantum numbers concerned. The formulas (3.15) may therefore be taken in this case to be a norm against which the results of other methods may be checked. It is especially pertinent to check, in that way, the results of the phase integral method based on the forms (1.5) and the normalizing factor (1.8).

When $V(x)=x^2$, we have $x_0=0$, and by (2.3) also $\sigma=0$. Thus $z=x$, and by (2.6) and (2.11) we find that $k=\frac{1}{4}\lambda E$, $\varphi=2x$, $\xi=\lambda x^2$, and $E_n=(2n+1)/\lambda$. Consider the case of the even quantum numbers n. Near $x=0$ the function $M_{(n/2)+1/4,-1/4}(\xi)$ differs from $\xi^{\frac{1}{4}}$ by higher powers of ξ. Hence

$$\{M_{(n/2)+1/4,\,-1/4}(\xi)/\varphi^{\frac{1}{2}}(z)\}_{x=0}=\lambda^{\frac{1}{4}}/2^{\frac{1}{2}},$$

and thus by (3.15)

$$u_n(0)=(-1)^{n/2}\{\lambda^{\frac{1}{4}}/\pi^{\frac{1}{4}}(n/2)!\}(n!/2^n)^{\frac{1}{2}}. \quad (3.17)$$

This is the exact result. The right-hand member of (1.5) at $x=0$, with C determined from (1.8), is readily found to give corresponding to this the approximation

$$u_n(0)=(-1)^{n/2}(2/\pi)^{\frac{1}{2}}(\lambda/(2n+1))^{\frac{1}{4}}. \quad (3.18)$$

The ratio of the values (3.18) and (3.17) is

$$(2^{n+1}/n!)^{\frac{1}{2}}\{(n/2)!/\{(2n+1)\pi\}^{\frac{1}{4}}\}. \quad (3.19)$$

By the use of Stirling's formula[5]

$$\lim_{n\to\infty}\{n!e^{n+1}/(n+1)^{n+\frac{1}{2}}(2\pi)^{\frac{1}{2}}\}=1,$$

this is easily shown to approach the value 1 as $n\to\infty$. For large quantum numbers, therefore, the approximation (3.18) is certainly good, as has, of course, been amply established. However, it is readily seen also that the ratio (3.19) is quite near 1 even when the quantum numbers are small. For instance, the ratios (3.19) corresponding to the numbers $n=0$, 2, 4, 6, are, respectively, 1.0623, 1.0046, 1.0015, and 1.0007. This corroborates the observations which have been made in this special case.[9]

[8] The given differential equation and its related equation are in this case the same. Thus the symbols u and y in (L) stand for the same functions, and the formulas (L (6)) apply exactly with u in the place of y.

[9] This paper was written while the author was on research leave under a grant from the Wisconsin Alumni Research Foundation.

Quantum-Theory Restrictions on the General Theory of Relativity

M. F. M. OSBORNE
Naval Research Laboratory, Washington, D. C.
(Received December 27, 1948)

The limitations set by the uncertainty principle on the measurement of the curvature of space are determined by passing a small test particle around a geodesic triangle. In measuring the curvature of space around a Schwarzschild-solution particle of finite size and physically realized density, it is found that the mass must be at least of the order of 10^4 kilograms, or the curvatures cannot be measured with an accuracy equal to the order of magnitude of the terms in the defining Eqs. $G_{ik}=0$. For mass points, the lower limit is 10^{-5} g. For smaller masses, the curvatures can only be measured with less accuracy and only over large regions of space. Similar limitations apply to alternative laws of gravitation involving higher derivatives of the metric. It is concluded that in any theory which attempts to unite quantum theory with the general theory of relativity, the relation of the metric to the energy momentum tensor, $G_{ik}-g_{ik}G/2=-KT_{ik}$, must appear only in the large and in a statistical sense, i.e., for large regions of space and large numbers of elementary particles.

IN this paper we endeavor to answer the question: What restrictions does the uncertainty principle place on the measurement of the curvature of space, and thus on the conceptions of the general theory of relativity? We shall do this by considering the definition of curvature as the ratio of the sum of the angles of a geodesic triangle minus π to its area in the limit of small area, and then determine the errors in measurement of angles and area when a small test particle or light quantum is passed around the triangle.

The basic measurements (to obtain the metric) of general relativity are coordinate and time. The basic measurements of quantum theory are coordinate and momentum. It is just the limitation of quantum theory on general relativity that coordinate and time cannot be determined alone, but must be tied up with a measurement of momentum or energy, which in turn are restricted by the uncertainty principle. As will be seen, this consideration becomes of especially simple and classical interpretation when one measures curvature in a time-like or xt plane.

We first recall the expressions for the curvatures of a space. The Riemannian curvature of a space, or product of the principal curvatures (Gauss curvature) of the surface formed by geodesics through a linear combination of two orthogonal directions at a point, is given by

$$M_{mn}=R_{ijkl}e_m{}^i e_n{}^j e_m{}^k e_n{}^l, \tag{1}$$

where R_{ijkl} is the Riemann-Christoffel tensor and $e_m{}^i$, $e_n{}^i$ are the contravariant components of the two orthogonal unit vectors $\mathbf{e}_m$, $\mathbf{e}_n$ which determine the surface.[1] The Riemannian curvature at a point is also definable as the ratio, in the limit of a small area, of the difference from π of the sum of the angles of a geodesic triangle to its area.

The sum of the Riemannian curvatures for all pairs of orthogonal directions formed with one given direction, is the mean curvature $\bar{M}_n$, given by

$$\bar{M}_n=\sum_m M_{mn}=-G_{ik}e_n{}^i e_m{}^k, \tag{2}$$

where G_{ik} is the Ricci-Einstein tensor.

The scalar or total curvature is the sum of all the mean curvatures

$$(M)_{\text{sc.}}=\sum_n \bar{M}_n=-G_{ik}g^{ik}. \tag{3}$$

We now ask what is the order of magnitude of these curvatures in a case of physical interest. To answer this question we observe that if one writes the Ricci-Einstein tensor in mixed form in (2), that is,

$$\bar{M}_n=-G_k{}^i e_n{}^k e_{ni}, \tag{4}$$

the dimensionality of the unit vectors cancels out. The same is true if (1) is written in mixed form. Furthermore, if the coordinate system and field is such that $G_i{}^k$ has only diagonal elements, these elements are the mean curvatures (ignoring sign) since the sum in (4) reduces to one term. Also, if $G_i{}^k$ is diagonal and expressed as a sum of terms, the individual terms are of the order of the Riemannian curvatures, or the elements of the Riemann-Christoffel tensor.

Exactly the conditions stated above are met in the fundamental example of greatest interest, the Schwarzschild solution of the equations of general relativity. Thus, if the metric is

$$ds^2=-\exp(\lambda)dr^2-r^2d\theta^2-r^2\sin^2\theta d\varphi^2+\exp(\nu)dt^2,$$

we easily find[2] for the $G_i{}^k$

$$\begin{aligned} G_1{}^1&=-\exp(-\lambda)(\nu''/2-\lambda'\nu'/4+\nu'^2/4-\lambda'/r),\\ G_2{}^2&=G_3{}^3=-\exp(-\lambda)(1+r(\nu'-\lambda')/2)/r^2+1/r^2,\\ G_4{}^4&=\exp(-\lambda)(-\nu''/2+\lambda'\nu'/4-\nu'^2/4-\nu'/r), \end{aligned} \tag{5}$$

[1] C. E. Weatherburn, *Riemannian Geometry and Tensor Calculus* (Cambridge University Press, London, 1938), p. 119.

[2] A. S. Eddington, *The Mathematical Theory of Relativity* (Cambridge University Press, London, 1923), p. 85. Also R. C. Tolman, *Relativity Thermodynamics and Cosmology* (Oxford University Press, London, 1934), p. 203.

and the Riemannian curvatures can be calculated to be

$$\begin{aligned} M_{12}&=M_{13}=-\exp(-\lambda)\lambda'/2r,\\ M_{14}&=\exp(-\lambda)(\nu''/2+\nu'^2/4-\nu'\lambda'/4),\\ M_{23}&=-(1-\exp(-\lambda))/r^2,\\ M_{24}&=M_{34}=\exp(-\lambda)\nu'/2r. \end{aligned} \tag{6}$$

To relate (5) and (6), using (2), one must use for directions along the three space-like axis, unit vectors whose co- and contravariant components are imaginary and of opposite sign. Thus $e_i=\delta_i{}^j g_{jj}{}^{\frac{1}{2}}$, $e^i=g^{ij}e_j$. This requirement is dictated by the use of an indefinite metric, so that lowering or raising subscripts changes signs along the first three axes, but the magnitude of unit vectors must be positive. (See reference 1, Eqs. (24)–(27), p. 46.)

It is known that the solution of Eqs. $G_i{}^k=0$ for λ, and ν is given by $\exp(\nu)=\exp(-\lambda)=1-2M/r$, and taking advantage of the fact that λ and ν are small, we have that

$$\nu''=2\nu/r^2, \quad \nu'=-\nu/r, \quad -\lambda=\nu=-2M/r.$$

This shows at once that there are two different orders of magnitude of terms which appear in (5) and (6),

$$\nu/r^2, \quad \nu^2/r^2, \tag{7}$$

or in c.g.s. units[3]

$$(GM/c^2r)(1/r^2), \quad (GM/c^2r)^2(1/r^2). \tag{8}$$

Terms of order $1/r^2$ also appear but always in combinations of order $(\exp(\nu)-1)/r^2\simeq\nu/r^2$. That there can be no terms $1/r^2$ directly in the Riemann-Christoffel tensor follows from the fact that for flat space and any coordinate system $R_{ijkl}\equiv 0$. Equations (7) and (8) give the orders of magnitude by which space, according to the general theory of relativity, differs from flatness. All of the curvatures in (6) are of the first order of magnitude. The second order of magnitude also appears directly in M_{14}.

Evidently for a complete determination of the curvature of space by triangulation, the curvature of the space is completely determined only if the error of observation is smaller than the second or smaller order of magnitude. We understand by "completely determined," a determination to the same accuracy as the defining differential equation $G_i{}^k=0$. Otherwise, the field will be incompletely determined. The curvature of a space is an observable in the sense of quantum mechanics if the errors, imposed by the uncertainty principle involved in determining it by triangulation with a test particle, are less than the smaller of the quantities (8). Otherwise, the curvature is unobservable or perhaps incompletely an observable.

We consider first the case that the quantities (8) are in decreasing order of magnitude, as will be the case so long as

$$(GM/c^2r)<1, \tag{9}$$

and we shall find that instructive information is obtained by considering the restrictions imposed by having the errors of observation separately less than these two different orders of magnitude.

Consider the errors imposed by the uncertainty principle on the measurement of curvature by passing a particle around a geodesic triangle, and measuring its angles and area. If the length of the side of the triangle is q, the position of the test particle will be uncertain within a band of width δq around the edges of the triangle. Hence, the uncertainty of the angle measurements will be of order $\delta q/q$. The curvature is

$$\kappa=\left(\sum_{i=1}^{3}\varphi_i-\pi\right)\Big/\text{area of triangle.} \tag{10}$$

If the area S is $\sim q^2$, the uncertainty δS in the area $\sim q\delta q$. Therefore, the uncertainty in the curvature is

$$\begin{aligned} \delta\kappa&=[\textstyle\sum(\delta\varphi_i/S)^2+((\sum\varphi_i-\pi)\delta S/S^2)^2]^{\frac{1}{2}}\\ &\simeq\delta q/q^3. \end{aligned} \tag{11}$$

This expression could also have been written down almost from inspection, on observing that the principal uncertainty in the curvature is due to the angle measurements, if the area of the band of uncertainty around the triangle is small compared to the total area of the triangle.

In the case that the triangle lies in the xt plane, the triangle is spanned by sending the test particle out along the axis and return (path ADA in Fig. 1), and measuring the time interval consumed. The angles are determined by velocity component (cf. momentum) measurements at the beginning and end of each side and these converted to angle measurements, using a cartesian-polar coordinate transformation. Imaginary units for t are used in the case of triangulation in the xt plane.

For the xt plane one has to distinguish between two cases, whether the velocity of the test particle is very much less than, or of order of, the velocity of light. For $v\ll c$ the area of the triangle ABC, Fig. 2, is of order qct, the uncertainty in the angles is $\sim\delta q/ct$. This follows from the fact that all the sides are of length $\sim ct$. Then the uncertainty in the curvature is $\sim\delta q/c^2t^2q$. For $v\sim c$ the area of the triangle ADC is $\sim c^2t^2$ and the uncertainty in angle is $\sim\delta q/ct$, so that the uncertainty in curvature $\sim\delta q/c^3t^3$.

We now have the following restrictions on the measurements of the test particle:

(A) The restriction of the uncertainty principle,

$$\delta p\delta q\gtrsim h. \tag{12}$$

[3] See reference 2, p. 202.

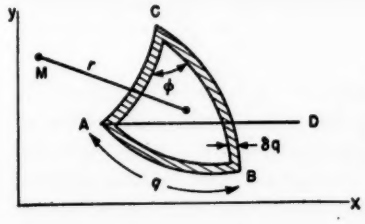

FIG. 1. Geodesic triangle to determine curvature of space at a distance r from a Schwarzschild particle of mass M.

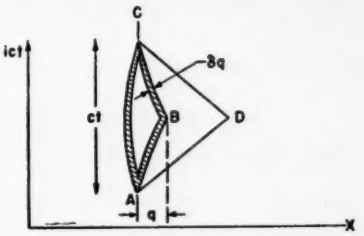

FIG. 2. Triangulation in the xt plane.

(B) A restriction in virtue of the fact that the basic measurements of relativity x and t (rods and clocks) and those of quantum theory (coordinate q and momentum p) are not independent. For the case that x and q are the same, we have

$$q=pt/m. \tag{13}$$

In the case that coordinates are deduced from direct measurements of momentum and time (as would be the case if one combined the momentum measurements made at the vertices of the triangles with time interval measurements, to determine angles and lengths of sides), Eq. (13) gives

$$\delta q/q \geq \delta p/p. \tag{14}$$

When the inequality sign is used, (14) can be roughly interpreted as a closure condition. This means that when the test particle is projected on the third side of the triangle, it will not return to its starting point or even remain in the plane of the first two sides within an error δq, unless the uncertainty in angle $\delta q/q$ is greater than the relative uncertainty in the momentum $\delta p/p$. We say "roughly" interpreted since p and δp, q and δq are not parallel but rather refer to average measurements at the three vertices of the triangle.

(C) The restriction

$$q \gg h/p. \tag{15}$$

This requires the triangle to be much more than one de Broglie wave-length on a side. Otherwise, the region of observation is not even defined to be a triangle as opposed to any other geometrical figure.

(D) The condition $q \ll r$. This requires that the dimensions of the triangle must be small compared to the distance to the particle whose field we are measuring. Otherwise one cannot properly speak of the measurement of the field $G_k{}^i$ at a point (actually average over a region of dimension q).

(E) The condition

$$mc^2 \ll Mc^2, \tag{16}$$

where m is the *total* mass of the test particle. This condition states that the gravitational effect of the test particle including its kinetic energy must be small compared to that of the Schwarzschild particle of rest mass M being measured. This condition, whether the test particle has a finite rest mass or is a light quantum, implies

$$p \ll Mc, \tag{17}$$

since for

$$v \ll c, \quad m \ll M, \quad p=mv \ll Mc,$$

or, if

$$v \sim c, \quad pc \sim mc^2 \ll Mc^2.$$

The form (16) will be useful for slow particles in measuring in the xt plane, otherwise the form (17) will be used.

Summarizing, we have that the error in measurement of the Riemannian curvature is $\delta\kappa \sim \delta q/q^3$ for curvatures in a space-like plane, and $\delta q/c^2t^2$, or $\delta q/c^3t^3$ for curvatures in a time-like plane as measured by slow ($v \ll c$) or fast ($v \sim c$) particles, respectively.

We have the following restrictions on the measurements

$$\begin{aligned} &\delta p \delta q \gtrsim h, && \text{(a)} \\ &\delta q/q \geq \delta p/p, && \text{(b)} \\ &q \gg h/p, && \text{(c)} \\ &q \ll r, && \text{(d)} \\ &m \ll M, \quad \text{or} \quad p \ll Mc. && \text{(e)} \end{aligned} \tag{18}$$

The first form of (e) implies the second, but not conversely.

We now ask what is implied by the condition that $\delta\kappa$ be much less than the larger of the two orders of magnitude (8) of the curvature itself. This requires, for a space-like section,

$$\delta q/q^3 \ll (GM/c^2r)(1/r^2). \tag{19}$$

Using (18) to eliminate δq, δp, q, p, r we find

$$(ch/GM^2) \ll 1. \tag{20}$$

Putting in numerical values for the physical constants, we find $M \gg 10^{-5}$ g. Thus 10^{-5} g is a lower limit for mass points, the space-like part of whose metric is observably different from flatness. It is also to be noted that once the critical mass is exceeded, the curvatures of this order of magnitude are *everywhere* defined. This is a consequence of the fact that q and r appear to the same power on both sides of (19) so that 18 (d) can eliminate them both at once. Physically, it means that the side of the measurement triangle q, and δq may be increased in just such a way, as the curvature decreases with increasing r, to make accurate observations always possible.

Let us now examine the restriction imposed by the second order of magnitude, for curvatures in space-like section. In this case we have

$$\delta q/q^3 \ll (GM/c^2r)^2(1/r^2), \tag{21}$$

which, when combined with (18), eventually gives

$$(c^2r/GM)(ch/GM^2) \ll 1. \tag{22}$$

When solved for r, (22) states that only within a sphere around the particle of the order of this radius is the curvature of space, or its departure from flatness, observable to the accuracy of the defining Eqs. $G_i^k=0$. If we combine this restriction with accepted possible values for density and ask for the limiting mass just outside of which the departure of the metric from flatness is completely observable, we find a lower limit of mass much greater than that obtained from the first order of magnitude. Let ρ be the density and r_0 a characteristic dimension of the particle. Then $M \simeq \rho r_0^3$, and for the curvature to be just completely observable at the surface ($r=r_0$) of the particle, we must have

$$(M/\rho)^{\frac{1}{3}} \ll G^2M^3/c^3h, \quad M \gg 10^7/\rho^{1/8} \text{ g}. \tag{23}$$

This is a quite severe restriction on the mass. As the density varies from 10^{-26} (density of interstellar space) to 10^{15} (density of nuclear matter) the limiting mass which can be thought to bend space definitively just outside itself varies from 10^{10} to 10^5 g.

One obvious implication of the restrictions above is that any relation between the metric of space and the tensor of matter, such as $G_{ik}-g_{ik}G/2 = -KT_{ik}$ must hold only in the statistical sense, and fail for elementary particles. Thus one should expect that in any unified field theory which attempts to unite quantum theory with the general theory of relativity, the curvature of space should arise as a statistical concept valid only for very large numbers of particles, since the above discussion shows that the curvature is simply not defined in the sense of measurements on elementary particles. A related viewpoint, which was perhaps first suggested by Mach and has also been discussed by Einstein,[4] is that the conception of mass requires the presence of other very large masses. One can have equivalence between inertial and gravitational mass, but the latter conception is simply not defined except in the presence of large masses.

Let us now consider the case where we carry out the triangulation in an xt plane. We must then have, in order to measure the curvature to first order for $v \ll c$,

$$\delta q/c^2t^2q \ll (GM/c^2r)(1/r^2). \tag{24}$$

[4] A. Einstein, *The Meaning of Relativity* (Princeton University Press, Princeton, 1945), p. 99 ff.

Eliminating t with (13), and using (18), one finds

$$h^2/GM^3r \ll 1, \tag{25}$$

or $r \gg h^2/GM^3$. In a time-like section, curvatures are defined to the first order only *outside* a sphere of this radius. If we express the inequality (25) in terms of the density ρ, as in (23), we can find a lower limit to the mass *everywhere* outside of which the curvature of a time-like section is defined to the first order. This is

$$M \gg (h^2\rho/G)^{3/10}, \tag{26}$$

or

$$M \gg 10^{-14}\rho^{3/10}. \tag{27}$$

Thus the lower limiting mass for this condition *increases* with increasing density. However, it should be noted that the restriction only applies for test particles of $v \ll c$, and so is not a completely binding one. In all cases the lower limit for the mass is exceedingly small, but is again, either for atomic or nuclear densities, much greater than the mass of one elementary particle. This conclusion, at first rather surprising, is still in keeping with the statistical point of view mentioned above, since, if the probability distribution (cf. ρ) of a particle of any mass is distributed thinly enough (i.e. over a large enough volume), everywhere *outside* this distribution it has (as shown below) an observable Newtonian gravitational field.

The inequality (25), which is independent of c, can also be deduced from the problem of measuring the classical gravitational attraction of a particle of mass M with a test particle of mass m by measuring the momentum change Δp_g when m passes M at a distance r. If one assumes the force $f \simeq GMm/r^2$ acts for a time $t \sim rm/p$ and imposes the condition (1), the change in momentum Δp_g, due to gravitational attraction, must be larger than the uncertainty in momentum Δp_u arising from the uncertainty principle, (2) $\delta q \ll r$, (3) $m < M$, (4) $\delta p \delta q \gtrsim h$, (5) $r \gg h/p$, exactly the inequality (25) is obtained. Thus the measurement of curvature to first order in the xt plane with slow particles is equivalent to the measurement of a classical gravitational potential.

While the above restriction is less severe than that obtained for the curvatures in a space-like plane, it does suggest that for elementary particles ($M \simeq 10^{-24}$) even the classical gravitational field is, in practice, not defined, since the distance and time required for the measurement is greater than the volume of the universe or its history can provide.

If we measure curvature in the xt plane with a particle of $v \sim c$, we must have for first order accuracy, $\delta q/c^3t^3 \ll (GM/c^2r)(1/r^2)$. Evidently this is exactly the same condition (19) obtained previously and leads to nothing new, since $ct \sim q$ for the triangle ADC in Fig. 2.

For second order accuracy for slow particles in an xt plane, we have

$$\delta q/c^2t^2q \ll (GM/c^2r)^2(1/r^2), \tag{28}$$

and using (13) and (18), we find $ch/GM^2 \ll 1$. This is the same as (20) for first order accuracy in an xy plane, so that this situation leads to nothing new. Also, nothing new is obtained by considering second order accuracy for particles with $v \sim c$ as we again obtain (21).

We can summarize all of the above by showing that they follow from the two basic inequalities (9) and (22):

$$(GM/c^2r) < 1, \tag{29}$$

$$(c^2r/GM)(ch/GM^2) \ll 1. \tag{30}$$

Multiplying (30) by successive powers of (29) we find a series of inequalities, (30) to (34), each of which implies, with (29), or (30) all those that follow it.

$$ch/GM^2 \ll 1, \tag{31}$$

$$h/Mcr \ll 1, \tag{32}$$

$$Gh/c^3r^2 \ll 1. \tag{33}$$

Equation (31) is the same as (20), as the condition for measuring curvature to the first order. (32) states that the field of a mass point is defined only for distances greater than its Compton wave-length, in practice not a very severe restriction. (33) gives a lower limit to the distance of definition independent of the mass, which is also exceedingly small.

Equations (29), (31) to (33) are respectively independent of h, r, G, and M. A fifth inequality independent of c can be obtained by multiplying (33) and (30).

$$h^2/GrM^3 \ll 1. \tag{34}$$

This is the same as (25), for measuring Newtonian potentials, or curvatures in the xt plane with slow particles.

We can discuss here a question raised by Eddington.[5] How shall we choose for the law of gravitation between different tensors whose divergence vanishes identically? $G_k{}^i$ involves only the second derivatives of the metric, hence, to measure it completely, only second order accuracy is required. Other possible tensors involve higher derivatives. For nth order accuracy, in triangulating to obtain the curvature, it follows from (7) and (8) that one must have

$$\delta q/q^3 < (GM/c^2r)^n(1/r^2), \tag{35}$$

which leads to

$$(c^2r/GM)^{n-1}(ch/GM^2) < 1, \tag{36}$$

$n=1$, 2 giving just (31) and (30).

[5] See reference 2, pp. 141–143.

For $n=3$, as required by Eddington's alternative, and introducing the density from $r_0^3 \sim M/\rho$, we find, for third order accuracy, in the curvature to be measurable just outside a particle of mass M

$$(c^2M^{\frac{1}{3}}/GM\rho^{\frac{1}{3}})^2(ch/GM^2) \ll 1, \quad M \gg 10^{14}/\rho^{1/5} \text{ g}. \tag{37}$$

From this, one can conclude that the distinction between the different proposals of Eddington for the gravitational law could not be measured, save for extremely large masses.

All of the above discussion was predicated on the assumption that $GM/c^2r < 1$. For $GM/c^2r > 1$ the orders of magnitude are reversed. This only occurs for extremely large masses and densities. Using $M \sim \rho r_0^3$, we find that for the orders of magnitude to be reversed at the surface of a particle of mass M,

$$M > c^3/G^{\frac{3}{2}}\rho^{\frac{1}{2}}, \quad M > 2 \cdot 10^{42}/\rho^{\frac{1}{2}}. \tag{38}$$

Such a situation is realized, if ever, only in the initial stages of an expanding universe.

In closing this discussion we may consider the case where curvature is *given*, say that for some very large mass, and we ask for the relation between the size of the triangle and the properties of the test particle in order that this given curvature may be measured. If $1/R^2$ is the given Gauss curvature, we must have

$$\delta q/q^3 \ll 1/R^2, \tag{39}$$

and using the first three of the inequalities (18) (the remaining ones are not applicable), we find

$$h/pq^3 \ll 1/R^2. \tag{40}$$

Evidently this inequality can always be satisfied by making p and q large, but it is instructive to consider a few examples. Suppose we are triangulating in the neighborhood of the sun with optical light $h/p = \lambda \sim 10^{-5}$ cm. For the first order, $M = 2 \cdot 10^{33}$ g, $r = 7 \cdot 10^{10}$ cm,

$$1/R^2 \simeq GM/c^2r^3 \simeq 10^{-27} \text{ cm}^{-2}. \tag{41}$$

It is essentially a curvature of this order of magnitude which is measured by an Einstein light deflection experiment. Equation (40) gives, with $h/p = 10^{-5}$ cm,

$$q \gg 10^7 \text{ cm} \tag{42}$$

as the side of the measurement triangle.

For a particle of mass one gram moving with a velocity of one centimeter per second, one finds the side of the triangle must be $q \gg 1$ cm.

As a further example, consider the measurement of the radius of curvature of the universe. This is certainly not less than 10^{28} cm, so we have

$$h/pq^3 \ll 1/R^2 \simeq 10^{-56}. \tag{43}$$

For optical light $\lambda \sim 10^{-5}$ we find

$$q \gg 10^{17} \text{ cm} \sim 0.1 \text{ light year.} \quad (44)$$

The important conclusion from these examples is not that a given curvature can always be measured somehow, but that (a) the curvature is defined (in the sense of the limitations of quantum-theory measurement) only in the *large*, and (b) the domain of largeness is fundamentally determined by the momentum of the test particle with which the curvature is measured. Here we are led again to the idea that the conception of curvatures and, when these are equated in the form $G_{ik}+\frac{1}{2}g_{ik}G$ to the stress tensor KT_{ik}, the conceptions of energy, mass, and momentum, are only defined for quite large masses and large volumes of space.

PHYSICAL REVIEW VOLUME 75, NUMBER 10 MAY 15, 1949

Theoretical Analysis of Ionization Chamber Data on Large Air Showers*

JOHN M. BLATT
Laboratory for Nuclear Science and Engineering, Massachusetts Institute of Technology, Cambridge, Massachusetts
(Received September 20, 1948)

The decoherence curve of large air showers is analyzed under the simplifying assumption of a constant lateral structure function for all air showers. The following results emerge: (1) Contrary to statements found in the literature, ordinary shower theory leads one to expect a rise in the decoherence curve at distances much less than the characteristic lateral distance r_1. (2) The theoretical decoherence curve calculated under the assumption of a constant structure function rises *more* sharply near the origin than the experimental points. This indicates that the effective structure function is less peaked than the one we used (due to Molière). (3) The dependence of the structure function upon the age of the shower tends to lessen this discrepancy. However, quantitative estimates make it appear doubtful that one can get agreement between theory and experiment without assuming a rather high multiplicity of the event which starts the shower.

(1) QUALITATIVE CONSIDERATIONS CONCERNING THE LATERAL STRUCTURE OF AIR SHOWERS

THE experiments which are to be interpreted here are connected with the so-called *decoherence curve* of large air showers. Two ionization chambers are placed a distance $2a$ apart. The chambers are biased so that they only respond if more than a certain amount of ionization is produced in each chamber, the bias being the same for both chambers. If the dimensions of the chambers can be neglected compared with their separation, the bias can be interpreted as meaning that each chamber responds only if the *density* of shower electrons passing through it is greater than a certain minimum amount, which we call ρ.

One then measures the coincidence counting rate W as a function of this minimum density ρ and of the half-distance a between the chambers. *A curve of $W(\rho, a)$ vs. a (keeping the bias constant) is called a decoherence curve.* We shall call a curve of $W(\rho, a)$ *vs.* ρ (keeping the separation a constant) a *density response curve.*

Historically, decoherence curves were measured first with Geiger-Müller counters.[1] It can be shown that a set of Geiger-Müller counter measurements giving the coincidence rate as a function of the distance between the counter trays and of the area of the counter trays (keeping the number of counters in each tray constant) is mathematically equivalent to a set of ionization chamber data, giving their coincidence rate as a function of the distance between the chambers and of the chamber bias. However, ionization chamber data are much preferable for the following reasons:

(1) A single set of measurements, in which pulses of different sizes are recorded, is required instead of a large number of measurements with counter trays of different areas.

(2) In Geiger-Müller counter measurements, there often exists the possibility of getting spurious counts from a single particle traveling horizontally, since one particle can easily produce a pulse. In ionization chamber measurements, ten to twenty particles must pass through the chamber before a pulse is recorded; hence, there are no spurious counts due to that source.

(3) For the same reason, statistical fluctuations are much less important in ionization chamber data.

(4) The mathematical analysis is incomparably simpler.

In discussing large air showers, we shall consider only the electron-photon component, since this component accounts for most of the ionizing radiation observed without heavy shielding on top of the detecting equipment. There seems to be reason to believe[2] that there are on the average about fifty electrons for every heavy ionizing particle in big air showers. (The word "electron" is used for both negatrons and positrons.)

We assume that the shower is started by an "initiating electron" near the top of the atmosphere.

* Assisted by the joint program of the ONR and the AEC.

[1] Auger, Maze, Ehrenfest, and Freon, J. de phys. et rad. 1, 39 (1939).

[2] G. Cocconi and K. Greisen, Phys. Rev. **74**, 62 (1948); J. E. Treat and K. Greisen, Phys. Rev. **74**, 414 (1948).

The initiating electron is very probably *not* a primary particle.[3] Since observations are mostly carried on below a considerable atmospheric depth (twenty radiation units in our case), the observations do not distinguish whether the initiating particle is an electron or a photon, nor can we tell just where the shower starts, as long as it is within a few radiation units from the top of the atmosphere. Recently, it has been suggested[4] that the event which initiates the shower is of a highly multiple character. The consequences of this hypothesis will be discussed in Section 6.

The usual shower theory treats the average longitudinal development of a shower under the assumption that the particles are all concentrated around the shower axis (the direction of the initiating particle). The effects (neglected in the usual shower theory) which lead to a lateral displacement of the shower particles from the axis of the shower are:

(1) scattering of electrons by air nuclei (Coulomb scattering);

(2) scattering of photons by electrons in air molecules (Compton scattering);

(3) the angular deviation of the particle in pair production from the direction of the parent photon;

(4) the angular deviation of the Bremsstrahlung photon from the direction of the parent electron.

One can estimate the angles involved in these processes. It turns out that the scattering of electrons by air nuclei gives most of the effect so that the other processes (2), (3), and (4), may be neglected. The scattering is predominantly multiple; i.e., deflections through a finite angle are mostly due to many successive scattering events, each event involving a very small angle, rather than to a single scattering event. The mean square angle of deviation $\langle\theta^2\rangle_{Av(dt)}$ due to multiple Coulomb scattering of a particle of energy E passing through a layer of matter of thickness dt (measured in radiation lengths) is given by[5]

$$\langle\theta^2\rangle_{Av(dt)}=(E_s/E)^2dt. \tag{1.1}$$

The "scattering energy" E_s is 21 Mev.

Qualitatively, the development of a shower may be described as follows: The initiating electron defines the axis of the shower. Before the maximum is reached, the number of particles rapidly increases while their average energy decreases. Beyond the maximum, the average energy of the particles stays roughly constant (at about the critical energy $\epsilon=86$ Mev in air), while the total number of particles decreases until the shower dies.

The lateral distribution of electrons is different for electrons of different energies. The root-mean-square Coulomb scattering angle is inversely proportional to the energy of the electrons. Hence, high energy electrons are found close to the shower axis, while low energy electrons are spread out over much larger lateral dimensions. The high energy electrons form a dense *shower-core*. The density of particles in the core of the shower is determined by the number of high energy electrons in the shower, *not* by the total number of electrons in the shower.

We can estimate the mean square distance $\langle r^2(E)\rangle$ of an electron of energy E from the shower axis in the following way. First, we observe that the parent of this electron was a particle of much higher energy (about three to ten times as much). Hence, on a first approximation, we can neglect the spreading of the ancestors of the electron in question. (This is true for E greater than the critical energy ϵ; we will see later that it is not true for $E\lesssim\epsilon$.) The mean square scattering angle per radiation unit of matter traversed is given by (1.1). The mean square lateral displacement can be estimated by taking the mean square angle over the range of the particle, and multiplying by the square of the range; i.e.,

$$\langle r^2\rangle\sim\langle\theta^2\rangle_{Av(\text{range})}\cdot[\text{range}]^2. \tag{1.2}$$

The range of high energy electrons in air showers is of the order of magnitude of one radiation length, the distance in which the energy is on the average reduced to $1/e$ of its original value by radiation processes. We therefore get the rough estimate

$$\langle r^2(E)\rangle\sim(E_sX_0/E)^2 \text{ for } E\gtrsim\epsilon. \tag{1.3}$$

For electrons of the critical energy ϵ, (1.3) gives

$$\langle r^2(\epsilon)\rangle\sim(E_sX_0/\epsilon)^2\equiv r_1^2, \tag{1.4}$$

The *characteristic lateral unit of length* r_1 defined by (1.4) gives an idea of the lateral extent of a shower over most of its length. For air, r_1 is about one-fifth of a radiation unit. At Echo Lake, Colorado, r_1 is about one hundred meters.

For electrons below the critical energy, it is not permissible to neglect the ionization loss. Indeed, the range of an electron of energy $E<\epsilon$ is of order $(E/\epsilon)X_0$, not of order X_0. If we put this into (1.2), we get

$$\langle x^2(E)\rangle\sim(E_s/E)^2(E/\epsilon)(EX_0/\epsilon)^2=(E/\epsilon)r_1^2. \tag{1.5}$$

This result must be interpreted with care. $\langle x^2(E)\rangle$ is *not* the mean square distance from the shower axis, but rather the mean square lateral distance from the position of the parent particle. Since $\langle x^2(E)\rangle$ *decreases* with decreasing energy, *one is not justified in neglecting the distribution of the ancestry of electrons of below critical energy*. This is borne out by more detailed calculations of $\langle r^2(E)\rangle$.[6]

[3] R. I. Hulsizer and B. Rossi, Phys. Rev. **73**, 1402 (1948).
[4] H. W. Lewis, J. R. Oppenheimer, and S. A. Wouthuysen, Phys. Rev. **73**, 127 (1948).
[5] B. Rossi and K. Greisen, Rev. Mod. Phys. **13**, 240 (1941).
[6] L. Landau, J. Phys. U.S.S.R. **3**, 237 (1940); S. Z. Belenky, J. Phys. U.S.S.R. **8**, 9 (1944).

The above considerations lead to the following qualitative picture of a shower. The shower first spreads out as it goes down into the atmosphere. The more energetic particles stay near the axis, their less energetic offspring spread out somewhat, *their* offspring spread even farther, etc. This makes the shower appear like a fir tree. This behavior does not persist, however. After a few radiation units, electrons of about the critical energy make up most of the population of the shower (this happens long before the average energy is reduced to ϵ). These low energy electrons have a limited range and do not spread any more. Hence, after a few radiation units, the shower does not spread out any more, its lateral dimensions staying constant, of order of magnitude r_1, (1.4). From then on, the shower looks like a cylinder, provided we measure all distances in radiation units. If we measure distances in meters, the cylinder becomes compressed as it goes down into the atmosphere since the radiation unit is proportional to the density of the air. In other words, the cylinder becomes a funnel.

The core of the shower is made up of energetic particles ($E \sim 10^9 - 10^{11}$ ev). The relative number of these energetic particles decreases as the shower passes through its maximum and gets older. The number of electrons of energy greater than E ($E > \epsilon$) passes through a maximum *before* the shower as a whole passes through its maximum. For a shower initiated by an electron of energy 10^{16} ev, the maximum of the shower as a whole occurs about 17.5 radiation units down. The maximum of electrons of energies larger than 10^9 ev occurs about two radiation units before that. We see that the relative importance of the core of the shower decreases with age.

In what follows, we shall restrict ourselves to the *average* development of air showers. At first sight, one might think that correlations of density fluctuations in the shower introduce large errors into the comparison of theory and experiment. This is true for the longitudinal development of the shower, but is *not* true for measurements of the lateral structure at any one level in the atmosphere, provided that many particles are required to set off the ion chambers. The reason is the difference in the "memory" and "amplification" properties of the shower for longitudinal and lateral fluctuations. In the longitudinal development, we have a cumulative process in which a given fluctuation is not only "remembered" for many radiation lengths but exerts an "amplified" effect because of the multiplication along the shower. In the lateral development, the electrons observed at a given distance from the shower axis go there almost entirely in the last few radiation lengths. Furthermore, once they get out from the core by an appreciable distance, they are already close to critical energy and do not multiply by a very large factor. Hence, the lateral development of the shower features both a short "memory" and a small "amplification" for fluctuations.

It is therefore reasonable to expect that the fluctuations in the lateral structure of the shower have a distribution not too far from the distribution which follows from the assumption that all the particles are statistically independent. If this is true, the root-mean-square deviation from the mean number of particles N expected at a given place will be of the order of $N^{\frac{1}{2}}$. We require at least twenty particles through the chamber before it responds. Hence, the fluctuations in density have an effect of the order of twenty-five percent on an individual count. Since we are dealing with a statistical distribution (the decoherence curve) rather than with each shower separately, this fluctuation is likely to be averaged out to a large extent. It is therefore permissible to work with average values and to neglect fluctuations from the average *provided that we restrict ourselves to events in one plane of observation perpendicular to the shower axis.* Fluctuations may interfere badly as soon as we try to correlate the experimental information at the plane of observation with hypotheses about the distribution-in-energy and in place-of-origin of the initiating particles of the shower.

We shall also assume that all showers come in vertically. This assumption can be checked experimentally by triggering a cloud chamber in coincidence with the ionization chambers. This experiment was done.[7] The result is that the angles involved are of order 20° or less for most showers.

The angles are expected to be small because a shower hitting at a large angle has to go through a thick layer of atmosphere compared to a vertical shower. There are fewer showers which can do this.

The large angle showers *do* contribute importantly to the decoherence curve at really large separations (500 to 1000 meters). The reason is that the effective chamber separation is less for showers coming in at an angle than for vertical showers. The two effects compensate in such a way that the maximum contribution comes not from the vertical direction but from some intermediate angle. This is especially so because a shower which can set off two counters separated by many times r_1 is necessarily a giant shower which is not affected much by the path length through the atmosphere (indeed, the shower may be so large that it does not even reach its maximum going straight down, in which case a bigger path length is even helpful). These considerations are due to Cocconi.[8] We shall not treat this subject here since we are interested in the decoherence curve for small separations between the chambers.

(2) THE LATERAL STRUCTURE FUNCTION OF AN AIR SHOWER

Let $\rho(E_0,t,r)$ be the average density of all shower electrons, irrespective of energy, per unit area per-

[7] R. W. Williams, Phys. Rev. **74**, 1689 (1948).
[8] G. Cocconi, Phys. Rev. **72**, 350 (1947).

pendicular to the axis of the shower at a distance r from the shower axis. We assume the shower was started by an initiating electron of energy E_0, a distance t radiation units above the plane of observation. Then the total number of electrons at this depth in the atmosphere is, in the notation of Rossi and Greisen,[5]

$$\Pi(E_0,0,t)=\int_0^\infty \rho(E_0,t,r)2\pi r dr. \qquad (2.1)$$

In order to correlate theory with experiment, we should not consider electrons down to zero energy, but rather we should make the lower limit on E equal to the minimum energy necessary to penetrate the wall of the ionization chamber. This does not make a significant difference for the experiments in question.

We now define the *lateral structure function* $f(E_0,t,r)$ of the shower by

$$f(E_0,t,r)\equiv \rho(E_0,t,r)/\Pi(E_0,0,t). \qquad (2.2)$$

It follows from this definition and (2.1) that the integral of the structure function over the whole plane of observation is unity:

$$\int_0^\infty f(E_0,t,r)2\pi r dr=1. \qquad (2.3)$$

Our qualitative considerations have shown that the structure function depends upon the age of the shower. A young shower, before it reaches its maximum, has a large proportion of high energy particles, hence a dense core. This makes the structure function peaked near the origin. As the shower becomes older, the core becomes less dense; hence the peak of the structure function becomes relatively less important.

For values of $r\ll r_1$ and t not much beyond $t_{\max}$, electrons of energy $E\gg\epsilon$ give most of the contribution to the structure function $f(E_0,t,r)$. In that case, one can give a rough estimate of the behavior of the structure function:[9]

$$f(E_0,t,r)\sim r^{s-2} \text{ provided } r\ll r_1, \qquad (2.4)$$

where s is a quantity defined by Eq. (2.104), reference 5. s is related to the "age" of the shower, being smaller than one before the maximum and larger than one after the maximum. Thus, for young showers, the peak is very strong; for showers at their maximum, the structure function is inversely proportional to the radial distance (for $r\ll r_1$); for very old showers, s approaches 2 and the above estimate breaks down (electrons of critical energy then determine the behavior of the structure function for all values of r, not just for $r\gtrsim r_1$).

[9] I. Pomeranchuk, J. Phys. U.S.S.R., **8**, 17 (1944). A. Migdal, J. Phys. U.S.S.R., **9**, 183 (1945).

The only detailed calculation of a structure function available at this time is due to Molière.[10] Molière restricts himself to the maximum of the shower. He starts by calculating the structure function for particles of a single energy E under the assumptions described as "approximation A" in the review paper by Rossi and Greisen;[5] i.e., Molière calculates the partial structure function $f(E_0,E,t_{\max}r)$ for electrons of energy $E\gg\epsilon$. It is somewhat difficult to estimate the accuracy of the Molière function, since long numerical computations are involved and the calculation has not been reported in detail so far. The fact that the distribution-in-angle (an intermediate step in the calculation) turns out to be negative for angles near $\theta=3(E_s/E)$,[11] is not encouraging. On the other hand, Molière's value for the mean square distance $\langle r^2\rangle(E_0,E,t_{\max})$ of particles of energy E from the shower axis at the shower maximum turns out to be correct within about 15 percent.

Molière himself states the value of $\langle r^2(E_0,E,t_{\max})\rangle$ implied by his partial structure function. It is

$$\langle r^2(E_0,E,t_{\max})\rangle=0.835(E_sX_0/E)^2. \qquad (2.5)$$

This can also be seen by differentiating his Fourier transform $\varphi(\rho)$ twice, and setting $\rho=0$. While this value of $\langle r^2(E_0,E,t_{\max})\rangle$ is supposedly appropriate to the maximum of the shower, actually the only property of the shower-distribution used was that $\pi(E_0,E,t_{\max})\sim E^{-2}$ (the notationis as in reference 5). This, however, is just the behavior of the track-length $z_\pi(E_0,E)$. Hence Molière's $\langle r^2(E_0,E,t_{\max})\rangle$ can be compared directly with $\langle r^2(E_0E)\rangle$ computed on a track-length basis; i.e.,

$$\langle r^2(E_0E)\rangle\equiv\int_0^\infty\langle r^2(E_0,E,t)\rangle\pi(E_0,E,t)dt/\int_0^\infty\pi(E_0,E,t)dt, \qquad (2.6)$$

This latter quantity can be calculated accurately under approximation A by a method due to Landau[6] or alternatively by an equivalent method due to Nordheim.[5,12] The result in either case is

$$\langle r^2(E_0E)\rangle=0.723(E_sX_0/E)^2 \text{ provided } E\ll E_0. \qquad (2.7)$$

The near agreement between (2.5) and (2.7) confirms Molière's basic calcalution. (2.7) differs somewhat from the result of Landau and Belenky in spite of the fact that we used their own method of calculation. The reason is that they employed approximate expressions for the track-lengths which are valid for $E\ll E_0$ but not for $E\sim E_0$. It turns out that an accurate expression for $z_\pi(E_0,E)$ for values of $E\sim E_0$ is essential to obtain the correct answer, even though the answer itself refers to an energy $E\ll E_0$. The result (2.7) was derived using the Rossi-Greisen Mellin transform directly.

The expression (2.7) still needs a correction because we express $\langle r^2\rangle$ in units of the radiation length X_0, and X_0 decreases as we go down into the atmosphere. We define the fractional decrease in X_0 per radiation length, q, by

$$q\equiv -X_0^{-1}(dX_0/dt). \qquad (2.8)$$

$q=0.041$ at Echo Lake, and it is roughly proportional to t^{-1}. If we neglect this altitude variation of q, the coefficient in

[10] G. Molière, *Cosmic Radiation*, ed. by W. Heisenberg (Dover Publications, New York, 1946), Chapter 3.

[11] The author thanks Drs. H. A. Bethe and L. Eyges for calling his attention to this point.

[12] L. W. Nordheim, Phys. Rev. **59**, 929 (1941). J. Roberg, Phys. Rev. **62**, 304 (1942). J. Lanossy, *Cosmic Rays* (Oxford University Press, London, 1948), Chapter VIII.

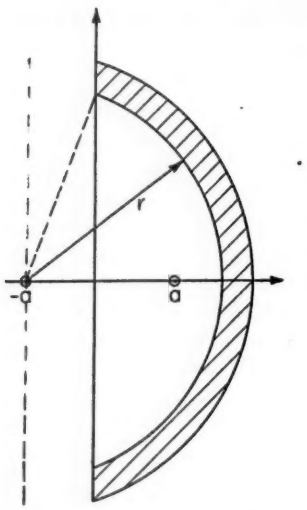

FIG. 1. Two ionization chambers, 1 and 2, are placed at $x=\pm a$, $y=0$. A shower whose core hits in the right half-plane will be counted provided it has sufficient density at the position of chamber 2.

Eq. (2.7) (called Q from here on) is given by

$$Q=0.723\frac{1-0.87q+0.43q^2}{(1-0.99q+0.19q^2)(1-1.99q+0.74q^2)}. \quad (2.9)$$

We can understand the dependence of Q upon q as follows: Since the particles which we measure at a given lateral distance from the shower axis got their lateral displacement somewhat earlier, we should replace X_0 in (2.7) by X_0 measured some distance Δt above the place of observation. This means $X_0(t)$ is replaced by $X_0(t-\Delta t)\cong X_0(t)[1+q\Delta t]$. Since X_0 enters squared, Q is given approximately by

$$Q\cong Q_0[1+2q\Delta t],$$

where $Q_0=0.723$ is the value computed by neglecting this effect. Expansion of (2.9) shows that $\Delta t\leqq 1.05$ radiation units; i.e., *the high energy particles which we observe got their lateral displacement on the average one radiation unit above the place of observation.* This agrees with Janossy's result. This effect is not negligible. It amounts to a ten percent increase in Q at Echo Lake. Indeed, at Echo Lake we find that $\langle r^2(E_0E)\rangle$ is given by

$$\langle r^2(E_0E)\rangle=0.786(E_sX_0/E)^2. \quad (2.10)$$

Even if Molière's partial structure function for particles of a single energy were rigorously correct for high energy ($E\gg\epsilon$) particles, his over-all structure function, summing the contributions of electrons of *all* energies, might still be in error. Molière states that he used Arley's approximation[13] to find the total number of low energy electrons. This approximation is quite poor,[14,15] and it would falsify his over-all structure function even if he had at his disposal the exact partial structure function for low energy electrons.

An even more serious error in Molière's calculation comes from the fact that he did not use the correct partial structure function for electrons near the critical energy. Rather he extrapolated the high energy partial structure function right down to the critical energy. It can be shown[15a] that this procedure overestimates the lateral spread of these low energy electrons considerably ($\langle r^2(E)\rangle$ is too large by about a factor of two at $E=\epsilon$). Since electrons of about critical energy make up most of the population of the shower, this error in the partial structure function is preserved in the total structure function.

Underestimation (a la Arley) of the number of low energy electrons is likely to make Molière's structure function more peaked than the true one. On the other hand, the incorrect partial structure function for low energies will make Molière's structure function less peaked (extending farther out) than the true one. A rough estimate[15a] shows that the over-all effect makes the Molière function *less* peaked than the true one. Just how much more is not known at this time.

It must be emphasized that Molière's calculation, even though we have no estimate of error for it, is the best one available at this time.** For this reason we shall choose it as the basis for comparison between theory and experiment. We shall assume that the Molière structure function represents the lateral structure of all showers. This assumption implies that *we disregard the variation of the structure function with age.* An estimate of the error thus introduced will be given in Section 6. It may be appropriate at this point to emphasize that the main merit of the theory to be developed here lies in the qualitative understanding of the main features of the decoherence curve, not in the quantitative results.

The over-all structure function of Molière can be approximated for small values of r by an analytic expression due to H. A. Bethe.[16]

$$\left.\begin{aligned} &f(E_0,t_{\max},r)=r_1^{-2}\phi(r/r_1),\\ &\phi(x)\cong Cx^{-1}(1+4x)\exp[-4x^{\frac{1}{2}}] \text{ for } x\lesssim 0.5.\end{aligned}\right\} \quad (2.11)$$

r_1 is the characteristic lateral unit of length (1.4). C is a constant, $C\cong 0.450$. Since we are concerned with distances of the order of one to ten meters while r_1 is 106 meters at Echo Lake, we can use (2.11) without introducing a large error. (Roughly ninety percent of the contribution to the counting rate of two chambers even twelve meters apart comes from showers whose cores hit no farther than fifty meters ($r/r_1\cong 0.5$) away.)

We see that the Molière function has the pre-

[13] N. Arley, Proc. Roy. Soc. **A168**, 519 (1938).
[14] S. Z. Belenky, Comptes Rendus, U.S.S.R. **30**, 608 (1941).
[15] M. Schonberg, Ann. Acad. Brasil. Sci. **12**, 281 (1940).
[15a] J. Roberg and L. Nordheim, Phys. Rev. **75**, 444 (1949). The author wishes to thank Professor Nordheim for calling his attention to this point and for giving him the numerical results of the above paper prior to its publication.
** Pomeranchuk and Migdal, reference 9, put the proper emphasis on the age-dependence of the structure function, but their work is more qualitative in character.
[16] H. A. Bethe, private communication.

dicted r^{-1} dependence near the origin. It should be emphasized, though, that the exponential factor is very important. It gives an appreciable deviation from the r^{-1} law already at distances of order $(r/r_1)\sim 0.01$ (i.e., one meter at Echo Lake).

(3) THE THEORETICAL FORMULA FOR THE COUNTING RATE NEGLECTING THE DIMENSIONS OF THE CHAMBER. THE INVERSION THEOREM

Let $S(N)$ be the number of showers crossing the plane of observation per unit time, with their axes falling within a unit area, such that the total number of particles crossing the plane is greater than N. We want to determine $W(\rho, a)$, the coincidence counting rate of two ionization chambers of dimensions much smaller than a, and biased so that a particle density greater than ρ is necessary before either chamber will register.

One can see from Fig. 1 that the recording of showers whose cores pass through the half-plane $x>0$ will be limited by the ionization chamber at $x=-a$. That is, if it registers, the other one will certainly register. (We are neglecting fluctuations.) Similarly, showers whose core passes through the half-plane $x<0$ will be limited by the chamber at $x=+a$.

Consider those showers whose cores pass through the shaded circular strip in Fig. 1. They will be recorded provided

$$Nf(r)\geqslant \rho. \tag{3.1}$$

The area of the circular strip is

$$dA=2 \text{ arc } \cos(a/r)rdr. \tag{3.2}$$

There are $S[\rho/f(r)]$ such showers per unit time. We get the contribution of the right half-plane to the counting rate $W(\rho, a)$ by summing over all these circular strips; i.e., by integrating from $r=a$ to $r=\infty$. By symmetry, the showers whose cores pass through the left half-plane give the same result. Hence

$$W(\rho, a)=\int_a^\infty 4r \text{ arc } \cos(a/r)S[\rho/f(r)]dr. \tag{3.3}$$

(3.3) is an integral equation connecting the experimental function $W(\rho, a)$ of ρ and a with the unknown function $S[\rho/f(r)]$ of ρ and r. It turns out that (3.3) has an explicit solution. This is due to the fact that the kernel involves only the ratio of r to a. The solution is

$$S[\rho/f(r)]=(2\pi)^{-1}\int_r^\infty (a^2-r^2)^{-\frac{1}{2}}(\partial^2 W/\partial a^2)da. \tag{3.4}$$

The kernel $(a^2-r^2)^{-\frac{1}{2}}$ has an infinite (but integrable) peak at the lower limit $a=r$. *Therefore, $S[\rho/f(r)]$ is essentially proportional to the second derivative of $W(\rho, a)$ with respect to a, at the point $r=a$.* This is a rather unfortunate fact. It means that *it is practically impossible to get the detailed behavior of $f(r)$ from the experimental data.* The statistical accuracy necessary before the second derivative of W has any meaning would require years of taking data. Conversely, this result explains the agreement between theory and experiment, found by investigators who *assumed* a structure function $f(r)$, and a frequency function $S(N)$ and determined the corresponding $W(\rho, a)$ from (3.3). In the light of this discussion, such agreement is to be expected for any reasonable choice of $f(r)$, but it proves very little about the correctness of this choice of $f(r)$.

(4) THE BEHAVIOR OF THE DECOHERENCE CURVE AT SMALL DISTANCES

The experiments[7] show that the coincidence counting rate $W(\rho, a)$ has approximately a power law dependence upon ρ; i.e.,

$$W(\rho, a)\cong \rho^{-\gamma}V(a), \tag{4.1}$$

where the exponent γ is a slowly varying function of a. In order to discuss the asymptotic behavior of the decoherence curve near $a=0$, we shall assume that γ is constant. Some evidence in favor of this assumption comes from the experiments of Cocconi[17] who investigated the distribution-in-density of showers somewhat smaller than the ones considered here. The results of Cocconi can be interpreted to mean that $S(N)\sim N^{-1.5}$ for N of order 10^3-10^5. Since showers of this order of magnitude contribute most of the counting rate in Williams' experiments for separations less than a meter, we can infer that the assumption

$$S(N)=\sigma N^{-\gamma}=\sigma N^{-1.5} \tag{4.2}$$

will give a good approximation to the behavior of the decoherence curve near zero separation.

We now show that $V(a)$ behaves in the following way for small values of a:

$$V(a)\cong V(0)-ka^{2-\gamma}. \tag{4.3}$$

Referring back to Fig. 1, we see that the region between the dotted line and the y axis would contribute to the counting rate of the left-hand chamber if the other chamber were moved over to $x=-a$. Hence, we must integrate $S[\rho/f(r)]$ over the area of this strip and multiply by 2 to get the differene between $W(\rho, 0)$ and $W(\rho, a)$. We introduce polar coordinates to get

$$W(\rho, 0)-W(\rho, a)=2\int_{-\pi/2}^{\pi/2}d\phi\int_0^{a\sec\phi} rdrS[\rho/f(r)].$$

We use Eq. (4.2) and the limiting form of the

[17] G. Cocconi, A. Loverdo, and V. Tongiorgi, Phys. Rev. 70, 846 (1946).

structure function for small values of r:

$$f(r) \cong C/r_1 r. \tag{4.4}$$

Equation (4.2) then gives

$$W(\rho, 0) - W(\rho, a) = \rho^{-\gamma}[V(0) - V(a)],$$

where

$$V(0) - V(a) = 2\sigma \int_{-\pi/2}^{\pi/2} d\phi \int_0^{a \sec\phi} r dr f^{\gamma}(r). \tag{4.5}$$

If we now substitute (4.4), we find that

$$V(0) - V(a) \cong \left[4\sigma (C/r_1)^{\gamma} (2-\gamma)^{-1} \int_0^{\pi/2} (\sec\phi)^{2-\gamma} d\phi \right] a^{2-\gamma}.$$

The coefficient in brackets is the k of Eq. (4.3). The importance of this result does not lie in the value of the coefficient. It lies in the fact that *the theory predicts an extremely sharp rise in the decoherence curve for small distances.* Indeed, formula (4.3) implies an infinite slope of $V(a)$ at $a=0$.

We have already seen that predictions like this cannot be trusted for very small distances. First of all, the chambers are *not* infinitely small—this will be discussed in Appendix A. Second, the structure function is *not* the Molière function for these small distances. This will be discussed in Section 6.

However, the qualitative result stands. *From ordinary shower theory, one should expect a rise in the decoherence curve for distances considerably less than the characteristic lateral unit* r_1. The usual argument against this is that most of the counts are due to showers whose cores hit far away. This is not true for very small separations. Essentially there are two effects here: (1) the cores of showers of a given number of particles N have to pass through an area which becomes smaller as N becomes smaller, and (2) the total number of showers per second per unit area is a rapidly decreasing function of N. The two effects work against each other. The net result depends upon the exponent γ in the power law of the distribution-in-number $S(N)$. For γ between one and two, we get a sharp peak at the center.

A few remarks may be in order here concerning Molière's calculation of the decoherence curve for Geiger-Müller counters. Molière finds that the theoretical decoherence curve should flatten off at distances of the order of three meters, in contradiction with the experimental data. On the other hand, a lengthy but elementary argument of the general nature of the one just given enables us to state that the result (4.3) also holds for Geiger-Müller counter decoherence curves; the only difference lies in the coefficient k.

A possible explanation for Molière's result is that he did not use a power law distribution for $S(N)$, but rather a power law for the distribution-in-energy of assumed primary electrons. The resulting $S(N)$ is not a pure power law. In particular, it rises less rapidly for small values of N. Hence, our assumption of a pure power law for $S(N)$ gives a larger rise of the decoherence curve near zero than Molière's assumption. However, it is doubtful that even under this assumption the decoherence curve should flatten off quite that rapidly. One is tempted to believe in an error in Molière's calculation, stemming either from the use of approximate functions for $\Pi(E_0,0,t)$ or from the very complicated numerical integrations involved in this method.

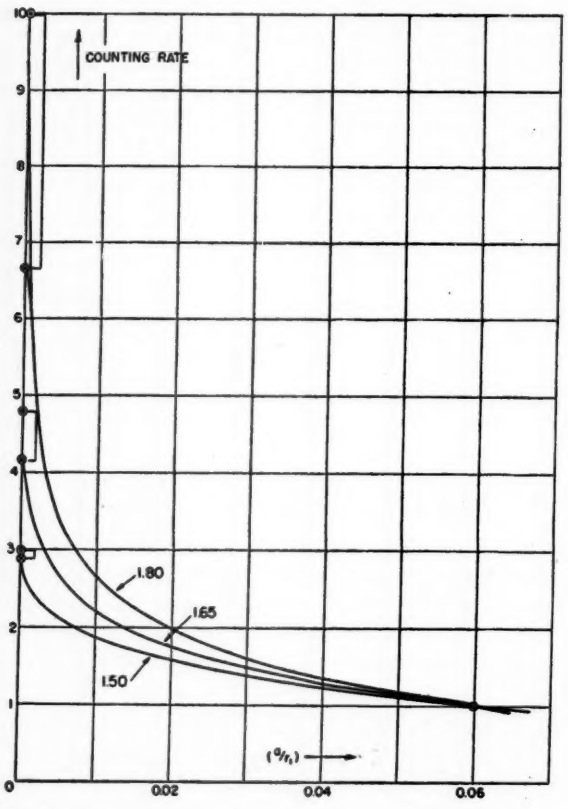

FIG. 2. Ordinate: Counting rate. Abscissa: Half-separation a between the chambers in units of the characteristic lateral distance r_1. The values of the exponents γ in the distribution-in-number $S(N)$ are indicated next to the curves. The correction for the point at $a=0$ is discussed in Appendix A.

The asymptotic form (4.4) of the structure function is not very accurate. $V(a)$, as defined by (4.1), was therefore calculated numerically from the Molière function (2.11) for various values of γ.

The results are given in Fig. 2. They are normalized to unity at $a=0.06$ (twelve meters separation at Climax). For each value of γ there are two points at zero separation. The upper one is uncorrected for the finite size of the chamber. The lower one is corrected for this effect. (See Appendix A.) The numbers next to the curves show what values of γ were assumed.

The theoretical decoherence curves show a drop of 2 or 3 (depending upon γ) between $a=0.01$ and $a=0.06$ (i.e., 2 and 12 meters chamber separation at Echo Lake). A factor of this order is observed experimentally.[7] On the other hand, the theoretical curves definitely disagree with experiment for very short distances. There the experimental curves

flatten off whereas the theoretical ones keep rising, even after one takes the finite chamber size into account. This will be discussed in the next section.

We would only like to point out here that the existence of this disagreement is not in contradiction with the remarks of Section 3. $S[\rho/f(r)]$ is proportional to the second derivative of W only where $f(r)$ is regular. In the present case, the theory predicts not only an infinite second derivative at $a=0$, but also an infinite first derivative. The experiments, even with rather poor statistics, can distinguish between a finite and an infinite slope, and they give a finite slope.

(5) THE DISTRIBUTION-IN-NUMBER $S(N)$

We start by recalling the experimental data[7] concerning the exponent γ in Eq. (4.1). These data are summarized in Table I. We see that the effective exponent γ_{eff} of the density response curves increases with chamber separation; $\gamma_{\text{eff}}=1.5$ for chambers close together, $\gamma_{\text{eff}}=1.9$ for chambers separated by twelve meters ($a\cong 0.06r_1$).

This behavior of γ_{eff} takes place because the size of the showers which contribute most to the counting rate depends upon the chamber separation. As the chamber separation increases, showers containing increasingly larger numbers of particles make the major contribution to the counting rate $W(\rho, a)$.

There are two reasons for γ_{eff} to vary with the number of particles in the showers which contribute most to the counting rate: (1) the distribution-in-number $S(N)$ of the showers may not follow a pure power law; (2) the structure function may be (and we know it actually is) age-dependent.

The first effect needs no explanation. In order to understand the second effect, let us assume for the moment that the distribution-in-number $S(N)$ follows a pure power law, $S(N)=\sigma N^{-\gamma}$. The age-dependence of the structure function implies that we overestimate the sharpness of the peak in old showers by using the Molière function. Since the structure function is normalized by Eq. (2.3), a smaller peak near zero implies that $f(r)$ has larger values for larger values of r. This situation is shown schematically in Fig. 3.

If the event which originates the shower is known both as to kind and height above the equipment, then the number of particles N in the shower also defines the age of the shower. We may therefore consider the structure function as a function of N and r:

$$f=f(N, r). \tag{5.1}$$

We define the minimum effective number of particles $\bar{N}=\bar{N}(\rho, r)$ by

$$\bar{N}f(\bar{N}, r)=\rho. \tag{5.2}$$

TABLE I. Effective exponent γ_{eff} as a function of chamber separation, for a bias $\rho=460$ electrons/m².

Chamber separation in meters at Echo Lake	a/r_1	γ_{eff}
0.015	0.0007	1.50
0.36	0.0017	1.67
1.0	0.0047	1.56
7.0	0.0332	1.85
12.2	0.0575	1.90

We shall assume that Eq. (5.2) has a unique solution for every r and ρ of interest. Then Eq. (3.3) becomes

$$W(\rho, a)=\int_a^\infty 4r \arccos(a/r)S[\bar{N}(\rho, r)]dr. \tag{5.3}$$

Next, we determine the dependence of $\bar{N}$ upon ρ. For a constant structure function, $\bar{N}$ is of course proportional to ρ (see Eq. (3.1)). Figure 3 shows that for *small* values of r, $f(N, r)$ increases with N, while for large values of r, $f(N, r)$ decreases with N. Over a small interval in ρ, N may be assumed to behave like ρ^α where α is less than unity for small r, greater than unity for large r.

We now substitute a pure power law for $S(N)$. Since most of the contribution to W comes from distances r of order of magnitude a, we conclude that the dependence of $W(\rho, a)$ upon ρ is roughly

$$W(\rho, a)\sim\rho^{-\alpha\gamma}, \tag{5.4}$$

with α evaluated at $r=a$. This shows that even a pure power law for $S(N)$ will lead to *effective exponents γ_{eff} which increase with increasing separation due to the age-dependence of the structure function.*

Since we have no quantitative information about the age-dependence of the structure function, we shall neglect effect (2) altogether in the quantitative discussion of this section, restricting ourselves to

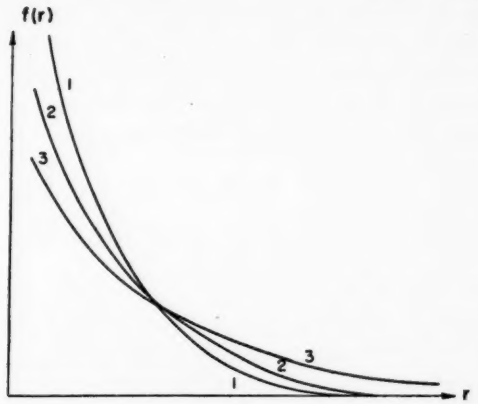

FIG. 3. Schematic picture of the age-dependence of the structure function. Curves 1, 2, and 3 are in order of increasing age of the shower. The structure function decreases with age for small values of r, increases with age for large values of r.

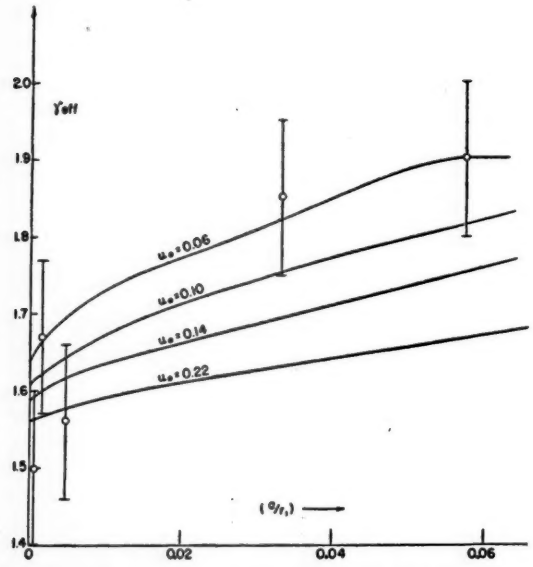

FIG. 4. Ordinate: Effective exponent γ_{eff} of $W(\rho, a)$ as a function of ρ. Abscissa: Half-distance a between the chambers in units of the characteristic lateral distance r_1. The curves are computed from formula (5.6). The experimental data are taken from Table I.

pointing out the qualitative changes introduced by this effect. Some very rough quantitative estimates will be given in Section 6.

We therefore assume that the structure function is still the same for all showers, but $S(N)$ is not a pure power law any more. This latter assumption is rather appealing, for the following reason: if we assume a power law for the distribution-in-*energy* of the initiating electrons, the distribution-in-number $S(N)$ at the place of observation will *not* be a power law throughout the range of N. It will be approximately a power law over small ranges of N, with exponents γ which depend upon N. γ will equal the exponent of the initiating distribution-in-energy for those values of N and the initiating energy for which the shower just reaches its maximum at Echo Lake. For bigger N (and therefore bigger E_0 and younger showers) γ will be larger. For smaller N (older showers past their maximum at Echo Lake) γ will be less.

We recall that Cocconi[17] found a power law for $S(N)$ with an exponent $\gamma \cong 1.5$. The showers which he observed were on the average smaller than the ones observed by Williams.[7] It is therefore reasonable to assume that $S(N)$ goes like $N^{-1.5}$ for low N (of order 10^3-10^5) and then drops off more steeply. The value of γ_{eff} for the largest separations used by Williams is of order 1.9. We therefore make the following assumption for the distribution-in-number $S(N)$:

$$\left.\begin{aligned} S(N)&=\sigma_0 N^{-1.5} \text{ for } N<N_0,\\ S(N)&=\sigma_1 N^{-1.9} \text{ for } N>N_0.\end{aligned}\right\} \tag{5.5}$$

From the definition of $S(N)$, it follows that it must be a continuous function. This determines the ratio of σ_0 to σ_1 for any given choice of the "breakpoint" N_0. It is an easy matter to substitute the assumption (5.5) into the basic formula (3.3) for the counting rate. We define the "breakpoint distance" u_0 by

$$f(u_0)\equiv \rho/N_0, \tag{5.6}$$

and the function $T(a, u, \gamma)$ by

$$\left.\begin{aligned} T(a,u,\gamma)&\equiv \int_u^\infty 4r \arccos(a/r) f^\gamma(r)dr \quad \text{for} \quad u>a,\\ T(a,u,\gamma)&\equiv T(a,a,\gamma) \quad \text{for} \quad u\leqslant a.\end{aligned}\right\} \tag{5.7}$$

We observe that $T(a, a, \gamma)$ is proportional to the counting rate for a pure power-law $S(N)$. Furthermore, $T(a, u, \gamma)$ can be obtained by a very small amount of numerical work once the pure power-law functions have been computed.

With these definitions, the coincidence counting rate becomes

$$W(\rho,a)=\sigma_0\rho^{-1.5}[T(a,a,1.5)-T(a,u_0,1.5)] +\sigma_1\rho^{-1.9}T(a,u_0,1.9). \tag{5.8}$$

The effective exponent γ_{eff} can be defined by

$$\gamma_{eff}=-(\rho/W)(\partial W/\partial\rho). \tag{5.9}$$

This definition means that γ_{eff} is the (negative) slope of a plot of $\log W$ against $\log\rho$. It follows that γ_{eff} is given by

$$\gamma_{eff}=\frac{1.5f(u_0)^{-1.5}[T(a,a,1.5)-T(a,u_0,1.5)]+1.9f(u_0)^{-1.9}T(a,u_0,1.9)}{f(u_0)^{-1.5}[T(a,a,1.5)-T(a,u_0,1.5)]+f(u_0)^{-1.9}T(a,u_0,1.9)}. \tag{5.10}$$

In Fig. 4, we have plotted γ_{eff} *vs.* a for various values of u_0. (a and u_0 are measured in units of the characteristic lateral shower-distance r_1.) Also shown in the figure are the experimental values. We have assigned an error of ± 0.10 to the values of γ_{eff} in Table I. This is somewhat less than the limit of error from a differential plot (see reference 7), but it is felt that ± 0.10 is a reasonable estimate of the probable error of the coefficient obtained from an integral plot.

We see that the points fall on a smooth curve within the experimental error. Unfortunately, none of the theoretical curves is a very good fit. A value of $u_0 \cong 0.06$ is a good fit for the points at 7 and 12 meters separation, while $u_0 \cong 0.14$ is a better fit for the smaller separations.

We point out that a function $S(N)$ which goes from $N^{-1.5}$ to $N^{-1.9}$ more gradually than our simple assumption (5.5) would make the theoretical curves in Fig. 4 even flatter.

The age-dependence of the structure function makes γ_{eff} smaller for small separations, larger for large separations (see (5.4)); hence the theoretical curves in Fig. 4 will become steeper if this effect is taken into account, in better agreement with the experimental data. However, it is uncertain whether the effect will be pronounced enough to lead to quantitative agreement between theory and experiment.

Showers near their maximum (for which the Molière $f(r)$ is presumably a reasonable approximation) contribute proportionately more to the counting rate at 7 meters and 12 meters than at close distances. We therefore choose the "best" value of the breakpoint distance u_0 to fit the points farther away; i.e., $u_0=0.06$. One can then assume that the discrepancy between the theoretical and observed values of γ_{eff} at small separations is due to the age-dependence of the structure function (see the next section, however, for another important effect).

A value of $u_0=0.06$ with a minimum density $\rho=460$ particles per m^2 corresponds, according to (5.6) to a breakpoint N_0 of 1.03×10^6, or within the accuracy involved here,

$$N_0=10^6 \text{ particles.} \tag{5.11}$$

We now compare the theoretical and experimental *decoherence* curves under the assumptions (5.5) and (5.11) (γ_{eff} was related to the density response curve). We shall determine the coefficient $\sigma_0 N_0^{-1.5}=\sigma_1 N_0^{-1.9}$ in front of the distribution by fitting the points at 7 and 12 meters. The result is shown in Fig. 5.

We see that the trend of the curve is correct except at very small separations (less than one meter). The theoretical curve drops by a factor of two, approximately, between $a/r_1=0.01$ and $a/r_1=0.05$ (i.e., between 2 meters and 10 meters chamber separation). The experimental points are in rough agreement with this.

On the other hand, there is decided disagreement for $(a/r_1)<0.01$. The theoretical curve rises sharply up to a value of 1.73 at zero separation. (This is already corrected for the finite chamber size; see Appendix A.) The experimental points indicate a flattening off. (The indication that the curve actually drops for small distances must not be taken seriously.) This discrepancy can again be attributed to the age-dependence of the structure function and is again explained qualitatively by the smaller peak if the structure function for older showers. It will be discussed quantitatively in Section 6.

It may be of interest to put down some numbers here for $S(N)$. We obtain

$$\left.\begin{aligned} S(N)&=1.8\times10^{-3}(N/10^6)^{-1.5}, \quad N<10^6,\\ S(N)&=1.8\times10^{-3}(N/10^6)^{-1.9}, \quad N>10^6,\end{aligned}\right\} \tag{5.12}$$

where $S(N)$ *is in* $(meter)^{-2}$ $(hour)^{-1}$. In particular, (5.12) tells us that there are 0.0018 showers per hour whose cores hit within one square meter and which have more than 10^6 particles at the place of observation. It hardly needs to be emphasized that *(5.12) is only an order-of-magnitude estimate.* In view of the uncertainty in the theory, we prefer not to give any estimate of error at all. The reader is referred to Appendix B for an alternative way of determining $S(N)$ which gives a result different by more than a factor of two from (5.12).

The qualitative agreement between theory and experiment in Fig. 5 for larger distances cannot be used as an argument in favor of the Molière function, in view of our remarks in Section 3.

(6) SOME ESTIMATES CONCERNING THE INFLUENCE OF THE AGE-DEPENDENCE OF THE STRUCTURE FUNCTION AND SOME SPECULATIONS ABOUT MULTIPLE PRODUCTION

We shall now discuss in more detail whether the discrepancies between the theoretical and experi-

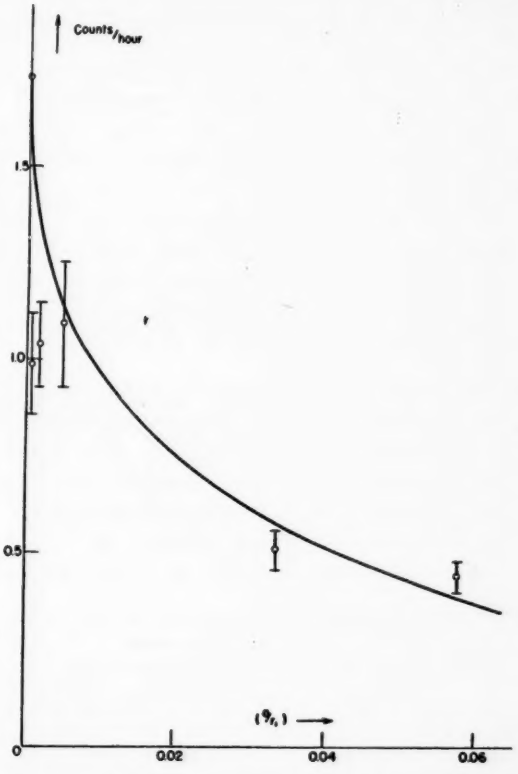

FIG. 5. The decoherence curve. Ordinate: Counts per hour with a bias of 460 particles/m². Abscissa: Half-separation between chambers in units of r_1. The experimental data are due to R. W. Williams. (See reference 7.) The theoretical curve is fitted to the points at $a=0.0332$ and $a=0.0575$.

mental values of $W(\rho, a)$ at small distances can be accounted for by the age-dependence of the structure function, under various assumptions about the way large air showers are initiated.

We shall use the estimate of Pomeranchuk and Migdal[9] for the behavior of the structure function at small distances

$$f(r) \sim r^{s-2}, \tag{6.1}$$

where s defines the age of the shower. $s=1$ corresponds to the shower maximum. In Section 4 we have derived the asymptotic form of the decoherence curve, (4.3). The "γ" in (4.3) came from the $[f(r)]^\gamma$ in the integral (4.5), under the assumption that $f(r)$ behaves like r^{-1}. If $f(r)$ behaves like r^{s-2} instead, the asymptotic behavior of the decoherence curve near $a=0$ becomes

$$V(a) \cong V(0) - ka^{2-(2-s)\gamma}. \tag{6.2}$$

Of course, the constant k is also changed.

For $s=1$ (showers at their maximum), this reduces to (4.3), as it must. But now consider older showers for which

$$2-(2-s)\gamma > 1, \quad s > 2-\gamma^{-1}. \tag{6.3}$$

Then $V(a)$ will come in horizontally at $a=0$, rather than with a vertical tangent. Since we are talking about older showers, it is reasonable to use Cocconi's[17] result for γ; i.e., $\gamma \cong 1.5$. *We then classify a shower as "old" if* $s > 4/3$.

It may be worth while to point out that this classification involves not merely the properties of any one shower, but also their distribution-in-number. Unless we know something about the exponent γ, we do not know which showers we are to classify as "old" for our purposes.

It is useful to put a few numbers in here, just to get an idea of the orders of magnitude involved. We shall make two different assumptions:

(1) The shower is initiated by an electron at the top of the atmosphere.

(2) The shower is initiated by a (secondary) electron four radiation units (144 g/cm^2) below the top of the atmosphere. We choose this number because the absorption length of the N radiation[18] in the atmosphere is of this order of magnitude.

We can determine which shower has $s=1.33$ under these two assumptions, by using formula (2.104) of reference 5. We then estimate what regions of the decoherence curve will be affected seriously by these showers. A shower containing only a few particles cannot affect the counting rate of two ionization chambers if they are placed far enough apart. Indeed, the largest possible half-separation $a_{\max}$ is given by

$$Nf(a_{\max}) = \rho \tag{6.4}$$

where ρ is the chamber bias. This corresponds to the case where the shower hits just midway between the chambers.

Unfortunately, we cannot use (6.1) here for $f(r)$ since the constant in front is important. We therefore have to fall back upon the Molière distribution. The results are given in Table II. The first column is the distance over which the shower develops, the second is the energy of the initiating electron for $s=1.33$, the third the number of particles at the place of observation. The fourth and fifth columns give the maximum chamber separations over which the shower can be effective.

These numbers are disconcertingly small. On Fig. 5, the experimental results start deviating from the theoretical curve at distances of the order of one meter, probably even two meters if we want to get a smooth curve.

Of course, the Molière function, being too large at the origin, will falsify the numbers in Table II, but the schematic Fig. 6 illustrates that we are likely to overestimate $a_{\max}$ in this way. For large enough values of (ρ/N), the true intersection point P gives a lower value of $a_{\max}$ than the intersection point Q with the Molière function. Since the values of r involved here are extremely small, we are very probably in that region of ρ/N.

It is not possible to say at this time whether a correct calculation will improve the situation or whether the qualitative discrepancy in Fig. 5 will remain. The estimates given here make us inclined to believe that under either one of the two assumptions about the generation of the shower presented so far, a mathematically correct application of shower theory will not yield agreement between theory and experiment. (We emphasize that the disagreement we are talking about here is in the opposite direction from the one sometimes referred to in the literature.[19,9] The theoretical curve rises too steeply near the origin.)

This leads us to believe that we may have been underestimating the age of the showers which are responsible for our counting rates. Suppose that air showers are not produced in an event involving only one initiating electron (or photon), but rather in an event of high multiplicity ν, involving elec-

TABLE II. (6.1) Maximum chamber separations over which an "old" shower can produce a count.

$t-t_0$ (radiation units)	E_0 (ev)	N	$(a_{\max}/r_1)$	Chamber separation at Echo Lake (meters)
16	3.23×10^{12}	1.42×10^{3}	1.5×10^{-4}	0.03
20	3.70×10^{13}	1.18×10^{4}	10^{-3}	0.20

[18] B. Rossi, Rev. Mod. Phys. **20**, 537 (1948).

[19] L. Janossy, *Cosmic Rays* (Oxford University Press, London, 1948), Chapter VIII.

trons (or photons) originating in the same place and in roughly the same direction. In that case, the value of N in Table II have to be multiplied by ν. If ν is of order 10^2 to 10^3, we are right in the region of N which contributes most to the counting rate for moderate separations. In that case, the flattening off of the decoherence curve becomes eminently understandable.

There is another effect of multiple production tending to make the decoherence curve come in with zero slope at $r=0$. This is the granular structure of such a many-core shower. After all, the initiating particles do not all have exactly the same directions. Whereas the angles are small, the distance to the place of observation is large.

It is not certain just how one should estimate the angles involved in such a multiple-production process. We shall assume that a primary (presumably a proton) creates a large number ν of short-lived mesons, each of which then generates a shower. In analogy with electron pair creation,[5] we shall assume that the mesons get sidewise momenta of order μc, where μ is the meson mass. (We shall assume $\mu c^2=160$ Mev; i.e., the mass of a π-meson.) The angle between the meson and the primary is then of order $\mu c^2/E$ where E is the energy of the meson. If the total energy of each meson goes into the shower, we can relate E to the total number of particles N at the place of observation in the following way. The number of particles in each component shower of this many-core air shower is N/ν. This determines E through

$$N/\nu=\Pi(E, 0, t), \tag{6.5}$$

where $\Pi(E, 0, t)$ is given by formula (2.104), reference 5 We shall assume $t=16$ radiation units; i.e., the showers are created 4 radiation units (144 g/cm^2) below the top of the atmosphere.

The result of this estimate is shown in Fig. 7, in which we have drawn lines of constant (estimated) core-separation in the N-ν-plane.

The figure shows that showers of 10^5 particles have cores separated by distances of order 10 cm if $\nu=10$, of order 0.9 meter if $\nu=100$, of order 5 meters if $\nu=1000$. Williams observed a few events with his "arrangement A" in which there were about that number of particles in the shower, with an apparent unique core over distances of one meter. A multiplicity of order 20–40 would not contradict this result, yet it would already give an appreciable structure to the shower core. True, the equipment used in the experiments could not resolve such a granular structure explicitly. But the structure would appear through the substitution of a much flatter "effective" structure function instead of our $f(r)$. This helps to explain the flattening off of the decoherence curve.

We want to emphasize that these estimates are very rough and are based upon an assumption (sidewise momentum of order μc) which may well be completely wrong. In addition, our estimate of the multiplicity ν depends upon the assumed effective height of shower-production, becoming smaller as this height increases. We have also indicated in Fig. 7 the curve of multiplicity *vs.* number of particles predicted by the Oppenheimer-Lewis theory.[4] These multiplicities are somewhat high, if we use our estimate of the angles involved, since showers of 10^5 particles contribute appreciably to the counting rate near zero separation, and these showers would have core-separations of order 1 meter.

We remark that the Oppenheimer-Lewis theory itself would give much larger angles than we have estimated, but this has been disproven experimentally.[7] It appears to the author that it is not justifiable to dismiss the possibility of high multiplicity, but small angles, on the grounds of theoretical arguments which involve rather doubtful meson field theories.

Since we do not accept the Oppenheimer-Lewis estimate of the angles involved in the production process, there is no obvious reason to accept their prediction for the multiplicity of production. Indeed, it is likely that the Oppenheimer-Lewis multiplicity provides an upper limit for what we can expect. A somewhat lower multiplicity, with ordinary relativistic angles of production, seems consistent with the data analyzed here.

In conclusion, the following points emerge from our analysis:

(1) *Contrary to statements found in the literature, ordinary shower theory leads one to expect a rise in the decoherence curve at distances much less than the characteristic lateral distance* r_1.

(2) *The theoretical decoherence curve calculated under the assumption of a constant structure function rises more sharply near the origin that the experi-*

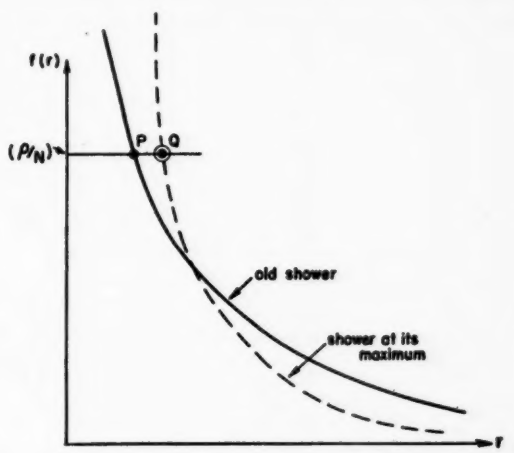

FIG. 6. The Molière structure function is likely to overestimate the area of influence of an old shower.

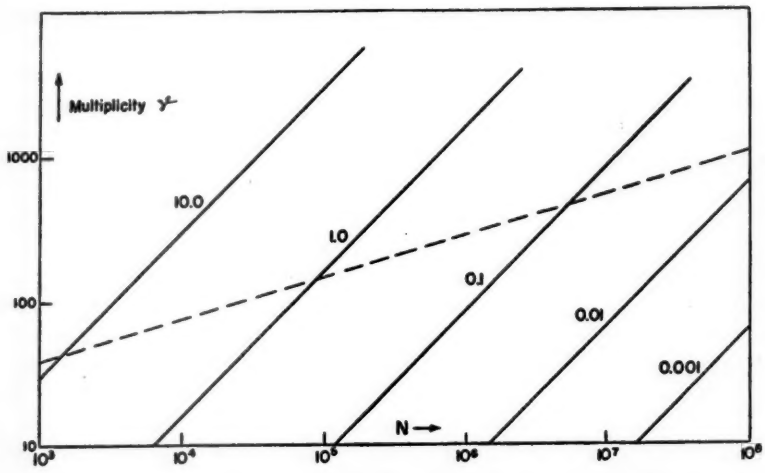

FIG. 7. Estimate of the granular structure of many-cored showers. Ordinate: Multiplicity of production ν. Abscissa: Total number of particles in the shower at the place of observation. The straight lines are lines of constant separation between cores, given in meters. The dashed curve is the multiplicity-number relation predicted by the Oppenheimer-Lewis theory. (See reference 4.)

mental points. This indicates that the effective structure function is less peaked than the Molière function.

(3) *While the age-dependence of the structure function tends to lessen this discrepancy, the quantitative estimates of Section 6 make it appear doubtful that one can get agreement between theory and experiment without assuming a rather high multiplicity of the event which starts the shower.*

ACKNOWLEDGMENTS

It is a pleasure to acknowledge many helpful discussions on this subject with Professor B. Rossi and R. W. Williams of M.I.T., H. A. Bethe of Cornell University, and L. W. Nordheim of Duke University.

APPENDIX A

The Correction for the Finite Dimensions of the Chambers

We recall that the chambers are biased so that they record only if the ionization exceeds a certain minimum amount. The chambers used were of cylindrical shape, about half a meter long and ten centimeters in diameter. We shall therefore neglect the width of the chambers, but not their length. A minimum value of the ionization can then be interpreted as a minimum number of particles which have to pass through the chamber before it records.

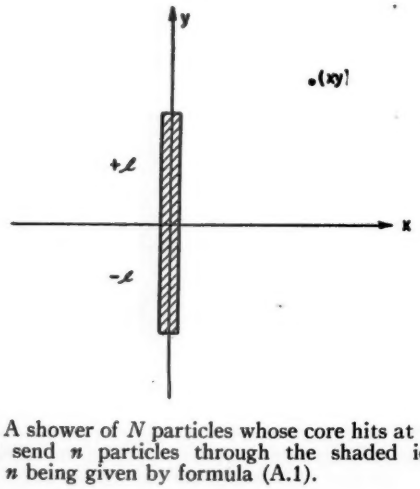

FIG. 8. A shower of N particles whose core hits at the point (xy) will send n particles through the shaded ionization chamber, n being given by formula (A.1).

We shall determine $W(\rho, a)$ for $a=0$, i.e., for a single chamber. Consider Fig. 8. If the core of a shower of N particles with a density function $\rho(r)=Nf(r)$ passes through the point (xy), the number of particles n passing through the chamber is

$$n=\int_{\text{Area of Chamber}}\int dx'dy'\rho[((x-x')^2+(y-y')^2)^{\frac{1}{2}}]. \qquad (A.1)$$

If we neglect the width of the chamber, the double integral becomes a single integral over y' between $-l$ and l with x' set equal to zero and $\int dx'$ replaced by T, the width of the chamber. Assuming a constant structure function,

$$\rho(r)=Nf(r),$$

(A.1) becomes

$$n=Ng(xy) \qquad (A.2)$$

where

$$g(xy)=T\int_{-l}^{l} dy' f[(x^2+(y-y')^2)^{\frac{1}{2}}]. \qquad (A.3)$$

Let r_0 ($\sim 0.01 r_1$) be the largest value of r for which (4.4) is an adequate approximation for our purposes. If both $r \ll r_0$ and $l \ll r_0$, we can replace $f(r)$ in (A.3) by the expression (4.4). The integral can then be evaluated explicitly, with the result

$$g(x, y) \cong (2lT)(C/r_1R)\cdots r \ll r_0 \text{ and } l \ll r_0 \qquad (A.4)$$

where the variable R is defined by

$$R^{-1} \equiv (2l)^{-1} \log\left(\frac{[x^2+(y-l)^2]^{\frac{1}{2}}-(y-l)}{[x^2+(y+l)^2]^{\frac{1}{2}}-(y+l)}\right). \qquad (A.5)$$

R is zero at $x=y=0$; for large values of x and y, R approaches $r \equiv (x^2+y^2)^{\frac{1}{2}}$.

For values of x and y much larger than l, the dimensions of the chamber can be neglected. In that case, formula (A.3) gives

$$g(xy) \cong (2lT)f(r), \quad r \gg l. \qquad (A.6)$$

We now observe that both (A.4) and (A.6) can be written as

$$g(xy) \cong (2lT)f(R). \qquad (A.7)$$

In practice the condition $l \ll r_0$ is satisfied, since $l \leqq 0.003 r_1$ for the chambers used. Equation (A.7) then holds for $R \ll r_0$ and for $R \gg l$. Since these two regions of validity overlap, it is evidently a good approximation to assume that (A.7) holds for all values of R.

Since $S(N)\cdot dx\cdot dy$ showers of more than N particles have cores which pass through the elementary area $dx\cdot dy$, per second, and since (A.2) implies that N must exceed $n/g(xy)$ in order that a count be recorded, we conclude that the

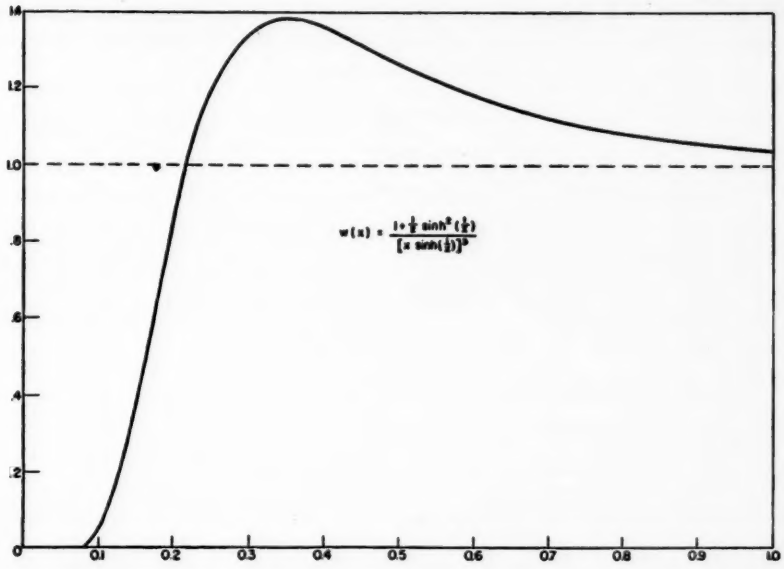

FIG. 9. Ordinate: Weight function $w(x)$ in formulas (A.11), (A.12). Abscissa: $x=R/l$.

counting rate $W(n, 0)$ of a single chamber is given by

$$W(n, 0)= \int\int S[n/g(xy]dxdy, \quad \text{(A.8)}$$

where the integral extends over the whole xy plane.

We now make the approximation (A.7) and introduce the notation

$$\rho \equiv n/2lT \quad \text{(A.9)}$$

for the average particle density through the chamber. We then get

$$W(\rho, 0) \cong \int_0^\infty S[\rho/f(R)]A(R)dR, \quad \text{(A.10)}$$

where $A(R)dR$ is the area in the xy plane enclosed between R and $R+dR$. A lengthy but elementary calculation gives the result

$$A(R)dR=w(R/l)2\pi RdR, \quad \text{(A.11)}$$

where the weight function w is given by

$$w(x)=[1+\tfrac{1}{2}\sinh^2(1/x)]\cdot[x\sinh(1/x)]^{-3}. \quad \text{(A.12)}$$

The weight function $w(x)$ is shown graphically in Fig. 9. We see that $w(x)\to 0$ as $x\to 0$. This cuts out the influence of the very small showers, as expected.

We proceed to calculate the correction ΔW to the counting rate for zero separation. We define

$$\Delta W=[W(\rho, 0)]_l-[W(\rho, 0)]_{l\to 0}. \quad \text{(A.13)}$$

We observe that we can obtain the limiting case of a point chamber from (A.10) and (A.11) by letting l go to zero (this is of course obvious from the start), in which case the weight function w becomes simply unity. We therefore have

$$\Delta W \cong \int_0^\infty S[\rho/f(r)][w(R/l)-1]2\pi RdR. \quad \text{(A.14)}$$

We remark that the integral extends from zero to infinity only formally. Practically, the factor $[w(R/l)-1]$ approaches zero for $R>l$ quite rapidly. Indeed, $w(R/l)=1+(7/120)(l/R)^4+\cdots$ for $R>l$. Hence, the main contribution to (A.14) comes from the region $R\lesssim\frac{3}{2}l$. For the chambers used $\frac{3}{2}l$ is about 0.40 meter, i.e., $4\times 10^{-3}r_1$ at Climax.

The asymptotic expression (4.4) for $f(r)$ is good out to r of order $10^{-2}r_1$. Hence, it is permissible to replace $f(r)$ by its asymptotic form (4.4) in the integral (A.14) for ΔW.

We again assume a power law for $S(N)$, i.e., $S(N)=\sigma N^{-\gamma}$. We then get

$$\Delta W=\rho^{-\gamma}\Delta V;$$

$$\Delta V \cong \sigma(C/r_1)^\gamma \int_0^\infty R^{-\gamma}[w(R/l)-1]2\pi RdR, \quad \text{(A.15)}$$

We can introduce $x=R/l$ as variable of integration, getting the *final result*

$$\Delta V \cong \sigma(C/r_1)^\gamma l^{2-\gamma} \int_0^\infty x^{-\gamma}[w(x)-1]2\pi xdx. \quad \text{(A.16)}$$

This formula for the correction has the advantage that it gives the dependence of ΔV upon r_1 and l explicitly. The dependence upon γ is not quite explicit, part of it being contained in the definite integral. The integral is a smooth function of γ, however. In Table III we give values of the integral for various values of γ. The integral is negative, indicating that the correction is in such a direction as to decrease the counting rate for a single chamber of finite size compared to a point chamber. This was, of course, to be expected.

APPENDIX B

The Counting Rate of the Triangle Arrangement

In order to check the Molière structure function experimentally, three of the four ionization chambers were placed

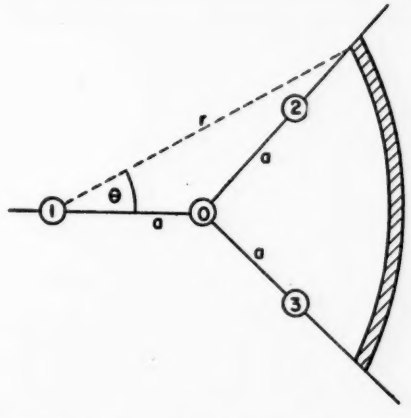

FIG. 10. A shower whose core passes through the shaded circular strip will be counted if it has sufficient density at the position of chamber 1.

TABLE III.

γ	$\int_0^\infty x^{-\gamma}[w(x)-1]2\pi x dx$
1.50	−2.08
1.60	−5.84
1.70	−10.42

at the corners of an equilateral triangle, with the fourth chamber in the center of the triangle.

We shall not discuss here the method used to test the validity of the Molière function. Suffice it to say that the Molière function agrees with experiment within the (rather large) experimental error, for the distances used (the side-length of the equilateral triangle was 12.2 meters).

We merely intend to derive the formula for the absolute counting rate of this arrangement. Consider Fig. 10. If all four chambers are biased to the same minimum density ρ, the showers whose core passes through the shaded circular strip will be counted if they have sufficient strength to set off chamber number one. This is true since chambers two, three, and four are nearer than chamber one for any point of the strip. The strip is defined by segments of circles centered at chamber number one, with radii between r and $r+dr$. The area of this strip is $2\theta r dr$, where θ is the angle indicated on the figure. The sine law of trigonometry gives the identity

$$r\sin((\pi/3)-\theta)=a\sin(2\pi/3),$$
$$\theta=(\pi/3)-\arcsin[(\sqrt{3}/2)(a/r)]. \quad \text{(B.1)}$$

If the core of a shower hits within the shaded area, it will be recorded provided its total number of particles N is big enough to give a sufficient density ρ at chamber one, a distance r away:

$$N \geqslant \rho/f(r)$$

The number of such showers per unit area per second is $S(N)=S[\rho/f(r)]$. We cover one-third of the plane by letting r vary from a to ∞. We therefore have for the absolute counting rate $W(\rho, a)$ of the triangle arrangement

$$W(\rho,a)=\int_a^\infty S[\rho/f(r)]\cdot\left[2\pi-6\arcsin\left(\frac{\sqrt{3}}{2}\frac{a}{r}\right)\right]rdr. \quad \text{(B.2)}$$

We again assume a power law for $S(N)$, $S(N)=\sigma N^{-\gamma}$; this gives

$$W(\rho,a)=\rho^{-\gamma}V(a),$$
$$V(a)=\sigma\int_a^\infty f^\gamma(r)\left[2\pi-6\arcsin\left(\frac{\sqrt{3}}{2}\frac{a}{r}\right)\right]rdr. \quad \text{(B.3)}$$

The integral has been evaluated numerically, for $\gamma=1.9$.

The observed counting rate was 47 counts in 325 hours, at a minimum density $\rho=616$ particles/m². If we assume a single power law for $S(N)$ with exponent $\gamma=1.9$ (this agrees with the density response curve at the distances involved; see Table I), we obtain the following result for the absolute number of showers per square meter per hour, containing more than N particles, at Climax, Colorado:

$$S(N)=8.4\times10^{-4}(N/10^6)^{-1.9}(\text{meter})^{-2}(\text{hour})^{-1}. \quad \text{(B.4)}$$

We have seen before (Section 5) that a single power law is not expected to be a good approximation to $S(N)$ for all values of N. The values of the exponents γ_{eff} at various distances (see Table I) make it appear reasonable to assume

$$S(N)=\begin{cases}\sigma_0 N^{-1.5} \text{ for } N<10^6,\\ \sigma_1 N^{-1.9} \text{ for } N>10^6,\end{cases} \quad \text{(B.5)}$$

where σ_0, σ_1 are adjusted so as to make $S(N)$ a continuous function. The subsequent analysis is exactly analogous to that of Section 5. The result is:

$$S(N)=8.4\times10^{-4}(N/10^6)^{-1.5}(\text{meter})^{-2}(\text{hour})^{-1},\ N<10^6$$
$$S(N)=8.4\times10^{-4}(N/10^6)^{-1.9}(\text{meter})^{-2}(\text{hour})^{-1},\ N>10^6. \quad \text{(B.6)}$$

The coefficient is the same in (B.4) and (B.6), indicating that the showers with less than 10^6 particles contribute a very small part (actually about 5 percent) of the total counting rate.

(B.6) is directly comparable with (5.8). We see that there is a discrepancy of slightly more than a factor of two. Since the experimental inaccuracies cannot account for such a large error, this discrepancy must be ascribed to the rough nature of the theory used here.

The discrepancy is probably due to two causes: (1) The Molière structure function is too spread out; the true structure function, being more concentrated, will lead to a decoherence curve falling off more rapidly with distance. Since the measurements with the triangle arrangement count showers at a larger effective distance this will improve the comparison between (B.6) and (5.8). The fact that the triangle arrangement was used to count showers with greater minimum particle densities will also work in the same direction. (2) It is rather likely that $S(N)$ of (B.6), does not vary rapidly enough for very large N. The effective exponent for very large N is likely to be considerably greater than 1.9. A qualitative argument shows that this effect will also improve the agreement between (B.6) and (5.8).

Whether these two effects are sufficient to remove the discrepancy altogether cannot be determined at this time. Without a knowledge of the true structure function, one cannot even make a sensible estimate.

Thermionic and Photoelectric Emission with Moderate Applied Electric Fields, Employing a Two-Step Potential Barrier*

THOMAS H. JACOBI
Physics Department, Saint Louis University, St. Louis, Missouri
(Received December 29, 1948)

The present paper presents a theoretical analysis of electron emission, both thermionic and photoelectric, with moderate applied electric fields, based on a two-step potential barrier, a shape not employed hitherto as far as can be determined. An expression is obtained for thermionic emission current density with applied electric field containing two arbitrary constants, V_1 and a, the height and width of the first step of the barrier. Comparison of this expression with the experimental results of Phipps and Seifert yields reasonable values for the two constants. An expression is obtained also for photoelectric emission employing the same barrier shape in which insertion of the same values of V_1 and a results in a periodic deviation of photo-current with applied electric field.

The present theoretical results for the photo-current *vs.* applied electric field are compared with those of Guth and Mullin.

THE present paper presents a theoretical analysis of electron emission, both thermionic and photoelectric, with moderate applied electric fields, based on a two-step potential barrier, a shape not employed hitherto as far as can be determined.

An early application of quantum mechanics to electron emission was made by Nordheim[1] who assumed for metals a single step rectangular surface potential barrier of height V_2, and obtained the following expression for J, the thermionic current density

$$J=AT^2\exp(-V_2-E_0/\theta)4(\theta/E_0)^{\frac{1}{2}}\times[(\pi)^{\frac{1}{2}}/2-2(\theta/E_0)^{\frac{1}{2}}-\cdots], \quad (1)$$

where A is the Richardson emission constant, 120.4 amp/cm² deg.²K; E_0 is the maximum energy of an electron within the metal at 0°K; and θ is written for kT. The factor,

$$4(\theta/E_0)^{\frac{1}{2}}[(\pi)^{\frac{1}{2}}/2-2(\theta/E_0)^{\frac{1}{2}}-\cdots],$$

can be considered as an average electron transmission coefficient, and is considerably lower than the value of 0.5 obtained experimentally.

Phipps[2,3] with various other workers, in a series of experimental investigations of Schottky emission at elevated temperatures found a periodic deviation of thermionic emission current density with applied electric field about the straight line predicted by simple Schottky theory. Mott-Smith[4] suggested that the observed effect might be due to partial reflection of electrons incident on the surface potential barrier. Guth and Mullin[5] obtained theoretical results in good agreement with Phipps' work, assuming a barrier of near parabolic shape. They extended their work to include photoelectric emission and predicted a periodic deviation in photo-current as shown by Fig. 1.

Some preliminary experiments here[6] have indicated a variation of photo-current about a straight Schottky line, and this work is being continued for various geometries. In connection with this experimental research, a somewhat different approach has been made to the theory. Because of the resulting mathematical simplicity, a two-step rectangular potential barrier, shown by Fig. 2, was

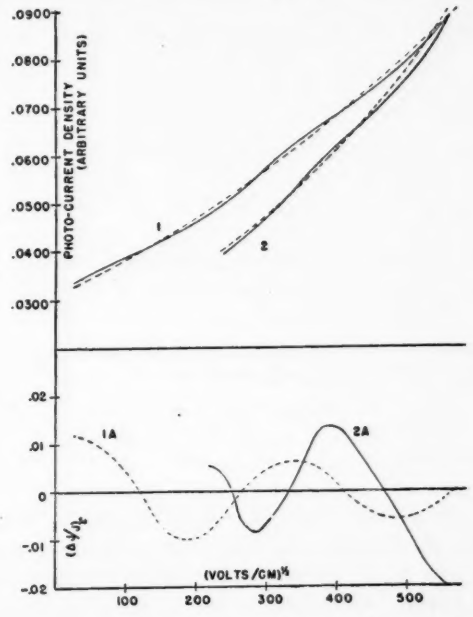

FIG. 1. Comparison of Eq. (7) with results of Guth-Mullin Theory. Curve 1 represents the total photo-current density compared with the non-periodic part of the photo-current density *vs.* (applied electric field)$^{\frac{1}{2}}$ in each case (from Eq. (7)); curve 1*A* is drawn to magnify the periodic nature of the variation. Curves 2 and 2*A* are the corresponding results obtained by Guth and Mullin.

* The research reported in this paper was supported by the ONR, Electronics Branch, under Contract N7 onr-320, Project No. NR 072 531.

[1] L. Nordheim, Zeits. f. Physik **46**, 833 (1927–28).
[2] T. E. Phipps and R. L. E. Seifert, Phys. Rev. **56**, 652 (1939).
[3] T. E. Phipps and D. Turnbull, Phys. Rev. **56**, 663 (1939).
[4] H. M. Mott-Smith, Phys. Rev. **56**, 668 (1939).
[5] E. Guth and C. J. Mullin, Phys. Rev. **59**, 575, 897 (1941).
[6] V. P. Jacobsmeyer, S.J., Phys. Rev. **69**, 50 (1946).

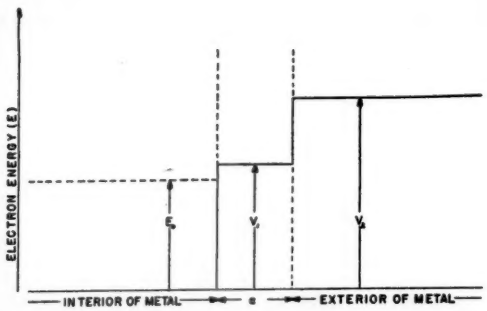

FIG. 2. Shape of potential barrier assumed. E_0 is the maximum energy of an electron at 0°K.

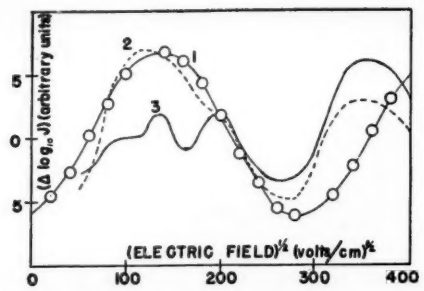

FIG. 3. Periodic variation of thermionic emission current density *vs.* (applied electric field)$^{\frac{1}{2}}$. Curve 1 is that predicted by a two-step potential barrier for tungsten with V_1 and a set equal to E_0 and 2.27×10^{-6} cm, respectively. Curves 2 and 3 were obtained by Phipps and Seifert for two samples of tungsten at temperatures of 1600° to 1700°K.

assumed. Such a shape, while better than the single-step barrier of Nordheim, is admittedly a coarser approximation to reality than the parabolic or Guth-Mullin type. For this two-step barrier, the following expression is found for the thermionic emission current density J_ε with applied electric field, using the approximation that all emission is due to electrons whose energy is within 1 electron volt of the barrier height, and dropping terms whose magnitude is less than one percent of the total.

$$J_\varepsilon = AT^2\left[\exp\frac{(E_0-V)}{\theta}\right]\frac{4(\pi V\theta)^{\frac{1}{2}}}{2V-V_1}\times\left\{\left(1+\frac{3\theta}{4V}-\frac{3\theta}{2V-V_1}\right)-\frac{V_1}{2V-V_1}\left(1+\frac{2ma^2\theta^2}{\hbar^2(V-V_1)}\right)^{-\frac{1}{2}}\times\cos\left[\frac{3\phi}{2}+\frac{2a}{\hbar}(2m(V-V_1))^{\frac{1}{2}}\right]\right\}, \quad (2)$$

in which

$$\phi=\tan^{-1}(a\theta/\hbar(V-V_1))(2m(V-V_1))^{\frac{1}{2}}, \quad (3)$$

$$V=V_2-\varepsilon^{\frac{1}{2}}e^{\frac{1}{2}}, \quad (4)$$

where ε is the electric field at the emitting surface and V_1, V_2, E_0, and a are defined by Fig. 2. The other symbols have their customary meaning.

So far, V_1 and a are arbitrary constants. However, it is possible to make some simple comparison of the theory with an experiment which gives information about one or the other of these two constants. If V_1 is arbitrarily put equal to E_0, a of Eqs. (2) and (3) can be found by trial from a good fit of Eq. (2) with the experimental results of Seifert and Phipps[2] for thermionic current density *vs.* applied electric field strength. The fit yielding $a=2.27\times10^{-6}$ cm is exhibited by Fig. 3.

With the constants V_1 and a adjusted by using experimental thermionic emission data, it is possible to derive the photoelectric analog of Eq. (2). This is accomplished by assuming that all electrons have equal probability of absorbing a photon and having their energy increased by $h\nu$. If the fraction of the electrons whose energy is thus increased is denoted by k, the electron flux can be written as[7]

$$\text{flux}=K(4\pi m\theta/h^3)\int_{V_2}^{\infty}\times\ln(1+\exp[(E_0+h\nu-E)/\theta])TdE, \quad (5)$$

where T, the transmission coefficient for the two-step barrier, is given by

$$T=\frac{8(E-V_2)^{\frac{1}{2}}E^{\frac{1}{2}}(E-V_1)}{(E-V_1)(2E-V_1)+V_1(V_2-V_1)\cos(2a/\hbar)2m(E-V_1)}. \quad (6)$$

Upon integration of Eq. (5), again dropping terms of magnitude less than one percent, the following is obtained for the photo-current density with applied electric field

$$J_\varepsilon=K_0[4/15(E_0+h\nu-V)^{5/2}-2/5K_2(E_0+h\nu-V)^{7/2}+K_1\cos b(d)^{\frac{1}{2}}\frac{2\pi^{\frac{1}{2}}d^{\frac{1}{2}}}{b^{\frac{1}{2}}}S\left(\frac{b(E_0+h\nu-V)}{(d)^{\frac{1}{2}}}\right)^{\frac{1}{2}}+K_1\sin b(d)^{\frac{1}{2}}\frac{2\pi^{\frac{1}{2}}d^{\frac{1}{2}}}{b^{\frac{1}{2}}}C\left(\frac{b(E_0+h\nu-V)}{d^{\frac{1}{2}}}\right)^{\frac{1}{2}} \quad (7)$$

where

$$K_0=K(4\pi me/h^3),$$
$$K_1=(E_0+h\nu-V)(V_1/2V-V_1),$$
$$K_2=[V_1+V/2V(V-V_1)],$$
$$b=(2a/\hbar)(2m)^{\frac{1}{2}},$$
$$d=V-V_1;$$

and S and C are used to indicate Fresnell integrals,

[7] A. H. Wilson, *The Theory of Metals* (Cambridge University Press, London, 1936), p. 251.

defined by

$$S_x=\int_0^x \sin(\pi/2)u^2du \quad \text{and} \quad C_x=\int_0^x \cos(\pi/2)u^2du$$

which are available in tabulated form.[8] Equation (7) is plotted on Fig. 1 for comparison with the Guth and Mullin theory. It is seen that the two theories predict somewhat different results, but that both theories yield a variation of the emission current about the straight line obtained in simple Schottky theory. It is hoped that experimental work in progress here will soon permit a test of the two theories compared in Fig. 3.

The author wishes to thank Dr. Roy Thomas who suggested this problem and aided materially in its completion and Professor A. H. Weber for frequent discussions and continued interest in the progress of the work.

[8] Jahnke and Emde, *Tables of Functions with Formulae and Curves* (Dover Publications, New York, 1948), pp. 34 and 35.

PHYSICAL REVIEW VOLUME 75, NUMBER 10 MAY 15, 1949

What Led to the Founding of the American Physical Society*

FREDERICK BEDELL**
Pasadena, California
(Received January 10, 1949)

ON a bright day in May, 1899, a group of physicists met at Columbia University to consider the forming of a physical society. I well remember the occasion. After a welcome from Professor M. I. Pupin, and a discussion of aims and policies, it was resolved that "a physical society be formally organized." A committee was appointed to draft a constitution, officers were elected, and the American Physical Society was founded. It was as simple as that! But *why*, in the gay nineties, was the Society founded? Difficult then was it to have foreseen the founding of the Society and its fifty years of continuous development of which we are now so proud. These I will not attempt to recite, but would call attention to early incidents within my own memory, some not of record, that may throw light upon its founding.

First let us look back to the year 1876, and later to the eighteen nineties, gay indeed for science as well as for society.

It was in 1876 that Henry A. Rowland, destined later to become the first president of our Society, was appointed professor of physics at the newly started Johns Hopkins University. Although physics at that time was highly developed in Europe, it was scarcely known in this country as a separate science, as it slowly emerged from the broader field of natural philosophy. Little known was the work of Rowland, so few were there to recognize its value.

Abroad, Rowland's work had been immediately appreciated by Clerk Maxwell who at once saw to its publication in England. It is reported that when the managers of Johns Hopkins University asked advice in Europe as to whom they should make their professor of physics, he was pointed out in all quarters as the best man for the place. In that position, Rowland was a leader in the development of physics and of graduate research in America. "Rowland's law of the magnetic circuit," corresponding to Ohm's law of the electric circuit, stood high in my student memories.

It was also in the year 1876 that the great Centennial Exposition was held in Philadelphia on the one hundredth anniversary of American independence. Long known as "The Centennial," it marked the beginning of what proved to be a great development of science in America, the forerunner of events that led to the formation of the American Physical Society. Even as a small boy, I sensed the Centennial's importance. Going to the Centennial and living in a hotel for the first time was itself a great adventure. Eagerly each day I started out afresh with my father to see more of the exposition —always more. There was much, of course, that I could not understand, but this very fact proved stimulating. Some of my memories of the exhibits stand clear. These, and others less clear until refreshed by later knowledge, well justify my taking the year 1876 as the datum line from which to measure the successive advances in the years that followed.

I was entranced with Machinery Hall, dominated by the huge Corliss engine with its sixteen hundred horsepower, a marvel of its time, from which I could scarcely draw away. There on exhibit were the first incandescent lamp by Thomas A. Edison, the first telephone by Alexander Graham Bell, and, in operation, the first dynamo made in America, made the preceding year by Professor William A.

* Presented by invitation at a Meeting of the American Physical Society at Berkeley, California, February 4, 1949.
** Professor of Physics, Emeritus, Cornell University.

Anthony with some of his associates at Cornell University, exhibits that typified the future of physics in industry and in education in which the Physical Society was destined to play its part.

Little did I know that in coming years I would have associations with Edison, Bell, and Anthony: with Edison, at his laboratory verifying with A. E. Kennelly the possibility of operating a 3-wire system from the windings of a single transformer, now so simple; with Bell, sitting beside him in New York and listening in with head phones as he first telephoned across the continent to Professor H. J. Ryan in California; and with Anthony with whom I had many close associations, using equipment which he himself had devised or built.

It is to Edison and Bell that credit is due for the place now held by physics research in industry, as witnessed by the great laboratories that bear their names. What a development from the early days when Edison was struggling with his first stock ticker and Bell started his research program with one assistant, Mr. Watson, on half time! What a difference between then and now, when organized research in industry is a recognized necessity!

Anthony was a leader in the development of research in technical education, combining manual skill with theory. The dynamo made by him saw fifty years of service before its retirement as a museum piece. He was a leader in standardization, constructing from necessity his own standards, and many were the instruments sent to him for standardization. Noteworthy was the "Great Tangent Galvanometer," with precision coils one meter in diameter, built by him and housed on the Cornell campus in the special-built "copper house," away from any magnetic disturbance. This I used long in the nineties. There was a growing need for a bureau of standards. This came later through the efforts of Professor S. W. Stratton. One of the first acts of the Physical Society after its founding was to send a memorial to Congress advocating its establishment.

Long after the close of the Centennial, it continued to send a reverberating thrill through the population. On meeting a friend one was asked: "What did you see at the Centennial?" or, "Did you go to the Centennial?" A distinction was at once made between the "hads" and the "had nots." Direct results during the next decade were the introduction of the trolley car and of electric lights. Gas lights, and the picturesque lamp-lighter carrying his ladder as he turned lights on and off, were disappearing from the streets.

In industry here and there, small direct current motors were finding a place, but to these there were two limitations. The direct current commutator was a source of trouble, and the low voltage limited the range of economic operation of direct current motors.

Within a decade, however, both of these limitations had been met: first, by Nikola Tesla, who, with his alternating current induction motor got rid of the commutator entirely; and second, by William Stanley, who, with his alternating current transformers operating in parallel from a high potential (500-volt) line, opened the way for the economical transmission of power at higher voltages and to greater distances.[1] Without these developments, how dwarfed would be our modern civilization!

Aside from their inventions, both Tesla and Stanley had marked influence on the times through their personalities, Tesla highly imaginative, Stanley practical. I recall a Sunday with Tesla at the house of a friend when for hours he would scarcely get down to earth, and a day with Stanley at Pittsfield, Massachusetts, discussing practical matters regarding a new type of condenser he was sending me for a test.

Gay, indeed, were the following years in the early nineties with their rapid developments in science and technology. The increasing amount of fundamental research at the universities, with increase of staff and equipment, was stimulating, and there arose a need for journals in specialized fields. The need for a journal devoted entirely to physics was early seen by Professor Edward L. Nichols, who, in 1893, with the support of Cornell University, founded the Physical Review. Professor Ernest Merritt was closely associated with Professor Nichols in its planning. Aside from the publication of the Review, the varied activities of Professors Nichols and Merritt had marked influence on events that led to the Society's founding. Before the first issue of the Review had left the press, I received an appointment as associate editor, when my stay at Cornell University was assured. The Physical Review was thus conducted by a board of three editors until its transfer to the Society twenty years later. Then for ten years more, under the Society's control, I served as its managing editor.

Of great significance in the summer of 1893, was the International Electrical Congress, held in

[1] Using six transformers connected to his 500-volt line, Stanley in 1885–6 supplied power for the operation of 150 fifty-volt lamps in Great Barrington at a distance of 4000 feet. It is interesting to note the objections then raised to the introduction of such a system, a system which is the basis of our present practice. It had been maintained that such parallel operation from a constant potential line was not practicable and that a separate line would be needed for each transformer. The patent office had once held it impossible to take more current from the secondary of a transformer than was put into the primary! Distribution by a high potential 500-volt power circuit was considered a fire hazard and danger to life, and, as alternating current was held to be more deadly than direct, it is reported that a bill was introduced (but not passed) in the Virginia legislature to limit alternating current distribution to 200 volts.

Chicago. On looking over the Proceedings of the Congress and noting the names of the eminent scientists from all over the world who participated in it, one might well believe it to be an International Congress of Physics, or a congress sponsored by the American Physical Society—had such a society been then in existence,—or, perhaps, to be a preview of a meeting of the Society yet to come.

The congress was truly international, the following official delegates from abroad taking part in its proceedings:

England
Sir Wm. H. Preece
Professor W. E. Ayrton
Professor S. P. Thompson
Alexander Siemens

Mexico
Senior Don A. W. Chavez

Germany
Dr. H. von Helmholtz
Dr. Otto Lummer

Italy
Professor Galileo Ferraris

Sweden
M. Wennman

Switzerland
Dr. A. Palaz
M. Reve Thury

France
Professor E. Mascart
Professor E. Hospitalier
M. De la Touanne
Dr. S. Leduc
Professor T. Violle

Among the participants in the congress were Anthony, Edison, and Tesla, whose earlier influences have already been noted. The demonstration of the famous Tesla Oscillator, given before the congress, might well have been given before a congress of physicists.

It is interesting to note that among the officers active in organizing the congress were Rowland, Nichols, and Webster, all so active later in organizing the Physical Society. Rowland and Nichols were on the program committee of the congress; Rowland was President and Nichols Secretary of the official Chamber of Delegates, and Webster, chairman of the Pure Theory Section. It was at this congress that I first became acquainted with Rowland and Webster, as we presented papers of common interest. This was the start of our life-long friendships.

As the nineties rolled on, the need in America for specialized societies in various fields was becoming more and more obvious. In the American Association for the Advancement of Science, while I was serving as Secretary of the Council and as General Secretary of the Association, the question kept arising as to what connection there might be between these specialized societies and the association. There seemed to be no general solution. I can recall no particular mention of physics in this connection. In private conversation, however, the desire for such a society was frequently expressed.

During these same years, I had an opportunity to view the scene from the other side of the Atlantic, while participating in meetings of the British Association for the Advancement of Science and the Physical Society of London, where similar questions were arising. A strong interest was shown regarding the coming developments of science in America and the possible part that the British societies might take therein. There was informal discussion for at least two years as to whether the Physical Society of London might have an American section, or a foreign secretary, but seemingly, the matter was dropped. Viewed from either side of the Atlantic, there seemed to be a need for some society for physicists in America. There were few laboratories equipped for research, either in the universities or elsewhere. The number of physicists was small and their facilities were meager, so there was question as to when, and in what way, this need could best be met.

To find an answer to this question, Professor Arthur G. Webster took vigorous action, and, as chairman of a representative committee, sent out a call for the meeting already referred to, held at Columbia University on May 20, 1899. The answer was *then* and *there* and the Society for which the need had long been growing, now had its being.

The officers elected at that first meeting of the Society, and the members attending, were as follows:

President	Henry A. Rowland
Vice President	Albert A. Michelson
Secretary	Ernest Merritt
Treasurer	William A. Hallock

Elected members of the Council:

Joseph S. Ames	Edward L. Nichols
Henry S. Carhart	Benjamin O. Peirce
William F. Magie	Michael I. Pupin

Arthur G. Webster

Other founding members:

Cleveland Abbe	George A. Hoadley
William C. Andrews	Marcia A. Keith
Wilder D. Bancroft	Arthur L. Kimball
Carl Barus	A. Stanley Mackenzie
Frederick E. Beach	Howard McClenahan
Frederick Bedell	Herschel C. Parker
Henry A. Bumsted	John S. Shearer
LeRoy C. Cooley	Allison W. Slocum
Morris B. Crawford	Isabelle Stone
Bergen Davis	Elihu Thomson
William C. Day	Charles C. Trowbridge
Thomas W. Edmondson	Franklin L. Tufts
Charles S. Hastings	Frank A. Waterman
Daniel W. Herring	

The second meeting of the Society, held October 28, 1899, was opened by the Presidential address of Professor Henry A. Rowland—"The Highest Aim of the Physicist." This was followed by the adoption of a constitution and the presentation of papers by Rowland, Pupin, and Webster. Thus speedily was the Society on its way.

Professor Rowland's address was most inspiring. I remember the thrill it gave me as he pointed out, with classic illustrations, that there is no such thing as absolute truth and that every theory or law is in its proper compartment, indicating the probability of its truth. The address is one that should be read and re-read by every member of the Society. At this fiftieth anniversary, it might well be reprinted[2] in full to make it accessible; no abstract would be adequate. As we left the meeting together, Rowland talked about the future of the Society and of physics, continuing at the station as we waited for our respective trains. Rowland took active interest in the meetings of the Society until his early death in 1901.

There were fifty-nine members of the Society by December, 1899. Although the number of members rapidly doubled, and redoubled in the following three years to 144 and in six years to 282, this total membership was woefully small, small indeed compared with the present membership of about eight thousand.

A very active part was taken by Professor Merritt not only in the founding of the Physical Society, but also in its successful continuance during its early years when, as secretary, he carried much of the load of its operation. Upon him fell the immediate task of arranging a program for four meetings a year, not so easy with so small a membership. Sometimes a telegram from Merritt was the first intimation a member received that he was on the program! Despite these difficulties, he arranged for the presentation of some excellent papers, as witnessed by the early issues of the Bulletin of the American Physical Society in which they appeared. The task of issuing the Bulletin, published quarterly, fell to the secretary. Its publication in its original form was discontinued after nine issues.

The relations between the Physical Review and the Physical Society were very cordial and for some years there was an arrangement whereby members of the Society received the Review at a reduced price. Merritt, who was active in the founding of the Review and of the Society, now had a dual roll as editor of one and secretary of the other. He had the interests of the two at heart and was continually striving for their betterment and dreamed of the time their union might be effected. However, he realized full well that while the Review was running with a deficit and the Society was still weak, such a union might spell disaster.

Later, as the Review and the Society grew stronger, Merritt saw his dream come true, and a proposal from the editors of the Review that its full control be transferred to the Society was finally approved. This became effective January 1, 1913. Thus, the twenty years of the First Series of the Physical Review, under the control of its three editors, was ended. Then, under the Society's control, began the Second Series of the Review, and for another ten years I had the pleasure of continuing on as its managing editor. A detailed account of the transfer may be found in the first issue of the Second Series. The long and noteworthy service of Professor Merritt is unique. As secretary of the society during its critical years, and then as its president and as councillor, he served continuously as an officer of the Society for over forty-nine years, with the Society's interest ever in mind. Prone to self-effacement, he never sought a selfish end, as I can vouch for after years of closest contact.

The Society is indebted, too, to Columbia University, not only for the warm welcome extended to it by genial Professor Pupin at its first meeting, but also for the hospitality that has been extended to it for fifty years by the members of the University's physics department. I would like to add my own personal appreciation of the valued service of the treasurer and the secretary of the Society now in office there. I trust that a full history of the Society since its founding may be prepared by those who have the information close at hand.

In illustrating the growing need for the Physical Society, I have reviewed some events preceding its founding that, by chance, came within my own range of vision. Other events might be added without materially changing the picture. I was fortunate in having known so long and so well those who played the major parts in the founding and in the events that preceded it. Happy am I to have witnessed not only the launching of the Physical Society but also the fifty years of its continuous development.

[2] Rowland's address was printed in an early issue of the Bulletin of the Society of which few copies are in existence.

Letters to the Editor

PUBLICATION of brief reports of important discoveries in physics may be secured by addressing them to this department. The closing date for this department is five weeks prior to the date of issue. No proof will be sent to the authors. The Board of Editors does not hold itself responsible for the opinions expressed by the correspondents. Communications should not exceed 600 words in length.

The Polarization of Starlight by Interstellar Dust Particles in a Galactic Magnetic Field

LEVERETT DAVIS, JR.
California Institute of Technology, Pasadena, California
AND
JESSE L. GREENSTEIN
Mount Wilson and Palomar Observatories, California
March 24, 1949

IN important recent communications Hall[1] and Hiltner[2] have reported that the light of distant stars shows detectable polarization with the electric vector in the plane of the galaxy. The light of these stars has been considerably dimmed and reddened in its passage through the dust which occurs near the galactic plane. Present evidence indicates that the polarization is not a property of the star but is produced while the light is traversing extensive regions of interstellar space. We must include the effect of matter in space since it is improbable that anisotropic galactic gravitational, electric, or magnetic fields could produce polarization. We wish to consider whether or not it is possible for non-spherical dust grains to produce the observed effects by preferentially weakening the transmitted light whose plane of vibration is parallel to the galactic magnetic field.

Four main points are involved in this explanation. (1) Interstellar space contains non-spherical dust grains. (2) There exists a general galactic magnetic field whose lines of force are perpendicular to the galactic plane in our part of the galaxy. (3) There is an appreciable tendency for the long axes of the dust grains to be oriented parallel to lines of force. (4) Light transmitted through a cloud of such oriented grains will be polarized. There is little doubt about the first and last of these assumptions. The second is a not unreasonable assumption which is a prominent feature of current speculation on the origin of cosmic rays; it would be greatly strengthened if it provides an explanation of the polarization. The assumption that the grains could be oriented now requires examination.

Because of collisions with interstellar hydrogen gas, which has a density of the order of 1 atom/cm^3 and a kinetic temperature of 10,000°K, the dust grains would be expected to attain the equipartition energy of about 10^{-12} erg for each of the six translational and rotational degrees of freedom in about 10^4 years (a short time on the galactic time scale). Taking 10^{-6} cm as the average radius of a grain and unity as its density, it follows that if nothing hinders rotation, the grains must have an angular velocity of the order of 10^9 radians/sec. in order to have this much rotational kinetic energy. The associated large centrifugal force should have important consequences in the theory of the formation of the dust grains from the gaseous interstellar medium. If the long axes of an appreciable fraction of the grains are to be oriented parallel to the weak galactic magnetic field, **B**, it is necessary that some mechanism be found that will reduce this angular velocity to zero. The braking mechanism must produce an average deceleration of 10 radians/sec. since it must remove the 10^6 radians/sec. imparted by an average collision in 10^5 sec., the average time between collisions of a hydrogen atom with a dust particle.

Of those braking mechanisms which we have considered, hysteresis comes closest to being adequate. The effects of eddy currents, for example, are unimportant for small grains unless $B>1$ gauss. The internal temperature of the grains is near 3°K and is maintained by radiation; heating by collision is negligible. Their composition is now supposed to be mainly frozen H_2O, CH_4 and NH_3 with metallic impurities. From the stellar abundances we estimate that iron will form 2 percent of the grain. If it is supposed that the grain as a whole exhibits hysteresis, due probably to the presence of small ferromagnetic regions, it is plausible to assume that at each revolution it loses due to hysteresis a kinetic energy equal to $f(B^2/8\pi)$ times its volume, where f is a fraction depending on the properties of the grain. In this case the deceleration would be independent of angular velocity and would be equally effective for large and small grains. To produce enough deceleration requires $fB \geq 2\times10^{-5}$ gauss. It appears then that the acceptance of the hypothesis will depend on discovering some hysteresis mechanism having very large f or some other powerful decelerating mechanism.

If the rotation of the grains can be stopped, it is to be expected that the grains, whether diamagnetic or paramagnetic, would be oriented with their long dimension parallel to **B** and hence normal to the galactic plane. The theory developed by Gans[3] for the scattering and absorption of light by small ellipsoidal particles can now be applied. The induced electric moment is greatest when the plane of the electric vector in the incident light is parallel to the long axis of the grain. Hence such light is most strongly scattered and absorbed while light polarized so that the electric vector lies in the plane of the galaxy is more easily transmitted. Stars whose light loss has been observed to be 98 percent show that 5 percent polarization[1] with the electric vector in the plane of the galaxy. This is about what would be expected on the basis of the theory if the ratio of long to short axes of the grains is 4/3 and if 1/6 of them are oriented. The observed variation of the plane of polarization with the position of the star is also not unexpected if it depends on the average **B** in the region between the star and the earth.

Details of this investigation will be published in the Astrophysical Journal.

[1] J. S. Hall, Science **109**, 166 (1949).
[2] W. A. Hiltner, Science **109**, 165 (1949); Nature **163**, 283 (1949).
[3] R. Gans, Ann. d. Physik **37**, 881 (1912).

Erratum: Phenomenological Theory of Exchange Currents in Nuclei

[Phys. Rev. **74**, 433 (1948)]
R. G. SACHS
University of Wisconsin, Madison, Wisconsin

THE operators*

$$(\mathrm{div}\,\mathbf{r})^n \quad \text{and} \quad \mathbf{r}(\mathrm{div}\,\mathbf{r})^{n-1} \tag{1}$$

which appear in Eqs. (39) and (43) and in the equation for U following Eq. (46) should be replaced by

$$\Sigma_{\alpha,\beta,\cdots\gamma}\frac{\partial}{\partial r_\alpha}\frac{\partial}{\partial r_\beta}\cdots\frac{\partial}{\partial r_\gamma}r_\alpha r_\beta\cdots r_\gamma, \tag{2}$$

there being n factors, and by

$$\Sigma_{\alpha,\beta,\cdots\gamma}\frac{\partial}{\partial r_\alpha}\frac{\partial}{\partial r_\beta}\cdots\frac{\partial}{\partial r_\gamma}r_\alpha r_\beta\cdots r_\gamma \mathbf{r} \tag{3}$$

with $n-1$ factors. In the sums α, β, $\cdots\gamma$ each takes on the values 1, 2, 3 corresponding to the three components of the vector **r**. Equations (1) differ from Eqs. (2) and (3) in that the differential operators in (1) do not act on all of the factors **r**, as they should.

* The subscripts j, k, which denote the pair of particles referred to by r have been dropped for the sake of simplicity.

Measurement of the Internal Friction of Solids

R. KAMEL
Fouad 1. University, Cairo, Egypt
January 5, 1949

VERY limited work has been done on internal friction by transverse vibrations at frequencies in the sonic and infrasonic range. The only important investigation in this respect is perhaps that of Bennewitz and Rötger.[1]

In the present inquiry, the internal friction of a number of solids in the form of wires having diameters or thicknesses between 0.025 cm and 0.1 cm, and lengths between 1 cm and 15 cm, was determined from transverse vibrations at frequencies between 10 and 1000 c.p.s. Two methods were employed *viz.*, the decay of free lateral vibrations and the width of resonance.

In the case of insulating materials, damped vibrations were initiated by gentle blows. In the case of conducting materials, damped as well as maintained vibrations were excited by electrostatic means. Experiments were carried out at a pressure of 0.001 cm. of mercury, and the maximum amplitudes were of the order of 0.0005 cm. and were estimated from the depth of the modulations introduced by the vibrating end of the wire on an intense beam of light. A photoelectric cell circuit incorporating a low noise amplifier, a cathode-ray tube, and a beat-frequency oscillator were used to detect and measure the vibrations. Oscillograms of damped vibrations were obtained by a moving film.

Experiments show that, even at low air pressure, the presence of boundaries near the vibrating specimen increases the decrement appreciably unless the distance is greater than about 0.5 cm. The behavior of steel, zinc, lead, glass, brass, and tin as regards the existence of a frequency corresponding to a maximum value for the internal friction confirms Zener's theory,[2] which attributes the internal friction in polycrystalline solids primarily to thermal currents. The curves in Fig. 1 give

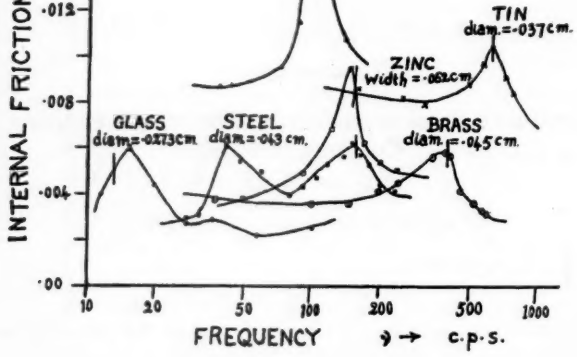

FIG. 1.

a summary of the results. The position of the calculated maxima are marked by vertical lines. Steel shows two maxima, the first of which is probably due to the contribution of ferromagnetism.

It has been observed that the transitional elements, nickel, palladium, and platinum, when subjected to forced vibrations, show two closely coupled maxima in the resonance curves from which it was not possible to calculate the internal friction.

[1] K. Bennewitz and H. Rötger, Physik. Zeits. **37**, 578 (1936).
[2] C. Zener, Phys. Rev. **52**, 230 (1937); Proc. Phys. Soc. London **52**, 152 (1940).

Absence of Photo-Conductivity in Tungstate Phosphors

CLIFFORD C. KLICK AND JAMES H. SCHULMAN
Naval Research Laboratory, Washington, D. C.
April 1, 1949

SCHEELITE ($CaWO_4$) has recently received considerable attention because of its efficiency in scintillation counting applications.[1] The tungstates are furthermore of general interest since they are among the comparatively few "pure" materials that give efficient room-temperature luminescence.[2] The similarity of the emission spectra of various tungstates strongly suggests that the tungstate ion is the luminescent center, and recent work by Kröger[3] gives added support to this viewpoint. Because of the rapid decay of the tungstate fluorescence ($\sim 10^{-6}$ sec.) it has generally been assumed that absorption of ultraviolet radiation, at least in the region of the first lattice absorption bands, produces only excitation of the tungstate ion, and that free electrons are not formed. Randall and Wilkins,[4] however, claim to have found photo-conductivity in pressed powders of $CaWO_4$ under 2650A and 3650A excitation, an observation which calls for a revision of the tacitly accepted picture of tungstate absorption and luminescence.

Since synthetic single crystals of a few efficient tungstate phosphors have recently become available,[5] it was thought worth while to search for photo-conductivity in these crystals. Crystals of $CaWO_4$ and $CdWO_4$, grown from the melt by the Crystal Section, NRL, and a crystal of $CaWO_4$ grown by the Linde Air Products Company were examined. Excitation, emission, and absorption spectra were also measured on the same crystals used in the photo-conductivity experiments.

For investigation of the photo-conductivity over the range 2200A to 4000A the light source was a hydrogen discharge lamp, the radiation being dispersed by a Gaertner quartz monochromator. Spot checks at 2537A were also made using a low pressure mercury arc lamp focused directly on the crystals. Care was taken to avoid illuminating the electrodes with the exciting light, because experiment indicated that spurious photo-currents resulted when the electrodes were irradiated with ultraviolet. The use of carbon electrodes, rather than metallic ones, was likewise found necessary in order to eliminate a small amount of photo-emission from the electrodes. With these precautions no photo-current was observed in either $CaWO_4$ or $CdWO_4$, with 225 volts applied to the crystals, using an instrument capable of detecting 5×10^{-15} ampere. This current is less than one-thousandth that observed with the photo-conductive crystals AgCl and TlCl under similar conditions.

Randall and Wilkins have also reported that $CaWO_4$ is faintly luminescent under 3650A excitation. We observed no luminescence in powders or single crystals of this material by visual or photographic examination under radiation from a "360BL" lamp equipped with an appropriate filter (Sylvania "Blacklight" lamp).

The excitation spectrum of $CdWO_4$, uncorrected for the energy distribution of the hydrogen lamp or for the transmission of the monochromator, has a peak at 3100A and a long-wave-length limit of 3350A. The excitation spectrum of $CaWO_4$, likewise uncorrected, peaks at 2600A and has a long-wave-length limit of 2850A. Kröger[3] reports an excitation limit of 2600A for pure $CaWO_4$, which shifts to about 3000A on the addition of 1 mole percent of lead. We therefore suspected lead contamination in our single crystals of $CaWO_4$. Spectroscopic analyses, capable of detecting 0.008 mole percent of lead, showed no lead in these crystals, however. Furthermore, a transmission spectrogram of one of the $CaWO_4$ crystals showed an absorption edge at 2720A with a long-wave-length extension of the edge to about 2800A, in fairly good agreement with our excitation data.

Our experiments indicate, then, no basis for concluding that free electrons are produced when tungstates are excited by ultraviolet light. The 3650A-excited luminescence and the photo-conductivity of $CaWO_4$ observed by Randall and Wilkins may have been due to impurities. Also, photo-emission for the electrodes may have played a part in their photo-conductivity measurements.

We wish to thank Esther W. Claffy for the spectrographic analyses; Robert J. Ginther for the transmission spectrogram of $CaWO_4$; and Stewart Slawson for the cutting and polishing of the crystals. Acknowledgment is also expressed to the Linde Air Products Company for their kindness in providing a specimen of their synthetic scheelite.

[1] R. J. Moon, Phys. Rev. **73**, 1210 (1938).
[2] N. F. Mott, and R. W. Hurney, *Electronic Processes in Ionic Crystals* (Oxford University Press, New York, 1940), pp. 203–204.
[3] F. A. Kroger, *Some Aspects of the Luminescence of Solids* (Elsevier Publishing Company, New York, 1948).
[4] J. T. Randall, and M. H. F. Wilkins, Proc. Roy. Soc. **184**, 347 (1945).
[5] S. Zerfoss, L. Johnson, and O. Imber, Phys. Rev. **75**, 320 (1949).

Infra-Red Absorption of Oxygen and Nitrogen Induced by Intermolecular Forces

M. F. Crawford, H. L. Welsh, and J. L. Locke*
McLennan Laboratory, University of Toronto, Toronto, Canada
April 4, 1949

An unperturbed homonuclear diatomic molecule can exhibit no rotation-vibrational absorption due to dipole transitions. However, in an attempt to detect $(O_2)_2$ complexes by infra-red absorption, we have found in liquid and compressed gaseous oxygen a marked absorption with a maximum at the vibrational frequency of the O_2 molecule, 1556 cm^{-1}. An investigation of compressed gaseous nitrogen showed a similar absorption at the N_2 vibrational frequency, 2331 cm^{-1}. The intensity-pressure relationships for both gases and for mixtures of the two gases prove conclusively that the absorption cannot be due to stable complexes or to quadrupole transitions. The effect must have its origin in dipole transitions induced by intermolecular forces during collisions.

The absorptions of the gases at pressures up to sixty atmospheres in a path length of 85 cm were measured with a Perkin-Elmer spectrometer. For pure oxygen at constant temperature, the absorption coefficient at all frequencies in the band was found to vary as the square of the pressure, as shown for two frequencies in Fig. 1. The shape of the absorption band, absorption coefficient *vs.* cm^{-1} (Fig. 2), is therefore independent of pressure. When nitrogen is added to the absorption cell and the partial pressure of oxygen is held constant, the oxygen absorption increases linearly with the partial pressure of nitrogen. The absorption observed in pure nitrogen has approximately the same intensity and shape as the oxygen band. In this case also, the absorption coefficient increases as the square of the pressure.

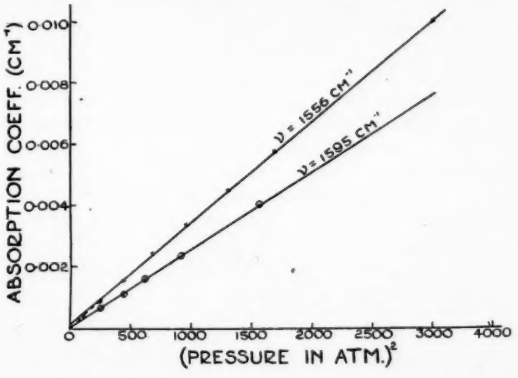

Fig. 1. Variation of the absorption coefficient with pressure at two points in the oxygen band.

These results are immediately explained on the assumption that the molecule absorbs during a collision with either a like molecule or a foreign gas molecule. The perturbation of the molecule by the strong intermolecular forces effective during the collision must produce a finite transition probability. Condon[1] has shown that the dipole induced in a molecule by a static electric field should give rise to transitions obeying the Raman rather than the infra-red selection rules. The polarization of the molecule by a colliding molecule will undoubtedly produce the same effect. Thus, the intensity distribution for the induced absorption in oxygen should be given by the Raman selection rules for rotation, $\Delta J=0, \pm 2$. This is compared with the experimental curve in Fig. 2. The envelope of the theoretical *O*- and *S*-branches matches well the intensity contour in the wings of the band. The integrated intensity of the *O*- and *S*-branches is found to be 0.7 of the total intensity of the band. This is very close to 0.75, the value of the theoretical ratio for the anisotropic part of the Raman scattering for a diatomic molecule. There seems, therefore, to be very little intensity in the *Q*-branch corresponding to isotropic Raman scattering. The intensity contour observed for liquid oxygen is consistent with that observed for the gas when the change in the Boltzmann factor with temperature is taken into consideration.

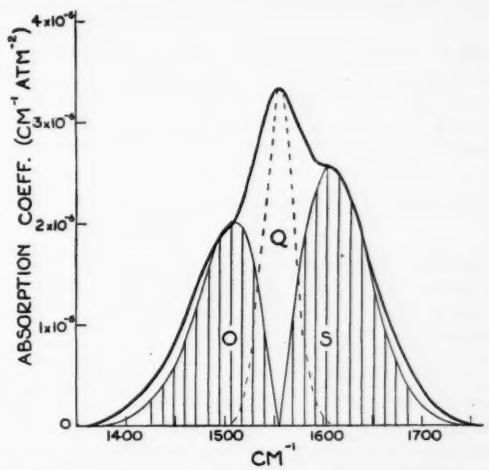

Fig. 2. The induced rotation-vibrational absorption of gaseous oxygen. The heavy curve is the experimental contour; the light curve is the theoretical envelope of the *O*- and the *S*-branch. The residual, *Q*-branch, intensity is shown as a broken line.

Discrete rotational lines were not observed. This is not unexpected, since the collisions postulated for the origin of the band should broaden the lines considerably. It is significant that the perturbation is sufficient to alter the transition probabilities but has negligible effect on the vibrational frequency.

The induced absorption established here should be a characteristic property of all molecules but is, of course, most readily detected for vibrations which are not otherwise infra-red active. It is probable that the infra-red absorption in hydrogen reported by Herzberg,[2] and attributed by him to quadrupole transitions, is due in part at least to induced transitions. The quadrupole intensity would introduce a linear term in the variation of the absorption coefficient with pressure. There seems to be an indication of this quadrupole term in oxygen at low pressures (Fig. 1).

* Holder of a scholarship under the Ontario Research Council, 1947–49.
[1] E. U. Condon, Phys. Rev. **41**, 759 (1932).
[2] G. Herzberg, Nature **163**, 170 (1949).

On the Transmission Coefficient of a Circular Aperture

C. J. BOUWKAMP
Laboratorium voor Wetenschappelijk Onderzoek, N. V. Philips' Gloeilampenfabrieken, Eindhoven, Nederland
February 28, 1949

RECENTLY Levine and Schwinger[1] developed a theory for approximately solving the problem of diffraction of a scalar plane wave by an aperture in an infinite plane screen. In particular they obtained for the transmission coefficient of a circular aperture, in the case of normal incidence, the approximate expression

$$t^{(2)}=(8/27\pi^2)(ka)^4[1+0.32(ka)^2+0.047823(ka)^4+\cdots], \quad (1)$$

which was then compared with my previous result,[2]

$$t=(8/27\pi^2)(ka)^4[1+0.32(ka)^2+0.027427(ka)^4 -0.004393(ka)^6+\cdots], \quad (2)$$

obtained by the method of spheroidal wave functions.

For a long time, however, I doubted the correctness of the last two numerical coefficients in (2). In fact both are wrong, and in view of the interesting results of Levine and Schwinger, it may be worth while to mention the correct expression. This reads

$$t=(8/27\pi^2)(ka)^4[1+0.32(ka)^2+0.0507755(ka)^4 +0.0002613(ka)^6+\cdots]. \quad (3)$$

It is to be observed that the approximation of (1) to (3) is far better than to (2). On the other hand, however, it is remarkable that the first-order approximation of Levine and Schwinger, *viz.*,

$$t^{(1)}=(8/27\pi^2)(ka)^4[1+0.32(ka)^2+0.049061(ka)^4+\cdots], \quad (4)$$

is closer to the correct expression (3) than is the second-order approximation (1).

I derived Eq. (3) in two completely different ways. First, by the method of spheroidal wave functions as before. As I have shown,[2] one has, up to and including terms of the order of $(ka)^{10}$,

$$t=(8/27\pi^2)(ka)^4[b_1{}^4X_1{}^2(1)][\{X_1'(0)\}^4+4(ka)^6b_1{}^4/81\pi^2]^{-1}, \quad (5)$$

in which[3]

$$b_1=1-(3/2\cdot5^4\cdot7)(ka)^4+(2/3\cdot5^6\cdot7)(ka)^6+\cdots,$$
$$X_1(1)=1+(1/5^2)(ka)^2-(3/2\cdot5^3\cdot7^2)(ka)^4 -(641/2\cdot3^4\cdot5^5\cdot7^2)(ka)^6+\cdots,$$
$$X_1'(0)=1-(3/2\cdot5^2)(ka)^2+(51/2^3\cdot5^3\cdot7^2)(ka)^4 +(6641/2^4\cdot3^4\cdot5^5\cdot7^2)(ka)^6+\cdots.$$

Inserting these expressions in (5), and expanding in powers of ka, we obtain (3). The exact values of the coefficients are $311/5^3\cdot7^2=0.0507755$, $2612/3^4\cdot5^3\cdot7^2-4/81\pi^2=0.0002613$.

In the second method, we do not use properties of spheroidal wave functions; it proceeds rather along the lines of Levine and Schwinger's paper cited. I shall briefly indicate the new approach, details of which will be published elsewhere.

Let $\exp(ikz)/ik$ represent a plane wave impinging normally upon the screen. Then the resultant wave field in the aperture may be determined from an integro-differential equation.[1] This aperture field can be developed in ascending powers of ika, *viz.*,

$$\varphi=\sum_{n=0}^{\infty}\varphi_n(ika)^n,$$

in which the coefficients depend on ρ, the distance to the center of the aperture. Setting

$$\varphi_n=\sum_{m=0}^{\infty}B_{n,m}P_{2m+1}[1-(\rho/a)^2]^{\frac{1}{2}},$$

in which P denotes the Legendre polynomial, while

$$B_{n,m}=0\begin{cases}m>n/2, & n \text{ even},\\ m>(n-3)/2, & n \text{ odd},\end{cases}$$

I obtained the recurrence relation

$$B_{n,m}=(-1)^{m+1}(m+\tfrac{3}{4})\frac{\Gamma(m+1)}{\Gamma(m+\frac{3}{2})}\sum_{\sigma=0}^{n-2}\sum_{\tau=0}^{\infty}(-1)^{\tau}\frac{\Gamma(\tau+\frac{3}{2})}{\Gamma(\tau+1)} \times\frac{\Gamma[-(\sigma/2)+(n-1/2)]\Gamma[-(\sigma/2)+(n+1)/2]}{\Gamma[-(\sigma/2)+\tau+(n+2)/2-m]\,\Gamma[-(\sigma/2)-\tau+(n+2)/2+m] \times\Gamma[-(\sigma/2)+\tau+(n+5)/2+m]\,\Gamma[-(\sigma/2)-\tau+(n-1)/2-m]}B_{\sigma,\tau},$$

from which the coefficients $B_{n,m}$ can be obtained successively, in virtue of

$$B_{0,0}=-2/\pi; \quad B_{0,m}=0(m>0); \quad B_{1,m}=0(m\geq0).$$

The transmission coefficient then becomes

$$t=Re\left[2ika\int_0^a\varphi(\rho)\rho d\rho\right]=\frac{2}{3}\sum_{n=0}^{\infty}(-1)^nB_{2n+3,0}(ka)^{2n+4},$$

which leads to (3) because

$$B_{3,0}=4/9\pi^2; \quad B_{5,0}=-32/225\pi^2; \quad B_{7,0}=1244/55125\pi^2;$$
$$B_{9,0}=16/729\pi^4-10448/4465125\pi^2.$$

[1] H. Levine and J. Schwinger, Phys. Rev. **74**, 958 (1948).
[2] C. J. Bouwkamp, Thesis, Groningen (1941).
[3] J. Math. Phys. **26**, 79 (1947).

On the Transmission Coefficient of a Circular Aperture

HAROLD LEVINE AND JULIAN SCHWINGER
Lyman Laboratory of Physics, Harvard University, Cambridge, Massachusetts
March 25, 1949

IN connection with the accompanying letter of Bouwkamp,[1] a few remarks appear desirable as a sequel to our paper.[2] A small numerical error in one term of an expansion for the second variational approximation to the transmission coefficient requires correction; the first two variational approximations, with an additional term in each beyond those given previously, are

$$t^{(1)}=(8/27\pi^2)(ka)^4[1+0.32(ka)^2 +0.0490612(ka)^4-0.0008054(ka)^6+\cdots],$$
$$t^{(2)}=(8/27\pi^2)(ka)^4[1+0.32(ka)^2 +0.0507755(ka)^4+0.0002613(ka)^6+\cdots].$$

The latter result is identical with the exact expression (3) of Bouwkamp, for all powers of ka retained.

A statement of the accuracy incorporated in any transmission coefficient $t^{(N)}$ of the foregoing sequence is readily obtained. By virtue of the stationary property of the coefficient, its deviations are proportional to the square of the error in the aperture wave function. Thus, with a wave function of the form $(1-(\rho^2/a^2))^{\frac{1}{2}}$ (or the first-order Legendre polynomial with argument $(1-(\rho^2/a^2))^{\frac{1}{2}}$), the expansion for $t^{(1)}$ is in error by a term of relative order $(ka)^4$, since the error in the wave function is of relative order $(ka)^2$ (see Bouwkamp). Similarly, with a wave function of the form

$$A_1(1-(\rho^2/a^2))^{\frac{1}{2}}+A_2(1-(\rho^2/a^2))^{\frac{3}{2}}$$

(or a linear combination of the first- and third-order Legendre polynomials with argument as before), the expansion for $t^{(2)}$ is in error by a term of relative order $(ka)^8$, since the error in the wave function is of relative order $(ka)^4$. In general, a wave function constructed from a linear combination of the first N odd Legendre polynomials with argument $(1-(\rho^2/a^2))^{\frac{1}{2}}$ yields a variational transmission coefficient $t^{(N)}$ whose expansion is exact through terms of relative order $(ka)^{4N-2}$. Furthermore, the stationary property of the transmission coefficient leads

one to expect that the inexact numerical factor of the term $(ka)^{4N}$ will be in close accord with the correct value.

[1] C. J. Bouwkamp, this issue.
[2] H. Levine and J. Schwinger, Phys. Rev. **74**, 958 (1948).

Two-Component Wave Equations

HERBERT JEHLE
*Brace Laboratory of Physics, University of Nebraska, Lincoln, Nebraska**
April 4, 1949

RECENTLY some interest has come up in two-component wave equations. As is well known, those wave equations, in contrast to the four-component Dirac equation, can only be made covariant with respect to the Lorentz group, not including covariance with respect to reflections.

The following antilinear two-component equation presents some interest,

$$\gamma^\kappa(\partial/\partial x^\kappa - i\varphi_\kappa)\psi = \mu\psi^*, \tag{1}$$

(ψ^* = conjugate complex of ψ), where

$$\tfrac{1}{2}(\gamma^{\kappa *}\gamma^\lambda + \gamma^{\lambda *}\gamma^\kappa) = -g^{\kappa\lambda}1, \tag{2}$$

with $g^{00}=+1$, $g^{11}=g^{22}=g^{33}=-1$. In the case $\varphi_\kappa=0$, we obtain by iteration the ordinary linear second-order wave equation. Equation (2) can be satisfied with

$$\gamma^0=\begin{pmatrix}0 & -1\\ 1 & 0\end{pmatrix},\quad \gamma^1=\begin{pmatrix}i & 0\\ 0 & i\end{pmatrix},\quad \gamma^2=\begin{pmatrix}0 & 1\\ 1 & 0\end{pmatrix},$$

$$\gamma^3=\begin{pmatrix}1 & 0\\ 0 & -1\end{pmatrix}. \tag{3}$$

With the Bargmann operator

$$\alpha = -\tilde{\alpha} = \begin{pmatrix}0 & -1\\ 1 & 0\end{pmatrix}, \tag{4}$$

we can form a real current vector

$$s^\kappa = \psi^\dagger\alpha\gamma^\kappa\psi \tag{5}$$

($\psi^\dagger$ = Hermitian conjugate).

Let us denote a Lorentz transformation by

$$\partial/\partial x^{\lambda'} = a_\lambda{}^\kappa \partial/\partial x^\kappa, \quad s^\lambda = a_\kappa{}^\lambda s^{\kappa'}. \tag{6}$$

Lorentz covariance of Eqs. (1) and (5) can be formulated in the following way. Let us take α and γ^κ as a *fixed* set of matrices (3) and (4) and transform the other quantities so that (1) and (5) go over into

$$\gamma^\kappa(\partial/\partial x^{\kappa'} - i\varphi_{\kappa'})\psi' = \mu\psi^{*\prime}, \tag{7}$$

$$s^{\kappa'} = \psi^{\dagger\prime}\alpha\gamma^\kappa\psi'. \tag{8}$$

If ψ transforms under the Lorentz transformation (6) as

$$\psi' = S^{-1}\psi, \tag{9}$$

the covariance of Eqs. (1) and (7) demands

$$\gamma^\kappa a_\kappa{}^\nu = S^{*-1}\gamma^\nu S, \tag{10}$$

and the covariance of (5) and (8) requires

$$\alpha = S^\dagger\alpha S^*, \tag{11}$$

Eq. (11) implies S to be an unimodular, i.e., $|S|=1$. Therefore, the matrix S contains only 3 complex parameters which is sufficient to satisfy Eq. (10) with 6 real parameters $a_\kappa{}^\nu$ of the Lorentz group.

A transformation $S^{*-1}\gamma^\nu S$ with any matrix S, applied to the γ^ν will preserve the relations (2), i.e., any set of matrices differing from Eq. (3) by an arbitrary S transformation will lead to nothing new.

The set of matrices

$$\gamma^0=\begin{pmatrix}0 & -1\\ 1 & 0\end{pmatrix},\quad \gamma^1=\begin{pmatrix}-i & 0\\ 0 & -i\end{pmatrix},\quad \gamma^2=\begin{pmatrix}0 & 1\\ 1 & 0\end{pmatrix},$$

$$\gamma^3=\begin{pmatrix}1 & 0\\ 0 & -1\end{pmatrix} \tag{12}$$

however, is another solution of (2), not differing from (2) by an S transformation. If Eqs. (1) and (3) represent the motion of a positive charge in the potential φ_κ, then Eqs. (1) and (12) represent the motion of a negative charge in the same potential φ_κ, which is readily seen by forming the conjugate complex of Eqs. (1) and (12) and comparing it with Eqs. (1) and (3).

The wave equation (1) is covariant with respect to gauge transformations $\varphi_\kappa'' = \varphi_\kappa + \partial\Lambda/\partial x^\kappa$,

$$\left.\begin{aligned} &\psi''=S^{-1}\psi,\quad \gamma^{\kappa\prime\prime}=S^{*-1}\gamma^\kappa S,\quad \alpha''=S^\dagger\alpha S^*\\ \text{with}\quad &S=1\exp(-i\Lambda),\end{aligned}\right\} \tag{13}$$

i.e., a not unimodular S. It is readily seen that $s^{\kappa\prime\prime}=s^\kappa$.

The charge conservation law

$$\partial s^\kappa/\partial x^\kappa = 0 \tag{14}$$

follows from Eq. (5) by differentiation, observing that the left-hand side is, as s^κ, a real quantity and the right-hand side, by virtue of Eq. (1), purely imaginary.

We are investigating solutions of the *set* of Eqs. (1) with any matrices γ^ν satisfying Eq. (2). If ψ_1 and ψ_2 are two solutions of Eqs. (1) and (2), we can superimpose them with arbitrary real coefficients provided we have first adjusted their relative phases by a transformation (13) to the same gauge, i.e., to the same matrices γ^ν. In this theory, therefore, the phase relations between superimposable ψ-functions are fixed.

* Research carried out at the Institute for Advanced Study and University of Pennsylvania, Philadelphia, Pennsylvania.

Neutron Diffraction by Gases

N. Z. ALCOCK AND D. G. HURST
Division of Atomic Energy Research, National Research Council of Canada, Chalk River, Ontario, Canada
April 5, 1949

BY use of a modified crystal spectrometer at the heavy water pile to select neutrons of 0.07-ev energy, the intensity of neutrons scattered from gases was measured in the angular range 5° to 90°. The gases studied, oxygen and carbon dioxide, were contained in a steel vessel at room temperature and approximately 60 atmospheres pressure. A schematic diagram of the experimental arrangement is shown in Fig. 1.

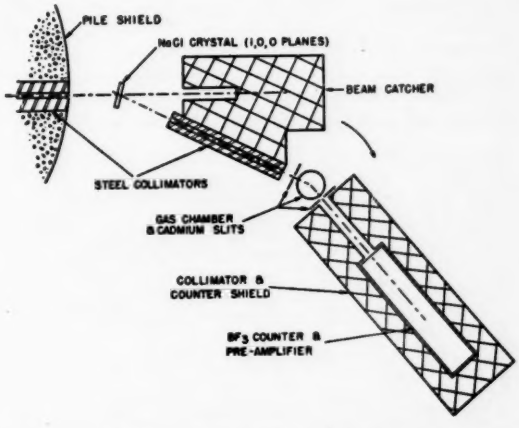

FIG. 1. Schematic diagram of neutron crystal spectrometer as modified for gas scattering experiments.

Since the scattering was not very intense, precautions were taken to reduce the background of fast neutrons penetrating the counter shield and slow neutrons scattered from the steel walls of the gas cell. The latter would be serious if the steel were not crystalline with a powder diffraction pattern. As there is no line of this pattern inside an angle of 30°, at small

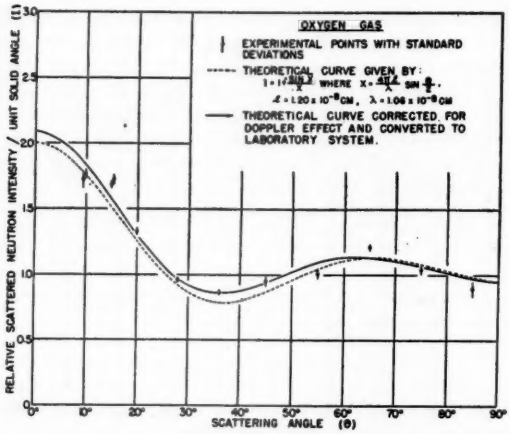
OXYGEN GAS
EXPERIMENTAL POINTS WITH STANDARD DEVIATIONS
THEORETICAL CURVE GIVEN BY:
THEORETICAL CURVE CORRECTED FOR DOPPLER EFFECT AND CONVERTED TO LABORATORY SYSTEM.
RELATIVE SCATTERED NEUTRON INTENSITY / UNIT SOLID ANGLE (I)
SCATTERING ANGLE (θ)

FIG. 2. Angular distribution of 0.07-ev neutrons scattered from oxygen gas.

angles the counter may be exposed to steel which is in the neutron beam without receiving too large a background. For angles above 30° baffles were arranged to prevent neutrons singly scattered from the steel from reaching the counter. Despite these precautions, at most angles background counts and true counts were approximately equal. The background from doubly scattered neutrons is appreciable (~10 percent), and an approximately calculated correction has been applied. No attempts were made to reduce it in the work here reported, but for work on other gases a system of baffles inside the gas cell has been planned.

In Figs. 2 and 3 are plotted the experimental results together with simple theoretical curves for both gases. (The vertical scale has been arbitrarily adjusted to fit the curves to the experimental points.) It will be seen that there is evidence of a pattern due to the form of the molecule.

The quantum-mechanically correct method of calculating the scattering requires a separate calculation for each possible rotational transition of the molecule (inelastic, elastic, and superelastic), and the summation of intensities after allowing for Doppler effect and the motion of the center of mass.[1] For a heavy molecule this requires a very large computational effort and has not been attempted. The curves drawn in Figs. 2 and 3 were obtained by a semiclassical calculation in which the neutron is represented by a wave, but the molecule is replaced by a rigid system of point scatterers. The method assumes elastic scattering only and is the same as the normal procedure for x-ray scattering,[2] with the atomic structure factors replaced by constants. No account has been taken of paramagnetism in the oxygen molecule,[3] but small corrections

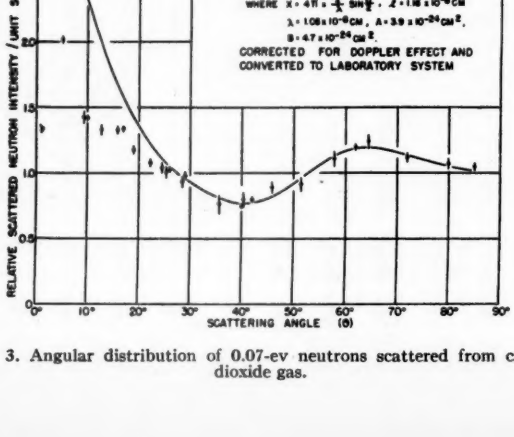
CARBON DIOXIDE GAS
EXPERIMENTAL POINTS WITH STANDARD DEVIATIONS
THEORETICAL CURVE GIVEN BY
CORRECTED FOR DOPPLER EFFECT AND CONVERTED TO LABORATORY SYSTEM
RELATIVE SCATTERED NEUTRON INTENSITY / UNIT SOLID ANGLE (I)
SCATTERING ANGLE (θ)

FIG. 3. Angular distribution of 0.07-ev neutrons scattered from carbon dioxide gas.

have been applied for Doppler effect and conversion to the laboratory system of coordinates. The good agreement with experiment in the case of oxygen leads one to expect that the exact formulas condense, to a close approximation, to the semiclassical result.[4] Of interest in this connection is a forthcoming letter by J. A. Spiers on the scattering of slow neutrons by deuterium gas.

Carbon dioxide, unlike oxygen, shows a marked deficiency in intensity at small angles. A possible cause of this is intermolecular interference, which in a liquid causes the scattering to be small for angles between zero and the first diffraction ring. The carbon dioxide in our experiment is near the liquid phase, and, as shown by Eisenstein and Gingrich[5] for x-ray scattering from argon, the vapor pattern may exhibit features characteristic of the liquid. If our conditions are compared with theirs, by the Law of Corresponding States, it is found that the deficiency in scattering is in good agreement but that the carbon dioxide shows no excess scattering corresponding to the liquid peak found for argon.

The study of gas scattering was suggested by Dr. B. W. Sargent. The spectrometer was the work of Mr. A. J. Pressesky, Mr. P. R. Tunnicliffe, and one of us (DGH).

[1] J. Schwinger and E. Teller, Phys. Rev. **52**, 286 (1937); M. Hamermesh and J. Schwinger, Phys. Rev. **69**, 145 (1946).
[2] See A. H. Compton and S. K. Allison, *X-rays in Theory and Experiment* (D. Van Nostrand Company, Inc., New York, 1935), second edition, p. 159.
[3] O. Halpern, Phys. Rev. **72**, 746 (1947).
[4] See E. Fermi and L. Marshall, Phys. Rev. **71**, 666 (1947), Section 4.
[5] A. Eisenstein and N. S. Gingrich, Phys. Rev. **62**, 261 (1942).

Inelastic Scattering of 14.5-Mev Neutrons by Lead*

H. T. GITTINGS, H. H. BARSCHALL, AND G. G. EVERHART
University of California, Los Alamos Scientific Laboratory, Los Alamos, New Mexico
April 7, 1949

ACCORDING to the statistical theory of nuclei[1] half the collisions of neutrons of wave-length short compared to the nuclear radius will result in inelastic scattering or absorption. The inelastically scattered neutrons are expected to have an approximately Maxwellian distribution in energy corresponding to the temperature of the residual nucleus.[2]

Previous investigations of the inelastic scattering by heavy nuclei of neutrons of energy above 3 Mev have been carried out by Grahame and Seaborg,[3] Soltan,[4] and Amaldi *et al.*[5] The results indicate reasonable agreement with theory for the magnitude of the cross section for inelastic scattering and absorption, but Grahame and Seaborg find for a Ra-Be source almost no inelastically scattered neutrons between the energies of 3 and 7 Mev, and Soltan finds no inelastically scattered neutrons between 3 and 11 Mev for Li+D neutrons.

The availability of 14.5-Mev neutrons with an energy spread of only ±0.5 Mev permits measurements of inelastic scattering in which the previous difficulties caused by the distribution in energy of the primary neutrons are not present. 14.5-Mev neutrons were obtained by bombarding a thick tritium gas target with deuterons from the Los Alamos electrostatic generator.

A lead sphere of radius about one-half mean free path for energy loss by the neutrons (4 cm) was constructed with a small central spherical cavity in which threshold detectors could be placed. In such a spherical geometry the effects of elastic scattering do not need to be considered since just as many neutrons are elastically scattered into the detector as are elastically scattered out, if the radius of the sphere is small compared with the distance from the source (40 cm). The threshold detectors were prepared in the form of long, thin foils which were rolled up tight to approximate a pseudosphere when placed in the cavity and which could be unrolled and wrapped helically around a Geiger tube.

A threshold detector should have, ideally, zero detection

cross section below a threshold energy and an approximately constant cross section above this energy. The aluminum (n,p) reaction has a threshold of about 3 Mev, a cross section above threshold of 0.03 barn and a half-life of 10.2 minutes. $Cu^{63}(n,2n)$ has a threshold of about 11 Mev, a cross section of 0.25 barn, and a half-life of 10.4 minutes.

The experimental procedure consisted of placing the sphere with the internal detector in the neutron beam for 10 minutes and then counting the induced foil activity. A second 10-minute run was then made with a duplicate detector but without the sphere. Normalization of the neutron flux was accomplished by placing a monitor foil of the same material as the detector foil in a standard position far enough from the sphere to minimize back-scattering. After irradiation the monitor foil and the detector foil were counted simultaneously on two Geiger counters for 10 minutes. Careful observations showed that only the 10-minute half-lives were excited. In this case, the ratio of total counts above background is the same as the ratio of foil activities at the end of irradiation.

The cross section for absorption and for inelastic scattering to below the detector threshold is given by

$$\sigma_{in} = -(1/Nr)\ln T$$

where N is the number of atoms per cc and r is the thickness of material between source and detector. T is the transmission and, using detector foils of equal mass and monitor foils of equal mass, is the ratio of the foil activities, A_d, with the sphere in and out, normalized to the same neutron flux by the ratio of monitor foil activities, A_m,

$$T = (A_d/A_m)\text{ in}/(A_d/A_m)\text{ out}.$$

When the transmission is computed in this fashion, the irradiation time, the waiting time, and the counting time do not need to be known.

The cross section of lead as determined by the aluminum detector was measured to be 2.20 ± 0.17 barns, and for the copper detector 2.29 ± 0.12 barns. The cross section is essentially the same for both detectors, which suggests that the inelastically scattered neutrons which are degraded in energy below the copper threshold are also degraded below the aluminum threshold, or, a 14.5-Mev neutron loses over 11 Mev in its first inelastic collision in lead. This result agrees with the findings of Grahame and Seaborg[3] for Ra-Be neutrons, and of Soltan[4] for Li+D neutrons. The absolute value of the cross section for inelastic scattering and absorption is in excellent agreement with the results of other workers,[3-5] and is about 10 percent less than one-half the total cross section, indicating a sticking probability of less than unity.

* This paper is based on work performed at Los Alamos Scientific Laboratory of the University of California under government contract W-7405-eng-36.

[1] H. A. Bethe, Phys. Rev. **57**, 1125 (1940).
[2] V. F. Weisskopf, Phys. Rev. **52**, 295 (1937).
[3] D. C. Grahame and G. T. Seaborg, Phys. Rev. **53**, 795 (1938).
[4] A. Soltan, Nature **142**, 252 (1938).
[5] E. Amaldi, D. Bocciarelli, B. N. Cacciapuoti, and G. C. Trabacchi, *Fundamental Particles* (Physical Society, London, 1947), p. 97.

On the Question of Atmospheric Ammonia*

M. V. MIGEOTTE** AND R. M. CHAPMAN
Mendenhall Laboratory of Physics, Ohio State University, Columbus, Ohio
March 14, 1949

IN a letter to the editor of the Physical Review,[1] Mohler, Goldberg, and McMath reported spectroscopic evidence for ammonia in the earth's atmosphere, based on close agreement, to within ±0.05 cm^{-1}, between 8 intense lines in the ammonia spectrum and features of the solar spectrum in the 2μ-region.

Since these lines would be components of combination bands of the ammonia spectrum, it would, therefore, seem desirable to verify the existence of NH_3 in the earth's atmosphere, by investigating one or more of the fundamental bands at 2.92, 2.99, 6.14, and 10.5μ, since they are certainly more intense than the combination bands.

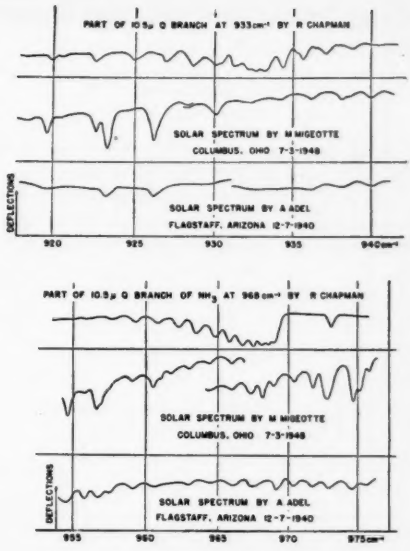

FIG. 1. Spectrograms for comparison.

The 2.9μ-region of the solar spectrum is complicated by the presence of many water vapor lines and will be investigated when winter water vapor conditions are most favorable. The 6.14μ-band of ammonia is almost impossible to detect, under any conditions, due to the very heavy water vapor absorption in this region. Fortunately, the 10.5μ-band of ammonia falls in a region of the solar spectrum where there are only a very few lines.

Comparison of our recent solar spectrograms and those of A. Adel,[2] published in 1941, with our laboratory spectrograms of the 10.5μ-band of ammonia, reveals no evidence of the two well-known Q branches, at 931 and 968 cm^{-1}, in the solar spectrum.

Figure 1 presents the spectrograms concerned, and, except for one or two lines, there is a good agreement between the records of Adel and Migeotte.

It has been determined by D. L. Wood of our laboratories that 1-mm pressure of ammonia in a 10-cm cell is detectable in this region. This fact and the lack of evidence for any absorption of NH_3 in the 10.5μ-region of the solar spectrum, indicate that only trace amounts of ammonia are present in the earth's atmosphere, and it is doubtful that the lines identified as ammonia lines in the 2μ-region arise from atmospheric absorption.

It is possible, however, that a local concentration of ammonia near the point of observation would give rise to an apparent atmospheric absorption.

* The work described in this letter was carried out, in part, under contract between Wright-Patterson Air Force Base of the Air Materiel Command and the Ohio State University Research Foundation.
** Now at the University of Liege, Belgium.
[1] Mohler, Goldberg, and McMath, Phys. Rev. **74**, 352 (1948).
[2] A. Adel, Astrophys. J. **94**, 451 (1941).

Erratum: The Detection of Gamma-Rays with Thallium-Activated Sodium Iodide Crystals

[Phys. Rev. **75**, 796 (1949)]

ROBERT HOFSTADTER
Palmer Physical Laboratory, Princeton University, Princeton, New Jersey

ON page 799 the symbol TlI (standing for thallium iodide) should have appeared after "100 milligrams of" in place of the symbol Tl, which appeared inadvertently.

Beryllium-Proton Reactions and Scattering

R. G. THOMAS, S. RUBIN, W. A. FOWLER, AND C. C. LAURITSEN
Kellogg Radiation Laboratory, California Institute of Technology, Pasadena, California
March 28, 1949

THE cross sections of the reactions $Be^9(p,d)Be^8$, $Be^9(p,\alpha)Li^6$, and $Be^9(p,p)Be^9$ have been measured at a laboratory angle of 138° for bombarding energies from 250 to 1300 kev using a high resolution double-focusing 180° magnetic spectrograph for reaction particle analysis.[1] Figure 1

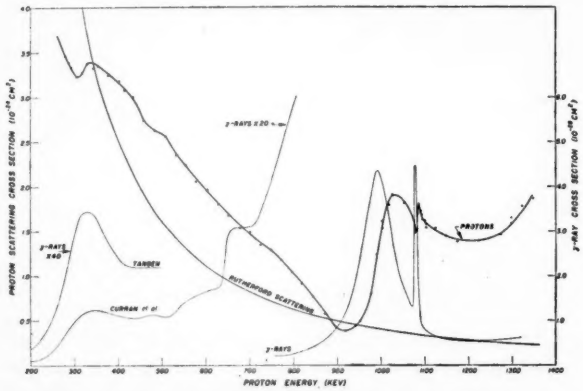

FIG. 1. Cross section for scattering of protons by beryllium at 138° (142° in center of mass coordinates). The energy scale should be increased by 0.32 percent. The cross section is 4π times the differential cross section per unit solid angle.

shows the proton scattering cross section and, for comparison, the $Be^9(p,\gamma)B^{10}$ data of Tangen,[2] Curran,[3] and Fowler, Lauritsen, and Lauritsen,[4] are included. The cross sections shown are 4π times the differential cross section per unit solid angle in center of mass coordinates. The energy scale was calibrated[2] by measurements on the strong $F^{19}(p\alpha',\gamma)$ resonance at 873.5 kev.[5] Particle detection was by means of an ionization chamber and linear amplifier. By observing the Rutherford scattering of protons from copper, it was found that counting was reliable down to 180 kev, where the pulses began to fall into the background noise. Figure 2 shows the reaction cross sections for disintegration into alpha-particles and deuterons. Below 750-kev bombarding energy, the alphas and deuterons could not be resolved magnetically since they have nearly the same curvature in the field, so it was necessary to use amplifier pulse size discrimination, a procedure which involves some error due to the straggling of the alpha-particles and deuterons in the target and chamber windows.

In measuring the alpha-particle cross section, the spectrograph field was adjusted for counting He^{++} ions; consequently, it was necessary to correct the yields for the number of He^+ ions which were not counted. Henderson,[6] Briggs,[7] and Rutherford[8] have studied the capture and loss exchange between He^+ and He^{++} in various substances. Their results

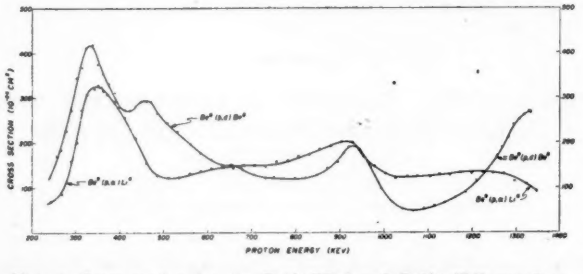

FIG. 2. Cross section for the $Be^9(pd)Be^8$ and $Be^9(p\alpha)Li^6$ reactions at 138°. The energy scale should be increased by 0.32 percent. The cross section is 4π times the differential cross section per unit solid angle.

show that although the equilibrium ratio of these two ions varies considerably with velocity, it is not a function of the substance penetrated. This is consistent with the calculations made by Bohr,[9] which indicate that the ratio of capture and loss cross sections is proportional to the inverse one-third power of the atomic number of the stopping material. Thin contamination layers of carbon and oxygen on the beryllium actually determine the ratio of the two types of ions in our case. We have used the experimental results for mica. No correction was made for the number of neutral helium atoms, as the equilibrium ratio of neutral to doubly charged alpha-particles is very small for the velocities dealt with here. No experimental data are available on the capture-and-loss ratio for protons and deuterons in the energy range with which we were concerned, so no correction was made. The analysis by Bohr indicates a ratio of neutral to singly charged protons of less than 5 percent for proton energies greater than 120 kev.

The yield of particles at each bombarding voltage was obtained by adjusting the field of the magnetic spectrograph so that only particles from a thin layer of the target somewhat below the surface were counted. The advantages of such a procedure are that surface contamination layers are avoided and that even though thick targets are employed a thin target yield curve is obtained, the target thickness in energy units being determined by the over-all resolution of the apparatus.

The over-all resolution, taking into account spectrograph resolution, size of the incident beam, spread in energy of the incident particles, straggling in the target, and change in energy of the scattered particles with angle of scattering, corresponded to a small effective spread in incident particle energy. This appreciably affected only the shape of proton interference at the narrow resonance at 1087 kev. At this energy the resolution was such that for a fixed bombarding energy and spectrograph setting protons were accepted by the spectrograph whose energy before scattering had a spread of 1 kev. From γ-ray studies[4] this resonance is found to have a natural width of 3–4 kev. The cross section is proportional to the yield multiplied by the stopping cross section of the target atoms.

The proportionality factor involves the ratio of the solid angle of the entrance window of the spectrograph to the energy interval accepted at the exit window. This was obtained by measuring the yield of protons scattered by copper and assuming the Rutherford formula for the cross section to hold. The stopping cross section for copper as a function of proton energy was obtained from the data of Mano,[10] while that for beryllium was obtained from the recent measurements by Madsen and Venkateswarlu.[11]

The proton scattering cross section shows prominent anomalies near 998 and 1087 kev, where marked resonance occurs in the cross section for the $Be^9(p\gamma)B^{10}$ reaction. Interference effects predicted for elastic scattering by the Breit-Wigner formula are indicated. Deviations from Rutherford scattering over the entire low energy region, especially near 330 kev, are also indicated. The alpha-particle and deuteron cross sections differ from customary results in that there is no indication of the rapid increase with bombarding energy usually attributed to barrier penetration factors. Anomalous effects appear at 330 and 900–1000 kev in the alpha-particle and deuteron reactions and, in addition to these energies, at 440 kev in the deuteron reaction. It is not clear whether the anomalies in the region 900–1000 correspond to interference effects from the 998-kev resonance or to resonance effects from a new level at 930 kev. A careful study of the alpha- and deuteron yield near 1087 kev was made with no indication of anomalous results similar to that in the elastic scattering. If an assignment of $J=0$ and even parity is made for the state at 1087 kev in B^{10}, then a strict selection rule forbidding alpha- or deuteron emission from this state follows. This is consistent with the known fact that this state does not radiate[4] to the

ground state of B^{10} and with the recent assignment of $J=3$ to the ground state since an octopole transition is then involved. The observed width is consistent with p-wave proton capture, formation of the state by s-wave capture not being possible since Be^9 has a spin of $\frac{3}{2}$. A more detailed theoretical discussion of these results will be given in a forthcoming publication by E. R. Cohen and R. F. Christy. This work was assisted by the joint program of the ONR and AEC.

[1] Snyder, Lauritsen, Fowler, and Rubin, Phys. Rev. **74**, 1564 (1948).
[2] Hole, Holtsmark, and Tangen, Naturwiss. **28**, 335 (1940).
[3] Curran, Dee, and Petrzilka, Proc. Roy. Soc. (London) **169**, 269 (1939).
[4] Fowler, Lauritsen, and Lauritsen, Rev. Mod. Phys. **20**, 236 (1948).
[5] Herb, Snowden, and Sala, Phys. Rev. **75**, 246 (1949). The figures were prepared on the basis of 440 kev for the first resonance in $Li^7(p\gamma)$. A correction of +0.32 percent is necessary to change to the $F^{19}(p\alpha', \gamma)$ scale.
[6] G. H. Henderson, Proc. Roy. Soc. (London) **109**, 157 (1925).
[7] G. H. Briggs, Proc. Roy. Soc. (London) **A114**, 341 (1927).
[8] E. Rutherford, Phil. Mag. **47**, 277 (1924).
[9] N. Bohr, Kgl. Danske Vid. Sels. Math.-Fys. Medd. **XVIII**, 8.
[10] G. Mano, J. de phys. et rad. **5**, 628 (1934).
[11] C. B. Madsen and P. Venkateswarlu, Phys. Rev. **74**, 648 (1948).

Radioactive Silver Isotopes Produced by Photo-Disintegration of Cadmium*

R. B. Duffield and J. D. Knight
Department of Physics, University of Illinois, Urbana, Illinois
March 10, 1949

In the silver fraction isolated from cadmium, which had been irradiated with 21-Mev betatron x-rays, we have found evidence of two hitherto unassigned silver activities of half-lives 5.3 hr. and 20 min. Their counting rates, calculated to saturation and compared with those of the 3.2-hr. Ag 112 and the 7.6-day Ag 111 produced by (γ,p) reactions in the same irradiation, gave the relative yields shown in Table I.

The cadmium was irradiated in the form of reagent grade cadmium nitrate tetrahydrate; the silver fraction was precipitated as AgCl, dissolved and reprecipitated in the presence of inactive Cd^{++} solution to minimize contamination by the rather strong cadmium activities produced in the original sample.

Counts taken with the silver source mounted between the poles of a permanent magnet showed the 5.3-hr. and 20-min. activities to be β-emitters. The mass assignments of these periods were made by similar irradiations and treatment of samples of cadmium oxide enriched in Cd 114 and Cd 116.[1]

The decay curves are shown in Figs. 1 and 2.

The silver from the Cd 114 decayed with a half-life of 5.3 hr. over five half-lives, thus establishing that it was Ag 113 made by Cd 114 (γ,p). An aluminum absorption curve, evaluated by the Feather method, gave a beta-ray energy of 2.1 ± 0.2 Mev. No gamma-ray was detected. A period of similar half-life and beta-ray energy has been reported for a fission product silver by Turkevich.[2]

In the same manner, the 20-min. silver activity was found to be Ag 115 made by Cd 116 (γ,p). An aluminum absorption curve of the radiation showed the beta-ray energy to be approximately 3 Mev. No gamma-radiation was detected. Unfortunately, the low activity level of the sample prevented the positive identification of either the 43-day or 2.3-day Cd 115 daughters which would be expected to grow in. The half-life and beta-ray energy are very close to those reported for a fission-product silver by Turkevich[2] and by Seelmann-Eggebert and Strassman.[3]

Irradiation of the Cd 114 sample with fast neutrons from 10-Mev deuterons on beryllium produced a 2-min. β^--emitter which was chemically identified as silver. As a check on the possibility that this activity may have been due to 2.3-min. Ag 108 from a possible silver impurity in the cadmium, the latter was irradiated with slow neutrons and counted. No period of this half-life was found. A second possibility, that the 2-min. period may have been a metastable Cd $113m$,[4] formed by Cd 114 $(n,2n)$, was excluded by the chemical separation and by the observed hardness of the electrons. It is probable, therefore, that the period we find is that of Ag 114 produced by Cd 114 (n,p).

We are indebted to Professor P. G. Kruger and the crew of the University of Illinois cyclotron and to Professor A. L. Hughes and the crew of the Washington University cyclotron for the neutron irradiations.

Table I.

Activity	Half-life	Relative yield
Ag 111	7.6 day	2.7
Ag 112	3.2 hr.	1.00
Ag	5.3 hr.	1.15
Ag	20 min.	0.18

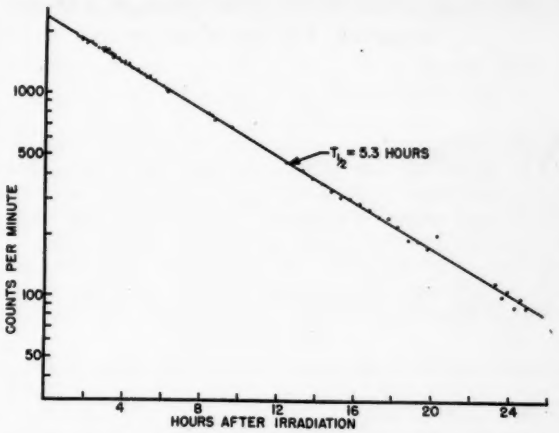

Fig. 1. Decay of silver activity produced by 21-Mev x-rays on cadmium containing 94 percent Cd 114.

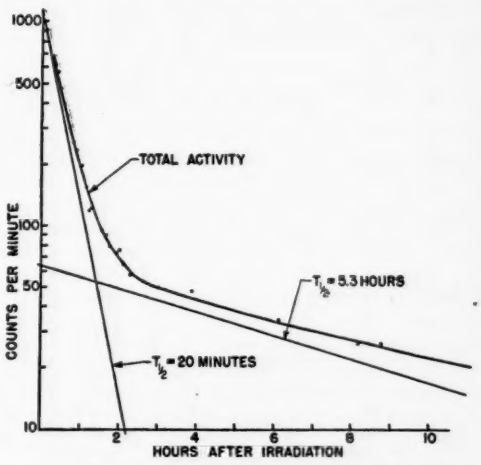

Fig. 2. Decay of silver activity produced by 21-Mev x-rays on cadmium containing 71 percent Cd 116, 18 percent Cd 114.

* Assisted by the joint program of the ONR and AEC.
[1] The enriched Cd 114 and Cd 116 used in this investigation were supplied by Carbide and Carbon Chemicals Corporation, Y-12 Plant, Oak Ridge, Tennessee, and obtained on allocation from the Isotopes Division of the AEC.
[2] A. Turkevich, Plutonium Project Report ANL-4010 quoted by G. T. Seaborg and I. Perlman, Rev. Mod. Phys. **20**, 585 (1948).
[3] W. Seelmann-Eggebert and F. Strassman, Zeits. F. Naturforschung **2a**, 80 (1947).
[4] A. C. Helmholz and C. L. McGinnis, Phys. Rev. **74**, 1559 (1948).

Microwave Resonance Absorption in a Paramagnetic Organic Compound

A. N. HOLDEN, C. KITTEL, F. R. MERRITT, AND W. A. YAGER
Bell Telephone Laboratories, Murray Hill, New Jersey
April 4, 1949

MICROWAVE resonance absorption was observed at 24,446 Mc/sec. at room temperature in a powdered crystal specimen of an organic free radical compound. Free radicals are organic compounds which have an odd number of electrons and thus have an unpaired electron spin. The unpaired spin leads to paramagnetism. The compound with which we have worked has the chemical formula $ON(C_6H_5)C(CH_3)_2CH_2C(CH_3)N(C_6H_5)O$ and is a substituted nitrogen oxide. Its paramagnetic properties were reported by Kenyon and Sugden,[1] who found that the value of the Curie constant corresponded closely to a spin of $\frac{1}{2}$. This is compatible with our microwave results. Approximate measurements of the magnetic susceptibility at liquid air, dry ice, and room temperatures by Mr. E. A. Nesbitt of this laboratory show the expected Curie-type behavior.

The compound, named β-(phenyl nitrogen oxide)-β-methyl pentane-δ-one oxime *N*-phenyl ether, was prepared by the method used by Banfield and Kenyon.[2] It forms bright red crystals which are stable at room temperature. The microwave measurements were made by placing about 1 cc of the crystals in a wave guide between the pole pieces of an electromagnet. The transmitted power was measured as a function of the intensity of the static magnetic field. It was observed that the insertion dielectric loss of the specimen was much smaller than that of the hydrated paramagnetic salts with which we have previously worked.

The change in transmitted power as a function of the intensity of the static magnetic field is plotted in Fig. 1. The resonance peak is exceptionally strong and sharp; in fact it is by far the sharpest peak yet reported for electronic paramagnetic resonance. The half-width at half-power is 20 oersteds. The g value as calculated from the resonance condition $\hbar\omega = g\mu_B H$ is 2.02. Our present experimental accuracy in the determination of absolute magnetic field intensity is about 1 percent, so that the free spin g value of 2.00 is within the present experimental error. It is possible to determine the center of our line to a relative precision of 2 oersteds or less, whereas the relativistic radiation reaction shift would amount to about 10 oersteds. This proposed application assumes that spin-orbit coupling effects do not contribute sensibly to the measured g value; a provisional argument can be suggested in support of this assumption, based on the apparent lack of anisotropy in the g value, despite the high structural anisotropy of the molecule itself.

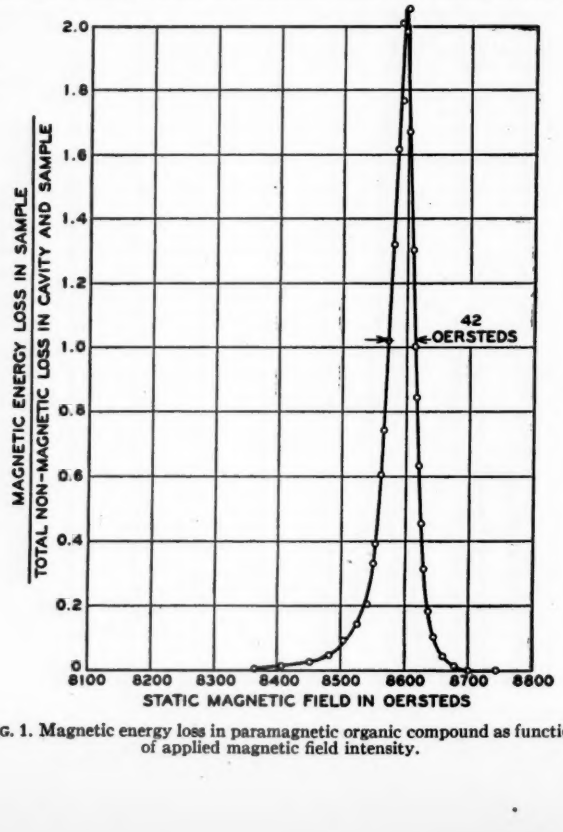

FIG. 1. Magnetic energy loss in paramagnetic organic compound as function of applied magnetic field intensity.

The sharpness of the resonance is probably accounted for by the low value of the spin ($S=\frac{1}{2}$) and by the relatively great magnetic dilution of the material. Measurements at a 3-cm wave-length are in agreement with the measurements at 1 cm.

We wish to thank Mr. E. A. Nesbitt for making the susceptibility determinations.

[1] J. Kenyon and S. Sugden, J. Chem. Soc. 170–171 (1932).
[2] F. H. Banfield and J. Kenyon, J. Chem. Soc. 1612–1629 (1926).

Strings, Poles, and the Electron

JOHN A. ELDRIDGE
State University of Iowa, Iowa City, Iowa
February 18, 1949

A COMPARISON of Dirac's treatment of magnetic poles with strings[1] and Wilson's discussion of the single pole[2] is of interest. Dirac considers the relation between a charge e and a pair of magnetic poles $\pm g$. The poles are connected by a "string" so as to introduce a solenoidal field (which I represent by **B**) as well as an irrotational field (which I represent by **H**). **B** and **H** have the properties of the conventional magnetic fields and so the string represents a region of magnetic polarization **M**. $\mathbf{B}=\mathbf{H}+4\pi\mathbf{M}$. For purpose of comparison we modify Dirac's development. We suppose the string to be a straight line between the poles. Since **B** is solenoidal it has a vector potential **A** which encircles the string. Consider a particle with mass m and charge e at a distance r from a line passing through the poles (the string or its extension). Its momentum is $m\mathbf{v}+e\mathbf{A}/c$ and its angular momentum about the line is $m\mathbf{r}\times\mathbf{v}+e\mathbf{r}\times\mathbf{A}/c$. We are interested in the second term which is the angular momentum associated with the cross products of the electric and magnetic fields. The magnetic moment per unit length in the string is g. For an infinitely long string $A=2g/r$ and the angular momentum in the field is $2eg/c$. We now assume that when e, g have the elementary values e_0, g_0 the angular momentum is $\hbar$. Therefore $g_0=\hbar c/2e_0$, which is Dirac's conclusion. The derivation demands infinitely long strings. Since the poles are at infinity it is g_0, linear density of magnetic moment along the string, which now appears to be the quantity of physical interest.

Wilson considers the relation between a charge and a single pole. Again the momentum of the system is the momentum of the particles plus the momentum of the crossed fields. There is now no solenoidal field and hence no vector potential but Wilson shows that the angular momentum of the field about a line joining the charge and pole in eg/c. He assumes that when the charges and poles have their elementary values that the angular momentum is $\frac{1}{2}\hbar$. This gives $g_0=\hbar c/2e_0$ for the elementary pole.

It seems likely that poles must exist in pairs. For a system consisting of a charge and a pair of opposite poles the angular momentum in the field will not have a definite value but will approach zero if the distance between the poles is made small in comparison with their distances from the charge. The result becomes definite if the poles have an infinite separation with the charge at a finite distance from their line of separation. The angular momentum associated with the fields of the in-

dividual poles now combine to give a field momentum of $2e_0g_0/c$. Setting this equal to $\hbar$ again gives the value of g_0.

The angular momentum of a charge and a pair of poles with finite separation has a definite magnitude in the special case that the charge and poles are colinear. Then the angular momentum is $\hbar$ if the charge lies between the poles and 0 if it does not.

One might suppose that an electron could be represented by a charge e_0 and two magnetic poles $\pm g_0$. If the distance between poles is e_0^2/mc^2, a value sometimes given for the electron diameter, the magnetic moment has the correct value but the angular momentum is $\hbar$ instead of $\hbar/2$. The correct spin is obtained if the charge spends only half its time between the poles.

[1] P. A. M. Dirac, Phys. Rev. **74**, 817 (1948).
[2] H. A. Wilson, Phys. Rev. **75**, 309 (1949).

Search for the Transition of Streamer to Townsend Form of Spark in Air

L. H. Fisher and B. Bederson
New York University, University Heights, New York
March 11, 1949

THE present view of the mechanism of spark discharge in air is that a streamer process is effective at atmospheric pressure and that a Townsend mechanism is active at lower pressures.[1] The Townsend mechanism in air may be secondary emission of electrons by positive ion bombardment of the cathode, or photoelectric emission at the cathode. There is little or no evidence to decide between these two mechanisms at low pressure, but Loeb[2] has expressed the opinion that the former is probably the predominating process. It thus may be possible to determine the transition region from the streamer to the Townsend mechanism by a study of the formative time lags of spark breakdown as a function of pressure and gap length.

Experiments were undertaken to measure these lags, using voltages as close to the static breakdown as possible. Previous measurements of formative time lags in air have been made with overvoltages of at least one percent, and usually much more.[3]

The cathode of a one-centimeter plane parallel gap was illuminated by ultraviolet light, and an approach voltage below but close to the static breakdown was applied. Then an additional small square voltage pulse (rise time 0.1 μsec.) was applied across the gap. The pulse started the sweep of a Sylvania P4 synchroscope. An electrode surrounding the transmission line to the chamber actuated the vertical deflection plates (no amplification) and thus allowed detection of the spark. The primary photoelectric current was about 50 electrons/μsec.

The results for 0.2 percent overvoltage are shown as a function of pressure in Fig. 1. These are average results. Minimum values follow a curve of the same shape, but lower at this particular overvoltage by a factor of about two. The distribution of results obtained at any given pressure and overvoltage shows that the measured lags are not statistical. The formative time lags are very long, although the lags decrease rapidly with increasing overvoltage. With an overvoltage of about one percent, the formative time lags are a small fraction of a microsecond *at all pressures* studied.

The immediate problem of separating streamer from Townsend mechanism cannot be answered. Indeed, the results obtained indicate the desirability of a general reexamination of the breakdown mechanisms when more data of this kind are available.

The ripple in the power supply (0.1 percent) prevented measurements from being made much closer than 0.2 percent above threshold. The ripple probably accounts in large measure for the distribution of results at a given pressure and overvoltage.

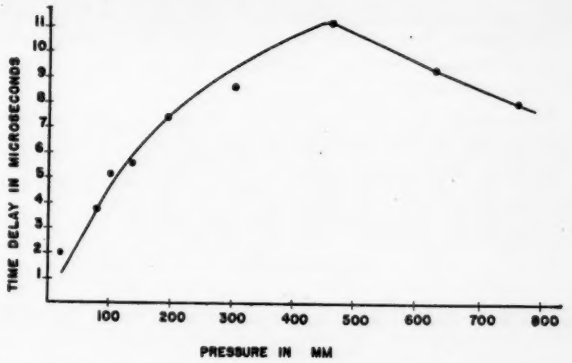

FIG. 1. Average formative time lag of spark breakdown in air as a function of pressure for 0.2 percent overvoltage in a one-cm gap.

Acknowledgment is made to the Research Corporation for a grant in support of this work, and to Professor L. B. Loeb of the University of California for the loan of the discharge chamber.

[1] L. B. Loeb and J. M. Meek, *The Mechanism of the Electric Spark* (Stanford University Press, Stanford, 1941).
[2] L. B. Loeb, Proc. Phys. Soc., London, **60**, 561 (1948).
[3] See for example Harry J. White, Phys. Rev. **49**, 507 (1936); Robert R. Wilson, Phys. Rev. **50**, 1082 (1936).

Decay of 8-Day Iodine^{131} to a Metastable State of Xenon^{131} *

A. R. Brosi, T. W. DeWitt,** and H. Zeldes
Oak Ridge National Laboratory, Oak Ridge, Tennessee
March 31, 1949

A RADIOACTIVE gas with a half-life of approximately 12 days has been found associated with the 8-day I^{131} produced at Oak Ridge National Laboratory. This radioactive gas is present in I^{131} preparations whether these are made from fission products or from neutron-bombarded tellurium. Removal of gas from a sample of I^{131} at intervals has shown the gaseous activity to be the daughter of a parent with an 8-day half-life. Inertness to calcium vapor indicates that this daughter is a radio-isotope of a noble gas.

Lead and tantalum absorption curves show that the 12-day activity decays with an approximately 165-kev gamma-ray as well as softer x-radiation. Tin and antimony absorption curves indicate that the x-rays are the K radiation of xenon. Lead absorption curves taken with a coincidence counter show that electrons are coincident with x-rays but not with gamma-rays. Assuming that the electrons are monoenergetic conversion electrons, the aluminum absorption curve indicates a strong component with an energy of approximately 130 kev and a much weaker component with an energy of approximately 160 kev. These energies differ from the observed gamma-ray energy by K and L binding energies of xenon.

Comparison of the electron disintegration rate of daughter 12-day xenon activity with the absolute disintegration rate of parent 8-day iodine, indicates that about one percent of the I^{131} atoms decay to this excited state of xenon^{131}. A rough calibration of the counter used for counting efficiency of 165-kev gamma-rays gives an internal conversion coefficient, N_e/N_q, of approximately 20.

The 12-day xenon^{131} isomer reported here is probably the same one that Camac[1] obtained by fast neutron bombardment of xenon. It may also be the same as the approximately 14-day xenon activity found in 0.03 percent fission yield by Chackett.[2] In a beta-ray spectrometer study of 8-day iodine^{131}, Owen, More, and Cook[3] found conversion electrons with an energy of 128 kev which were not found by Metzger and Deutch.[4] It is believed that these electrons were from the 12-day xenon daughter trapped in their source. The results reported here

lend support to the suggestion of Owen, Moe, and Cook that a small fraction of the 8-day iodine^{131} atoms, which decay with a 600-kev beta-ray, emit a 286-kev gamma-ray followed by a 165-kev gamma-ray.

* This document is based on work performed under Contract No. W 7405. Eng 26, for the Atomic Energy Project at Oak Ridge National Laboratory.
** Now at Mellon Institute, Pittsburgh, Pennsylvania.
[1] M. Camac, Metallurgical Project Report CC-2409 (1944).
[2] W. J. Arrol, K. F. Chackett, and S. Epstein, Canadian Research Council Report No. 297 (1947).
[3] Owen, Moe, and Cook, Phys. Rev. **74**, 1879 (1948).
[4] F. Metzger and M. Deutch, Phys. Rev. **74**, 1640 (1948).

A Time-of-Flight Mass Spectrometer with Varying Field

J. A. Hipple and H. A. Thomas
National Bureau of Standards, Washington, D. C.
March 15, 1949

Of several time-of-flight mass spectrometers that have been proposed recently, only that of Goudsmit[1] gives promise of attaining very high resolution because of the favorable focusing property. The perfect focusing in this instrument can be considered a special case of that obtained in uniform crossed electric and magnetic fields[2] with $E=0$ in this case. It has been recognized that the crossed-field instrument with E having a constant value other than zero could also be used as a time-of-flight instrument in the manner proposed by Goudsmit, but this does not possess some of the advantages of the method proposed here.

In Fig. 1, there is a uniform magnetic field H in the x direction and a uniform electric field E in the z direction. The field E has the value E_0 at $t=0$ and decreases linearly with time to the value $E=-E_0$ at $t=T$. In a coordinate system moving with the proper varying velocity, the ions describe circular paths in which the time for one revolution is given as in Goudsmit's case by

$$T_1=670M/H \text{ microseconds},$$

where M is the mass of the ion in atomic weight units and H the magnetic field in gauss. The y component of the velocity of the moving coordinate system is independent of the initial conditions and the mass of the ions. The z component of this velocity is also independent of the initial conditions, but does depend on the mass of the ions (the present discussion is concerned with singly charged positive ions). However, the distance B in the z direction to the exit slit is chosen only large enough to allow the beam to miss the electrode structure around the source and receiver and to provide sufficient space for the source and receiver.

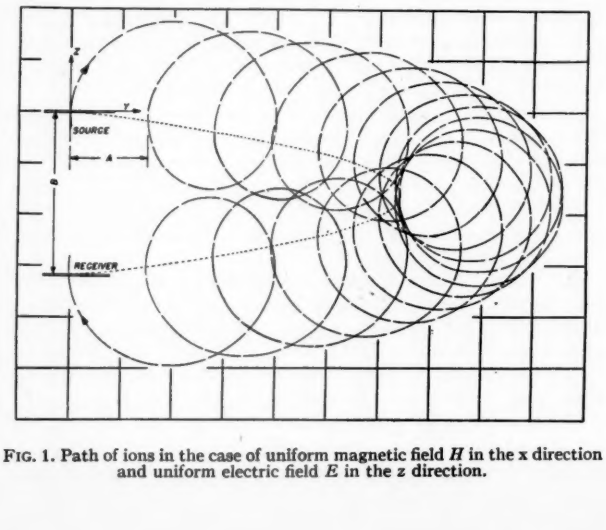

FIG. 1. Path of ions in the case of uniform magnetic field H in the x direction and uniform electric field E in the z direction.

The field E is adjusted so that a selected reference mass M_0 passes through the exit slit after an integral number of cycles n_0. Except for the small z dispersion which has an almost negligible effect in this application but which may be calculated, other ions having the proper mass to undergo an integral number of revolutions n_1 will also be perfectly focused regardless of the initial conditions. Ions having made a non-integral number of revolutions, n, when the moving coordinate system has returned to $y=0$, will be dispersed slightly in the y direction when n does become an integer. This may not be too serious as the exit slit may be made quite wide when a pulsed ion beam is used and the transit time measured in the manner of Goudsmit's instrument. However, as it may be possible to make n_0 very large by a modification of the method of varying E which will be described later, its value could be chosen so that n for the ion being measured will be fairly close to an integer when M_0 is detected. The value n_0 for the reference mass M_0 can be measured experimentally, and the nearest whole number to n may be calculated from the approximate known value of the mass M. The experiment then determines the deviation of n from this whole number by measuring the difference in the arrival times of M_0 and M.

By changing the variation of E with time, the transit time could be increased; for instance, E might be kept at zero at the turning point (maximum value of y) for a period of time while the ions revolve in the magnetic field before increasing E in the negative direction to bring the ions back to the collector. With this technique, the extent of the magnetic field in the y direction may be decreased; in fact, if the variation in E is made in a time less than that for one cycle, a ring-shaped magnet could be used. The displacement of the ion beam might be effected by a small variation in the magnetic field although this compromises somewhat the perfect focusing condition.

The chief difficulties with this scheme appear to be the long ion path and the lack of focusing in the direction of the magnetic field. However, the possibility of detecting some of the ions after a fairly long transit time looks sufficiently promising to justify some exploratory experiments. Furthermore, it appears to be possible to incorporate weak axial focusing if E is kept at zero for an appreciable portion of the time.

A very attractive variation would be to decrease E to zero, allowing the ions to spin at the maximum y displacement of the moving coordinate system and subsequently displace them in a helical path by a weak electrostatic field in the direction of the magnetic field. With this arrangement, perfect focusing is obtained for all masses except for the small z dispersion which is unimportant since this is a time-of-flight device. Using the proton moment[3] to measure the value of the magnetic field, this device could be used to determine e/M (and from it the Faraday) with good accuracy since all measurements would involve only time. Preliminary plans have been completed for the construction of the equipment to do this.

[1] S. A. Goudsmit, Phys. Rev. **74**, 622 (1948).
[2] W. Bleakney and J. A. Hipple, Phys. Rev. **53**, 521 (1938).
[3] Thomas, Driscoll, and Hipple, Phys. Rev. **75**, 902 (1949).

Search for Stable Pd^{100}, W^{178}, and Pb^{202} *

Henry E. Duckworth, Robert F. Black, and Richard F. Woodcock
Scott Laboratory, Wesleyan University, Middletown, Connecticut
April 8, 1949

It has been pointed out[1] that the stability curve got by plotting the mass of the lightest isotope against atomic number shows marked linearity among the heavier elements of even atomic number. Since the breaks in such a stability curve must have significance in a precise theory of nuclear

forces, it is desirable to locate their position accurately. The breaks occurring at palladium, tungsten and lead have been checked by using the Wesleyan University mass spectrograph to search for certain unobserved isotopes of these elements, namely, Pd^{100}, W^{178} and Pb^{202}.

The isotopic constitution of palladium was determined by Dempster[2] in 1935 and an electrical measurement of the isotopic abundances was made by Sampson and Bleakney[3] in the following year. The faintest isotope, Pd^{102}, was found to have an abundance of 0.8 percent. In the present search for Pd^{100}, palladium ions were obtained from a high frequency spark between palladium electrodes. With an exposure of three hours no isotopes of palladium lighter than Pd^{102} were observed on the mass spectrum. On the other hand, Pd^{102} was clearly visible with an exposure of ten seconds. It is concluded that the hypothetical Pd^{100} exists to less than 0.0007 percent. The same limit of abundance can be assigned to Pd^{98}, Pd^{99} and Pd^{101}.

Tungsten is known to consist of five isotopes with mass numbers 180, 182, 183, 184 and 186. Of these, W^{180}, first observed by Dempster[4] in 1937, is much the rarest, constituting, according to Inghram,[5] 0.12 percent of normal tungsten. Although the hypothetical W^{178} has been shown by Inghram to exist to less than 0.002 percent, because of its unique position on the stability curve, a further search for it was made. Tungsten ions were obtained from a high frequency spark between two tungsten electrodes. An exposure of one minute showed the faint W^{180} while an exposure of two hours failed to reveal any isotopes lighter than this. It is concluded that the limit of abundance of W^{178} is 0.001 percent. Also, Inghram's limits of abundance can be lowered to 0.001 percent for both W^{179} and W^{181}.

Lead has four isotopes of which the lightest, Pb^{204}, is the least abundant, constituting, according to Nier,[6] 1.5 percent of normal lead. Using a spark between pure lead electrodes as a source of lead ions, a two-hour exposure failed to reveal any isotopes lighter than Pb^{204}. Pb^{204} itself was clearly visible with an exposure of one second. The limit of abundance of the hypothetical Pb^{202} is reckoned to be 0.0004 percent. The same limit holds for Pb^{203}, Pb^{201} and Pb^{200}.

On the basis of this search it seems reasonable to conclude that stable Pd^{100}, W^{178} and Pb^{202} do not exist. Such a conclusion permits the accurate location of three breaks in the above-mentioned stability curve.

The authors wish to thank Mr. Clifford Geiselbreth for his help in the making of electrodes.

* This letter is based on work done at Wesleyan University under Contract AT(30-1)-451 with the Atomic Energy Commission.

[1] H. E. Duckworth, Phys. Rev. **75**, 1438 (1949).
[2] A. J. Dempster, Nature **136**, 65 (1935).
[3] Milo B. Sampson and Walter Bleakney, Phys. Rev. **50**, 732 (1936).
[4] A. J. Dempster, Phys. Rev. **52**, 1074 (1937).
[5] M. G. Inghram, Phys. Rev. **70**, 653 (1946).
[6] A. O. Nier, J. Am. Chem. Soc. **60**, 1571 (1938).

Concentrating Holes and Electrons by Magnetic Fields

H. SUHL AND W. SHOCKLEY
Bell Telephone Laboratories, Murray Hill, New Jersey
March 24, 1949

IN the Hall effect for electrons alone or holes alone the carriers flow parallel to the specimen and the electric field has a transverse component. When both carriers are present, the net transverse current is zero due to compensating flows of holes and electrons to the same side. For low electric fields, recombination and generation keep the concentrations at their equilibrium values. Holes injected by transistor action at e in Fig. 1 were largely concentrated on one side of the germanium filament by virtue of the high electric fields ($\sim$20 v/cm) and small dimensions employed.

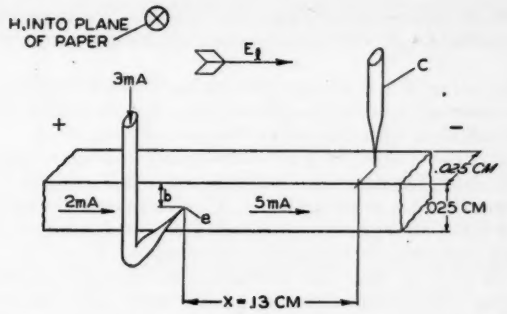

FIG. 1. Experimental arrangement of specimen, currents, and electric and magnetic fields.

The hole concentration at a distance x from the emitter was measured with the aid of a collector point c operated in the reverse direction so as to draw 10 μa. Figure 2 shows the conductance of this point *versus* H for the current conditions shown in Fig. 1. The conductance in excess of the value for $H=-20{,}000$ gauss is considered as proportional to hole concentration and is denoted by g on the left scale. Plus magnetic fields tend to concentrate holes on the collector side and the admittance rises; however, for $H>10{,}000$, the holes are concentrated near the surface and recombine with electrons on the surface so that the hole current decays before reaching c, and g decreases. For minus H, the holes are deflected away from c and g decreases monotonically.

The equations for p, the concentration of holes, are readily derived for: (1) hole concentration much less than electron concentration, (2) equal mobilities and concentrations for holes and electrons; in this case the space charges cancel, producing no transverse field. For (1) the transverse forces on the holes are approximated by a transverse electric field $E_2=E_l\sin(\theta_p+\theta_n)\cong E_l(\theta_p+\theta_n)$, where E_l is the longitudinal electric field $\theta_{p,n}=10^{-8}(R\sigma)_{p,n}H$ and $(R\sigma)_{n,p}=$mobility for electrons and holes ($\cong$1700 cm^2/v sec. for holes), and H is the magnetic field. (For (2), $E_2\cong E_l\theta_p$.) $\varphi=eE_2b/2kT\equiv KE_lH$, where $2b$ is the width of the filament, is a measure of the transverse concentration.

Recombination of holes with electrons on the surface of the filament takes place according to the law (component of hole flux normal to surface) $=s$ times (concentration of holes at the surface). For $H=0$ the concentration across the filament varies as $\cos\beta y$, where y is measured from the center and $\beta b\tan\beta b=sb/D\equiv\psi$, where $D=$diffusion constant.

For the following limiting cases, the values of p are:

for $\varphi\ll 1$	$p=1+\varphi+(\varphi/\psi)\sin^2\beta b$,
large $+H$, $\varphi>1$	$p_+=[(4\varphi/\psi)-2]\exp[-A\psi(2\varphi-1)]$,
large $-H$	$p_-=p_+[1-(\psi/\varphi)]\exp(2\psi-4\varphi)$,

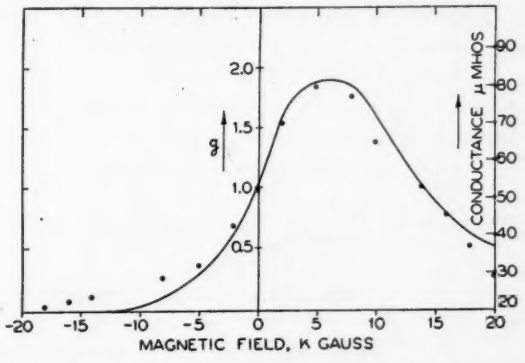

FIG. 2. Conductance of collector point, taken as measure of hole density, *versus* magnetic field.

where $A=(kTx/eE_1b^2)$. The curve of Fig. 2 corresponds to $A=2$, $\psi=0.43$, $K=10^{-5}$ cm/v gauss, assuming p proportional to g.

The value of s is about 1500 cm/sec., which implies that since thermal velocity is 10^7 cm/sec., a hole makes about 1500 collisions with the surface before being captured.

For H more negative than -8000 gauss, the curve does not fit the data. The difference is attributed to holes generated on the same surface as the collector. If these gave a contribution g_0 for $H=0$, they should contribute $g_0\psi/2\varphi$ for large negative H and thus give the hyperbolic tail observed.

It is evident that this technique, in addition to demonstrating concentration by magnetic fields and measuring surface recombination, can be used in the intrinsic range to measure ratios of holes to electrons and volume recombination constants.

The reduction of hole lifetime by strong magnetic fields accounts for large apparent magnetoresistive effects under conditions of hole injection.

We are indebted to G. L. Pearson whose development of and experiments with the filament technique suggested this experiment, and to J. R. Haynes and other colleagues at the Laboratories for many helpful suggestions.

Angular Correlations in Successive Nuclear α-γ-Emission and the Excited State of Li^7 *

BERNARD T. FELD
Physics Department and Laboratory for Nuclear Science and Engineering, Massachusetts Institute of Technology, Cambridge, Massachusetts
March 31, 1949

THE ~480-kev excited state of Li^7 has been observed in a variety of nuclear reactions.[1] Most of the data are consistent with the Li^7 level scheme (1) of Fig. 1. However, as pointed out by Inglis,[2] the α-particle branching, in the reaction $B^{10}(n,\alpha)Li^{7*}$, Li^7, is inconsistent with scheme (1); Inglis has suggested scheme (2), to explain this reaction.

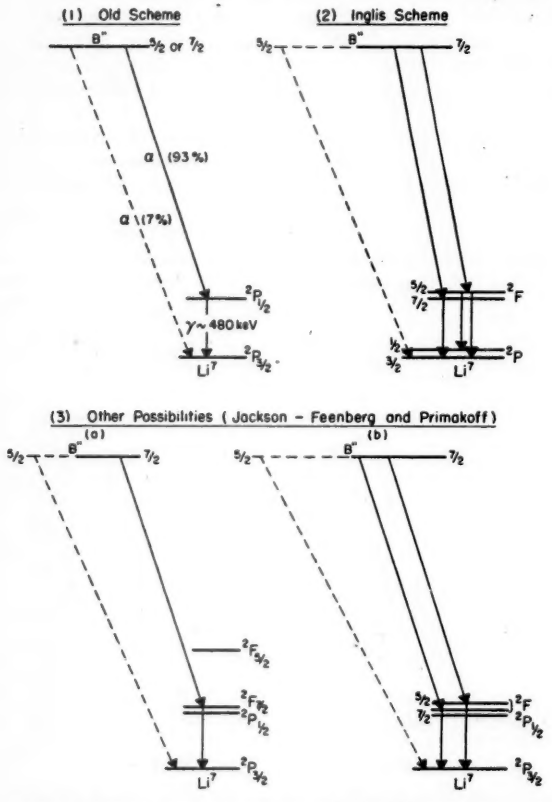

FIG. 1. Proposed level schemes for the $B^{10}(n,\alpha)Li^7$ reaction.

TABLE I. Theoretical angular correlations in successive α-γ-emission.

Initial (B^{11}) spin	α-particle angular momentum (L)	Intermediate (Li^{7*}) spin	γ-ray type	Final (Li^7) spin	$W(\theta)$
5/2 or 7/2	any	½	any	3/2	1
7/2	1	7/2	El. Quad.	3/2	$1-0.508\cos^2\theta$
7/2	1	5/2	El. Quad.	3/2	$1+0.079\cos^2\theta$
7/2	1	5/2	El. Quad.	1/2	$1+0.231\cos^2\theta$
7/2	1	5/2	El. Quad.	3/2 or 1/2	$1+0.197\cos^2\theta$
7/2	1	5/2	Mag. Dip.	3/2	$1-0.143\cos^2\theta$

Scheme (2) is, however, incapable of explaining the observed (~10 percent) branching in the Be^7 (K capure) Li^{7*}, Li^7 disintegration.[3] Scheme (3a) of Fig. 1, suggested by J. D. Jackson and by E. Feenberg and H. Primakoff,[4] has the advantage that it is consistent with the observations in both of the aforementioned reactions; scheme (3b), while less likely, is also consistent. However, these schemes depend on a fortuitous near-degeneracy of a number of levels.

It is the purpose of this note to suggest a method for distinguishing between the various suggested level schemes. Since the lifetime of the Li^{7*} state produced by the (thermal neutron) $B^{10}(n,\alpha)$ reaction is short ($<2\times10^{-13}$ sec.),[5] compared to the period associated with the Li^7 hyperfine structure splitting ($\sim10^{-9}$ sec.),[6] the angular correlation between the directions of emission of the short-range α-particle (by B^{11}) and the ~480-kev γ-ray (by Li^{7*}), should depend on the spins of the states involved and on the angular momentum properties of the α-particle and γ-ray. Table I summarizes the expected angular correlations for the various possibilities shown in Fig. 1. $W(\theta)$ represents the relative number (per unit solid angle) of γ-rays emitted at an angle θ with respect to the preceding α-particle. The angular correlations were computed by the method of Hamilton,[7] suitably modified to take into account that the first particle emitted is an α-particle.

Of the schemes shown in Fig. 1, only (1) and (3a) lead to unambiguous answers. Scheme (1)—$^2P_{\frac{1}{2}}$ excited state—leads to $W(\theta)=1$, irrespective of the properties of the other two states or of the nature of the emitted particles, because of the symmetry associated with the spin ½. Scheme (3a) results in a large angular correlation, with $W(0)/W(\pi/2)=0.492$, which should be easily observable.

The correlations for schemes (2) and (3b) depend on the relative branching of the α-particles to the two states of the F doublet. The branching of the γ-rays from the $^2F_{5/2}$ state to the P doublet (scheme 2) is uniquely determined by the properties of these states and the "sum rule";[8] the effect of this branching is shown in the last row of Table I. However, because the nature of the B^{11} state is not uniquely determined, the α-particle branching cannot be decided on purely theoretical grounds. Assuming relative probabilities of a and $(1-a)$, respectively, for the $7/2\rightarrow5/2$ and $7/2\rightarrow7/2$ transitions, we obtain

$$W(\theta)=1+(0.705a-0.508)\cos^2\theta, \text{ for scheme (2),}$$

and

$$W(\theta)=1+(0.587a-0.508)\cos^2\theta, \text{ for scheme (3b).}$$

Unfortunately, both of these possibilities lead to small angular correlations over certain ranges of values of a. If a difference of less than 10 percent between the correlations at angles 0 and $\pi/2$ were unobservable, the ranges $a=0.58-0.86$ for scheme (2) and $a=0.7-1.0$ for scheme (3b) would lead to apparent spherical symmetry. However, over most of the range of possible values of a, the angular correlation is easily observable.

Experiments are now under way at this laboratory to measure the α-γ-angular correlation in the $B^{10}(n,\alpha)Li^{7*}$ reaction. The α-particles are detected in a proportional

counter having a thin B^{10} deposit on one of the plates; the γ-rays are detected in a scintillation counter, the position of which can be changed relative to the direction of the emitted α-particles.

* Assisted by the joint program of the ONR and the AEC.

[1] W. F. Hornyak and T. Lauritsen, Rev. Mod. Phys. **20**, 191 (1948): See also, Zaffarano, Kern, and Mitchell, Phys. Rev. **74**, 105 (1948); F. N. D. Kurie and M. Ter-Pergossian, Phys. Rev. **74**, 677 (1948); Buechner. Strait, Stergeopoulos, and Sperduto, Phys. Rev. **74**, 1569 (1948); L. G. Elliott and R. E. Bell, Phys. Rev. **74**, 1869 (1948); Rasmussen, Lauritsen, and Lauritsen, Phys. Rev. **75**, 199 (1949).
[2] David R. Inglis, Phys. Rev. **74**, 1876 (1948).
[3] Rumbaugh, Roberts, and Hafstad, Phys. Rev. **54**, 657 (1938).
[4] Private communications.
[5] L. G. Elliott and R. E. Bell, Phys. Rev. **74**, 1869 (1948).
[6] Kusch, Millman, and Rabi, Phys. Rev. **57**, 765 (1940).
[7] Donald R. Hamilton, Phys. Rev. **58**, 122 (1940).
[8] E. U. Condon and G. H. Shortley, *Theory of Atomic Spectra* (Cambridge University Press, London, 1935), pp. 238, 241–243, 253.

Stars Built on the Shell Source Model

CHUSHIRO HAYASHI
Department of Cosmophysics, Kyoto University, Kyoto, Japan
March 28, 1949

PREVIOUSLY, it was shown[1] that C–N reactions can also explain the energy generation of the two well-known giant stars, Capella A and ζ Aurigae K, if they are built on the Gamow shell-source model,[2] and that in their envelopes the hydrogen content must be $\sim$35 percent by weight if helium is neglected. Based on this chemical composition and the C–N reactions, possible structures of stars, which have given masses, 8 $M_\odot$ and $M_\odot$, but dehydrogenized isothermal cores of various masses have been investigated.

Under widely different assumptions as to luminosity, L, and radius, R, the usual four equations of stellar equilibrium[3] for p (pressure), T (temperature), $M(r)$ (mass inside the radius r), and $L(r)$ (energy flow across the surface of radius r) are numerically integrated inward. The following assumptions are made: In the envelopes the hydrogen content is 35 percent and the remainder is a Russell mixture which contains 1 percent of carbon and nitrogen, while in the cores hydrogen is replaced by helium; for the mean molecular weight, μ, and the opacity, values tabulated by Strömgren[4] and Morse[5] are used; in the convective regions, temperature gradients are given by the formula of an adiabatic change of matter and radiation.[3]

Values of p, T, and $M(r)$ at the points where $L(r)$ vanishes are compared with those of the Emden solutions of the isothermal cores. Here, it is convenient to use the functions U, V, and ψ (measure of electron degeneracy), which determine the core's solutions apart from the homologous transformations, defined by

$$U=4\pi r^3\rho/M(r), \quad V=GM(r)\rho/rp_g,$$

$$\rho/\mu_e m_H=(4\pi/h^3)(2m_e kT)^{\frac{3}{2}}\int_0^\infty u^{\frac{1}{2}}[\exp(-\psi+u)+1]^{-1}du,$$

where ρ, p_g, and μ_e are density, gas pressure, and mean molecular weight of the electron, respectively. In our case, suitable conditions for the outer and inner solutions are given by the continuity of U/μ, V/μ, and $\psi+\log_e(\mu_e/\mu)$. Appropriate solutions thus obtained by interpolation determine L, R, and internal conditions of stars in a series of one parameter ψ_c, the value of ψ at the center.

The results are similar for the two masses as shown in Figs. 1 and 2. Calculated ranges of ψ_c are from -5.4 to $+23.3$ for 8 $M_\odot$ and from -2.3 to $+11.5$ for $M_\odot$. They correspond to slight increases of the core's temperatures, from 3.5×10^7 to 5.2×10^7 °K for 8 $M_\odot$ and from 2.1×10^7 to 2.4×10^7 °K for $M_\odot$, and large increases of the central densities, from 10 to 5.1×10^5 g/cm³ for 8 $M_\odot$ and from 1.5×10^2 to 5.5×10^4 g/cm³ for $M_\odot$. For minimum values of ψ_c, the core's masses M^* are nearly zero and the stars lie within the main sequence. L and R increase with ψ_c when $\psi_c<0$ (perfect gas state), and then

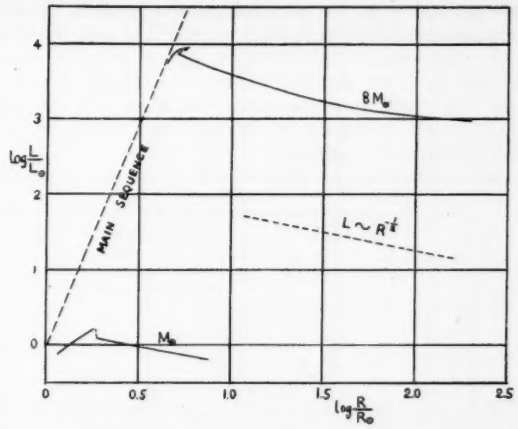

FIG. 1. Luminosity-radius relations for stars of masses, 8 $M_\odot$ and $M_\odot$.

change abruptly when $\psi_c\simeq0$ (incipient degeneracy). Further increases of ψ_c (strong degeneracy) give rapid increases of R, while increases of M^* are relatively small and consequently the Eddington's relation $L\sim R^{-1}$ is approximately satisfied. Together with the earlier results,[1] these will give the general features of giants of any mass. Further, from their observed distribution and the above smallness of changes in M^*, the co-existence of many invisible stars of still larger R may be expected. The small variations of L over the entire range of R will explain the empirical mass-luminosity relation on the basis of the same chemical composition.

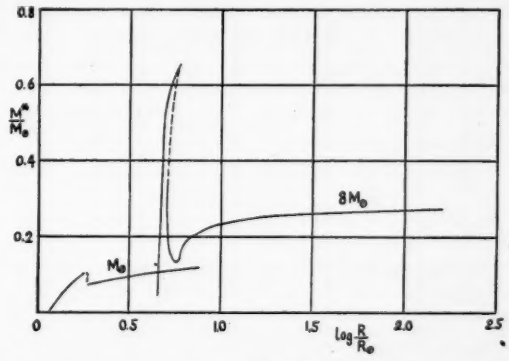

FIG. 2. Relations between the radii and the core's masses of the stars.

The author wishes to express his deep gratitude to Professor H. Yukawa for his continued interest in this work.

[1] C. Hayashi, Prog. Theor. Phys. **2**, 127 (1947).
[2] G. Gamow, Phys. Rev. **67**, 120 (1945); G. Gamow and G. Keller, Rev. Mod. Phys. **17**, 125 (1945).
[3] See, for example: S. Chandrasekhar, *An Introduction to the Study of Stellar Structure* (University of Chicago Press, Chicago, 1939).
[4] B. Strömgren, Zeits. f. Astrophys. **7**, 22 (1931).
[5] P. M. Morse, Astrophys. J. **92**, 27 (1940).

Discrepancies between Physically and Chemically Determined Atomic Weights for the Elements between Silver 47 and Iodine 53

J. R. WHITE AND J. H. BUCK
Research and Development Department, Socony-Vacuum Laboratories, Paulsboro, New Jersey
March 16, 1949

THIS letter describes an observation which may prove only an interesting error coincidence. In the region of the periodic table between silver 47 and iodine 53 all available physical data lead to higher chemical atomic weights than accepted chemical data. A deviation curve for the atomic

weights derived from the two independent sources possesses a maximum coincident with mass number 115 and coincident with the unexplained minimum in abundances of isotope species derived from uranium fission. One possible resolution of these discrepancies requires the postulate of a presently excluded second minimum in the packing fraction curve of naturally distributed isotopes.

Precise, natural isotopic distributions have been determined for each of the elements from silver 47 to iodine 53. Two, remote observers are in essential accord in assigning isotopic distributions for the elements, silver 47, cadmium 48, indium 49, and tellurium 52. One observer has contributed the abundance assignments for tin 50 and antimony 51. Additionally, there are older mass spectrographic determinations involving photometry of a photographic plate whose precision does not warrant their being given equal weight in this consideration, but which, for non-complex elements, are in fair accord with recent work.

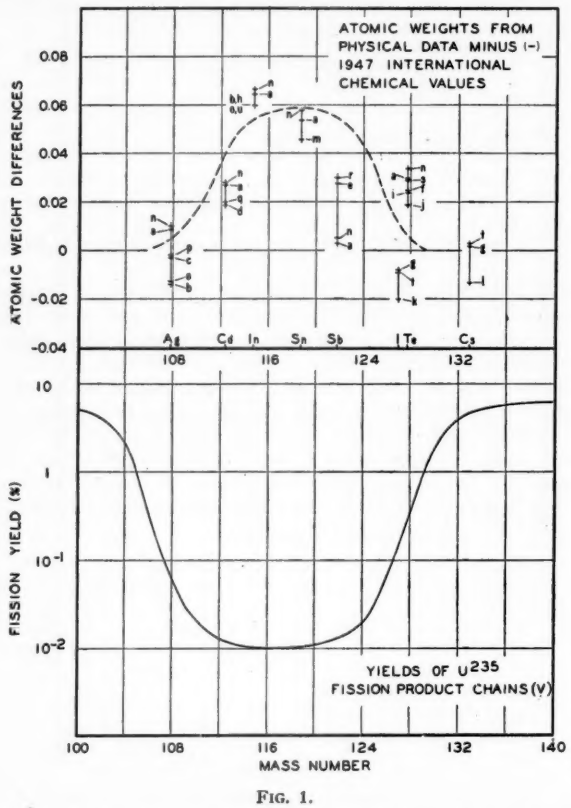

FIG. 1.

[a] Packing fraction from Flügge and Mattauch's adjusted table, Physik. Zeits. **44**, 181 (1943); abundances from White and Cameron, Phys. Rev. **74**, 991 (1948).
[b] Packing fraction from Flügge and Mattauch, reference a; abundances from Aston, Nature **133**, 684 (1934); Proc. Roy. Soc. **A149**, 396 (1935).
[c] Packing fraction from Flügge and Mattauch, reference a; abundances from Paul, Naturwiss. **31**, 419 (1943).
[d] Packing fraction from Flügge and Mattauch, reference a; abundances from Nier, Phys. Rev. **73**, 1206 (1948).
[e] Packing fraction from Flügge and Mattauch, reference a; abundances from Aston, Proc. Roy. Soc. **A132**, 492 (1931).
[f] Packing fraction from Flügge and Mattauch, reference a; abundances from Williams and Yuster, Phys. Rev. **69**, 556 (1946).
[g] Packing fraction from Flügge and Mattauch, reference a; singly isotopic.
[h] Packing fraction from Flügge and Mattauch, reference a; abundances from Sampson and Bleakney, Phys. Rev. **50**, 456 (1936).
[i] Packing fraction from Aston, Proc. Roy. Soc. **A132**, 487 (1931); abundances from White and Cameron, reference a.
[j] Packing fraction from Aston, reference i; abundances from Williams and Yuster, reference f.
[k] Packing fraction from Aston, Proc. Roy. Soc. **A115**, 487 (1927); singly isotopic.
[l] Packing fraction from Aston, Proc. Roy. Soc. **A134**, 574 (1931); singly isotopic.
[m] Packing fraction from Aston, Proc. Roy. Soc. **A163**, 391 (1937); abundances from White and Cameron, reference a.
[n] Packing fraction from Dempster, Phys. Rev. **53**, 869 (1938); abundances from White and Cameron, reference a.
[o] Packing fraction from Dempster, reference n; abundances from Aston, reference b.
[p] Packing fraction from Dempster, reference n; abundances from Paul, reference c.
[q] Packing fraction from Dempster, reference n; abundances from Nier, reference d.
[r] Packing fraction from Dempster, reference n; abundances from Aston, reference e.
[s] Packing fraction from Dempster, reference n; abundances from Williams and Yuster, reference f.
[t] Packing fraction from Dempster, reference n; singly isotopic.
[u] Packing fraction from Dempster, reference n; abundances from Sampson and Bleakney, reference h.
[v] The Plutonium Project, Rev. Mod. Phys. **18**, 513 (1946).

The abundance assignments for each element and each observer have been combined with packing fractions, either measured directly by Dempster, Graves, Aston and Flügge and Mattauch or interpolated from their curves, to enable computation of chemical atomic weights. In these computations a physical to chemical scale conversion factor of 1.000275 has been employed. These computed chemical weights have then been compared with International Chemical weights determined by chemical means; the differences (chemical weights computed from physical data—International Chemical values) have been plotted against the chemical weights as in Fig. 1. While the shape of this curve may be questioned; a positive deviation from the expected scattering about the ordinate zero is not anticipated. A more interesting coincidence is evident when the yields of U^{235} fission product chains are plotted on the same abscissa.

Resolution of the deviation curve of Fig. 1 by packing fraction reassignment will require that a second sharp minimum appear in the packing fraction curve in a manner to coincide with mass 115 and the minimum in the yield of U^{235} fission product chains. Present packing fraction assignments exclude such a minimum.

It appears that the discrepancies in atomic weights here described should be resolved by reexamination of chemical data or physical data, or both.

The Forces between Ammonia Molecules and the Second Virial Coefficient for Ammonia

VERNON MYERS
Department of Physics, Pennsylvania State College, State College, Pennsylvania
April 8, 1949

STOCKMAYER[1] has calculated the second virial coefficient for ammonia on the basis of a point dipole model; however such a model was shown to be inadequate for water.[2] The author has included the quadrupole moment in the computation of the long range attractive forces. The ratio of the quadrupole term to the dipole term for NH_3 was assumed to be the same as that for H_2O.[2] This assumption may be somewhat in error, but it seems more reasonable than the extreme one of point dipoles. The dipole moment for ammonia was taken to be $1.48 \cdot 10^{-18}$ e.s.u.[3] Optical dispersion data[4] yield a static polarizability of $2.15 \cdot 10^{-24}$ cm^3, an oscillator strength of 2.72, and a resonance energy of 11.8 ev. Making use of the notation of reference (2):

Alignment effect, $V = -(1.37/R^3 + 3.31/R^5) f(\theta_1, \theta_2, \phi)$ ev (R in A).
Induction effect, $V = -(5.9/R^6 + 14/R^8)$ ev.
Dispersion effect, $V = -(40.9/R^6 + 133/R^8)$ ev.

TABLE I. A comparison of the experimental and theoretical second virial coefficients for ammonia.

Temp. °K	Classical virial cm³/mole	Quantum correction cm³/mol	Theoretical virial cm³/mol	Experimental virial cm³/mol	Percent difference
300	−315	9	−306	−270	−13.3
400	−124	2	−122	−119	−2.5
500	−65.0	0.7	−64.3	−66.6	3.5
600	−37.0	0.4	−36.6	−40.6	9.9

The short range repulsive forces were approximated by a hard sphere model. The molecular diameter was chosen so as to give the best agreement between the observed and calculated second virial coefficients in the temperature interval from 300°K to 600°K. The following intermolecular potential was used:

$$V=\begin{cases}\infty \text{ if } R<3.16\text{A},\\ -(1.37/R^3+3.31/R^5)f(\theta_1,\theta_2,\phi)-(46.8/R^6+147/R^8)\text{ ev.}\\ \qquad\qquad \text{if } R>3.16\text{A}.\end{cases}$$

In the computation of the second virial coefficient, the quantum correction due to the exchange gf energy between the translational and rotational motions must be included. This correction was taken into account using Kirkwood's method.[5] Table I shows the results. The measured values for the second virial coefficient are those of Keyes.[6] Better agreement with experiment could probably be obtained if a repulsive potential of the form $A\exp-(R/b)$ were introduced, however this was not considered to be worth while in view of the uncertainty in regard to the estimation of the quadrupole effect.

[1] Walter H. Stockmayer, J. Chem. Phys. **9**, 398 (1941).
[2] H. A. Margenau and V. W. Myers, Phys. Rev. **66**, 307 (1944).
[3] H. H. Uhlig, J. G. Kirkwood, and F. G. Keyes, J. Chem. Phys. **1**, 155 (1933).
[4] K. L. Wolf and K. F. Herzfeld, *Handbuch der Physik* (Verlag. Julius Springer, Berlin, 1928).
[5] John G. Kirkwood, J. Chem. Phys. **1**, 597 (1933).
[6] Frederick G. Keyes, J. Am. Chem. Soc. **60**, 1761 (1938).

Solid Solubility Effect of Metallic Surface Friction

KWAI UMEDA AND YOSHIHIRO NAKANO
Department of Physics, Faculty of Science, Hokkaido University, Sapporo, Japan
March 17, 1949

ON improving the "Bowden method,"[1] we have obtained the following temperature dependence of the surface friction coefficient μ for a number of metal pairs.

At first for the pair of the same metal, μ remains nearly constant with temperature θ until it vanishes suddenly at the melting point of the metal.

For a pair of different metals, we had expected that μ would vanish probably at the lower of the melting points of the component metals. In reality, if the metal pair is of a limited solubility type (a typical example is Sn-Pb, Fig. 1),

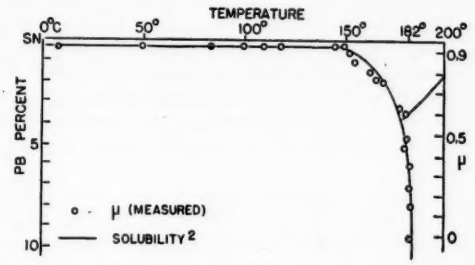

FIG. 1.

μ vanishes at neither of the melting points (Sn: 232°C, Pb: 327°C) but at a far lower temperature (182°C), which coincides well with the eutectic point of the binary system. At this temperature a liquid state can be observed along the rubbed trace. This indicates the formation of the eutectic alloy at the friction boundary, and supports Bowden's "local melting theory." Further the full course of the friction coefficient *vs.* temperature curve is so similar to the solubility *vs.* temperature curve on the side of the lower melting point metal in the binary alloy phase-diagram, that an empirical

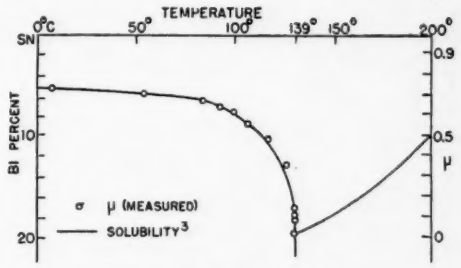

FIG. 2.

linear relation is found to hold:

$$\mu_\theta=(\alpha_{\text{eutec}}-\alpha_\theta)/k. \qquad (1)$$

The quantity k, quite remarkably, is found to have a constant value 10, if α is the solubility of the metal of lower melting point expressed in weight percentage; however, when Bi is a component, k has the exceptional value of 20, when α the solubility of Bi is taken, no matter what the other component may be. A typical example is Bi-Sn, Fig. 2. Data from many metal pairs which were examined are collected in Table I.

TABLE I. Temperature of vanishing friction coefficient and value of coefficient k in Eq. (1) for several metal pairs of limited solubility.

Metal pair	Lower melt. pt.	Eutec. pt.	Temp. $\mu=0$	k for weight %	k for atomic %
Sn–Pb	232°C	182°C	182°C	10	5.9
Sn–Bi	232	139	139	20	12
Sn–Cd	232	182	182	10	10.4
Sn–Zn	232	199	199	10	10
Sn–Tl	232	170	170	10	10
Bi–Pb	271	125	125	20	20
Bi–Cd	271	148	148	*	*
Bi–Zn	271	254	254	*	*
Tl–Cd	302	204	204	10	10
Cd–Pb	321	247	247	10	10
Cd–Zn	321	255	255	10	16.5
Pb–Sb	327	258	291**	10	16.5

* Solubility is too small to determine the value of k.
** This coincides with the knick point of the solidus line.

For the simple eutectic systems (Sn-Ag, Sn-Al, Sn-Zn, Pb-Ag, and Cd-Bi are examined), the systems with intermetallic compound (Sn-Mg_2Sn, Pb-Mg_2Pb, and $MgZn_2$-$MgZn_5$) and the systems with many intermediate phases (In-Ag, In-Cu, Zn-Ag, Zn-Cu, Cd-Ag, and Sn-Sb), the feature is essentially similar. It is also for pairs with solidified mercury (Hg-Tl, Hg-Rb, and Hg-Te) slightly observable.

We should like to call the correspondence between the friction coefficient and the solid solubility, here observed, the "solid solubility effect" of the metallic surface friction. This effect also gives a guiding suggestion to the determination of the phase-diagram of binary alloy, for example to the existence of the minute solubility or to the preference of the exact solubility curve.

Full results will be published soon in the Journal of the Faculty of Science of Hokkaido University of Japan.

[1] F. P. Bowden, Proc. Roy. Soc. London **169**, 371 (1939).
[2] K. Honda and H. Abe, Sci. Rep. Tōhoku Univ. Japan **19**, 315 (1939).
[3] Y. Matsunashi and T. Satō, J. Japan Inst. Metal **2**, 596 (1938).

The Electron Spectrum of Iodine[131]

J. M. CORK, H. B. KELLER, J. SAZYNSKI, W. C. RUTLEDGE, AND A. E. STODDARD
University of Michigan, Ann Arbor, Michigan
March 25, 1949

BECAUSE of its extensive use in medicine, the radioactivity of iodine 131 is of interest. Several reports have appeared recently[1–5] giving the energies of the gamma-rays of this isotope. Three of these investigations employed electron

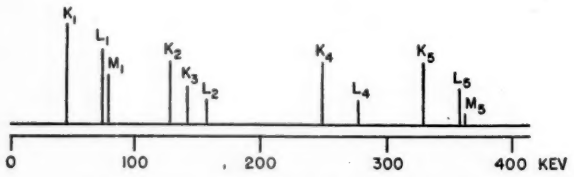

FIG. 1. Energy of the electron lines from iodine 131.

lens spectrometers with their accompanying low resolving power to evaluate the energy of the conversion electrons. J. DuMond and associates[4] have observed the unconverted gamma-rays in a crystal spectrometer and report energies of 80.13, 284.13, and 364.18 kev. We had, by means of photographic spectrometers, observed these and other gamma-rays with good relative precision but, due to the uncertainty in the absolute value of the magnetic field, entertained some doubt of the absolute accuracy. It is of interest to note that our previously published values for the strong higher energy lines were reported[3] as 284.8 and 365.0 kev, values consistently slightly greater than those of DuMond. It is now possible to calibrate the magnetic fields in an absolute manner in terms of DuMond's energies.

The complete electron spectrum as now obtained from carrier-free specimens procured from Oak Ridge is shown in Fig. 1, and the energies are collected in Table I. This shows

TABLE I. The electron spectrum of iodine 131.

Observed line	Identification	Gamma-energy
45.6 kev	K_1	80.1 kev
74.7	L_1	80.1
79.0	M_1	80.1
129.1	K_2	163.6
142.5	K_3	177.0
158.2	L_2	163.6
249.6	K_4	284.1
278.7	L_4	284.1
329.7	K_5	364.2
358.8	L_5	364.2
363.1	M_5	364.2

clearly four electron line sets with energy differences characteristic of xenon. A single additional electron line at 142.5 kev is interpreted as a K line. In all, there are five gamma-rays whose energies are 80.1, 163.6, 177.0, 284.1, and 364.2 kev.

A higher energy line was observed with less accuracy by absorption in lead. This had been reported by Deutsch as having an energy of 638 kev. It is now possible to propose a satisfactory level scheme incorporating the new lines, as shown in Fig. 2, provided both the lower energy beta-limit and the high energy gamma-ray are less energetic than reported by

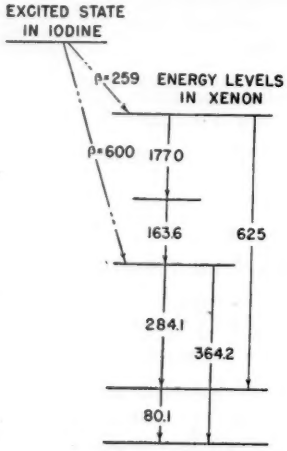

FIG. 2. A possible level scheme associated with iodine 131.

Deutsch. On observing the curves as presented this would seem to be not impossible.

This investigation was supported jointly by the AEC and the ONR.

[1] M. Deutsch and E. Metzger, Phys. Rev. **74**, 1640 (1948).
[2] Owen, Moe, and Cook, Phys. Rev. **74**, 1879 (1948).
[3] J. M. Cork, Nucleonics **4**, 24 (1949).
[4] Lind, Brown, Klein, Muller, and DuMond, Phys. Rev. **75**, 1633 (1949).
[5] Zaffarano, Mitchell, and Kern, Phys. Rev. **75**, 1632 (1949).

Microwave Absorption of Some Organic Vapors

BÖRGE BAK, ERIK STENBERG KNUDSEN, AND ERHARDT MADSEN
Department of Chemistry, University of Copenhagen, Denmark
April 4, 1949

A MICROWAVE spectrograph for the 1.25-cm region has been built. The Hughes-Wilson technique[1] was applied. The klystron is a frequency-modulated 2K33 which radiates in the 22,600–25,700-mc region. Unfortunately, the coverage is not total, as the klystron is of a somewhat deteriorated war-surplus quality. The regions 24320–24270, 22860–22820 plus smaller, scattered regions are generally inaccessible. The gas cell is a 3-m K-band wave guide, vacuum-tight sealed by mica windows and placed with the broad side downwards. The modulation electrode is placed on the bottom of the cell, insulated from the guide by paper. It is kept straight by two weights placed outside the cell and connected with the electrode by violin strings, carried vacuum-tight through the mica windows. To ensure that the electrode follows the bottom of the guide, the latter is placed in a slightly curved position. The distance electrode-upper wave guide wall seems to be quite constant judging from the sharpness of e.g., the cos line at 24326 mc. This electrode has the advantage of being easy to place but the cell-electrode capacity is high, which gives rise to trouble in the construction of a stable square-wave generator, desirable as modulator element. So far, a d.c. voltage between 50 and 300 volts, superimposed by a sine wave with amplitude ±40 volts and frequency 0.22–0.24 mc, has been used. The narrow band communication receiver (~2 kc) following the 1N26 crystal is tuned to the frequency of the sine oscillator. The radio output, after passing an RC-filter, is displayed on an oscilloscope screen and simultaneously listened to via a loudspeaker. Signals, indicating absorption, are easily distinguished from the different types of noise in the way they look and sound, and in that they disappear when the sine oscillator is interrupted. Wavelengths are measured by a wave meter of the absorption type calibrated against NH_3, all the lines of which were quoted in literature[2] in the 22600–25700-mc region were observed, as were the lines of BrCN,[3] and cos.[3] Our wave-length measuring technique seems good to ±5 mc, which is rather poor in these days. While a suitable frequency-measuring system is being constructed, we have investigated a number of organic gases to get an impression of the possibilities of the microwave technique.

Organic vapors hitherto investigated are CH_3OH,[4–6] CH_3NH_2,[5] CH_3Cl, CH_3Br, CH_3J,[7] CH_3CN,[8] CH_3NC,[8] CH_3NO_2,[6] and $(CH_2)_2O$.[9,10] More organic vapors were tried by us. In the case of acetaldehyde, acetic acid, dimethyl and diethyl-ether, nitrobenzene, pyridin, anilin, furan, and methyl-eneiodide, no absorption was found. Our positive results are:

C_6H_5Br (bromobenzene; gas pressure 0.3 mm, Stark d.c. voltage 100) 23742–23690–[22050] mc.

C_2H_5OH (ethyl alcohol; pressure 0.16 mm, d.c. voltage 120) 25069–24385–24369–24295–23605–23555–23148–23081–22820 mc.

$(CH_3)_2CO$ (acetone; pressure 0.19 mm, d.c. voltage 100) 24758–24691–24646–24102–23934–23839–23827–23793–23778–23749–23661–23603–23339–22940–[22560]–[22500]–[22410] mc.

CH_3NO_2 (nitromethane; pressure 0.07 mm, d.c. voltage 125) 25412–25391(25400)–24599(24603)–24448–(24320)–24428–24017(24047)–23706–23483–23467–23330–(23250)–23021–[22620]–[22580]–[21970] mc.

CH_3OH (methyl alcohol; pressure 0.1 mm, d.c. voltage 50) 25349–25332–25312–(25300)–25289–25151–25131(25132)–25110–25038(25050)–25021(25018)–24997–24977–24960 (24954)–24928(24929)–24913–24901–(24317–24081–24040)–23857(23861)–23457(23450)–(23415)–23122(23121) mc.

Numbers in square brackets are very roughly estimated values, numbers in parenthesis are from reference 6. The substances used were of high purity. Spectra of probable contaminations were investigated.

[1] R. H. Hughes and E. B. Wilson, Jr., Phys. Rev. **71**, 562 (1947).
[2] W. E. Good and D. K. Coles, Phys. Rev. **71**, 385 (1947).
[3] Townes, Holden, and Merritt, Phys. Rev. **74**, 1113 (1948).
[4] Donald K. Coles, Phys. Rev. **74**, 1194 (1948).
[5] W. D. Hershberger and J. Turkevich, Phys. Rev. **71**, 554 (1947).
[6] B. P. Dailey and E. B. Wilson, Jr., Phys. Rev. **72**, 522 (1947).
[7] Simmons, Gordy, and Smith, Phys. Rev. **74**, 1246 (1948).
[8] Ring, Edwards, Kessler, and Gordy, Phys. Rev. **72**, 1269 (1947).
[9] Shulman, Dailey, and Townes, Phys. Rev. **74**, 846 (1948).
[10] Cunningham, Le Van, and Gwinn, Phys. Rev. **74**, 1537 (1948).

On the External Polarization of the Vacuum

HARTLAND S. SNYDER*
Brookhaven National Laboratory, Upton, Long Island, New York

April 4, 1949

WE consider here the motion of an electron (positron) in an arbitrary external electromagnetic field determined by the potentials $\phi(\mathbf{r}, t)$, $\mathbf{A}(\mathbf{r}, t)$. The equation of motion for the electron-positron field is

$$i\hbar(\partial\psi/\partial t) = \{-\boldsymbol{\alpha}\cdot[i\hbar\boldsymbol{\nabla} + (e/c)\mathbf{A}]c + mc^2\beta + e\phi\}\psi. \quad (1)$$

We denote by $U_k(\mathbf{r}, t, t_0)$ solutions of (1) which reduce to plane waves on the surface $t=t_0$. The solutions $U_k(\mathbf{r}, t, t_0)$ will then form a complete orthogonal set of function. For convenience in writing, we will also treat these solutions as if they could be normalized to unity. We now split the solutions $U_k(\mathbf{r}, t, t_0)$ into two sets $U_{k+}(\mathbf{r}, t, t_0)$ and $U_{k-}(\mathbf{r}, t, t_0)$, which are defined so that $H_0U_k(\mathbf{r}, t_0, t_0) = \epsilon_k U_k(\mathbf{r}, t_0, t_0)$ with $H_0 = -i\hbar c\boldsymbol{\alpha}\cdot\boldsymbol{\nabla} + mc^2\beta$ has $\epsilon_{k+} > 0$ and $\epsilon_{k-} < 0$. The general solution of (1) may now be written

$$\psi = \Sigma a_k U_k(\mathbf{r}, t, t_0), \quad (2)$$

in which the operators a_k are independent of time. If the field, ψ, is Fermi quantized, then the a_k and a_k^* satisfy the anti-commutation relations $[a_k, a_{k'}]_+ = 0$, $[a_k, a_{k'}^*]_+ = \delta_{kk'}$. We now define charge density and current density operators by

$$\begin{aligned}\rho(\mathbf{r}, t, t_0) = {} & \Sigma a_{k+}^* a_{k'+} U_{k+}^*(\mathbf{r}, t, t_0) U_{k'+}(\mathbf{r}, t, t_0) \\ & + \Sigma a_{k+}^* a_{k'-} U_{k+}^*(\mathbf{r}, t, t_0) U_{k'-}(\mathbf{r}, t, t_0) \\ & + \Sigma a_{k-}^* a_{k'+} U_{k-}^*(\mathbf{r}, t, t_0) U_{k'+}(\mathbf{r}, t, t_0) \\ & - \Sigma a_{k'-} a_{k-}^* U_{k-}^*(\mathbf{r}, t, t_0) U_{k'-}(\mathbf{r}, t, t_0).\end{aligned} \quad (3)$$

$$\begin{aligned}\mathbf{S}(\mathbf{r}, t, t_0) = {} & \Sigma a_{k+}^* a_{k'+} U_{k+}^*(\mathbf{r}, t, t_0)\boldsymbol{\alpha} U_{k'+}(\mathbf{r}, t, t_0) \\ & + \Sigma a_{k+}^* a_{k'-} U_{k+}^*(\mathbf{r}, t, t_0)\boldsymbol{\alpha} U_{k'-}(\mathbf{r}, t, t_0) \\ & + \Sigma a_{k-}^* a_{k'+} U_{k-}^*(\mathbf{r}, t, t_0)\boldsymbol{\alpha} U_{k'+}(\mathbf{r}, t, t_0) \\ & - \Sigma a_{k'-} a_{k-}^* U_{k-}^*(\mathbf{r}, t, t_0)\boldsymbol{\alpha} U_{k'-}(\mathbf{r}, t, t_0).\end{aligned}$$

The charge and current density operators as defined by (3) are obviously gauge invariant. They, at least formally, transform covariantly under Lorentz transformations. If we define the vacuum, as was done by Schwinger,[1] by the condition that the states $U_{k+}(\mathbf{r}, t, t_0)$ are empty and the states $U_{k-}(\mathbf{r}, t, t_0)$ are full as $t_0 \to -\infty$, then the a_{k+} are annihilation operators for electrons and the a_{k-} are creation operators for positrons. If we take the state in which there are no positrons or electrons present at $t=t_0$, then the expectation values $\langle\rho(\mathbf{r}, t, t_0)\rangle = 0$ and $\langle\mathbf{S}(\mathbf{r}, t, t_0)\rangle = 0$. The above expectation values are independent of t and t_0. We have thus obtained a result which is in disagreement with the infinite results of Schwinger and others. The result we have here obtained is an exact consequence of the equations of motion (1) and of the initial conditions used. We thus see that the problem of positron-electron field in a given external field is not a dynamical problem, it is entirely the problem of the appropriate definition of which states are electron states and which states are positron states.

* Research carried out at Brookhaven National Laboratory, Upton, Long Island, under the auspices of the AEC.
[1] Julian Schwinger, Phys. Rev. **75**, 651 (1949).

Proceedings of the American Physical Society

MINUTES OF THE MEETING AT CLEVELAND, MARCH 10–12, 1949

THE 291st meeting of the American Physical Society was held on Thursday, Friday, and Saturday, March 10, 11, and 12, 1949, in the buildings of the Western Reserve University and the Case Institute of Technology. By inserting a meeting in March into our seasonal schedule, we returned approximately to the prewar system under which a meeting toward the end of February was interpolated between the Winter and Spring Conventions. This was a very agreeable and successful meeting of moderate size (257 registrants) and leisurely pace, and it seemed to justify itself fully. Mainly it consisted of papers in solid-state physics; our Division of that field held its Annual Meeting as a portion of ours and arranged a large and notable Symposium, and assisted also in the procurement of many ten-minute papers, so that for once in modern history nuclear physics found itself overshadowed (13 contributed papers in nuclear physics, 27 in solid-state physics, and 9 in other fields). It was welcome to many to find the balance redressed in this fashion. A small session of invited papers, preceded by an address of welcome by the President (T. Keith Glennan) of Case Institute of Technology, was introduced to diversify the meeting; and our members also had the opportunity of attending a lecture by H. L. Dryden ("Turbulent Fluid Motion Challenges the Physicist") before the Cleveland Physics Society. We owe a debt of gratitude to the Local Committee headed by E. Hutchisson and R. S. Shankland for making general arrangements and for providing meeting rooms at Case, and to the President of Western Reserve University for enabling us to meet also in the excellent Allen Memorial Library Auditorium.

The dinner of the Society was held on the Friday evening in the Hollenden Hotel with a regrettably small attendance, so that too few by far listened to the after-dinner speech by Frederick Seitz and witnessed the display of magic by William Shockley.

The Council met on the Saturday morning, and elected eight candidates to Fellowship and 166 to Membership; their names are appended.

The Society has received reports of the loss through death of our members E. H. Colpitts (Bell Telephone Laboratories, retired), J. H. Cross (Texas Technological College), C. K. Edmunds (Pomona), and H. C. Rentschler (Westinghouse, retired).

Elected to Fellowship: P. G. Bergmann, Charles Kittel, Henry Primakoff, R. W. Pringle, R. D. Sard, Bernard Waldman, E. A. Walker, M. W. White.

Elected to Membership: Henry Celler Alberts, Charles Leonard Albright, W. K. Allan, Mrs. Sue Gray Al-Salam, Lester Marchant Baggett, Robert T. Bayard, James H. Becker, Wallace Birnbaum, Martin M. Block, Roger W. Boom, Lynn Joseph Brady, Herbert J. Bramson, Philip James Bray, Roy John Britten, Harold L. Brode, Harold Dean Brown, William Bruenner, William E. Brundage, John W. Buttrey, Jr., David O. Caldwell, Palmer W. Carlin, Herman Y. Carr, Robert Carter, Faye Ruth Chabrow, Mirza Sikandar Beg Chaghtai, Thomas K. Chatham, Milton Chorvinsky, Patrick Joseph Clinton, Simon Cohen, B. Collinge, Frank Charles Collins, Reuben Copperman, Frederic Rudolph Crownfield, Jr., Robert V. Crum Jr., Daniel R. Curran, A. E. Douglas, Russell E. Duff, D. N. F. Dunbar, Paul F. Dunn, Dorris M. Ehret, Adelaide T. Emory, James H. Foster, Robert H. Fox, Robert A. Freiberg, Carl-Erik Froberg, James E. Garvey, Louis A. Giamboni, Thomas L. Gilbert, Robert J. Ginther, Clyde P. Glover, Edwin L. Goldwasser, Roland H. Good, Jr., John Van Nuys Granger, Robert W. Green, Paul M. Griffin, Rafael Grinfeld, Ralph S. Halford, William Halpern, William H. Hamill, Fred T. Harris, Hunter C. Harris, Jr., R. C. Hawkings, John T. Hayward, Harry H. Heckman, Jr., Eugene B. Herman, Jane M. Heslin, Frank Hirst, Isidore Hodes, Milan Holzknecht, Richard J. Howard, Robert A. Howard, Harmon W. Hubbard, Ralph A. Jack, John C. Johnson, Robert E. Johnson, Jr., James E. Johnston, Elliot A. Kearsley, Wallace D. Kilpatrick, Robert E. King, Jay Kleinbard, Melvin Klerer, Robert M. Kloepper, Edward B. D. Lambe, Lewis M. Lawton, Jr., Jules S. Levin, Bernard L. Lewis, Donald R. Lewis, Edgar Lipworth, Holbrook M. MacNeille, Bertram J. Malenka, Myron S. Malkin, Clifford Mannal, Walter H. Manning, Jr., Charles D. Maunsell, Kenneth B. McAfee, Jr., Allen S. McDonald, Jr., Alexander W. Merrison, Walter J. Merz, Richard E. Miller, James H. Moon, Henry B. Moore, Jack B. Morgan, Robert W. Morse, Eugene J. Moscaret, David E. Muller, Rollie J. Myers, Jr., Donald J. Neil, Fred L. Niemann, J. Burton Nichols, John A. Northrop, John C. Noyes, Clifford Orman, John B. Orr, Everett D. Palmatier, Henry W. Parker, Thomas E. Phipps, Jr., Gerald S. Picus, Charles A. Reed, Frederick Reif, Carlton D. Schrader, Thomas S. Schreiber, William E. Scott, Kenneth Shaftan, William T. Sharp, Noah Sherman,

James J. Shipman, Maurice B. Shurman, Robert T. Siegel, John C. Simons, Jr., Robert L. Smith, Ronald K. Smith, Frederick Sobel, David W. Sparks, Godfrey H. Stafford, Adolph Stern, R. Walter Steur, Forrest C. Strome, Jr., George L. Stukenbroeker, Kuan Han Sun, John M. Teem, Jack R. Tessman, David G. Thomas, Robert N. Thorn, Jay T. Thomas, John W. Townsend, Jr., John E. Van Hoomissen, J. Van den Handel, Kenneth L. Vander Sluis, Samuel S. Verner, Ralph Vinegar, S. Visvanathan, G. A. Voetelink, Edward L. Wagner, Frank C. Walz, A. H. Wapstra, Roger W. Warren, John W. Weil, Max M. Weiss, Howard A. Wilcox, Perry W. Williams, W. F. Williams, John J. Windle, Oliver C. Yonts, Donald R. Young, Alfred Zajac, James P. Zietlow.

KARL K. DARROW, *Secretary*
American Physical Society
Columbia University
New York 27, N. Y.

Invited Papers on the General Programme

Electromagnetic properties of nucleons. L. L. FOLDY, *Case Institute of Technology.*

Nuclear scattering. J. H. WILLIAMS, *University of Minnesota.*

Studies of internal motion and molecular structure by electron diffraction. ISABELLA KARLE, *Naval Research Laboratory.*

Linguistics of solid-state physics. K. K. DARROW, *Bell Telephone Laboratories.*

Symposium of the Division of Solid-State Physics

Ferromagnetism and rubber elasticity. EUGENE GUTH, *University of Notre Dame.*

Nuclear magnetic resonance in studies of solids. G. E. PAKE, *Washington University.*

Recent developments in ferromagnetism. CHARLES KITTEL, *Bell Telephone Laboratories.*

Influence of atomic order on magnetic properties. J. E. GOLDMAN, *Westinghouse Research Laboratories.*

Recent developments in knowledge of order-disorder phenomena. R. SMOLUCHOWSKI, *Carnegie Institute of Technology.*

Brittle fracture of triaxial stresses. E. OROWAN, *Cambridge University.*

Multiplication of electrons in crystals by high electrostatic fields. F. SEITZ, *Carnegie Institute of Technology.*

Some electrical and photoelectric studies of *p*—*n* junctions in silicon and germanium. F. S. GOUCHER, *Bell Telephone Laboratories.*

Resistivity of germanium samples at liquid-helium temperatures. I. ESTERMANN, *Carnegie Institute of Technology.*

Grain and interphase boundaries in metals. C. S. SMITH, *University of Chicago.*

New techniques in high-pressure research. A. W. LAWSON, *University of Chicago.*

Optical interference phenomena and cinema-micrography of barium titanate crystals. A. P. DE BRETTEVILLE, N. J. FIELD, AND S. B. LEVIN, *Squier Signal Laboratory.*

Solid-State Physics

B1. Thermal Expansion of $Li_2SO_4 \cdot H_2O$. CHARLES S. SMITH AND H. H. LANDON, *Case Institute of Technology.*—The complete thermal expansion characteristics of the monoclinic crystal $Li_2SO_4 \cdot H_2O$ have been determined by x-ray diffraction measurements of thermal strains in a number of crystallographic directions for the temperature interval $-30°C$ to $+25°C$. The thermal expansion coefficient in an arbitrary direction in the crystal is given by $\alpha_{33}' = C_{13}^2\alpha_{11} + C_{23}^2\alpha_{22} + C_{33}^2\alpha_{33}$, where the α's are the principal expansion coefficients and the C's are the direction cosines of the arbitrary direction with respect to the principal axes. The results are, in units of 10^{-6} reciprocal °C, $\alpha_{11} = 16.3$, $\alpha_{22} = 27.5$, $\alpha_{33} = -2.9$ with $\psi = 2.7°$. The direction of α_{11} lies at angle ψ with respect to the c axis of the unit cell[1] and in the obtuse angle between c and a. The direction of α_{22} is, by symmetry, the b axis of the unit cell. The thermal expansion is thus negative in a 45° range roughly normal to c in the $a-c$ plane.

[1] G. E. Ziegler, Z. Kristallogr. **89**, 456–461 (1934).

B2. Primary and Secondary Pyroelectric Effect in Lithium Sulfate Monohydrate. HANS JAFFE, *The Brush Development Company.*—Data on thermal expansion of lithium sulfate crystals[1] permit calculation of the secondary pyroelectric effect, i.e., the piezoelectric moment due to a set of stresses that would produce elastic strains equal to the thermal expansion. Further information needed are the piezoelectric coefficients relating to the polar axis for which we found $d_{21} = -4.0$, $d_{22} = 16.0$, $d_{23} = 1.5$, $d_{25} = -5.3 \cdot 10^{-12}$ coulomb/newton, and several elastic constants.[2] The resulting secondary pyroelectric constant is $21 \cdot 10^{-6}$ coulomb/m² °C, while the observed total pyroelectric effect[3] is $76 \cdot 10^{-6}$ coulomb/m² °C. The strong electromechanical coupling in lithium sulfate (about 0.35) therefore accounts for only 30 percent of its exceptionally high pyroelectric effect.

[1] C. S. Smith, preceding paper.
[2] Some of these were obtained privately from W. P. Mason.
[3] *International Critical Tables* VI (McGraw-Hill Book Company, Inc., New York), p. 212.

B3. Propagation of Elastic Waves in Some Cubic Crystals as a Function of External Pressure. DAVID LAZARUS, *University of Chicago.*—Measurements of velocity of sound in single crystal specimens of CuZn, KCl, and NaCl have been made, using a pulsed ultrasonic technique, over a pressure range of 10,000 bars. From observation of the velocities of longitudinal and transverse waves in both (100) and (110) crystals of each material, the elastic constants can be computed, with two internal checks. The measured percentage change in velocity of sound for 10,000-bars pressure is given for various velocities in the table. Good correlations are found between computed compressibilities and those measured by Bridgman. The decrease in

	Longitudinal		Transverse	
Material	$V_{(100)[010]}$ (%)	$V_{(110)[011]}$ (%)	$V_{(100)[010]}$ (%)	$V_{(110)[011]}$ (%)
CuZn	+1.83	+1.77	+1.59	+1.21
KCl	+14.9	+10.0	−3.71	+15.8
NaCl	+12.5	+7.0	+1.05	+12.6

the (100) 010 shear velocity for KCl can be explained by consideration of short-range exchange forces, as shown by

Zener.* Comparison is made between pressure effects and the previously measured effects of temperature on elastic constants.

* C. M. Zener, Phys. Rev. 71, 846 (1947).

B4. Apparatus for Rapid Measurement of Internal Friction. HERBERT I. FUSFELD, *Frankford Arsenal.*—This paper describes apparatus for measuring internal friction which satisfies the conditions: (a) low induced stress amplitude to preclude any effects due to the measurements, (b) ability to install specimen within a few minutes after treatment, (c) rapidity of measurement, at a rate of ten to twenty per minute, (d) accuracy of at least 1 percent. Longitudinal vibrations are induced by an eddy-current drive, similar to one previously described in the literature,[1] satisfying (a) and (b) above. Conditions (c) and (d) are obtained by measuring the decay time of free vibrations using vacuum tube trigger circuits and a counter chronograph. As the counter records times on the order of 0.010 second with considerable accuracy, satisfactory measurements can be made with push-button rapidity and simplicity.

[1] R. H. Randall, F. C. Rose, and C. Zener, Phys. Rev. 56, 343 (1939).

B5. A Calculation of the Effects Produced by Soluble Impurities on the Damping of Metals. J. S. KOEHLER, *Carnegie Institute of Technology.**—The ideas of Cottrell[1] and of Mott and Nabarro[1] are used to calculate that portion of the damping which is associated with plastic deformation. It is assumed that the damping arises from an interaction of a moving dislocation with the crystal lattice. It is assumed that this interaction gives rise to a certain amount of energy loss each time a dislocation of unit length moves through one atomic distance. The dislocations are taken to be anchored at the impurity atoms in the manner proposed by Cottrell. The application of an external alternating stress then causes the portion of the dislocation between two impurity atoms to oscillate on its slip plane much like a stretched string. The resonant frequency for such a system is calculated very roughly to be in the megacycle range. The damping in the kilocycle range is calculated to vary inversely as the square of the concentration of impurities; hence the large effects of traces of hydrogen on the damping of copper and of bismuth on the damping of lead can be understood. It is pointed out that at very low frequencies the force exerted by dislocations under external stress on the impurity atoms may lead to a motion of the impurity atom.

* This research was supported by the ONR.
[1] A Conference on the Strength of Solids (Bristol Conference) London Physical Society (1948).

B6. Effect of Dissolved Hydrogen on the Decrement and the Elastic Constants of Copper.* J. MARX, *Carnegie Institute of Technology.*—Measurements made on the damping and elastic constants of single crystals of 99.999 percent copper shows that samples, grown and previously annealed to constant decrement in vacuo, exhibit a very marked decrease in decrement when heated in dry hydrogen at 500°C. Decrements were observed to change from 4.8×10^{-3} to 5.7×10^{-4} at strain amplitudes of 2.5×10^{-7}. A simultaneous *increase* of about 3 percent occurred in the axial Young's modulus of the specimens. This latter change is in the opposite direction to that observed by Koster[1] for the case of *metallic* impurities in copper.

* This research was supported by the ONR.
[1] W. Koster and W. Ravscher, Zeitz, f. Metallkunde 39, 111 (1948).

B7. Longitudinal Vibration of Bars with Non-Linear Internal Friction. A. S. NOWICK, *Columbia University.*—In investigations of internal friction of plastic origin,[1] the measured decrement of crystalline bars has been found to be dependent on amplitude of vibration. This result means that the partial differential equation of motion of the bar is non-linear. Thus far, it has always been assumed implicitly that this equation of motion can be linearized with negligible error. To test this assumption a Maxwell model with non-Newtonian dashpot is chosen and the appropriate non-linear integro-differential equation for longitudinal motion is derived. An approximation method is described for solving this equation for the case of steady-state forced vibration near a resonant frequency, under the assumption of small damping. It is found that all odd normal modes appear. Approximate numerical solution for the amplitudes of the first three modes is then obtained on the assumption of dissipative velocities proportional to the third, fifth, and seventh powers of the applied stress. It is found that the equation of motion cannot be linearized to good approximation if powers higher than the third appear appreciably in the relation between dissipative velocity and applied stress. The analogous calculation for a more general model is briefly discussed.

[1] See, for example, T. A. Read, Phys. Rev. 58, 371 (1940).

B8. On the Mechanism of the Embrittlement of Copper by Bismuth. T'ING-SUI KÊ, *University of Chicago.*—The embrittlement of copper by small amount of bismuth has been known for many years. Voce and Hallowes[1] proposed recently that the agent responsible for embrittlement is bismuth present in the form of a thin film at the grain boundaries of copper. In order to examine this picture from a different angle, measurements on internal friction and elastic modulus were made on copper specimens free from and containing bismuth. These specimens were heat-treated to cause embrittlement according to Voce and Hallowes. Measurements were made with a frequency of transverse vibration of about 1000 cycles per second from −50°C to 550°C. It has been found: (1) There is no abrupt change in elastic modulus of the copper-bearing specimens in passing through the melting point of bismuth (271°C). (2) Each bismuth-bearing specimen gives an internal friction peak around 290°C and the height of the peak varies approximately linearly with the bismuth content. (3) The internal friction peak (around 500°C) associated with the stress relaxation across copper grain boundaries was reduced by the presence of bismuth. These observations indicate that the bismuth causing embrittlement of copper does not form a thin film along copper grain boundaries.

[1] E. Voce and A. P. C. Hallowes, J. Inst. Metals 14, 323 (1947).

B9. Precipitation from Supersaturated Solid Solutions of C and N in α-Iron.* CHARLES A. WERT, *The University of Chicago.*—The formation of precipitates from the solid solutions of C and N in α-iron has been studied by means of the internal friction peak associated with the interstitial diffusion of the solute atoms. A transformation law of the type first proposed by Johnson and Mehl[1] for recrystallization has been found to fit the experimental data. The data are interpreted as showing the following: (1) Fe_3C precipitates in the shape of spheres; (2) an intermediate phase in

the precipitation of nitrogen forms in the shape of disks; (3) there is no incubation time for nucleation of these precipitates; and (4) within experimental error there is no continuous nucleation. Using the results of a derivation made by Zener (as yet unpublished), the mean distance between nuclei is calculated for Fe_3C. This distance is found to be about 800, 2000, and 7000 angstroms at 27°C, 102°C, and 312°C, respectively. With appropriate experimental conditions the temperature dependence of the precipitation rate is found to be about the same as the temperature dependence of the diffusion rate of the solute atoms.

* This research was supported by the ONR.

[1] Johnson and Mehl, "Reaction kinetics in processes of nucleation and growth," AIME 135, 416 (1939).

B10. The Diffusion of Carbon in Alpha-Iron. JAMES K. STANLEY, *Westinghouse Research Laboratories* (*Introduced by* J. E. Goldman).—The diffusion of carbon in alpha- (body-centered cubic) iron was determined using two methods. The first method consisted of diffusing carbon from a saturated well (actually fine pearlite; carbon content 0.7 percent) into an essentially carbon-free material. The second method consisted of diffusing carbon from a "high" carbon sample (0.008 percent) to a sample of lower carbon (0.001 percent), both samples being in the ferritic phase. Both methods gave similar results when the carbon distribution curves were analyzed by Fick's law of diffusion. The data can be represented by the following equation: $D=3.8\times10^{-3}e^{-(16{,}800/RT)}$ cm²/sec. The diffusion coefficient of carbon in alpha-iron is considerably faster than that for carbon in gamma-iron;[1] for example, at 725°C the diffusion coefficient is about 125 times greater.

[1] C. Wells and R. F. Mehl, AIME **145**, 279 (1941).

B11. Plastic Deformation of Crystals. DONALD WAHL, *Massachusetts Institute of Technology.*—A review of past work on plastically bent single crystals (primarily NaCl) showed a great deal unexplained. In the past, crystals were bent without regard to uniformity during deformation. Attention was paid only to the end product (that is, an arc of a circle). A simple device has been built to bend crystal specimens uniformly at speeds and to radii within wide ranges. Preliminary x-ray investigations of deformed crystals (primarily alkali halides) by the Laue transmission method, have been found inconclusive. Instead it appears that a series of exposures taken with a monochromatic beam, making different angles with the crystal "face," yields more information through a type of specialized pole figure for nearly perfect single crystals. It is expected that with the use of these new tools a better understanding of the processes allowing deformation will be obtained.

B12. Mechanism of Steady-State Creep in Metals. B. G. RIGHTMIRE, *Massachusetts Institute of Technology.*—The experimental results of Dushman[1] show that in the steady-state creep of metals the logarithm of the strain rate varies linearly with stress. From the slopes of these curves he deduces that the unit of flow comprises about 1000 atoms. It is here pointed out that Dushman's values of energy of activation suggest that the unit of flow contains only about 10 atoms. To explain this apparent contradiction it is proposed that the flow units are dislocations that move segmentally, rather than as rigid structures. Each segment is assumed to be one atomic diameter in length. It is postulated that if one of these segments jumps to a new position of equilibrium the others follow in tandem. With the aid of this concept, absolute-reaction-rate theory enables one to estimate the number of atoms per dislocation, and the concentration and velocity of the dislocations. Computations have been made for aluminum, silver, and platinum. It is found that aluminum contains relatively few, fast-moving dislocations, which may account for the observed slip bands.

[1] S. Dushman, L. W. Dunbar, and H. Huthsteiner "Creep of metals," J. App. Phys. **15**, 108–124 (1944).

B13. Surface Energies for a Free Electron Metal. H. B. HUNTINGTON, *Rensselaer Polytechnic Institute.*—If one chooses as an idealized model for a metal a region enclosing free electrons with a square barrier, the expression for the surface energy turns out to be relatively independent of barrier height, providing the barrier is so placed that there is no excess or deficit of electrons. The value so obtained, however, is more than twice a corresponding result calculated for a particular metal, sodium, using the self-consistent potential developed by Bardeen.[1] The same procedures are applied to the situation of two metal surfaces separated by a displacement comparable to the distance between planes of closest packing. Particular attention is paid to the cohesive forces between the surfaces. A possible application exists if a supersaturated solution of lattice vacancies in a metal should precipitate to form a plate-like void. From a knowledge of the cohesive forces one can estimate an upper limit to the size to which such a plate might grow before collapsing.

[1] J. Bardeen, Phys. Rev. **49**, 653 (1936).

Papers Not Classed Elsewhere

F1. Transition Temperatures of Methyl methacrylate Polymers at Ultrasonic Frequencies. THOMAS F. PROTZMAN, *Ohio State University.*—The velocity of sound in methyl methacrylate polymers (Plexiglas) has been measured at temperatures from 24 to 90°C, and frequencies from three to eleven megacycles. Optical diffraction methods were used to determine the sound velocity within a maximum error of 1 percent. This low experimental error made possible a detailed study of the sound velocity-temperature relationships. A previously unreported transition of a new type has been found. The sound velocity decreases linearly with increasing temperature, with an abrupt increase of slope occurring when a transition temperature is reached. The transition temperature is found to decrease linearly with frequency, falling from 64°C at three megacycles to 49°C at eleven megacycles. The observed transitions apparently are not manifestations of elastic relaxational effects, and are tentatively attributed to the excitation of some mode of molecular motion, for example, molecular vibrations.

F2. Measurements of Ultrasonic Absorption in Viscous Liquids. JOSEPH L. HUNTER, *John Carroll University.*—Measurements of ultrasonic absorption in several liquids ranging in viscosity from 40 to 400 cp have been made in an interferometer having an air-liquid interface as a reflector.[1] The measurements were made at room tempera-

ture in four different liquids at frequencies of 3, 4, and 5 megacycles. The measured value was in each case higher than that predicted by the Stokes-Kirchoff expression, being on the average somewhat less than twice as great. The measurements may therefore be taken as support for Liebermann's suggestion of a dilational term in the viscosity which causes the absorption to be greater than that expected when only shear viscosity is considered.

[1] J. L. Hunter, Phys. Rev. **74**, 1228 (1948).

F3. The X-Ray K-Absorption Edge of Calcium in the Metal and Some Compounds. MARCELLA COOPER PETREE AND W. W. BEEMAN, *University of Wisconsin.*—The calcium K-absorption edges of the element and of $CaCl_2$, CaF_2, $Ca(OH)_2$, and calcite have been measured using a double crystal vacuum spectrometer and Geiger counter recording. The resolving power was about 0.3 e.v. in the 3-angstrom region. The absorption edge of calcium metal shows fair agreement with the single crystal photographic work of Sanner,[1] and displays a remarkable complexity of structure in comparison with the potassium edge.[2] The curves for the compounds exhibit the similarities to be expected among examples of ionic binding. The fact that the spectrometer was equipped with calcite crystals made it possible to investigate the shift of the reflection curve with respect to the absorption curve of calcite in a region of anomalous dispersion. The shifts observed were of the order of 2 e.v.

[1] Hugo Sanner, *Thesis*, Upsala (1941).
[2] J. B. Platt, Phys. Rev. **69**, 337 (1945).

F4. On the Existence of Micelles in Organic Acid Monolayers. H. T. EPSTEIN, *University of Michigan.*—Electron micrographs of fatty acid monolayers show an organization of the molecules into clusters, or micelles, of the order of 100A in diameter. Because the substrates used have had irregularities of the same order of magnitude, the establishment of the micelle as a property of the monolayer molecules must be based on the observation of systematic variations in the micelles as external conditions are correspondingly varied. Such variations have now been observed; the micelle diameter, for example, is found to vary with the length of the molecule. Additional evidence is available from electron diffraction experiments, and these results will be included in a summary of the evidence for the reality of the micelles. A model for the structure within a micelle has been developed which permits the calculation of relationships between the micelle diameter, the length of the molecules, and the characteristic tilt of the molecules as measured by electron diffraction. Predictions of the model have been tested and a qualitative agreement between theory and experiment has been obtained.

F5. A Sector Type Double Focusing Magnetic Spectrometer. E. S. ROSENBLUM, *Case Institute of Technology.*—The analysis, by Shull and Dennison,[1] of the motion of electrons in an annular magnetic field which varies approximately with $1/r^{\frac{1}{2}}$, has been extended to allow the field to cover an arbitrary sector, and to allow arbitrary location of the source outside the field. Considering small variations from equilibrium values, in the coordinates and momentum of incident particles, it is found that an image of a source can be obtained in the space beyond the field boundaries. An analogy to a thick-lens optical system is developed, from which the location of principal points, coordinates of conjugate foci, the magnification and dispersion can be determined. A second order analysis gives more information on image size and resolution. It is found that with any given field angle and equal object and image distances, the magnification and dispersion are the same as that given by Shull and Dennison,[1] and the resolution is of the same order of magnitude. For smaller object distances, image size and dispersion both increase, so that the resolution varies only slightly. However, the flexibility of the instrument, accessibility of source and counter, and their location in field-free space, should make the instrument a useful one.

[1] Shull and Dennison, Phys. Rev. **71**, 681 (1947).

F6. Noise Spectrum Analyzer.* B. R. RUSSELL, R. DICKSON, AND P. H. MILLER, JR., *University of Pennsylvania.*—An analyzer having twelve band-pass amplifier channels each with its own square law detector and indicator has been set up for the purpose of measuring flicker noise (noise power per c.p.s. $\alpha\nu^{-1}$) in the range 10^2 to 5×10^5 c.p.s.[1] Day to day calibration is achieved by means of the shot noise from a 931A photo-multiplier tube which has instead of a load resistor an RC network adjusted so that its impedance varies nearly as $\nu^{-\frac{1}{2}}$ in the range covered by the instrument. In this way the frequency independent shot noise of the photo-multiplier[2] is attenuated to match the flicker type noise for which the instrument was designed. Results of the measurements of the noise in crystal rectifiers, electrolytic condensers and tired batteries will be presented.

* This work supported by Bureau of Ships, US Navy.
[1] R. H. Thomas, Technical Report No. 8, February 1, 1948, BuShips Contract NObs-34144.
[2] R. D. Sard, J. App. Phys. **17**, 768 (1946).

F7. High Current Pulse Generator Using Mechanical Energy Storage, R. I. STROUGH AND E. F. SHRADER, *Case Institute of Technology.*—Construction of a high current d.c. generator of the series unipolar type employing no iron in its magnetic "circuit" is in progress. This machine is being studied as a possible energy storage system for an air core betatron, and as a possible cloud-chamber field supply. The rotor of the machine serves as a flywheel for energy storage and is driven up to speed between current pulses by means of compressed air jets acting on turbine buckets cut in the rotor. The present model employing a $5\frac{3}{4}$ inch diameter rotor weighing 11 lbs. will store 64,000 joules at 30,000 r.p.m. quite safely. To obtain the negative resistance characteristic necessary for current build-up in the machine, it is essential that the brush resistance be kept extremely small. For this reason a brush system employing mercury flowing between amalgamated surfaces is being investigated. Static model tests indicate that such brushes may be operated at current densities of the order of 10^4 amperes per square cm with a contact resistance of the order of a few micro-ohms cm^2.

F8. New Phenomena of Radiation in Magnetic Fields. FELIX EHRENHAFT, *University of Vienna, Austria.*—The initiative for the following experiments the results of which are well known in full extent since Christmas 1947 has been given by the hypothesis of unipolar magnetic charge. F. Ehrenhaft, R. F. K. Herzog, M. J. Higatsberger, F. P. Viehböck, and P. M. Weinzierl found, using the metallic connected north and south pole of an electromagnet as cathode of a gas-discharge, that besides the gas-discharge

between cathode and anode a radiation becomes visible and can be photographed reaching from pole shoe to pole shoe; the pole shoes have to be covered with a thin layer of some isolating material f.i. apiezon-oil. Under these conditions this radiation becomes visible in discrete light traces following the direction of the magnetic lines of force. This radiation is not caused by high frequent oscillations[1] and it also exists if the space between the pole shoes is surrounded with a Faraday-cage to screen off the influence of the electric field of the anode. Under certain conditions one part of the radiation between the poles forks to the anode. A sufficient explanation of these phenomena by means of moving electric charges is not possible. At my institute F. Blaha and J. A. Schedling using as cathode a permanent magnet got the same results.

[1] A. Righi, Physik. Zeits. **11**, 158 (1910) and **15**, 529 (1914); J. Ives, Phys. Rev. **9**, 349 (1917).

F9. The Electron Does Not Exist. BAYARD P. PEAKES.—The discovery of the electron was apparently a sound advancement in theoretical physics. But let's review the conditions under which it exists. The beam in the cathode-ray tube was first thought to be light, until it was found that it could be bent by electric or magnetic fields. The beam's reaction to magnetic and electric fields identified the rays as being composed of tiny particles having a negative charge, electrons. Yet, these electrons occurred only when the pressure in the tube was about 10^{-3} mm Hg. When there was no air in the tube, conduction was most difficult, and there were no electrons. Hence, if a certain pressure is needed for electrons, these electrons must be derived from that air, and be the cause of them. A complete, careful study of electrical phenomena will reveal electricity as being some form of kinetic energy. Conductors, or maintainers of it, are hot glass, a flame, or light. Electricity *could* be a wave disturbance, made by intermittent attraction between magnet and copper conductor. After many months of working over physics books, one can get this definition of electricity: it is a supersonic motivation, of necessity a wave disturbance, and is created and persists only where there is a contrast, or potential difference, between two points in its line of propogation.

Order-Disorder, Structure, Magnetism, Semi-Conductors

U1. Short Range Order in Cu_3Au.* J. M. COWLEY, *Massachusetts Institute of Technology*.—At temperatures greater than the critical temperature, the long range order of Cu_3Au is zero but considerable short-range order remains. This short-range order gives rise to a diffuse scattering of x-rays with maxima at the positions of the sharp super-structure reflections given by the ordered lattice. A three-dimensional Fourier analysis of the diffuse scattering power, plotted as a periodic function in reciprocal lattice space, gives directly the short-range order coefficients α_{lmn} which determine the probability of either copper atoms or gold atoms being at the lattice points with coordinates l, m, n with respect to a given atom. Values of these short-range order coefficients have been calculated from measurements of the intensities of x-ray scattering from a single crystal of Cu_3Au held at various temperatures above the critical temperature, using a Geiger counter spectrometer with a bent-crystal monochromator. The results indicate a tendency for like and unlike atoms to arrange themselves in alternate shells about a given atom with a distribution analogous to that of atoms in a liquid. The dependence of the short-range order coefficients on temperature, and their relation to long range order are discussed.

* Supported in part by the ONR.

U2. Structure and Short Range Order for Low Temperature Ag_3Al.* B. W. ROBERTS, JR., *Massachusetts Institute of Technology*.—The low temperature phase of Ag_3Al has been reported in space group O^7-P4_132 as simple cubic with random positioning of the twenty atoms per unit cell. The atom arrangement was reported identical with that of beta-manganese and several isomorphous alloys all of which have valence electron to atom ratios of 3:2. In an investigation of the short range order in Ag_3Al a forbidden line and several intensity changes were observed on powder x-ray diffraction photographs. These dictated a change in space group to lower symmetry and an adjustment of the atom positions. The new space group was found to be T^4-P2_13 with twenty atoms in two (4a) and one 12(b) equivalent positions. Since a satisfactory intensity agreement is obtained from a random arrangement of the 15 Ag and the 5 Al atoms in the twenty cell positions, there is no evidence for a long range order in Ag_3Al. Measurements of total diffuse x-ray scattering from flat powder samples indicate that a small amount of short range order exists in low temperature Ag_3Al.

* Supported in part by the ONR.

U3. Long Range Order in β-Brass.* B. E. WARREN AND D. CHIPMAN, *Massachusetts Institute of Technology*.—A single crystal of β-brass cut parallel to (100) is mounted in a heating unit on a Geiger counter spectrometer. Using either crystal monochromated CuKα or CuKβ radiation the integrated intensity of the superstructure line (100) is measured at various temperatures up to T_c. Comparison with (111) of NaCl shows the long range order to be nearly perfect at room temperature. With increasing temperature the measured long range order drops continuously to zero at T_c. The drop is somewhat steeper near the critical temperature than the variation predicted from current theories. The use of crystal monochromated CuKβ rather than CuKα radiation increases the integrated intensity of (100) β-brass by a factor of 4, but does not give as accurate a measure of long range order because of the uncertainty in $(f_{Zn}-f_{Cu})$.

* Supported in part by the ONR.

U4. Superlattice Lines of the Second Kind and Their Relation to the Apparent Discrepancy in the X-Ray Analysis of the Structure of Heusler Alloy. LOUIS GOLD, *Brown University*.—A new aspect of order-disorder transformations has been uncovered in connection with what at first appeared to be a discrepancy in the x-ray analysis of the structure of Heusler alloy. It was found that the assigned structure* could not account for the weak series of lines as characteristic of the ordered form of the alloy. An explanation which accounts for the odd index lines of the weak series appearing not only as a distinct group, but also with considerably lower intensity than the even index superlattice lines, is to be associated with what may be termed superlattice lines of the second kind. These lines are attributable to intermediate order only, vanishing when

the alloy is completely ordered or disordered. An analysis of conditions for the existence of superlattice lines of the second kind reveals that the effect is a perfectly general one and is not limited to Heusler alloy. Systems in which atoms have several degrees of freedom for interchange may be expected to exhibit diffraction lines characteristic of the intermediate state of order, the actual occurrence of such superlattice lines being predictable from an examination of the structure factor for any degree of order.

* A. J. Bradley and J. W. Rodgers, "The crystal structure of Heusler alloys," Proc. Roy. Soc. London **144A**, 340–359 (1934).

U5. Structure of Ferroelectric $BaTiO_3$.* G. C. DANIELSON AND R. E. RUNDLE, *Iowa State College.*—Megaw[1] has shown from x-ray powder photographs that $BaTiO_3$ is tetragonal in the ferroelectric state with unit cell dimensions at 20°C of $a_0=3.9946$A, $c_0=4.0335$A. It has been reported by one of us[2] that x-ray diffraction of a single domain crystal at 20°C indicates that the titanium ion is displaced from the center of the unit cell and in the direction of the c axis by about 0.16A, in agreement with the displacement to be expected from Hulm's[3] measurement of the spontaneous polarization. Recently, Mason and Matthias[4] have made reference to this displacement of the titanium ion in developing a theory to explain the ferroelectric behavior of $BaTiO_3$. The previous x-ray determination was based on the relatively high intensity of x-ray scattering from the (00 11) plane as shown by a Weissenberg pattern using molybdenum radiation. The interpretation of this high intensity is open to question, however. By using Ag radiation from a demountable gas tube, and single domain crystals grown by E. G. Grimsal and F. A. Halden (using Matthias' method,) it now appears that the displacement of the titanium ion must be much less that previously reported and even less than 0.1A at 20°C. Still shorter wave-length radiation seems to be necessary for an exact determination.

* This work was done in part in the Ames Laboratory of the Atomic Energy Commission.
[1] Megaw, Proc. Roy. Soc. **189**, 261 (1947).
[2] Danielson, Matthias, and Richardson, Phys. Rev. **74**, 986 (1948).
[3] Hulm, Nature **160**, 126 (1947).
[4] W. P. Mason and B. T. Matthias, Phys. Rev. **74**, 1622 (1948).

U6. An X-Ray Investigation of Iron-Rich Iron Tungsten Alloys. DAVID D. VAN HORN, *Case Institute of Technology.*—Debye-Scherrer diffraction patterns in the back-reflection region have been used to investigate the solid-solubility of tungsten in iron. Standard techniques have been used, with modifications in some cases, to obtain accurate determination of lattice parameters. Incidental to these determinations of the lattice parameter of alloys of various compositions, the lattice parameter of pure α-iron (at 20°C) was found to be $a_0=2.8603_1\pm0.00004kX$ units, which is in essential agreement with Jette and Foote.* The lattice parameter *vs.* composition curve of the α-phase iron-tungsten solid solution has been obtained. It has been possible from this information to determine the variation in the solubility of tungsten in iron with temperature in a number of solution heat treated and aged iron-tungsten alloys.

* Jette and Foote, J. Chem. Phys. **3**, 605 (1935).

U7. The Limiting Sensitivity of Instruments for Displaying the Magnetic Hysteresis Loops of Small Specimens. E. C. CRITTENDEN, JR. AND R. I. STROUGH, *Case Institute of Technology.*—The factors limiting the ultimate attainable sensitivity have been studied and an instrument constructed which approaches this limit. The instrument is of the type[1,2] which displays on a CRO screen the integrated signal from a pair of bucked flux coils *vs.* the magnetizing field. Circuit noise at the preamplifier input and at the integrator output and the perfection of balance of the two flux coils limit the usable sensitivity. Since the preamplifier signal is multiplied by $1/\omega$ because of integration, low frequency noise reduction is important. Use of electrometer tube circuits in the preamplifier reduces integrated noise output 45 db. A magnetizing current wave form containing first and third harmonics with adjustable amplitude and phase reduces the number of Fourier components in the signal for most specimens. This greatly reduces the integrator noise difficulty by permitting higher preamplifier gain and reducing the band width needed in the second amplifier. Special construction of magnetizing and flux coils reduces stray field noise. The instrument as constructed gives a signal equal to noise for 1.5×10^{-4} Maxwells flux change.

* This work was supported by the ONR.
[1] Crittenden, Smith, and Olson, Rev. Sci. Inst. **17**, 372 (1946).
[2] M. O. Scherb, Rev. Sci. Inst. **19**, 411 (1948).

U8. Microwave Magnetic Resonance Absorption in Chrome Alum at 1.25 cm. W. A. YAGER, F. R. MERRITT, A. N. HOLDEN, AND C. KITTEL, *Bell Telephone Laboratories.*—Magnetic resonance absorption at a frequency of 24,446 mc/sec. was observed in a crystal of ammonium chrome alum at room temperature as a function of the intensity of the static magnetic field applied in the [111] direction. Previous measurements have been reported on this salt at lower frequencies, by the Oxford, Rutgers, and Pittsburgh groups. We observed five absorption lines, at 7210, 8220, 8770, 9220, and 10,290 oersteds. Using the theory given by Broer[1] and by P. R. Weiss[2] we find a g-value of 1.99 from the position of the central line; while from the difference of the lowest and highest lines we find a zero field energy level splitting of 0.143 cm^{-1}. The results are in good agreement with theory and with results reported by other workers at lower frequencies.

[1] L. J. F. Broer, Physica **9**, 547 (1942).
[2] P. R. Weiss, Phys. Rev. **73**, 470 (1948).

U9. Quantum Theory of Ferromagnetic Resonance. J. M. RICHARDSON, *Bell Telephone Laboratories.*—Luttinger and Kittel[1] have given a quantum mechanical derivation of the Kittel equation (first derived classically), $\Delta E=g\mu_B(BH_i)^{\frac{1}{2}}$, giving the separation between large adjacent eigen values of the Hamiltonian for a plane specimen of ferromagnetic material with the static field parallel to the plane. They actually used the more general Hamiltonian for an elliptical specimen $\mathcal{H}=aJ_z+bJ_z^2+cJ_x^2$, in which J_x and J_z are the x and z components of the angular momentum operator, and in which the 1st term arises from the static field applied in the x direction and the 2nd and 3rd terms arise from demagnetizing effects. Their derivation was based upon the approximate solution of the secular equation using an explicit representation in which J_z is diagonal. In this paper it is shown how to derive the result more simply using formal operator algebra and no explicit representation. First, the commutators of $\mathcal{H}$ with J_y and J_z are computed. Assuming $J_z\simeq\langle J_z\rangle_{Nl}$, these commutators can be linearly combined so that $[J_y\pm i\alpha J_z, \mathcal{H}]=\mp\hbar\omega(J_y\pm i\alpha J_z)$, in which $\omega=(a+2(b-c)$

$\times\langle J_z\rangle_{Av})^{\frac{1}{2}}(a+2b\langle J_z\rangle_{Av})^{\frac{1}{2}}$, which is just the classical relation, and $\alpha=(a+2(b-c)\langle J_z\rangle_{Av})^{\frac{1}{2}}(a+2b\langle J_z\rangle_{Av})^{-\frac{1}{2}}$.

[1] J. M. Luttinger and C. Kittel, Helv. Phys. Acta. 21, 480-482 (1948).

U10. Conductivity of Sintered and Single Crystals of Zinc Oxide Semiconductor.* E. E. HAHN, B. R. RUSSELL, AND P. H. MILLER, JR., *University of Pennsylvania.*—Room temperature measurements of electrical conductivities, σ, and Hall constants, R, give carrier mobilities ~100 to 200 cm^2 volt^{-1} sec.$^{-1}$ in single crystals of ZnO[1] and ~5 to 60 cm^2 volt^{-1} sec.$^{-1}$ in sintered samples.[2] σ and the sample type show no correlation. Measured by usual methods, poorly sintered samples invariably show low σ and are usually frequency dependent ($\nu\sim10^7$ c.p.s.). Sintered samples therefore probably consist of semiconducting microcrystals surrounded by lower conductivity layers; measured conductivities are largely determined by the layers. Theory of measurement[3] of R indicates the layers negligibly affect R because of the shorting-out effect of the microcrystals; measured R values for sintered samples are therefore characteristic of the microcrystals. Assuming the mobility in a single crystal having dimensions ~0.1 cm is the same as in a sintered sample microcrystal having the same number of impurities, the experimental discrepancy in mobilities is attributed to erroneous σ-values and indicates that σ of sintered ZnO microcrystals cannot be determined accurately by usual methods.

* Work supported by Bureau of Ships, USN.
[1] Supplied by New Jersey Zinc Co., Palmerton, Pa.; spectroscopic check indicates presence of lead impurities.
[2] For other measurements see P. H. Miller, Jr., Phys. Rev. 60, 890 (1941); O. Fritsch, Ann. d. Physik 22, 375 (1935).
[3] I. Isenberg, B. R. Russell, and R. F. Greene, Rev. Sci. Inst. 19, 684 (1948).

U11. Theory of Photovoltaic Effect of $P-N$ Barrier in a Semi-Conductor. H. Y. FAN, *Purdue University.**—Sosnowski has treated the $P-N$ barrier on the basis of penetration of the barrier by electrons. Such treatment applies to very narrow barriers with thickness comparable to the mean free path of the electrons. We shall consider thick barriers where the diffusion theory applies. If the activation energies of both types of impurities are so small that they are almost completely ionized, a condition true for germanium over wide temperature range, then we can write for the divergences of electron (i_1) and hole current (i_2) in the barrier $-(1/e)(di_1/dx)=(1/e)(di_2/dx)=H+L-rn_1n_2$, where H is the rate of transition (per unit volume) of electrons from the filled band to the conduction band under thermodynamical equilibrium conditions, L is the rate of additional transition (per unit volume) due to light absorption, r is the recombination coefficient of conduction electrons and holes, n_1 and n_2 are the concentrations of conduction electrons and holes respectively. It can be shown that if the light beam is wide compared with the barrier thickness then the change in potential difference between the two boundaries A and B of the barrier due to the illumination is: $\Delta V_{AB}=\log(n_{1A}'n_{1B}^0/n_{1B}'n_{1A}^0)=\log(n_{2B}'n_{2A}^0/n_{2A}'n_{2B}^0)$, where superscript zero refers to the normal condition and superscript prime refers to the condition under illumination. If the increase in n_1 and n_2 is small compared with normal values of n_1 in the N region and n_2 in the P region of the semiconductor, then the open circuit photovoltage is given by: $V_P=(kT/e)\log(H+L/H)$.

* This work was assisted by a Signal Corps contract.

U12. Theory of Resistivity and Hall Effect in Semi-Conducting Anisotropic Crystals.* V. A. JOHNSON, *Purdue University.*—In anisotropic crystals the effective mass of a free electron (or hole) has a tensor characteristic. This property of the mass produces a tensor character in the resistivity, which has been investigated experimentally[1] and also theoretically.[2] By extending the treatment of tensor resistivity due to Bronstein, explicit expressions are obtained for the tensor resistivity in an intrinsic semiconductor (both holes and electrons) and also for the resistivity due to scattering by ionized impurities; the latter is influenced by the tensor properties of both mass and dielectric constant. Derivation of the Hall effect in anisotropic crystals shows that the Hall coefficient is independent of crystal orientation in the magnetic field as long as carriers of one sign only are present, but the Hall coefficient will have a directional dependence if both holes and electrons conduct and if the effective mass ratio has a directional dependence.

* This work was assisted by a Signal Corps contract.
[1] V. E. Bottom, Bull. Am. Phys. Soc. 24 (January) 1949.
[2] M. Bronstein, Physik. Zeits. d. Sowjetunion 2, 28 (1932).

U13. Photovoltaic Effect of $P-N$ Barriers Produced in Germanium by α- and Deuteron Bombardment.* M. BECKER AND H. Y. FAN, *Purdue University.*—$P-N$ barriers can be created in N-type germanium by α- or deuteron bombardment of a part of the surface.[1] The photovoltaic effect has been studied quantitatively for a number of such barriers.[2] The experimental arrangement consisted of a 100 watt Western Union Concentrated Arc whose light was first focused on a rotating slotted disk which passed light pulses of 0.001 sec. at a 0.05 duty cycle. It was then made parallel and passed through fixed diaphragms whose diameters determined the intensity of the final light spot which was 1 mm in diameter. The open circuit photovoltage pulses were amplified and displayed on an oscilloscope. It is found that excluding the visible light by a No. 88 Wratten filter has little effect upon the magnitude of the photovoltage, hence the effective spectral region is in the infra-red. Over a range of 1:1024 in intensity and a range of 1:104 in photovoltage, the equation derived by one of the authors in an accompanying paper $e^{eV/kT}-1=\alpha I$, is closely satisfied for all the barriers studied. In the above equation V is the open circuit photovoltage and I is the light intensity and α a constant.

* This work was assisted by a Signal Corps contract.
[1] K. Lark-Horovitz, E. Bleuler, R. Davis, and D. Tendam, Phys. Rev. 23, 1256 (1948).
[2] The authors wish to thank Mr. J. Forster for preparing some of the samples.

U14. Resistivity of Germanium Samples at Liquid Helium Temperatures. I. ESTERMANN, A. FONER, AND J. E. ZIMMERMAN, *Carnegie Institute of Technology.**—The resistivity of several germanium samples with different amounts of added impurities was measured between 4°K and 20°K. Samples with high impurity content, in which the electron gas is degenerated below 100°K, do not change their resistivity in this temperature range. Another sample, which has a degeneracy temperature of 20°K, computed from Hall Effect measurements, showed the same behavior. Two other samples, which did not become degenerate above 20°K, exhibited a moderate increase in resistivity (20 and 80 percent respectively) between 20°K and 4°K. Two "pure" samples, i.e., without added impurities,

showed a very strong increase of resistivity below 20°K, increasing from about 2 ohm-cm at 20°K to more than 3×10^5 ohm-cm at 4.7°K. At these low temperatures, however, the resistance depends strongly on the applied electric field, and this effect requires further study.[1]

* This paper is to be given as L1 in the Symposium; the abstract is printed here for the record.
[1] Work assisted by the ONR and the Research Corporation.

Nuclear Physics

V1. Preliminary Investigation of Radiations from I^{124}. J. LAWRENCE MEEM, JR. AND FRED MAIENSCHEIN, *Indiana University.*—I^{124} (4-day) was made by bombarding antimony with 23-Mev alpha-particles in the Indiana University cyclotron. Absorption of positrons in aluminum indicate a beta-ray end point of 2.45 Mev. Coincidence absorption of Compton electrons ejected from aluminum show that the maximum energy gamma-ray is approximately 2 Mev. Beta-gamma-coincidences are present and the number of beta-gamma-coincidences per recorded beta-ray is independent of the energy of the beta-rays. This work was assisted by the joint program of the ONR and AEC.

V2. Disintegration of Iodine^{131}. DANIEL J. ZAFFARANO, ALLAN C. G. MITCHELL, AND BERNARD D. KERN,* *Indiana University.*—The beta- and gamma-rays of I^{131} obtained from Oak Ridge have been examined with a magnetic lens spectrometer. Gamma-rays of energy 80, 163, 282, 363, and 637 kev have been found, of which all except the last one are internally converted. The beta-end point is 605 kev, and a plot using exact Fermi functions indicates a second group at 238 kev with perhaps a third at lower energy. The gamma-ray at 163 kev is weak and was not reported by Metzger and Deutsch,[1] but was found by Owen, Moe, and Cook.[2] A decay scheme similar to that given in reference 1 is proposed which gives better agreement with our measurement of the energy of the second beta-group and incorporates the 163-kev gamma-ray also reported in reference.[2] This work was assisted by the joint program of the ONR and the AEC.

* Atomic Energy Commission Fellow.
[1] F. Metzger and M. Deutsch, Phys. Rev. **74**, 1640 (1948).
[2] G. Owen, D. Moe, and C. Cook, Phys. Rev. **74**, 1879 (1948).

V3. Coincidence Studies on Au^{199}. FRED MAIENSCHEIN AND J. LAWRENCE MEEM, JR., *Indiana University.*—The activity of Au^{199} (3.3 days), obtained from Oak Ridge, has been studied by absorption and coincidence counting techniques. Absorption of the beta-rays in aluminum indicate a beta-ray end point of 0.32 Mev. Coincidence absorption of photoelectrons give an energy of 0.211 Mev for the highest energy gamma-ray, in agreement with Peacock and Wilkinson.[1] A small, but definitely positive, gamma-gamma-coincidence rate was observed. The beta-gamma-coincidence rate was found to be independent of the energy of the beta-rays. Coincidences between internal conversion electrons and beta-rays indicates that the most energetic conversion electrons have an energy of about 120 kev. A search was made for a metastable state of Hg^{199} growing from Au^{199}. There is no evidence for the formation of a state of half-life 43 min. formerly attributed[2] to Hg^{199}. This work was assisted by the joint program of the ONR and the AEC.

[1] C. Peacock and R. Wilkinson, Phys. Rev. **75**, 329 (1949).
[2] M. Friedlander and C. Wu, Phys. Rev. **63**, 227 (1943); R. Sherr, K. T. Bainbridge, and H. H. Anderson, Phys. Rev. **60**, 473 (1941).

V4. Energy Distribution of Fission Fragments from U^{235} and U^{233}. D. C. BRUNTON AND G. C. HANNA, *Chalk River Laboratory.*—Measurements have been made of the energy distributions of fission fragments from U^{235} and U^{233} irradiated with slow neutrons. A coincident pulse technique was employed using a double "back-to-back" ionization chamber. The chamber was filled with $A+3$ percent CO_2 and pulses were obtained by electron collection with Frisch grids shielding the collecting electrodes. Pulses lying in a fixed energy interval were selected in one side of the chamber by an electronic "gate" and the energy distribution of the coincident pulses in the other side was measured on a thirty-channel pulse analyzer. Runs with a wide open gate yield the normal double-peaked curve of fragment energy distribution. A narrow energy gate was moved progressively across the double peaked curve and for each setting the coincident distribution was measured. These gated distributions are surprisingly independent of the gating energy. The mean position and the width of the distribution shift only a few Mev for a 20-Mev change in gating energy. A comparison of the fragment energies for U^{235}, U^{233}, and Pu^{239} * will be given. The asymmetry of the fission process appears to decrease with increasing mass number of the fissile nucleus. The total kinetic energy is found to be a maximum at a mass ratio of 1.25.

* M. Deutsch and M. Ramsey, MDDC-945.

V5. Range Distribution of the Charged Particles from the $D-D$ Reactions for 10-Mev Deuterons: Differential Elastic Scattering Cross Section at 40 Degrees, 30 Degrees, and 20 Degrees in the Laboratory System. L. ROSEN, F. K. TALLMADGE, AND J. H. WILLIAMS, *Los Alamos.*—Photographic plates were used to determine the range distribution of all charged particles from the $D-D$ reactions as well as the absolute intensity of the elastically scattered deuterons for 10-Mev deuterons from the Los Alamos cyclotron. These measurements were made at 40 degrees, 30 degrees, and 20 degrees (laboratory coordinate system) with respect to the incident beam which was focused on a "thin" deuterium gas target 15 feet from the cyclotron. At 40 degrees all of the charged particles from above reactions (protons, tritons, He^3's, and elastically scattered deuterons) were clearly resolved. At 20 degrees the triton and deuteron mean ranges differed by less than three percent and hence could not be resolved. Slit systems were used to define the number of tracks originating in a given swath across the photographic plate. This, together with the high degree of resolution of scattered deuterons from other charged particles (at 20 degrees the energy width at half-maximum of the scattered deuterons was three percent), permitted precise determinations of the differential $D-D$ scattering cross section. Accurate determinations of beam direction, beam energy, maximum beam energy spread, and purity of target gas were made from the same plates which yielded the cross-section determinations.

V6. Angular Distribution of Photo-Neutrons.* EDWIN P. MEINERS, JR., DAVID R. SMITH, AND LEWIS SLACK,

Washington University.—A study has been made of the angular distribution of photo-neutrons obtained by the action of Na^{24} γ-rays (2.76 Mev) on deuterium under approximately ideal conditions of low neutron scattering. Sources of Na^{24} of about one curie initial activity were prepared by bombarding metallic sodium with deuterons in the Washington University cyclotron. A BF_3 ionization chamber was used as detector, which together with the source, was hung from a frame tower on top of the Washington University physics building. Results were obtained at 0° and 90° angles for three glass spheres, 0.95, 1.27, and 1.50 cm in diameter, filled with D_2O; and extrapolation made to a sphere of zero diameter. The final calculation gives a value for the ratio of the photo-magnetic cross section to the photoelectric cross section $\sigma_m/\sigma_e=0.286 \pm 0.034$, a value which is in excellent agreement with theory. This work was confirmed by repeating the measurements using, as method of neutron detection, the Szilard-Chalmers reaction in calcium permanganate solution. This latter method possesses the advantage of being completely insensitive to γ-rays. Work is now in progress on the angular distribution of photo-neutrons from beryllium bombarded by Na^{24} γ-rays.

* Assisted by the ONR.

V7. Depolarization of Neutrons During Diffusion. OTTO HALPERN, *University of Southern California.*—Rigorous[1] or asymptotic[2] solutions of the transport equation for neutrons incident upon a plate of infinite or finite thickness have been used to determine the change in polarization of the reflected and transmitted beams. The method is particularly suited to the physically most interesting case of small depolarization per collision. The solutions of the transport equation obtained differ by varying amounts (15 percent to 100 percent) from those given by Borowitz and Hamermesh.[3] The intensities of the reflected and transmitted beams are in many cases of practical interest (thickness$\sim$5–10 mean free paths) of the same order of magnitude contrary to the statements of the authors quoted. Measurement of the depolarization of returning beams seems most promising in some cases; formulae for this effect are given for every angle of return.

[1] O. Halpern, R. Luneburg, and O. Clarke, Phys. Rev. **53**, 173 (1938).
[2] O. Halpern and R. Luneburg (to be published).
[3] S. Borowitz and N. Hamermesh, Phys. Rev. **74**, 1285 (1948).

V8. Variation of the Equilibrium Radius with Time in a Flux-Forced Field-Biased Betatron.* E. C. GREGG, JR., *Case Institute of Technology.*—An analysis of the magnetic and electric circuits of a flux-forced field-biased betatron shows that the influence of imperfect feedback is equivalent to a time varying phase shift between flux and guiding field if the core is driven to saturation. For the case where core linearity is maintained, a constant phase shift results. Further, such an effect causes the true equilibrium radius to depend not only on the time in the acceleration cycle but also the relative injection phase (bias). Calculations show that for a phase shift of 30′, the variation in radius will range from -3.5 percent to $+6$ percent as the injection phase is varied from 0 to $-60°$. Typical operating conditions of the Case Institute 30-Mev betatron showed that a phase shift of 11′ should result while an actual phase shift of 30′ was measured. The difference is due to inner pole tip saturation which has a further effect of reducing the $H\sim 1/r^n$ range. Such considerations are of importance in proper gun and nominal equilibrium orbit locations for optimum performance.

* Supported in part by funds from the Research Corporation of New York and the Thomas White Fund of The Cleveland Foundation.

V9. Single Production of Mesons by γ-Rays Near Threshold. L. L. FOLDY, *Case Institute of Technology.*—The cross section for single charged meson production through absorption of a γ-ray in a γ-ray-nucleon collision has been calculated to order g^2 in the charged scalar meson theory (scalar coupling) and charged pseudoscalar meson theory (pseudovector coupling). The nucleon was assumed to be infinitely heavy thus restricting the validity of the results to γ-ray energies small compared to the nucleon rest energy and therefore to the energy region just above threshold. In the scalar theory the process can take place only through an intermediate state, but in the pseudoscalar theory, as a consequence of the currents associated with the emission of a meson by the nucleon, a direct transition from initial to final state is possible. Since the matrix element for the latter transition is not proportional to the meson momentum, the cross section in the pseudoscalar theory varies with a lower power of the energy above threshold (ΔE^1) than does the cross section for the scalar theory (ΔE^3), contrary to the usual behavior. Very near threshold the angular distribution of the mesons is proportional to $\sin^2\theta$ in the scalar theory and is uniform in the pseudoscalar theory. In both theories at energies 50 percent above threshold, the cross sections are of order 10^{-28} cm^2.

V10. Positon Theory. FREDERIK J. BELINFANTE, *Purdue University.*—Schroedinger's theory describing electrons by antisymmetric functions in configuration space follows from general quantized field theory by Fock's theory of second quantization. This theory is generalized so as to describe also positon-negaton theory in configuration space. The Schroedinger functions are products of separate antisymmetric functions for positons and for negatons, each necessarily a superposition of Slater-determinants of solutions of only one energy sign in field-free space. This holds in presence of external fields, too, as follows from Schwinger's relativistic splitting of the quantized electron $\psi(x)$ in interaction representation into two parts. The hydrogen atom then shows a superposition of states with N positons and $(N+1)$ negatons, with non-vanishing probability for any N. Then $\psi(x_0)$ as operator changes a state with n negatons and p positons into a superposition of a state with one negaton removed at x_0, and another state with one positon added with wave function $\Sigma\varphi_i(x)\varphi_i^*(x_0)$, where φ_i are positive energy solutions of Dirac's equation in field-free space. This distinction of states of either energy sign enables one to reformulate familiar subtraction formalisms and also to generalize Pauli's "*Handbuch* quantum-electrodynamics without gauge-dependent quantities" to positon theory, introducing suitable operators of pair creation and annihilation.

V11. Precision Gamma-Ray Wave-Length Measurements on I^{131} with the 2-Meter Curved Crystal Focusing Spectrometer.* DAVID A. LIND, JAMES BROWN, DAVID

KLEIN, DAVID MULLER, AND JESSE DUMOND, *California Institute of Technology.*—Using a "carrier free" source of I^{131} five independent precision measurements of the 364 kev and two on the 80-kev lines had been made when news of the new disintegration scheme of F. Metzger and M. Deutsch[1] showing at least two additional lines reached us. In spite of source decay we were still able to obtain one precision measurement of the 284-kev line. The results are: measured wave-lengths in cm $(34.033\pm0.01)\cdot10^{-11}$, $(154.671\pm0.01)\cdot10^{-11}$, $(43.622\pm0.02)\cdot10^{-11}$; calculated energies in kev 364.18 ± 0.1, 80.133 ± 0.005, 284.13 ± 0.1. The sum of the quantum energies of the 284- and 80-kev lines agrees to a part in 4500 with that of the 364-kev line thus giving strong evidence for the correctness of Metzger and Deutsch's cascade scheme but unfavorable to a more recent four line double cascade proposal of G. E. Owen, D. Moe, and C. S. Cook.[2]

* Assisted by the joint program of the AEC and ONR.
[1] F. Metzger and M. Deutsch, Phys. Rev. **74**, 1640 (1948).
[2] G. E. Owen, D. Moe, and C. S. Cook, Phys. Rev. **74**, 1879 (1948).

V12. Diffraction of Slow Neutrons by Liquid D_2O. S. J. CZYZAK AND A. WATTENBERG, *Argonne National Laboratory.*—An investigation has been made of the relative differential scattering cross section of heavy water in an attempt to obtain information concerning interatomic distances in water. A curve has been obtained at 25°C covering a range in $(\sin\theta)/\lambda$ from 0.1 to 0.9. Only one pronounced maximum is present at a value of $(\sin\theta)/\lambda=0.16$ in agreement with previous x-ray diffraction work.[1]

[1] J. Morgan and B. E. Warren, J. Chem. Phys. **6**, 666 (1938).

SUPPLEMENTARY PROGRAMME

SP1. On the Scattering of Low Energy γ-Rays by Protons. L. L. FOLDY, *Case Institute of Technology.**—As a consequence of the coupling of the proton to the meson field one would expect that a proton could scatter a low energy γ-ray ($\hbar k \ll Mc^2$) through polarization of its meson charge cloud as well as through the usual Thomson scattering. The highest order term of this type in the transition matrix element would be expected to be of order $(g^2/\hbar c)(M/\mu)$ compared to the Thomson scattering term. An attempt to calculate this effect to the indicated order was made employing the charged scalar meson theory (scalar coupling) and the charged pseudoscalar meson theory (pseudovector coupling). In the scalar theory, the process may occur through two or three intermediate states, while in the pseudoscalar theory processes involving only one intermediate state are also possible. All quantities are finite in the scalar theory, but the matrix elements corresponding to processes with two and three intermediate states are equal and of opposite sign and lead to cancellation of any effect to this order. In the pseudoscalar theory the contributions arising from transitions involving an even and an odd number of intermediate states, now separately divergent, are again equal and of opposite sign leading again to cancellation of any effect. The cancellation in both cases occurs only after the summation over all intermediate momentum states for the meson. It is therefore difficult to attribute the null result in the two cases to some simple underlying selection rule.

* To be given after Session V if the Chairman rules that time permits.

Author Index to Papers Presented at the Cleveland Meeting.

Becker, M. and H. Y. Fan—No. U13
Belinfante, Frederik—No. V10
Brunton, D. C. and G. C. Hanna—No. V4
Cowley, J. M.—No. U1
Crittenden, E. C. Jr. and R. I. Strough—No. U7
Czyzak, S. J. and A. Wattenberg—No. V12
Danielson, G. C. and R. E. Rundle—No. U5
Darrow, K. K.—No. A4
de Bretteville, A. P., N. J. Field, and S. B. Levin—No. L4
Ehrenhaft, Felix—No. F8
Epstein, H. T.—No. F4
Estermann, I.—No. L1
——**A. Foner, and J. E. Zimmerman**—No. U14
Fan, H. Y.—No. U11
Foldy, L. L.—Nos. A1, V9, SP1
Fusfeld, Herbert I.—No. B4
Gold, Louis—No. U4
Goldman, J. E.—No. G4
Goucher, F. S.—No. K4
Gregg, E. C. Jr.—No. V8
Guth, Eugene—No. G1
Hahn, E. E., B. R. Russell, and P. H. Miller, Jr.—No. U10
Halpern, Otto—No. V7
Hunter, Joseph L.—No. F2
Huntington, H. B.—No. B13
Jaffe, Hans—No. B2
Johnson, V. A.—No. U12
Karle, Isabella—No. A3
Kê, T'ing-Sui—No. B8
Kittel, Charles—No. G3
Koehler, J. S.—No. B5
Lawson, A. W.—No. L3
Lazarus, David—No. B3
Lind, David A., James Brown, David Klein, David Muller, and Jesse DuMond—No. V11
Maienschein, Fred and J. Lawrence Meem, Jr.—No. V3
Marx, J.—No. B6
Meem, J. Lawrence Jr. and Fred Maienschein—No. V1
Meiners, Edwin P. Jr., David R. Smith, and Lewis Slack—No. V6
Nowick, A. S.—No. B7

Orowan, E.—No. K2
Pake, G. E.—No. G2
Peakes, Bayard P.—No. F9
Petree, Marcella Cooper and W. W. Beeman—No. F3
Protzman, Thomas F.—No. F1
Richardson, J. M.—No. U9
Rightmire, B. G.—No. B12
Roberts, B. W. Jr.—No. U2
Rosen, L., F. K. Tallmadge, and J. H. Williams—No. V5
Rosenblum, E. S.—No. F5
Russell, B. R., R. Dickson, and P. H. Miller, Jr.—No. F6
Seitz, F.—No. K3
Smith, C. S.—No. L2
Smith, Charles S. and H. H. Landon—No. B1
Smoluchowski, R.—No. K1
Stanley, James K.—No. B10
Strough, R. I. and E. F. Shrader—No. F7
Van Horn, David D.—No. U6
Wahl, Donald—No. B11
Warren, B. E. and D. Chipman—No. U3
Wert, Charles A.—No. B9
Williams, J. H.—No. A2
Yager, W. A., F. R. Merritt, A. N. Holden, and C. Kittel—No. U8
Zaffarano, Daniel J., Allan C. G. Mitchell, and Bernard D. Kern—No. V2

PHYSICAL REVIEW VOLUME 75, NUMBER 10 MAY 15, 1949

Proceedings of the American Physical Society

Minutes of the Meeting of the Metropolitan Section at the Bell Telephone Laboratories, Murray Hill, New Jersey on March 25, 1949

THE sixteenth annual meeting of the Metropolitan Section was held at Murray Hill on March 25, 1949. About one hundred members and guests were present. The morning session consisted of:

Welcoming Remarks by O. E. Buckley, *Bell Telephone Laboratories, Murray Hill, New Jersey.*

Radar Techniques in High Speed X-Ray Moving Pictures. Donald Dickson, *Westinghouse Electric Corporation, East Pittsburgh, Pennsylvania.*

Wave Propagation in Dipole Arrays. W. E. Kock, *Bell Telephone Laboratories, Murray Hill, New Jersey.*

Physics in an Industrial Laboratory. O. S. Duffendack, *Philips Laboratories, Inc., Irvington-on-Hudson, New York.*

In the afternoon short descriptions were given by D. H. Wenny, F. S. Malm, and W. C. Jones of the work in their laboratories at Murray Hill. The remainder of the afternoon was spent in tours by the members to the Free Space Room and many other laboratories.

Officers of the Section elected for the 1949–50 season are:

President	J. B. Johnson
Vice-President	W. W. Havens, Jr.
Secretary-Treasurer	I. Fankuchen
Committee Members	O. S. Duffendack
	Y. Beers

W. F. C. Ferguson
Secretary-Treasurer

THE PHYSICAL REVIEW

Characteristics of the Fi
On the g/ Values of the A
Magnetic Moment of the
Production of π-Mesons i
Reactions Induced by Slo
. . . . . .
Interpretation of the Reson
. . . . . .
Relativistic Terms in the
Microwave Asborption Sp
Radiations from Ge^{77} and
Neutrons in the Extensive
Analysis of Neutrons in
Precision Measurements
. . . . . .
On the Origin of Solar Ra
Transmission of Elastic P
Ferromagnetic Resonance
. . . . . .
Equations of State of Ma
. . . . . .
On the Wave Equation whi
Quantum-Theory Rectifi
Theoretical Analysis of Ion
Thermionic and Photoelec
Barrier . . . . . .
What Led to the Founding
Letters to the Editor:
Polarization of S
. . . . . .
Erratum: Phot
Measurement of
Absence of Photo-
. . . . . .
Infra-Red Absorp
. . . . . .
On the Transmi
On the Transmi
Two-Component
Neutron Diffract
Inelastic Scatteri
. . . . . .
On the Question
Erratum: The Det
. . . . . .
Beryllium-Proton
. . . . . .
Radioactive Silv
. . . . . .
Microwave Reson
. . . . . .
Strings, Poles, a
Search for the
. . . . . .
Decay of 8-Day
. . . . . .
Time-of-Flight M
Search for Stabl
. . . . . .
Concentrating H
Angular Correlat
. . . . . .
Stars Built on th
Discrepancies
between
Forces between
. . . . . .
Solid Solubility
Electron Spectr
. . . J.
Microwave Abso
. . . . . .
On the External
Proceedings of the Amer
Minutes of the
Minutes of the
New J

LANCASTER PRESS, INC.